

MULTIMODALITY IMAGING IN ACUTE CORONARY SYNDROME

EDITED BY: Jinwei Tian, Zhao Wang and Minjie Lu
PUBLISHED IN: Frontiers in Cardiovascular Medicine





frontiers

Frontiers eBook Copyright Statement

The copyright in the text of individual articles in this eBook is the property of their respective authors or their respective institutions or funders. The copyright in graphics and images within each article may be subject to copyright of other parties. In both cases this is subject to a license granted to Frontiers.

The compilation of articles constituting this eBook is the property of Frontiers.

Each article within this eBook, and the eBook itself, are published under the most recent version of the Creative Commons CC-BY licence.

The version current at the date of publication of this eBook is CC-BY 4.0. If the CC-BY licence is updated, the licence granted by Frontiers is automatically updated to the new version.

When exercising any right under the CC-BY licence, Frontiers must be attributed as the original publisher of the article or eBook, as applicable.

Authors have the responsibility of ensuring that any graphics or other materials which are the property of others may be included in the CC-BY licence, but this should be checked before relying on the CC-BY licence to reproduce those materials. Any copyright notices relating to those materials must be complied with.

Copyright and source acknowledgement notices may not be removed and must be displayed in any copy, derivative work or partial copy which includes the elements in question.

All copyright, and all rights therein, are protected by national and international copyright laws. The above represents a summary only. For further information please read Frontiers' Conditions for Website Use and Copyright Statement, and the applicable CC-BY licence.

ISSN 1664-8714

ISBN 978-2-88976-425-9

DOI 10.3389/978-2-88976-425-9

About Frontiers

Frontiers is more than just an open-access publisher of scholarly articles: it is a pioneering approach to the world of academia, radically improving the way scholarly research is managed. The grand vision of Frontiers is a world where all people have an equal opportunity to seek, share and generate knowledge. Frontiers provides immediate and permanent online open access to all its publications, but this alone is not enough to realize our grand goals.

Frontiers Journal Series

The Frontiers Journal Series is a multi-tier and interdisciplinary set of open-access, online journals, promising a paradigm shift from the current review, selection and dissemination processes in academic publishing. All Frontiers journals are driven by researchers for researchers; therefore, they constitute a service to the scholarly community. At the same time, the Frontiers Journal Series operates on a revolutionary invention, the tiered publishing system, initially addressing specific communities of scholars, and gradually climbing up to broader public understanding, thus serving the interests of the lay society, too.

Dedication to Quality

Each Frontiers article is a landmark of the highest quality, thanks to genuinely collaborative interactions between authors and review editors, who include some of the world's best academicians. Research must be certified by peers before entering a stream of knowledge that may eventually reach the public - and shape society; therefore, Frontiers only applies the most rigorous and unbiased reviews.

Frontiers revolutionizes research publishing by freely delivering the most outstanding research, evaluated with no bias from both the academic and social point of view. By applying the most advanced information technologies, Frontiers is catapulting scholarly publishing into a new generation.

What are Frontiers Research Topics?

Frontiers Research Topics are very popular trademarks of the Frontiers Journals Series: they are collections of at least ten articles, all centered on a particular subject. With their unique mix of varied contributions from Original Research to Review Articles, Frontiers Research Topics unify the most influential researchers, the latest key findings and historical advances in a hot research area! Find out more on how to host your own Frontiers Research Topic or contribute to one as an author by contacting the Frontiers Editorial Office: frontiersin.org/about/contact

MULTIMODALITY IMAGING IN ACUTE CORONARY SYNDROME

Topic Editors:

Jinwei Tian, The Second Affiliated Hospital of Harbin Medical University, China

Zhao Wang, University of Electronic Science and Technology of China, China

Minjie Lu, Chinese Academy of Medical Sciences and Peking Union Medical College, China

Citation: Tian, J., Wang, Z., Lu, M., eds. (2022). Multimodality Imaging in Acute Coronary Syndrome. Lausanne: Frontiers Media SA.
doi: 10.3389/978-2-88976-425-9

Table of Contents

- 06 Editorial: Multimodality Imaging in Acute Coronary Syndrome**
Yining Wang, Zhao Wang, Jinwei Tian and Minjie Lu
- 10 Role of Cardiovascular Computed Tomography in Acute Coronary Syndromes During the COVID-19 Pandemic-Single Center Snapshot Study**
Mirvat Alasnag, Waqar Ahmed, Ibrahim Al-Nasser and Khaled Al-Shaibi
- 15 Impact of Concomitant Impairments of the Left and Right Ventricular Myocardial Strain on the Prognoses of Patients With ST-Elevation Myocardial Infarction**
Wei Lai, He Jie, Dong Jian-Xun, Kong Ling-Cong, Zeng Jun-Tong, Shi Bo-Zhong, An Dong-Ao-Lei, Chen Bing-Hua, Ding Song, Li Zheng, Yang Fan, Yang Yi-Ning, Yan Fu-Hua, Xiu Jian-Cheng, Wang Hu-Wen, Xu Jian-Rong, Ge Heng and Pu Jun
- 27 Correlation of Myocardial Strain and Late Gadolinium Enhancement by Cardiac Magnetic Resonance After a First Anterior ST-Segment Elevation Myocardial Infarction**
Shiqin Yu, Jinying Zhou, Kai Yang, Xiuyu Chen, Yucong Zheng, Kankan Zhao, Jialin Song, Keshan Ji, Peng Zhou, Hongbing Yan and Shihua Zhao
- 36 Elevated Serum Levels of Soluble ST2 Are Associated With Plaque Vulnerability in Patients With Non-ST-Elevation Acute Coronary Syndrome**
Guqing Luo, Yuxuan Qian, Xincheng Sheng, Jiateng Sun, Zhinan Wu, Fei Liao, Qi Feng, Yan Yin, Song Ding and Jun Pu
- 45 A Novel Computed Tomography-Based Imaging Approach for Etiology Evaluation in Patients With Acute Coronary Syndrome and Non-obstructive Coronary Angiography**
Runjianya Ling, Lihua Yu, Zhigang Lu, Yuehua Li and Jiayin Zhang
- 54 Focal Geometry and Characteristics of Erosion-Prone Coronary Plaques in vivo Angiography and Optical Coherence Tomography Study**
Muhua Cao, Tianyu Wu, Jiawei Zhao, Zhuo Du, Zhuozhong Wang, Lulu Li, Guo Wei, Jinwei Tian, Haibo Jia, Gary S. Mintz and Bo Yu
- 65 Usefulness of Diastolic Function Score as a Predictor of Long-Term Prognosis in Patients With Acute Myocardial Infarction**
SungA Bae, Hyun Ju Yoon, Kye Hun Kim, Hyung Yoon Kim, Hyukjin Park, Jae Yeong Cho, Min Chul Kim, Yongcheol Kim, Youngkeun Ahn, Jeong Gwan Cho and Myung Ho Jeong
- 77 Research Progress of Imaging Methods for Detection of Microvascular Angina Pectoris in Diabetic Patients**
Yiming Qi, Lihua Li, Guoquan Feng, Chen Shao, Yue Cai and Zhongqun Wang
- 86 Sex Differences in the Non-infarct-Related Artery-Based Quantitative Flow Ratio in Patients With ST-Elevation Myocardial Infarction: A Retrospective Study**
Hongli Hou, Qi Zhao, Chao Qu, Meng Sun, Qi Liu, Xingtao Huang, Xuedong Wang, Ruoxi Zhang, Lifeng Du, Jingbo Hou and Bo Yu

- 94 Relationship Between Immunoinflammation and Coronary Physiology Evaluated by Quantitative Flow Ratio in Patients With Coronary Artery Disease**
Chengzhe Liu, Zhiyao Yu, Huaqiang Chen, Jun Wang, Wei Liu, Liping Zhou, Yueyi Wang, Hu Chen, Huixin Zhou, Zhihao Liu, Jiapeng Han, Hong Jiang and Lilei Yu
- 104 Advances in CT Techniques in Vascular Calcification**
Lijie Zhang, Lihua Li, Guoquan Feng, Tingpan Fan, Han Jiang and Zhongqun Wang
- 113 Coronary Computed Tomography Angiography Assessment of High-Risk Plaques in Predicting Acute Coronary Syndrome**
Guanyu Lu, Weitao Ye, Jiehao Ou, Xinyun Li, Zekun Tan, Tingyu Li and Hui Liu
- 125 Combined Use of Multiple Intravascular Imaging Techniques in Acute Coronary Syndrome**
Takashi Kubo, Kosei Terada, Yasushi Ino, Yasutsugu Shiono, Shengxian Tu, Tien-Ping Tsao, Yundai Chen and Duk-Woo Park
- 130 Comparison of Myocardial Layer-Specific Strain and Global Myocardial Work Efficiency During Treadmill Exercise Stress in Detecting Significant Coronary Artery Disease**
Jingru Lin, Lijian Gao, Jia He, Mengyi Liu, Yuqi Cai, Lili Niu, Ying Zhao, Xiaoni Li, Jiangtao Wang, Weichun Wu, Zhenhui Zhu and Hao Wang
- 141 Coronary Computed Tomography Angiographic Predictors of Non-culprit Territory Unrecognized Myocardial Infarction Assessed by Cardiac Magnetic Resonance in Non-ST-elevation Acute Coronary Syndrome**
Kazuki Matsuda, Masahiro Hoshino, Yoshihisa Kanaji, Tomoyo Sugiyama, Toru Misawa, Masahiro Hada, Tatsuhiko Nagamine, Kai Nogami, Kodai Sayama, Yun Teng, Hiroki Ueno, Taishi Yonetsu, Tetsuo Sasano and Tsunekazu Kakuta
- 152 Knowledge of Hyperemic Myocardial Blood Flow in Healthy Subjects Helps Identify Myocardial Ischemia in Patients With Coronary Artery Disease**
Lijuan Lyu, Jichen Pan, Dumin Li, Xinhao Li, Wei Yang, Mei Dong, Chenghu Guo, Peixin Lin, Yeming Han, Yongfeng Liang, Junyan Sun, Dexin Yu, Pengfei Zhang and Mei Zhang
- 165 Artificial Intelligence—A Good Assistant to Multi-Modality Imaging in Managing Acute Coronary Syndrome**
Ming-hao Liu, Chen Zhao, Shengfang Wang, Haibo Jia and Bo Yu
- 176 Predictors of Near-Infrared Spectroscopy-Detected Lipid-Rich Plaques by Optical Coherence Tomography-Defined Morphological Features in Patients With Acute Coronary Syndrome**
Eisuke Usui, Taishi Yonetsu, Mari Ohmori, Yoshinori Kanno, Masahiko Nakao, Takayuki Niida, Yuji Matsuda, Junji Matsuda, Tomoyuki Umemoto, Toru Misawa, Masahiro Hada, Masahiro Hoshino, Yoshihisa Kanaji, Tomoyo Sugiyama, Tsunekazu Kakuta and Tetsuo Sasano

184 *Protective Value of Aspirin Loading Dose on Left Ventricular Remodeling After ST-Elevation Myocardial Infarction*

Camilla Calvieri, Nicola Galea, Francesco Cilia, Giacomo Pambianchi, Giuseppe Mancuso, Domenico Filomena, Sara Cimino, Iacopo Carbone, Marco Francone, Luciano Agati and Carlo Catalano

195 *Deceleration Capacity Improves Prognostic Accuracy of Relative Increase and Final Coronary Physiology in Patients With Non-ST-Elevation Acute Coronary Syndrome*

Jun Wang, Chengzhe Liu, Fuding Guo, Zhen Zhou, Liping Zhou, Yueyi Wang, Huaqiang Chen, Huixin Zhou, Zhihao Liu, Shoupeng Duan, Ji Sun, Qiang Deng, Saiting Xu, Hong Jiang and Lilei Yu



Editorial: Multimodality Imaging in Acute Coronary Syndrome

Yining Wang¹, Zhao Wang^{2*}, Jinwei Tian^{3*} and Minjie Lu^{1,4*}

¹ Department of Magnetic Resonance Imaging, Fuwai Hospital, State Key Laboratory of Cardiovascular Disease, National Center for Cardiovascular Diseases, Chinese Academy of Medical Sciences and Peking Union Medical College, Beijing, China, ² School of Electronic Science and Engineering, University of Electronic Science and Technology of China, Chengdu, China, ³ Department of Cardiology, The Second Affiliated Hospital of Harbin Medical University, Harbin, China, ⁴ Laboratory of Cardiovascular Imaging (Cultivation), Chinese Academy of Medical Sciences, Beijing, China

Keywords: cardiac computed tomographic imaging, cardiac magnetic resonance imaging (CMR), echocardiography, multi-modality imaging, acute coronary syndrome (ACS)

Editorial on the Research Topic

Multimodality Imaging in Acute Coronary Syndrome

Acute coronary syndrome (ACS) is a group of clinical syndromes caused by acute myocardial ischemia, mainly including ST-segment elevation myocardial infarction (STEMI), non-STEMI (NSTEMI), and unstable angina. It is commonly attributed to the rupture of atherosclerotic plaques and secondary acute intracoronary thrombosis, and patients may die from acute myocardial ischemia after experiencing chest discomfort and dyspnea (1). Each year, more than 7 million people are diagnosed with ACS worldwide (2). With such a large base population, timely diagnosis and intervention are crucial for saving lives. For clinicians, understanding the characteristics and capabilities of each imaging modality can help in the rapid selection of appropriate examination within the prime time window. Imaging is essential for providing the comprehensive assessment of the anatomy and physiology of coronary arteries in the diagnosis, monitoring, prognostic evaluation of ACS, and beyond to maximize patient benefit.

Selected papers in this research theme discuss recent advances in multi-modality imaging (MMI) of ACS including both non-invasive and invasive techniques, which provide great insight into the etiology and pathology of ACS, and also demonstrate application of new technologies to refine the existing diagnostic system for ACS.

ECHOCARDIOGRAPHY

As the preferred screening tool for patients with suspected coronary artery disease (CAD), stress echocardiography can increase diagnostic efficacy and reduce medically induced injury but still with unsatisfactory specificity and sensitivity (3). Lin et al. reported the enhanced effect of global myocardial work efficiency (GWE) as a novel parameter of left ventricular function measurement, affirming the improved diagnostic ability of GWE in combination with myocardial layer-specific strain for CAD.

Left ventricular systolic and diastolic dysfunction suggests possible structural myocardial injury, and the predictive role of a single left ventricular diastolic function (LVDF) marker for the occurrence of adverse events in patients with post-acute myocardial ischemia (AMI) is well-established. Bae et al. described how the sum of the abnormal diastolic function markers was measured by transthoracic echocardiography, from which the left ventricular wall motion score index (WMSI) was calculated. They emphasized the application of this comprehensive scoring method for long-term prognosis and risk stratification of CAD.

OPEN ACCESS

Edited by:

Sebastian Kelle,
Deutsches Herzzentrum
Berlin, Germany

Reviewed by:

Georgios Benetos,
National and Kapodistrian University
of Athens, Greece

*Correspondence:

Minjie Lu
coolkan@163.com
Jinwei Tian
tianjinweidr2009@163.com
Zhao Wang
zhaowang92@gmail.com

Specialty section:

This article was submitted to
Cardiovascular Imaging,
a section of the journal
Frontiers in Cardiovascular Medicine

Received: 09 May 2022

Accepted: 18 May 2022

Published: 27 May 2022

Citation:

Wang Y, Wang Z, Tian J and Lu M
(2022) Editorial: Multimodality Imaging
in Acute Coronary Syndrome.
Front. Cardiovasc. Med. 9:939428.
doi: 10.3389/fcvm.2022.939428

CONTRAST ENHANCED CARDIAC COMPUTED-TOMOGRAPHY

Approximately 6% of AMI patients do not exhibit acute coronary obstruction (4). There are also a large number of patients who are unable to undergo cardiovascular magnetic resonance (CMR) due to contraindications or equipment unavailability. Using a novel CT-based imaging approach, Ling et al. provided comprehensive assessment of coronary structure and function in the above population. With the add-on of late iodine enhancement (LIE) for myocardial scar identification, dynamic computed tomography myocardial perfusion imaging (CT-MPI) combined with coronary computed tomographic angiography (CCTA) is not only equivalent to CMR in etiologic assessment, but also provides additional visualization of coronary artery wall and luminal structures to guide clinical intervention and prognostic management of patients with ACS. CCTA assessment of functional coronary stenosis is challenging and requires myocardial blood flow (MBF) as a complement to physiological information, which is generally obtained by positron emission tomography (PET) and magnetic resonance imaging (MRI). However, CT-MPI, also as a MBF assessment tool, has limited use in clinical practice. The study by Lyu et al. obtained MBF cut-off values for dynamic CT-MPI which can differentiate healthy subjects from patients with functional myocardial ischemia, establishing the basis for the development of future universal datasets.

Unrecognized myocardial infarction (UMI) accounts for approximately more than 50% of all myocardial infarctions and is difficult to recognize due to its asymptomatic syndromes (5, 6). In this setting, late gadolinium enhancement (LGE) is able to detect unrecognized myocardial scar in a subset of STEMI patients, but has limited evidence in NSTEMI patients. Matsuda et al. demonstrated the ability of CCTA to detect non-infarct-related UMI before invasive coronary angiography.

Intravascular ultrasound (IVUS) or optical coherence tomography (OCT) enables high resolution imaging of atherosclerotic plaques but is limited by its invasive nature. With the rapid development of non-invasive imaging technologies, it would be interesting to see whether non-invasive methods can approach the diagnostic accuracy of invasive methods for plaque characterization. Luo et al. validated the ability of serum soluble suppression of tumorigenicity-2 (sST2) to predict plaque tissue composition in patients with NSTEMI using standard CCTA and coronary angiography. Assessment of coronary lesions by inflammatory factors combined with imaging techniques may be one of the key future directions.

The diagnostic value of CCTA on unstable plaques and surrounding environment was likewise confirmed by Lu et al. CCTA stood out when clinicians need an “one-stop shop” examination to assess coronary anatomy, histological features of atherosclerotic plaques and hemodynamics. It can comprehensively evaluate the condition of almost all coronary arteries and branches macroscopically, while identifying the characteristics of high-risk atherosclerotic plaques with high precision. The authors discussed the application of CCTA in

predicting the occurrence of ACS and patient risk assessment, and provided an overview of some emerging techniques such as computational fluid dynamics.

The predictive function of coronary calcification on cardiovascular morbidity and mortality has been confirmed by previous studies and CT is considered the gold standard. Zhang et al. enumerated the diagnostic performance of different types of CT techniques in the assessment of vascular calcification including coronary calcification. Multi-slice spiral CT and dual-energy CT are commonly used in clinical practice to detect and quantify the extent of arterial calcification and assess high-risk plaque features. Emerging CT techniques including multi-slice spiral CT, micro CT, ultra-high resolution CT and etc., aim to enhance the detection of microcalcification by improving the imaging resolution.

The Coronavirus Disease 2019 (COVID 19) pandemic challenges traditional ACS assessment pathways, and it is sometimes of high demand to limit the spread of infection by avoiding unnecessary invasive procedures and curtailing the length of patient stay. Based on the GRACE Score, hemodynamics, and patients' COVID19 status, Alasnag et al. established the ACS cardiac computed tomography (CCT) protocol and treatment strategy, and validated the role of CCT in the evaluation of low risk ACS. Although this study is only a single-center trial, it has demonstrated the role of CCT in the anatomical risk stratification and has encouraged us to take on new challenges in special settings when working with conventional imaging.

CARDIAC MAGNETIC RESONANCE IMAGING (CMR)

As LGE has become an established technique for marking infarcted myocardium *in vivo*, CMR can be used for risk stratification and prognostic management of patients with STEMI (7, 8). Subtle and localized myocardial dysfunction can be further detected by strain analysis, but the correlation of cardiac MRI signature tracing with conventional CMR parameters is not yet known. Yu et al. demonstrated that strain not only correlates closely with LGE performance, but also detects alterations in myocardial function that are missed by left ventricular ejection fraction (LVEF) assessment and myocardial enhancement.

Left ventricular remodeling after STEMI is associated with adverse cardiovascular events in patients, and current guidelines recommend that patients improve their prognosis by taking aspirin prior to percutaneous coronary intervention (PCI) (7, 9). Calvieri et al. demonstrated the role of CMR in assessing the efficacy of cardioprotective therapies. CMR feature tracking analysis (CMR-FT), which is able to quantitatively assess subtle deformation in response to myocardial motion, detected adverse ventricular remodeling at an early stage.

Impairment of LV strain predicts possible subsequent ventricular remodeling and worsening ejection fraction, raising concerns among clinicians. With the development of new therapies, short-term mortality in patients with STEMI has decreased substantially, however, long-term prognosis varies

widely. Accurate and clinical available indicators for risk stratification are able to aid in the early identification of high-risk patients. Lai et al. affirmed the established role of CMR myocardial strain measurements for adverse events and the prognostic significance of the combined assessment of both left and right ventricular strain indexes.

CARDIAC NUCLEAR MEDICINE

Complications of diabetes often involve the microcirculatory system, and patients can develop angina secondary to microcirculatory dysfunction. Qi et al. reviewed the progress of commonly used imaging methods in detecting coronary microvascular angina. Both single-photon emission computed tomography (SPECT) and PET-MPI quantify myocardial blood flow, with the latter being more sensitive and specific. CMR is sensitive to early lesions and allows qualitative and quantitative visualization of coronary microcirculation. Myocardial contrast echocardiography is commonly used for preliminary screening and in recent years has also been developed for therapeutic purposes. CT allows for a comprehensive assessment of non-coronary ischemic heart disease (INOCA).

IVUS, OCT, FFR, AND QFR

Kubo et al. evaluated the combined use of multiple intravascular imaging techniques in ACS with their respective strengths and weaknesses. Both IVUS and OCT provide cross-sectional images of coronary arteries. IVUS provides better penetration, and can assess the size of both the lumen and external elastic lamina of the vessel, and therefore is valuable for assessing plaque burden. OCT has higher resolution but shallower penetration depth, and can detect thin cap fibroatheroma, also known as vulnerable plaque (10, 11), which has a large necrotic core and a thin fibrous cap often with macrophage infiltration. OCT can differentiate all major types of atherosclerotic plaques including lipid, calcification, fibrous plaques and etc. Near-infrared spectroscopy (NIRS) can detect the lipid component of plaques. They emphasized that any single technique has limitations in assessing the pathology of ACS and that a combination of multi-modality imaging techniques is needed to perform a comprehensive assessment and guide lesion-specific treatment. Usui et al. demonstrated that the examination results between OCT and NIRS are correlated, offering the possibility of assessing the morphological and molecular characteristics of lipid-rich plaques by a single system.

Cao et al. used OCT to evaluate the predictors of erosion-prone plaques, and found that some atherosclerotic plaques with certain features and geometry are more prone to develop secondary plaque erosion, which is one of the most common causes of coronary thrombosis.

Several studies have shown that there are anatomical, pathological and clinical differences between male and female CAD patients, and using the same cardiovascular assessment criteria does not provide appropriate treatment recommendations and prognostic assessments. Hou et al. clarified the gender difference of quantitative flow ratio

(QFR) in patients with STEMI, providing evidence for future establishment of a personalized treatment system. They focused on patients with poorer prognosis for non-infarct-related arterial disease (NIRA), who may require a more aggressive treatment approach.

Previous studies have shown that both the immune system and inflammatory cells promote plaque progression and aggravate coronary artery stenosis (12, 13). Liu C. et al. demonstrated that immunoinflammatory biomarkers such as interleukin (IL)-6, tumor necrosis factor (TNF)- α , and interferon (IFN)- γ were associated with a high risk of QFR ≤ 0.8 . It is suggested that combining inflammatory markers with imaging parameters can significantly improve the identification of functional severe CAD by predicting functional ischemia and anatomic stenosis.

PCI is the one of the routine treatments for STEMI, but approximately 20% patients who fail functional revascularization still experience adverse coronary events after the procedure. FFR can predict patient prognosis by evaluating functional stenosis of the coronary arteries. Wang et al. found that coronary physiology and deceleration capacity (DC) combined with QFR were able to improve the predictive accuracy of major adverse cardiac and cerebrovascular events.

ARTIFICIAL INTELLIGENCE (AI)

The comprehensive assessment of ACS often involves multiple imaging modalities, demanding real-time, objective and precise diagnosis. Liu M-h. et al. discussed the advantages of AI combined with MMI in filling the gaps of ACS management strategies. With massive data collection and powerful processing capabilities, AI, in particular deep learning, learns and extracts hierarchical features from clinical data automatically and is valuable for lesion identification and segmentation, disease classification, clinical recommendation, and prognosis prediction. With the help of AI, diagnostic performance can be significantly improved ranging from non-invasive imaging techniques such as CT and CMR to invasive imaging techniques such as coronary angiography (CAG), OCT and IVUS.

CONCLUSION AND FUTURE PERSPECTIVES

It's thrilling to see the fast pace multimodality imaging technologies have been developed in the evaluation of ACS for the past decade. In addition, the advances of new technologies can further help physicians and bring benefits to patients. The combination of multiple imaging modalities, the addition of AI technology and the joint application of biological markers and imaging techniques have already evolved into mainstream directions for future research, which may bring fundamental changes to the diagnosis and management of ACS.

AUTHOR CONTRIBUTIONS

YW wrote the first draft of the manuscript. ZW, JT, and ML wrote sections of the manuscript. All authors contributed to manuscript revision, read, and approved the submitted version.

FUNDING

This work was supported by the Construction Research Project of the Key Laboratory (Cultivation) of Chinese Academy of Medical Sciences (2019PT310025), National Natural Science Foundation of China (81971588),

Youth Key Program of High-level Hospital Clinical Research (2022-GSP-QZ-5), the Applied Technology Research and Development Plan of Heilongjiang Province (GY2020YF0039 to JT) and the Fok Ying-Tong Education Foundation for Young Teachers (171032 to JT).

REFERENCES

- Anderson JL, Morrow DA. Acute Myocardial Infarction. *N Engl J Med*. (2017) 376:2053–64. doi: 10.1056/NEJMra1606915
- Reed GW, Rossi JE, Cannon CP. Acute myocardial infarction. *Lancet*. (2017) 389:197–210. doi: 10.1016/S0140-6736(16)30677-8
- Task Force Members, Montalescot G, Sechtem U, Achenbach S, Andreotti F, Arden C, et al. 2013 ESC guidelines on the management of stable coronary artery disease: the Task Force on the management of stable coronary artery disease of the European Society of Cardiology. *Eur Heart J*. (2013) 34:2949–3003. doi: 10.1093/eurheartj/ehz296
- Smilowitz NR, Mahajan AM, Roe MT, Hellkamp AS, Chiswell K, Gulati M, et al. Mortality of myocardial infarction by sex, age, and obstructive coronary artery disease status in the ACTION Registry-GWTG (acute coronary treatment and intervention outcomes network registry-get with the guidelines). *Circ Cardiovasc Qual Outcomes*. (2017) 10:e003443. doi: 10.1161/CIRCOUTCOMES.116.003443
- Antiochos P, Ge Y, Steel K, Bingham S, Abdullah S, Mikolich JR, et al. Imaging of clinically unrecognized myocardial fibrosis in patients with suspected coronary artery disease. *J Am Coll Cardiol*. (2020) 76:945–57. doi: 10.1016/j.jacc.2020.06.063
- Acharya T, Aspelund T, Jonasson TF, Schelbert EB, Cao JJ, Sathya B, et al. Association of unrecognized myocardial infarction with long-term outcomes in community-dwelling older adults: the ICELAND MI Study. *JAMA Cardiol*. (2018) 3:1101–6. doi: 10.1001/jamacardio.2018.3285
- Ibanez B, James S, Agewall S, Antunes MJ, Bucciarelli-Ducci C, Bueno H, et al. 2017 ESC Guidelines for the management of acute myocardial infarction in patients presenting with ST-segment elevation: the Task Force for the management of acute myocardial infarction in patients presenting with ST-segment elevation of the European Society of Cardiology (ESC). *Eur Heart J*. (2018) 39:119–77. doi: 10.1093/eurheartj/ehx393
- Schulz-Menger J, Bluemke DA, Bremerich J, Flamm SD, Fogel MA, Friedrich MG, et al. Standardized image interpretation and post-processing in cardiovascular magnetic resonance - 2020 update : Society for Cardiovascular Magnetic Resonance (SCMR): Board of Trustees Task Force on Standardized Post-Processing. *J Cardiovasc Magn Reson*. (2020) 22:19. doi: 10.1186/s12968-020-00610-6
- Funaro S, La Torre G, Madonna M, Galiuto L, Scarà A, Labbadia A, et al. Incidence, determinants, and prognostic value of reverse left ventricular remodelling after primary percutaneous coronary intervention: results of the Acute Myocardial Infarction Contrast Imaging (AMICI) multicenter study. *Eur Heart J*. (2009) 30:566–75. doi: 10.1093/eurheartj/ehn529
- Uemura S, Ishigami K, Soeda T, Okayama S, Sung JH, et al. Thin-cap fibroatheroma and microchannel findings in optical coherence tomography correlate with subsequent progression of coronary atheromatous plaques. *Eur Heart J*. (2012) 33:78–85. doi: 10.1093/eurheartj/ehz284
- Jinnouchi H, Sato Y, Torii S, Sakamoto A, Cornelissen A, Bhoite RR, et al. Detection of cholesterol crystals by optical coherence tomography. *Eurointervention*. (2020) 16:395–403. doi: 10.4244/EIJ-D-20-00202
- Hansson GK. Inflammation, atherosclerosis, and coronary artery disease. *N Engl J Med*. (2005) 352:1685–95. doi: 10.1056/NEJMra043430
- Chávez-Sánchez L, Espinosa-Luna JE, Chávez-Rueda K, Legorreta-Haquet MV, Montoya-Díaz E, Blanco-Favela F. Innate immune system cells in atherosclerosis. *Arch Med Res*. (2014) 45:1–14. doi: 10.1016/j.arcmed.2013.11.007

Conflict of Interest: The authors declare that the research was conducted in the absence of any commercial or financial relationships that could be construed as a potential conflict of interest.

Publisher's Note: All claims expressed in this article are solely those of the authors and do not necessarily represent those of their affiliated organizations, or those of the publisher, the editors and the reviewers. Any product that may be evaluated in this article, or claim that may be made by its manufacturer, is not guaranteed or endorsed by the publisher.

Copyright © 2022 Wang, Wang, Tian and Lu. This is an open-access article distributed under the terms of the Creative Commons Attribution License (CC BY). The use, distribution or reproduction in other forums is permitted, provided the original author(s) and the copyright owner(s) are credited and that the original publication in this journal is cited, in accordance with accepted academic practice. No use, distribution or reproduction is permitted which does not comply with these terms.



Role of Cardiovascular Computed Tomography in Acute Coronary Syndromes During the COVID-19 Pandemic-Single Center Snapshot Study

Mirvat Alasnag^{1*}, Waqar Ahmed¹, Ibrahim Al-Nasser² and Khaled Al-Shaibi¹

¹ Cardiac Center, King Fahd Armed Forces Hospital, Jeddah, Saudi Arabia, ² Radiodiagnostics Department, King Fahd Armed Forces Hospital, Jeddah, Saudi Arabia

OPEN ACCESS

Edited by:

Minjie Lu,

Chinese Academy of Medical Sciences and Peking Union Medical College, China

Reviewed by:

Mamas Mamas,

Keele University, United Kingdom

Ankush Gupta,

Military Hospital Jaipur, India

*Correspondence:

Mirvat Alasnag
mirvat@jeddacath.com

Specialty section:

This article was submitted to Cardiovascular Imaging, a section of the journal Frontiers in Cardiovascular Medicine

Received: 08 February 2021

Accepted: 12 April 2021

Published: 11 May 2021

Citation:

Alasnag M, Ahmed W, Al-Nasser I and Al-Shaibi K (2021) Role of Cardiovascular Computed Tomography in Acute Coronary Syndromes During the COVID-19 Pandemic-Single Center Snapshot Study. *Front. Cardiovasc. Med.* 8:665735. doi: 10.3389/fcvm.2021.665735

Background: In clinical practice, cardiac computed tomography (CCT) has a limited role in acute coronary syndromes (ACS). Several trials evaluated CCT in low and intermediate risk patients presenting to the emergency room (ER) and noted that it was both safe and feasible. During the COVID19 pandemic, it is imperative to adopt a pathway for the evaluation of ACS that permits early discharge, reduces invasive coronary angiography and limits exposure of healthcare workers. Here, we present a single center experience by which CCT was incorporated in the clinical pathway of patients presenting to the ER with chest pain and ACS.

Methods: This is a snapshot study of the first 27 patients who underwent CCT immediately after the lockdown in the city of Jeddah. ST elevation myocardial infarctions and hemodynamically unstable patients were excluded. Those with unstable angina or a Non-ST elevation myocardial infarction were screened for COVID19. The patients' COVID19 status and the results of the CCT were then used to determine the treatment strategy. Patient predisposition, hospital stay and exposure of staff are collected and reported.

Results: All CCT images were interpretable with no limitations or significant artifact. CCT identified critical disease in 7 patients (26%), normal epicardial coronary arteries in 11 (41%) and mild to moderate disease in 9 (33%). All patients with normal or mild to moderate disease were assigned to a conservative strategy and discharged within 24 h. Those with a NSTEMI and critical anatomy were assigned to an additional invasive evaluation with subsequent revascularization. During the course of this study, no transmission to healthcare workers occurred.

Conclusion: CCT enabled 80% of patients to be discharged within the first 24 h, the majority of whom were discharged from the emergency room. It was able to identify critical anatomy facilitating appropriate revascularization. This snapshot study warrants exploration of the role of CCT in ACS further particularly since the latest European Society of Cardiology's Non-STEACS guidelines suggest a role for CCT in the evaluation of low risk ACS.

Keywords: cardiac computed tomography, COVID-19, acute coronary syndrome, infection, revascularization

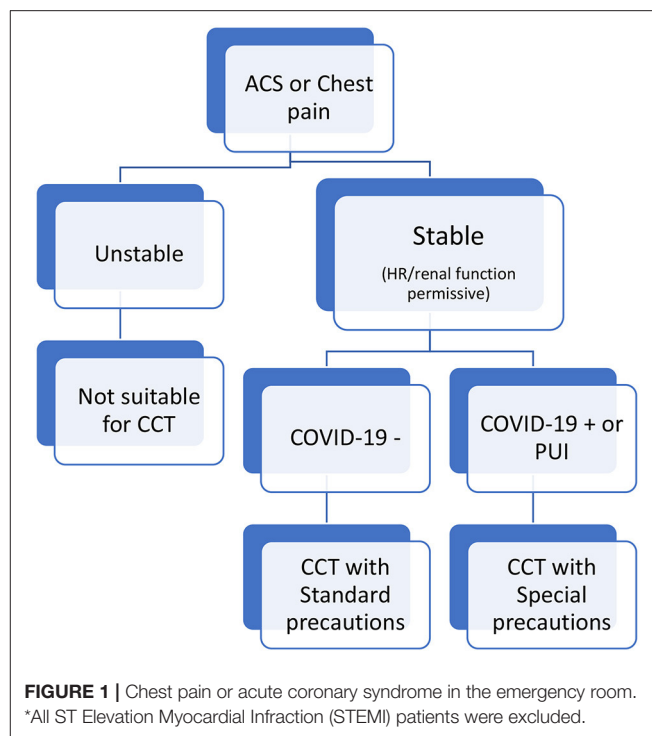
INTRODUCTION

The SARS-CoV-2 [Corona Virus Disease 2019 (COVID19)] pandemic has posed new challenges to the global cardiovascular community. The goals of any tertiary cardiac center are 2-fold: limit transmission of the infection to the public and healthcare personnel while providing timely and safe care to patients with acute coronary syndromes (ACS). Conventionally, the role of cardiovascular computed tomography (CCT) in ACS has been minimal as the majority of these patients commonly undergo an early invasive strategy. COVID19 created a new reality in many healthcare systems where an invasive strategy is limited by the availability of healthcare workers, personal protective equipment (PPE) and beds. In this study we review the evolving role of CCT in ACS in a tertiary cardiac center in Saudi Arabia during the COVID19 pandemic.

METHODS

This is a single center snapshot study of the first 27 consecutive patients who presented with chest pain or ACS and underwent CCT evaluation at the Cardiac Center of King Fahd Armed Forces Hospital (KFAFH) after the lockdown in the city of Jeddah (March 23, 2020). Research and ethics committee approval was obtained prior to the data collection. Total CCT studies, patient disposition and healthcare personnel's infection rates were prospectively collected from the center's key performance indicator database, infection control database and employee health records. All baseline characteristics, assigned strategy, outcome and COVID19 status were obtained from the patients' electronic medical record.

All elective admissions to the cardiac center were canceled. Only patients requiring acute cardiac care were transferred from outlying hospitals provided the COVID19 screen was negative. Patients presenting to KFAFH's emergency room with an ACS were screened for COVID19 symptoms in particular fever, cough and shortness of breath. If there was no suspicion of COVID19, the usual guideline directed ACS protocols were adopted. However, those with a suspicion based on symptoms or referral source were placed in isolation and a screening test was requested. The COVID19 polymerase chain reaction (PCR) was sent to an on-site laboratory and results were obtained in 3–4 h. The ACS CCT protocol adopted is defined in **Figure 1**. Those with chest pain or an ACS were risk stratified according to the GRACE Score and hemodynamics. If patients were unstable, had an ST elevation myocardial infarction (STEMI) or had prohibitive renal dysfunction, they were excluded and did not undergo a CCT. Stable patients with chest pain or an ACS underwent CCT. The precautions employed for those with a COVID19 negative screen were standard universal precautions. Those under investigation or positive for COVID19 underwent CTA in a dedicated Siemens 128 Flash CT Scanner with special precautions. During the CCT study, staffing in the room was minimized to the nurse who placed the electrodes, connected the intravenous cannula and positioned the patient. The nurse wore PPE as recommended by the WHO including an N95 mask. The imaging expert and radiographer remained in the control



room. The patient was transported with a regular surgical mask directly to the one designated CT scanner bypassing the holding and recovery areas.

Patients' COVID19 status and the results of the CCT were then used to determine the treatment strategy as illustrated in **Figure 2**. Patients who had a negative COVID19 PCR and a normal CCT were discharged home immediately. Those with critical anatomy were admitted for an invasive coronary angiogram. Critical anatomy was defined as stenosis >70% in major epicardial coronary vessels or Left main stenosis. Those with mild or moderate distal or branch vessel disease were discussed with the main responsible physician and patient to consider medical therapy and early discharge. As for those who were COVID19 positive or under investigation, normal or mild to moderate coronary disease on CCT allowed discharge of the patients to an isolation facility. Critical anatomy required hospitalization in an isolation unit. A case by case discussion ensued in a heart team format to determine the most appropriate course of action (conservative, surgical or percutaneous revascularization).

The CCT study was performed using standard imaging protocols for coronary evaluation and included the lung fields. Two-dimensional maximum intensity projections and multiplanar reformatted images as well as three-dimensional images were evaluated on a Syngo Via workstation by an imaging expert. Coronary artery calcium score, coronary stenosis and the lung parenchyma were all assessed and reported. Quadruple rule outs for pulmonary embolism, myocardial perfusion, coronary anatomy and parenchymal lung involvement were employed whenever possible.

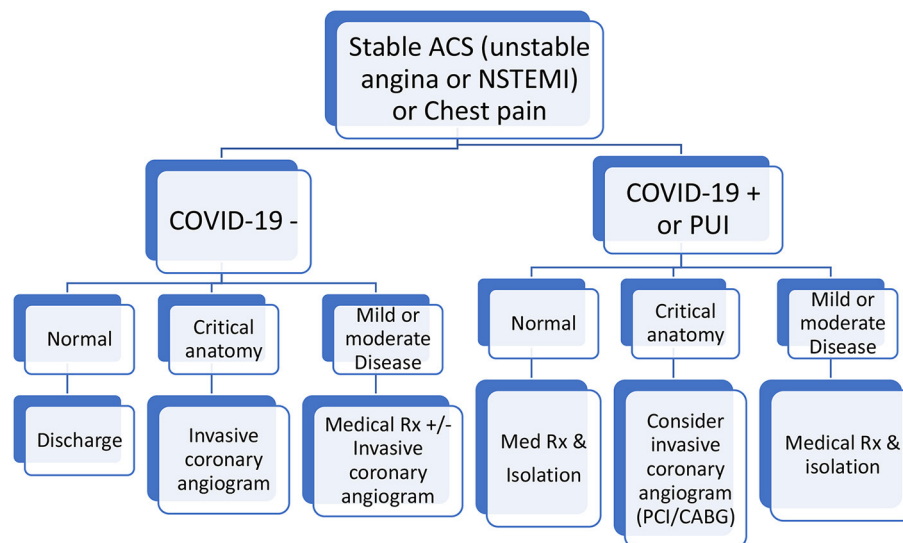


FIGURE 2 | Chest pain or acute coronary syndrome clinical pathway. *All ST elevation myocardial infarction (STEMI) and unstable patients were excluded.

TABLE 1 | Summary of results.

General characteristics	Total 27
Age (years)	Range 20–73 (Mean 52)
Gender – Female	14 (52 %)
ASCVD risk factors	
0	6
1	6
2	8
>3	7
Presentation of ACS	
Chest pain/Unstable Angina	14
NSTEMI	13
CT findings	
Normal	11
Mild to Moderate	9
Critical	7
Treatment strategy	
PCI (In-patient)	4
CABG (In-patient)	1
CABG (Deferred)	2
Conservative	20
EF (mean)	Range 15–65 % (Mean 50%)
Length of Hospital Stay	0–5 days (Mean 1 day)
Chest pain/Unstable Angina	0–2 days (Mean 0 days)
NSTEMI	0–5 days (Mean 1.6 days)

Statistical Analysis

In this prospective analysis the continuous variables are presented as mean and range. The qualitative variables are presented in percentages.

RESULTS

This cohort comprises the first 27 patients evaluated in the emergency room immediately after the COVID19 lockdown in Jeddah, March 15, 2020 who presented with acute onset chest pain consistent with angina of which 13 had a positive high sensitivity troponin I assay. The results are summarized in **Table 1**. The mean age was 52 years (range 20–73 years). Fifty-two percent were women. Six patients had no known atherosclerotic cardiovascular risk factors and seven had 3 or more risk factors. The mean left ventricular ejection fraction was 50% (range 15–65%). All CCT images were interpretable with no limitations or significant artifact. CCT identified critical disease in 7 patients (26%) all of whom had presented with a NSTEMI, normal epicardial coronary arteries in 11 (41%) and mild to moderate disease in 9 (33%). All patients with normal or mild to moderate disease were assigned to a conservative strategy and discharged within 24h. Those with a NSTEMI and critical anatomy were assigned to an additional invasive evaluation of which four underwent *ad hoc* percutaneous coronary interventions (PCI) for the Left anterior descending artery (3) and Left Circumflex artery (1), 1 had in-hospital coronary artery bypass grafting (CABG) for distal Left Main disease and two were deferred for elective CABG at a later date for three vessel disease. Examples of obstructive disease detected by CCT and treated by PCI are illustrated in **Supplementary Figures 1, 2**.

DISCUSSION

CCT has an established role in the assessment of patients with stable coronary syndromes which has been validated in multiple randomized clinical trials (1–3). Its role in the evaluation of patients in the emergency room has also been studied in several

randomized trials the most notable being the ROMICAT I and II trials (4–7). However, the patients in these trials were low to intermediate risk with negative initial cardiac serum markers and electrocardiograms. In the ROMICAT cohorts, both the feasibility and safety of such a strategy were confirmed. The average length of stay was significantly reduced with no increase in major adverse cardiac events at 28 days.

During the current COVID19 pandemic, utilization of healthcare resources including beds and PPE in addition to exposure of HCW to COVID19 is a priority (8, 9). This must be balanced against a timely designation of the treatment strategy for ACS patients. We, therefore, included those with positive serum markers who had either confirmed or suspected COVID19 infection. The results of this snapshot study indicated that 80% of patients were discharged within 24 h, the majority directly from the emergency room signifying very efficient bed utilization. Fifty per centage of those were discharged the same day and carried a low Grace Score. The overall low Grace Score of the study population, including those who presented with a NSTEMI, suggests such a strategy of non-invasive assessment of the coronary arteries and rapid discharge planning may be applicable only to a low or intermediate risk populations. This is in line with the previously mentioned ROMICAT studies enrolling similar populations and excluded high risk, STEMI and patients in shock. There was a marked reduction in invasive angiography and subsequently less consumption of PPE and exposure of catheterization personnel. None of the staff in the CCT department or catheterization laboratory were infected.

Furthermore, troponin elevation in critically ill patients is frequently due to Type II myocardial infarction unrelated to obstructive epicardial coronary artery disease. This protocol was able to identify those with critical anatomy that required invasive angiography and revascularization. Those who didn't have critical anatomy, the CCT was able to furnish additional information such as evaluation of the lung fields for COVID19 pneumonitis, myocarditis and pulmonary embolism all which could raise troponins and have been reported in COVID19 cases.

There is ample evidence that the negative predictive value (NPV) of CCT exceeds 90% sensitivity and specificity of 96.5 and 72.4% respectively. It is noteworthy that the NPV is not impacted by the clinical risk scores (10). The utility in low risk ACS has been added to the European Society of Cardiology's Non-ST elevation Myocardial Infarction Guidelines (ESC NSTEMI) elaborated in August 2020 suggesting a wider role for this technology in select patients. Our experience during the COVID19 adds to the growing experience with streamlining care using CCT in low risk ACS (11). It should be noted that even the ESC guidelines recognize that non-obstructive coronary disease carries prognostic implications. Intracoronary imaging and cardiac magnetic resonance imaging have been recommended in the evaluation of those with myocardial infarction and non-obstructive coronary arteries (MINOCA). Establishing protocols that permit expeditious inpatient or outpatient assessment of such cases is important.

Limitations

This is a snapshot study with a small number of patients. The study only serves as a pilot that requires further validation through large scale randomized trials. There is no long term follow up available. However, during such an outbreak the goal of all centers is to provide acute care for a surge of COVID19 patients that can overwhelm the system. Furthermore, it should be noted that the ROMICAT trials reported outcome data at 28 days only. The purpose of pathways that include CCT is to enable cardiac centers to further risk stratify patients and allow early discharge. CT scanners are often shared by the cardiology and radiology services. Therefore, adoption of these pathways would require coordination between the departments. In addition, during such an outbreak it is necessary to prioritize studies for all patients with both cardiac and non-cardiac needs.

CONCLUSIONS

COVID19 presented a unique opportunity for CCT to assist in providing anatomic risk stratification for those with ACS allowing expedited discharge of those with low risk anatomy and preserving beds during the outbreak. It also reduced invasive procedures and exposure of catheterization laboratory personnel with conservation of PPE in lower risk patients. Nevertheless, individualized case by case decisions are still necessary to ensure patient outcomes for the higher risk categories. This snapshot warrants exploring the role of CCT in ACS further through larger randomized studies. It is in keeping with the latest ESC NSTEMI guidelines.

DATA AVAILABILITY STATEMENT

The raw data supporting the conclusions of this article will be made available by the authors, without undue reservation.

ETHICS STATEMENT

The studies involving human participants were reviewed and approved by Ethics Committee of King Fahd Armed Forces Hospital. Written informed consent for participation was not required for this study in accordance with the national legislation and the institutional requirements.

AUTHOR CONTRIBUTIONS

All authors listed have made a substantial, direct and intellectual contribution to the work, and approved it for publication.

SUPPLEMENTARY MATERIAL

The Supplementary Material for this article can be found online at: <https://www.frontiersin.org/articles/10.3389/fcvm.2021.665735/full#supplementary-material>

REFERENCES

- Budoff MJ, Dowe D, Jollis JG, Gitter M, Sutherland J, Halamert E, et al. Diagnostic performance of 64-multidetector row coronary computed tomographic angiography for evaluation of coronary artery stenosis in individuals without known coronary artery disease: results from the prospective multicenter ACCURACY (assessment by coronary computed tomographic angiography of individuals undergoing invasive coronary angiography) trial. *J Am Coll Cardiol.* (2008) 52:1724–32. doi: 10.1016/j.jacc.2008.07.031
- Min JK, Dunning A, Lin FY, Achenbach S, Al-Mallah M, Budoff MJ, et al. Age- and sex-related differences in all-cause mortality risk based on coronary computed tomography angiography findings results from the international multicenter CONFIRM (coronary CT angiography evaluation for clinical outcomes: an international multicenter registry) of 23,854 patients without known coronary artery disease. *J Am Coll Cardiol.* (2011) 58:849–60. doi: 10.1016/j.jacc.2011.02.074
- Nazir MS, Nicol E. The SCOT-HEART trial: cardiac CT to guide patient management and improve outcomes. *Cardiovas Res.* (2019) 115:e88–90. doi: 10.1093/cvr/cvz173
- Hoffmann U, Bamberg F, Chae CU, Nichols JH, Rogers IS, Seneviratne SK, et al. Coronary computed tomography angiography for early triage of patients with acute chest pain: the ROMICAT (rule out myocardial infarction using computer assisted tomography) trial. *J Am Coll Cardiol.* (2009) 53:1642–50. doi: 10.1016/j.jacc.2009.01.052
- Hoffmann U, Truong Q, Schoenfeld D, Chou E, Woodard P, Nagurney J, et al. Coronary CT angiography versus standard evaluation in acute chest pain. *N Engl J Med.* (2012) 367:299–308. doi: 10.1056/NEJMoa1201161
- Schlett CL, Banerji D, Siegel E, Bamberg F, Lehman SJ, Ferencik M, et al. Prognostic value of CT angiography for major adverse cardiac events in patients with acute chest pain from the emergency department: 2-year outcomes of the ROMICAT trial. *JACC Cardiovasc Imaging.* (2011) 4:481–91. doi: 10.1016/j.jcmg.2010.12.008
- Hoffmann U, Truong QA, Fleg JL, Goehler A, Gazelle S, Wiviott S, et al. Design of the rule out myocardial ischemia/infarction using computer assisted tomography: a multicenter randomized comparative effectiveness trial of cardiac computed tomography versus alternative triage strategies in patients with acute chest pain in the emergency department. *Am Heart J.* (2012) 163:330–8. doi: 10.1016/j.ahj.2012.01.028
- Choi AD, Abbata S, Branch KR, Feuchtnner GM, Ghoshhajra B, Nieman K, et al. Society of cardiovascular computed tomography guidance for use of cardiac computed tomography amidst the COVID-19 pandemic. *J Cardiovasc Comp Tomog.* (2020) 14:101–4. doi: 10.1016/j.jcct.2020.03.002
- American College of Radiology Recommendations for the Use of Chest Radiography and Computed Tomography (CT) for Suspected COVID-19 Infection. Available online at: <https://www.acr.org/Advocacy-and-Economics/ACR-PositionStatements/Recommendations-for-ChestRadiography-and-CT-for-Suspected-COVID19-Infection> (accessed March 22, 2020).
- Linde JJ, Kelbæk H, Hansen TF, Sigvardsen PE, Torp-Pedersen C, Bech J, et al. Coronary CT angiography in patients with non-ST-segment elevation acute coronary syndrome. *J Am Coll Cardiol.* (2020) 75:453–63. doi: 10.1016/j.jacc.2019.12.012
- Collet JP, Thiele H, Barbato E, Barthélémy O, Bauersachs J, Bhatt DL, et al. ESC scientific document group, 2020 ESC guidelines for the management of acute coronary syndromes in patients presenting without persistent ST-segment elevation: the task force for the management of acute coronary syndromes in patients presenting without persistent ST-segment elevation of the European society of cardiology (ESC). *Eur Heart J.* (2020) ehaa575.

Conflict of Interest: The authors declare that the research was conducted in the absence of any commercial or financial relationships that could be construed as a potential conflict of interest.

Copyright © 2021 Alasnag, Ahmed, Al-Nasser and Al-Shaibi. This is an open-access article distributed under the terms of the Creative Commons Attribution License (CC BY). The use, distribution or reproduction in other forums is permitted, provided the original author(s) and the copyright owner(s) are credited and that the original publication in this journal is cited, in accordance with accepted academic practice. No use, distribution or reproduction is permitted which does not comply with these terms.



Impact of Concomitant Impairments of the Left and Right Ventricular Myocardial Strain on the Prognoses of Patients With ST-Elevation Myocardial Infarction

OPEN ACCESS

Edited by:

Minjie Lu,
Chinese Academy of Medical
Sciences and Peking Union Medical
College, China

Reviewed by:

Yucheng Chen,
Sichuan University, China
Erhan Tenekecioglu,
University of Health Sciences, Turkey

*Correspondence:

Ge Heng
dr.geheng@foxmail.com
Pu Jun
pujun310@hotmail.com

[†]These authors have contributed
equally to this work

Specialty section:

This article was submitted to
Cardiovascular Imaging,
a section of the journal
Frontiers in Cardiovascular Medicine

Received: 27 January 2021

Accepted: 30 April 2021

Published: 31 May 2021

Citation:

Lai W, Jie H, Jian-Xun D,
Ling-Cong K, Jun-Tong Z,
Bo-Zhong S, Dong-Ao-Lei A,
Bing-Hua C, Song D, Zheng L, Fan Y,
Yi-Ning Y, Fu-Hua Y, Jian-Cheng X,
Hu-Wen W, Jian-Rong X, Heng G and
Jun P (2021) Impact of Concomitant
Impairments of the Left and Right
Ventricular Myocardial Strain on the
Prognoses of Patients With
ST-Elevation Myocardial Infarction.
Front. Cardiovasc. Med. 8:659364.
doi: 10.3389/fcvm.2021.659364

Wei Lai^{1†}, He Jie^{1†}, Dong Jian-Xun¹, Kong Ling-Cong¹, Zeng Jun-Tong¹, Shi Bo-Zhong¹,
An Dong-Ao-Lei², Chen Bing-Hua², Ding Song¹, Li Zheng¹, Yang Fan¹, Yang Yi-Ning³,
Yan Fu-Hua⁴, Xiu Jian-Cheng⁵, Wang Hu-Wen⁶, Xu Jian-Rong², Ge Heng^{1*} and Pu Jun^{1*}

¹ Department of Cardiology, School of Medicine, Renji Hospital, Shanghai Jiao Tong University, Shanghai, China,

² Department of Radiology, School of Medicine, Renji Hospital, Shanghai Jiao Tong University, Shanghai, China, ³ The First
Affiliated Hospital, Xinjiang Medical University, Ürümqi, China, ⁴ Department of Radiology, School of Medicine, Ruijin Hospital,
Shanghai Jiao Tong University, Shanghai, China, ⁵ Nanfang Hospital, Southern Medical University, Guangzhou, China,

⁶ School of Public Health, Shanghai Jiaotong University, Shanghai, China

Background: The impact of concomitant impairments of left and right ventricular (LV and RV) strain on the long-term prognosis of acute ST-elevation myocardial infarction (STEMI) is not clear.

Methods: We analyzed CMR images and followed up 420 first STEMI patients from the EARLY Assessment of MYOcardial Tissue Characteristics by CMR in STEMI (EARLY-MYO-CMR) registry (NCT03768453). These patients received timely primary percutaneous coronary intervention (PCI) within 12 h and CMR examination within 1 week (median, 5 days; range, 2–7 days) after infarction. Global longitudinal strain (GLS), global radial strain (GRS), and global circumferential strain (GCS) of both ventricles were measured based on CMR cine images. Conventional CMR indexes were also assessed. Primary clinical outcome was composite major adverse cardiac and cerebrovascular events (MACCEs) including cardiovascular death, re-infarction, re-hospitalization for heart failure and stroke. In addition, CMR data from 40 people without apparent heart disease were used as control group.

Results: Compared to controls, both LV and RV strains were remarkably reduced in STEMI patients. During follow-up (median: 52 months, interquartile range: 29–68 months), 80 patients experienced major adverse cardiac and cerebrovascular events (MACCEs) including cardiovascular death, re-infarction, heart failure, and stroke. LV-GCS > −11.20% was an independent predictor of MACCEs ($P < 0.001$). RV-GRS was the only RV strain index that could effectively predict the risk of MACCEs (AUC = 0.604, 95% CI [0.533, 0.674], $P = 0.004$). Patient with RV-GRS ≤ 38.79% experienced more MACCEs than those with preserved RV-GRS (log rank $P < 0.001$). Moreover, patients

with the concomitant decrease of LV-GCS and RV-GRS were more likely to experience MACCEs than patients with decreased LV-GCS alone (log rank $P = 0.010$). RV-GRS was incremental to LV-GCS for the predictive power of MACCEs (continuous NRI: 0.327; 95% CI: 0.095–0.558; $P = 0.006$). Finally, tobacco use ($P = 0.003$), right coronary artery involvement ($P = 0.002$), and LV-GCS $> -11.20\%$ ($P = 0.012$) was correlated with lower RV-GRS.

Conclusions: The concomitant decrease of LV and RV strain is associated with a worse long-term prognosis than impaired LV strain alone. Combination assessment of both LV and RV strain indexes could improve risk stratification of patients with STEMI.

Trial Registration: ClinicalTrials.gov, NCT03768453. Registered 7 December 2018 - Retrospectively registered, <https://clinicaltrials.gov/ct2/show/NCT03768453>.

Keywords: ST-elevation myocardial infarction, cardiac magnetic resonance, myocardial strain analysis, right ventricle, prognostic implications

INTRODUCTION

The in-hospital mortality rate of patients with acute ST-elevation myocardial infarction (STEMI) has greatly declined (1). However, the long-term prognosis of patients with STEMI is quite varied (2). Therefore, the early risk stratification of patients with STEMI is essential. Accurate and clinically applicable indicators are needed.

The left ventricle (LV) function is a key prognostic factor for patients with STEMI (2). Although LV ejection fraction (LVEF) is regularly used as a measurement of LV function, it is less sensitive for the detection of regional or subtle myocardial impairments, which are common in the early phase of myocardial infarction and occur as the very beginning of subsequent adverse cardiac remodeling (3). For the past decade, myocardial strain measurements have been used to determine LV function. Myocardial strain demonstrates the absolute magnitude of myocardial deformation in each segment compared to the global estimation of conventional LVEF (3). Recent studies have shown that the impairments of LV strains measured by echocardiography and cardiac magnetic resonance (CMR) in the acute phase of STEMI are closely related to future LV remodeling, sustained deterioration of LVEF, and the occurrence of adverse events (4–6).

The impairment of right ventricular (RV) function may also help determine the prognosis of patients with STEMI (7–9). However, the irregular anatomic morphology renders the visualization of the RV so that accurate measurement of its strains by echocardiography remains challenging. The inter- and intra-variability of the measurements found in echocardiographic studies likely attributes to the conflicting results (10). Therefore, the prognostic impact of concomitant RV dysfunction in STEMI patients remains undetermined.

In this study, we used feature-tracking (FT) technology based on the CMR cine images of patients with STEMI obtained within their first week of hospitalization and followed the prognosis of each patient. We aimed to investigate the prognostic implication of combinative assessment of both LV and RV strain indexes in patients with STEMI.

METHODS

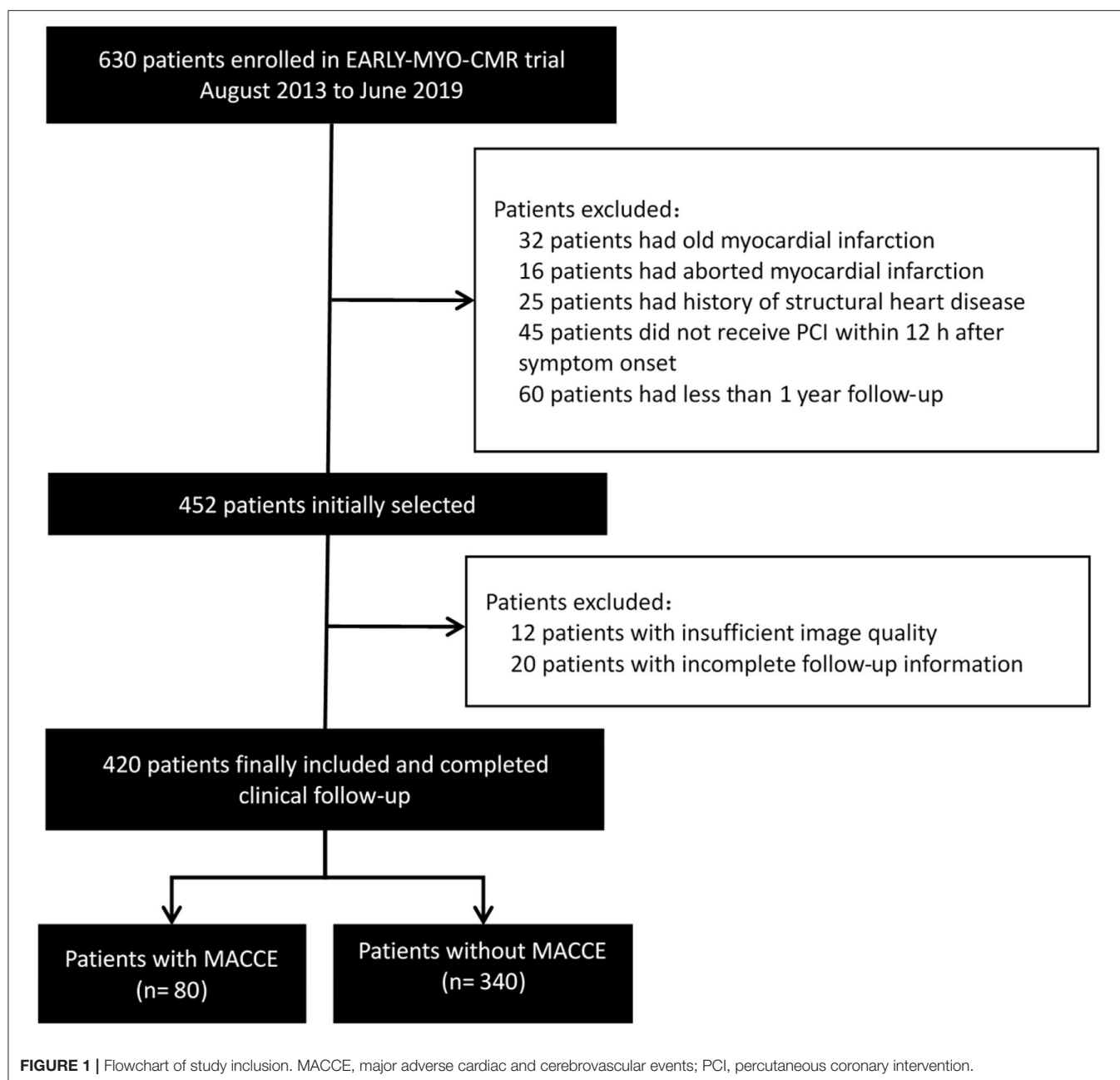
Study Design and Subjects

We used patient data obtained from the Early Assessment of Myocardial Tissue Characteristics by CMR in STEMI Registry (EARLY-MYO-CMR, NCT03768453). The multi-center registry prospectively includes all-comer patients with STEMI who have undergone CMR imaging (11). The inclusion criteria for the current study were as follows: first-time STEMI (as diagnosed by typical ischemic syndrome and electrocardiography (EKG) manifestation of ST elevation in at least two contiguous precordial (≥ 2 mm) or peripheral leads (≥ 1 mm), primary percutaneous coronary intervention (PCI) within 12 hours after symptom onset, and CMR imaging within the first week of STEMI onset. All patients received standard medical care (2). The flowchart of study inclusion is seen in **Figure 1**. In addition, CMR data from 40 people without apparent heart disease were used as control group.

CMR Imaging and Analysis

CMR imaging was performed using 3.0-Tesla scanners (Achieva TX, Philips Healthcare, Netherlands). All sequences were acquired in breath-hold with a default field of view (FOV) at 350×350 mm². A balanced, steady-state free precession (SSFP) sequence was used to produce cine images (TR/TE 3.2/1.6 ms, 30 phases, flip angle 45°, voxel size $2.0 \times 1.6 \times 8$ mm³). A short-tau inversion-recovery spin echo sequence was used to produce T2-weighted black-blood images (TR/TE 2 R-R intervals/75 ms, voxel size $2.0 \times 1.6 \times 8$ mm³). Ten minutes after the administration of 0.1 mmol/kg gadopentetate dimeglumine (Magnevist, Bayer HealthCare Pharmaceuticals Inc., Wuppertal, Germany), late gadolinium enhancement (LGE) images were acquired using an inversion recovery segmented SSFP sequence with a proper inversion time (TR/TE 3.5/1.7 ms, flip angle 25°, temporal resolution 190 ms, voxel size $1.5 \times 1.7 \times 10$ mm³ interpolated into $0.74 \times 0.74 \times 5$ mm³).

Images were analyzed offline by an experienced reader blinded to the patients' clinical data using commercial software (CVI42,



Circle Cardiovascular Imaging, Inc., Calgary, Canada). Contours were acquired according to an established protocol in the core lab (11, 12). The software automatically delineated the borders of the epicardium, endocardium, infarction, intramyocardial hemorrhage (IMH), and microvascular obstructions (MVO). All contours were inspected and manual corrections were made when necessary. Volumetric parameters, such as LVEF, were calculated using short-axis cine images covering the whole heart. Infarction was determined as hyperenhanced myocardium (a signal intensity > 5 SDs of normal myocardium). The extent of the infarction and MVO were quantified as a percentage

of left ventricular myocardial mass (%LV). FT analysis was performed based on the cine images according to previously reported protocols (5, 13). For LV strain, data were derived from contiguous short-axis images (slice thickness: 8 mm, gap: 0 mm) and single-slice long-axis views (2-chamber, 3-chamber, and 4-chamber planes). The software calculated segmental peak strains on a 16-segment model. Subsequently, the global strains, including global longitudinal strain (GLS), global radial strain (GRS), and global circumferential strain (GCS), were calculated as the mean of the respective segmental peak values. The RV-GLS, GRS, and GCS and the RVEF were measured using the short-axis,

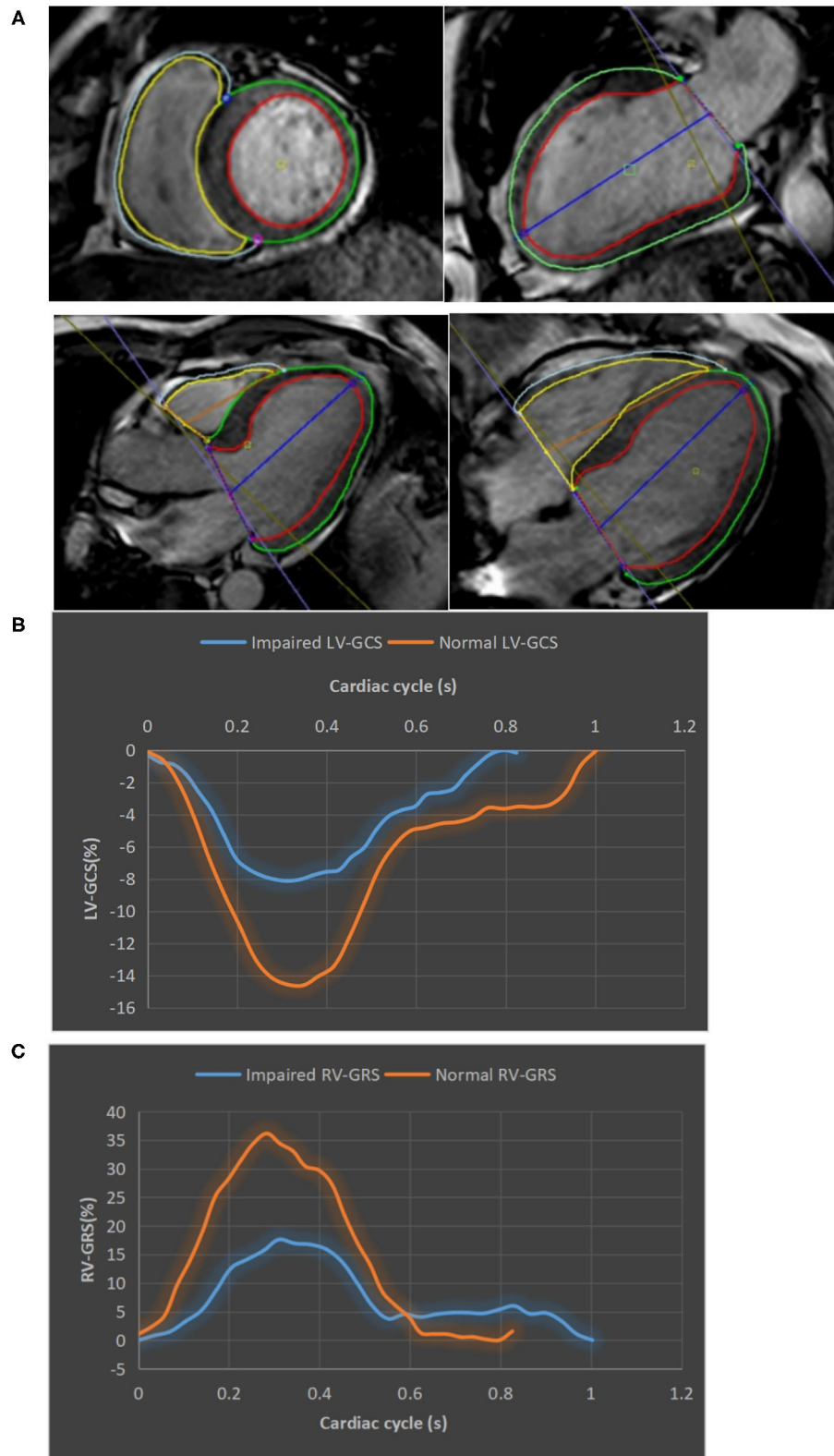


FIGURE 2 | The measurement of LV/RV strains. **(A)** LV and RV tracking in cine CMR short axis, two-, three-, and four-chamber views. The epicardial and endocardial contour of LV/RV were delineated by green, red, gray, and yellow lines, respectively. **(B)** Strain curves of a patient with impaired LV-GCS (-8.13%) and a patient with normal LV-GCS (-14.62%). **(C)** Strain curves of a patient with impaired RV-GRS (17.61%) and a patient with normal RV-GRS (36.15%). CMR, cardiac magnetic resonance; GCS, global circumferential strain; GRS, global radial strain.

TABLE 1 | Clinical characteristics of patients with STEMI.

Parameter	All (<i>n</i> = 420)	Non-MACCE (<i>n</i> = 340)	MACCE (<i>n</i> = 80)	<i>P</i> -value
Age, y	60 (54, 65)	60 (54, 65)	59 (54, 65)	0.754
Male, <i>n</i> (%)	375 (89.3)	306 (90.0)	69 (86.3)	0.329
BMI, kg/m ²	24.96 (22.86, 26.67)	24.82 (22.76, 26.57)	25.10 (22.90, 27.68)	0.379
Total ischemic time, h	4.50 (3.23, 5.85)	4.50 (3.14, 5.71)	4.70 (3.75, 6.44)	0.185
Hypertension, <i>n</i> (%)	234 (55.7)	176 (51.8)	58 (72.5)	0.001
Diabetes, <i>n</i> (%)	129 (30.7)	99 (29.1)	30 (37.5)	0.144
Smoking, <i>n</i> (%)	245 (58.3)	192 (56.5)	53 (66.3)	0.110
Hyperlipidemia, <i>n</i> (%)	261 (62.1)	212 (62.4)	49 (61.3)	0.855
Systolic blood pressure on admission, mmHg	136 (122, 150)	136 (122, 150)	137 (123, 150)	0.991
Heart rate on admission, bpm	78 (68, 88)	77 (67, 87)	80 (72, 88)	0.059
Killip classification on admission, <i>n</i> (%)				0.016
1	391 (93.0)	324 (95.3)	67 (83.8)	
2	19 (4.6)	13 (3.8)	6 (7.5)	
3	6 (1.4)	2 (0.6)	4 (5.0)	
4	4 (1.0)	1 (0.3)	3 (3.7)	
TIMI flow pre-PCI, <i>n</i> (%)				0.436
0–1	242 (57.6)	199 (58.5)	43 (53.8)	
2–3	178 (42.4)	141 (41.5)	37 (46.3)	
TIMI flow post-PCI, <i>n</i> (%)				0.007
0–2	40 (9.5)	26 (7.6)	14 (17.5)	
3	380 (90.5)	314 (92.4)	66 (82.5)	
Culprit vessel, <i>n</i> (%)				0.410
LAD	247 (58.8)	195 (57.4)	52 (65.0)	
LCX	37 (8.8)	32 (9.4)	5 (6.3)	
RCA	136 (32.4)	113 (33.2)	23 (28.8)	
Number of affected vessels, <i>n</i> (%)				0.651
1	188 (44.8)	154 (45.3)	34 (42.5)	
≥2	232 (55.2)	186 (54.7)	46 (57.5)	
Number of stents, <i>n</i> (%)				0.045
0–1	315 (75.0)	262 (77.1)	53 (66.3)	
≥2	105 (25.0)	78 (22.9)	27 (33.8)	
Peak hs-CRP, mg/L	10.40 (3.30, 25.70)	9.46 (3.32, 23.35)	13.70 (3.05, 36.10)	0.064
Peak CK, U/L	2,223 (1,029, 3,792)	1,967 (896, 3,471)	3,429 (1,853, 5,151)	<0.001
Peak CK-MB, U/L	229.24 (94.08, 372.88)	198.15 (81.63, 339.43)	376.10 (235.13, 568.28)	0.025
Peak hs-cTnI, ng/ml	26.57 (6.76, 55.79)	23.80 (6.86, 49.93)	36.29 (5.02, 99.21)	<0.001
Peak D-dimer, ug/ml	0.13 (0.09, 0.24)	0.13 (0.09, 0.24)	0.16 (0.11, 0.27)	0.060
HbA _{1c} , %	5.8 (5.4, 6.7)	5.8 (5.4, 6.6)	5.8 (5.4, 7.0)	0.427
LDL-C, mmol/L	3.15 (2.57, 3.78)	3.13 (2.54, 3.78)	3.20 (2.72, 3.74)	0.469
Scr, umol/L	74.00 (65.13, 85.85)	74.00 (66.00, 85.30)	71.95 (61.13, 86.75)	0.386
ALT, U/L	35.00 (22.00, 54.00)	34.10 (22.00, 51.53)	38.55 (25.25, 66.43)	0.067

ALT, alanine transaminase; BMI, body mass index; BNP, B-type natriuretic peptide; CK, creatine kinase; CK-MB, MB isoenzyme of creatine kinase; HbA_{1c}, glycosylated hemoglobin; hs-CRP, high-sensitivity C-reactive protein; hs-cTnI, high-sensitivity cardiac troponin I; LAD, left anterior descending artery; LCX, left circumflex artery; LDL-C, low density lipoprotein cholesterol; MACCE, major adverse cardiac and cerebrovascular events; PCI, percutaneous coronary intervention; RCA, right coronary artery; Scr, serum creatinine; STEMI, ST-elevation myocardial infarction; TIMI, thrombolysis in myocardial infarction. *P*-values of factors with bold values are less than 0.05.

3-chamber and 4-chamber long-axis images. Contours of the RV endocardium and epicardium were manually delineated. **Figure 2** shows the measurement of LV/RV strain and typical strain changes in patients with normal or impaired LV/RV function. Besides, 10% of the cases were randomly selected to test the intra- and inter-observer variability of the CMR analysis.

Angiographic Assessments

Angiographic assessments, including the thrombolysis in myocardial infarction (TIMI) myocardial flow grading (TFG) (14), were performed according to their standard protocols. An experienced interventional cardiologist analyzed all of the images.

TABLE 2 | CMR indexes of patients with STEMI.

Parameter	All (n = 420)	Non-MACCE (n = 340)	MACCE (n = 80)	P-value
LV-GRS, %	18.66 (13.85, 24.55)	19.57 (15.18, 25.15)	14.38 (10.10, 19.94)	<0.001
LV-GCS, %	-14.20 (-17.08, -11.51)	-14.72 (-17.25, -12.23)	-11.60 (-14.20, -8.70)	<0.001
LV-GLS, %	-8.39 (-10.70, -6.52)	-8.61 (-10.85, -6.63)	-7.68 (-9.33, -6.15)	0.018
RV-GRS, %	41.84 (33.10, 54.29)	43.88 (34.05, 55.74)	37.23 (29.95, 47.17)	0.004
RV-GCS, %	-13.09 (-15.74, -10.49)	-13.17 (-15.76, -10.27)	-12.57 (-15.72, -10.79)	0.801
RV-GLS, %	-11.49 (-14.14, -8.32)	-11.72 (-14.21, -8.47)	-10.57 (-13.91, -7.90)	0.239
LV-EDV, ml	115.64 (99.72, 134.56)	114.78 (98.62, 131.96)	121.69 (101.10, 146.46)	0.028
LV-ESV, ml	46.85 (36.12, 61.75)	45.20 (35.82, 58.08)	57.77 (38.48, 83.92)	<0.001
LV-SV, ml	66.71 (55.23, 76.94)	67.63 (55.81, 77.45)	64.09 (51.63, 75.40)	0.095
LV-EF, %	58.48 (50.26, 65.45)	59.63 (52.01, 65.79)	52.94 (41.82, 63.92)	<0.001
RV-EDV, ml	84.60 (68.74, 104.64)	84.62 (68.96, 105.07)	84.14 (66.85, 102.35)	0.618
RV-ESV, ml	35.46 (26.21, 45.17)	35.53 (26.65, 45.40)	34.79 (23.41, 42.67)	0.485
RV-SV, ml	48.78 (36.18, 63.12)	48.78 (36.36, 63.66)	48.53 (33.95, 59.86)	0.483
RV-EF, %	58.26 (50.10, 65.30)	58.35 (50.14, 64.98)	58.07 (49.79, 68.49)	0.918
LV-IS, % of LVMM	24.50 (17.31, 33.32)	23.52 (16.71, 31.00)	30.68 (20.97, 41.75)	<0.001
LV-MVO, % of LVMM	1.10 (0, 2.90)	0.90 (0, 2.60)	2.04 (0.15, 5.54)	0.001
LV IMH, n (%)	236 (56.2)	185 (54.4)	51 (63.8)	0.130
LV thrombus, n (%)	34 (8.1)	22 (6.5)	12 (15.0)	0.012
LV aneurysm, n (%)	114 (27.1)	82 (24.1)	32 (40.0)	0.004

EDV, end-diastolic volume; EF, ejection fraction; ESV, end-systolic volume; GCS, global circumferential strain; GLS, global longitudinal strain; GRS, global radial strain; IMH, Intramyocardial hemorrhage; IS, infarct size; LVMM, left ventricular myocardial mass; MVO, microvascular obstruction; SV, stroke volume; MACCE, major adverse cardiac and cerebrovascular events. P-values of factors with bold values are less than 0.05.

Clinical End Points and Follow-Up

The clinical end point of the study was the incidence of composite major adverse cardiac and cerebrovascular events (MACCEs). MACCEs were defined as cardiovascular death, non-fatal myocardial re-infarction, hospitalization for heart failure, and stroke after discharge (15). Clinical follow-up was performed through telephone or clinical interviews by two study nurses blinded to the research data at day 30 and months 3, 6, and 12 post-STEMI, and every 6 months thereafter. Reported MACCEs were confirmed using the patients' electronic medical records.

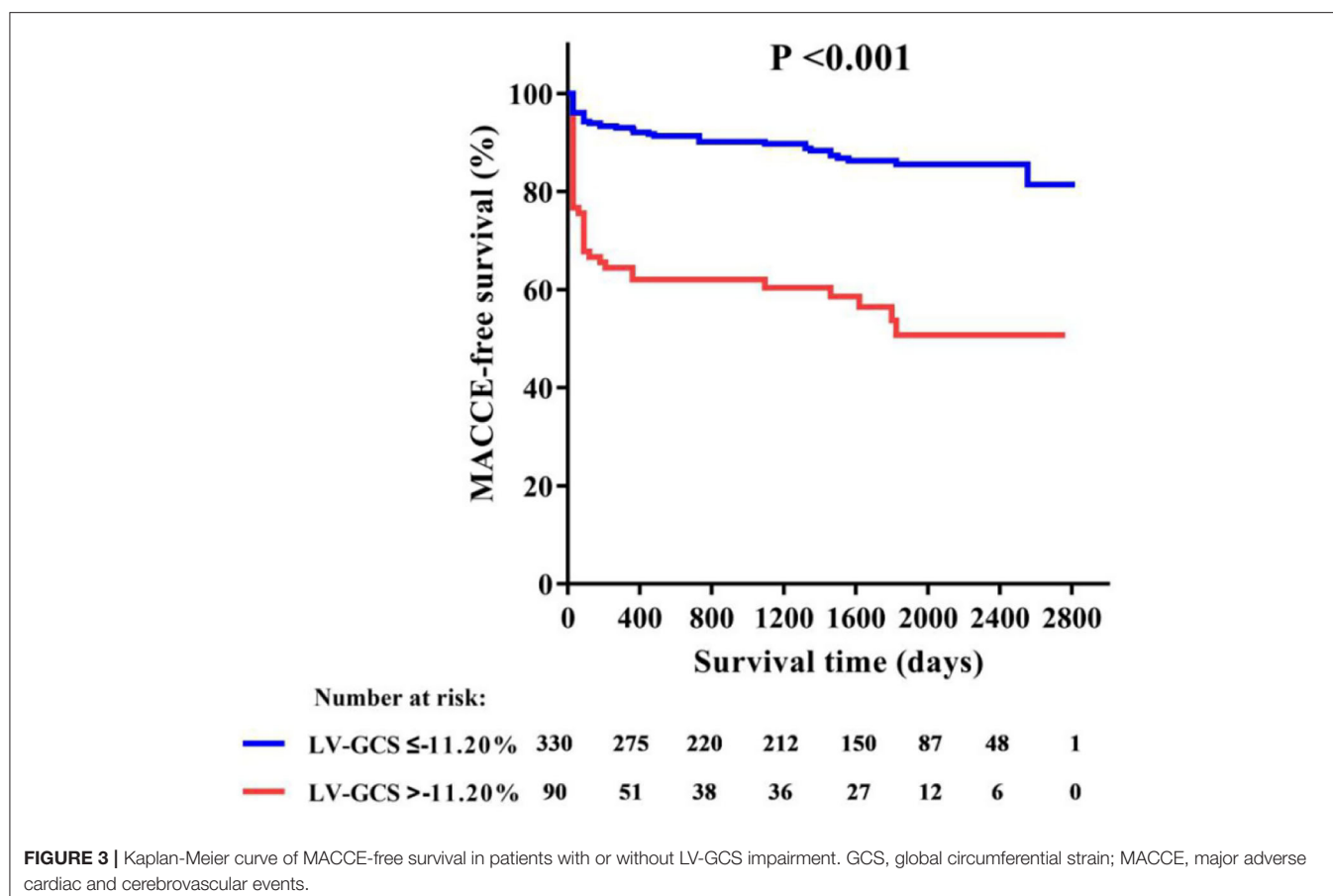
TABLE 3 | Cox regression analysis of predictors for MACCE.

Parameter	Univariate analysis		Multivariate analysis	
	HR (95% CI)	P	HR (95% CI)	P
LV-GCS, %	1.212 (1.140, 1.287)	<0.001	1.157 (1.082, 1.237)	<0.001
LV-GRS, %	0.919 (0.887, 0.952)	<0.001		
LV-GLS, %	1.085 (1.013, 1.162)	0.020		
RV-GCS, %	1.013 (0.957, 1.071)	0.661		
RV-GRS, %	0.989 (0.975, 1.002)	0.105		
RV-GLS, %	1.042 (0.986, 1.101)	0.143		
Male, n (%)	0.695 (0.368, 1.315)	0.264		
Age	1.000 (0.976, 1.025)	0.984		
Hypertension, n (%)	2.301 (1.408, 3.760)	0.001	1.913 (1.105, 3.311)	0.020
Diabetes, n (%)	1.414 (0.899, 2.224)	0.134		
Smoking, n (%)	1.254 (0.787, 1.997)	0.342		
Heart rate on admission, bpm	1.016 (1.001, 1.032)	0.039		
Killip classification on admission, n (%)				
1	Ref	–		
2	1.893 (1.166, 3.075)	0.010		
3	2.621 (1.232, 5.575)	0.012		
4	2.932 (0.709, 12.122)	0.137		
TIMI flow post-PCI, n (%)				
0–2	1.989 (1.117, 3.543)	0.020		
3	Ref	–		
Culprit vessel, n (%)				
LAD	Ref	–		
LCX	0.579 (0.231, 1.449)	0.243		
RCA	0.761 (0.466, 1.243)	0.275		
Peak hs-cTnl, ng/ml	1.011 (1.005, 1.017)	<0.001		
LV-EDV, ml	1.008 (1.001, 1.014)	0.018		
LV-EF, %	0.960 (0.945, 0.976)	<0.001		
LV-IS, % LVMM	1.045 (1.027, 1.062)	<0.001		
LV-MVO, % LVMM	1.153 (1.096, 1.213)	<0.001	1.079 (1.016, 1.147)	0.013
LV thrombus, n (%)	2.301 (1.244, 4.253)	0.008		
LV aneurysm, n (%)	2.066 (1.319, 3.235)	0.002		

EDV, end-diastolic volume; EF, ejection fraction; GCS, global circumferential strain; GLS, global longitudinal strain; GRS, global radial strain; hs-cTnl, high-sensitivity cardiac troponin I; LVMM, left ventricular myocardial mass; MACCE, major adverse cardiac and cerebrovascular events; MVO, microvascular obstruction; PCI, percutaneous coronary intervention; TIMI, thrombolysis in myocardial infarction; IS, infarct size. Factors with bold values are included in the multivariate analysis.

Statistical Analysis

The distribution of data was determined using the Kolmogorov-Smirnov test. Normally distributed continuous variables are presented as mean \pm SD and compared using the Student's *t*-test. Variables without normal distribution are presented as median and interquartile range (IQR) and compared using the Wilcoxon rank sum test. Categorical variables are presented as number



of cases with corresponding percentages and the differences were compared using the Chi-square test or the Fisher's exact test. The correlation between two continuous variables was evaluated using the Spearman's coefficient. The intra- and inter-observer variability of CMR analysis was assessed using intra-class correlation coefficients (ICC) and Bland-Altman analysis. An ICC > 0.74 was considered high consistency.

The factors influencing the right ventricular strain were determined using logistic regressions. Kaplan-Meier curves were used to illustrate event-free rates, and the differences were compared using the log-rank test. The predictors of MACCEs were determined using multivariable Cox regression analysis. Statistically significant ($p \leq 0.05$) variables in the univariate Cox regression model and other clinically significant variables were included in the multivariate analysis. The discriminative power of the predictors of MACCEs were further assessed using receiver operating characteristic analyses with the optimal cutoff points of continuous MACCEs predictors estimated by the Youden Index. All analyses in this study were performed using SPSS version 23.0 (SPSS Inc., Chicago, Illinois). The additional predictive power of the incidence of MACCEs for concomitantly impaired LV-GCS and RV-GRS compared with that of impaired LV-GCS alone was further assessed using the reclassification analyses (R package PredictABLE software, R version 3.6.2, the R Foundation, Vienna, Austria). The continuous net reclassification improvement

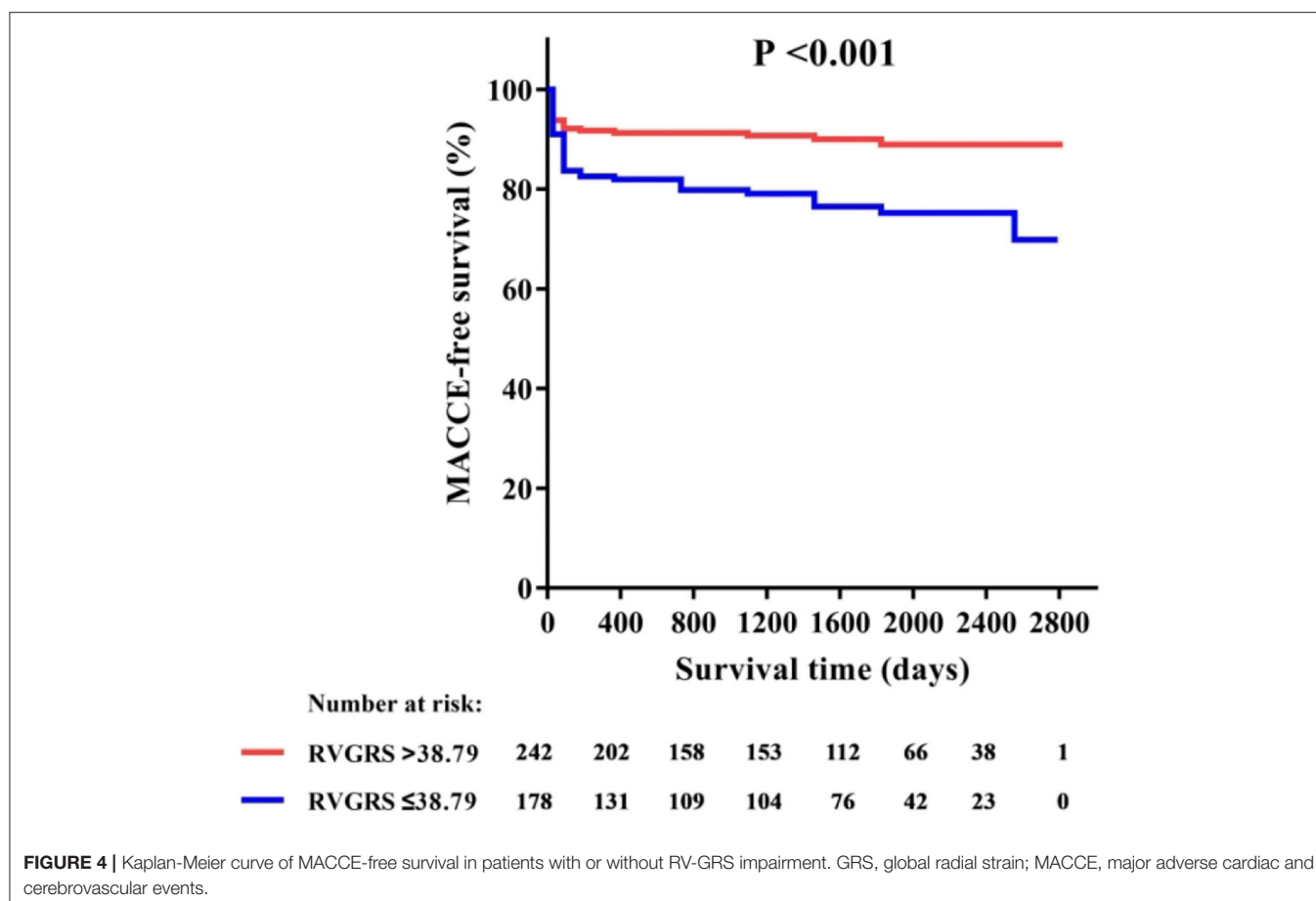
(NRI), which indicates improvement of the prediction, was determined. Statistical significance was set at $P < 0.05$.

RESULTS

A total of 420 patients in the Early-MYO-CMR database met the inclusion criteria of this analysis (**Figure 1**). Among them, 310 patients had been included in a previous analysis (15). CMR imaging was performed a median of 5 days (range: 2–7 days) after symptom onset.

Clinical Characteristics and MACCEs

During a median follow-up of 52 months (IQR: 29–68 months), 80 patients (19.0%) experienced MACCEs, including 8 cardiovascular deaths (1.9%), 19 myocardial re-infarctions (4.5%), 46 admissions for heart failure (10.9%), and 7 strokes (1.7%). **Table 1** shows the patients' clinical characteristics. Patients who experienced MACCEs had a higher prevalence of hypertension, higher Killip classification on admission, and worse TFG after PCI. The peak concentrations of creatine kinase, the MB isoenzyme of CK, and high-sensitivity cardiac troponin I were significantly higher in patients who experienced MACCEs. Patients who experienced MACCEs received more stents than those who did not.



CMR Indexes and MACCEs

Compared to the control group, participants with STEMI had significantly lower LV and RV strains (LVGLS: -8.39% vs. -13.07% , $P < 0.001$; LVGRS: 18.66% vs. 33.65% , $P < 0.001$; LVGCS: -14.20% vs. -20.81% , $P < 0.001$; RVGLS: -11.49% vs. -22.54% , $P = 0.010$; RVGRS: 41.84% vs. 54.38% , $P < 0.001$; RVGCS: -13.09% vs. -18.93% , $P = 0.017$).

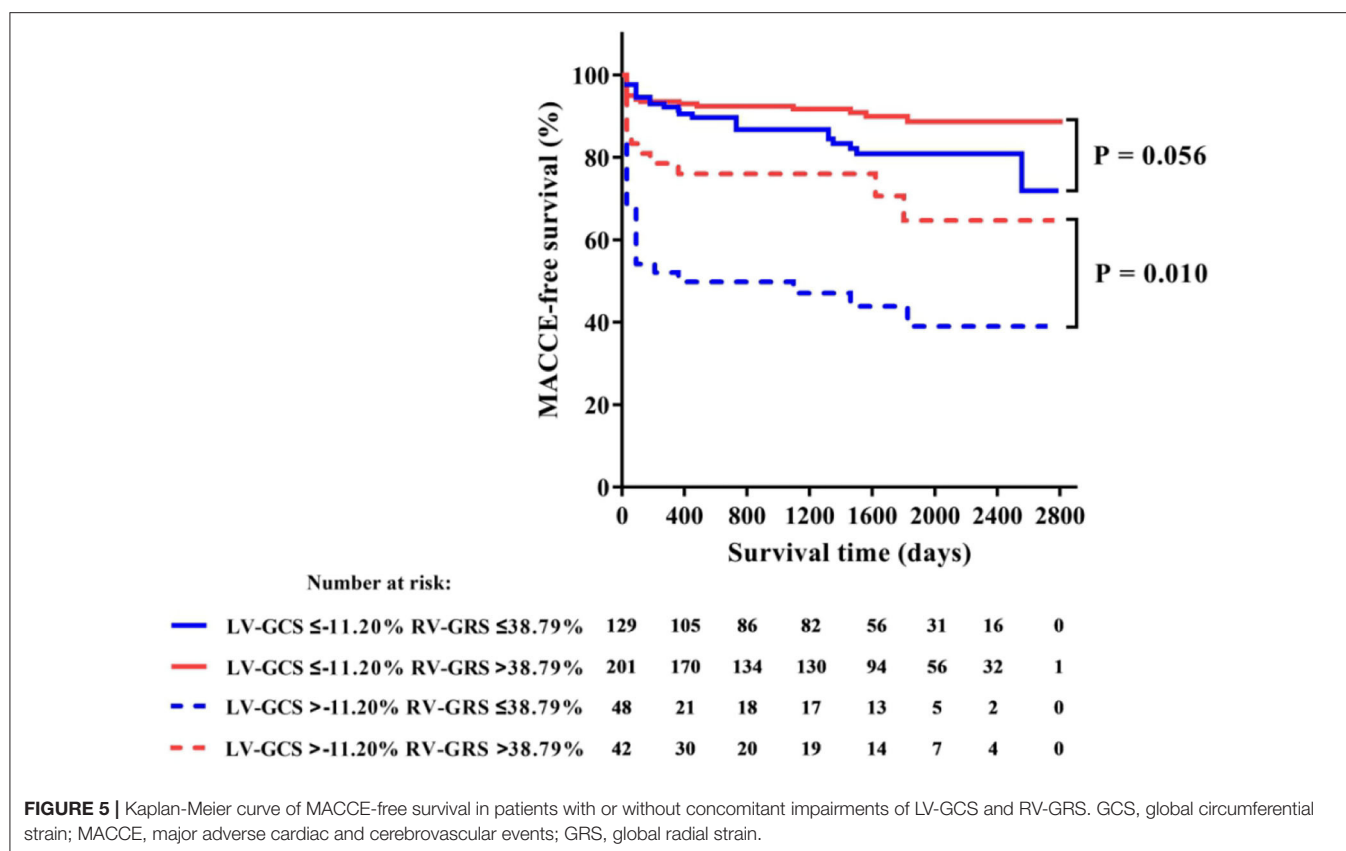
Table 2 shows the patient's CMR indexes. In general, the patients who developed MACCEs presented with a higher degree of LV enlargement, lower LVEF, more extensive infarctions and MVO, and a higher incidence of aneurysms and thrombus formation in the LV. All 3 LV strain indexes and RV-GRS were significantly decreased in those patients. LV-GCS was found to be an independent predictive factor of MACCEs in the multivariate Cox regression models adjusting for clinical characteristics and CMR indexes (**Table 3**). The ROC analysis determined that the optimal cut-off point of LV-GCS to predict MACCEs was -11.20% (Youden's index: 0.703; 95% CI: 0.634–0.772; $P < 0.001$), with a sensitivity of 48.75% and a specificity of 85.00%. Patients with LV-GCS $> -11.20\%$ were significantly more likely to experience MACCEs than patients with LV-GCS $\leq -11.20\%$ (43.3% vs. 12.4% , $P < 0.001$). The predictive power of LV-GCS for MACCEs at this cutoff was more accurate than that of LVEF (area under the curve: 0.703 and 95% CI: 0.634–0.772 vs. 0.630 and 95% CI: 0.557–0.703, $P = 0.003$). The Kaplan-Meier curves

for MACCEs-free survival were significantly different between patients with LV-GCS beyond or below the cutoff ($P < 0.001$ by log-rank test) (**Figure 3**).

Among all RV strains, RV-GRS appeared to effectively predict MACCEs in this study (Youden index: 0.604; 95% CI: 0.533–0.674; $P = 0.004$), the optimal cut-off point was 38.79%. The MACCEs-free survival rate was significantly different between patients with RV-GRS beyond or below the cutoff (log rank $P < 0.001$) (**Figure 4**). Forty-eight patients had concomitantly reduction of RV-GRS and LV-GCS, these patients had a significantly worse prognosis than the 42 patients with reduced LV-GCS alone ($P = 0.010$). Patients with reduced RV-GRS but preserved LV-GCS also seemed to have a worse prognosis than patients with higher RV-GRS, but was not statistically significant ($P = 0.056$) (**Figure 5**). The addition of RV-GRS to LV-GCS improved the predictive power for MACCEs compared to LV-GCS alone (continuous NRI: 0.327; 95% CI: 0.095–0.558; $P = 0.006$).

Factors That Influence RV-GRS

The incidence of reduced RV strain ($<38.79\%$) in patients with occlusions in the left anterior descending branch (LAD), left circumflex branch (LCX), and right coronary artery (RCA) were 37.8, 37.5, and 51.5%, respectively. Tobacco use (67.4% of patients with decreased RV-GRS; $P = 0.003$), an occluded RCA



(39.4% of patients with decreased RV-GRS; $P = 0.002$), and LV-GCS $> -11.20\%$ (27.1% of patients with decreased RV-GRS; $P = 0.012$) was significantly correlated with decreased RV-GRS (Table 4).

Reproducibility of CMR Measurements

We found a high consistency in both intra- and inter-observer variabilities of the CMR measurements. Detailed Intraclass correlation coefficient data and Bland-Altman graphics can be found in Supplementary Table 1 and Supplementary Figure 1.

DISCUSSION

This study focused on the relationship between CMR-derived myocardial strain data and STEMI prognosis. We found that post-STEMI LV strain is a key determinant of patient prognosis and that LV-GCS $> -11.20\%$ in the acute phase of STEMI is an independent predictor of long-term MACCEs. We also found that concomitantly reduction of RV-GRS and LV-GCS resulted in a worsened prognosis. Combinative assessment of RV-GRS to LV-GCS significantly improved the predictive power for MACCEs than LV-GCS alone. Besides, tobacco use, occlusions in the RCA, and impaired LV-GCS were associated with the decrease of RV strain.

Patients with STEMI have a highly diverse prognosis. Myocardial strain has emerged as a more useful marker than LVEF to reflect both global and regional myocardial function

(3). Echocardiography is the most convenient method to measure myocardial strain. However, due to the high-quality images and computer-oriented imaging in comparison to echocardiography (5, 10), CMR-based strain measurements are more reliable and have become the reference method of strain assessment (16, 17).

Almost all studies focusing on myocardial strain have demonstrated that LV strain is a determining factor in the prognosis of patients with STEMI. In our study, LV-GLS, LV-GCS, and LV-GRS were significantly reduced in patients who experienced MACCEs compared to those who did not, and LV-GCS was identified as an independent predictor of MACCEs. This result is consistent with those of Nucifora's study (18). In other studies, CMR-derived LV-GLS had been reported to independently predict long-term prognosis (4, 5). The varied predictive powers of the three individual LV-strain indexes among studies have not been clarified yet. However, LV-GCS is more accurate and reproducible than the other two indexes when compared with CMR tagging measurement (18–20). As demonstrated by Buss, the CMR-derived LV-GCS could distinguish an infarction area similar to that recognized by LGE (21). Neizel also found that LV-GCS could predict LVEF changes 6 months after the occurrence of STEMI (22). Both of them are well-recognized determinants for STEMI prognosis.

In contrast, the role of the RV function in the risk stratification of STEMI patients had only limited evidences that mostly provided by echocardiographic studies. In the current study, we found that lower RV strain was associated with increased

TABLE 4 | Logistic regression analysis of RV-GRS impairment.

Parameter	Univariate analysis		Multivariate analysis	
	HR (95% CI)	P	HR (95% CI)	P
Age, y	1.027 (1.005, 1.050)	0.016		
Male, n (%)	0.407 (0.200, 0.828)	0.013		
Hypertension, n (%)	0.840 (0.568, 1.242)	0.383		
Diabetes, n (%)	1.344 (0.878, 2.056)	0.173		
Smoking, n (%)	0.547 (0.366, 0.818)	0.003	0.532 (0.353, 0.801)	0.003
Killip classification on admission, n (%)				
1	ref	–		
2	1.047 (0.655, 1.675)	0.847		
3	1.550 (0.648, 3.706)	0.324		
4	0 (0, –)	0.999		
TIMI flow post-PCI, n (%)				
0–2	0.504 (0.260, 0.974)	0.042		
3	ref	–		
Culprit vessels, n (%)				
LAD	Ref	–	Ref	–
LCX	0.992 (0.487, 2.023)	0.983	0.942 (0.453, 1.957)	0.873
RCA	0.569 (0.373, 0.870)	0.009	0.484 (0.309, 0.758)	0.002
Peak CK, U/L	1.000 (1.000, 1.000)	0.041		
Peak hs-cTnI, ng/ml	0.996 (0.990, 1.001)	0.141		
Peak BNP, pg/ml	1.000 (1.000, 1.001)	0.380		
LV-GRS, %	1.011 (0.985, 1.037)	0.424		
LV-GCS, %	0.953 (0.907, 1.002)	0.059	0.934 (0.886, 0.985)	0.012
LV-GLS, %	0.982 (0.924, 1.045)	0.569		
LV-EDV, ml	0.999 (0.993, 1.005)	0.782		
LV-ESV, ml	0.997 (0.990, 1.005)	0.492		
LV-EF, %	1.008 (0.992, 1.025)	0.309		
LV-IS, % LVMM	0.992 (0.976, 1.007)	0.288		
LV-MVO, % LVMM	0.935 (0.873, 1.001)	0.055		
LV IMH, n (%)	1.147 (0.776, 1.694)	0.491		

BNP, B-type natriuretic peptide; CK, creatine kinase; EDV, end-diastolic volume; EF, ejection fraction; ESV, end-systolic volume; GCS, global circumferential strain; GLS, global longitudinal strain; GRS, global radial strain; hs-cTnI, high-sensitivity cardiac troponin I; IMH, Intramyocardial hemorrhage; LVMM, left ventricular myocardial mass; MVO, microvascular obstruction; PCI, percutaneous coronary intervention; TIMI, thrombolysis in myocardial infarction; IS, infarct size; SV, stroke volume. Factors with bold values are included in the multivariate analysis.

MACCEs and improved the accuracy of risk stratification only based on the impairment of LV strain. Besides, our finding that reduction of RV strain could be found in all-location infarctions may be an important supplement to previous studies that had only researched RV strain in patients with RV or inferior infarctions (23, 24). The mechanism of RV strain impairments in non-inferior infarctions might be similar to right heart dysfunction due to left heart failure (25). Interestingly, we also found that tobacco use is associated with RV dysfunction. Since

chronic obstructive pulmonary disease (COPD) in patients who smoke can cause pre-existing RV strain impairment (26), our results suggest that STEMI patients who smoke are more likely to have RV dysfunction, which do not conflict with the “smoker’s paradox” theory claiming that smoking can lead to a more favorable left ventricular remodeling process (27).

The finding that concomitant reduction of RV and LV strain resulted in a worse prognosis than LV strain alone has important clinical implications. Although LV dysfunction is the most critical determinant for a patient’s prognosis, our results suggest that a combinative assessment of RV function using CMR imaging analysis further increases the accuracy of risk stratification, especially in patients with decreased LV function.

LIMITATIONS

This study has several limitations. First, the CMR images of study population were not consecutively included due to loss of follow-up, poor image quality, etc. Second, the follow-up CMR data of study population was limited, which hampered the dynamic monitoring of myocardial strain. Finally, this study didn’t possess the images of quantitative T1 mapping as well as T2* mapping which had been proposed for advanced infarct characterization with potential for improved risk stratification post-STEMI.

CONCLUSIONS

In conclusion, concomitant impairment of both LV and RV strain is associated with a worse long-term prognosis than impaired LV strain alone. A combinative assessment of both RV and LV strains based on CMR images could improve risk stratification of patients with STEMI.

DATA AVAILABILITY STATEMENT

The original contributions presented in the study are included in the article/**Supplementary Material**, further inquiries can be directed to the corresponding author/s.

ETHICS STATEMENT

The studies involving human participants were reviewed and approved by Shanghai Jiaotong University School of Medicine, Renji Hospital Ethics Committee. The patients/participants provided their written informed consent to participate in this study.

AUTHOR CONTRIBUTIONS

WL and HJ: analyzed images and data and drafted the manuscript. GH: concept development and critical review of the manuscript. DJ-X, ZJ-T, SB-Z, and YF-H: image analysis and critical review of the manuscript. AD-A-L, CB-H, XJ-R, and YY-N: collected images and critical review of the manuscript. DS, LZ, and WH-W: statistical analysis and critical review of the manuscript. PJ: all aspects of study. All authors read and

approved the final manuscript and worked in the design or data collection of EARLY-MYO-CMR (NCT03768453) registry.

FUNDING

This work was supported by the National Key Research and Development Program of China (2018YFC1312802), National Science Fund for Distinguished Young Scholars (81625002), National Natural Science Foundation of China (81930007 and 81770238), Shanghai Outstanding Academic Leaders Program (18XD1402400), Shanghai Shen Kang Hospital Development Center (16CR3034A), Shanghai Municipal Education Commission Gaofeng Clinical Medicine Grant (20152209), Shanghai Jiao Tong University School of Medicine (DLY201804 and YG2016MS45), and Innovative Research

Team of High-Level Local Universities in Shanghai and Clinical Research of Renji hospital (PY2018-III-06).

ACKNOWLEDGMENTS

We are grateful to Ms. Wang Ji-Hong and Mr. Xie Yao-fei for their works in patients' follow-up. We would like to thank Editage (www.editage.cn) for English language editing.

SUPPLEMENTARY MATERIAL

The Supplementary Material for this article can be found online at: <https://www.frontiersin.org/articles/10.3389/fcvm.2021.659364/full#supplementary-material>

REFERENCES

1. Szummer K, Wallentin L, Lindhagen L, Alfredsson J, Erlinge D, Held C, et al. Improved outcomes in patients with ST-elevation myocardial infarction during the last 20 years are related to implementation of evidence-based treatments: experiences from the SWEDEHEART registry 1995-2014. *Eur Heart J*. (2017) 38:3056–65. doi: 10.1093/eurheartj/ehx515
2. Ibanez B, James S, Agewall S, Antunes MJ, Bucciarelli-Ducci C, Bueno H, et al. 2017 ESC Guidelines for the management of acute myocardial infarction in patients presenting with ST-segment elevation: the Task Force for the management of acute myocardial infarction in patients presenting with ST-segment elevation of the European Society of Cardiology (ESC). *Eur Heart J*. (2018) 39:119–77. doi: 10.1093/eurheartj/ehx393
3. Smiseth OA, Torp H, Opdahl A, Haugaa KH, Urheim S. Myocardial strain imaging: how useful is it in clinical decision making? *Eur Heart J*. (2016) 37:1196–207. doi: 10.1093/eurheartj/ehv529
4. Gavara J, Rodriguez-Palomares JF, Valente F, Monmeneu JV, Lopez-Lereu MP, Bonanad C, et al. Prognostic value of strain by tissue tracking cardiac magnetic resonance after ST-segment elevation myocardial infarction. *JACC Cardiovasc Imaging*. (2018) 11:1448–57. doi: 10.1016/j.jcmg.2017.09.017
5. Reindl M, Tiller C, Holzknecht M, Lechner I, Beck A, Plappert D, et al. Prognostic implications of global longitudinal strain by feature-tracking cardiac magnetic resonance in ST-elevation myocardial infarction. *Circ Cardiovasc Imaging*. (2019) 12:e009404. doi: 10.1161/CIRCIMAGING.119.009404
6. Ersboll M, Valeur N, Mogensen UM, Andersen MJ, Moller JE, Velazquez EJ, et al. Prediction of all-cause mortality and heart failure admissions from global left ventricular longitudinal strain in patients with acute myocardial infarction and preserved left ventricular ejection fraction. *J Am Coll Cardiol*. (2013) 61:2365–73. doi: 10.1016/j.jacc.2013.02.061
7. Pfisterer M. Right ventricular involvement in myocardial infarction and cardiogenic shock. *Lancet*. (2003) 362:392–4. doi: 10.1016/S0140-6736(03)14028-7
8. Park SJ, Park JH, Lee HS, Kim MS, Park YK, Park Y, et al. Impaired RV global longitudinal strain is associated with poor long-term clinical outcomes in patients with acute inferior STEMI. *JACC Cardiovasc Imaging*. (2015) 8:161–9. doi: 10.1016/j.jcmg.2014.10.011
9. Stiermaier T, Backhaus SJ, Matz J, Koschalka A, Kowallick J, de Waha-Thiele S, et al. Frequency and prognostic impact of right ventricular involvement in acute myocardial infarction. *Eur Heart J*. (2020) 41:ehaa946.1609. doi: 10.1093/ehjci/ehaa946.1609
10. Kirkpatrick JN, Vannan MA, Narula J, Lang RM. Echocardiography in heart failure: applications, utility, new horizons. *J Am Coll Cardiol*. (2007) 50:381–96. doi: 10.1016/j.jacc.2007.03.048
11. He J, Kong LC, Zeng JT, Shi BZ, An DA, Chen BH, et al. Comparison of direct stenting with conventional strategy on myocardial impairments in ST-segment elevation myocardial infarction: a cardiac magnetic resonance imaging study. *Int J Cardiovasc Imaging*. (2020) 36:1167–75. doi: 10.1007/s10554-020-01812-w
12. Ge H, Ding S, An D, Li Z, Ding H, Yang F, et al. Frame counting improves the assessment of post-reperfusion microvascular patency by TIMI myocardial perfusion grade: evidence from cardiac magnetic resonance imaging. *Int J Cardiol*. (2016) 203:360–6. doi: 10.1016/j.ijcard.2015.10.194
13. Liu B, Dardeer AM, Moody WE, Edwards NC, Hudsmith LE, Steeds RP. Normal values for myocardial deformation within the right heart measured by feature-tracking cardiovascular magnetic resonance imaging. *Int J Cardiol*. (2018) 252:220–23. doi: 10.1016/j.ijcard.2017.10.106
14. Sheehan FH, Braunwald E, Canner P, Dodge HT, Gore J, Van Natta P, et al. The effect of intravenous thrombolytic therapy on left ventricular function: a report on tissue-type plasminogen activator and streptokinase from the Thrombolysis in Myocardial Infarction (TIMI Phase I) trial. *Circulation*. (1987) 75:817–29. doi: 10.1161/01.CIR.75.4.817
15. Leng S, Ge H, He J, Kong L, Yang Y, Yan F, et al. Long-term prognostic value of cardiac MRI left atrial strain in st-segment elevation myocardial infarction. *Radiology*. (2020) 296:299–309. doi: 10.1148/radiol.20200176
16. Bodi V. Strain by feature tracking: a short summary of the journey of CMR in STEMI. *JACC Cardiovasc Imaging*. (2019) 12(Pt. 1):1199–201. doi: 10.1016/j.jcmg.2018.08.009
17. Eitel I, Stiermaier T, Lange T, Rommel KP, Koschalka A, Kowallick JT, et al. Cardiac magnetic resonance myocardial feature tracking for optimized prediction of cardiovascular events following myocardial infarction. *JACC Cardiovasc Imaging*. (2018) 11:1433–44. doi: 10.1016/j.jcmg.2017.11.034
18. Nucifora G, Muser D, Tioni C, Shah R, Selvanayagam JB. Prognostic value of myocardial deformation imaging by cardiac magnetic resonance feature-tracking in patients with a first ST-segment elevation myocardial infarction. *Int J Cardiol*. (2018) 271:387–91. doi: 10.1016/j.ijcard.2018.05.082
19. Schuster A, Hor KN, Kowallick JT, Beerbaum P, Kutty S. Cardiovascular magnetic resonance myocardial feature tracking: concepts and clinical applications. *Circ Cardiovasc Imaging*. (2016) 9:e004077. doi: 10.1161/CIRCIMAGING.115.004077
20. Augustine D, Lewandowski AJ, Lazdam M, Rai A, Francis J, Myerson S, et al. Global and regional left ventricular myocardial deformation measures by magnetic resonance feature tracking in healthy volunteers: comparison with tagging and relevance of gender. *J Cardiovasc Magn Reson*. (2013) 15:8. doi: 10.1186/1532-429X-15-8
21. Buss SJ, Krautz B, Hofmann N, Sander Y, Rust L, Giusca S, et al. Prediction of functional recovery by cardiac magnetic resonance feature tracking imaging in first time ST-elevation myocardial infarction. Comparison to infarct size and transmural by late gadolinium enhancement. *Int J Cardiol*. (2015) 183:162–70. doi: 10.1016/j.ijcard.2015.01.022
22. Neizel M, Korosoglou G, Lossnitzer D, Kuhl H, Hoffmann R, Ocklenburg C, et al. Impact of systolic and diastolic deformation indexes assessed by strain-encoded imaging to predict persistent severe myocardial dysfunction

- in patients after acute myocardial infarction at follow-up. *J Am Coll Cardiol.* (2010) 56:1056–62. doi: 10.1016/j.jacc.2010.02.070
23. Ivey-Miranda JB, Almeida-Gutierrez E, Borrayo-Sanchez G, Antezana-Castro J, Contreras-Rodriguez A, Posada-Martinez EL, et al. Right ventricular longitudinal strain predicts acute kidney injury and short-term prognosis in patients with right ventricular myocardial infarction. *Int J Cardiovasc Imaging.* (2019) 35:107–16. doi: 10.1007/s10554-018-1447-5
 24. Smarz K, Zaborska B, Jaxa-Chamiec T, Tysarowski M, Budaj A. Right ventricular systolic function as a marker of prognosis after ST-elevation inferior myocardial infarction 5-year follow-up. *Int J Cardiol.* (2016) 221:549–53. doi: 10.1016/j.ijcard.2016.07.088
 25. Ponikowski P, Voors AA, Anker SD, Bueno H, Cleland JGF, Coats AJS, et al. 2016. ESC Guidelines for the diagnosis treatment of acute chronic heart failure: The Task Force for the diagnosis treatment of acute chronic heart failure of the European Society of Cardiology (ESC) Developed with the special contribution of the Heart Failure Association (HFA) of the ESC. *Eur Heart J.* (2016) 37:2129–200. doi: 10.1093/eurheartj/ehw128
 26. Goedemans L, Hoogslag GE, Abou R, Schalijs MJ, Marsan NA, Bax JJ, et al. ST-segment elevation myocardial infarction in patients with chronic obstructive pulmonary disease: prognostic implications of right ventricular systolic dysfunction as assessed with two-dimensional speckle-tracking echocardiography. *J Am Soc Echocardiogr.* (2019) 32:1277–85. doi: 10.1016/j.echo.2019.05.016
 27. Symons R, Masci PG, Francone M, Claus P, Barison A, Carbone I, et al. Impact of active smoking on myocardial infarction severity in reperfused ST-segment elevation myocardial infarction patients: the smoker's paradox revisited. *Eur Heart J.* (2016) 37:2756–64. doi: 10.1093/eurheartj/ehv738

Conflict of Interest: The authors declare that the research was conducted in the absence of any commercial or financial relationships that could be construed as a potential conflict of interest.

Copyright © 2021 Lai, Jie, Jian-Xun, Ling-Cong, Jun-Tong, Bo-Zhong, Dong-Ao-Lei, Bing-Hua, Song, Zheng, Fan, Yi-Ning, Fu-Hua, Jian-Cheng, Hu-Wen, Jian-Rong, Heng and Jun. This is an open-access article distributed under the terms of the Creative Commons Attribution License (CC BY). The use, distribution or reproduction in other forums is permitted, provided the original author(s) and the copyright owner(s) are credited and that the original publication in this journal is cited, in accordance with accepted academic practice. No use, distribution or reproduction is permitted which does not comply with these terms.



Correlation of Myocardial Strain and Late Gadolinium Enhancement by Cardiac Magnetic Resonance After a First Anterior ST-Segment Elevation Myocardial Infarction

OPEN ACCESS

Edited by:

Jinwei Tian,

The Second Affiliated Hospital of
Harbin Medical University, China

Reviewed by:

Lian-Ming Wu,

Shanghai JiaoTong University, China
Grigoris Korosoglou,
GRN Klinik Weinheim, Germany

*Correspondence:

Shihua Zhao
cjrzhaozhishua2009@163.com
Hongbing Yan
hbyanfuwai2018@163.com

[†]These authors have contributed
equally to this work

Specialty section:

This article was submitted to
Cardiovascular Imaging,
a section of the journal
Frontiers in Cardiovascular Medicine

Received: 05 May 2021

Accepted: 01 June 2021

Published: 02 July 2021

Citation:

Yu S, Zhou J, Yang K, Chen X,
Zheng Y, Zhao K, Song J, Ji K,
Zhou P, Yan H and Zhao S (2021)
Correlation of Myocardial Strain and
Late Gadolinium Enhancement by
Cardiac Magnetic Resonance After a
First Anterior ST-Segment Elevation
Myocardial Infarction.
Front. Cardiovasc. Med. 8:705487.
doi: 10.3389/fcvm.2021.705487

Shiqin Yu^{1†}, Jinying Zhou^{2†}, Kai Yang¹, Xiuyu Chen¹, Yucong Zheng¹, Kankan Zhao³,
Jialin Song¹, Keshan Ji¹, Peng Zhou², Hongbing Yan^{2,4*} and Shihua Zhao^{1*}

¹ State Key Laboratory of Cardiovascular Disease, MR Center, Fuwai Hospital, National Center for Cardiovascular Diseases, Chinese Academy of Medical Sciences and Peking Union Medical College, Beijing, China, ² State Key Laboratory of Cardiovascular Disease, Coronary Heart Disease Center, Fuwai Hospital, National Center for Cardiovascular Diseases, Chinese Academy of Medical Sciences and Peking Union Medical College, Beijing, China, ³ Paul C. Lauterbur Research Center for Biomedical Imaging, Shenzhen Institutes of Advanced Technology, Chinese Academy of Sciences, SZ University Town, Shenzhen, China, ⁴ Fuwai Hospital, Chinese Academy of Medical Sciences, Shenzhen, China

Objectives: To investigate the correlation of cardiac magnetic resonance (CMR) feature-tracking with conventional CMR parameters in patients with a first anterior ST-segment elevation myocardial infarction (STEMI).

Methods: This sub-analysis of OCTAMI (Optical Coherence Tomography Examination in Acute Myocardial Infarction) registry included 129 patients who finished a CMR examination 1 month after a first anterior STEMI. Cine images were applied to calculate both global and segmental left ventricular peak strain parameters. The patients were divided into two groups by left ventricular ejection fraction (LVEF) and compared with 42 healthy controls. Segmental late gadolinium enhancement (LGE) was graded according to LGE transmural as follows: (1) >0 to ≤25%; (2) >25 to ≤50%; (3) >50 to ≤75%; (4) >75%. Left ventricle was divided into infarcted, adjacent, and remote regions to assess regional function.

Results: Compared with controls, global radial ($28.39 \pm 5.08\%$ vs. $38.54 \pm 9.27\%$, $p < 0.05$), circumferential ($-16.91 \pm 2.11\%$ vs. $-20.77 \pm 2.78\%$, $p < 0.05$), and longitudinal (-13.06 ± 2.15 vs. -15.52 ± 2.69 , $p < 0.05$) strains were impaired in STEMI patients with normal LVEF ($\geq 55\%$). Strain parameters were strongly associated with LGE (radial: $r = 0.65$; circumferential: $r = 0.69$; longitudinal: $r = 0.61$; all $p < 0.05$). A significant and stepwise impairment of global strains was observed in groups divided by LGE tertiles. Furthermore, segmental strain was different in various degrees of LGE transmural especially for radial and circumferential strain. Strains of adjacent region were better than

infarcted region in radial and circumferential directions and worse than remote region in all three directions.

Conclusion: Global and regional strain could stratify different extent and transmural of LGE, respectively. Although without LGE, adjacent region had impaired strains comparing with remote region.

Keywords: ST-segment elevation myocardial infarction, magnetic resonance imaging, strain, late gadolinium enhancement, left ventricle

INTRODUCTION

Cardiac magnetic resonance (CMR) imaging is considered a gold standard for quantification of cardiac function integrating myocardial tissue characterization (1). Left ventricular ejection fraction (LVEF) assessment is indicated for risk stratification and prognostic management in ST-segment elevation myocardial infarction (STEMI) patients (2). However, LVEF is neither able to detect regional variations in myocardial contractility nor identify subtle but important contractile abnormalities (3, 4). Moreover, patients with heart failure can present a preserved LVEF. Late gadolinium enhancement (LGE) provides delineation of infarcted myocardium *in vivo* of which myocardial contractility is unlikely restored after coronary revascularization (5).

Moreover, myocardial deformation can be evaluated by CMR. Recently, strain analysis by CMR feature-tracking, using routinely acquired cine images, has been increasingly conducted to detect subtle and regional myocardial dysfunction in a variety of cardiovascular diseases including myocardial infarction (6, 7). Unlike LVEF which reflects contractile function by volumetric changes, strain is a more in-depth evaluation studying three different directions of myocardial deformation corresponding to geometry of myocardial fibers. In this regard, CMR feature-tracking is a potential supplement to LVEF and LGE for assessment in STEMI patients.

Therefore, we aimed to investigate whether strain analysis by CMR feature-tracking could provide complementary evaluation value in STEMI patients on top of conventional CMR parameters including LVEF and LGE. We hypothesized that myocardial strain assessed by CMR feature-tracking could be more sensitive to detect early decline in left ventricular (LV) function with preserved LVEF, quantify regional dysfunction, and discriminate different degrees of myocardial infarction assessed by LGE.

METHODS

Study Population

The present retrospective study was a sub-analysis from OCTAMI (Optical Coherence Tomography Examination in Acute Myocardial Infarction) registry (clinical trial unique identifier: NCT03593928), which continuously enrolled a prospective cohort of STEMI patients for evaluating culprit lesions by optical coherence tomography. The major inclusion criteria for OCTAMI were as follows: (1) age ≥ 18 years; (2) presented with persistent chest pain lasting more than 30 min with ST-segment elevation >0.1 mV in at least two

contiguous leads or new left bundle-branch block on the 18-lead electrocardiogram and elevated troponin I level (2); (3) referred to primary percutaneous coronary intervention. Patients were qualified for the current study if they (1) presented with a first STEMI due to left anterior descending coronary artery and (2) finished a CMR examination at 1 month after index procedure. Forty-two age- and sex-matched healthy subjects were recruited as controls. This study was approved by the review board of the local hospital and all participants provided written informed consent.

CMR Imaging

CMR imaging was performed on a 3.0-Tesla scanner (Discovery MR750; GE Healthcare, Milwaukee, USA) with a phased-array cardiovascular coil, using electrocardiographic and respiratory gating. The protocol mainly consisted of cine imaging and LGE imaging for analysis. Cine images were acquired in three long-axis views (LV two-chamber, three-chamber, and four-chamber) and short-axis views encompassing the entire LV using balanced steady-state free precession sequence (b-SSFP). Typical imaging parameters were field of view = 320×320 mm, matrix = 224×192 , repetition time (TR) = 3.3 ms, echo time (TE) = 1.7 ms, flip angle = 50° , temporal resolution = 46–60 ms, slice thickness = 8 mm, and slice gap = 2 mm. LGE images were acquired 10–15 min after intravenous administration of gadolinium-DTPA (Magnevist; Bayer, Berlin, Germany) at a dose of 0.2 mmol/kg, using a segmented phase-sensitive inversion recovery sequence at the same views as cine images in end diastole. Typical imaging parameters were field of view = 360×360 mm, matrix = 224×192 , TR = 6.0 ms, TE = 2.8 ms, flip angle = 25° , slice thickness = 8 mm, slice gap = 2 mm, and TI = 300 ms.

CMR Analysis

All the analyses were conducted using commercial software CVI42 (Circle Cardiovascular Imaging, Calgary, Canada) by investigators with more than 3 years' experience. Endocardial and epicardial contours of LV myocardium were manually traced on short-axis cine at end diastole and end systole, respectively, and cardiac functional parameters were computed automatically. Papillary muscles were assigned to the LV volume. For quantification of contrast enhancement, outline of left ventricular myocardium was manually depicted and LGE was detected by +5 SDs over the signal intensity of normal myocardium (8, 9). LGE results were recorded as percentage of enhanced myocardial volume of left ventricle. Feature-tracking

performed on three long-axis cines and short-axis cine to calculate LV peak strain parameters, including global radial strain (GRS), global circumferential strain (GCS), and global longitudinal strain (GLS). All endocardial and epicardial borders of LV throughout the cardiac cycle were automatically tracked by contours manually delineated at end diastole. After that, all the boundary points were checked and the contours would be adjusted if necessary. American Heart Association (AHA) 16-segment model was used to generate segmental results (10). Segments were graded according to LGE transmural in end-diastole as follows: (1) >0 to $\leq 25\%$, (2) >25 to $\leq 50\%$, (3) >50 to $\leq 75\%$, and (4) $>75\%$. Because the culprit lesion was left anterior descending coronary artery in present patients, we divided LV into three regions by combining the method described by Götte et al. (11) and AHA 16-segment model: infarcted region (segments 1, 2, 7, 8, 13, 14)—LGE distributed region, adjacent region (segments 3, 6, 9, 12, 15, 16)—contiguously to the infarcted region, and remote region (segments 4, 5, 10, 11)— 180° opposite from the infarct. Two radiologists with 3- and 5-year experience of CMR imaging assessed strain parameters in 15 random patients independently for inter-observer analysis. 3 months later, one of the investigators repeated assessment to determine the intra-observer variability.

Statistical Analyses

Continuous variables were expressed as mean \pm SD or median values with interquartile range (IQR) depending on normality variables. Correspondingly, *t*-test or Mann-Whitney *U* test was applied to compare two groups; one-way ANOVA with *post hoc* LSD tests or Kruskal-Wallis *H* test was performed for comparisons of three groups. Categorical variables were reported as exact numbers with percentages and χ^2 test or Fisher exact test was conducted for comparison. Linear regression analyses were performed to determine the association between strain parameters and LGE. Receiver operating characteristics analysis was used to define the optimal cut-off values by the Youden Index and to quantify discriminative power. Inter- and intra-observer analyses were conducted by intraclass correlation coefficient. Statistical analyses were performed using IBM SPSS Statistics 23.0 (Armonk, NY) and MedCalc 16.8.4 (Ostend, Belgium). A two-tailed *p*-value <0.05 was considered statistically significant.

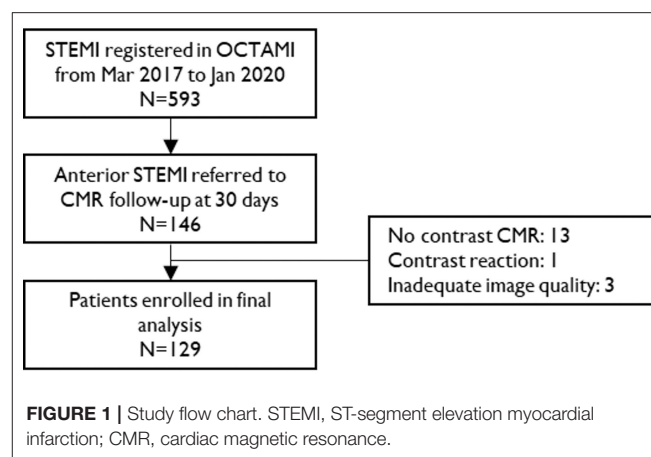
RESULTS

Baseline Characteristics

A total of 129 STEMI patients (age 55 years, IQR, 48–63 years; 112 men) and 42 healthy controls (age 53 years, IQR, 48–60 years; 37 men) were included in the study (Figure 1). Table 1 summarizes the baseline characteristics of patients' population. Patients had a high prevalence of hyperlipidemia (72%) and 87% of the patients were male. All participants presented with a first anterior STEMI due to left anterior descending artery. However, 47 patients (36%) had two diseased vessels and 33 (26%) had three diseased vessels.

CMR Parameters

CMR examinations were conducted 33 (IQR, 30–38) days after index events. The STEMI patients were divided into two



groups by LVEF ($\geq 55\%$) and compared with healthy subjects. An overview of assessed CMR parameters is presented in Table 2. LGE distribution was consistent with left anterior descending coronary territory. Compared with controls, all the CMR parameters were impaired in the whole STEMI group (all $p < 0.001$). Conventional cardiac function parameters (except cardiac output) were similar between patients with LVEF $\geq 55\%$ and controls (all $p > 0.05$), but GRS, GCS, and GLS were impaired in patients with LVEF $\geq 55\%$ (Supplementary Figure 1, all $p < 0.001$). Furthermore, all strain parameters of STEMI patients with LVEF $< 55\%$ were much worse than LVEF $\geq 55\%$ group (Supplementary Figure 1, all $p < 0.001$). It is worth noting that the percentage of LGE in LVEF $< 55\%$ group was significantly more than LVEF $\geq 55\%$ group ($p < 0.001$). Therefore, the correlation of myocardial strain and extent of LGE was investigated further.

Association Between LV Strain and LGE

As Figure 2 shows, all global strain parameters were strongly associated with LGE extent (GRS: $r = 0.65$, $\beta = -0.41$, $p < 0.001$; GCS: $r = 0.69$, $\beta = 0.21$, $p < 0.001$; GLS: $r = 0.61$, $\beta = 0.15$, $p < 0.001$). When dividing the patients by LGE tertiles, the increase in LGE extent was correlated to a significant and stepwise impairment of global strains (Figure 3): the average strain values for LGE tertiles were 26.82, 22.82, and 17.41% for GRS; -16.3 , -14.39 , and -11.57% for GCS; and -13.34 , -11.24 , and -9.78% for GLS.

For segmental results, the receiver operating characteristic curve analysis demonstrated that all segmental strain parameters were good discriminators for segmental LGE $> 50\%$ (Figure 4), and radial strain [cut-off value: 12.89%, sensitivity: 77%, specificity: 88%, area under curve (AUC): 0.902] and circumferential strain (cut off value: -10.20% , sensitivity: 80%, specificity: 85%, AUC: 0.903) performed better than longitudinal strain (cut-off value: -9.98% , sensitivity: 72%, specificity: 69%, AUC: 0.763). Furthermore, Figure 5 illustrates that segmental strain was different in various degrees of LGE transmural especially for radial and circumferential strain. The more transmural the segmental LGE, the worse the segmental strain.

TABLE 1 | Baseline characteristics of the study population.

	Total STEMI (n = 129)	LVEF <55% (n = 85)	LVEF ≥55% (n = 44)	P-value
Age, years	55 (48–63)	52 (46–63)	56 (50–62)	0.26
Male, n (%)	112 (87)	71 (84)	41 (93)	0.12
Body mass index, kg/m ²	25.4 (23.8–27.7)	25.5 (23.8–27.9)	25.4 (23.2–27.1)	0.52
Hypertension, n (%)	64 (50)	44 (52)	20 (46)	0.50
Hyperlipidemia, n (%)	93 (72)	61 (72)	32 (73)	0.91
Diabetes mellitus, n (%)	40 (31)	25 (29)	15 (34)	0.59
Smoker, n (%)	92 (71)	57 (67)	35 (80)	0.14
Ischemia time, h	5.0 (3.0–7.8)	5.0 (3.0–7.3)	5.0 (3.0–8.0)	0.81
TIMI flow pre-PCI, n (%)				0.02
0	71 (55)	54 (63)	17 (39)	
1	10 (8)	6 (7)	4 (9)	
2	15 (12)	10 (12)	5 (11)	
3	33 (25)	15 (18)	18 (41)	
TIMI flow post-PCI, n (%)				1.00
0	2 (1)	1 (1)	1 (2)	
1	0 (0)	0 (0)	0 (0)	
2	1 (1)	1 (1)	0 (0)	
3	126 (98)	83 (98)	43 (98)	
Number of diseased vessels				0.63
1	49 (38)	32 (38)	17 (39)	
2	47 (36)	31 (36)	16 (36)	
3	33 (26)	22 (26)	11 (25)	
Admission creatinine, μmol/L	74.6 (65.2–85.2)	74.8 (65.0–86.0)	73.1 (66.2–84.4)	0.88
Peak cTnI, ng/mL	27.0 (9.5–53.3)	33.5 (18.2–60.1)	13.5 (6.6–31.6)	0.001
Time of peak cTnI, h	20 (14–27)	21 (15–27)	19 (12–27)	0.38
Peak NT-proBNP, pg/mL	1,364.5 (729.1–2,889.1)	1,666.1 (915.9–3,215.3)	914.7 (404.7–2,072.2)	0.001
Time of peak NT-proBNP, h	29 (22–42)	32 (24–49)	26 (19–32)	0.004

PCI, percutaneous coronary intervention; cTnI, cardiac troponin I; NT-proBNP, N terminal pro B type natriuretic peptide.

TABLE 2 | CMR parameters of the study population.

	STEMI			Controls (n = 42)
	Total (129)	LVEF <55% (n = 85)	LVEF ≥55% (n = 44)	
LVEF, %	51 (42–57)*	45 (38–51) [†]	60 (56–63) [‡]	63 (59–67)
SV, mL	72.58 ± 17.48*	68.71 ± 16.56 [†]	80.05 ± 16.96 [‡]	83.66 ± 15.03
EDV, mL	150.54 ± 34.13*	159.10 ± 34.25 [†]	134.02 ± 27.41 [‡]	132.50 ± 23.62
ESV, mL	71.9 (57.5–96.3)*	88.4 (71.2–107.0) [†]	54.8 (43.6–63.9) [‡]	47.4 (41.1–57.3)
CO, L/min	4.70 ± 1.19*	4.57 ± 1.25 [†]	4.96 ± 1.00 [†]	6.02 ± 1.09
LGE, %	12.04 (5.80–19.82)	17.14 (9.67–24.14)	6.38 (1.88–11.60) [‡]	–
GRS, %	22.39 ± 6.60*	19.28 ± 4.95 [†]	28.39 ± 5.08 ^{†‡}	38.54 ± 9.27
GCS, %	–14.11 ± 3.19*	–12.66 ± 2.64 [†]	–16.91 ± 2.11 ^{†‡}	–20.77 ± 2.78
GLS, %	–11.46 ± 2.64*	–10.64 ± 2.50 [†]	–13.06 ± 2.15 ^{†‡}	–15.52 ± 2.69

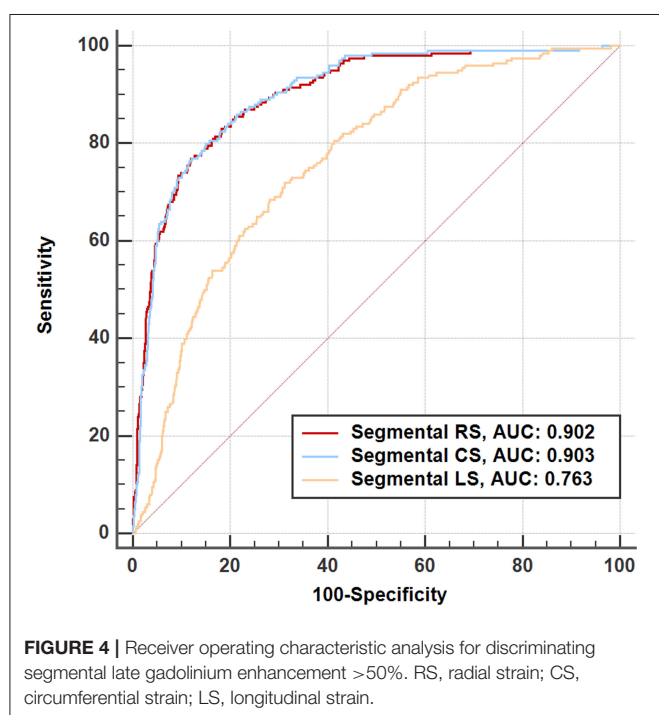
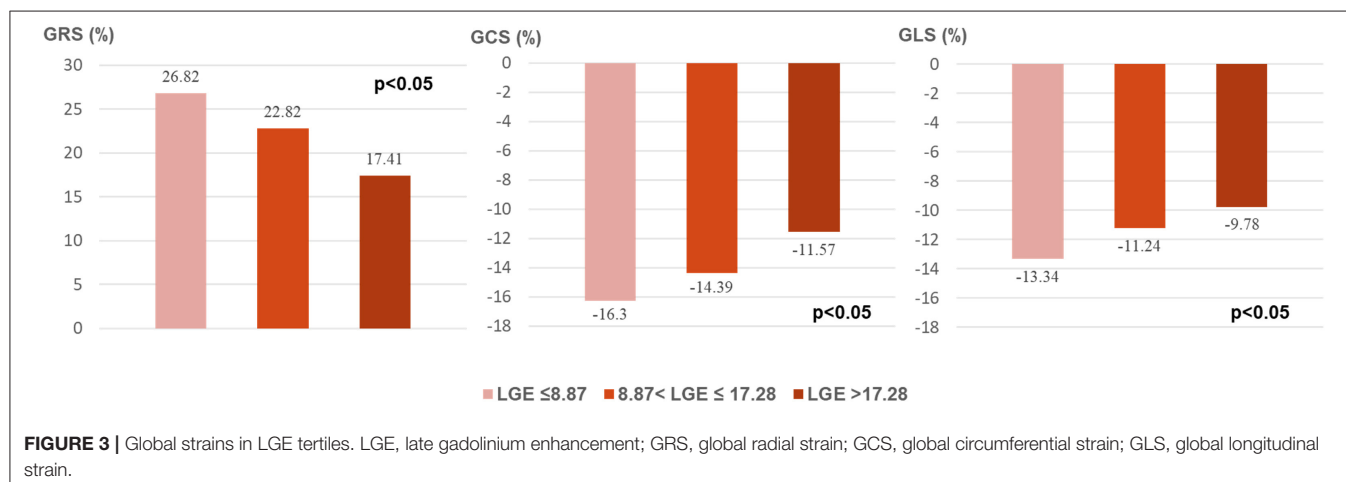
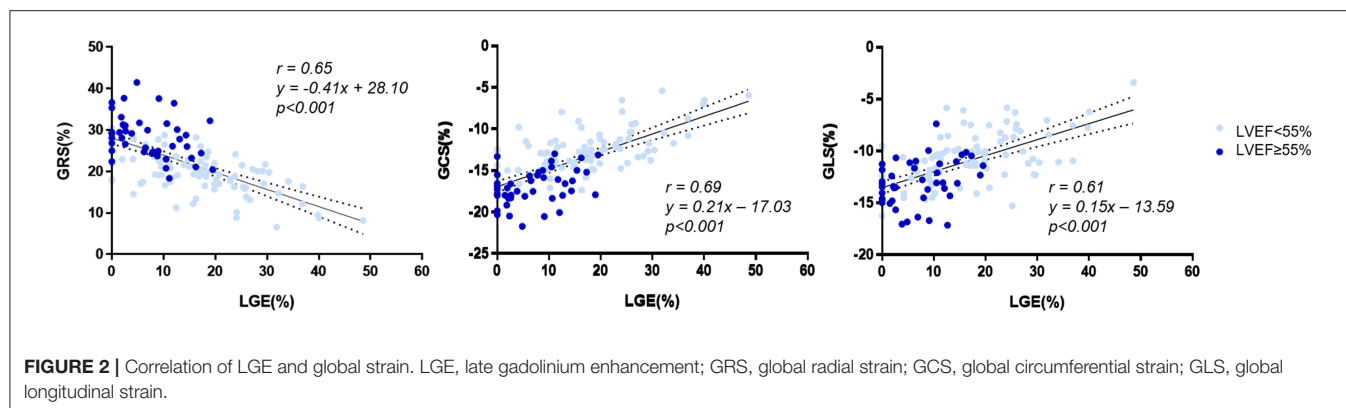
CMR, cardiac magnetic resonance; STEMI, ST-segment elevation myocardial infarction; LVEF, left ventricular ejection fraction; SV, stroke volume; EDV, end-diastolic volume; ESV, end-systolic volume; CO, cardiac output; LGE, late gadolinium enhancement; GRS, global radial strain; GCS, global circumferential strain; GLS, global longitudinal strain.

* $p < 0.05$ when compared with the controls between 2 groups (the total STEMI group and the controls). [†] $p < 0.05$ when compared with the controls among three groups (the STEMI LVEF <55% group, the STEMI LVEF ≥55% group, and the controls). [‡] $p < 0.05$ when compared with the STEMI (LVEF <55%) group among three groups (the STEMI LVEF <55% group, the STEMI LVEF ≥55% group, and the controls).

Strain Parameters in Different Regions

The strain of remote region, adjacent region, and infarcted region presented a significant and stepwise impairment in

radial (median value: 29.30, 22.84, and 19.90%, respectively, $p < 0.001$) and circumferential (median value: –17.85, –15.09, and –13.66%, respectively, $p < 0.001$) directions (**Figure 6**).



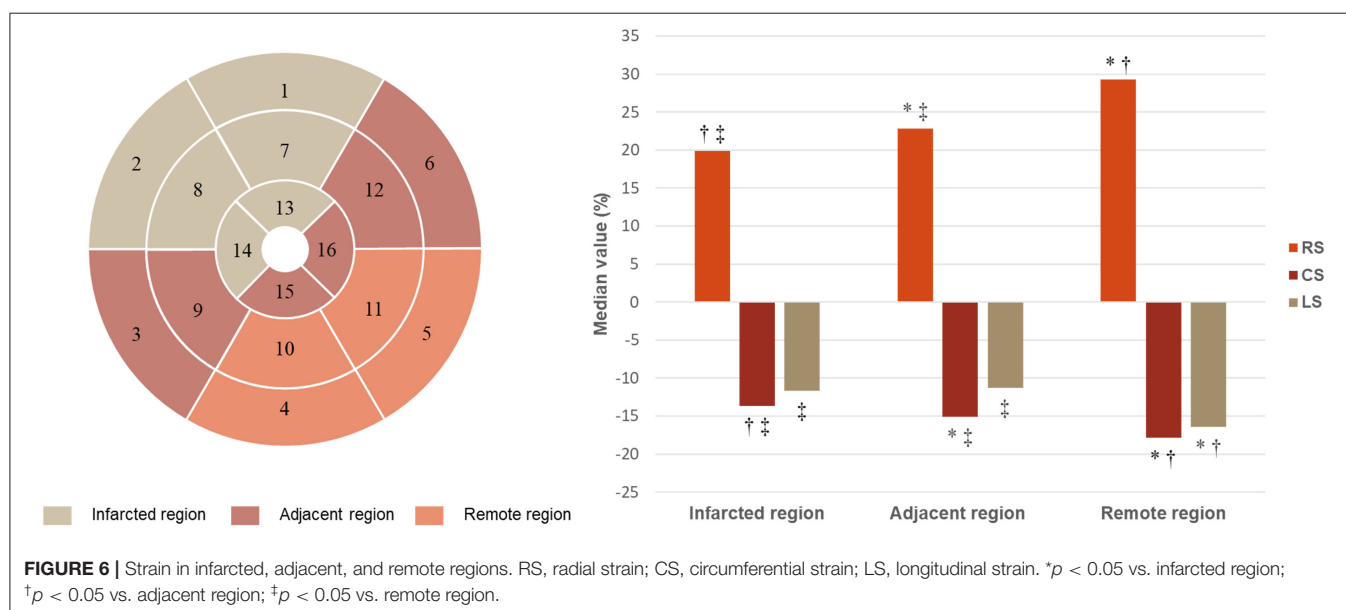
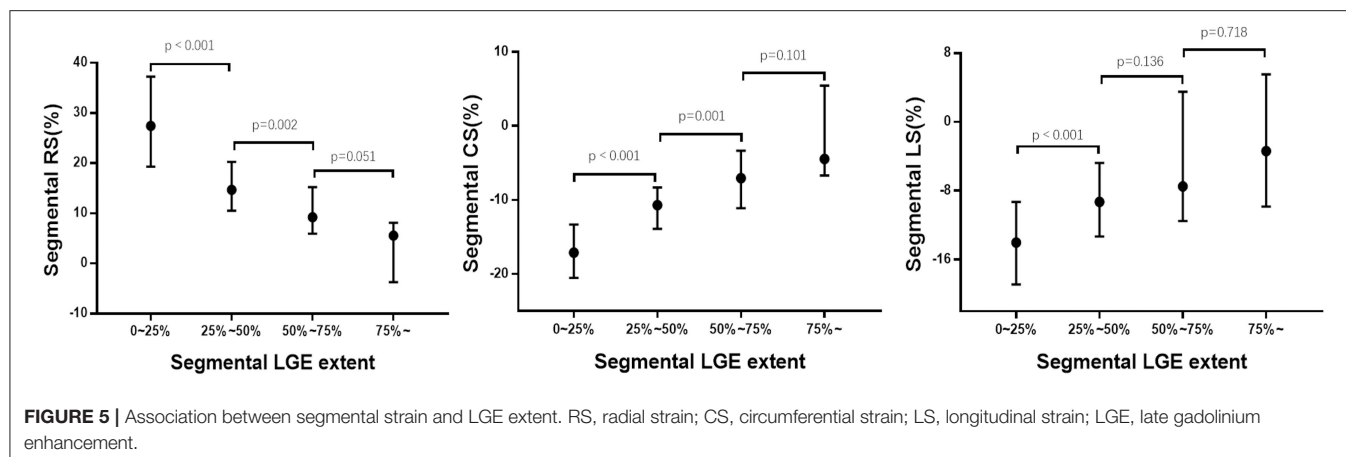
Longitudinal strain was similar between infarcted and adjacent region (−11.66 vs. −11.29%, $p > 0.05$) but both significantly worse than remote region (−16.45%; both $p < 0.001$).

Intra-observer and Inter-observer Variability

Reproducibility was excellent for all strain parameters given in Table 3. The intraclass correlation coefficients ranged from 0.859 to 0.979 for intra-observer agreement and ranged from 0.749 to 0.954 for inter-observer agreement.

DISCUSSION

The present study investigated the additional value and correlation of myocardial strain assessed by CMR feature-tracking to conventional CMR parameters in patients with a first anterior STEMI at 1 month after index procedure. The main findings were as follows: (1) compared with healthy controls, CMR feature-tracking detected impaired global strains in STEMI patients with normal LVEF; (2) strain was closely associated with infarcted myocardium detected by LGE, and global and regional strain could stratify different extent and transmural of myocardial infarction respectively; (3) although without LGE,



adjacent region had impaired strains comparing with remote region—deformation reduced successively from remote region to adjacent region and infarcted region.

Recently, myocardial strain analysis is considered as a powerful tool to quantify subtle and regional myocardial dysfunction over ejection fraction (6, 12). Speckle tracking echocardiography is a convenient way for strain analysis but is limited by inherent weakness of echocardiography, including angle-dependent, low signal/noise ratio and inter-vendor differences (13, 14). CMR tagging, requiring specific sequence, is time consuming and confined for clinical application. CMR feature-tracking analysis is a rapid and semi-automated approach performed offline on routine cine images, which has been popularly applied to research in cardiovascular diseases. Moreover, the feasibility of CMR feature-tracking and agreements with speckle tracking echocardiography, tagging, and strain-encoded MRI have been confirmed in several studies (15–18). However, better reproducibility of CMR feature-tracking was observed in global strain than segmental strain (19, 20). Also,

a few studies showed a lower reproducibility of segmental strain by CMR feature-tracking than acquisition-based techniques including tagging and strain-encoded MRI (21, 22). Therefore, global deformation was more frequently applied in literatures. Fent et al. demonstrated that GLS was reduced in patients with previous myocardial infarction in the context of normal LVEF (4). However, they only conducted strain analysis on two-chamber and four-chamber cines to calculate longitudinal strain for 40 patients and 40 controls. Further, our study applied on three long-axis cines and short-axis cine stacks of LV demonstrated that GRS, GCS, and GLS were already declined in STEMI patients with normal LVEF, implying that these patients were supposed to receive active treatment to prevent further deterioration of cardiac function. Moreover, assessment of regional myocardial dysfunction is necessary and helpful for clinical strategy. Shah et al. demonstrated that about one-fifth of dysfunctional and thinned segments presented with negative LGE could recover from revascularization (23). In short, strain parameters are practicable and provide information about both

TABLE 3 | Inter- and intra-observer variability of CMR feature tracking derived global and regional strain parameters.

	Intra-observer		Inter-observer	
	ICC	95% CI	ICC	95% CI
RS, %				
Global	0.916	0.773 to 0.971	0.9	0.736 to 0.965
Basal	0.859	0.578 to 0.953	0.749	0.416 to 0.907
Mid	0.924	0.788 to 0.974	0.883	0.693 to 0.959
Apical	0.869	0.651 to 0.954	0.886	0.690 to 0.960
CS, %				
Global	0.913	0.764 to 0.970	0.856	0.607 to 0.950
Basal	0.905	0.741 to 0.967	0.885	0.692 to 0.960
Mid	0.929	0.808 to 0.975	0.884	0.612 to 0.963
Apical	0.902	0.732 to 0.966	0.834	0.577 to 0.941
LS, %				
Global	0.924	0.716 to 0.976	0.913	0.679 to 0.973
Basal	0.979	0.921 to 0.993	0.954	0.871 to 0.984
Mid	0.9	0.736 to 0.965	0.886	0.637 to 0.963
Apical	0.92	0.768 to 0.973	0.9	0.732 to 0.965

ICC, intraclass correlation coefficient; RS, radial strain; CS, circumferential strain; LS, longitudinal strain.

global and regional myocardial dysfunction which is different from LVEF and may guide early therapy for better prognosis.

Previous studies demonstrated that strain parameters within 1 week post-STEMI showed moderate to strong correlation with LGE (r ranged from 0.32 to 0.64) and provided prediction of prognosis (24–26). However, edema and hemorrhage may result in overestimated infarct size by LGE soon after STEMI (27). The present study scheduled CMR examination 1 month after index event (the presence and extent of edema/hemorrhage were much less than acute period), and the results showed a strong association between strain parameters and LGE (GRS: $r = 0.65$; GCS: $r = 0.69$; GLS: $r = 0.61$). Moreover, the present study investigated the correlation of myocardial strain and LGE in detail. Our study showed that regional and global strain could discriminate different transmural and extent of LGE, and segmental strains were good discriminators for LGE >50% (AUC: 0.763–0.903). A previous study reported that segments with >50% LGE extent were hard to recover despite successful revascularization (5). Therefore, it is an alternative to evaluate myocardial infarction without contrast administration and it is predominant for patients with contraindications to contrast agents. In addition, a few studies demonstrated that GLS provides incremental prognostic value to LGE (24, 25). Hence, strain parameters could provide useful information for clinical strategy.

Last but not the least, strain analysis could provide regional function of segments with different conditions. Götte et al. compared regional function between the infarcted and remote region and found significant differences by CMR tissue tagging but not by wall thickening analysis (11). An animal study, quantifying regional mechanical changes 2 weeks after index procedure by tagged cine, also presented similar results, in

which circumferential strain was $-1.5 \pm 0.5\%$, $-4.5 \pm 0.8\%$, and $-5.5 \pm 1.4\%$ in infarct zone, transition zone, and remote zone, respectively (direct comparison was not performed) (28). Our study performed in a larger human population and by a more convenient method (CMR feature-tracking) showed that strains in adjacent region were better than infarcted region and worse than remote region. The possible explanations were as follows: (1) under the background of function decline in infarcted region, kinetic coordination and synchrony of myocardium in adjacent region were impaired; (2) myocardial cells in adjacent region might be slightly edematous without LGE presence; (3) multivessel disease could have a chronic impact on the blood supply of uninvolved myocardium and impair the contractility of uninvolved myocardium. Also, strain impairment of ischemic segments has been demonstrated by a recent study, which investigated the discriminating ability of circumferential and longitudinal strain among ischemic, infarcted, and negative myocardium in patient and segmental levels (29). Furthermore, we speculated that considerably declined strain in adjacent region might contribute to negative remodeling of LV in long term, and the reduced deformation in adjacent region should be alerted.

Study Limitations

There were several limitations in the present study. First, sample size was relatively small. Second, the study only focused on patients with first anterior STEMI so that it limited the ability to extrapolate the findings in a general acute coronary syndrome or STEMI population. Third, CMR parameters were retrospectively analyzed from a prospective cohort with LGE 1 month after percutaneous coronary intervention as study endpoint—T2/T2* mapping was not scheduled so that edema and hemorrhage in the patients were not available; dynamic changes of CMR characteristics could not be observed; however, functional recovery, LV remodeling, and long-term functional outcome were valuable and could be assessed in follow-up CMR examinations (6 or 12 months). Moreover, prognostic results were not reported in the present study since the event rate was low. Therefore, the prognostic association between strain and LGE could not be investigated. Further prospective study with large numbers of patients might be warranted.

CONCLUSION

Global and regional strain could stratify different extent and transmural of LGE, respectively. Although without LGE, adjacent region had impaired strains comparing with remote region.

DATA AVAILABILITY STATEMENT

The original contributions presented in the study are included in the article/supplementary material, further inquiries can be directed to the corresponding author/s.

ETHICS STATEMENT

The studies involving human participants were reviewed and approved by The Review Board of Fuwai Hospital. The patients/participants provided their written informed consent to participate in this study.

AUTHOR CONTRIBUTIONS

SY conception and design of study, analyzed images, and drafted the article. JZ conception and design of study, acquired clinical data, and drafted the article. KY, YZ, JS, and KJ analyzed images and critically revised the article. XC, HY, and SZ conception and design of study and critically reviewed the article. KZ performed statistical analysis and critically reviewed the article. PZ acquired clinical data and critically reviewed the article. All authors read and approved the final article for publication.

REFERENCES

- Schulz-Menger J, Bluemke DA, Bremerich J, Flamm SD, Fogel MA, Friedrich MG, et al. Standardized image interpretation and post-processing in cardiovascular magnetic resonance - 2020 update : Society for Cardiovascular Magnetic Resonance (SCMR): Board of Trustees Task Force on Standardized Post-Processing. *J Cardiovasc Magn Reson.* (2020) 22:19. doi: 10.1186/s12968-020-00610-6
- Ibanez B, James S, Agewall S, Antunes MJ, Bucciarelli-Ducci C, Bueno H, et al. 2017 ESC Guidelines for the management of acute myocardial infarction in patients presenting with ST-segment elevation: the Task Force for the management of acute myocardial infarction in patients presenting with ST-segment elevation of the European Society of Cardiology (ESC). *Eur Heart J.* (2018) 39:119–77. doi: 10.1093/eurheartj/ehx393
- Elias J, van Dongen IM, Hoebers LP, Ouweneel DM, Claessen B, Ramunddal T, et al. Recovery and prognostic value of myocardial strain in ST-segment elevation myocardial infarction patients with a concurrent chronic total occlusion. *Eur Radiol.* (2020) 30:600–8. doi: 10.1007/s00330-019-06338-x
- Fent GJ, Garg P, Foley JRJ, Dobson LE, Musa TA, Erhayiem B, et al. The utility of global longitudinal strain in the identification of prior myocardial infarction in patients with preserved left ventricular ejection fraction. *Int J Cardiovasc Imaging.* (2017) 33:1561–9. doi: 10.1007/s10554-017-1138-7
- Kim RJ, Wu E, Rafael A, Chen EL, Parker MA, Simonetti O, et al. The use of contrast-enhanced magnetic resonance imaging to identify reversible myocardial dysfunction. *N Engl J Med.* (2000) 343:1445–53. doi: 10.1056/NEJM200011163432003
- Mangion K, McComb C, Auger DA, Epstein FH, Berry C. Magnetic resonance imaging of myocardial strain after acute ST-segment-elevation myocardial infarction: a systematic review. *Circ Cardiovasc Imaging.* (2017) 10:e006498. doi: 10.1161/CIRCIMAGING.117.006498
- Kraigher-Krainer E, Shah AM, Gupta DK, Santos A, Claggett B, Pieske B, et al. Impaired systolic function by strain imaging in heart failure with preserved ejection fraction. *J Am Coll Cardiol.* (2014) 63:447–56. doi: 10.1016/j.jacc.2013.09.052
- Ibanez B, Aletas AH, Arai AE, Arheden H, Bax J, Berry C, et al. Cardiac MRI endpoints in myocardial infarction experimental and clinical trials: JACC scientific expert panel. *J Am Coll Cardiol.* (2019) 74:238–56. doi: 10.1016/j.jacc.2019.05.024
- Mastrodicasa D, Elgavish GA, Schoepf UJ, Suranyi P, van Assen M, Albrecht MH, et al. Nonbinary quantification technique accounting for myocardial infarct heterogeneity: feasibility of applying percent infarct mapping in patients. *J Magn Reson Imaging.* (2018) 48:788–98. doi: 10.1002/jmri.25973
- Cerqueira MD, Weissman NJ, Dilsizian V, Jacobs AK, Kaul S, Laskey WK, et al. Standardized myocardial segmentation and nomenclature for

FUNDING

This study was co-funded by National Natural Science Foundation of China (Nos. 81930044, 81620108015, and 81970308), the Chinese Academy of Medical Sciences Innovation Fund for Medical Sciences (2016-I2M-1-009), and the Fund of Sanming Project of Medicine in Shenzhen (No. SZSM 201911017).

SUPPLEMENTARY MATERIAL

The Supplementary Material for this article can be found online at: <https://www.frontiersin.org/articles/10.3389/fcvm.2021.705487/full#supplementary-material>

Supplementary Figure 1 | Comparison of global strain. * $p < 0.05$ for comparison between two groups.

- tomographic imaging of the heart. A statement for healthcare professionals from the Cardiac Imaging Committee of the Council on Clinical Cardiology of the American Heart Association. *Circulation.* (2002) 105:539–42. doi: 10.1161/hc0402.102975
- Gotte MJ, van Rossum AC, Twisk JWR, Kuijter JPA, Marcus JT, Visser CA. Quantification of regional contractile function after infarction: strain analysis superior to wall thickening analysis in discriminating infarct from remote myocardium. *J Am Coll Cardiol.* (2001) 37:808–17. doi: 10.1016/S0735-1097(00)01186-4
- Khan JN, Nazir SA, Singh A, Shetye A, Lai FY, Peebles C, et al. Relationship of myocardial strain and markers of myocardial injury to predict segmental recovery after acute ST-segment-elevation myocardial infarction. *Circ Cardiovasc Imaging.* (2016) 9:e003457. doi: 10.1161/CIRCIMAGING.115.003457
- Kirkpatrick JN, Vannan MA, Narula J, Lang RM. Echocardiography in heart failure: applications, utility, and new horizons. *J Am Coll Cardiol.* (2007) 50:381–96. doi: 10.1016/j.jacc.2007.03.048
- Mirea O, Pagourelas ED, Duchenne J, Bogaert J, Thomas JD, Badano LP, et al. Intervendor differences in the accuracy of detecting regional functional abnormalities: a report from the EACVI-ASE strain standardization task force. *JACC Cardiovasc Imaging.* (2018) 11:25–34. doi: 10.1016/j.jcmg.2017.02.014
- Barreiro-Perez M, Curione D, Symons R, Claus P, Voigt JU, Bogaert J. Left ventricular global myocardial strain assessment comparing the reproducibility of four commercially available CMR-feature tracking algorithms. *Eur Radiol.* (2018) 28:5137–47. doi: 10.1007/s00330-018-5538-4
- Khan JN, Singh A, Nazir SA, Kanagala P, Gershlick AH, McCann GP. Comparison of cardiovascular magnetic resonance feature tracking and tagging for the assessment of left ventricular systolic strain in acute myocardial infarction. *Eur J Radiol.* (2015) 84:840–8. doi: 10.1016/j.ejrad.2015.02.002
- Obokata M, Nagata Y, Wu VC, Kado Y, Kurabayashi M, Otsuji Y, et al. Direct comparison of cardiac magnetic resonance feature tracking and 2D/3D echocardiography speckle tracking for evaluation of global left ventricular strain. *Eur Heart J Cardiovasc Imaging.* (2016) 17:525–32. doi: 10.1093/ehjci/jev227
- Backhaus SJ, Metschies G, Zieschang V, Erley J, Mahsa Zamani S, Kowallik JT, et al. Head-to-head comparison of cardiovascular MR feature tracking cine versus acquisition-based deformation strain imaging using myocardial tagging and strain encoding. *Magn Reson Med.* (2021) 85:357–68. doi: 10.1002/mrm.28437
- Dobrovie M, Barreiro-Perez M, Curione D, Symons R, Claus P, Voigt JU, et al. Inter-vendor reproducibility and accuracy of segmental left ventricular strain measurements using CMR feature tracking. *Eur Radiol.* (2019) 29:6846–57. doi: 10.1007/s00330-019-06315-4
- Almutairi HM, Boubertakh R, Miquel ME, Petersen SE. Myocardial deformation assessment using cardiovascular magnetic

- resonance-feature tracking technique. *Br J Radiol.* (2017) 90:20170072. doi: 10.1259/bjr.20170072
21. Wu L, Germans T, Guclu A, Heymans MW, Allaart CP, van Rossum AC. Feature tracking compared with tissue tagging measurements of segmental strain by cardiovascular magnetic resonance. *J Cardiovasc Magn Reson.* (2014) 16:10. doi: 10.1186/1532-429X-16-10
 22. Bucius P, Erley J, Tanacli R, Zieschang V, Giusca S, Korosoglou G, et al. Comparison of feature tracking, fast-SENC, and myocardial tagging for global and segmental left ventricular strain. *ESC Heart Fail.* (2020) 7:523–32. doi: 10.1002/ehf2.12576
 23. Shah DJ, Kim HW, James O, Parker M, Wu E, Bonow RO, et al. Prevalence of regional myocardial thinning and relationship with myocardial scarring in patients with coronary artery disease. *JAMA.* (2013) 309:909–18. doi: 10.1001/jama.2013.1381
 24. Reindl M, Tiller C, Holzknecht M, Lechner I, Beck A, Plappert D, et al. Prognostic implications of global longitudinal strain by feature-tracking cardiac magnetic resonance in ST-elevation myocardial infarction. *Circ Cardiovasc Imaging.* (2019) 12:e009404. doi: 10.1161/CIRCIMAGING.119.009404
 25. Eitel I, Stiermaier T, Lange T, Rommel KP, Koschalka A, Kowallick JT, et al. Cardiac magnetic resonance myocardial feature tracking for optimized prediction of cardiovascular events following myocardial infarction. *JACC Cardiovasc Imaging.* (2018) 11:1433–44. doi: 10.1016/j.jcmg.2017.11.034
 26. Yoon YE, Kang SH, Choi HM, Jeong S, Sung JM, Lee SE, et al. Prediction of infarct size and adverse cardiac outcomes by tissue tracking-cardiac magnetic resonance imaging in ST-segment elevation myocardial infarction. *Eur Radiol.* (2018) 28:3454–63. doi: 10.1007/s00330-017-5296-8
 27. Dall'Armellina E, Karia N, Lindsay AC, Karamitsos TD, Ferreira V, Robson MD, et al. Dynamic changes of edema and late gadolinium enhancement after acute myocardial infarction and their relationship to functional recovery and salvage index. *Circ Cardiovasc Imaging.* (2011) 4:228–36. doi: 10.1161/CIRCIMAGING.111.963421
 28. Karthikeyan B, Sonkawade SD, Pokharel S, Preda M, Schweser F, Zivadinov R, et al. Tagged cine magnetic resonance imaging to quantify regional mechanical changes after acute myocardial infarction. *Magn Reson Imaging.* (2020) 66:208–18. doi: 10.1016/j.mri.2019.09.010
 29. Zhao L, Zhang C, Tian J, DeLano M, Ma X. Myocardial deformation assessed by MR feature tracking in groups of patients with ischemic heart disease. *J Magn Reson Imaging.* (2021). doi: 10.1002/jmri.27588. [Epub ahead of print].

Conflict of Interest: The authors declare that the research was conducted in the absence of any commercial or financial relationships that could be construed as a potential conflict of interest.

Copyright © 2021 Yu, Zhou, Yang, Chen, Zheng, Zhao, Song, Ji, Zhou, Yan and Zhao. This is an open-access article distributed under the terms of the Creative Commons Attribution License (CC BY). The use, distribution or reproduction in other forums is permitted, provided the original author(s) and the copyright owner(s) are credited and that the original publication in this journal is cited, in accordance with accepted academic practice. No use, distribution or reproduction is permitted which does not comply with these terms.



Elevated Serum Levels of Soluble ST2 Are Associated With Plaque Vulnerability in Patients With Non-ST-Elevation Acute Coronary Syndrome

OPEN ACCESS

Edited by:

Zhao Wang,
University of Electronic Science and
Technology of China, China

Reviewed by:

Ruizheng Shi,
Central South University, China
Jinwei Tian,
The Second Affiliated Hospital of
Harbin Medical University, China

*Correspondence:

Song Ding
dingsong1105@163.com
Jun Pu
pujun310@hotmail.com

†These authors have contributed
equally to this work

Specialty section:

This article was submitted to
Cardiovascular Imaging,
a section of the journal
Frontiers in Cardiovascular Medicine

Received: 31 March 2021

Accepted: 04 June 2021

Published: 22 July 2021

Citation:

Luo G, Qian Y, Sheng X, Sun J, Wu Z,
Liao F, Feng Q, Yin Y, Ding S and Pu J
(2021) Elevated Serum Levels of
Soluble ST2 Are Associated With
Plaque Vulnerability in Patients With
Non-ST-Elevation Acute Coronary
Syndrome.
Front. Cardiovasc. Med. 8:688522.
doi: 10.3389/fcvm.2021.688522

Guqing Luo^{1†}, Yuxuan Qian^{1†}, Xincheng Sheng¹, Jiateng Sun¹, Zhihan Wu¹, Fei Liao¹,
Qi Feng², Yan Yin², Song Ding^{1*} and Jun Pu^{1*}

¹ Department of Cardiology, School of Medicine, Renji Hospital, Shanghai Jiaotong University, Shanghai, China, ² Department of Radiology, School of Medicine, Renji Hospital, Shanghai Jiaotong University, Shanghai, China

Background: Recent studies have suggested that soluble suppression of tumorigenicity-2 (sST2), an inflammation-related protein receptor, is associated with atherosclerotic diseases. This study aimed to investigate the potential predictive value of sST2 on plaque vulnerability by assessing whether elevated serum levels of sST2 are associated with vulnerable plaque features in patients with non-ST-elevation acute coronary syndrome (ACS).

Methods: A total of 120 patients with non-ST-elevation ACS (167 lesions) were prospectively enrolled and evaluated by standard coronary computed tomography angiography (CCTA) and coronary angiography in this study. Serum sST2 levels were measured by ELISA (Presage[®] ST2 Assay Kit, Critical Diagnostics), and semiautomated software (QAngioCT, Medis) was used to quantify coronary plaques.

Results: The included patients were divided into 4 groups by serum sST2 level quartiles. Volumetric analysis of the whole lesion revealed that patients with higher sST2 levels had a larger absolute necrotic core (NC) volume (Quartile 4 vs. Quartile 1, 86.16 ± 59.71 vs. 45.10 ± 45.80 mm³, $P = 0.001$; Quartile 4 vs. Quartile 2, 86.16 ± 59.71 vs. 50.22 ± 42.56 mm³, $P = 0.002$) and a higher NC percentage (Quartile 4 vs. Quartile 1, 35.16 ± 9.82 vs. $23.21 \pm 16.18\%$, $P < 0.001$; Quartile 4 vs. Quartile 2, $35.16 \pm 9.82\%$ vs. $22.50 \pm 14.03\%$, $P < 0.001$; Quartile 4 vs. Quartile 3, $35.16 \pm 9.82\%$ vs. $25.04 \pm 14.48\%$, $P < 0.001$). Correlation analysis revealed that serum sST2 levels were positively correlated with the NC ($r = 0.323$, $P < 0.001$) but negatively correlated with dense calcium ($r = -0.208$, $P = 0.007$). Furthermore, among those with plaque calcification, patients with spotty calcification exhibited higher serum sST2 levels than those with large calcification (26.06 ± 16.54 vs. 17.55 ± 7.65 ng/mL, $P = 0.002$). No significant differences in plaque components at the level of the minimal lumen area (MLA) were found among the groups.

Conclusions: Serum sST2 levels were correlated with different coronary plaque components in patients with non-ST-elevation ACS. A higher serum level of sST2 was correlated with plaque vulnerability.

Clinical Trial Registration: www.ClinicalTrials.gov, identifier: NCT04797819.

Keywords: coronary computed tomography angiography, coronary plaque, plaque vulnerability, soluble ST2, non-ST elevation acute coronary syndromes

INTRODUCTION

Rupture of vulnerable plaques and subsequent thrombosis are the main triggers of acute coronary syndrome (ACS), and researchers are becoming increasingly interested in the early identification of vulnerable plaques. Standard intracoronary imaging methods, such as intravascular ultrasound (IVUS) and optical coherence tomography (OCT), are used to quantify the distribution and severity of coronary plaques but are limited by their invasive features. Coronary computed tomographic angiography (CTA) is a sensitive and non-invasive modality widely used for the diagnosis of coronary artery disease. QAngioCT can quantitatively analyze stenosis, plaque burden, and specific intraplaque components of coronary CTA (CCTA) images by obtaining 3-dimensional centerline of coronary artery and reconstructing coronary artery volume via a fast vessel-tracking algorithm (1, 2). Furthermore, several studies supported the feasibility of non-invasive quantitative CCTA (QCCTA) via QAngioCT software to assess plaque burden and plaque components when compared to quantitative coronary angiography (QCA) or virtual histology (VH)-IVUS analysis (1–3).

Inflammation plays an essential role in the pathogenesis of plaque vulnerability (4). sST2, a soluble form of ST2, can modulate the inflammatory response and exert proinflammatory effects when secreted into the circulation (4, 5). Elevated serum levels of sST2 have been observed in patients with several inflammatory and autoimmune diseases, including inflammatory bowel disease, asthma, and rheumatoid arthritis. Several studies have focused on the association between serum sST2 and cardiovascular diseases. Previous studies demonstrated that elevation of serum sST2 levels was associated with poor prognosis in patients with myocardial infarction (MI) or heart failure (HF) (6–8). An animal study has reported that administration of sST2 exacerbated atherosclerosis development in a mouse model (9). Consistent with that, a recent study by Zhang et al. showed that serum sST2 levels were elevated in patients with ACS, especially in those with complex lesions (4). In this study, we aimed to investigate the relationships between serum sST2 levels and CCTA-based plaque components in patients with non-ST-elevation ACS. We hypothesized that elevated serum sST2 level might be closely related to vulnerable plaque features, serving as a reliable sensor of coronary immune-inflammatory disorder and a simple indicator for coronary plaque vulnerability.

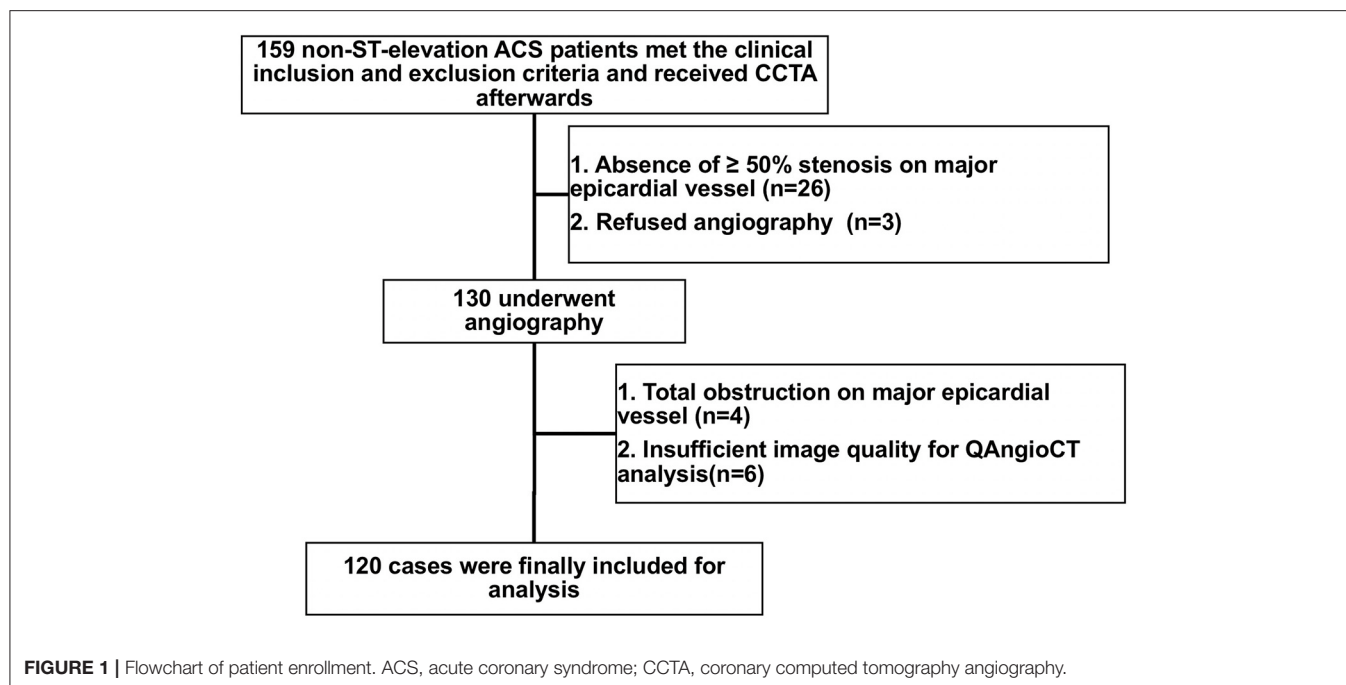
METHODS

Study Population

Patients with non-ST-elevation ACS who required an immediate (<2 h) or early invasive strategy (<24 h) according to guidelines, including those who presented with hemodynamic instability or cardiogenic shock, life-threatening arrhythmias or cardiac arrest, mechanical complications, acute heart failure, dynamic ST or T wave changes, or a Global Registry of Acute Coronary Events (GRACE) score > 140, were excluded (10). In addition, subjects with a previous history of coronary artery bypass graft surgery or percutaneous coronary intervention (PCI), immune system disorder, cancer, acute/chronic infection, statin use within 3 months, atrial fibrillation, end-stage renal failure, or iodine-containing contrast allergy were excluded. Between January 2019 and December 2019, a total of 159 patients with non-ST-elevation ACS (non-ST-elevation myocardial infarction or unstable angina) aged 18–75 years who underwent CCTA were prospectively enrolled in this study. After CCTA, we also excluded patients with no significant ($\geq 50\%$) stenosis of major epicardial vessels ($n = 26$) and those who refused subsequent angiography ($n = 3$). Among the 130 remaining patients who received angiography, those with total obstruction of major epicardial vessels ($n = 4$) or insufficient image quality for QAngioCT analysis ($n = 6$) were excluded. Finally, a total of 120 patients with 167 lesions were included in our study for the final analysis (Figure 1). The baseline features and cardiovascular risk factors of the study subjects were documented. This study was approved by the Institutional Review Board of Renji Hospital, and all subjects provided written informed consent.

Serum sST2 and Other Biochemical Indicators Measurement

At admission, four milliliters of venous blood were collected from the antecubital veins of patients hospitalized for the angiography procedure into EDTA-containing tubes. The blood was centrifuged at 3,000 g for 5 min within 1 h of collection, and the serum was immediately separated and stored at -80°C for further testing. Serum sST2 levels were measured with a commercial ELISA kit (Presage[®] ST2 Assay Kit, REF#BC-1065, Critical Diagnostics, San Diego, CA) according to the manufacturer's instructions. Following standard laboratory techniques, other serum biochemical indicators including alanine transaminase (ALT), serum creatinine (Scr), high-sensitivity



C-reactive protein (hs-CRP), and low-density lipoprotein (LDL) were analyzed at hospital admission as well.

Enhanced Coronary CTA

Enhanced coronary CT scans were obtained from all of the included patients on a 320-slice CT scanner (Aquilion ONE, Toshiba Medical Systems, Otawara, Japan). To optimize the imaging quality, oral metoprolol was administered to patients with a heart rate >75 beats/min prior to the CT scan. The tube voltage and current for each patient was determined by Toshiba integrated dose reduction technique (SureExposure 3D). Electrocardiograms were used for retrospective gating to eliminate motion interference. Imaging data were reconstructed at a slice thickness of 0.5 mm and a reconstruction interval of 0.25 mm. All the results were interpreted by radiologists with board certifications for cardiac CT interpretation.

Plaque Characteristics Analysis

CCTA data were transferred to offline workstations. Plaque characteristics were semiautomatically analyzed using QAngioCT software (Medis® QAngio CT V3.1, Medis Medical Imaging Systems, Leiden, the Netherlands). All lesions with a stenosis of $\geq 50\%$ underwent quantitative analysis (11–13). Plaque characteristics were analyzed by two trained observers who were blinded to the clinical characteristics of the corresponding patients. QAngioCT software was used for the automated 3-dimensional reconstruction of the coronary artery volume to determine the contours of the vessel wall and lumen (Figure 2). Volumetric characterization of the plaque characteristics focused on the entire plaque volume under 3-dimensional reconstruction, while the cross-sectional characterization focused at the level of the minimal lumen area

(MLA) (2, 14). And in our study, the level of the MLA was automatically identified using the lumen contours detected on coronary CTA (2). Different plaque components on CCTA were distinguished by Hounsfield unit (HU) values, and different cut-off values were available in previous studies, which were obtained by comparing coronary CTA with VH-IVUS or histological examination (15, 16). For the current study, a density of $-30 \sim 75$ HUs indicated necrotic core (NC), while a density of $76 \sim 130$ HUs indicated fibrous fatty (FF), a density of $131 \sim 350$ HUs indicated fibrous tissue (FT), and a density >351 HUs indicated dense calcium (DC) (14, 17). The eccentricity index and remodeling index were automatically calculated by QAngioCT software. Eccentricity index was calculated as (maximal plaque thickness minus minimal plaque thickness) divided by maximal plaque thickness (2, 18, 19). At the level of the minimal lumen area, the remodeling index was calculated by dividing the cross-sectional vessel wall area by the corresponding reference area. The cross-sectional reference area was determined in the normal-appearing reference area as close as possible to the respective coronary lesion (2, 18, 20). Spotty calcification was defined when <3 mm in size on curved multiplanar reformation images and 1-sided on cross-sectional images. Large calcification was defined as the calcification larger than spotty calcification (21, 22).

Statistical Analysis

Statistical analyses were performed using IBM SPSS Statistics 23 (SPSS, Inc., Chicago, IL). Summary statistics of continuous data with symmetric distribution are expressed as the mean \pm standard deviation (SD), while categorical data are expressed as counts (percentages). Comparison of continuous variables between two groups was performed using the independent

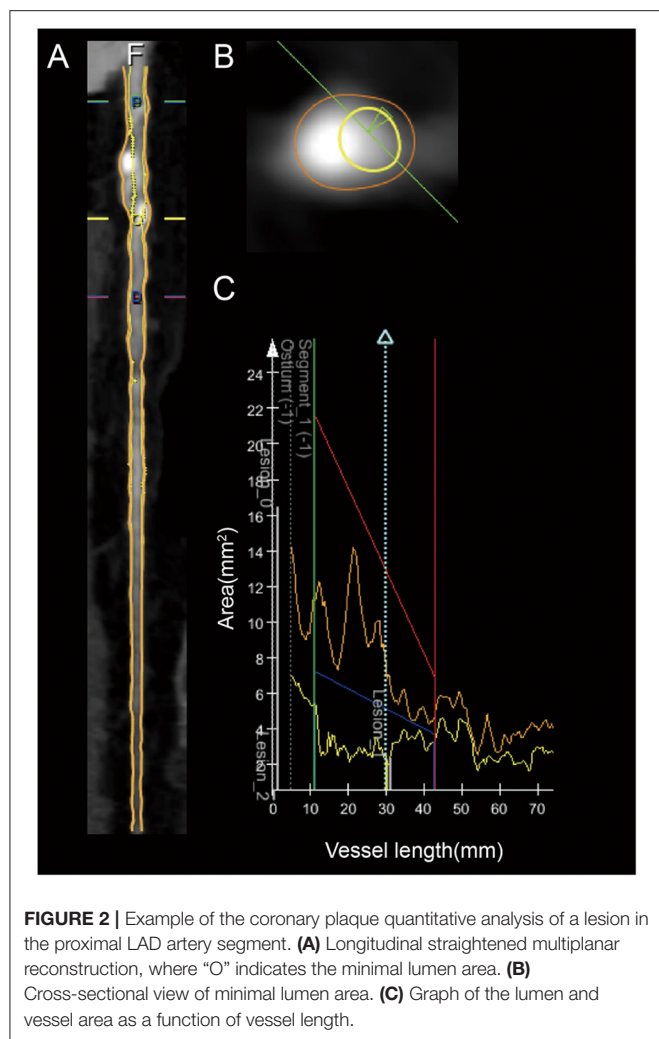


FIGURE 2 | Example of the coronary plaque quantitative analysis of a lesion in the proximal LAD artery segment. **(A)** Longitudinal straightened multiplanar reconstruction, where “O” indicates the minimal lumen area. **(B)** Cross-sectional view of minimal lumen area. **(C)** Graph of the lumen and vessel area as a function of vessel length.

sample *t*-test, while categorical variables were compared using the chi-squared test. Pearson’s chi-square test was used to compare the constituent ratios and to assess the correlations between two continuous variables. $P < 0.05$ indicate statistical differences. Furthermore, threshold level of significance for differences among groups were adjusted for multiple comparisons by Bonferroni’s correction. As 6 tests were performed among 4 groups, the differences were statistically significant when the observed *P*-values were less than the specified significance level (α) divided by the number of tests (K) = $0.05/6 < 0.0084$.

RESULTS

Baseline Characteristics

Out of 120 patients, 167 lesions were analyzed in our study. Eighty-two patients had one lesion undergoing analysis, while 29 patients had two lesions and 9 patients had three lesions undergoing analysis. Patients were classified into 4 groups according to the serum sST2 level quartiles (sST2 < 14.5 ng/mL,

Quartile 1; $14.5 \text{ ng/mL} \leq \text{sST2} < 20.5 \text{ ng/mL}$, Quartile 2; $20.5 \text{ ng/mL} \leq \text{sST2} < 25.9 \text{ ng/mL}$, Quartile 3; $\text{sST2} \geq 25.9 \text{ ng/mL}$, Quartile 4). A comparison of the baseline characteristics is shown in **Table 1**. Patients with higher serum sST2 levels were older (Quartile 4 vs. Quartile 2, 70.27 ± 8.38 vs. 64.17 ± 8.91 ng/mL, $P = 0.008$). There were no statistically significant differences in the sex, BMI, heart rate, blood pressure, incidence of hypertension, hyperlipemia, diabetes mellitus, chronic obstructive pulmonary disease, known valvular disease, ALT level, Scr level, hs-CRP level, or eGFR among the groups. The lesion distributions across the main coronary arteries were not significantly different.

Serum sST2 Level and Plaque Components in Volumetric Analysis of the Whole Lesion

As shown in **Table 2**, the relationships between the serum sST2 level and the absolute volumes or percentages of four different plaque components throughout the entire lesion were assessed. We found that patients with higher sST2 levels had a larger absolute NC volume (Quartile 4 vs. Quartile 1, 86.16 ± 59.71 vs. $45.10 \pm 45.80 \text{ mm}^3$, $P = 0.001$; Quartile 4 vs. Quartile 2, 86.16 ± 59.71 vs. $50.22 \pm 42.56 \text{ mm}^3$, $P = 0.002$) and a higher NC percentage (Quartile 4 vs. Quartile 1, $35.16 \pm 9.82\%$ vs. $23.21 \pm 16.18\%$, $P < 0.001$; Quartile 4 vs. Quartile 2, $35.16 \pm 9.82\%$ vs. $22.50 \pm 14.03\%$, $P < 0.001$; Quartile 4 vs. Quartile 3, $35.16 \pm 9.82\%$ vs. $25.04 \pm 14.48\%$, $P < 0.001$). On the contrary, patients with higher sST2 levels had a lower DC percentage (Quartile 4 vs. Quartile 1, $7.23 \pm 9.76\%$ vs. $18.07 \pm 22.13\%$, $P = 0.005$; Quartile 4 vs. Quartile 2, $7.23 \pm 9.76\%$ vs. $17.66 \pm 19.89\%$, $P = 0.003$). No differences were observed in the other plaque characteristics, including the mean plaque burden, maximal plaque thickness, FT and FF components. The serum sST2 level was positively correlated with both the absolute NC volume (Pearson’s $r = 0.323$, $P < 0.001$) and the NC percentage (Pearson’s $r = 0.425$, $P < 0.001$). In addition, the serum sST2 level was mildly negatively correlated with the absolute DC volume (Pearson’s $r = -0.208$, $P = 0.007$) and the DC percentage (Pearson’s $r = -0.275$, $P < 0.001$) (**Table 3**).

Serum sST2 Level and Plaque Components at the Level of the Minimal Lumen Area (MLA)

As shown in **Table 4**, there were no differences in the plaque components at the level of the minimal lumen area among the groups.

Soluble ST2 and Plaque Calcification

Different types of plaque calcification play different roles in plaque vulnerability. To further clarify the correlation between the serum sST2 level and coronary plaque calcification, we divided patients into two groups based on the existence of plaque calcification. The results showed no significant difference in the serum sST2 levels (22.87 ± 14.44 vs. $24.47 \pm 15.63 \text{ ng/mL}$, $P = 0.494$) between the calcification and non-calcification groups (**Figure 3A**). However, further division of the calcification group into two subgroups by the plaque calcification type revealed that patients with spotty calcification had higher sST2 levels

TABLE 1 | Baseline characteristics.

	Quartile 1 (N = 30) <14.5 ng/mL	Quartile 2 (N = 30) 14.5–20.5 ng/mL	Quartile 3 (N = 30) 20.5–25.9 ng/mL	Quartile 4 (N = 30) >25.9 ng/mL	P-value					
					Quartile 2 vs. Quartile 1	Quartile 3 vs. Quartile 1	Quartile 4 vs. Quartile 1	Quartile 3 vs. Quartile 2	Quartile 4 vs. Quartile 2	Quartile 4 vs. Quartile 3
Age, yrs	65.10 ± 8.48	64.17 ± 8.91	65.60 ± 6.78	70.27 ± 8.38	0.679	0.802	0.021	0.486	0.008	0.021
Sex, M/F	20/10	24/6	21/9	22/8	0.250	0.786	0.581	0.380	0.549	0.779
BMI, kg/m ²	25.15 ± 2.47	25.75 ± 4.05	24.66 ± 2.58	24.37 ± 3.42	0.488	0.458	0.320	0.219	0.160	0.711
HR, bpm	71.97 ± 10.94	75.20 ± 14.77	72.07 ± 11.54	69.00 ± 14.63	0.340	0.973	0.378	0.364	0.108	0.371
SBP, mmHg	136.17 ± 14.34	131.07 ± 14.64	135.87 ± 20.92	132.97 ± 24.85	0.178	0.949	0.544	0.308	0.720	0.627
HTN, n (%)	20 (66.7)	23 (76.7)	20 (66.7)	17 (56.7)	0.399	1.000	0.434	0.399	0.104	0.434
DM, n (%)	7 (23.3)	10 (33.3)	11 (36.7)	15 (50.0)	0.390	0.260	0.032	0.787	0.190	0.297
COPD, n (%)	3 (10.0)	4 (13.3)	3 (10.0)	5 (16.7)	0.688	1.000	0.448	0.688	0.718	0.448
Known valvular disease, n (%)	1 (3.3)	1 (3.3)	0 (0)	2 (6.7)	1.000	0.313	0.554	0.313	0.554	0.150
ALT, U/L	20.50 ± 7.44	20.90 ± 10.98	23.17 ± 18.29	27.77 ± 18.70	0.869	0.464	0.055	0.563	0.089	0.339
Scr, μmol/L	76.10 ± 21.89	73.50 ± 21.07	73.77 ± 23.22	73.93 ± 14.42	0.641	0.690	0.653	0.963	0.926	0.973
eGFR, mL/(min*1.73 m ²)	97.27 ± 16.18	101.63 ± 28.27	100.29 ± 30.73	94.37 ± 18.12	0.468	0.636	0.515	0.862	0.242	0.368
LDL, mmol/L	2.49 ± 0.69	2.32 ± 0.79	2.59 ± 0.83	2.29 ± 0.79	0.391	0.615	0.321	0.212	0.898	0.171
hs-CRP, mg/L	2.01 ± 1.74	3.38 ± 3.93	3.45 ± 4.12	6.31 ± 10.00	0.090	0.086	0.027	0.943	0.143	0.155
Coronary arteries	42	43	42	40	0.158	0.520	0.790	0.714	0.207	0.616
LAD, n (%)	16 (38.1)	22 (51.2)	20 (47.6)	18 (45.0)						
LCX, n (%)	8 (19.0)	11 (25.6)	9 (21.4)	6 (15.0)						
RCA, n (%)	18 (42.9)	10 (23.2)	13 (31.0)	16 (40.0)						

F, female; M, male; BMI, body mass index; HR, heart rate; SBP, systolic blood pressure; HTN, hypertension; DM, diabetes mellitus; COPD, chronic obstructive pulmonary disease; ALT, alanine transaminase; Scr, serum creatinine; eGFR, estimated glomerular filtration rate; LDL, low-density lipoprotein; hs-CRP, high-sensitivity C-reactive protein; LAD, left anterior descending artery; LCX, left circumflex artery; RCA, right coronary artery.

than those with large calcification (26.06 ± 16.54 vs. 17.55 ± 7.65 ng/mL, $P = 0.002$) (**Figure 3B**).

DISCUSSION

The main findings of this study are as follows: (a) Among the four coronary plaque component phenotypes assessed by CCTA, the serum sST2 level was correlated with the NC and DC components. The volume of the NC component was larger in patients with higher serum sST2 levels, while that of the DC was decreased in these patients. (b) Further subgroup analysis revealed that patients with spotty calcification had higher serum sST2 levels than those with large calcification.

Previous studies have shown that inflammation plays an essential role in atherosclerosis, especially in NC formation, and NC has been proven to be tightly correlated with plaque vulnerability (23–29). As an important inflammatory factor, sST2 exerts proinflammatory effects and regulates the pathogenesis of atherosclerosis. A recent study by Zhang et al., as mentioned above, demonstrated that patients with ACS had higher serum sST2 levels than those with stable angina pectoris (SAP), which suggested that sST2 is potentially associated with plaque vulnerability (4). In our study, we further investigated the correlation between the serum sST2 level and plaque

vulnerability by assessing the coronary plaque components in patients with non-ST-elevation ACS and revealed a positive correlation between the serum sST2 level and NC component in coronary lesions.

The role of calcification in plaque vulnerability remains controversial. Previous studies have reported a biphasic association between calcification and plaque vulnerability, as spotty calcification was more often found in ruptured plaques, while large calcification was more strongly related to stable plaques (30). Interestingly, patients with higher serum sST2 levels had smaller intraplaque calcification volumes in our study, and further subgroup analysis revealed that patients with spotty calcification had higher serum sST2 levels than those with large calcification. Furthermore, macrophages may play a role in the relationship between sST2 and calcification. Previous studies have demonstrated that sST2 may suppress the differentiation of macrophages toward the anti-inflammatory M2 phenotype (31). Proinflammatory M1 macrophages may facilitate microcalcification formation in plaque progression, leading to plaque rupture, while anti-inflammatory M2 macrophages are related to macrocalcification in plaque regression, suggesting plaque stability (32).

However, we did not observe associations between the serum sST2 level and plaque components at the level of the MLA.

TABLE 2 | Serum sST2 level and plaque components in volumetric analysis of the whole lesion.

	Quartile 1 (N = 30) <14.5 ng/mL	Quartile 2 (N = 30) 14.5–20.5 ng/mL	Quartile 3 (N = 30) 20.5–25.9 ng/mL	Quartile 4 (N = 30) >25.9 ng/mL	P-value					
					Quartile 2 vs. Quartile 1	Quartile 3 vs. Quartile 1	Quartile 4 vs. Quartile 1	Quartile 3 vs. Quartile 2	Quartile 4 vs. Quartile 2	Quartile 4 vs. Quartile 3
Analyzed lesions, <i>n</i>	42	43	42	40						
Plaque volume, mm ³	240.18 ± 209.36	217.95 ± 133.49	230.18 ± 181.63	220.45 ± 143.18	0.562	0.816	0.618	0.725	0.935	0.788
Mean plaque burden, %	60.34 ± 8.78	62.47 ± 7.71	60.86 ± 12.64	59.80 ± 9.35	0.238	0.829	0.787	0.480	0.160	0.666
Maximal plaque thickness, mm	2.57 ± 0.70	2.45 ± 0.74	2.41 ± 0.86	2.36 ± 0.50	0.421	0.352	0.110	0.844	0.512	0.718
Fibrous volume, mm ³	73.79 ± 40.17	75.36 ± 43.05	74.62 ± 57.81	73.73 ± 46.89	0.862	0.939	0.995	0.947	0.870	0.939
Fibrous volume, %	35.32 ± 13.42	38.97 ± 13.24	37.50 ± 16.72	34.80 ± 9.91	0.211	0.512	0.841	0.656	0.107	0.374
Fibrous fatty volume, mm ³	35.80 ± 19.47	35.49 ± 23.50	36.87 ± 30.42	37.34 ± 28.21	0.947	0.848	0.775	0.816	0.747	0.942
Fibrous fatty volume, %	18.25 ± 7.10	17.95 ± 7.15	18.18 ± 7.19	18.13 ± 7.26	0.848	0.964	0.937	0.885	0.914	0.973
Necrotic core volume, mm ³	45.10 ± 45.80	50.22 ± 42.56	62.65 ± 69.86	86.16 ± 59.71	0.595	0.178	0.001	0.326	0.002	0.105
Necrotic core volume, %	23.21 ± 16.18	22.50 ± 14.03	25.04 ± 14.48	35.16 ± 9.82	0.829	0.588	<0.001	0.415	<0.001	<0.001
Dense calcium volume, mm ³	74.21 ± 172.44	48.16 ± 78.62	39.11 ± 67.42	16.72 ± 26.96	0.376	0.225	0.039	0.570	0.017	0.051
Dense calcium volume, %	18.07 ± 22.13	17.66 ± 19.89	14.61 ± 18.40	7.23 ± 9.76	0.929	0.438	0.005	0.464	0.003	0.026

TABLE 3 | Correlation between serum sST2 and plaque components in volumetric analysis of the whole lesion.

Parameters	Pearson correlation	P-value
Plaque volume, mm ³	−0.019	0.807
Mean plaque burden, %	0.018	0.818
Maximal plaque thickness, mm	−0.071	0.363
Fibrous volume, mm ³	−0.059	0.446
Fibrous volume, %	−0.166	0.056
Fibrous fatty volume, mm ³	0.088	0.257
Fibrous fatty volume, %	0.093	0.230
Necrotic core volume, mm ³	0.323	<0.001
Necrotic core volume, %	0.425	<0.001
Dense calcium volume, mm ³	−0.208	0.007
Dense calcium volume, %	−0.275	<0.001

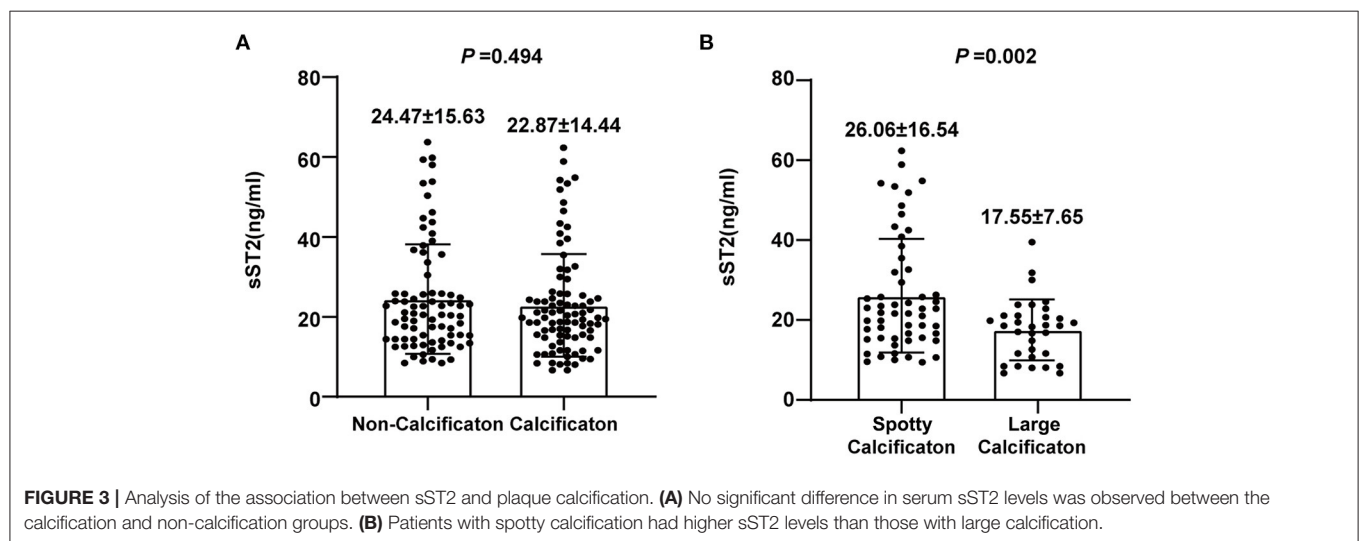
Perhaps the cross-sectional characteristics of the plaques at the level of the MLA were unable to reflect the characteristics of the whole plaque. Moreover, a similar conclusion was drawn in a previous study focused on carotid plaques, as no associations between serum sST2 levels and cross-sectional plaque characteristics were found on specimens from carotid endarterectomy (33).

In addition, we have observed that higher serum sST2 levels were correlated with older age in our study, which is consistent with previous studies (4, 34). Usually, aging is accompanied with alterations of cytokine expression toward a pro-inflammatory pattern (35–37). sST2, a modulator of the inflammatory response, might increase with age and exert a pro-inflammatory effect, while the underlying mechanisms need further study.

The current study does have some limitations. First, the study was observational in nature and was performed at a single center. Second, although this preliminary study has observed associations between serum sST2 levels and plaque vulnerability, only surrogate and not clinical endpoints were analyzed due to a relatively small sample size. Previous studies have demonstrated that elevation of serum sST2 levels were associated with poor prognosis in patients with myocardial infarction (MI) and heart failure (HF) (6–8). A larger sample size study is required in future to further investigate the predictive value of serum sST2 on long-term prognosis of patients with non-ST-elevation ACS. Third, although our study revealed that serum sST2 levels were correlated with NC and DC plaque components, the underlying mechanisms remain unclear. Previous study reported the role of sST2 in facilitating M1 macrophage polarization, which participated in the formation of spotty calcification and vulnerable plaque (31, 32, 38). However, the pathophysiological effects of sST2 on plaque vulnerability remain largely unknown, which need further mechanistic studies.

TABLE 4 | Serum sST2 and plaque components at the level of the MLA.

	Quartile 1 (N = 30) <14.5 ng/mL	Quartile 2 (N = 30) 14.5–20.5 ng/mL	Quartile 3 (N = 30) 20.5–25.9 ng/mL	Quartile 4 (N = 30) >25.9 ng/mL	P-value					
					Quartile 2 vs. Quartile 1	Quartile 3 vs. Quartile 1	Quartile 4 vs. Quartile 1	Quartile 3 vs. Quartile 2	Quartile 4 vs. Quartile 2	Quartile 4 vs. Quartile 3
Analyzed lesions, <i>n</i>	42	43	42	40						
Eccentricity index	0.65 ± 0.15	0.68 ± 0.22	0.71 ± 0.21	0.72 ± 0.26	0.602	0.174	0.182	0.453	0.420	0.897
Plaque burden, %	79.11 ± 12.21	81.43 ± 10.49	77.31 ± 14.23	76.93 ± 15.13	0.378	0.561	0.497	0.150	0.132	0.911
Remodeling index	1.01 ± 0.16	0.98 ± 0.11	0.97 ± 0.15	0.97 ± 0.19	0.285	0.166	0.392	0.966	0.983	0.989
Maximal plaque thickness, mm	1.96 ± 0.47	1.91 ± 0.49	2.08 ± 0.56	1.86 ± 0.63	0.627	0.320	0.428	0.148	0.702	0.107
Fibrous area, mm ²	3.24 ± 2.27	3.18 ± 1.89	2.94 ± 1.84	2.64 ± 1.88	0.899	0.538	0.222	0.574	0.209	0.483
Fibrous area, %	27.11 ± 16.02	26.26 ± 12.41	24.20 ± 14.14	27.45 ± 18.65	0.796	0.411	0.934	0.495	0.741	0.395
Fibrous fatty area, mm ²	2.86 ± 2.35	2.29 ± 1.29	2.37 ± 1.97	2.14 ± 1.41	0.203	0.340	0.119	0.831	0.625	0.560
Fibrous fatty area, %	21.92 ± 12.91	21.06 ± 11.88	18.24 ± 11.26	19.20 ± 10.32	0.764	0.197	0.322	0.282	0.458	0.699
Necrotic core area, mm ²	4.12 ± 2.28	4.00 ± 3.01	4.20 ± 3.21	3.33 ± 3.01	0.850	0.895	0.205	0.777	0.321	0.223
Necrotic core area, %	32.00 ± 15.17	33.24 ± 19.02	31.62 ± 20.14	28.99 ± 21.61	0.751	0.927	0.488	0.714	0.357	0.585
Dense calcium area, mm ²	1.11 ± 2.02	1.77 ± 2.77	2.00 ± 3.08	1.93 ± 2.92	0.232	0.146	0.165	0.732	0.809	0.917
Dense calcium area, %	9.69 ± 15.78	14.24 ± 20.60	15.59 ± 23.80	17.15 ± 23.69	0.279	0.213	0.116	0.789	0.564	0.776



CONCLUSIONS

Our study demonstrated that serum sST2 levels were correlated with different coronary plaque components in patients with non-ST-elevation ACS. Patients with higher serum sST2 levels had a larger NC plaque component. The serum sST2 level might be a useful

predictive marker of plaque vulnerability in patients with non-ST-elevation ACS.

DATA AVAILABILITY STATEMENT

The original contributions presented in the study are included in the article/supplementary

material, further inquiries can be directed to the corresponding author/s.

ETHICS STATEMENT

The studies involving human participants were reviewed and approved by Institutional Review Board of Renji Hospital. The patients/participants provided their written informed consent to participate in this study.

AUTHOR CONTRIBUTIONS

SD and JP conceived and designed the study and amended the manuscript. GL, YQ, ZW, and FL acquired clinical data. QF and YY analyzed QAngioCT data. XS and JS executed the statistical analysis. GL and YQ drafted the manuscript. All authors contributed to the interpretation of the data and approved the final version of this manuscript.

REFERENCES

- Boogers MJ, Schuijff JD, Kitslaar PH, van Werkhoven JM, de Graaf FR, Boersma E, et al. Automated quantification of stenosis severity on 64-slice CT: a comparison with quantitative coronary angiography. *JACC Cardiovasc Imaging*. (2010) 3:699–709. doi: 10.1016/j.jcmg.2010.01.010
- Boogers MJ, Broersen A, van Velzen JE, de Graaf FR, El-Naggar HM, Kitslaar PH, et al. Automated quantification of coronary plaque with computed tomography: comparison with intravascular ultrasound using a dedicated registration algorithm for fusion-based quantification. *Eur Heart J*. (2012) 33:1007–16. doi: 10.1093/eurheartj/ehv465
- Papadopolou SL, Neeffes LA, Garcia-Garcia HM, Flu WJ, Rossi A, Dharampal AS, et al. Natural history of coronary atherosclerosis by multislice computed tomography. *JACC Cardiovasc Imaging*. (2012) 5(3 Suppl):S28–37. doi: 10.1016/j.jcmg.2012.01.009
- Zhang Y, Fan Z, Liu H, Ma J, Zhang M. Correlation of plasma soluble suppression of tumorigenicity-2 level with the severity and stability of coronary atherosclerosis. *Coron Artery Dis*. (2020) 31:628–35. doi: 10.1097/MCA.0000000000000851
- Aimo A, Migliorini P, Vergaro G, Franzini M, Passino C, Maisel A, et al. The IL-33/ST2 pathway, inflammation and atherosclerosis: trigger and target? *Int J Cardiol*. (2018) 267:188–92. doi: 10.1016/j.ijcard.2018.05.056
- Aimo A, Vergaro G, Passino C, Ripoli A, Ky B, Miller WL, et al. Prognostic value of soluble suppression of tumorigenicity-2 in chronic heart failure: a meta-analysis. *JACC Heart Fail*. (2017) 5:280–6. doi: 10.1016/j.jchf.2016.09.010
- Aimo A, Vergaro G, Ripoli A, Bayes-Genis A, Pascual Figal DA, de Boer RA, et al. Meta-Analysis of soluble suppression of tumorigenicity-2 and prognosis in acute heart failure. *JACC Heart Fail*. (2017) 5:287–96. doi: 10.1016/j.jchf.2016.12.016
- Jenkins WS, Roger VL, Jaffe AS, Weston SA, AbouEzzeddine OE, Jiang R, et al. Prognostic value of soluble ST2 after myocardial infarction: a community perspective. *Am J Med*. (2017) 130:1112.e9–e15. doi: 10.1016/j.amjmed.2017.02.034
- Miller AM, Xu D, Asquith DL, Denby L, Li Y, Sattar N, et al. IL-33 reduces the development of atherosclerosis. *J Exp Med*. (2008) 205:339–46. doi: 10.1084/jem.20071868
- Roffi M, Patrono C, Collet JP, Mueller C, Valgimigli M, Andreotti F, et al. 2015 ESC guidelines for the management of acute coronary syndromes in patients presenting without persistent ST-segment elevation: task force for the management of acute coronary syndromes in patients presenting without persistent ST-segment elevation of the European Society of Cardiology (ESC). *Eur Heart J*. (2016) 37:267–315. doi: 10.1093/eurheartj/ehv320

FUNDING

This work was supported by grants from the National Key R&D Program of China (2018YFC1312802), National Natural Science Foundation of China (82070477 and 81800223), Shanghai ShenKang Hospital Development Center (SHDC12019X12), Shanghai Jiao Tong University School of Medicine Multi-center clinical research project DLY201804, and Shanghai Sailing Program (18YF1413500).

ACKNOWLEDGMENTS

The authors would like to acknowledge the core laboratory (CardHemo, Med-X Research Institute, Shanghai Jiao Tong University, Shanghai, China) for guidance and quality control of QAngioCT analysis.

- Fuchs S, Lavi I, Tzang O, Fuchs S, Brosh D, Bental T, et al. Necrotic core and thin cap fibrous atheroma distribution in native coronary artery lesion-containing segments: a virtual histology intravascular ultrasound study. *Coron Artery Dis*. (2011) 22:339–44. doi: 10.1097/MCA.0b013e3283467829
- Ito T, Terashima M, Kaneda H, Nasu K, Matsuo H, Ehara M, et al. Comparison of *in vivo* assessment of vulnerable plaque by 64-slice multislice computed tomography versus optical coherence tomography. *Am J Cardiol*. (2011) 107:1270–7. doi: 10.1016/j.amjcard.2010.12.036
- Deftereos S, Giannopoulos G, Kossyvakis C, Kaoukis A, Raisakis K, Panagopoulou V, et al. Association of soluble tumour necrosis factor-related apoptosis-inducing ligand levels with coronary plaque burden and composition. *Heart*. (2012) 98:214–8. doi: 10.1136/heartjnl-2011-300339
- de Graaf MA, Broersen A, Kitslaar PH, Roos CJ, Dijkstra J, Lelieveldt BP, et al. Automatic quantification and characterization of coronary atherosclerosis with computed tomography coronary angiography: cross-correlation with intravascular ultrasound virtual histology. *Int J Cardiovasc Imaging*. (2013) 29:1177–90. doi: 10.1007/s10554-013-0194-x
- Brodoefel H, Reimann A, Heuschmid M, Tsiflikas I, Kopp AF, Schroeder S, et al. Characterization of coronary atherosclerosis by dual-source computed tomography and HU-based color mapping: a pilot study. *Eur Radiol*. (2008) 18:2466–74. doi: 10.1007/s00330-008-1019-5
- Motoyama S, Sarai M, Harigaya H, Anno H, Inoue K, Hara T, et al. Computed tomographic angiography characteristics of atherosclerotic plaques subsequently resulting in acute coronary syndrome. *J Am Coll Cardiol*. (2009) 54:49–57. doi: 10.1016/j.jacc.2009.02.068
- Precht H, Kitslaar PH, Broersen A, Dijkstra J, Gerke O, Thygesen J, et al. Influence of adaptive statistical iterative reconstruction on coronary plaque analysis in coronary computed tomography angiography. *J Cardiovasc Comput Tomogr*. (2016) 10:507–16. doi: 10.1016/j.jcct.2016.09.006
- Mintz GS, Nissen SE, Anderson WD, Bailey SR, Erbel R, Fitzgerald PJ, et al. American college of cardiology clinical expert consensus document on standards for acquisition, measurement and reporting of Intravascular Ultrasound Studies (IVUS). a report of the american college of cardiology task force on clinical expert consensus documents. *J Am Coll Cardiol*. (2001) 37:1478–92. doi: 10.1016/s0735-1097(01)01175-5
- Higuma T, Soeda T, Abe N, Yamada M, Yokoyama H, Shibutani S, et al. A combined optical coherence tomography and intravascular ultrasound study on plaque rupture, plaque erosion, and calcified nodule in patients with st-segment elevation myocardial infarction: incidence, morphologic characteristics, and outcomes after percutaneous coronary intervention. *JACC Cardiovasc Interv*. (2015) 8:1166–76. doi: 10.1016/j.jcin.2015.02.026

20. Kröner ES, van Velzen JE, Boogers MJ, Siebelink HM, Schali J, Kroft LJ, et al. Positive remodeling on coronary computed tomography as a marker for plaque vulnerability on virtual histology intravascular ultrasound. *Am J Cardiol.* (2011) 107:1725–9. doi: 10.1016/j.amjcard.2011.02.337
21. Ehara S, Kobayashi Y, Yoshiyama M, Shimada K, Shimada Y, Fukuda D, et al. Spotty calcification typifies the culprit plaque in patients with acute myocardial infarction: an intravascular ultrasound study. *Circulation.* (2004) 110:3424–9. doi: 10.1161/01.CIR.0000148131.41425.E9
22. Motoyama S, Kondo T, Sarai M, Sugiura A, Harigaya H, Sato T, et al. Multislice computed tomographic characteristics of coronary lesions in acute coronary syndromes. *J Am Coll Cardiol.* (2007) 50:319–26. doi: 10.1016/j.jacc.2007.03.044
23. Wolf D, Ley K. Immunity and inflammation in atherosclerosis. *Circ Res.* (2019) 124:315–27. doi: 10.1161/CIRCRESAHA.118.313591
24. Grootaert MOJ, Schrijvers DM, Van Spaendonck H, Breynaert A, Hermans N, Van Hoof VO, et al. NecroX-7 reduces necrotic core formation in atherosclerotic plaques of ApoE knockout mice. *Atherosclerosis.* (2016) 252:166–74. doi: 10.1016/j.atherosclerosis.2016.06.045
25. Otsuka F, Yasuda S, Noguchi T, Ishibashi-Ueda H. Pathology of coronary atherosclerosis and thrombosis. *Cardiovasc Diagn Ther.* (2016) 6:396–408. doi: 10.21037/cdt.2016.06.01
26. Nasu K, Tsuchikane E, Katoh O, Vince DG, Virmani R, Sarmely JF, et al. Accuracy of *in vivo* coronary plaque morphology assessment: a validation study of *in vivo* virtual histology compared with *in vitro* histopathology. *J Am Coll Cardiol.* (2006) 47:2405–12. doi: 10.1016/j.jacc.2006.02.044
27. Pu J, Mintz GS, Brilakis ES, Banerjee S, Abdel-Karim AR, Maini B, et al. In vivo characterization of coronary plaques: novel findings from comparing greyscale and virtual histology intravascular ultrasound and near-infrared spectroscopy. *Eur Heart J.* (2012) 33:372–83. doi: 10.1093/eurheartj/ehs387
28. Pu J, Mintz GS, Biro S, Lee JB, Sum ST, Madden SP, et al. Insights into echo-attenuated plaques, echolucent plaques, and plaques with spotty calcification: novel findings from comparisons among intravascular ultrasound, near-infrared spectroscopy, and pathological histology in 2,294 human coronary artery segments. *J Am Coll Cardiol.* (2014) 63:2220–33. doi: 10.1016/j.jacc.2014.02.576
29. Ding S, Xu L, Yang F, Kong L, Zhao Y, Gao L, et al. Association between tissue characteristics of coronary plaque and distal embolization after coronary intervention in acute coronary syndrome patients: insights from a meta-analysis of virtual histology-intravascular ultrasound studies. *PLoS ONE.* (2014) 9:e106583. doi: 10.1371/journal.pone.0106583
30. Shi X, Gao J, Lv Q, Cai H, Wang F, Ye R, et al. Calcification in atherosclerotic plaque vulnerability: friend or foe? *Front Physiol.* (2020) 11:56. doi: 10.3389/fphys.2020.00056
31. Ono Y, Yoshino O, Hiraoka T, Akiyama I, Sato E, Ito M, et al. IL-33 exacerbates endometriotic lesions via polarizing peritoneal macrophages to M2 subtype. *Reprod Sci.* (2020) 27:869–76. doi: 10.1007/s43032-019-00090-9
32. Shioi A, Ikari Y. Plaque calcification during atherosclerosis progression and regression. *J Atheroscler Thromb.* (2018) 25:294–303. doi: 10.5551/jat.RV17020
33. Willems S, Quax PH, de Borst GJ, de Vries JP, Moll FL, de Kleijn DP, et al. Soluble ST2 levels are not associated with secondary cardiovascular events and vulnerable plaque phenotype in patients with carotid artery stenosis. *Atherosclerosis.* (2013) 231:48–53. doi: 10.1016/j.atherosclerosis.2013.08.024
34. Kohli P, Bonaca MP, Kakkar R, Kudanova AY, Scirica BM, Sabatine MS, et al. Role of ST2 in non-ST-elevation acute coronary syndrome in the MERLIN-TIMI 36 trial. *Clin Chem.* (2012) 58:257–66. doi: 10.1373/clinchem.2011.173369
35. Xia S, Zhang X, Zheng S, Khanabadi R, Kalionis B, Wu J, et al. An update on inflamm-aging: mechanisms, prevention, and treatment. *J Immunol Res.* (2016) 2016:8426874. doi: 10.1155/2016/8426874
36. Rea IM, Gibson DS, McGilligan V, McNerlan SE, Alexander HD, Ross OA. Age and age-related diseases: role of inflammation triggers and cytokines. *Front Immunol.* (2018) 9:586. doi: 10.3389/fimmu.2018.00586
37. Huang Y, Hu C, Ye H, Luo R, Fu X, Li X, et al. Inflamm-aging: a new mechanism affecting premature ovarian insufficiency. *J Immunol Res.* (2019) 2019:8069898. doi: 10.1155/2019/8069898
38. Ding S, Lin N, Sheng X, Zhao Y, Su Y, Xu L, et al. Melatonin stabilizes rupture-prone vulnerable plaques via regulating macrophage polarization in a nuclear circadian receptor ROR α -dependent manner. *J Pineal Res.* (2019) 67:e12581. doi: 10.1111/jpi.12581

Conflict of Interest: The authors declare that the research was conducted in the absence of any commercial or financial relationships that could be construed as a potential conflict of interest.

Copyright © 2021 Luo, Qian, Sheng, Sun, Wu, Liao, Feng, Yin, Ding and Pu. This is an open-access article distributed under the terms of the Creative Commons Attribution License (CC BY). The use, distribution or reproduction in other forums is permitted, provided the original author(s) and the copyright owner(s) are credited and that the original publication in this journal is cited, in accordance with accepted academic practice. No use, distribution or reproduction is permitted which does not comply with these terms.



A Novel Computed Tomography-Based Imaging Approach for Etiology Evaluation in Patients With Acute Coronary Syndrome and Non-obstructive Coronary Angiography

OPEN ACCESS

Edited by:

Zhao Wang,
University of Electronic Science and
Technology of China, China

Reviewed by:

Long Jiang Zhang,
Nanjing General Hospital of Nanjing
Military Command, China
Yining Wang,
Chinese Academy of Medical
Sciences and Peking Union Medical
College, China

*Correspondence:

Yuehua Li
driyuehua@126.com
Jiayin Zhang
andrewssmu@msn.com

[†]These authors have contributed
equally to this work

Specialty section:

This article was submitted to
Cardiovascular Imaging,
a section of the journal
Frontiers in Cardiovascular Medicine

Received: 02 July 2021

Accepted: 04 August 2021

Published: 24 August 2021

Citation:

Ling R, Yu L, Lu Z, Li Y and Zhang J
(2021) A Novel Computed
Tomography-Based Imaging
Approach for Etiology Evaluation in
Patients With Acute Coronary
Syndrome and Non-obstructive
Coronary Angiography.
Front. Cardiovasc. Med. 8:735118.
doi: 10.3389/fcvm.2021.735118

Runjianya Ling^{1†}, Lihua Yu^{1†}, Zhigang Lu², Yuehua Li^{1*} and Jiayin Zhang^{3*}

¹ Institute of Diagnostic and Interventional Radiology, Shanghai Jiao Tong University Affiliated Sixth People's Hospital, Shanghai, China, ² Department of Cardiology, Shanghai Jiao Tong University Affiliated Sixth People's Hospital, Shanghai, China, ³ Department of Radiology, Shanghai General Hospital, Shanghai Jiao Tong University School of Medicine, Shanghai, China

Objective: This study sought to investigate the diagnostic value of dynamic CT myocardial perfusion imaging (CT-MPI) combined with coronary CT angiography (CCTA) in acute coronary syndrome (ACS) patients without obstructive coronary angiography.

Methods: Consecutive ACS patients with normal or non-obstructive coronary angiography findings who had cardiac magnetic resonance (CMR) contraindications or inability to cooperate with CMR examinations were prospectively enrolled and referred for dynamic CT-MPI + CCTA + late iodine enhancement (LIE). ACS etiology was determined according to combined assessment of coronary vasculature by CCTA, quantified myocardial blood flow (MBF) and presence of LIE.

Results: Twenty two patients were included in the final analysis. CCTA revealed two cases of side branch occlusion and one case of intramural hematoma which were overlooked by invasive angiography. High risk plaques were observed in 6 (27.3%) patients whereas myocardial ischemia was presented in 19 (86.4%) patients with varied extent and severity. LIE was positive in 13 (59.1%) patients and microvascular obstruction was presented in three cases with side branch occlusion or spontaneous intramural hematoma. The specific etiology was identified in 20 (90.9%) patients, of which the most common cause was cardiomyopathies (41%), followed by microvascular dysfunction (14%) and plaque disruption (14%).

Conclusion: Dynamic CT-MPI + CCTA was able to reveal the potential etiologies in majority of patients with ACS and non-obstructive coronary angiography. It may be a useful alternative to CMR for accurate etiology evaluation.

Keywords: acute coronary syndrome, coronary, computed tomography angiography, myocardial perfusion imaging, late iodine enhancement

INTRODUCTION

Acute coronary syndrome (ACS) is one of the leading causes of morbidity and mortality worldwide (1). The concept of ACS usually includes ST-elevation myocardial infarction (STEMI), non-ST-elevation myocardial infarction (NSTEMI) and unstable angina (2). Although the major etiology of ACS lies in acute vessel obstruction secondary to plaque rupture, non-obstructive invasive coronary angiography (ICA) can also be seen in approximately 6% of acute myocardial infarction (AMI) patients (3, 4).

High-sensitivity cardiac troponin I (hs-cTnI) is the most sensitive biomarker for denoting the presence of ACS (5). However, elevation of hs-cTnI can be observed in different clinical scenarios other than AMI caused by coronary artery obstruction. Myocardial infarction with non-obstructive coronary arteries (MINOCA), myocarditis, Takotsubo syndrome and cardiomyopathies may also contribute to acute chest pain, elevated level of hs-cTnI, and similar electrocardiogram change (6).

The management of patients with ACS and non-obstructive coronary arteries depends on the evaluation of underlying etiology, in which cardiac magnetic resonance (CMR) plays an important role for precise diagnosis (7, 8). However, CMR has contraindications, such as claustrophobia and pacemaker implantation. The long acquisition duration and need for strict breath holding further impairs the feasibility of CMR in ACS patients, in whom the image quality is usually suboptimal. Besides, despite of the superiority of myocardial tissue characterization, CMR is unable to visualize the coronary vessel wall anatomy and plaque features which might also provide valuable information for ACS etiology (9, 10).

Dynamic CT myocardial perfusion imaging (CT-MPI) combined with coronary CT angiography (CCTA) has been introduced as a fast one-stop approach for functional and anatomical imaging of coronary artery disease (CAD) (11, 12). Its diagnostic performance for hemodynamic assessment has been validated against invasive fractional flow reserve (FFR) according to previous studies (13, 14). In addition, the clinical application of dynamic CT-MPI + CCTA in AMI patients has also been investigated with reference to CMR (15, 16). Those preliminary studies show promising results in terms of detection of myocardial infarction and microvascular obstruction (MVO) by this CT-based method. Therefore, we hypothesized that dynamic CT-MPI + CCTA might be helpful for etiology evaluation in ACS patients with patent coronary arteries. The aim of the current study was to investigate the diagnostic value of dynamic CT-MPI + CCTA in ACS patients without obstructive coronaries.

MATERIALS AND METHODS

Patient Population

The hospital ethic committee approved this prospective study and all patients gave informed consents. Between March 1st, 2019 and December 31st, 2020, consecutive ACS patients with normal or non-obstructive coronary angiography findings were screened

and those who had CMR contraindications or inability to cooperate with CMR examinations were prospectively enrolled. The exclusion criteria were: (1) patients with previous history of coronary revascularization; (2) patients with previous history of myocardial infarction; (3) image quality of dynamic CT-MPI or CCTA was significantly impaired.

The ACS was diagnosed if: (1) patients had acute onset of chest pain; and (2) elevated level of hs-cTnI (>99th percentile of the upper reference level); and (3) excluded other extra-cardiac causes of elevated troponin. Normal or non-obstructive coronary angiography was defined as that invasive coronary angiography (ICA) revealed absence of $\geq 50\%$ stenosis of any epicardial vessel. Subsequently, all patients underwent dynamic CT-MPI + CCTA within 7-days interval after ICA.

Dynamic CT-MPI + CCTA Acquisition

A third-generation dual source CT (SOMATOM Force, Siemens Healthineers) was used for image acquisition. An integrated protocol, which incorporated calcium score, dynamic CT-MPI, CCTA and late iodine enhancement (LIE), was employed (online **Supplement Figure 1**). In brief, coronary Agatston calcium score (CACS) was firstly performed to calculate the calcification burden of each epicardial vessels. Intravenous infusion of adenosine triphosphate (ATP) at $160 \mu\text{g/kg/min}$ was then administrated for 3 min before the triggering of dynamic CT-MPI acquisition. Dynamic CT-MPI was acquired using a shuttle mode technique and started 4 s after the begin of contrast injection. Dynamic acquisition was set at the end-systolic phase (triggered at 250 ms after the R wave in all patients) and scans were launched every second or third heart cycle according to patients' heart rate. CARE kV and CARE dose 4D was used to reduce radiation dose. The reference tube voltage and effective current was 80 kVp and 300 mAs respectively.

Nitroglycerin was given sublingually in all subjects 5 min after dynamic CT-MPI. Prospective ECG-triggered sequential acquisition was performed in all participants for CCTA. 5~7 min after CCTA (17, 18), LIE was acquired using targeted spatial frequency filtration averaging technique (17). The detailed parameters of contrast medium injection, dynamic CT-MPI, CCTA and LIE acquisition were given in online **Appendix**.

Image Analysis of CCTA

All CCTA was reconstructed with a smooth kernel (Bv 40) and third generation iterative reconstruction technique (strength 3, ADMIRE, Siemens Healthineers, Germany). Dataset with best image quality from all available phases were transferred to a commercially available workstation (SyngoVia VB 2.0, Siemens Healthineers, Germany) for further analysis. Conventional qualitative and quantitative plaque parameters were evaluated for all lesions on major epicardial arteries (diameter ≥ 2 mm) using a dedicated plaque analysis software (Coronary Plaque Analysis, version 4.3, Siemens Healthineers, Germany). The following indices were measured and recorded: (1) Diameter stenosis (DS); (2) remodeling index and the presence of positive remodeling (PR) (19); (3) low-attenuation plaque (LAP) (20); (4) spotty calcification (SC) (20); (5) Napkin-ring sign (NRS) as defined by previous study (19). The detailed definitions of the above

parameters were given in online **Appendix**. Lesions with at least two HRP features (PR, LAP, SC and NRS) were deemed high-risk plaques (21). The stenosis severity of individuals was evaluated according to Coronary Artery Disease–Reporting and Data System (CAD-RADS) (21).

All CCTA data was independently analyzed by two cardiovascular radiologists (with 12-year and 4-year experience of cardiac imaging) and any disagreement was resolved by consensus.

Image Analysis of CT-MPI and LIE

Dataset of dynamic CT-MPI was reconstructed with a dedicated kernel (Qr36) for reduction of iodine beam-hardening artifacts. A commercially available CT-MPI software package (Myocardial perfusion analysis, VPCT body, Siemens Healthineers, Forchheim, Germany) was used for further analysis. Motion correction was manually applied if breathing-related mis-registration of the left ventricle was present. The quantification of myocardial blood flow (MBF) was performed using a hybrid deconvolution model, as previously reported (22).

For measurement of absolute MBF, region of interest (ROI) was manually placed on short axis view on a segment base according to the 17-segment model with exclusion of apical segment (23). The segment-based MBF was manually measured with ROI covering the whole myocardial segment (with exclusion of endocardial and epicardial interface). According to the previous studies, MBF < 100 mL/min/100 mL was considered the presence of myocardial ischemia (13, 14).

The dataset of LIE was reconstructed with a dedicated kernel (Qr36) for reduction of iodine beam-hardening artifacts. The four image stacks were averaged to one final image stack using non-rigid registration processed with a volume software (Syngo CT Dynamic Angio, Siemens Healthineers, Germany) in order to reduce image noise. Further multiplanar reformation reconstruction using this fused image stack was made to acquire short axis view of left ventricle, with image thickness and interval of 3 mm. The presence of LIE was defined as focal enhancement with left ventricle myocardium by visual analysis. The LIE patterns were classified into subendocardial, subepicardial, intramural, and diffuse according to the involved areas. Microvascular obstruction (MVO) was defined as the non-enhancing area surrounded by myocardium with LIE (24).

All CT-MPI data was independently analyzed by two cardiovascular radiologists (with 12-year and 4-year experience of cardiac imaging) and any disagreement was resolved by consensus.

Statistical Analysis

A commercially available software (SPSS Statistics 25, IBM Corp., Armonk, New York) was used for statistical analysis. One-sample Shapiro-Wilk test was used to check the assumption of normal distribution. One-sample *t*-test was used for normally distributed data while Mann-Whitney U test was used for non-normally distributed data. Data for continuous variables were presented as mean ± SD, whereas those with non-normal distribution were presented as median and quartiles. Categorical variables are presented as frequencies and percentages.

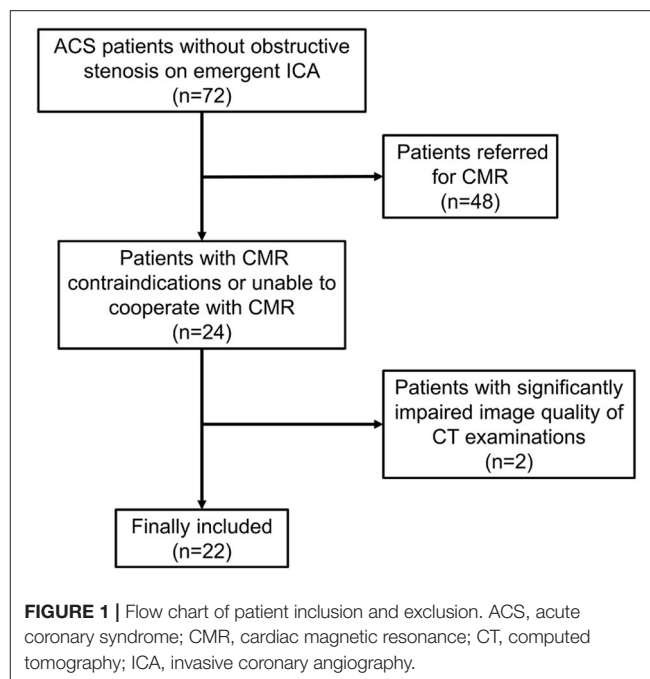


TABLE 1 | Clinical characteristics.

Characteristics	Overall
Patients (n)	22 (100 %)
Males (n)	13 (59.1 %)
Age (year)	59.50 ± 13.28
Risk factors (n)	
Current smoker	9 (40.9 %)
Hypertension	17 (77.3 %)
Diabetes mellitus	9 (40.9 %)
Dyslipidemia	3 (15.0 %)
CT Radiation dose (mSv)	6.48 ± 2.60
CKMB elevation (n)	8 (38.1 %)
CT contrast medium usage (ml)	94.73 ± 3.98
ECG change (n)	
ST-segment elevation	6 (28.6 %)
ST-segment depression	8 (38.1 %)
Non ST-segment change	7 (33.3 %)
hs-cTnI (ug/L)	
Onset value	1.07 ± 1.75
Highest value	5.87 ± 9.23

Values are mean ± SD, or n (%).

CKMB, creatine kinase isoenzyme-MB; ECG, electrocardiogram; hs-cTnI, high-sensitivity cardiac troponin I (normal range 0.00–0.03 ug/L).

RESULTS

Patient Characteristics

Between March 1st, 2019 and December 31st, 2020, 72 consecutive ACS patients were diagnosed as normal or non-obstructive stenosis on emergent ICA. Among them, 24 patients with CMR contraindications or unable to cooperate with CMR

TABLE 2 | Imaging findings of dynamic CT-MPI + CCTA.

	Overall	Cardiomyopathies	Acute myocarditis	Ischemic					Unclassified
				Vascular occlusion	Spontaneous intramural hematoma	CMD	Plaque disruption	MB	
Patients (n)	22 (100 %)	9 (40.9 %)	1 (4.5 %)	2 (9.1 %)	1 (4.5 %)	3 (13.6 %)	3 (13.6 %)	1 (4.5 %)	2 (9.1 %)
CT-MPI									
Myocardial ischemia (n)	19 (86.4 %)	9 (100 %)	0 (0 %)	2 (100 %)	1 (100 %)	3 (100 %)	3 (100 %)	1 (100 %)	0 (0 %)
Ischemic segments (n)	4.00 (2.75 - 6.00)	4.00 (2.50 - 10.50)	0	3.50 (2.25 - 3.00)	4	5.00 (3.00 - 5.00)	6.00 (4.00 - 6.00)	4	0
Mean MBF of ischemic segment (ml/100ml/min)	70.74 ± 10.02	74.44 ± 6.75	0	47.00 ± 4.24	63	74.17 ± 2.93	75.33 ± 2.31	72	0
LIE (n)									
Enhancement	13 (59.1 %)	5 (55.6 %)	1 (100 %)	2 (100 %)	1 (100 %)	0 (0 %)	3 (100 %)	1 (100 %)	0 (0 %)
Within vessel territory	7 (31.8 %)	0 (0 %)	0 (0 %)	2 (100 %)	1 (100 %)	0 (0 %)	3 (100 %)	1 (100 %)	0 (0 %)
MVO	3 (13.6 %)	0 (0 %)	0 (0 %)	2 (100 %)	1 (100 %)	0 (0 %)	0 (0 %)	0 (0 %)	0 (0 %)
Type (n)									
Subendocardial	1 (4.5 %)	0 (0 %)	0 (0 %)	0 (0 %)	0 (0 %)	0 (0 %)	1 (33.3 %)	0 (0 %)	0 (0 %)
Intramural	1 (4.5 %)	1 (11.1 %)	0 (0 %)	0 (0 %)	0 (0 %)	0 (0 %)	0 (0 %)	0 (0 %)	0 (0 %)
Subepicardial	1 (4.5 %)	0 (0 %)	1 (100 %)	0 (0 %)	0 (0 %)	0 (0 %)	0 (0 %)	0 (0 %)	0 (0 %)
Diffuse	10 (45.5 %)	4 (44.4 %)	0 (0 %)	2 (100 %)	1 (100 %)	0 (0 %)	2 (66.7 %)	1 (100 %)	0 (0 %)
CCTA (n)									
CAD-RADS category									
CAD-RADS 0	2 (9.1 %)	1 (11.1 %)	1 (100 %)	0 (0 %)	0 (0 %)	0 (0 %)	0 (0 %)	0 (0 %)	0 (0 %)
CAD-RADS 1	3 (13.6 %)	1 (11.1 %)	0 (0 %)	0 (0 %)	0 (0 %)	1 (33.3 %)	0 (0 %)	0 (0 %)	1 (50 %)
CAD-RADS 2	14 (63.6 %)	7 (77.7 %)	0 (0 %)	0 (0 %)	0 (0 %)	2 (66.7 %)	3 (100 %)	1 (100 %)	1 (50 %)
CAD-RADS 3	0 (0 %)	0 (0 %)	0 (0 %)	0 (0 %)	0 (0 %)	0 (0 %)	0 (0 %)	0 (0 %)	0 (0 %)
CAD-RADS 4	1 (4.5 %)	0 (0 %)	0 (0 %)	0 (0 %)	1 (100 %)	0 (0 %)	0 (0 %)	0 (0 %)	0 (0 %)
CAD-RADS 5	2 (9.1 %)	0 (0 %)	0 (0 %)	2 (100 %)	0 (0 %)	0 (0 %)	0 (0 %)	0 (0 %)	0 (0 %)
Plaque features (n)									
LAP	3 (13.6 %)	0 (0 %)	0 (0 %)	2 (100 %)	0 (0 %)	0 (0 %)	1 (33.3 %)	0 (0 %)	0 (0 %)
PR	11 (50.0 %)	2 (22.2 %)	0 (0 %)	2 (100 %)	0 (0 %)	3 (100 %)	3 (100 %)	0 (0 %)	1 (50 %)
SC	7 (31.8 %)	2 (22.2 %)	0 (0 %)	2 (100 %)	0 (0 %)	0 (0 %)	2 (66.7 %)	1 (100 %)	0 (0 %)
NRS	2 (9.1 %)	1 (11.1 %)	0 (0 %)	0 (0 %)	0 (0 %)	0 (0 %)	1 (33.3 %)	0 (0 %)	0 (0 %)
High-risk plaques	6 (27.3 %)	1 (11.1 %)	0 (0 %)	2 (100 %)	0 (0 %)	0 (0 %)	3 (100 %)	0 (0 %)	0 (0 %)

Values are mean ± SD, n (%), or median (interquartile range).

CCTA, coronary CT angiography; CMD, coronary microvascular dysfunction; LAP, low-attenuation plaque; LIE, late iodine enhancement; MB, myocardial bridge; MBF, myocardial blood flow; MPI, myocardial perfusion imaging; MVO, microvascular obstruction; NRS, napkin-ring sign; PR, positive remodeling; SC, spotty calcification.

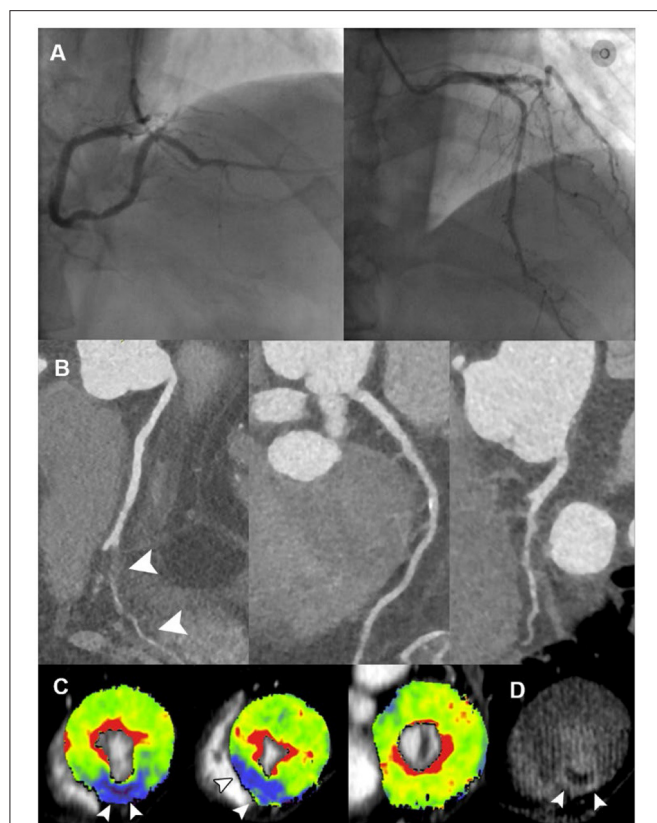


FIGURE 2 | Representative case of vessel occlusion with MVO in a 66-year-old male with ACS and non-obstructive ICA. **(A)** ICA revealed mild stenosis at middle LAD and distal RCA, without presence of obstructive lesion. **(B)** CPR images showed occlusion of PDA ostium (white arrowhead). **(C)** Short-axis views of CT-MPI showed significantly reduced myocardial blood flow within PDA territory (white arrowhead). **(D)** LIE image showed the transmural late enhancement with the presence of MVO within PDA territory (white arrowhead). ACS, acute coronary syndrome; CPR, curved planar reformation; CT, computed tomography; ICA, invasive coronary angiography; LAD, left anterior descending; LIE, late iodine enhancement; MPI, myocardial perfusion imaging; MVO, microvascular obstruction; PDA, posterior descending artery; RCA, right coronary artery.

examinations were referred for dynamic CT-MPI and CCTA. Two patients were further excluded due to significantly impaired image quality of CT examinations caused by severe motion artifact (**Figure 1**). Finally, 22 patients (mean age, 59.50 ± 13.28 years) were included in the current study, including 13 males (mean age, 62.46 ± 11.37 years) and 9 females (mean age, 55.22 ± 15.30 years). The mean radiation dose for dynamic CT-MPI + CCTA (including LIE) was 6.48 ± 2.60 mSv, using 0.014 as the conversion factor. Contrast medium induced nephropathy was not reported in the current study. Detailed demographic data were given in **Table 1**.

Imaging Findings of CCTA

Among ACS patients with normal or non-obstructive coronary angiography, CCTA findings were in line with ICA results in 86.4% (19/22) subjects. The mismatch between CCTA and ICA

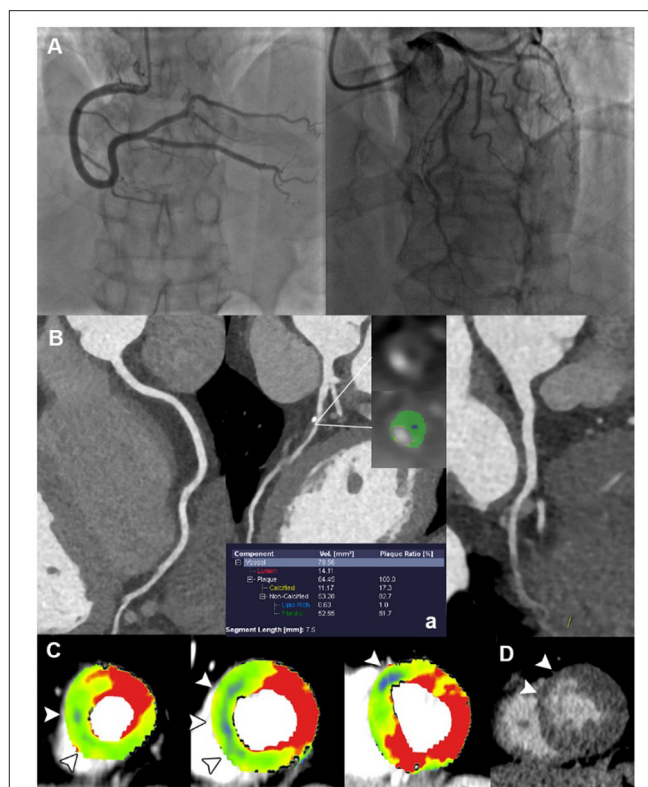


FIGURE 3 | Representative case of plaque disruption in a 61-year-old male with ACS and non-obstructive ICA. **(A)** ICA revealed mild stenosis at proximal LAD, without presence of obstructive lesion. **(B)** CPR images showed mixed plaque at proximal LAD with the presence of LAP, PR, NRS, and SC, indicating a typical HRP. **(C)** Short-axis views of CT-MPI showed significantly reduced myocardial blood flow within LAD territory (white arrowhead). **(D)** LIE image showed the subendocardial late enhancement within LAD territory (white arrowhead). ACS, acute coronary syndrome; CPR, curved planar reformation; CT, computed tomography; ICA, invasive coronary angiography; LAD, left anterior descending; LAP, low-attenuation plaque; LIE, late iodine enhancement; MPI, myocardial perfusion imaging; MVO, microvascular obstruction; NRS, napkin-ring sign; PR, positive remodeling; SC, spotty calcification.

was due to the overlook of side branch occlusion in two cases and side branch spontaneous intramural hematoma in one case by ICA (**Table 2**).

Overall, CCTA revealed normal coronary arteries (CAD-RADS 0) in 2 (9.1 %) patients, non-obstructive stenosis (CAD-RADS 1-2) in 17 (77.3 %) patients, and obstructive stenosis (CAD-RADS 3-5) in 3 (13.6 %) patients (**Table 2**). In terms of HRP features, PR and SC were commonly presented in the current population whereas HRP was observed in 6 (27.3%) patients (**Table 2**).

Imaging Findings of Dynamic CT-MPI

Myocardial ischemia was presented in 19 (86.4 %) patients with varied extent and severity. Lowest MBF was observed in the cases with overlooked side branch occlusion, followed by the case with spontaneous intramural hematoma (**Table 2**).

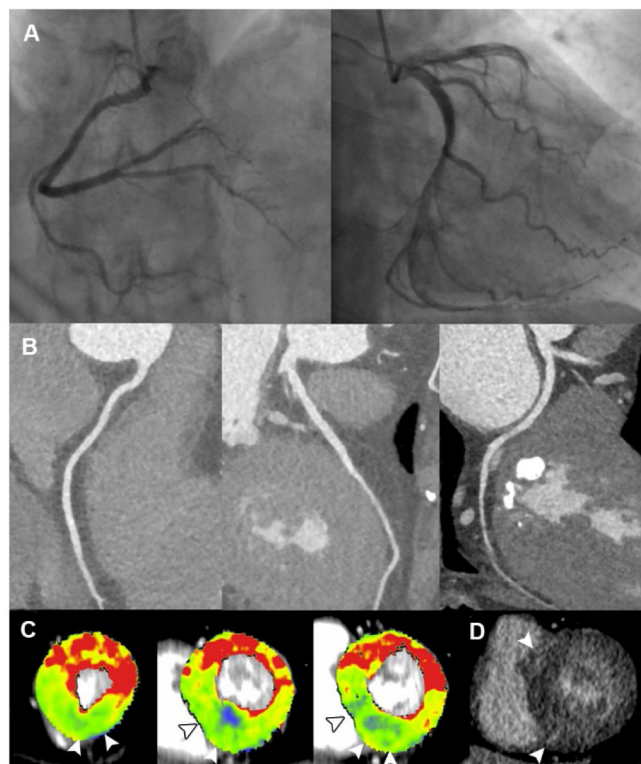


FIGURE 4 | Representative case of cardiomyopathy in a 60-year-old female with ACS and non-obstructive ICA. **(A,B)** ICA and CCTA revealed normal coronary vasculature. **(C)** Short-axis views of CT-MPI showed significantly reduced myocardial blood flow at apical inferior, mid septal, mid inferior, basal septal as well as basal inferior segments, with focal myocardial hypertrophy (white arrowhead). **(D)** LIE image showed the focal intra-mural late enhancement at RV insertion points (white arrowhead). The above findings were consistent with the diagnosis of hypertrophic cardiomyopathy. ACS, acute coronary syndrome; CCTA, coronary computed tomography angiography; CT, computed tomography; ICA, invasive coronary angiography; LAD, left anterior descending; LAP, low-attenuation plaque; LIE, late iodine enhancement; MPI, myocardial perfusion imaging; MVO, microvascular obstruction; RV, right ventricle.

In addition, LIE was positive in 13 (59.1 %) patients and diffuse LIE was the most common pattern (**Table 2**). LIE area complied with vessel-related territory in seven cases and randomly distributed in six cases. MVO was presented in three cases with side branch occlusion or spontaneous intramural hematoma.

Etiology of ACS According to Dynamic CT-MPI + CCTA

The underlying etiologies of ACS were subsequently classified into ischemic, cardiomyopathies, acute myocarditis and unclassified, according to the imaging findings of dynamic CT-MPI + CCTA (**Table 2**).

The specific ischemic causes of ACS could be further divided into vessel occlusion (defined as presence of side branch occlusion, reduced MBF and positive LIE within vessel territory, **Figure 2**), spontaneous intramural hematoma (defined as long segment of continuous filling defect within lumen, reduced MBF and positive LIE within vessel territory), plaque disruption (defined as presence of HRP features, non-obstructive stenosis, reduced MBF and positive LIE within vessel territory) (**Figure 3**), microvascular dysfunction (defined as reduced MBF

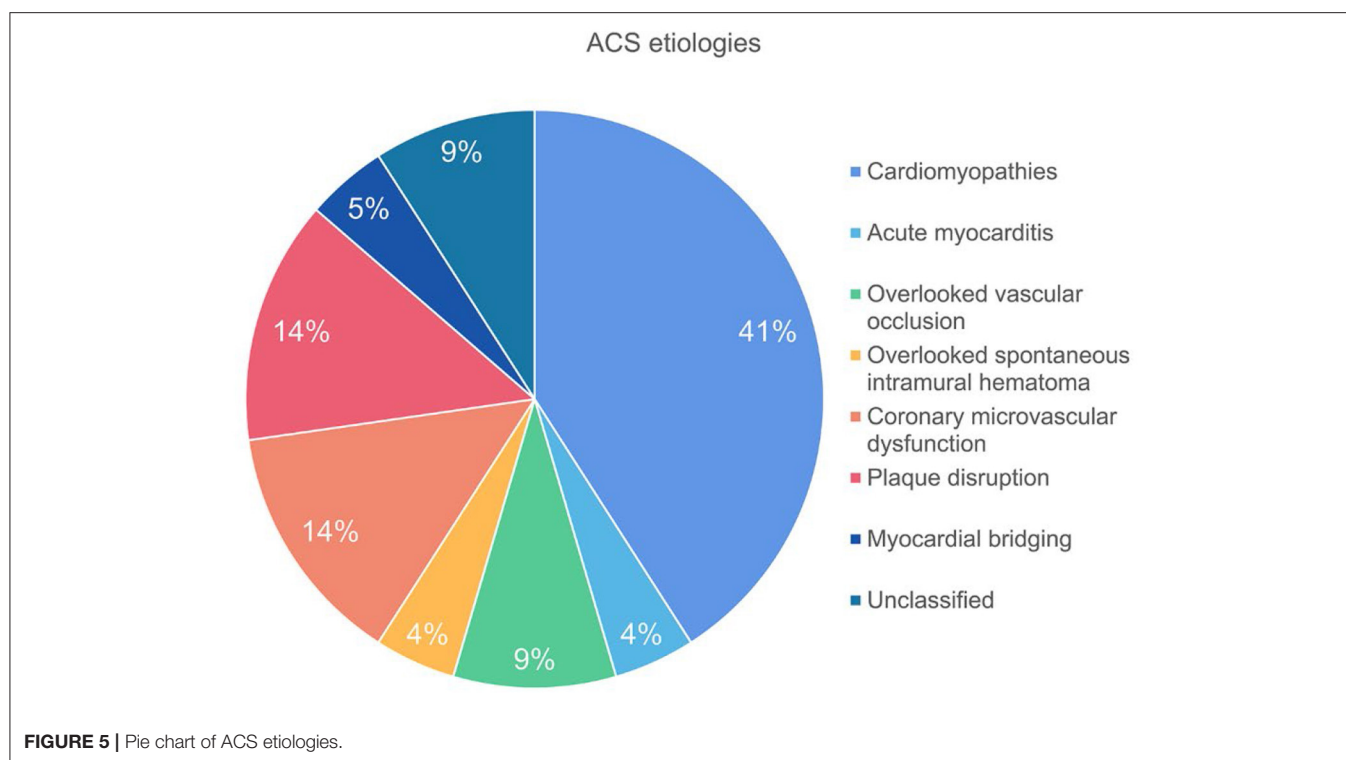
with random distribution and absence of LIE), and myocardial bridging (defined as reduced MBF and positive LIE within myocardial bridging territory). Other causes of ACS included cardiomyopathies (absence of obstructive stenosis, presence of hypertrophic or dilated left ventricle, with or without myocardial ischemia/LIE) (**Figure 4**) and acute myocarditis (absence of epicardial stenosis, normal myocardial perfusion, and presence of typical subepicardial LIE).

Finally, there were two cases diagnosed as “unclassified” due to the absence of imaging evidence of myocardial ischemia or injury. Thus, the specific etiology was identified in 20 (90.9 %) patients by dynamic CT-MPI + CCTA (**Figure 5**).

DISCUSSION

The major finding of the present study showed that dynamic CT-MPI + CCTA was able to uncover the underlying etiologies in majority of patients with ACS and non-obstructive coronary angiography.

Normal or non-obstructive ICA is not an uncommon finding in AMI patients (3, 4) and the specific etiologies in this cohort consist of not only coronary causes (epicardial causes,



including plaque disruption and coronary artery dissection, microvascular causes, such as microvascular dysfunction and coronary artery spasm), but also Takotsubo syndrome, acute myocarditis, and cardiomyopathies (7, 25). Identification of the underlying etiology in those subjects is of paramount importance because the clinical management and prognosis strongly depend on the precise diagnosis. According to a scientific statement from the American Heart Association regarding diagnosis and management of MINOCA, CMR is recommended as a key investigation in the diagnostic work-up because it can exclude myocarditis, takotsubo syndrome, and cardiomyopathies, as well as provide imaging confirmation of AMI (6). According to one recent study, CMR combined with optical coherence tomography (OCT) was able to identify potential mechanisms in 84.5% of women with a diagnosis of MINOCA (26). However, CMR and OCT are still not widely available imaging approaches and ACS patients might not be able to cooperate with the long acquisition time of CMR. Thus, developing an alternative imaging modality with the ability of assessing myocardial injury and potential etiology would be clinically beneficial.

The current study for the first time investigated the clinical value of dynamic CT-MPI + CCTA in the diagnostic workflow of ACS without obstructive coronary angiography. Thanks to the technical advantages of this “one-stop shop” imaging modality, this CT-based approach allows simultaneous assessment of coronary vasculature, myocardial perfusion, and myocardial injury as well. As one core part of the CT protocol, dynamic CT-MPI is able to accurately quantify MBF and diagnose myocardial ischemia (13, 14). LIE has also been proven to represent a useful alternative to late gadolinium enhancement to detect myocardial scar (27). Moreover, CCTA provides

comprehensive evaluation of coronary anatomy, including overlooked side branch occlusion, intramural hematoma, and HRP features of suspected culprit lesions. Although it is not a direct imaging method for diagnosis of plaque disruption, CCTA has been validated for identification of thin-cap fibroatheroma with reference to intravascular ultrasound (28). It complements dynamic CT-MPI for exploration of potential epicardial etiologies when myocardial injury is presented. With the help of the above comprehensive assessment, dynamic CT-MPI + CCTA was able to identify the specific etiology of ACS without obstructive ICA in 90.9% patients in the current cohort, which was similar to one previous CMR + OCT study (26).

In light of the above findings, the clinical role of dynamic CT-MPI + CCTA lies in the following aspects for ACS evaluation. First, this CT-based approach provides a useful alternative to CMR for etiology assessment in ACS patients without obstructive coronary angiography. Unlike CMR, which requires longer acquisition time and has more contraindications, dynamic CT-MPI + CCTA offers a faster way for functional and anatomical evaluation. Although dynamic CT-MPI + CCTA is currently unable to visualize myocardial edema, it is still a valuable complement in cases with CMR contraindications for etiology investigation. ACS patients without obstructive ICA may benefit from this CT-based method owing to specific etiology identification and precise treatment accordingly. Moreover, thanks to the technical development, the radiation exposure of CT-MPI + CCTA decreases significantly, from 13.1 to 6.3 mSv (13, 29). In the current study using third-generation dual source CT, the overall radiation dose of whole CT protocol (including LIE) was 6.48 mSv, which was reasonable and acceptable in clinical practice.

Despite the above promising results, the current study has several limitations. First, CMR and OCT validation were not available in the present study to confirm the diagnosis by dynamic CT-MPI + CCTA. Thus, the diagnostic accuracy of CT-based etiology evaluation could not be assessed. In addition, the overall sample size was small in this preliminary study with limited case number of different etiologies, which made inter-group analysis unavailable. The prognostic value of CT imaging was also unclear. Future studies with larger sample size are warranted to investigate the clinical impact of CT-based approach on guiding proper management and prognosis improvement. Finally, due to technical limitation, it is of note that dynamic CT-MPI + CCTA was unable to evaluate several pathological features, such as myocardial edema, systolic function of left ventricle, coronary emboli and coronary spasm. Therefore, some MINOCA etiologies, such as Takotsubo Syndrome, coronary thrombus and coronary spasm, cannot be assessed using this approach. Other imaging methods should be employed when these causes are suspected.

In conclusion, dynamic CT-MPI + CCTA was able to reveal the potential etiologies in majority of patients with ACS and non-obstructive coronary angiography. It may be an useful alternative to CMR for accurate etiology evaluation.

DATA AVAILABILITY STATEMENT

The raw data supporting the conclusions of this article will be made available by the authors, without undue reservation.

REFERENCES

- Eisen A, Giugliano RP, Braunwald E. Updates on acute coronary syndrome: a review. *JAMA Cardiol.* (2016) 1:718–30. doi: 10.1001/jamacardio.2016.2049
- Thygesen K, Alpert JS, Jaffe AS, Chaitman BR, Bax JJ, Morrow DA, et al. Fourth universal definition of myocardial infarction (2018). *J Am Coll Cardiol.* (2018) 72:2231–64. doi: 10.1016/j.jacc.2018.08.1038
- Smilowitz NR, Mahajan AM, Roe MT, Hellkamp AS, Chiswell K, Gulati M, et al. Mortality of myocardial infarction by sex, age, and obstructive coronary artery disease status in the ACTION registry-GWTG (Acute Coronary Treatment and Intervention Outcomes Network Registry-Get With the Guidelines). *Circ Cardiovasc Qual Outcomes.* (2017) 10:e003443. doi: 10.1161/CIRCOUTCOMES.116.003443
- Pasupathy S, Air T, Dreyer RP, Tavella R, Beltrame JF. Systematic review of patients presenting with suspected myocardial infarction and nonobstructive coronary arteries. *Circulation.* (2015) 131:861–70. doi: 10.1161/CIRCULATIONAHA.114.011201
- Agewall S, Giannitsis E, Jernberg T, Katus H. Troponin elevation in coronary vs. non-coronary disease. *Eur Heart J.* (2011) 32:404–11. doi: 10.1093/eurheartj/ehq456
- Tamis-Holland JE, Jneid H, Reynolds HR, Agewall S, Brilakis ES, Brown TM, et al. Contemporary diagnosis and management of patients with myocardial infarction in the absence of obstructive coronary artery disease: a scientific statement from the American heart association. *Circulation.* (2019) 139:e891–908. doi: 10.1161/CIR.0000000000000670
- Bhatia S, Anstine C, Jaffe AS, Gersh BJ, Chandrasekaran K, Foley TA, et al. Cardiac magnetic resonance in patients with elevated troponin and normal coronary angiography. *Heart.* (2019) 105:1231–6. doi: 10.1136/heartjnl-2018-314631
- Assomull RG, Lyne JC, Keenan N, Gulati A, Bunce NH, Davies SW, et al. The role of cardiovascular magnetic resonance in patients presenting with chest pain, raised troponin, and unobstructed coronary arteries. *Eur Heart J.* (2007) 28:1242–9. doi: 10.1093/eurheartj/ehm113
- Hayes SN, Kim ESH, Saw J, Adlam D, Arslanian-Engoren C, Economy KE, et al. Spontaneous coronary artery dissection: current state of the science: a scientific statement from the American Heart Association. *Circulation.* (2018) 137:e523–57. doi: 10.1161/CIR.0000000000000564
- Niccoli G, Scalzone G, Crea F. Acute myocardial infarction with no obstructive coronary atherosclerosis: mechanisms and management. *Eur Heart J.* (2015) 36:475–81. doi: 10.1093/eurheartj/ehu469
- Yu M, Shen C, Dai X, Lu Z, Wang Y, Lu B, et al. Clinical outcomes of dynamic computed tomography myocardial perfusion imaging combined with coronary computed tomography angiography versus coronary computed tomography angiography-guided strategy. *Circ Cardiovasc Imaging.* (2020) 13:e009775. doi: 10.1161/CIRCIMAGING.119.009775
- Yu L, Tao X, Dai X, Liu T, Zhang J. Dynamic CT myocardial perfusion imaging in patients without obstructive coronary artery disease: quantification of myocardial blood flow according to varied heart rate increments after stress. *Korean J Radiol.* (2021) 22:97–105. doi: 10.3348/kjr.2020.0249
- Li Y, Yu M, Dai X, Lu Z, Shen C, Wang Y, et al. Detection of hemodynamically significant coronary stenosis: ct myocardial perfusion versus machine learning ct fractional flow reserve. *Radiology.* (2019) 293:305–14. doi: 10.1148/radiol.2019190098
- Li Y, Dai X, Lu Z, Shen C, Zhang J. Diagnostic performance of quantitative, semi-quantitative, and visual analysis of dynamic CT myocardial perfusion imaging: a validation study with invasive fractional flow reserve. *Eur Radiol.* (2021) 31:525–34. doi: 10.1007/s00330-020-07145-5
- Yu M, Chen X, Dai X, Pan J, Wang Y, Lu B, et al. The value of low-dose dynamic myocardial perfusion CT for accurate evaluation of microvascular obstruction in patients with acute myocardial infarction. *AJR Am J Roentgenol.* (2019) 213:798–806. doi: 10.2214/AJR.19.21305

ETHICS STATEMENT

The studies involving human participants were reviewed and approved by Shanghai Jiaotong University Affiliated Sixth People's Hospital Ethics Committee. The patients/participants provided their written informed consent to participate in this study.

AUTHOR CONTRIBUTIONS

RL contributed to image analysis, statistical analysis, and manuscript drafting. LY contributed to image analysis and statistical analysis. ZL contributed to patient enrollment and image analysis. YL contributed to literature research and manuscript drafting. JZ contributed to study conception and design, image analysis, literature research, and manuscript drafting.

FUNDING

This study is supported by Shanghai Committee of Science and Technology (Grant No.: 21ZR1452200).

SUPPLEMENTARY MATERIAL

The Supplementary Material for this article can be found online at: <https://www.frontiersin.org/articles/10.3389/fcvm.2021.735118/full#supplementary-material>

16. Pan J, Yuan M, Yu M, Gao Y, Shen C, Wang Y, et al. Myocardial blood flow quantified by low-dose dynamic CT myocardial perfusion imaging is associated with peak troponin level and impaired left ventricle function in patients with st-elevated myocardial infarction. *Korean J Radiol.* (2019) 20:709–18. doi: 10.3348/kjr.2018.0729
17. Kurobe Y, Kitagawa K, Ito T, Kurita Y, Shiraishi Y, Nakamori S, et al. Myocardial delayed enhancement with dual-source CT: advantages of targeted spatial frequency filtration and image averaging over half-scan reconstruction. *J Cardiovasc Comput Tomogr.* (2014) 8:289–98. doi: 10.1016/j.jcct.2014.06.004
18. Ohta Y, Kitao S, Yunaga H, Fujii S, Mukai N, Yamamoto K, et al. myocardial delayed enhancement CT for the evaluation of heart failure: comparison to MRI. *Radiology.* (2018) 288:682–91. doi: 10.1148/radiol.2018172523
19. Motoyama S, Sarai M, Harigaya H, Anno H, Inoue K, Hara T, et al. Computed tomographic angiography characteristics of atherosclerotic plaques subsequently resulting in acute coronary syndrome. *J Am Coll Cardiol.* (2009) 54:49–57. doi: 10.1016/j.jacc.2009.02.068
20. Min JK, Shaw LJ, Devereux RB, Okin PM, Weinsaft JW, Russo DJ, et al. Prognostic value of multidetector coronary computed tomographic angiography for prediction of all-cause mortality. *J Am Coll Cardiol.* (2007) 50:1161–70. doi: 10.1016/j.jacc.2007.03.067
21. Cury RC, Abbara S, Achenbach S, Agatston A, Berman DS, Budoff MJ, et al. CAD-RADS™: Coronary artery disease - reporting and data system: an expert consensus document of the society of cardiovascular computed tomography (SCCT), the American College of Radiology (ACR) and the North American Society for Cardiovascular Imaging (NASCI). Endorsed by the American College of Cardiology. *J Am Coll Radiol.* (2016) 13:1458–66. doi: 10.1016/j.jacr.2016.04.024
22. Bamberg F, Klotz E, Flohr T, Becker A, Becker CR, Schmidt B, et al. Dynamic myocardial stress perfusion imaging using fast dual-source CT with alternating table positions: initial experience. *Eur Radiol.* (2010) 20:1168–73. doi: 10.1007/s00330-010-1715-9
23. Cerqueira MD, Weissman NJ, Dilsizian V, Jacobs AK, Kaul S, Laskey WK, et al. Standardized myocardial segmentation and nomenclature for tomographic imaging of the heart. A statement for healthcare professionals from the Cardiac Imaging Committee of the Council on Clinical Cardiology of the American Heart Association. *Circulation.* (2002) 105:539–42. doi: 10.1161/hc0402.102975
24. O'Sullivan JF, Leblond AL, O'Dea J, Hristova I, Kumar S, Martin K, et al. Multidetector computed tomography accurately defines infarct size, but not microvascular obstruction after myocardial infarction. *J Am Coll Cardiol.* (2013) 61:208–10. doi: 10.1016/j.jacc.2012.08.1014
25. Scalone G, Niccoli G, Crea F. Editor's Choice- Pathophysiology, diagnosis and management of MINOCA: an update. *Eur Heart J Acute Cardiovasc Care.* (2019) 8:54–62. doi: 10.1177/2048872618782414
26. Reynolds HR, Maehara A, Kwong RY, Sedlak T, Saw J, Smilowitz NR, et al. Coronary optical coherence tomography and cardiac magnetic resonance imaging to determine underlying causes of myocardial infarction with nonobstructive coronary arteries in women. *Circulation.* (2021) 143:624–40. doi: 10.1161/CIRCULATIONAHA.120.052008
27. Palmisano A, Vignale D, Benedetti G, Del Maschio A, De Cobelli F, Esposito A. Late iodine enhancement cardiac computed tomography for detection of myocardial scars: impact of experience in the clinical practice. *Radiol Med.* (2020) 125:128–36. doi: 10.1007/s11547-019-01108-7
28. Yuan M, Wu H, Li R, Yu M, Dai X, Zhang J. The value of quantified plaque analysis by dual-source coronary CT angiography to detect vulnerable plaques: a comparison study with intravascular ultrasound. *Quant Imaging Med Surg.* (2020) 10:668–77. doi: 10.21037/qims.2020.01.13
29. Bamberg F, Becker A, Schwarz F, Marcus RP, Greif M, von Ziegler F, et al. Detection of hemodynamically significant coronary artery stenosis: incremental diagnostic value of dynamic CT-based myocardial perfusion imaging. *Radiology.* (2011) 260:689–98. doi: 10.1148/radiol.11110638

Conflict of Interest: The authors declare that the research was conducted in the absence of any commercial or financial relationships that could be construed as a potential conflict of interest.

Publisher's Note: All claims expressed in this article are solely those of the authors and do not necessarily represent those of their affiliated organizations, or those of the publisher, the editors and the reviewers. Any product that may be evaluated in this article, or claim that may be made by its manufacturer, is not guaranteed or endorsed by the publisher.

Copyright © 2021 Ling, Yu, Lu, Li and Zhang. This is an open-access article distributed under the terms of the Creative Commons Attribution License (CC BY). The use, distribution or reproduction in other forums is permitted, provided the original author(s) and the copyright owner(s) are credited and that the original publication in this journal is cited, in accordance with accepted academic practice. No use, distribution or reproduction is permitted which does not comply with these terms.



Focal Geometry and Characteristics of Erosion-Prone Coronary Plaques *in vivo* Angiography and Optical Coherence Tomography Study

Muhua Cao^{1,2}, Tianyu Wu^{1,2}, Jiawei Zhao^{1,2}, Zhuo Du^{1,2}, Zhuozhong Wang^{1,2}, Lulu Li^{1,2}, Guo Wei^{1,2}, Jinwei Tian^{1,2}, Haibo Jia^{1,2}, Gary S. Mintz³ and Bo Yu^{1,2*}

¹ Department of Cardiology, The Second Affiliated Hospital of Harbin Medical University, Harbin, China, ² The Key Laboratory of Myocardial Ischemia, Chinese Ministry of Education, Harbin, China, ³ Cardiovascular Research Foundation, New York, NY, United States

OPEN ACCESS

Edited by:

Salah D. Qanadli,
University of Lausanne, Switzerland

Reviewed by:

Nicolas Amabile,
L'Institut Mutualiste
Montsouris, France
Christos Bourantas,
University College London,
United Kingdom

*Correspondence:

Bo Yu
dryu_hmu@163.com

Specialty section:

This article was submitted to
Cardiovascular Imaging,
a section of the journal
Frontiers in Cardiovascular Medicine

Received: 14 May 2021

Accepted: 11 August 2021

Published: 08 September 2021

Citation:

Cao M, Wu T, Zhao J, Du Z, Wang Z,
Li L, Wei G, Tian J, Jia H, Mintz GS
and Yu B (2021) Focal Geometry and
Characteristics of Erosion-Prone
Coronary Plaques *in vivo* Angiography
and Optical Coherence Tomography
Study.
Front. Cardiovasc. Med. 8:709480.
doi: 10.3389/fcvm.2021.709480

Objective: This study compared focal geometry and characteristics of culprit plaque erosion (PE) vs. non-culprit plaques in ST-segment elevated myocardial infarction (STEMI) patients in whom optical coherence tomography (OCT) identified PE as the cause of the acute event.

Background: Culprit PE is a distinct clinical entity with specific coronary risk factors and its own tailored management strategy. However, not all plaques develop erosion resulting in occlusive thrombus formation.

Methods: Between January 2017 and July 2019, there were 484 STEMI patients in whom OCT at the time of primary percutaneous intervention identified culprit lesion PE to be the cause of the event; 484 culprit PE were compared to 1,132 non-culprit plaques within 1,196 imaged vessels.

Results: Culprit PE were highly populated at “hot spots” within the proximal 40 mm in the left anterior descending artery (LAD) and tended to cluster proximal to a nearby bifurcation mainly in the LAD. Minimal lumen area (MLA) <2.51 mm² and AS (area stenosis) >64.02% discriminated culprit PE from non-culprit plaques. In the multivariable analysis, focal geometry (LAD location, distance from coronary ostium <40 mm, and location proximal to a nearby bifurcation), luminal narrowing (MLA <2.51 mm², AS > 64.02%), and TCFA phenotype were independent predictors of culprit PE overall. Cholesterol crystals were predictive of culprit PE with underlying LRP morphology while the absence of calcification and microchannels were risk factors for culprit PE with an underlying non-LRP. Similarities and differences in predictors of culprit PE were found between males and females; distance from coronary ostium <40 mm, MLA <2.51 mm², TCFA, and less spotty calcium were risk factors of culprit PE in males, but not in females while smaller RVD was associated with culprit PE only in females.

Conclusions: Irrespective of underlying lesion substrates and patient risk factors, there are lesion-specific and OCT-identifiable predictors of developing culprit PE in erosion-prone vulnerable patients.

Keywords: erosion-prone plaque, predictors, plaque erosion, optical coherence tomography, acute coronary syndrome

INTRODUCTION

Plaque erosion (PE) is a distinct pathological and clinical entity and the second most common cause of coronary thrombosis; it is responsible for 25–35% of acute coronary syndrome (ACS) and may have its own tailored management strategy (1). Furthermore, patients with culprit eroded plaques have a lower prevalence of rupture-related pancoronary, non-culprit lesion instability to include a lower prevalence of thin-cap fibroatheromas (TCFA), plaque ruptures, and high-risk plaques as defined in the CLIMA study (NCT02883088), regardless of systemic risk factor profiles (2).

Features of PE include detachment of the endothelium and platelet activation and aggregation. Flow disturbances appear first leading to chronic and persistent endothelial activation and injury (3). However, not all plaques in an erosion-prone vulnerable patient develop into erosions resulting in occlusive thrombus formation, suggesting that certain plaques may be at increased risk by virtue of their particular plaque features and focal geometry.

While there is ample evidence for risk factor predictors of an erosion-prone vulnerable patient (4–7), there is a scarcity of *in vivo* data regarding lesion-specific predictors for erosion-prone plaques within an erosion-prone vulnerable patient. Therefore, the present study compared plaque characteristics and focal geometry of culprit PE vs. non-culprit plaques in a large series of ST-segment elevation myocardial infarction (STEMI) patients in whom optical coherence tomography (OCT) identified plaque erosions as the cause of the acute event.

MATERIALS AND METHODS

Study Population

Between January 2017 and July 2019, 2,136 patients (≥ 18 years of age) presenting with STEMI were treated emergently with OCT imaging in the Cardiovascular Hospital of the 2nd Affiliated Hospital of Harbin Medical University (Harbin, China). Criteria for the diagnosis of STEMI have been described previously (8). Patients with OCT imaging of the culprit vessel after predilation ($n = 28$), who presented with in-stent restenosis or thrombosis ($n = 66$), or with suboptimal image quality or very short analyzable segment ($n = 81$) or incomplete demographic or clinical or imaging data ($n = 30$) were excluded. After excluding STEMIs caused by culprit plaque rupture, calcified nodule, and other culprit plaque phenotypes, 484 STEMI patients in whom the acute event was caused by culprit PE as identified by OCT imaging were included in the present study (Supplementary Figure 1).

Manual thrombectomy was performed in the setting of initial of thrombolysis in myocardial infarction (TIMI) flow grade ≤ 1 or extensive thrombus. OCT of the culprit artery was performed before percutaneous coronary intervention (PCI) while OCT of the non-culprit arteries was performed after the culprit lesion was treated. Accordingly, 1,132 non-culprit plaques were identified within 1,196 imaged vessels (single-, double-, and triple-vessel OCT imaging in 71, 114, and 299, respectively). Criteria for traditional risk factors have been included in the

Supplementary Materials. The present study complied with the Declaration of Helsinki and was approved by the Ethics Committee of the 2nd Affiliated Hospital of Harbin Medical University, and all patients provided written informed consent.

Coronary Angiography Analysis

Quantitative coronary angiography (QCA) analysis was performed using Cardiovascular Angiography Analysis System (CAAS, 5.10, Pie Medical Imaging B.V., Maastricht, The Netherlands). Coronary flow was assessed with the TIMI flow grade classification. QCA parameters including the reference vessel diameter (RVD), minimal lumen diameter (MLD), diameter stenosis (DS), and lesion length were measured post-thrombectomy from end-diastolic frames and calibration using the catheter tip (9). The distance from culprit or non-culprit lesions to the respective coronary ostium was measured in a non-foreshortened view (9). Lesions assessed angiographically were matched to OCT using fiducial sidebranches.

OCT Image Acquisition and Analysis

OCT imaging was acquired with a commercially available C7-XR or ILUMIEN OPTIS or OPTIS Integrated System (Abbott Vascular, Santa Clara, CA, USA) (2, 10, 11). As noted above, pre-intervention OCT of the culprit lesion was performed before and OCT imaging of non-culprits was performed after treatment of the infarct lesion. In case of long vessel segments, imaging was performed using multiple pullbacks that were then “stitched” together and overlapped to assess the entire vessel. OCT was performed in the mid or distal segments in most studied vessels (88.2% of left anterior descending artery [LAD]; 84.7% of right coronary artery [RCA] and 64.4% of left circumflex artery [LCX]). The total length of analyzed OCT pullbacks was 206.3 ± 35.5 mm (70.8 ± 25.5 in the LAD; 84.1 ± 19.1 in the RCA and 45.8 ± 15.5 in the LCX) (Supplementary Table 1).

All OCT images were submitted for core laboratory analyses that were carried out by two independent investigators (M.C. and T.W.) who were blinded to clinical, angiographic, and laboratory data using an offline review workstation (Abbott Vascular) (2, 10, 11). Any discordance was resolved by consensus with a third reviewer (Z.D.). Quantitative and qualitative analyses of all lesions were performed as previously described and as presented in the **Supplementary Material** (2, 8, 11, 12). Culprit lesions were identified based on angiographic findings, ECG changes, and/or left ventricular wall motion abnormalities (8). All plaques were identified by OCT as segments with a loss of the normal three-layered structure of the vessel wall. At least three consecutive 1 mm cross-sections with these features were necessary to define a plaque (2, 11, 12). A distance of at least 5 mm on the longitudinal view was necessary to consider two plaques as separate (12).

Based on established OCT diagnostic criteria, PE was identified by the presence of attached thrombus overlying an intact and visualized plaque, luminal surface irregularity at the culprit lesion in the absence of thrombus, or attenuation of the underlying plaque by thrombus without superficial lipid or calcification immediately proximal or distal to the site

of thrombus (**Supplementary Figure 2**) (8). Excellent intra-observer and inter-observer agreement was observed in the identification of culprit PE (κ , 0.93 and 0.89, respectively).

Quantitative analysis was performed at 1 mm intervals on cross-sectional OCT images. Proximal and distal references were the sites with the largest lumen area proximal and distal to the lesion, but within the same segment; and a mean reference lumen area was calculated. Minimal lumen area (MLA) was the smallest lumen area within the length of the lesion. For culprit PE and non-culprit plaque with thrombus, MLA was estimated excluding the thrombus and was used to determine luminal percent stenosis of the pre-thrombotic plaque [$100 \times (1 - \text{MLA}/\text{mean of reference areas})$]. The method for tracing lumen area and MLA has been presented in **Supplementary Figure 3**. For lesions without thrombus, percent area stenosis was calculated as [$100 \times (1 - \text{MLA}/\text{mean of reference areas})$]. Minimal flow area (MFA) was the smallest flow area within the length of the lesion (13). Percent area stenosis (AS) was calculated as $(([\text{Mean Reference Lumen Area} - \text{MLA}]/\text{Mean Reference Lumen Area}) \times 100)$.

The distance from each lesion to a nearby bifurcation was determined from the pre-thrombotic MLA site to the bifurcation (**Supplementary Figure 3**). “Nearby bifurcation” was a sidebranch (with an orifice diameter >1.0 mm measured by OCT) within 5 mm proximal or distal to the lesion (4).

Statistical Methods

Data distribution was assessed according to the Kolmogorov-Smirnov test. Continuous variables were expressed as mean \pm standard deviation or median (interquartile range), and compared using the independent samples Student's test or Mann-Whitney U test. Categorical data were presented as counts (proportions) and were compared using the Chi-square or Fisher's exact test. Receiver-operating characteristic (ROC) analysis and calculation of sensitivity and specificity were performed to test the ability of MLA and AS to differentiate culprit PE from non-culprit plaques. Comparisons of per-lesion data were performed using the generalized estimating equations (GEE) to take into account potential clustering of multiple plaques in a single patient. Predictors of culprit PE were analyzed by the multi-variable logistic regression model with GEE. Variables tested included location in the LAD, distance from coronary ostium <40 mm, location proximal to a nearby bifurcation, MLA <2.51 mm², AS $>64.02\%$, RVD, lipid rich plaque (LRP), TCFA, cholesterol crystals, macrophages, calcification, spotty calcium, and microchannels. Variables that showed $P < 0.10$ in the univariate model were entered into the multivariate model. Intra-observer and inter-observer differences were quantified using the κ coefficient of agreement for the culprit plaque identification. A two-sided $P < 0.05$ was considered statistically significant. Statistical analyses were performed using SPSS version 23.0 (IBM Corp, Armonk, NY).

RESULTS

Patient Characteristics

Baseline characteristics and laboratory findings of STEMI patients with culprit PE have been shown in **Table 1**.

TABLE 1 | Baseline characteristics and laboratory findings of STEMI patients with culprit plaque erosion.

Variables	Patients with culprit PE (n = 484)
Male	364 (75.2)
Age (years)	55.2 \pm 11.6
Age <50 years	165 (34.1)
Risk factors	
Diabetes mellitus	82 (16.9)
Dyslipidemia	243/462 (52.6)
Current smoker	281 (58.1)
Hypertension	203 (41.9)
CKD	42/483 (8.7)
Laboratory data	
TC (mg/dL)	178.1 \pm 40.6
Triglyceride (mg/dL)	118.3 (83.4–179.1)
LDL-C (mg/dL)	108.9 \pm 32.5
HDL-C (mg/dL)	50.1 \pm 12.2
TC/HDL ratio	3.7 \pm 1.2
HbA1c (%)	5.7 (5.4–6.1)
hs-CRP (mg/L)	4.5 (2.1–10.6)
Hemoglobin (g/L)	148.2 \pm 20.0
Previous history	
Previous MI	5 (1.0)
Previous PCI	1 (0.2)

Values shown are n (%), mean \pm SD, or median (25th–75th percentiles). CKD, chronic kidney disease; HDL-C, high-density lipoprotein cholesterol; hs-CRP, high-sensitive C-reactive protein; LDL-C, low-density lipoprotein cholesterol; MI, myocardial infarction; PCI, percutaneous coronary intervention; PE, plaque erosion; STEMI, ST-segment elevation myocardial infarction; TC, total cholesterol.

Angiographic Findings

QCA results including RVD, MLD, DS, and lesion length comparing culprit PE to non-culprit plaques have been presented in **Table 2**. Culprit PE were longer and had more severe diameter stenosis than non-culprit plaques.

OCT Findings

OCT findings comparing culprit PE to non-culprit plaques have been shown in **Table 2**. Culprit PE had smaller MLA and MFA and were longer than non-culprit plaques. Compared with non-culprit plaques, there were more TCFA (26.0% vs. 11.9%, $p < 0.001$) in culprit PE. Although LRPs were observed in both groups (53.5% of culprit PE and 37.9% of non-culprit plaques), LRPs underlying culprit PE had a larger mean and maximum lipid arc as well as a larger lipid index and more TCFA compared to non-culprit plaques. Other underlying plaque characteristics—including cholesterol crystals, macrophages and microchannels—were comparable between the two groups. While there was no difference in frequency of calcification or spotty calcium comparing culprit PE to non-culprit plaques, when present, calcium appeared to be more extensive in culprit PE than in non-culprit plaques.

TABLE 2 | QCA and OCT analysis of culprit and non-culprit plaques in patients with culprit plaque erosion.

Variables	Culprit PE (n = 484)	Non-culprit plaque (n = 1,132)	P-value
QCA analysis			
RVD (mm)	3.02 ± 0.63	2.92 ± 0.66	0.519
MLD (mm)	1.13 ± 0.43	1.70 ± 1.21	<0.001
DS (%)	63.4 (54.5–70.6)	42.0 (35.1–50.0)	<0.001
Lesion length (mm)	13.8 (10.4–18.0)	9.7 (7.4–13.3)	<0.001
OCT analysis			
Lesion length (mm)	19.9 ± 5.9	14.6 ± 6.0	<0.001
Proximal reference lumen area (mm ²)	8.7 ± 3.4	8.3 ± 3.3	0.682
Distal reference lumen area (mm ²)	7.1 ± 3.3	7.4 ± 3.3	0.238
MLA (mm ²)	2.2 ± 1.4	3.8 ± 2.0	<0.001
MFA (mm ²)	1.6 ± 1.2	3.8 ± 2.1	<0.001
AS (%)	72.0 ± 13.7	53.2 ± 14.2	<0.001
Lipid rich plaques			
Thinnest FCT (μm)	70.7 ± 32.7	84.8 ± 37.9	0.054
Mean lipid arc (°)	213.5 ± 61.5	163.3 ± 47.2	<0.001
Maximum lipid arc (°)	285.3 ± 80.9	205.4 ± 72.6	<0.001
Lipid core length (mm)	5.5 (3.2–8.5)	3.6 (2.0–6.1)	0.240
Lipid index	1105.2 (612.8–1812.1)	587.0 (281.5–1016.3)	0.008
TCFA	126 (26.0)	135 (11.9)	<0.001
Cholesterol crystal	169 (34.9)	189 (16.7)	0.055
Macrophage	302 (62.4)	608 (53.7)	0.124
Microchannel	97 (20.0)	312 (27.6)	0.512
Spotty calcium	110 (22.7)	276 (24.4)	0.103
Calcification	185 (38.2)	409 (36.1)	0.216
Calcification length	3.9 (2.1–7.9)	3.4 (1.7–6.4)	0.005
Mean calcification arc	77.1 ± 31.9	67.4 ± 33.0	0.004
Max calcification arc	109.3 (73.2–164.0)	88.6 (58.2–124.9)	<0.001
Calcification index	292.0 (122.0–614.9)	209.1 (91.2–447.0)	<0.001
Thrombus	436 (90.1)	49 (4.3)	<0.001
White	389 (89.2)	43 (87.8)	0.755
Red	47 (10.8)	6 (12.2)	

Values shown are n (%), mean ± SD, or median (25th–75th percentiles). AS, Area stenosis; DS, diameter stenosis; FCT, fibrous-cap thickness; MFA, minimal flow area; MLA, minimal lumen area; MLD, minimal lumen diameter; OCT, optical coherence tomography; PE, plaque erosion; QCA, quantitative coronary angiography analysis; RVD, reference vessel diameter; TCFA, thin-cap fibroatheroma.

Plaque Distribution

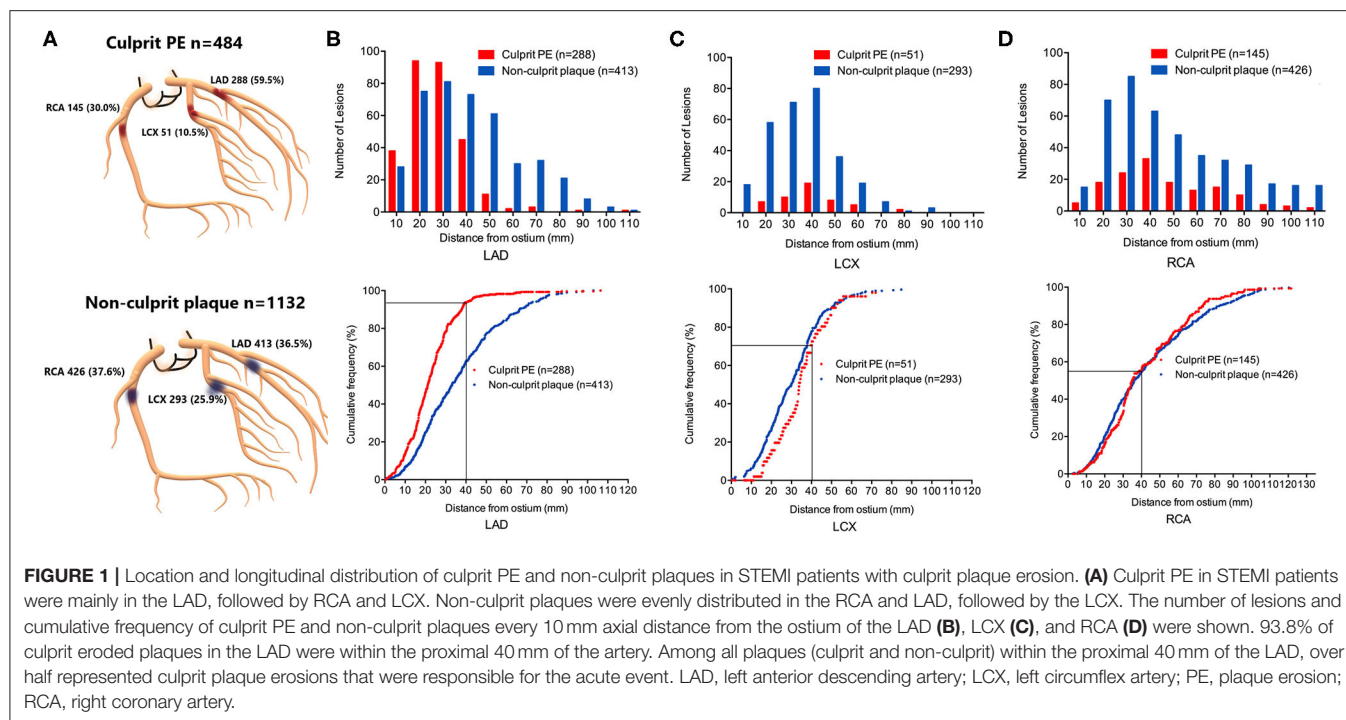
As shown in **Figure 1**, culprit PE was preferentially located in the LAD (288 of 484, 59.5%), followed by the RCA (145 of 484, 30.0%); they were least common in the LCX (51 of 484, 10.5%). Non-culprit plaques in the 484 patients with culprit PE were relatively evenly distributed in the RCA (426 of 1,132, 37.6%), LAD (413 of 1,132, 36.5%), and LCX (293 of 1,132, 25.9%) (**Figure 1A**).

Longitudinal mapping of both culprit PE and non-culprit plaques has been shown in **Figures 1B–D**. There was a gradient in the absolute number of culprit PE and non-culprit plaques from proximal to distal coronary segments mainly in the LAD and LCX while they were more evenly distributed in the RCA. Especially in the LAD, there was a strong proximal clustering of culprit PE compared with non-culprit plaques. Among all 527 culprit and non-culprit plaques within 40 mm of the LAD ostium,

more than half (270 of 527, 51.2%) were a culprit PE that was responsible for the acute event.

The cumulative frequency distribution curves demonstrated that 93.8% (270 of 288) of culprit PE in the LAD were within 40 mm of the LAD ostium (**Figure 1B**), 70.6% of culprit PE in the LCX were within 40 mm of the LCX ostium (**Figure 1C**), and 55.2% of culprit PE in the RCA were within 40 mm of the RCA ostium (**Figure 1D**).

Overall, 60.5% (293 of 484) culprit PE and 59.5% (673 of 1,132) non-culprit plaques were located near a bifurcation (**Figure 2A**). Among them, culprit PE showed a significant tendency to cluster proximal to a nearby bifurcation (proximal vs. distal: 61.1% vs. 37.5%, $p < 0.001$) while the trend was completely opposite in non-culprit plaques (proximal vs. distal: 25.0% vs. 68.8%, $p < 0.001$) (**Figure 2B**). This was especially true in the LAD where 70.3% of culprit PE were near a bifurcation, but it was



less common in the RCA (19.5%) or LCX (10.2%). In contrast, non-culprit plaques were near a bifurcation in 41.8% of LAD, 31.5% of RCA, and 26.7% of LCX (Figure 2B). Culprit PE that were located proximally were within 2.5 (1.6–3.6) mm from the nearby bifurcation while non-culprit PE that were located distally were within 1.7 (0.5–2.9) (Figure 2C).

Predictors of Culprit PE (vs. Non-culprit Plaques)

The inferred pre-thrombotic MLA was smaller and AS was more severe in culprit PE than in non-culprit plaques (Table 2). According to the ROC analysis, the optimal cut-off values of MLA $<2.51 \text{ mm}^2$ [area under the curve (AUC) = 0.766] and AS $>64.02\%$ (AUC = 0.833) could distinguish culprit PE from non-culprit plaques with a sensitivity of 76.4 and 77.7%, a specificity of 69.6 and 76.5%, a positive predictive value of 51.8 and 58.6%, a negative predictive value of 87.4 and 88.9%, and a diagnostic accuracy of 71.7 and 76.9% (Figures 3A–D).

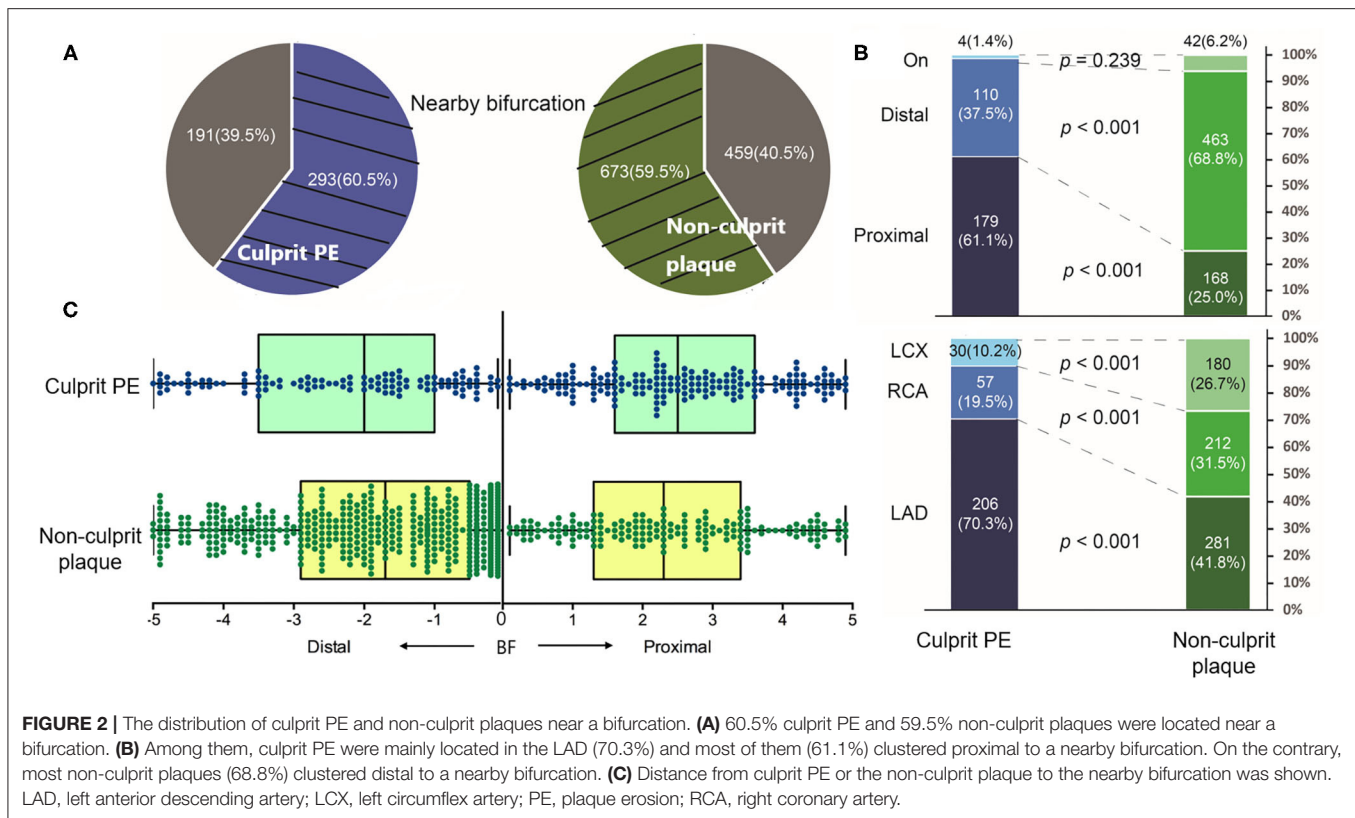
In the multivariable analysis, location in the LAD, distance from ostium $<40 \text{ mm}$, proximal to a nearby bifurcation, MLA $<2.51 \text{ mm}^2$, AS $>64.02\%$, and presence of TCFA were significantly associated with culprit PE (Figure 4, Supplementary Table 2). Subgroup analyses of different underlying phenotypes showed that location in the LAD, distance from ostium $<40 \text{ mm}$, proximal to a nearby bifurcation, MLA $<2.51 \text{ mm}^2$, and AS $>64.02\%$ were predictive of culprit PE, regardless of underlying plaque phenotype (LRPs or non-LRPs). TCFA and presence of cholesterol crystals were significantly associated with culprit PE in the subgroup with underlying LRP morphology while less calcification and microchannels were significantly associated

with culprit PE in the subgroup of non-LRPs (Figure 4, Supplementary Tables 3, 4).

In an exploratory analysis the predictors of culprit PE in male and female were then investigated (Figure 5, Supplementary Tables 5, 6). Location in the LAD, proximal to a nearby bifurcation, and AS $>64.02\%$ were common predictors for culprit PE, regardless of sex. Distance from coronary ostium $<40 \text{ mm}$, MLA $<2.51 \text{ mm}^2$, TCFA, and less spotty calcium were risk factors of culprit PE in males, but not in females. Smaller RVD was associated with culprit PE only in females. No co-linearity was found between MLA and AS, MLA $<2.51 \text{ mm}^2$ and AS $>64.02\%$ in overall plaques and subgroup of LRPs vs. non-LRPs and males vs. females.

DISCUSSION

This is the first study investigating characteristics and predictors of erosion-prone plaques in a comprehensive map of culprit and non-culprit sites in STEMI patients in whom the acute event was caused by culprit PE. The main findings were as follows. (1) Culprit PE were highly populated at “hot spots” within the proximal 40 mm of the LAD. (2) Culprit PE tended to develop proximal to a nearby bifurcation, especially in the LAD. (3) MLA $<2.51 \text{ mm}^2$ and AS $>64.02\%$ were the optimal cut-off values of luminal stenosis to discriminate culprit eroded plaques from non-eroded, non-culprit plaques. (4) Similarities and differences in predictors of culprit PE were found between different plaque phenotypes and between males and females.



Location and Spatial Distribution of Plaque Erosion

Like other high-risk plaques (ruptures and TCFAs) (14–16) and acute coronary occlusions (9), we found non-uniform PE distribution with proximal clustering (within 40 mm of the coronary ostium) in the LAD (93.8%) and LCX (70.6%). Notably, the present study confirmed and extended the results of our prior OCT studies (2, 4), verifying the presence of specific “hot spots” for culprit PE (within the proximal 40 mm of the LAD) where culprit PE accounted for more than half of all (culprit and non-culprit) plaques. Moreover, LAD location and distance from coronary ostium <40 mm were strong predictors of culprit PE.

The etiology for the LAD predominance and proximal clustering still remains unclear. Although the LAD and LCX taper more than the RCA, vessel size seems not to be a good explanation for proximal clustering because RVD was not significantly associated with culprit PE. Compared with other arterial segments, the proximal LAD has multiple sidebranches leading to marked variations in blood instability and shear stress. Furthermore, there is lower endothelial shear stress (ESS) in the proximal compared to the distal segment of the left coronary artery (17).

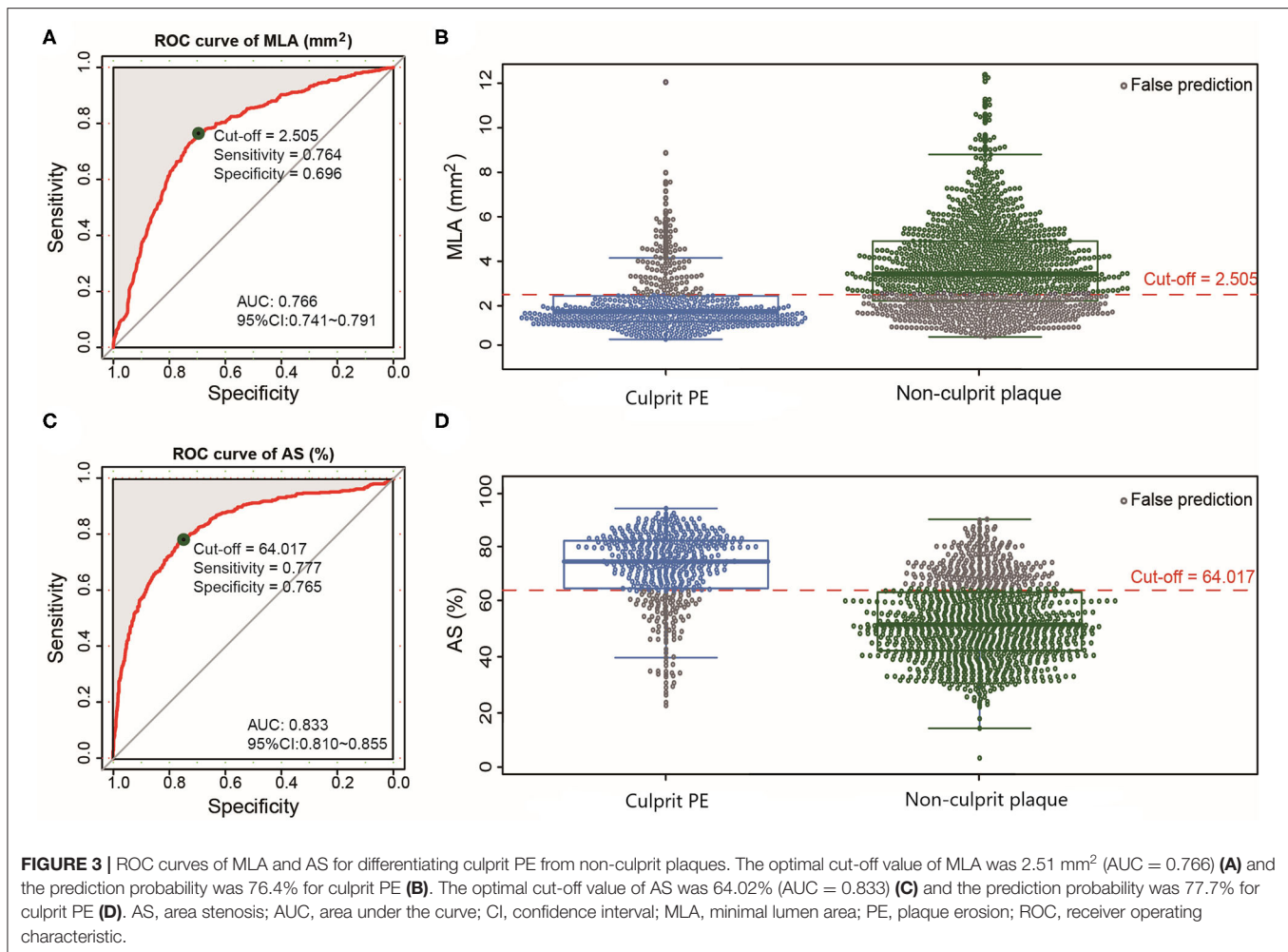
Nearby Bifurcation and Plaque Erosion

In the present study culprit PE tended to cluster proximal to a nearby bifurcation, a sharply distinct distribution pattern compared with non-culprit plaques. The magnitude of wall shear stress (WSS) and OSI around a bifurcation is very variable as

proved using computational fluid dynamics simulations (18). Disturbed flow and oscillatory WSS can influence the site of atherosclerotic plaque formation and development of culprit PE. Low ESS has been associated with lipid, and high ESS has been correlated with the site of acute erosion and thrombosis (19). Moreover, reduced ability to repair wounds of endothelial cells near sidebranches compared with non-branch regions might also facilitate culprit PE formation (20).

Luminal Narrowing and Plaque Erosion

Although OCT imaging cannot evaluate the extent of plaque burden due to its limited imaging depth, culprit PE presented with a higher degree of pre-existing luminal narrowing compared with non-culprit plaques. Although we do not really know the precise culprit PE luminal narrowing before thrombus formation, MLA and AS (excluding thrombus) were measured in the current study in order to approach the pre-thrombus culprit PE luminal narrowing as much as possible. The best cut-off values of MLA (<2.51 mm²) and AS (>64.02%) were found to be common and strong predictors of culprit PE, regardless of the underlying substrates. These results suggested that pre-existing severe lumen narrowing was still important for an erosion-prone plaque to turn into a culprit PE at geometrically predisposed areas. Whether erosion-prone plaques experience a rapid step-wise progression (21) at the onset of the acute coronary event remains unclear. Meanwhile, distinct level of ESS, ESS gradient (ESSG), and OSI have been found in upstream and downstream to the MLA at the location of eroded plaques and thrombus



(22); and the degree of luminal narrowing could further influence composition of thrombus (23) and healing in eroded plaques (24). Future prospective imaging studies and computational fluid dynamics studies are needed to establish association among dynamic luminal narrowing, shear stress, and clinical events caused by culprit erosion.

Predictors of Culprit PE

Besides luminal narrowing and focal geometry, the presence of TCFA remained one risk factor for culprit PE overall and in the subgroup with underlying LRP. Different from TCFA as a precursor for plaque rupture, TCFA in PE might merely represent greater lipid accumulation and not be pathophysiologically linked; there was more lipid, but comparable thinnest FCT. As a heterogeneous entity, underlying LRPs accounted for about half of culprit PE (2). Notably, cholesterol crystals were found to be independent predictors of culprit PE in the subgroup of LRPs. Cholesterol crystals are mainly taken up by macrophages and exert effects on different cell types such as neutrophils and endothelial and smooth muscle cells (25). Through stimulating neutrophil extracellular traps releasing

and activation of the complement system, cholesterol crystals could facilitate thrombosis (25). Because the role of cholesterol crystals has been mainly elucidated in plaque rupture, the exact physiological mechanisms of cholesterol crystals in PE remains unknown. Nevertheless, our results suggested that erosion-prone vulnerable patients might still benefit from statin therapy.

In the subgroup of non-LRPs (fibrous and fibrocalcific plaques), the absence of calcification and microchannels was a risk factor for culprit PE. The pattern and extent of calcification tended to differ sharply according to plaque phenotype (26). In line with our findings, previous pathological studies have reported less histological calcification in erosions and maximum calcification in fibrocalcific plaques compared with other phenotypes (26). On one hand, calcification has been strongly associated with adverse outcomes and represents increased risk of coronary artery disease (26, 27). On the other hand, in an erosion-prone vulnerable patient, calcification seemed to represent a lower risk for a plaque turning into a culprit PE. Microchannels or neoangiogenesis at non-culprit regions has been identified as potential predictors of angiographic plaque progression and multiple plaque ruptures through leak of

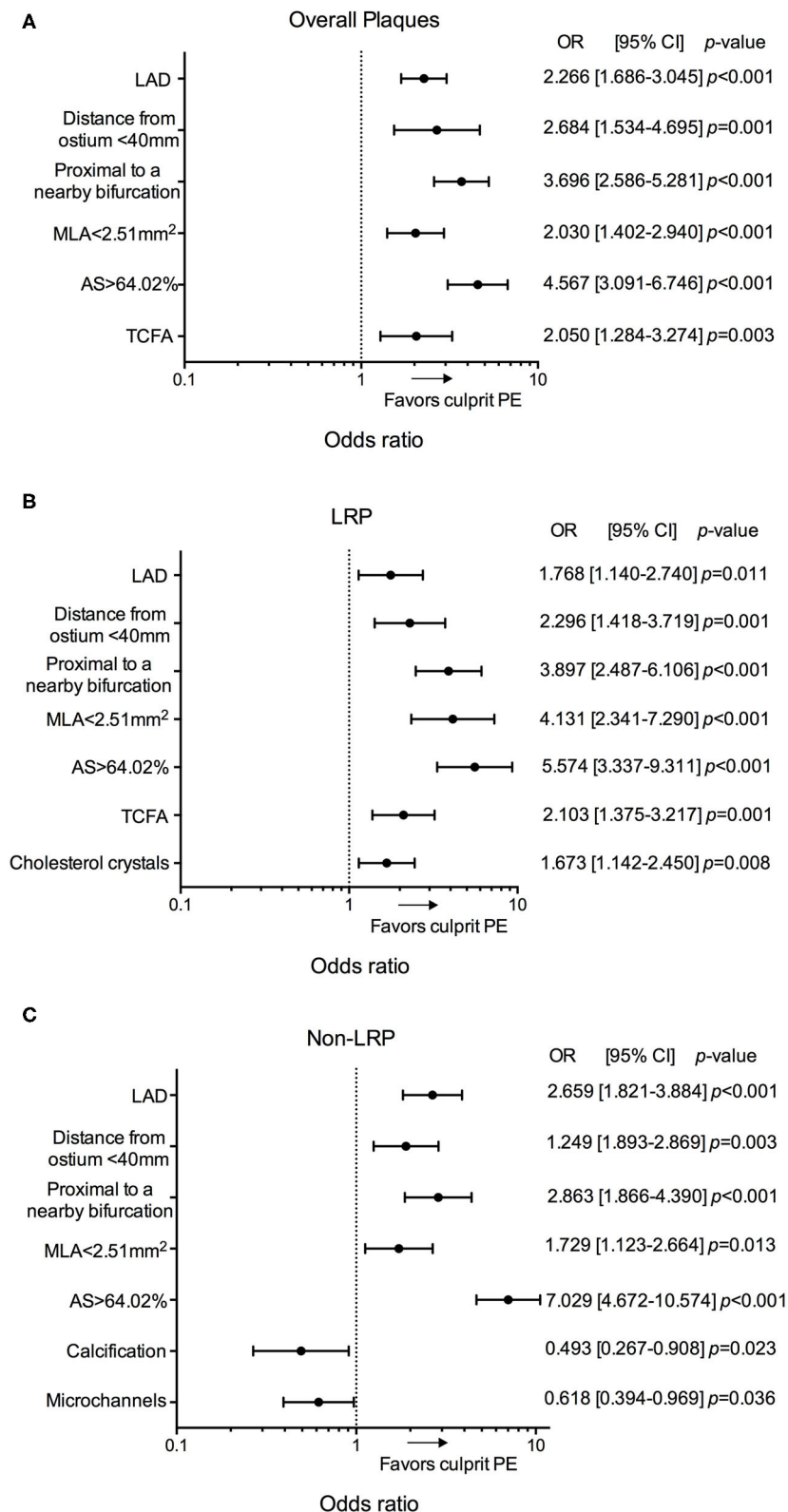
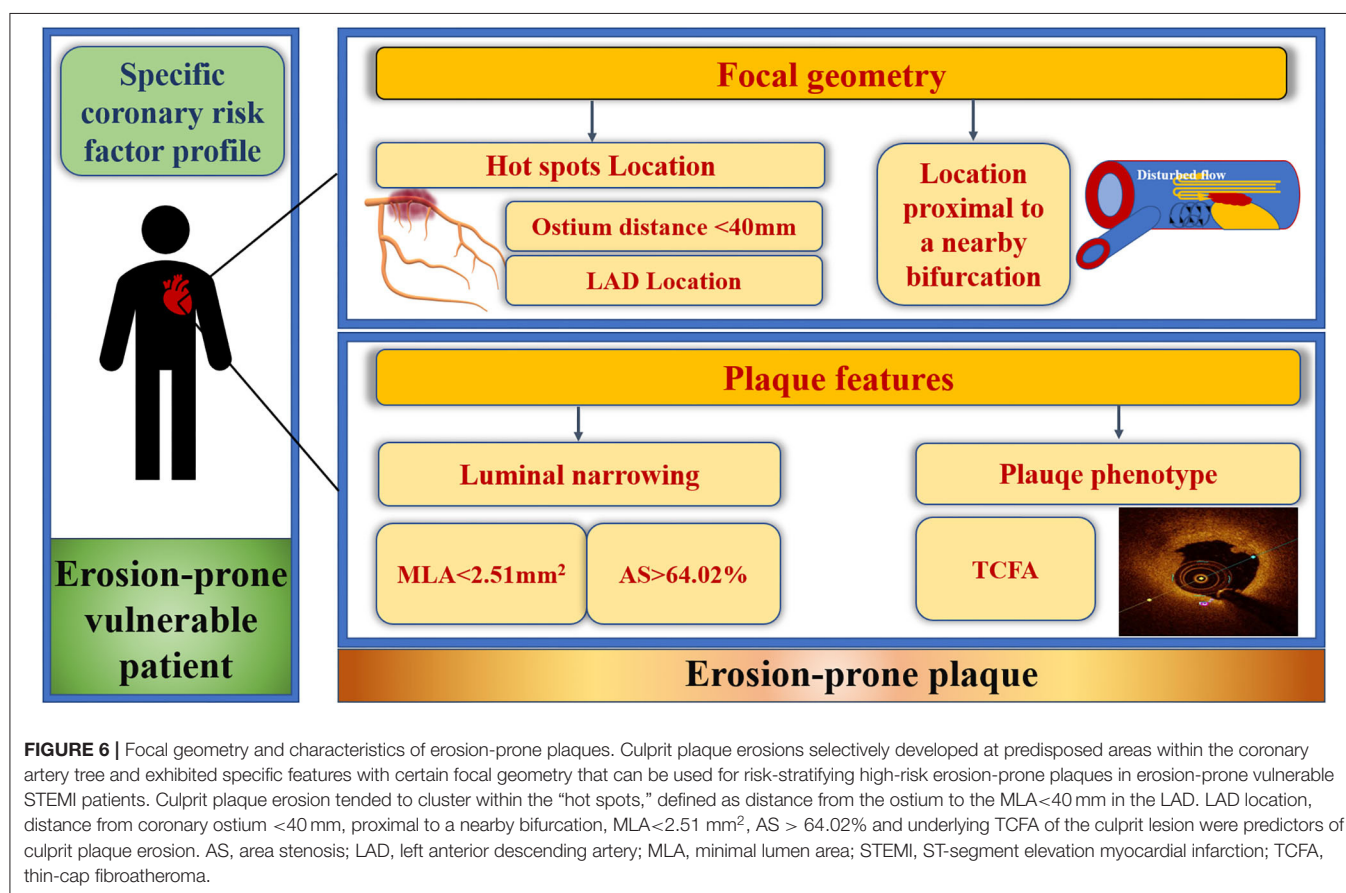
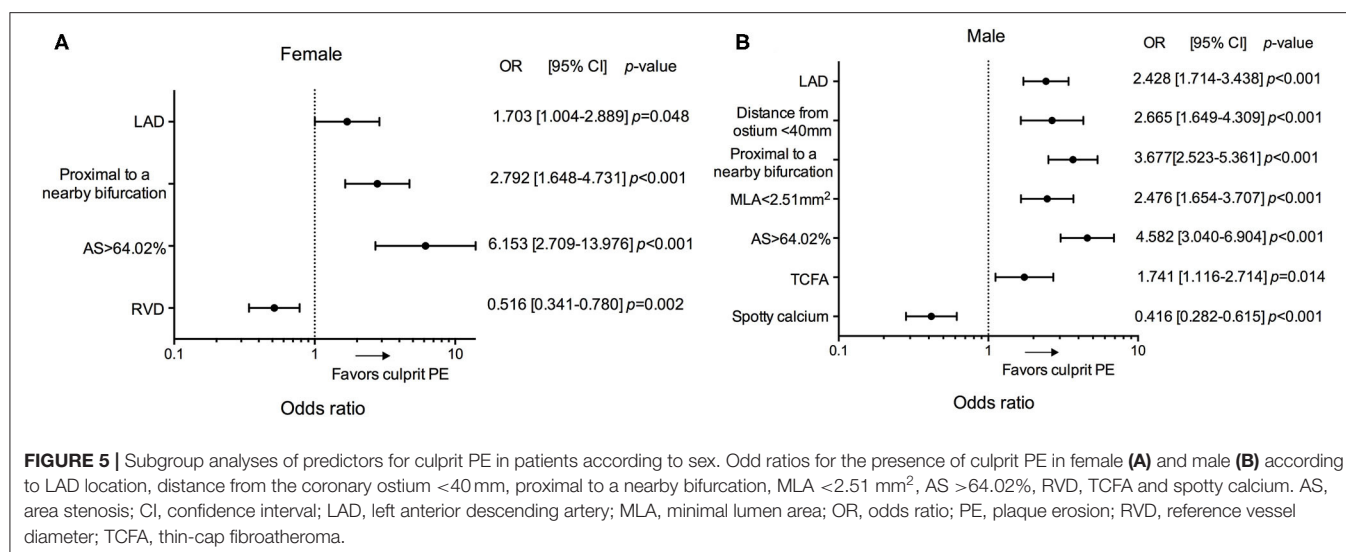


FIGURE 4 | Predictors for culprit PE in overall cohort of 484 patients. Odds ratios for the presence of culprit PE overall **(A)**, in LRPs **(B)**, and in non-LRPs **(C)** according to LAD location, distance from the coronary ostium <40 mm, proximal to a nearby bifurcation, MLA < 2.51 mm², AS > 64.02%, TCFA, presence of cholesterol crystals, calcification and microchannels. AS, area stenosis; CI, confidence interval; LAD, left anterior descending artery; LRP, lipid-rich plaque; MLA, minimal lumen area; OR, odds ratio; PE, plaque erosion; TCFA, thin-cap fibroatheroma.



inflammatory cells and cytokines (12, 28). However, pathological and imaging data about the association of microchannels with plaque erosion are still limited.

Sex Difference in Predictors of Culprit PE

Less non-culprit rupture and calcium content has been observed in females (29). Unlike in males, plaque phenotype, lipid content,

and micro-structures did not appear to be important for culprit PE in females while location and plaque burden were key predictors of culprit PE. Interestingly, smaller RVD was found to be a risk factor for culprit PE in females, but not in males. Females have significantly smaller epicardial coronary arteries together with higher baseline myocardial blood flow compared with males, resulting in an increase in ESS (29). In this case, vessel

segments with smaller RVD might be more sensitive to disturbed flow and rapid progression of plaque burden in females. Unlike rupture-prone vulnerability, our study found a negative role of spotty calcium in culprit PE in males.

Study Limitations

First, this was a retrospective observational analysis although data were collected prospectively. Second, consecutive patients undergoing OCT imaging of one, two, or three major epicardial coronary arteries were enrolled in order to minimize selection bias; and non-culprit plaques were analyzed in all of the imaged vessels. Had we included only patients with 3-vessel OCT, there would have been a different bias. Third, as the current OCT system cannot visualize individual endothelial cells, the OCT definition of culprit PE was in some ways an exclusion diagnosis. Fourth, the features of the culprit plaques were analyzed just after deocclusion; and correct underlying plaque analysis might be impeached due to the signal absorption caused by remnant thrombus. In the current study, the proportion of red thrombus was comparable between the two groups; and patients with massive thrombus in the culprit lesion were excluded. Fifth, manual thrombectomy could also alter the morphology of the culprit lesion by inducing dissection or iatrogenic rupture. Sixth, the data reflected the focal geometry and characteristics of erosion-prone coronary plaques of Chinese STEMI patients. Thus, the results may not be generalizable to other countries or ethnicities or to NSTEMI-ACS patients. Seventh, to date, there is no diagnostic definition for a plaque that is going to develop culprit PE and occlusive thrombus. Through providing comprehensive information of culprit PE and non-culprit lesions in other locations besides the culprit site, the present study only elucidated focal geometry and characteristics of erosion-prone coronary plaques in erosion-prone vulnerable patients. Finally, while not currently available, long-term follow-up of this large series of STEMI patients is in progress.

CONCLUSIONS

The current study elucidated particular focal geometry (anatomy and location) and characteristics for erosion-prone plaques. LAD location, distance from the coronary ostium <40 mm, location proximal to a nearby bifurcation, MLA <2.51 mm², AS >64.02%, and presence of TCFA were independent predictors for culprit PE overall, which can be used for risk-stratifying high-risk erosion-prone plaques in erosion-prone vulnerable patients (**Figure 6**). Cholesterol crystals were predictive of culprit PE with underlying LRP morphology while the absence of calcification and microchannels were risk factors for culprit PE

with an underlying non-LRP. Specific risk factors of erosion-prone plaques should be considered in men and women. Future prospective *in vivo* studies are required to validate the predictive value for clinical events or efficient therapeutic targets of plaque erosion.

DATA AVAILABILITY STATEMENT

The raw data supporting the conclusions of this article will be made available by the authors, without undue reservation.

ETHICS STATEMENT

The studies involving human participants were reviewed and approved by The Ethics Committee of the 2nd Affiliated Hospital of Harbin Medical University (Harbin, China). The patients/participants provided their written informed consent to participate in this study.

AUTHOR CONTRIBUTIONS

MC: conception and design of the research, acquisition, analysis and interpretation of data, manuscript drafting, and critical manuscript revision. TW, JZ, and ZD: substantial contribution to data acquisition and analysis. ZW and LL: contribution to statistical analysis. GW: substantial contribution to patients' enrollment and cardiac intervention. JT and HJ: critical manuscript revision. GM and BY: substantial contribution to the design of research and critical manuscript revision. All authors contributed to the article and approved the submitted version.

FUNDING

This work was supported by National Key R&D Program of China (grant No. 2016YFC1301100 to BY) and National Natural Science Foundation of China (grant No. 81827806).

ACKNOWLEDGMENTS

The authors sincerely thank all colleagues and patients who participated in this study.

SUPPLEMENTARY MATERIAL

The Supplementary Material for this article can be found online at: <https://www.frontiersin.org/articles/10.3389/fcvm.2021.709480/full#supplementary-material>

REFERENCES

- Libby P, Pasterkamp G, Crea F, Jang IK. Reassessing the mechanisms of acute coronary syndromes. *Circ Res.* (2019) 124:150–60. doi: 10.1161/CIRCRESAHA.118.311098

- Cao M, Zhao L, Ren X, Wu T, Yang G, Du Z, et al. Pancoronary plaque characteristics in STEMI caused by culprit plaque erosion versus rupture: 3-vessel OCT study. *JACC Cardiovasc Imaging.* (2021) 14:1235–45. doi: 10.1016/j.jcmg.2020.07.047

3. Crea F, Libby P. Acute coronary syndromes: the way forward from mechanisms to precision treatment. *Circulation*. (2017) 136:1155–66. doi: 10.1161/CIRCULATIONAHA.117.029870
4. Dai J, Xing L, Jia H, Zhu Y, Zhang S, Hu S, et al. *In vivo* predictors of plaque erosion in patients with ST-segment elevation myocardial infarction: a clinical, angiographical, and intravascular optical coherence tomography study. *Eur Heart J*. (2018) 39:2077–85. doi: 10.1093/eurheartj/ehy101
5. Sato A. Plaque erosion is a predictable clinical entity and tailored management in patients with ST-segment elevation myocardial infarction. *J Thorac Dis*. (2018) 10:S3274–5. doi: 10.21037/jtd.2018.08.103
6. Yamamoto E, Yonetsu T, Kakuta T, Soeda T, Saito Y, Yan BP, et al. Clinical and laboratory predictors for plaque erosion in patients with acute coronary syndromes. *J Am Heart Assoc*. (2019) 8:e012322. doi: 10.1161/JAHA.119.012322
7. Jinnouchi H, Virmani R, Finn AV. Are characteristics of plaque erosion defined by optical coherence tomography similar to true erosion in pathology? *Eur Heart J*. (2018) 39:2086–9. doi: 10.1093/eurheartj/ehy113
8. Jia H, Abtahian F, Aguirre AD, Lee S, Chia S, Lowe H, et al. *In vivo* diagnosis of plaque erosion and calcified nodule in patients with acute coronary syndrome by intravascular optical coherence tomography. *J Am Coll Cardiol*. (2013) 62:1748–58. doi: 10.1016/j.jacc.2013.05.071
9. Wang JC, Normand SL, Mauri L, Kuntz RE. Coronary artery spatial distribution of acute myocardial infarction occlusions. *Circulation*. (2004) 110:278–84. doi: 10.1161/01.CIR.0000135468.67850.F4
10. Dai J, Fang C, Zhang S, Li L, Wang Y, Xing L et al. Frequency, predictors, distribution, and morphological characteristics of layered culprit and nonculprit plaques of patients with acute myocardial infarction: *in vivo* 3-vessel optical coherence tomography study. *Circ Cardiovasc Interv*. (2020) 13:e009125. doi: 10.1161/CIRCINTERVENTIONS.120.009125
11. Sugiyama T, Yamamoto E, Bryniarski K, Xing L, Lee H, Isobe M, et al. Nonculprit plaque characteristics in patients with acute coronary syndrome caused by plaque erosion vs plaque rupture: a 3-vessel optical coherence tomography study. *JAMA Cardiol*. (2018) 3:207–14. doi: 10.1001/jamacardio.2017.5234
12. Vergallo R, Uemura S, Soeda T, Minami Y, Cho JM, Ong DS, et al. Prevalence and predictors of multiple coronary plaque ruptures: *in vivo* 3-vessel optical coherence tomography imaging study. *Arterioscler Thromb Vasc Biol*. (2016) 36:2229–38. doi: 10.1161/ATVBAHA.116.307891
13. Amabile N, Hammas S, Fradi S, Souteyrand G, Veugeois A, Belle L, et al. Intracoronary thrombus evolution during acute coronary syndrome: regression assessment by serial optical coherence tomography analyses. *Eur Heart J Cardiovasc Imaging*. (2015) 16:433–40. doi: 10.1093/ehjci/jeu228
14. Cheruvu PK, Finn AV, Gardner C, Caplan J, Goldstein J, Stone GW, et al. Frequency and distribution of thin-cap fibroatheroma and ruptured plaques in human coronary arteries: a pathologic study. *J Am Coll Cardiol*. (2007) 50:940–9. doi: 10.1016/j.jacc.2007.04.086
15. Wykrzykowska JJ, Mintz GS, Garcia-Garcia HM, Maehara A, Fahy M, Xu K, et al. Longitudinal distribution of plaque burden and necrotic core-rich plaques in nonculprit lesions of patients presenting with acute coronary syndromes. *JACC Cardiovasc Imaging*. (2012) 5:S10–8. doi: 10.1016/j.jcmg.2012.01.006
16. Araki M, Soeda T, Kim HO, Thondapu V, Russo M, Kurihara O, et al. Spatial distribution of vulnerable plaques: comprehensive *in vivo* coronary plaque mapping. *JACC Cardiovasc Imaging*. (2020) 13:1989–99. doi: 10.1016/j.jcmg.2020.01.013
17. Soulis JV, Farmakis TM, Giannoglou GD, Louridas GE. Wall shear stress in normal left coronary artery tree. *J Biomech*. (2006) 39:742–9. doi: 10.1016/j.jbiomech.2004.12.026
18. Lee SW, Antiga L, Spence JD, Steinman DA. Geometry of the carotid bifurcation predicts its exposure to disturbed flow. *Stroke*. (2008) 39:2341–47. doi: 10.1161/STROKEAHA.107.510644
19. Thondapu V, Mamon C, Poon EKW, Kurihara O, Kim HO, Russo M, et al. High spatial endothelial shear stress gradient independently predicts site of acute coronary plaque rupture and erosion. *Cardiovasc Res*. (2020) 117:1974–85. doi: 10.1093/cvr/cvaa251
20. Akong TA, Gotlieb AI. Reduced *in vitro* repair in endothelial cells harvested from the intercostal ostia of porcine thoracic aorta. *Arterioscler Thromb Vasc Biol*. (1999) 19:665–671. doi: 10.1161/01.atv.19.3.665
21. Jang IK. Plaque progression: slow linear or rapid stepwise? *Circ Cardiovasc Imaging*. (2017) 10:e006964. doi: 10.1161/CIRCIMAGING.117.006964
22. Yamamoto E, Thondapu V, Poon E, Sugiyama T, Fracassi F, Dijkstra J, et al. Endothelial shear stress and plaque erosion: a computational fluid dynamics and optical coherence tomography study. *JACC Cardiovasc Imaging*. (2019) 12:374–5. doi: 10.1016/j.jcmg.2018.07.024
23. Kurihara O, Takano M, Soeda T, Fracassi F, Araki M, Nakajima A, et al. Degree of luminal narrowing and composition of thrombus in plaque erosion. *J Thromb Thrombol*. (2020) 1:143–50. doi: 10.1007/s11239-020-02159-8
24. Vergallo R, Crea F. Atherosclerotic plaque healing. *N Engl J Med*. (2020) 383:846–57. doi: 10.1056/NEJMra2000317
25. Baumer Y, Mehta NN, Dey AK, Powell-Wiley TM, Boisvert WA. Cholesterol crystals and atherosclerosis. *Eur Heart J*. (2020) 41:2236–39. doi: 10.1093/eurheartj/ehaa505
26. Mori H, Torii S, Kutyna M, Sakamoto A, Finn AV, Virmani R. Coronary artery calcification and its progression: what does it really mean? *JACC Cardiovasc Imaging*. (2018) 11:127–42. doi: 10.1016/j.jcmg.2017.10.012
27. Puchner SB, Mayrhofer T, Park J, Lu MT. Differences in the association of total versus local coronary artery calcium with acute coronary syndrome and culprit lesions in patients with acute chest pain: the coronary calcium paradox. *Atherosclerosis*. (2018) 274:251–7. doi: 10.1016/j.atherosclerosis.2018.04.017
28. Uemura S, Ishigami K, Soeda T, Okayama S, Sung JH, Nakagawa H, et al. Thin-cap fibroatheroma and microchannel findings in optical coherence tomography correlate with subsequent progression of coronary atherosclerotic plaques. *Eur Heart J*. (2012) 33:78–85. doi: 10.1093/eurheartj/ehr284
29. Haider A, Bengs S, Luu J, Osto E, Siller-Matula JM, Muka T, et al. Sex and gender in cardiovascular medicine: presentation and outcomes of acute coronary syndrome. *Eur Heart J*. (2020) 41:1328–36. doi: 10.1093/eurheartj/ehz898

Conflict of Interest: GM has received research and fellowship support grants from Abbott; has been a consultant for and has received honoraria from Boston Scientific and Phillips; and has been a consultant for Terumo.

The remaining authors declare that the research was conducted in the absence of any commercial or financial relationships that could be construed as a potential conflict of interest.

Publisher's Note: All claims expressed in this article are solely those of the authors and do not necessarily represent those of their affiliated organizations, or those of the publisher, the editors and the reviewers. Any product that may be evaluated in this article, or claim that may be made by its manufacturer, is not guaranteed or endorsed by the publisher.

Copyright © 2021 Cao, Wu, Zhao, Du, Wang, Li, Wei, Tian, Jia, Mintz and Yu. This is an open-access article distributed under the terms of the Creative Commons Attribution License (CC BY). The use, distribution or reproduction in other forums is permitted, provided the original author(s) and the copyright owner(s) are credited and that the original publication in this journal is cited, in accordance with accepted academic practice. No use, distribution or reproduction is permitted which does not comply with these terms.



Usefulness of Diastolic Function Score as a Predictor of Long-Term Prognosis in Patients With Acute Myocardial Infarction

SungA Bae¹, Hyun Ju Yoon^{2*}, Kye Hun Kim², Hyung Yoon Kim², Hyukjin Park², Jae Yeong Cho², Min Chul Kim², Yongcheol Kim¹, Youngkeun Ahn², Jeong Gwan Cho² and Myung Ho Jeong²

¹ Division of Cardiology, Department of Internal Medicine, Yonsei University College of Medicine and Cardiovascular Center, Yonjin Severance Hospital, Yonjin, South Korea, ² Division of Cardiology, Chonnam National University Hospital, Chonnam National University Medical School, Gwangju, South Korea

OPEN ACCESS

Edited by:

Minjie Lu,
Chinese Academy of Medical
Sciences and Peking Union Medical
College, China

Reviewed by:

Kenya Kusunose,
Tokushima University Hospital, Japan
Mariana Paiva,
Centro Hospitalar Universitário de São
João (CHUSJ), Portugal

*Correspondence:

Hyun Ju Yoon
ann426@hanmail.net

Specialty section:

This article was submitted to
Cardiovascular Imaging,
a section of the journal
Frontiers in Cardiovascular Medicine

Received: 25 June 2021

Accepted: 19 August 2021

Published: 10 September 2021

Citation:

Bae S, Yoon HJ, Kim KH, Kim HY,
Park H, Cho JY, Kim MC, Kim Y,
Ahn Y, Cho JG and Jeong MH (2021)
Usefulness of Diastolic Function Score
as a Predictor of Long-Term
Prognosis in Patients With Acute
Myocardial Infarction.
Front. Cardiovasc. Med. 8:730872.
doi: 10.3389/fcvm.2021.730872

Background: Left ventricular diastolic function (LVDF) evaluation using a combination of several echocardiographic parameters is an important predictor of adverse events in patients with acute myocardial infarction (AMI). To date, the clinical impact of each individual LVDF marker is well-known, but the clinical significance of the sum of the abnormal diastolic function markers and the long-term clinical outcome are not well-known. This study aimed to investigate the usefulness of LVDF score in predicting clinical outcomes of patients with AMI.

Methods: LVDF scores were measured in a 2,030 patients with AMI who underwent successful percutaneous coronary intervention from 2012 to 2015. Four LVDF parameters (septal $e' \geq 7$ cm/s, septal $E/e' \leq 15$, TR velocity ≤ 2.8 m/s, and LAVI ≤ 34 ml/m²) were used for LVDF scoring. The presence of each abnormal LVDF parameter was scored as 1, and the total LVDF score ranged from 0 to 4. Mortality and hospitalization due to heart failure (HHF) in relation to LVDF score were evaluated. To compare the predictive ability of LVDF scores and left ventricular ejection fraction (LVEF) for mortality and HHF, receiver operating characteristic (ROC) curve and landmark analyses were performed.

Results: Over the 3-year clinical follow-up, all-cause mortality occurred in 278 patients (13.7%), while 91 patients (4.5%) developed HHF. All-cause mortality and HHF significantly increased as LVDF scores increased (all-cause mortality–LVDF score 0: 2.3%, score 1: 8.8%, score 2: 16.7%, score 3: 31.8%, and score 4: 44.5%, $p < 0.001$; HHF–LVDF score 0: 0.6%, score 1: 1.8%, score 2: 6.3%, score 3: 10.3%, and score 4: 18.2%, $p < 0.001$). In multivariate analysis, a higher LVDF score was associated with significantly higher adjusted hazard ratios for all-cause mortality and HHF. In landmark analysis, LVDF score was a better predictor of long-term mortality than LVEF (area under the ROC curve: 0.739 vs. 0.640, $p < 0.001$).

Conclusion: The present study demonstrated that LVDF score was a significant predictor of mortality and HHF in patients with AMI. LVDF scores are useful for risk stratification of patients with AMI; therefore, careful monitoring and management should be performed for patients with AMI with higher LVDF scores.

Keywords: diastolic function, left ventricular ejection fraction, myocardial infarction, mortality, heart failure

INTRODUCTION

Acute myocardial infarction (AMI) is characterized by regional myocardial injury that may lead to systolic and diastolic dysfunction due to left ventricular (LV) remodeling and dysfunction. Left ventricular diastolic function (LVDF), an aftermath of AMI, is an important predictor for major adverse events (1–3). The 2009 guidelines for diastolic dysfunction included many parameters and was perceived as overly complex (4). In 2016, the guidelines were revised to simplify the measurement of LVDF, thereby enhancing the usefulness of the guidelines in routine practice (5, 6). It recommended two separate algorithms. For patients with maintained left ventricular ejection fraction (LVEF $\geq 50\%$) and unknown diastolic function, Algorithm A is primarily used to classify normal and abnormal diastolic function, while Algorithm B is designed to estimate LV filling pressure and grade diastolic function of patients with a reduced ($<50\%$) or preserved LVEF and known or suspected diastolic dysfunction. However, if the patient's diagnosis is unknown or the LVEF is marginal (45–55%), there are problems in selecting an algorithm for LVDF evaluation. Therefore, there is a need for an LVDF assessment that can be easily applied to clinical practice by providers with different levels of expertise.

Recently, Oh et al. proposed a simplified and unified algorithm for LVDF assessment (7). This algorithm benefited by simplifying the assessment in clinical practice and avoiding problems with discordance and false calls of diastolic dysfunction to achieve high specificity. To date, the clinical impact of each individual LVDF marker is well-known, but the clinical significance of the sum of the abnormal diastolic function markers and the long-term clinical outcome are not well-known (8). This study aimed to investigate the usefulness of LVDF score in predicting clinical outcomes of patients with AMI.

MATERIALS AND METHODS

Patient Population

All patients with AMI registered at Chonnam National University Hospital from 2011 to 2015 were included in the study. Of the initial 3,009 patients, 2,030 patients who underwent successful primary percutaneous intervention (PCI)

and transthoracic echocardiography (TTE) were selected. Patients with moderate to severe mitral regurgitation (MR), mitral annular calcification, atrial fibrillation, those who did not undergo PCI, those who underwent suboptimal or failed PCI, those with no echocardiography findings, and those with insufficient TTE imaging or loss to follow-up were excluded (**Supplementary Figure 1**). AMI is defined as cardiomyocyte necrosis in a clinical setting consistent with acute myocardial ischemia (9). It was diagnosed by clinical presentation, serial changes on echocardiography suggesting infarction, and an increase in cardiac markers, preferably cardiac troponins, with at least one value above the 99th percentile of the upper reference limit. The study complies with the Declaration of Helsinki, and the local institutional review board (IRB) of the study center approved the study protocol (CNUH 05-49). Written informed consent was obtained from each study patient.

Echocardiographic Data and Study Definition

A comprehensive transthoracic echocardiogram was obtained within 48 h of admission for all patients. All TTE measurements were recorded during routine clinical practice according to the current American Society of Echocardiography (ASE/EACVI) recommendations (10). Left ventricular systolic function was assessed by LVEF obtained using the biplane method of disk summation, from the apical 2- and 4-chamber views, according to the modified biplane Simpson's method. To calculate the wall motion score index (WMSI), the LV was divided into 16 segments. Each segment was assessed and scored based on its motion and systolic thickening (1 = normokinesia, 2 = hypokinesia, 3 = akinesia, 4 = dyskinesia). The WMSI was calculated as the sum of the individual segment scores divided by the number of segments (11). Left atrial (LA) volume was assessed using the modified biplane Simpson's method, from the apical 2- and 4-chamber views, at end-systole and indexed to body surface area. In cases in which the Simpson's method could not be used due to missing or poor quality apical views, LA volume index (LAVI) was calculated using the Cube method (12). Peak early diastolic tissue velocity (e') was measured from the septal aspects of the mitral annulus, while mitral inflow velocity was assessed using the pulsed-wave Doppler from the apical 4-chamber view (5). The right ventricular (RV) functional measures were tricuspid annulus systolic tissue Doppler velocity (s') and RV dysfunction, which was defined as $s' < 10$ cm/s. Peak tricuspid regurgitation (TR) velocity was measured, and pulmonary artery systolic pressure (PASP) was estimated as $4 \times (\text{peak TR velocity})^2 + 5$ (5).

Abbreviations: AMI, acute myocardial infarction; AUC, area under the receiver operating characteristic curve; eGFR, estimated glomerular filtration rate; HF, heart failure; LAVI, left atrial volume index; LV, left ventricular; LVDF, left ventricular diastolic function; LVEF, left ventricular ejection fraction; LVH, left ventricular hypertrophy; PCI, percutaneous coronary intervention; RCA, right coronary artery; ROC, receiver operating characteristic; RV, right ventricular; STEMI, ST-segment elevation myocardial infarction; TR, tricuspid regurgitation; TTE, transthoracic echocardiography; WMSI, wall motion score index.

Four LVDF parameters (septal $e' \geq 7$ cm/s, septal $E/e' \leq 15$, TR velocity ≤ 2.8 m/s, and LAVI ≤ 34 ml/m²) were used for LVDF scoring (7). The presence of each abnormal LVDF parameter was scored as 1, and the total LVDF score ranged from 0 to 4 (normal filling pressure: LVDF score 0–1, indeterminate: LVDF score 2, increased filling pressure: LVDF score 3–4).

Clinical Data Collection

Demographic features and cardiovascular risk factors were obtained via patient interviews or review of medical records. During admission, findings of coronary angiography and detailed procedural characteristics of PCI, as well as data on discharge medications were collected. Patient treatment was performed according to current standard practice. After PCI, all patients were recommended to take aspirin indefinitely with clopidogrel or a potent P2Y₁₂ inhibitor, such as prasugrel or ticagrelor, for at least 1 year.

Clinical Outcomes

The incidence of mortality and hospitalization due to heart failure (HHF) in relation with the LVDF score over the 3-year study period were evaluated. All causes of death were considered cardiac unless an apparent non-cardiac cause was otherwise stated. Readmission for HF was defined as the patient showing signs and symptoms of HF upon admission and was treated with medications, including diuretic therapy (either intravenous diuretics or augmentation of oral diuretics), vasodilators, inotropic support, or ultrafiltration for HF during admission. All end points followed the definitions of the Academic Research Consortium (13).

Statistical Analyses

Continuous variables are presented as means \pm standard deviations or medians with interquartile ranges and compared using an unpaired *t*-test or Mann–Whitney rank sum test. Categorical variables are expressed as numbers with percentages and compared using Pearson's chi-square test or Fisher's exact test. Mortality and HHF were assessed using Kaplan–Meier curves according to the LVDF score. A multivariate Cox regression model was used for each of the above-mentioned cut-offs, with covariates that had $P < 0.05$ on univariate analysis or had predictive values [age ≥ 65 years, male sex, previous MI, estimated glomerular filtration rate (eGFR) $\leq 60\%$, LVEF, and cardiogenic shock, LV end-diastolic volume index, LV end-systolic volume index, LV geometry]. To compare the predictive abilities of LVDF scores and LVEF for mortality and HHF, receiver operating characteristic (ROC) curve analysis and DeLong's test were performed. In addition, comparisons of all-cause mortality between the LVDF score and LVEF according to the exploratory subgroups of interest were assessed using an ROC curve. For ROC curves, landmark analyses were used to compare LVDF scores and LVEF before and after 30 days of follow-up because 30 days following primary reperfusion is a critical period where the greatest degree of cardiac remodeling occurs (14).

All probability values were two-sided, and *p*-values < 0.05 were considered statistically significant. All statistical analyses were performed using R Core Team (2015). R: A language and environment for statistical computing (version 3.6.0, R Foundation for Statistical Computing, Vienna, Austria. URL <https://www.R-project.org/>).

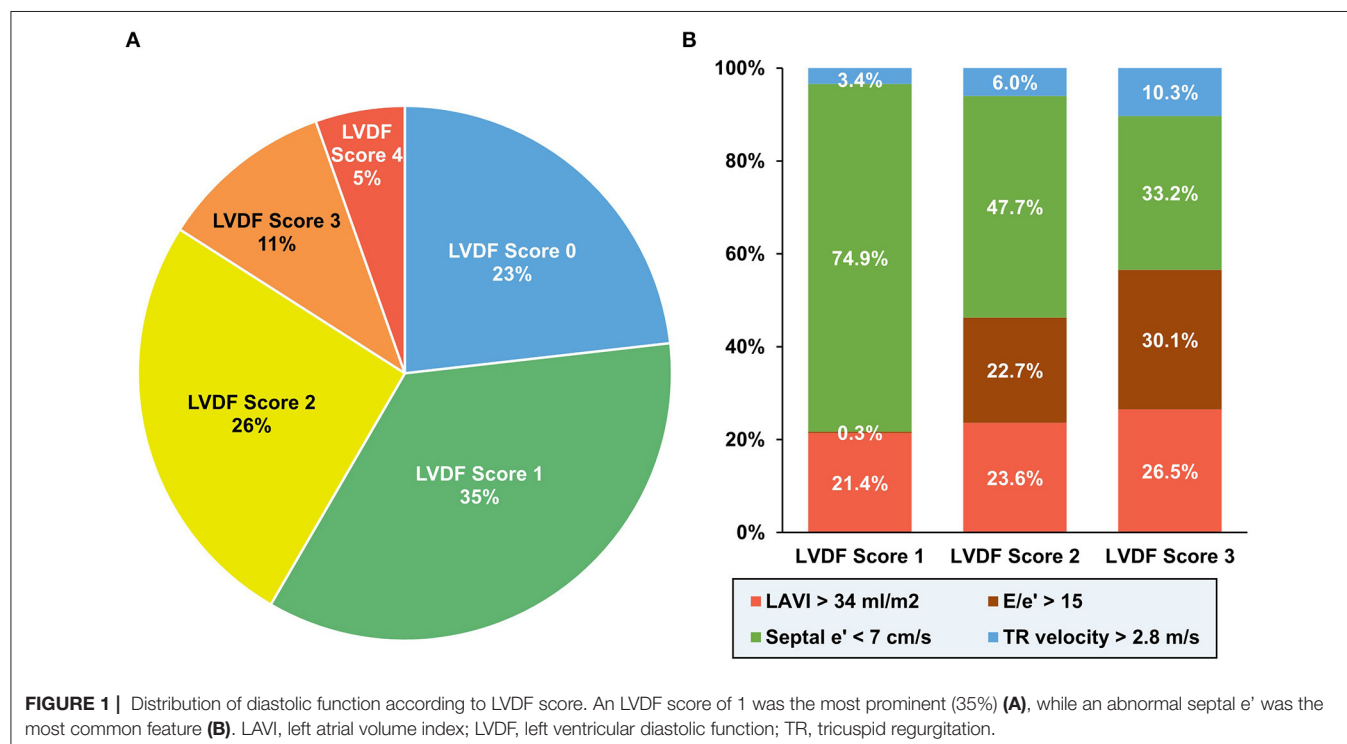


TABLE 1 | Baseline Clinical and Procedural-related Characteristics.

	Total (N = 2,030)	LVDF Score 0 (N = 471)	LVDF Score 1 (N = 714)	LVDF Score 2 (N = 521)	LVDF Score 3 (N = 214)	LVDF Score 4 (N = 110)	P-value
Demographics							
Age, years	64.6 ± 12.6	54.9 ± 11.0	64.2 ± 11.6	69.5 ± 10.9	71.0 ± 11.1	72.8 ± 9.6	<0.001
Male	1,471 (72.5%)	418 (88.7%)	565 (79.1%)	315 (60.5%)	118 (55.1%)	55 (50.0%)	<0.001
Body mass index	24.1 ± 3.3	24.1 ± 3.0	24.3 ± 3.4	23.9 ± 3.4	23.9 ± 3.5	23.2 ± 3.5	0.016
Comorbidities							
Hypertension	1,070 (52.7%)	131 (27.8%)	372 (52.1%)	333 (63.9%)	154 (72.0%)	80 (72.7%)	<0.001
Diabetes mellitus	618 (30.4%)	96 (20.4%)	206 (28.9%)	169 (32.4%)	86 (40.2%)	61 (55.5%)	<0.001
Dyslipidemia	156 (7.7%)	43 (9.1%)	61 (8.5%)	23 (4.4%)	22 (10.3%)	7 (6.4%)	0.015
Previous history of MI	169 (8.3%)	21 (4.5%)	65 (9.1%)	35 (6.7%)	28 (13.1%)	20 (18.2%)	<0.001
Previous history of CVA	122 (6.0%)	13 (2.8%)	38 (5.3%)	42 (8.1%)	17 (7.9%)	12 (10.9%)	0.001
Final diagnosis							
STEMI	846 (41.7%)	224 (47.6%)	322 (45.1%)	191 (36.7%)	75 (35.0%)	34 (30.9%)	<0.001
NSTEMI	1,184 (58.3%)	247 (52.4%)	392 (54.9%)	330 (63.3%)	139 (65.0%)	76 (69.1%)	
Examination and laboratory values							
Systolic pressure	124.9 ± 22.3	123.5 ± 19.7	125.4 ± 22.2	124.3 ± 23.8	126.6 ± 24.4	127.7 ± 22.2	0.076
Diastolic pressure	78.4 ± 14.3	78.4 ± 13.4	78.7 ± 14.0	77.3 ± 15.1	79.1 ± 15.3	80.9 ± 14.7	0.476
Mean arterial pressure	93.8 ± 16.6	93.3 ± 15.1	94.2 ± 16.3	92.9 ± 17.6	94.8 ± 17.9	96.4 ± 16.8	0.221
Heart rate	78.9 ± 17.0	78.3 ± 16.1	77.6 ± 15.6	79.1 ± 18.4	81.5 ± 18.7	83.8 ± 18.0	<0.001
Killip class	1.4 ± 0.8	1.2 ± 0.6	1.3 ± 0.7	1.4 ± 0.8	1.6 ± 0.9	1.8 ± 0.9	<0.001
Cardiogenic shock	172 (8.5%)	24 (5.1%)	59 (8.3%)	53 (10.2%)	25 (11.7%)	11 (10.0%)	0.017
eGFR, ml/min/1.73 m ²	96.2 ± 46.6	111.6 ± 40.9	99.4 ± 46.1	89.9 ± 49.3	83.4 ± 43.2	64.9 ± 38.5	<0.001
NT-proBNP, pg/ml	3474.2 ± 10216.1	860.1 ± 3230.2	2068.8 ± 5524.7	3051.8 ± 5816	6212.9 ± 8734.8	17068.7 ± 31162	<0.001
Lesion profiles							
Culprit vessel							0.286
Left main artery	52 (2.6%)	11 (2.3%)	17 (2.4%)	14 (2.7%)	5 (2.3%)	5 (4.5%)	
LAD artery	962 (47.4%)	226 (48.0%)	355 (49.7%)	228 (43.8%)	95 (44.4%)	58 (52.7%)	
Left circumflex artery	364 (17.9%)	75 (15.9%)	137 (19.2%)	97 (18.6%)	42 (19.6%)	13 (11.8%)	
Right coronary artery	652 (32.1%)	159 (33.8%)	205 (28.7%)	182 (34.9%)	72 (33.6%)	34 (30.9%)	
Three vessels disease	194 (9.6%)	27 (5.7%)	65 (9.1%)	60 (11.5%)	27 (12.6%)	15 (13.6%)	0.005
ACC/AHA B2/C lesion	1,893 (93.3%)	424 (90.0%)	668 (93.6%)	499 (95.8%)	197 (92.1%)	105 (95.5%)	0.006
Pre-PCI TIMI flow 0-1	1,035 (51.0%)	273 (58.0%)	360 (50.4%)	248 (47.6%)	103 (48.1%)	51 (46.4%)	0.01
Procedural characteristics							
Trans-radial approach	956 (47.1%)	222 (47.1%)	358 (50.1%)	239 (45.9%)	89 (41.6%)	48 (43.6%)	0.171
2nd generation DES	1,727 (85.1%)	418 (88.7%)	629 (88.1%)	433 (83.1%)	171 (79.9%)	76 (69.1%)	<0.001
Total number of stents	1.4 ± 0.9	1.4 ± 0.7	1.4 ± 0.8	1.5 ± 0.9	1.6 ± 1.0	1.4 ± 0.9	0.040
Medication at discharge							
Aspirin	2,029 (100.0%)	471 (100.0%)	714 (100.0%)	520 (99.8%)	214 (100.0%)	110 (100.0%)	0.575
P2Y12 inhibitor	2,028 (99.9%)	470 (99.8%)	714 (100.0%)	520 (99.8%)	214 (100.0%)	110 (100.0%)	0.716
Ticagrelor	460 (22.7%)	115 (24.4%)	165 (23.1%)	112 (21.5%)	45 (21.0%)	23 (20.9%)	
Prasugrel	516 (25.4%)	168 (35.7%)	206 (28.9%)	91 (17.5%)	34 (15.9%)	17 (15.5%)	
Clopidogrel	1,052 (51.8%)	187 (39.7%)	343 (48.0%)	317 (60.8%)	135 (63.1%)	70 (63.6%)	
ACE inhibitor or ARB	1,746 (86.0%)	408 (86.6%)	618 (86.6%)	450 (86.4%)	176 (82.2%)	94 (85.5%)	0.569
Beta-blocker	1,724 (84.9%)	411 (87.3%)	603 (84.5%)	432 (82.9%)	178 (83.2%)	100 (90.9%)	0.118
Statin	1,879 (92.6%)	447 (94.9%)	659 (92.3%)	482 (92.5%)	193 (90.2%)	98 (89.1%)	0.111

Values are mean ± SD or n (%). NT-proBNP, N-terminal pro-brain natriuretic peptide; ACC/AHA, American College of Cardiology/American Heart Association; ACEI, angiotensin-converting enzyme inhibitor; ARB, angiotensin-II receptor blocker; CVA, cerebrovascular accident; DES, drug-eluting stent; eGFR, estimated glomerular filtration rate; LAD, left anterior descending artery; LVDF, left ventricular diastolic function; NSTEMI, non ST-segment elevation myocardial infarction; STEMI, ST-segment elevation myocardial infarction; TIMI, Thrombolysis in Myocardial Infarction.

RESULTS

Baseline Characteristics

Of the 3,009 patients with AMI recruited for the study, 979 patients were excluded for following reasons: 39 with moderate to severe MR; 68 with mitral annular calcification; 194 with atrial fibrillation; 23 with failed or suboptimal PCI; 380 with no PCI; 93 with no TTE; 172 with insufficient TTE imaging; and 10

with follow-up loss (**Supplementary Figure 1**). The proportion of LVDF scores were as follows: 23.2% (score 0), 35.2% (score 1), 25.7% (score 2), 10.5% (score 3), and 5.4% (score 4) (**Figure 1A**). An LVDF score of 1 was the most prominent (35%), with an abnormal septal e' being the most common feature. $E/e' > 15$ showed an increasing pattern as the LVDF score increased (**Figure 1B**). The baseline demographics, final diagnosis, and risk factors were found to be significantly varied with the LVDF score

TABLE 2 | Transthoracic Echocardiographic Characteristics.

Variable	Total (N = 2,030)	LVDF score 0 (N = 471)	LVDF score 1 (N = 714)	LVDF score 2 (N = 521)	LVDF score 3 (N = 214)	LVDF score 4 (N = 110)	P-value
LV structure							
LVEDVi (ml/m ²)	72.0 ± 19.7	65.2 ± 14.2	67.9 ± 15.9	75.0 ± 20.0	84.7 ± 24.9	88.4 ± 23.6	<0.001
LVESVi (ml/m ²)	31.5 ± 16.2	25.1 ± 9.5	28.5 ± 11.7	33.6 ± 17.5	42.7 ± 23.0	44.9 ± 20.5	<0.001
LVEDD (cm)	50.2 ± 5.8	49.0 ± 4.7	49.4 ± 5.3	50.5 ± 5.9	52.9 ± 7.0	53.5 ± 6.2	<0.001
LVESD (cm)	34.7 ± 6.8	32.5 ± 5.0	33.8 ± 5.7	35.2 ± 7.1	38.7 ± 8.8	39.5 ± 7.7	<0.001
Septal wall thickness (cm)	9.4 ± 1.8	9.2 ± 1.6	9.4 ± 1.7	9.4 ± 2.0	9.6 ± 2.0	9.6 ± 1.9	0.003
Posterior wall thickness (cm)	9.5 ± 1.5	9.4 ± 1.4	9.5 ± 1.5	9.5 ± 1.5	9.8 ± 1.8	9.9 ± 1.7	<0.001
LV mass (g)	171.9 ± 47.6	160.3 ± 39.8	167.4 ± 42.9	173.3 ± 49.4	193.9 ± 56.4	199.2 ± 53.6	<0.001
LV mass index (g/m ²)	101.6 ± 26.8	91.1 ± 21.5	97.3 ± 23.0	104.6 ± 26.3	118.9 ± 31.0	124.5 ± 30.0	<0.001
RWT	0.39 ± 0.08	0.38 ± 0.07	0.39 ± 0.08	0.38 ± 0.07	0.38 ± 0.10	0.38 ± 0.09	0.056
LV geometry							
Normal	895 (48.2%)	268 (62.3%)	342 (52.4%)	198 (42.6%)	61 (31.0%)	26 (23.6%)	<0.001
Concentric remodeling	326 (17.6%)	100 (23.3%)	135 (20.7%)	66 (14.2%)	17 (8.6%)	8 (7.3%)	
Concentric hypertrophy	239 (12.9%)	24 (5.6%)	80 (12.3%)	73 (15.7%)	37 (18.8%)	25 (22.7%)	
Eccentric hypertrophy	395 (21.3%)	38 (8.8%)	96 (14.7%)	128 (27.5%)	82 (41.6%)	51 (46.4%)	
LV systolic function							
LVEF (%)	55.0 ± 11.3	59.2 ± 9.0	55.5 ± 10.2	54.3 ± 11.6	49.4 ± 12.8	47.8 ± 13.2	<0.001
≥50%	1434 (70.6%)	402 (85.4%)	520 (72.8%)	350 (67.2%)	112 (52.3%)	50 (45.5%)	
<50%	596 (29.4%)	69 (14.6%)	194 (27.2%)	171 (32.8%)	102 (47.7%)	60 (54.5%)	
TDI septal s' (cm/s)	6.7 ± 2.8	7.9 ± 1.8	7.0 ± 3.9	6.1 ± 1.6	5.6 ± 1.5	5.0 ± 1.7	<0.001
WMSI	1.4 ± 0.4	1.3 ± 0.3	1.4 ± 0.3	1.4 ± 0.4	1.6 ± 0.4	1.6 ± 0.4	<0.001
LV diastolic function							
E/A ratio	0.9 ± 2.1	1.0 ± 0.9	0.9 ± 3.3	0.8 ± 0.6	0.9 ± 0.6	1.4 ± 0.8	0.888
E wave (cm/s)	68.5 ± 21.1	70.0 ± 16.7	60.2 ± 17.6	66.9 ± 20.5	81.9 ± 20.3	98.4 ± 22.6	<0.001
A wave (cm/s)	80.2 ± 22.7	70.3 ± 18.4	78.8 ± 19.0	86.3 ± 22.6	92.4 ± 27.2	78.8 ± 31.3	<0.001
Deceleration time (ms)	205.0 ± 66.3	194.0 ± 54.2	211.4 ± 66.6	212.5 ± 67.3	202.6 ± 76.1	179.0 ± 73.6	0.831
TDI septal e' (cm/s)	5.8 ± 2.2	8.3 ± 2.0	5.7 ± 1.8	4.7 ± 1.3	4.3 ± 1.1	4.1 ± 1.1	<0.001
Septal E/e'	13.2 ± 6.8	8.6 ± 2.2	10.7 ± 2.4	15.0 ± 5.6	20.4 ± 8.7	25.4 ± 9.6	<0.001
LA size and function							
LA diameter (mm)	38.5 ± 5.8	35.3 ± 3.5	36.8 ± 5.2	39.7 ± 5.6	43.1 ± 5.0	46.4 ± 4.4	<0.001
LAVI (cm ² /m ²)	32.2 ± 14.7	23.7 ± 6.3	27.8 ± 11.6	35.1 ± 14.0	44.5 ± 14.7	54.5 ± 16.0	<0.001
TDI septal a' (cm/s)	9.0 ± 2.3	9.9 ± 2.4	9.3 ± 2.1	8.6 ± 2.0	7.9 ± 2.0	6.7 ± 2.1	<0.001
RV function							
TDI RV s' (cm/s)	12.4 ± 2.9	12.4 ± 2.4	12.3 ± 3.0	12.4 ± 3.1	12.5 ± 2.9	12.7 ± 3.3	0.445
Pulmonary pressure							
TR velocity (m/s)	2.1 ± 0.7	1.8 ± 0.7	1.9 ± 0.6	2.1 ± 0.7	2.5 ± 0.6	3.2 ± 0.3	<0.001
PASP (mmHg)	24.6 ± 11.7	20.2 ± 8.9	21.8 ± 9.0	24.9 ± 11.0	31.7 ± 11.9	46.8 ± 8.5	<0.001

Values are expressed as mean ± standard deviation or number (%).

A wave, peak late diastolic velocity of mitral inflow; AV, aortic valve; A' wave, peak late diastolic velocity of mitral septal annulus; DT, deceleration time of mitral inflow; E wave, peak early diastolic velocity of mitral inflow; E' wave, peak early diastolic velocity of mitral septal annulus; LAD, left atrium diameter; LVEDVi, left ventricular end-diastolic volume index; LVEDD, left ventricular end-diastolic diameter; LVEF, left ventricular ejection fraction; LVESVi, left ventricular end-systolic volume index; LVESD, left ventricular end-systolic diameter; MR, mitral regurgitation; PG, pressure gradient; PASP, pulmonary artery systolic pressure; RWT, relative wall thickness; s', peak systolic velocity of mitral septal annulus; TDI, tissue doppler imaging; TRV, tricuspid regurgitation velocity; WMSI, wall motion score index.

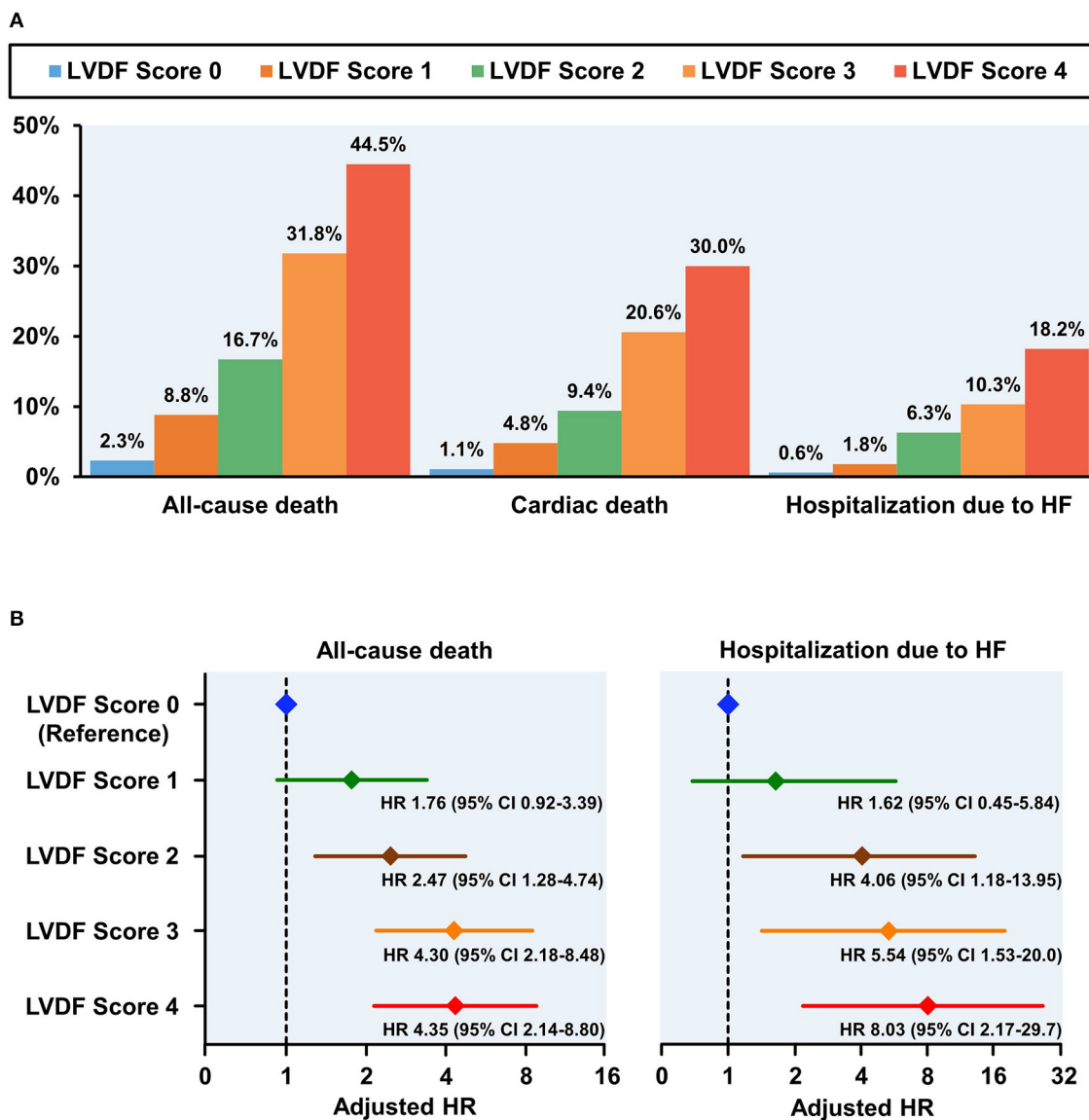
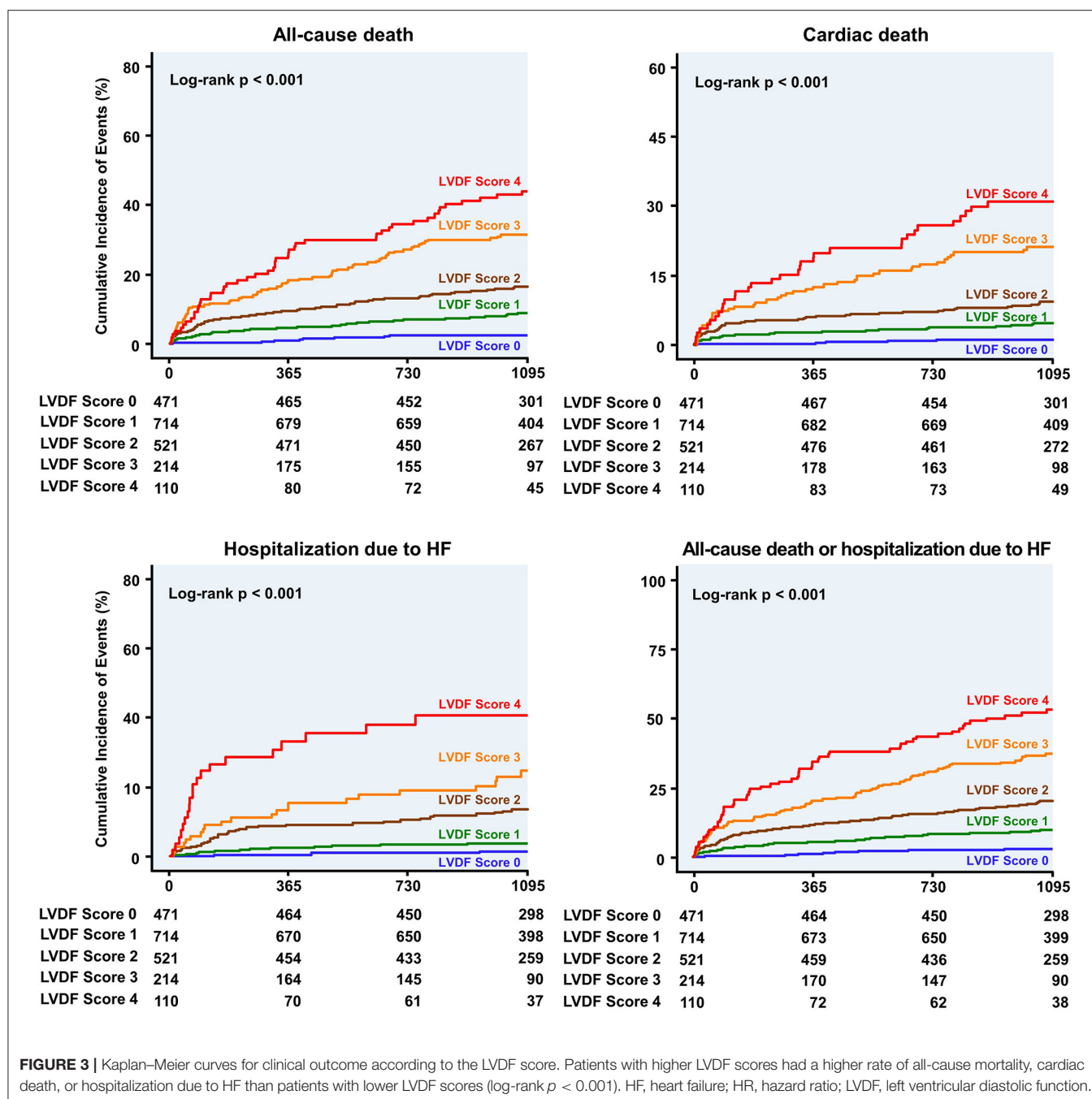


FIGURE 2 | Clinical outcomes according to LVDF scores **(A)** and adjusted HR plot for all-cause mortality and hospitalization due to HF **(B)**. All-cause mortality, cardiac death, and heart failure (HF) rehospitalization rates increased in a stepwise fashion from 2.3% (LVDF score 0) to 44.5% (LVDF score 4) ($p < 0.001$). Higher LVDF scores had incrementally higher adjusted HRs for all-cause mortality and hospitalization due to HF. CI, confidence interval; HF, heart failure; HR, hazard ratio; LVDF, left ventricular diastolic function.

(Table 1). A total of 2,030 patients with a mean age of 64.6 ± 12.6 years, including 1,471 males (72.5%), were included in this study. Co-morbidities such as hypertension and diabetes mellitus were found in 52.7 and 41.0% of patients, respectively. As the LVDF score increased, eGFR decreased while N-terminal pro-brain natriuretic peptide levels increased ($p < 0.001$). Second-generation drug-eluting stent was chosen as the most implanted intervention (85.1%), and the total number of stents was 1.4 ± 0.9 . Most patients were receiving aspirin, a P2Y12 inhibitor, ACE inhibitor or ARB, beta-blocker, or a statin.

Echocardiographic Characteristics

Based on the left ventricular mass index (LVMI) results and relative wall thickness, LV hypertrophy (LVH) was observed in 34.2% of patients (concentric: 12.9%, eccentric: 21.3%; Table 2). The prevalence of LVH increased as the LVDF score increased. The mean LVEF was $55.0 \pm 11.3\%$. As the LVDF score increased, the LVEF decreased and WMSI increased. The higher the LVDF score of patients, the higher the LAVI and septal E/e' TR velocity but the lower the septal e' .



Clinical Outcome

During a median follow-up period of 1,099 (interquartile range: 1,063–1,124) days, 278 patients (13.7%) died and 91 patients (4.5%) were readmitted for HF. All-cause mortality and HHF significantly increased as the LVDF score increased (all-cause mortality–LVDF score 0: 2.3%, score 1: 8.8%, score 2: 16.7%, score 3: 31.8%, and score 4: 44.5%, $p < 0.001$; HHF–LVDF score 0: 0.6%, score 1: 1.8%, score 2: 6.3%, score 3: 10.3%, and score 4: 18.2%, $p < 0.001$; **Figure 2A**). In multivariate analysis, a higher LVDF score was associated with significantly higher adjusted

hazard ratios (HR) for all-cause mortality and HHF (**Figure 2B**). Kaplan–Meier survival analysis revealed that patients with higher LVDF scores had a higher rate of all-cause mortality, cardiac death, and HHF than those with lower LVDF scores (log-rank $p < 0.001$; **Figure 3**). In various subgroups, the LVDF scores stratification had incrementally higher adjusted hazard ratio (HR) for all-cause mortality (**Supplementary Figure 2**).

LVDF score 2–4 and LVEF $< 40\%$ were independent predictors of all-cause death, and LVDF score 2–4, LVEF 40–50% and $< 40\%$ were independent predictors of HHF (**Table 3**).

TABLE 3 | Independent Predictors for All-cause Death And Hospitalization Due to HF.

	HR	95% CI	P-value
All-cause death			
LVDF score 1 (LVDF Score 0 as a reference)	1.761	0.915 – 3.387	0.090
LVDF score 2 (LVDF Score 0 as a reference)	2.468	1.284 – 4.743	0.007
LVDF score 3 (LVDF Score 0 as a reference)	4.299	2.180 – 8.475	<0.001
LVDF score 4 (LVDF Score 0 as a reference)	4.346	2.144 – 8.804	<0.001
LVEF 40-50% (LVEF \geq 50% as a reference)	1.325	0.963 – 1.823	0.083
LVEF < 40% (LVEF \geq 50% as a reference)	2.075	1.468 – 2.933	<0.001
Age > 65 years	5.338	3.518 – 8.100	<0.001
Male	1.190	0.919 – 1.542	0.187
Previous history of MI	1.819	1.312 – 2.522	0.001
eGFR < 60	2.241	1.752 – 2.868	<0.001
Cardiogenic shock	2.739	2.038 – 3.684	<0.001
LVEDVi \geq 31.5 ml/m ²	1.082	0.798 – 1.467	0.611
LV mass index \geq 101 ml/m ²	0.991	0.724 – 1.358	0.957
Abnormal LV geometry	1.263	0.925 – 1.726	0.142
Hospitalization due to HF			
LVDF score 1 (LVDF Score 0 as a reference)	1.624	0.451 – 5.838	0.458
LVDF score 2 (LVDF Score 0 as a reference)	4.064	1.183 – 13.95	0.026
LVDF score 3 (LVDF Score 0 as a reference)	5.535	1.531 – 20.00	0.009
LVDF score 4 (LVDF Score 0 as a reference)	8.031	2.169 – 29.73	0.002
LVEF 40-50% (LVEF \geq 50% as a reference)	1.773	1.018 – 3.086	0.043
LVEF < 40% (LVEF \geq 50% as a reference)	3.206	1.758 – 5.847	0.001
Age > 65 years	2.223	1.233 – 4.008	0.008
Male	0.862	0.551 – 1.348	0.515
Previous history of MI	1.268	0.692 – 2.321	0.442
eGFR < 60	2.798	1.826 – 4.289	<0.001
Cardiogenic shock	1.362	0.740 – 2.506	0.320
LVEDVi \geq 31.5 ml/m ²	1.219	0.702 – 2.117	0.482
LV mass index \geq 101 ml/m ²	0.830	0.468 – 1.470	0.523
Abnormal LV geometry	1.469	0.832 – 2.596	0.185

Hazard ratios and their 95% confidence intervals were calculated by multivariable Cox regression analysis.

Abbreviations are as in **Tables 1, 2**.

In addition, HR values for all-cause death and HHF were higher in LVDF score 4 than in LVEF < 40% {all-cause death—LVDF score 4: HR 4.346 [95% confidence interval (CI) 1.468–2.933], $p < 0.001$ vs. LVEF < 40%: HR 2.075 (95% CI 1.468–2.933), $p < 0.001$; HHF—LVDF score 4: HR 8.031 (95% CI 2.169–29.73), $p = 0.002$ vs. LVEF < 40%: HR 3.206 (95% CI 1.758–5.847), $p = 0.001$ }.

Prediction of Clinical Outcome: LVDF Score vs. LVEF

The ROC curve showed that the LVDF score was significantly better at predicting all-cause mortality and readmission for recurrent HF than LVEF (area under the ROC curve [AUC]: 0.743 vs. 0.676, Delong's test $p = 0.003$; AUC: 0.762 vs. 0.688, Delong's test $p = 0.046$; respectively; **Figure 4**).

Subgroup analysis showed that the LVDF score performed significantly better than LVEF in patients with

ST-segment elevation myocardial infarction (STEMI), LVEF \geq 50%, Killip class < 3, abnormal LV geometry (LV remodeling or LVH), and non-right coronary artery (RCA) target vessel (**Supplementary Figure 3**). Comparison of the predictive performance of the individual LVDF parameters and LVEF showed that E/e' ratio was the best predictor of all-cause death and HHF (**Supplementary Figure 4**).

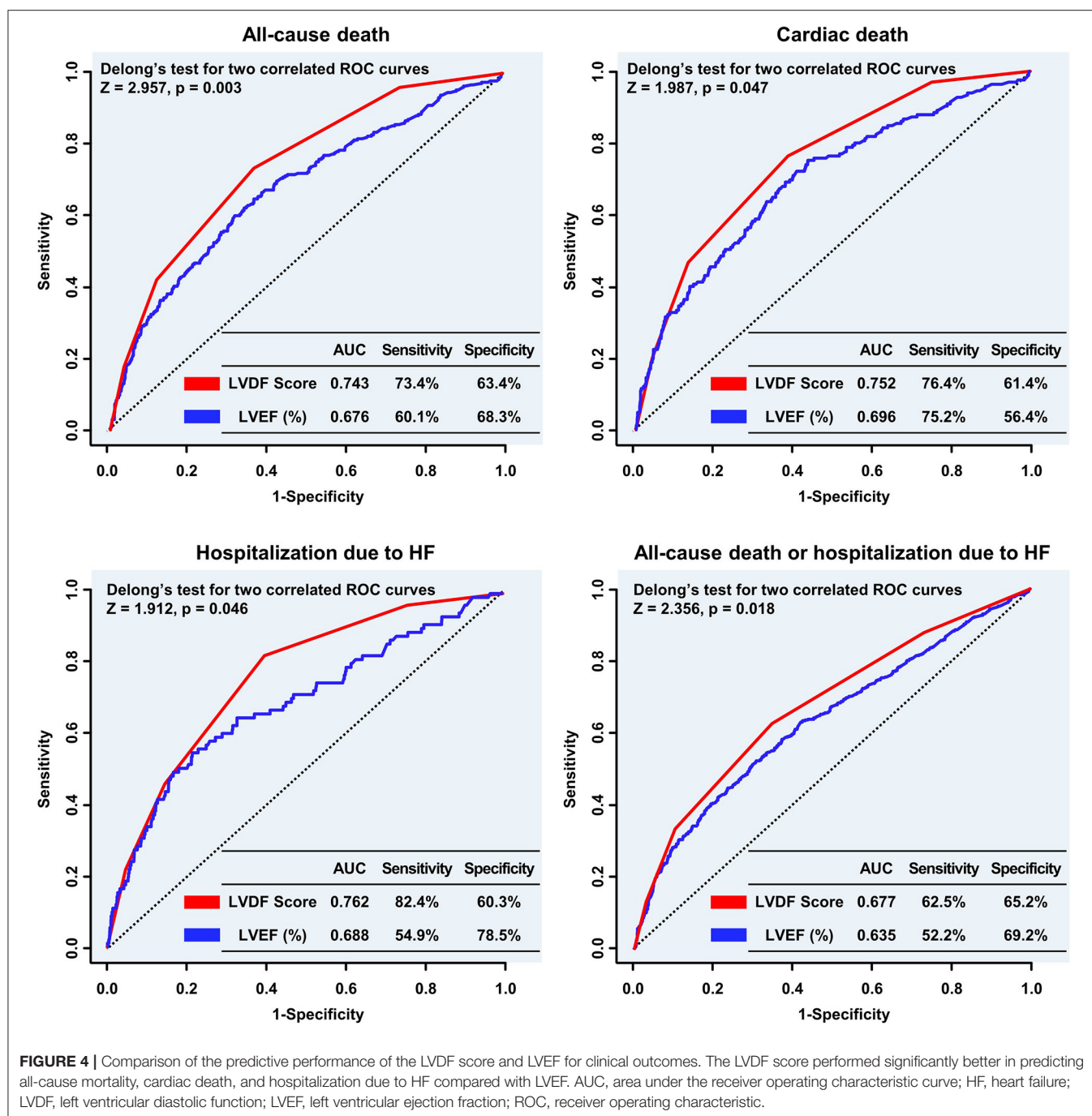
In landmark analysis, LVEF was the most predictive parameter for all-cause mortality within the first 30 days of follow-up (AUC: 0.801 vs. 0.704, $p = 0.045$), but between 30 days and 3 years of follow-up, the LVDF score was the better predictor (AUC: 0.739 vs. 0.640, $p < 0.001$) (**Figure 5**).

DISCUSSION

This study examined the construct validity of the unified LVDF algorithm, by demonstrating the ability of a simplified LVDF score to outperform LV systolic function in predicting long-term clinical outcomes in 2,030 patients with AMI. Patients with high LVDF scores had a significantly higher risk of all-cause mortality or readmission for recurrent HF than patients with low LVDF scores, which was consistently observed even after adjusting for baseline differences. The LVDF score performed significantly better in predicting all-cause mortality and readmission for recurrent HF compared with LVEF. Subgroup analysis showed that LVDF scores performed significantly better than LVEF in patients with STEMI, LVEF \geq 50%, Killip class < 3, abnormal LV geometry (LV remodeling or LVH), and non-RCA target vessels. In landmark analysis, LVDF scores were better in predicting all-cause mortality than LVEF in the long-term follow-up (30 days ~ 3 years).

Predicting Clinical Outcome Using the LVDF Score in Patients With Acute Myocardial Infarction

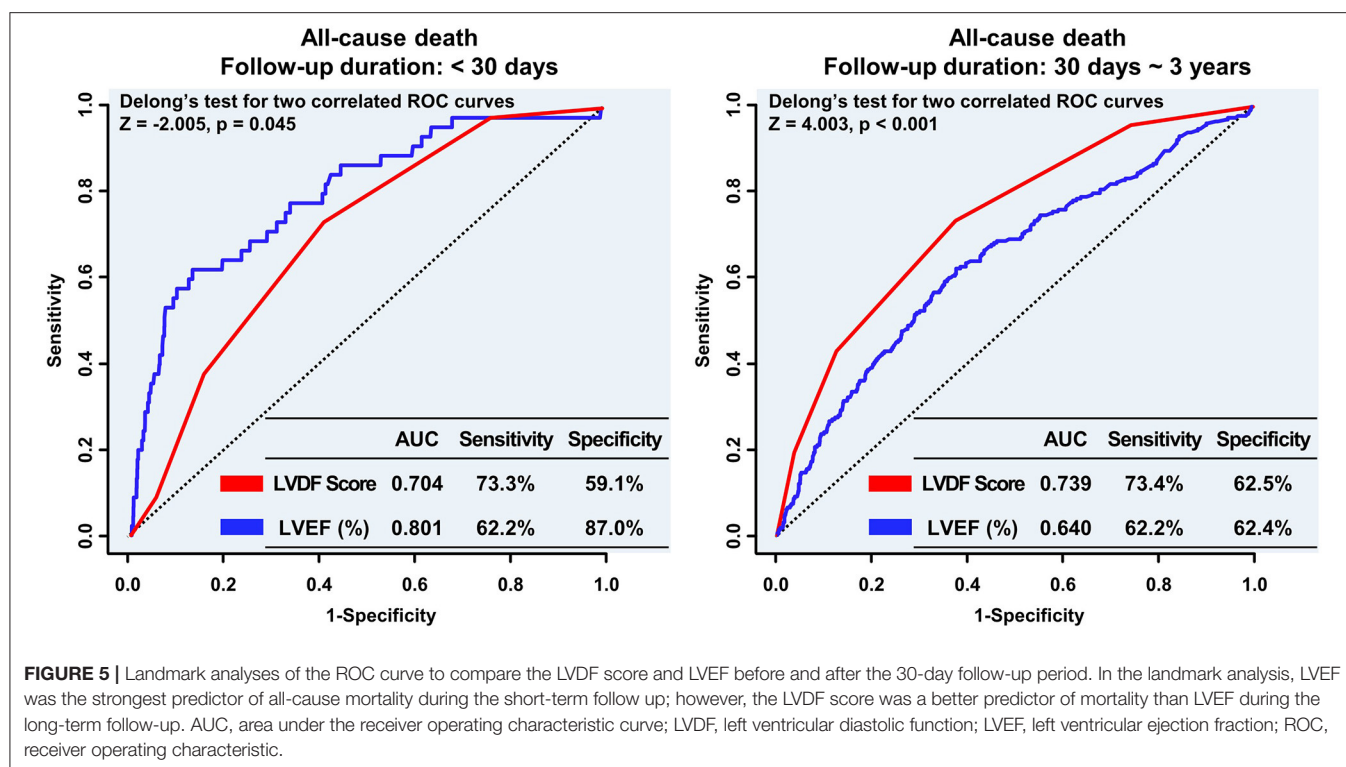
Previous studies have shown that in the 2016 ASE/EACVI guidelines, assessment of diastolic function was a strong independent predictor of outcomes for MI (15, 16). However, these studies excluded indeterminate variables and shock groups, had relatively smaller study subjects, and included limitations that were difficult to apply in a clinical setting. Contrastingly, the present study included patients with AMI with cardiogenic shock and indeterminate variables and found that the prognosis worsened as the LVDF score increased. Additionally, in the distribution of diastolic function, the most common in LVDF score 1 was septal e' < 7 cm/s. However, in LVDF score 2, the E/e' > 15 ratio increases, and thereafter, in LVDF score 3, the TR velocity > 2.8 m/s ratio increases. And among individual LVDF parameters, E/e' ratio and TR velocity were the best predictors of all-cause death and HHF. Therefore, clinical outcomes can be predicted simply by evaluating the LVDF scoring system, which is expected to be helpful in routine clinical practice for patients with AMI.



Comparison of LVDF Score to LVEF for Mortality Prediction

Prognosis of LV systolic dysfunction after AMI has been a major research focus for several decades (3). The insights from these studies have led to several therapeutic interventions that have improved outcomes. In addition to depressed systolic function, clinical and radiological evidence of HF is a consistent and powerful predictor of outcomes in patients with AMI (17). However, there have been no studies comparing mortality

between the two predictors, namely LV systolic function and current LVDF guidelines, in patients with AMI. In the present study, the LVDF score was found to be superior to LVEF in predicting mortality, especially in patients with AMI with STEMI, preserved LVEF ($\geq 50\%$), hemodynamic stable state (Killip class <3), abnormal LV geometry, and non-RCA target vessels. LVEF is a strong predictor for clinical outcomes; however, since each LVDF parameter, including septal e' , E/e' , TR velocity, and LAVI, is known as a strong independent prognostic factor in



HF and other diseases (18–21), the intersection of these four can be judged as a more powerful predictor for mortality. Especially, abnormal LV geometry (increased wall thickness and/or reduced end diastolic volume), which is a confounder for LVEF, makes it possible for LVEF to be unaltered despite significantly reduced LV function (22). In this study, as a result of analyzing the LV of patients with AMI, the normal LV geometry was less than half and the total LV mass index was $101.6 \pm 26.8 \text{ g/m}^2$, which was thicker compared with the LV wall of the normal population ($69.9 \pm 8.9 \text{ g/m}^2$) (23); thus, LVDF is considered to be a better predictor than LVEF.

The Importance of Evaluating LV Diastolic Function

There are prognostic reasons why LVDF evaluation is clinically important. From a diagnostic point of view, elevated LV filling pressure is an important cause of HF in patients with AMI (24). There are several studies focusing on optimal non-invasive assessment of left ventricular filling pressures that compared natriuretic peptide levels with Doppler against mean wedge pressure. Studies have shown that Doppler had a stronger correlation with mean wedge pressure, and the E/e' ratio tracked with changes in mean wedge pressure, whereas B-type natriuretic peptide levels did not (25). Similar results were seen in patients with ambulatory HF in which the E/e' ratio successfully tracked with changes in LA pressure (26). In this study, there was no significant difference in MAP in all groups ($p = 0.221$), but the LVDF score increased with the E/e' ratio ($p < 0.001$), leading to a decrease in coronary perfusion pressure, which is thought to be the cause of increased mortality and readmission for recurrent HF in the long term.

Interestingly, LVEF was superior to the LVDF score for predicting all-cause mortality during the short-term follow-up period (<30 days), but the LVDF score was superior to LVEF during the long-term follow-up (30 days ~ 3 years). As a consequence of AMI, the measurement of changes in LV size, shape, and the thickness of both infarcted and non-infarcted segments of the ventricle, collectively referred to as ventricular remodeling, is important in evaluating ventricular function and prognosis (27); however, several studies have shown that measurement of lesion size and left ventricular systolic function (28, 29) or alterations in post-infarction left ventricular remodeling (30) do not explain why patients with AMI have an increased tendency to develop long-term adverse outcomes. Therefore, in the acute stage, assessing prognosis based on LVEF is reasonable, and it is desirable to assess the prognosis using the LVDF score for patients undergoing long-term follow-up.

Study Limitations

This study had several limitations. First, despite its large sample size and granular data, this study had the potential for unmeasured confounders and lack of some data. Second, echocardiography-based estimates of hemodynamic measurements, such as the E/e' ratio, were used to measure LV filling pressures and TR velocity for pulmonary artery pressures, which are indirect measures. However, these correlate well with invasive measurements (31), and in clinical practice, diastolic function is evaluated mainly using echocardiography. Third, the 2016 ASE/EACVI guidelines recommended using the average of the lateral and septal velocities to measure LVDF, since these values are significantly different in certain situations such as left bundle branch block, regional wall motion abnormality, or significant right ventricular dysfunction, but only the septal e'

velocity was used. However, there is no evidence that the average e' velocity provides a more reliable assessment for diastolic function (7). Moreover, septal E/e' was found to be associated with a poor outcome in TOPCAT trial (32), whereas lateral E/e' did not differ between patients with heart failure with preserved ejection fraction who were and were not hospitalized in I-Preserve (33). In the present study, comparison of the predictive performance of the individual LVDF parameters showed that E/e' ratio was the best predictor of all-cause death and hospitalization due to HF (Supplementary Figure 4). Subgroup analysis was performed for factors that could affect septal e' (WMSI ≥ 2 , left bundle branch block or TDI RV $s' < 9.5$ cm/s) (Supplementary Figure 5). Therefore, consistent results were obtained.

CONCLUSION

The present study demonstrated that the LVDF score is a significant predictor of mortality and HHF in patients with AMI. The LVDF score can be useful in the risk stratification of patients with AMI; thus, careful monitoring and management should be provided to patients with AMI with higher LVDF scores.

DATA AVAILABILITY STATEMENT

The raw data supporting the conclusions of this article will be made available by the authors, without undue reservation.

REFERENCES

- Hillis GS, Møller JE, Pellikka PA, Gersh BJ, Wright RS, Ommen SR, et al. Noninvasive estimation of left ventricular filling pressure by E/e' is a powerful predictor of survival after acute myocardial infarction. *J Am Coll Cardiol*. (2004) 43:360–7. doi: 10.1016/j.jacc.2003.07.044
- Jons C, Joergensen RM, Hassager C, Gang UJ, Diken U, Johannesen A, et al. Diastolic dysfunction predicts new-onset atrial fibrillation and cardiovascular events in patients with acute myocardial infarction and depressed left ventricular systolic function: a CARISMA substudy. *Eur J Echocardiogr*. (2010) 11:602–7. doi: 10.1093/ejehocardiogr/jeq024
- Møller JE, Pellikka PA, Hillis GS, Oh JK. Prognostic importance of diastolic function and filling pressure in patients with acute myocardial infarction. *Circulation*. (2006) 114:438–44. doi: 10.1161/CIRCULATIONAHA.105.601005
- Nagueh SF, Appleton CP, Gillebert TC, Marino PN, Oh JK, Smiseth OA, et al. Recommendations for the evaluation of left ventricular diastolic function by echocardiography. *J Am Soc Echocardiogr*. (2009) 22:107–33. doi: 10.1016/j.echo.2008.11.023
- Nagueh SF, Smiseth OA, Appleton CP, Byrd BF 3rd, Dokainish H, Edvardsen T, et al. Recommendations for the evaluation of left ventricular diastolic function by echocardiography: an update from the American Society of Echocardiography and the European Association of Cardiovascular Imaging. *J Am Soc Echocardiogr*. (2016) 29:277–314. doi: 10.1016/j.echo.2016.01.011
- Nagueh SF. Left ventricular diastolic function: understanding pathophysiology, diagnosis, and prognosis with echocardiography. *JACC Cardiovasc Imaging*. (2020) 13(1 Pt 2):228–44. doi: 10.1016/j.jcmg.2018.10.038
- Oh JK, Miranda WR, Bird JG, Kane GC, Nagueh SF. The 2016 diastolic function guideline: is it already time to revisit or revise them? *JACC Cardiovasc Imaging*. (2020) 13(1 Pt 2):327–35. doi: 10.1016/j.jcmg.2019.12.004
- Almeida JG, Fontes-Carvalho R, Sampaio F, Ribeiro J, Bettencourt P, Flachskampf FA, et al. Impact of the 2016 ASE/EACVI recommendations on the prevalence of diastolic dysfunction in the general population. *Eur Heart J Cardiovasc Imaging*. (2018) 19:380–6. doi: 10.1093/ehjci/jex252
- Thygesen K, Alpert JS, Jaffe AS, Simoons ML, Chaitman BR, White HD, et al. Third universal definition of myocardial infarction. *Eur Heart J*. (2012) 33:2551–67. doi: 10.1093/eurheartj/ehs184
- Lang RM, Bierig M, Devereux RB, Flachskampf FA, Foster E, Pellikka PA, et al. Recommendations for chamber quantification: a report from the American Society of Echocardiography's Guidelines and Standards Committee and the Chamber Quantification Writing Group, developed in conjunction with the European Association of Echocardiography, a branch of the European Society of Cardiology. *J Am Soc Echocardiogr*. (2005) 18:1440–63. doi: 10.1016/j.echo.2005.10.005
- Lang RM, Badano LP, Mor-Avi V, Afilalo J, Armstrong A, Ernande L, et al. Recommendations for cardiac chamber quantification by echocardiography in adults: an update from the American Society of Echocardiography and the European Association of Cardiovascular Imaging. *J Am Soc Echocardiogr*. (2015) 28:1–39.e14. doi: 10.1016/j.echo.2014.10.003
- Lang RM, Bierig M, Devereux RB, Flachskampf FA, Foster E, Pellikka PA, et al. Recommendations for chamber quantification. *Eur J Echocardiogr*. (2006) 7:79–108. doi: 10.1016/j.euje.2005.12.014
- Garcia-Garcia HM, McFadden EP, Farb A, Mehran R, Stone GW, Spertus J, et al. Standardized end point definitions for coronary intervention trials: the Academic Research Consortium-2 Consensus Document. *Circulation*. (2018) 137:2635–50. doi: 10.1161/CIRCULATIONAHA.117.029289
- Daubert MA, White JA, Al-Khalidi HR, Velazquez EJ, Rao SV, Crowley AL, et al. Cardiac remodeling after large ST-elevation myocardial infarction in the current therapeutic era. *Am Heart J*. (2020) 223:87–97. doi: 10.1016/j.ahj.2020.02.017

ETHICS STATEMENT

The studies involving human participants were reviewed and approved by the study complies with the Declaration of Helsinki, and the Chonnam national university hospital institutional review board of the study center approved the study protocol (CNUH 05-49). The patients/participants provided their written informed consent to participate in this study.

AUTHOR CONTRIBUTIONS

SB performed the statistical analysis. SB and HY drafted the manuscript. KK, HK, HP, JC, MK, YK, YA, JC, and MJ reviewed/edited the manuscript and contributed to the interpretation of data. KK conceptualized the overall study design and supervised all aspects of the study and revised the manuscript critically. All authors have read and approved the manuscript.

FUNDING

This study was supported by a grant of Chonnam National University Hospital Biomedical Research Institute (BCRI19039).

SUPPLEMENTARY MATERIAL

The Supplementary Material for this article can be found online at: <https://www.frontiersin.org/articles/10.3389/fcvm.2021.730872/full#supplementary-material>

15. Prasad SB, Lin AK, Guppy-Coles KB, Stanton T, Krishnasamy R, Whalley GA, et al. Diastolic dysfunction assessed using contemporary guidelines and prognosis following myocardial infarction. *J Am Soc Echocardiogr.* (2018) 31:1127–36. doi: 10.1016/j.echo.2018.05.016
16. Prasad SB, Guppy-Coles KB, Holland D, Stanton T, Krishnasamy R, Whalley G, et al. Echocardiographic predictors of all-cause mortality in patients with left ventricular ejection fraction >35%: value of guideline based assessment of diastolic dysfunction. *Int J Cardiol Heart Vasc.* (2019) 24:100407. doi: 10.1016/j.ijcha.2019.100407
17. Killip T 3rd, Kimball JT. Treatment of myocardial infarction in a coronary care unit. A two year experience with 250 patients. *Am J Cardiol.* (1967) 20:457–64. doi: 10.1016/0002-9149(67)90023-9
18. Shah AM, Cikes M, Prasad N, Li G, Getchevski S, Claggett B, et al. Echocardiographic features of patients with heart failure and preserved left ventricular ejection fraction. *J Am Coll Cardiol.* (2019) 74:2858–73. doi: 10.1016/j.jacc.2019.09.063
19. Benfari G, Miller WL, Antoine C, Rossi A, Lin G, Oh JK, et al. Diastolic determinants of excess mortality in heart failure with reduced ejection fraction. *JACC Heart Fail.* (2019) 7:808–17. doi: 10.1016/j.jchf.2019.04.024
20. Tennøe AH, Murbræck K, Andreassen JC, Fretheim H, Garen T, Gude E, et al. Left ventricular diastolic dysfunction predicts mortality in patients with systemic sclerosis. *J Am Coll Cardiol.* (2018) 72:1804–13. doi: 10.1016/j.jacc.2018.07.068
21. Bae S, Kim KH, Yoon HJ, Kim HY, Park H, Cho JY, et al. Clinical impact of echocardiography-defined pulmonary hypertension on the clinical outcome in patients with multiple myeloma. *Medicine.* (2020) 99:e22952. doi: 10.1097/MD.00000000000022952
22. Stokke TM, Hasselberg NE, Smedsrud MK, Sarvari SI, Haugaa KH, Smiseth OA, et al. Geometry as a confounder when assessing ventricular systolic function: comparison between ejection fraction and strain. *J Am Coll Cardiol.* (2017) 70:942–54. doi: 10.1016/j.jacc.2017.06.046
23. Mizukoshi K, Takeuchi M, Nagata Y, Addetia K, Lang RM, Akashi YJ, et al. Normal values of left ventricular mass index assessed by transthoracic three-dimensional echocardiography. *J Am Soc Echocardiogr.* (2016) 29:51–61. doi: 10.1016/j.echo.2015.09.009
24. Somaratne JB, Whalley GA, Gamble GD, Doughty RN. Restrictive filling pattern is a powerful predictor of heart failure events postacute myocardial infarction and in established heart failure: a literature-based meta-analysis. *J Card Fail.* (2007) 13:346–52. doi: 10.1016/j.cardfail.2007.01.010
25. Dokainish H, Zoghbi WA, Lakkis NM, Al-Bakshy F, Dhir M, Quinones MA, et al. Optimal noninvasive assessment of left ventricular filling pressures: a comparison of tissue Doppler echocardiography and B-type natriuretic peptide in patients with pulmonary artery catheters. *Circulation.* (2004) 109:2432–9. doi: 10.1161/01.CIR.0000127882.58426.7A
26. Edelmann F, Wachter R, Schmidt AG, Kraigher-Krainer E, Colantonio C, Kamke W, et al. Effect of spironolactone on diastolic function and exercise capacity in patients with heart failure with preserved ejection fraction: the Aldo-DHF randomized controlled trial. *JAMA.* (2013) 309:781–91. doi: 10.1001/jama.2013.905
27. van der Laan AM, Nahrendorf M, Piek JJ. Healing and adverse remodelling after acute myocardial infarction: role of the cellular immune response. *Heart.* (2012) 98:1384–90. doi: 10.1136/heartjnl-2012-301623
28. Stone PH, Muller JE, Hartwell T, York BJ, Rutherford JD, Parker CB, et al. The effect of diabetes mellitus on prognosis and serial left ventricular function after acute myocardial infarction: contribution of both coronary disease and diastolic left ventricular dysfunction to the adverse prognosis. The MILIS Study Group. *J Am Coll Cardiol.* (1989) 14:49–57. doi: 10.1016/0735-1097(89)90053-3
29. Woodfield SL, Lundergan CF, Reiner JS, Greenhouse SW, Thompson MA, Rohrbeck SC, et al. Angiographic findings and outcome in diabetic patients treated with thrombolytic therapy for acute myocardial infarction: the GUSTO-I experience. *J Am Coll Cardiol.* (1996) 28:1661–9. doi: 10.1016/S0735-1097(96)00397-X
30. Solomon SD, St John Sutton M, Lamas GA, Plappert T, Rouleau JL, Skali H, et al. Ventricular remodeling does not accompany the development of heart failure in diabetic patients after myocardial infarction. *Circulation.* (2002) 106:1251–5. doi: 10.1161/01.CIR.0000032313.82552.E3
31. Kampaktsis PN, Kokkinidis DG, Wong SC, Vavuranakis M, Skubas NJ, Devereux RB. The role and clinical implications of diastolic dysfunction in aortic stenosis. *Heart.* (2017) 103:1481–7. doi: 10.1136/heartjnl-2017-311506
32. Shah AM, Claggett B, Sweitzer NK, Shah SJ, Anand IS, O'Meara E, et al. Cardiac structure and function and prognosis in heart failure with preserved ejection fraction: findings from the echocardiographic study of the Treatment of Preserved Cardiac Function Heart Failure with an Aldosterone Antagonist (TOPCAT) Trial. *Circ Heart Fail.* (2014) 7:740–51. doi: 10.1161/CIRCHEARTFAILURE.114.001583
33. Carson PE, Anand IS, Win S, Rector T, Haass M, Lopez-Sendon J, et al. The hospitalization burden and post-hospitalization mortality risk in heart failure with preserved ejection fraction: results from the I-PRESERVE trial (Irbesartan in Heart Failure and Preserved Ejection Fraction). *JACC Heart Fail.* (2015) 3:429–41. doi: 10.1016/j.jchf.2014.12.017

Conflict of Interest: The authors declare that the research was conducted in the absence of any commercial or financial relationships that could be construed as a potential conflict of interest.

Publisher's Note: All claims expressed in this article are solely those of the authors and do not necessarily represent those of their affiliated organizations, or those of the publisher, the editors and the reviewers. Any product that may be evaluated in this article, or claim that may be made by its manufacturer, is not guaranteed or endorsed by the publisher.

Copyright © 2021 Bae, Yoon, Kim, Kim, Park, Cho, Kim, Kim, Ahn, Cho and Jeong. This is an open-access article distributed under the terms of the Creative Commons Attribution License (CC BY). The use, distribution or reproduction in other forums is permitted, provided the original author(s) and the copyright owner(s) are credited and that the original publication in this journal is cited, in accordance with accepted academic practice. No use, distribution or reproduction is permitted which does not comply with these terms.



Research Progress of Imaging Methods for Detection of Microvascular Angina Pectoris in Diabetic Patients

Yiming Qi¹, Lihua Li², Guoquan Feng³, Chen Shao¹, Yue Cai¹ and Zhongqun Wang^{1*}

¹ Department of Cardiology, Affiliated Hospital of Jiangsu University, Zhenjiang, China, ² Department of Pathology, Affiliated Hospital of Jiangsu University, Zhenjiang, China, ³ Department of Radiology, Affiliated Hospital of Jiangsu University, Zhenjiang, China

OPEN ACCESS

Edited by:

Jinwei Tian,
The Second Affiliated Hospital of
Harbin Medical University, China

Reviewed by:

Fausto Rigo,
Hospital of Venice, Italy
Xiaodan Xia,
Guangzhou Medical University, China

*Correspondence:

Zhongqun Wang
wangtsmc@126.com

Specialty section:

This article was submitted to
Cardiovascular Imaging,
a section of the journal
Frontiers in Cardiovascular Medicine

Received: 24 May 2021

Accepted: 27 August 2021

Published: 21 September 2021

Citation:

Qi Y, Li L, Feng G, Shao C, Cai Y and
Wang Z (2021) Research Progress of
Imaging Methods for Detection of
Microvascular Angina Pectoris in
Diabetic Patients.
Front. Cardiovasc. Med. 8:713971.
doi: 10.3389/fcvm.2021.713971

Diabetes is a complex metabolic disease characterized by hyperglycemia. Its complications are various, often involving the heart, brain, kidney, and other essential organs. At present, the number of diabetic patients in the world is growing day by day. The cardiovascular disease caused by diabetes has dramatically affected the quality of life of diabetic patients. It is the leading cause of death of diabetic patients. Diabetic patients often suffer from microvascular angina pectoris without obstructive coronary artery disease. Still, there are typical ECG ischemia and angina pectoris, that is, chest pain and dyspnea under exercise. Unlike obstructive coronary diseases, nitrate does not affect chest pain caused by coronary microvascular angina in most cases. With the increasing emphasis on diabetic microvascular angina, the need for accurate diagnosis of the disease is also increasing. We can use SPECT, PET, CMR, MCE, and other methods to evaluate coronary microvascular function. SPECT is commonly used in clinical practice, and PET is considered the gold standard for non-invasive detection of myocardial blood flow. This article mainly introduces the research progress of these imaging methods in detecting microvascular angina in diabetic patients.

Keywords: microvascular angina, diabetes, diagnosis, imaging methods, research progress

INTRODUCTION

Diabetes is a complex metabolic disease characterized by hyperglycemia (1). It affects all organs of the body, and there are many kinds of complications. According to the World Health Organization, there are more than 100 kinds of complications in patients with diabetes, including vascular and non-vascular complications. Blood vessel complications can be divided into macrovascular and microvascular complications, and many diabetic patients have vascular complications in the early diagnosis of diabetes (2). Diabetic microvascular angina is a kind of microvascular disease caused by diabetes. Kemp (3) first described this syndrome with typical angina pectoris symptoms and myocardial ischemia, but with normal coronary angiography as “cardiac X syndrome.” Until 1985, Cannon called this disease coronary microvascular angina (CMVA). Although people have a deep understanding of the obstructive coronary disease, they lack understanding of non-obstructive angina caused by coronary microvascular dysfunction (CMVD). von Scholten et al. (4) showed that the incidence of CMVD in patients with type 2 diabetes was significantly higher than

that in people without diabetes. Diabetic patients have a higher risk of developing obstructive coronary artery disease (5), but coronary CMVD should not be ignored (6). The latter can lead to coronary microvascular angina pectoris, resulting in angina symptoms. Still, coronary angiography shows no apparent stenosis. The severity of this disease in women is higher than that in men, this may be related to female unique aldosterone hyperresponsiveness (7). CFR is a recognized index for evaluating CMVD. In addition, we can also use the index of microcirculatory resistance (IMR) to evaluate CMVD (8). More than 490,000 invasive coronary angiography (ICA) operations were performed in Japan, according to a 2019 JROAD report. However, the number of percutaneous coronary interventions was only 271,000 (9). This demonstrates that many invasive examinations are unnecessary, many patients do not have severe obstructive coronary disease. Therefore, we need to pay more attention to non-invasive ways. At present, the standard imaging diagnosis methods are SPECT, PET, CMR, and MCE. Accurate diagnosis of diabetic microvascular angina is of great help to the treatment and prognosis of patients.

DIABETIC MICROVASCULAR DYSFUNCTION

Coronary microcirculation determines 95% of the myocardial blood flow resistance, while the epicardial coronary artery only accounts for 5% (10). So microcirculation plays a significant role in regulating myocardial blood supply. Coronary microcirculation is composed of anterior arterioles, arterioles, and capillaries. It regulates capillaries' blood flow through specific mechanisms to meet the dynamic demand of myocardial blood supply (11), including the endothelium-dependent mechanism and endothelium-independent mechanism. When the body is suffering from diabetes, coronary microcirculation will be affected by a series of factors such as hyperglycemia, inflammatory reaction, cardiac autonomic nerve dysfunction, etc. It leads to myocardial ischemia, eventually CMVA.

Studies have shown that this injury is similar in patients with type 1 and type 2 diabetes, and chronic hyperglycemia is a crucial factor leading to CMVD (12). The main feature of CMVD in diabetic patients is endothelial dysfunction, which leads to the impairment of endothelial-dependent mechanisms. In some cases, endothelial-independent mechanisms may also be affected as well (13). In people with diabetes, microcirculation first occurs functional changes, then structural changes (14). These functional changes include endothelial dysfunction, autonomic nerve dysfunction, etc. Structural changes include thickening of the arterial wall, capillary basement membrane, formation of deposits in the small artery wall, and small coronary artery wall fibrosis. Recently, some scholars suggested that (15) endothelial dysfunction is related to the down-regulation of MCT4. Hyperglycemia and inflammatory factors can downregulate the expression of MCT4. This results in lactic acid transport disorder and intracellular pH imbalance, eventually leading to endothelial cell apoptosis and endothelial dysfunction.

The incidence of CMVA is high, but because there is no imaging performance of obstructive coronary disease, it is easy to cause misdiagnosis and missed diagnosis, which has seriously affected people's lives. The COVADIS conducted multinational, multiracial, and multicenter prospective observational studies in 14 research centers in 4 continents, 7 countries to explore the clinical characteristics and prognosis of patients with MVA and the impact of gender and race on patients CMVA (16). From June 2015 to December 2018, the study prospectively included 688 MVA patients, with all patients not receiving trial treatment during the observation phase. The results showed that MVA patients had a high risk of MACE regardless of gender and race, with an average MACE rate of 7.7% years. However, Caucasian whites were significantly higher than Asian populations and were associated with hypertension and previous coronary heart disease, with poor quality of life in women compared to men.

To better develop treatment strategies, CMVD can be divided into four different types. Ca Mici and Filippo (17) divided coronary microvascular dysfunction into four types: type I: CMVD without myocardial disease and coronary stenosis; type II: CMVD caused by myocardial disease; type III: coronary artery occlusion combined with CMVD; type IV: iatrogenic CMVD. In patients with diabetes, due to some unique pathophysiological mechanisms, Type I and type III CMVD are most likely to occur, and type I CMVD is the earliest in patients with diabetes (13).

DIAGNOSIS OF CMVA

At present, the diagnostic criteria of CMVA are proposed by COVADIS, including the following four items: (1) The presence of symptoms indicating myocardial ischemia; (2) There was objective evidence of myocardial ischemia; (3) No obstructive coronary disease; (4) Evidence of coronary microvascular dysfunction. When the four conditions are met, coronary microvascular angina can be diagnosed; when there are standards 1 and 3, but standards 2 and 4 have only one item, It can only be diagnosed as suspected coronary microvascular angina (18).

Because the current technology does not allow us to observe coronary microcirculation directly (19), we can only indirectly evaluate the microcirculation function through some methods to obtain evidence of myocardial ischemia. Myocardial ischemia can be caused by epicardial coronary artery occlusion or CMVD. When both of them have dysfunction, it can also cause myocardial ischemia (20).

Coronary flow reserve (CFR) is a recognized index to evaluate coronary blood flow. Gould KL first proposed CFR in 1974. It refers to the ratio of mean blood flow in the congestive phase to mean blood flow at rest after the application of vasodilator. The normal value of CFR is between 2 and 2.5 (21). The coronary microvascular disease can cause a decrease in CFR (≤ 2). CFR is determined by both large and microvessels of the coronary artery. Therefore, the reduction is caused by CMVD when CAD is excluded. Some studies have shown that the causes of CFR decrease in patients with diabetes are different in different periods. In patients with early diabetes, the reduction of CFR is mainly caused by increased baseline blood flow velocity.

In contrast, the decrease of CFR in patients with advanced diabetes mellitus is mainly caused by decreased blood flow velocity during hyperemia (22). It is crucial to determine CFR in diabetic patients. Even in patients with diabetes without known CAD, their Cardiac Mortality is comparable to non-diabetic patients with known CAD if CFR is impaired (23). At present, CFR can be measured by both invasive and non-invasive methods. The former is mainly coronary Doppler flow guide wire, while the latter includes SPECT, CMR, and PET explicitly. MCE has also been proved to be able to evaluate coronary microcirculation (24).

TIMI myocardial imaging grading can also evaluate coronary microcirculation. Its principle is to analyze the time required for contrast agents to enter myocardial tissue, divided into 0–3 grades (25). TIMI can be used as a semi-quantitative index to reflect the perfusion state of coronary microcirculation. However, TIMI grading is limited by observer variability. Studies have shown that (26) when measured by two independent laboratories, the coincidence rate of TIMI assessment is only 83%. When the results of the third laboratory exist, the coincidence rate further decreases. When the TFC of the left anterior descending artery was modified with 1.7, we can obtain corrected TIMI classification (CTFC). Compared with TIMI flow classification, CTFC is more objective and repeatable. It can evaluate microvascular dysfunction in patients with microvascular angina pectoris. Ding et al. (27) proposed a new index TMP frame counting (TMP-FC) based on TIMI, myocardial angiography was quantified by frame counting. Ge et al. (28) suggested that $\text{TMP-FC} \geq 95.5$ was an independent predictor of MVD ($\text{OR} = 11.61$, $P < 0.001$). Moreover, the sensitivity and negative predictive value of TMP-FC in the diagnosis of CMVD were significantly improved. TMP-FC was directly proportional to the degree of CMVD progression, so that it can present disease progression.

RESEARCH PROGRESS OF IMAGING METHODS FOR DETECTION OF MICROVASCULAR ANGINA PECTORIS

Single-Photon Emission Computed Tomography

SPECT usually uses thallium-201 (^{201}Tl) or technetium-99m ($^{99\text{m}}\text{Tc}$) labeled tracers (29) to record the radioactivity of the myocardium under resting and loading conditions. According to the phenomena of myocardial perfusion decrease and defect in the two states, we can diagnose CMVD after eliminating the epicardial coronary artery stenosis. The advantage of SPECT in diagnosing CMVD is its higher sensitivity. Compared with PET, SPECT is cheaper (30), so it is more frequently-used in the clinic.

In recent years, solid-state detector technology based on cadmium-zinc telluride (CZT) has become a hot spot in SPECT development. Recently, the CZT-SPCET has achieved a commodified supply. Two cardiac-centered CZT cameras are available commercially-Discovery NM530c and D-SPECT. CZT-SPECT has gradually expanded the scope of clinical applications due to the technical advantages. The traditional anger camera is limited by low photon sensitivity and low inherent spatial

resolution and needs a high radioisotope dose to ensure image quality. CZT-SPECT uses a semiconductor solid-state detector, directly converting gamma rays into electrical signals at room temperature (31). CZT crystal has higher photon sensitivity and higher energy resolution, so using a lower dose of radioactive tracer can also ensure image quality (32). The research of Duvall et al. (33) shows that the new single-photon emission tomography CZT camera technology can significantly reduce the radiation exposure and acquisition time on the premise of ensuring the imaging quality. CZT-SPECT can also lessen the injection dose of examiners. Nakazato et al. (34) applied CZT detector SPECT-MPI to 79 patients with the guarantee of image quality. When the acquisition time of the experimental group was 14 min, the average injection dose of the experimental group could be reduced to 92.5 MBq (2.5mCi). This is beneficial for protecting patients' health and improving the working efficiency of hospitals.

Due to the technical limitations, the standard semi-quantitative evaluation of myocardial perfusion cannot assess subtle changes in myocardial blood flow (MBF) regulation. The MPR obtained by CZT-SPECT can help to overcome the limitations of semi-quantitative MPI. CZT detector allows dynamic acquisition and quantification of MBF, Konstantin et al. (35) compared the ability of invasive coronary angiography and dynamic CZT-SPECT to assess myocardial blood flow. They found that CFR obtained by dynamic CZT-SPECT is consistent with CFR obtained by the invasive method. Acampa et al. (36) compared the ability of CZT-SPECT and PET imaging to evaluate myocardial absolute blood flow and blood flow reserve. It is found that there is a significant correlation between the latter and positron emission tomography. Therefore, CZT-SPECT can provide a more accurate myocardial blood flow. Because it can adopt a semi-automatic method, CZT-SPECT reduces the errors caused by operators and improves the accuracy and repeatability of diagnosis (37).

Interestingly, the advent of the CZT camera made the Simultaneous dual isotope $^{201}\text{Tl}/^{99\text{m}}\text{Tc}$ myocardial perfusion imaging possible. ^{201}Tl is more linearly related to myocardial blood flow leading to an accurate identification of mild-ischemia. $^{99\text{m}}\text{Tc}$ labeled tracers have nearly ideal physical imaging properties for gamma cameras, so it has a better imaging quality (38). However, it was found in Bernard Songy's studies that defect size in 20% of patients would be underestimated. This is mainly due to the lack of good scattering correction methods (39). But this at least proves that the goal is not out of reach. Moreover, with the appearance of the CZT camera, it is possible to reuse an old tracer, $^{99\text{m}}\text{Tc}$ -Teboroxime, which has a high extraction rate in a wide range of coronary blood flow rates and is seldom used because of its short half-life. However, it may show unique advantages in clinics with the progress of technology (40).

The image reconstruction of dynamic SPECT is complicated. Because the camera rotates slowly, the dynamic data must be reconstructed from the projection, and the attenuation should be corrected appropriately. Therefore, Debasis Mitra developed a Spline Initialized Factor Analysis of Dynamic Structures (SIFADS) algorithm (41), which performed well in animal and human experiments and significantly reduced image noise and

improved image quality. In addition, deep learning technology is developing rapidly and shows excellent potential in image acquisition and processing, which may be widely used in the future (42).

Positron Emission Computed Tomography

PET is considered the gold standard for the non-invasive detection of myocardial blood flow (43). PET myocardial perfusion imaging (MPI) is a powerful tool for diagnosing coronary artery disease (44), which is widely used to detect cardiovascular function. Compared with SPECT-MPI, PET-MPI has higher sensitivity and specificity, can quantify myocardial blood flow more accurately (45), and provides higher quality images (46). Nevertheless, at the same time, it also has a higher inspection cost. The basic principle of PET-MPI is to dynamically analyze the signal of radionuclide tracer injected into a human body. If microcirculation disturbance occurs, it will show the perfusion defect at the corresponding position. At present, the commonly used tracers are mainly $^{15}\text{O-H}_2\text{O}$, $^{13}\text{N-NH}_3$, and $^{82}\text{Rb-RbCl}$. CFR can be obtained by detecting tracer signals at rest and under stress, respectively. If CFR decreases after eliminating obstructive coronary disease, CMVD is indicated.

Wanli et al. (47) evaluated the value of $^{13}\text{N-NH}_3$ PET-MPI in the diagnosis of microvascular diseases. They found that the MBF of diabetic patients was lower than that of non-diabetic patients [(2.63 ± 0.98) and (3.62 ± 1.28) ml·min⁻¹·g⁻¹; $t = -2.758$, $P = 0.008$], and diabetes may be a risk factor for the decrease of MBF (OR = 0.254, 95% CI: 0.073–0.887), so diabetes is closely related to the occurrence of coronary microvascular disease. Studies have shown that PET-derived MBF and CFR are powerful tools for predicting future major adverse cardiac events. For example, a CFR decrease (<1.6) on ^{13}N -ammonia PET and ^{82}Rb PET is an independent factor to predict MACE and early revascularization (48). We know that CFR in diabetic patients is closely related to cardiac death. PET is the gold standard for quantitative myocardial blood flow, so the use of PET is of great clinical significance for the accurate quantification of myocardial blood flow in diabetic patients.

It should be noted that the half-life of tracers used at present is very short, which requires hospitals to have cyclotrons to make tracers, which further increases the detection cost and has higher requirements for hospitals (49). PET tracer should have the characteristics of high specificity to molecular targets, high metabolic stability, high affinity to target tissues, low cost, and good safety (50). The new generation tracer ^{18}F -flurpiridaz has a long half-life (110 min), low cost, and good imaging quality. Although it is still in the clinical trial stage, it has shown excellent performance (51). Compared with other PET radionuclides, ^{18}F has the shortest positron range in tissues (52). It improves spatial resolution and may be widely used in microvascular imaging in the future. ^{18}F -labeled ^{18}F -FDG is a radiolabeled glucose analog. As with glucose, ^{18}F -FDG passes into the cells through a glucose transport mechanism. However, ^{18}F -FDG cannot participate in glycolysis and cannot be metabolized and excreted from cells. Ischemic sites can be imaging by using differences in ^{18}F -FDG absorption in normal and ischemic myocardium (53). Because the glucose metabolism of cardiac muscle cells varies

greatly in different physiological situations, strict control of the metabolic environment is required to accurately diagnose myocardial ischemia (54). In any case, the application of ^{18}F -FDG contributes to the diagnosis of microvascular angina.

The unique feature of detecting microcirculation using PET is that PET obtains information on the molecular level (55). It can reflect the degree of damage to myocardial cells. For instance, [^{18}F]FEDAC is commonly used in non-invasive visualization of neuroinflammation, inflammation of the lung, acute liver injury, and liver fibrosis (56), but recent studies have found that [^{18}F] FEDAC also has good results in assessing the myocardial ischemic injury. Myocardial ischemia leads to myocardial cell mitochondrial dysfunction, then downregulation of translocator protein TSPO expression. Luo et al. (57) synthesized an ^{18}F -labeled PET probe, N-benzyl-N-methyl-2-[7,8-dihydro-7-(2-[^{18}F]fluoroethyl)-8-oxo-2-phenyl-9Hpurin-9-yl]acetamide ([^{18}F]FEDAC), with a high binding affinity for TSPO. They injected FEDAC into two groups of mice and analyzed the differences in TSPO expression using PET. Ischemic tissue uptake decreased, with normal-to-ischemic uptake ratios of 10.47 ± 3.03 (1.5 min) and 3.92 ± 1.12 (27.5 min) ($P = 0.025$). The reduction in [^{18}F] FEDAC uptake in the PET image is consistent with the observed histopathological features. This suggests that this technique has good specificity and sensitivity in assessing the ischemic distribution, but more research should be needed to verify this technique.

However, the shortcomings of PET myocardial perfusion imaging in detecting coronary microvascular angina pectoris are that its spatial resolution is relatively low (58). The tracer used will inevitably cause radiation to patients. Compared with two-dimensional PET, the new high-sensitivity 3D positron emission tomography scanner adopts a three-dimensional acquisition method with a small radiation dose, which shows promising results in the experiment. It may diagnose CMVA more accurately (59).

Cardiac Magnetic Resonance Imaging

Compared with radioactive tracer imaging, MRI has higher spatial resolution and temporal resolution (60), has the characteristics of no ionizing radiation, multi-parameter imaging, and good imaging of soft tissue, and is a powerful tool for clinical diagnosis of coronary artery diseases (61). After injection of contrast media, the signal intensity in areas with good coronary microcirculation increased uniformly, while in areas with myocardial ischemia, the signal intensity increased slowly. The MBF at rest and filling state can be obtained by analyzing the signal intensity by computer. Then CFR can be calculated. The research results of Raksha Indorkar (62) show that CFR derived from CMR is an independent predictor of major adverse cardiovascular events (MACE). CMR can observe coronary microcirculation in a non-quantitative or quantitative way. Quantitative CMR can accurately detect coronary microvascular dysfunction. This point has been confirmed by Zorach et al. (63). In addition, CMR is sensitive to early coronary microvascular lesions. Levelt et al. (64) performed adenosine stress and resting T1 mapping on 31 T2DM patients and 16 healthy controls. All patients were excluded from the obstructive coronary heart

disease. They found that the myocardial perfusion reserve index (MPRI) of T2DM patients was lower than that of the control group (1.60 ± 0.44 vs. 2.01 ± 0.42 , $P = 0.008$). During adenosine stress, patients with T2DM showed decreased non-contrast T1 response to relative stress vs. control group. So CMR can detect subclinical coronary microvascular dysfunction without gadolinium contrast agent injection. Studies suggest that CMR has a high application value in practice because the quantification of adenosine stress T1 CMR can accurately distinguish obstructive epicardial CAD from microvascular dysfunction without using contrast media (65).

Recently, in the diagnosis of microvascular diseases, Chatzantonis et al. (66, 67) introduced a new cardiovascular magnetic resonance (CMVD) parameter named “myocardial transit-time” (MyoTT), which is defined as the blood circulation time from the orifice of the coronary artery to the collection of the coronary sinus. MyoTT reflects the transmission time of gadolinium in myocardial microvascular. Therefore, it can be used for the diagnosis of CMVD. Compared with CFR, MyoTT has the advantages of not prolonging the examination time of patients, being easy to operate. It considers the heterogeneity of microvascular’s functional lesions and can quickly evaluate the overall pathological changes of myocardial infarction microvasculature. However, due to the lack of research on MyoTT, it is necessary to evaluate its diagnostic performance in the future further.

Though little research has been done using perfusion CMR, recent studies have shown that MPRI derived from CMR, expressed as the hyperemic-to-resting myocardial perfusion ratio, can evaluate the prognosis of patients. In a retrospective study of 218 patients by Zhou et al. (68), 91% of the patients had an MPRI value of <2.0 . During the 5.5-year follow-up, 34 MACEs occurred, an MPRI cut-off value of <1.47 was identified as the optimal prognostic threshold for predicting MACE.

Patients with cardiac electronic implant devices undergoing CMR may develop arrhythmia or even cardiac arrest. This is a major safety issue for CMR testing. Canadian Heart Rhythm Society and Canadian Association of Radiologists has detailed the precautions and taboos of CMR checks in the statement (69). With these electronic implantable devices being upgraded, their compatibility with CMR is also improved. As long as the manufacturer’s agreement is strictly followed and supervision is done during the inspection, the inspection can be implemented. Another safety issue is that some patients are allergic to agents, but this can be solved by taking a skin test before injection or through drug replacement.

In addition, compared with 1.5T semi-quantitative CMR, 3T high-resolution CMR can identify CMVD with high precision. It shows better diagnosis performance in experiments (70) and improves the image signal-to-noise ratio (71). With the development of technology, high-resolution CMR will hopefully be widely used in the clinical diagnosis of CMVD in the future. At present, the disadvantage of magnetic resonance is the inability to provide examinations for patients with metal implants, high prices and long imaging time. So CMR equipment’s development direction in the future is to solve the

compatibility between metal implants and CMR, reduce the detection cost and time, and find simpler and feasible parameters to diagnose CMVD.

Myocardial Contrast Echocardiography

The appearance of an acoustic contrast agent makes it possible to evaluate cardiac microcirculation by ultrasound. These contrast agents are composed of microbubbles similar to red blood cells. They can freely pass through the pulmonary circulation after entering the human body and enter the coronary microvasculature. In the myocardium with good coronary microvasculature, microbubbles can flow normally. Then imaging can be obtained through the scattering effect of microbubbles. However, images of abnormal myocardium are different from normal.

MCE uses microbubbles as contrast agents, so selecting suitable microfoam materials impacts diagnostic efficacy significantly. Xu et al. (72) designed platelet membrane-coated particles with a porous polylactic-co-glycolic acid (PLGA) core coated with a platelet membrane shell, platelet membrane can bind to myocardial ischemia-reperfusion areas. Injury areas of the mouse cardiac muscle were evaluated using ultrasound. They found a significantly increased signal strength in the risk area, a technique that may contribute to the diagnosis of early myocardial injury. Current ultrasonic microbubbles are used in various materials, but people mostly make improvements around the stability and toxicity of microbubbles, so it is necessary to find microbubble materials targeted to myocardial ischemia.

For a long time, the accuracy of CMVD detection by MCE has been controversial (73). In fact, its reliability and accuracy have been confirmed, and its diagnostic performance is comparable to that of positron emission tomography, but it lacks the approval of relevant regulatory authorities (74). Yang et al. (75) performed quantitative MCE of adenosine triphosphate (ATP) stress on 227 patients with chest pain and no obvious coronary artery stenosis ($<50\%$) to evaluate CFR. They found that diabetic patients have a higher possibility of cardiovascular adverse events and considered that quantitative MCE of ATP stress could be used to evaluate coronary artery microcirculation. CFR obtained by ultrasound has assignable significance for the prediction of adverse events. Cortigiani et al. (76) administered Dipyridamole Stress Echocardiography in 1,130 patients (including 341 diabetic and 789 non-diabetic patients) and assessed their left anterior descending CFR. They found the annual event rate in the diabetic and non-diabetic patients was 9.3 and 5.1%, respectively. Patients with abnormal CFR significantly increased event rates over patients with normal CFR ($p < 0.0001$). This fully affirms the prognostic value of ultrasound in patients with diabetes.

Ultrasound may have a unique therapeutic function due to its biological effects. Moccetti et al. (77) found that the cavitation effect produced by ultrasound microbubbles can make myocardial microcirculation release ATP and increase microcirculation blood flow. In primates, blood flow increases up to double. Given the portability of the ultrasound device, it is possible to use it to control the area of myocardial infarction. In addition, we can use microbubbles to transport some drugs and promote their absorption. Acidic fibroblast growth factor

TABLE 1 | Comparison and progress of various equipment for the diagnosis of myocardial ischemia (87).

Device	Accuracy	Practicability	Developments
SPECT	Common	Good	CZT camera improves imaging quality and reduce radiation The new algorithm SIFADS can improve image quality
PET	Good	Common	A new generation of tracer ^{18}F -flurpiridaz is promising to be widely used in clinics [^{18}F]FEDAC reflects the damage degree of cells
CMR	Good	Good	New parameter MyoTT increases the value of CMR 3T High Resolution CMR may be widely used in clinic
MCE	Bad	Common	Microbubbles can combine targeted drugs to improve microvascular function
CCTA	Common	Common	DTI and EAT _{thickness} increase the value of CCTA in the diagnosis of coronary microvascular disease

(FGF1) can resist oxidative damage, induce endothelial smooth muscle cell proliferation and promote angiogenesis. Lei Zheng et al. (78) delivered FGF1 to the myocardium of diabetic rats by using FGF1-loaded nanoliposomes combined with ultrasonic targeted microbubble destruction. Cavitation and mechanical effect produced by microbubble destruction can promote drug absorption, and improve myocardial microcirculation. This achieves good results in preventing diabetic cardiomyopathy. The limitation of MCE in evaluating coronary microvascular function is that its accuracy is interfered with by many factors, such as the technical level of operators and patient's situation (79). In a word, MCE is a potential technology with advantages of low cost, simple operation, and no ionizing radiation, these makes it play a unique role in the preliminary screening of coronary microvascular angina pectoris.

Coronary Computed Tomography Angiography

Coronary computed tomography angiography (CCTA) is a reliable method for clinical coronary stenosis (80). However, the diagnosis effect of coronary microvascular abnormality is not good (81). What is essential is that CT can implement the “one-stop-shop” imaging of INOCA (82). The vascular functional information provided by Dynamic CT-MPI is combined with the vascular anatomical information provided by CCTA, which is beneficial for detecting the function of microvessels and the identification of sizeable vascular obstruction. Yu et al. (83) also found that the MBF measured by CT-MPI was associated with the heart rate, when the heart rate increment is >20 , the MBF will increase dramatically. Therefore, the effect of the heart rate also needs to be considered when referring to the MBF.

Intracavity attenuation gradient (TAG) is a new CT parameter, which is defined as the linear regression coefficient between

TABLE 2 | Characteristics of various imaging methods for microvascular angina.

Device	Advantages	Disadvantages
SPECT	Low costs Good practicability	Low sensitivity and specificity Radiation exposure
PET	Accurate quantification of MBF Molecular-level research	High costs Radiation exposure Higher requirements for hospital
CMR	No radiation exposure Sensitive to subtle changes Assessment without contrast agents	High costs Limited by metal implants Time consuming
MCE	Low costs, Suitable for screening Biological effect	Bad reliability
CCTA	Assessment of epicardial vessels and microvascular	Insensitive to microvascular disease Radiation exposure

the attenuation of intracavity contrast agent and axial distance (84). Recently, based on the attenuation gradient (TAG), Kojima et al. (85) put forward a new diagnostic index, the Dynamic TAG Index (DTI), which overcomes the disadvantage that TAG is easily affected by other non-ischemic factors. When there is coronary ischemia, DTI will obviously increase. So DTI increases the value of CCTA in diagnosing functional coronary diseases. The result shows that DTI combined with CCTA has good consistency with PET-MPI and shows comparable performance. However, there are few samples in this study, and it needs to be verified in a giant sample experiment. In addition, Alam et al. (86) found that the increased epicardial adipose tissue (EAT) measured by CT was significantly correlated with MFR. It was proposed that the cut-off value of EAT_{thickness} >5.6 mm was the best value for detecting abnormal coronary microvascular function. This may provide a new reference direction for the examination of coronary microvascular function.

Comparison of microvascular angina pectoris detected by various imaging methods (Tables 1, 2)

CONCLUSION

The cardiovascular complications are prevalent in diabetic patients., And a large proportion of patients have vascular diseases in the early stage of diabetes. Rapid and accurate diagnosis of CMVA can help patients' treatment strategies. Imaging equipment such as SPECT, PET, CMR, and MCE have played an essential role in the non-invasive evaluation of CMVA. Non-invasive methods are more acceptable to patients than invasive methods and can reduce unnecessary waste of resources. Simultaneously, the use of cheap screening techniques also contributes to early intervention in asymptomatic patients. With the development of science and technology, the reliability of these methods will be continuously improved. The emergence of new technologies and new parameters will enable them to

provide a better basis for the diagnosis of CMVA. Despite the relevant advantages of non-invasive techniques, we should recognize some limitations. Vasodilators used in non-invasive techniques only evaluate their own ability to dilate blood vessels. Also, obstructive CAD must be excluded before the diagnosis of CMVD. Given the high incidence of obstructive angina pectoris in diabetic patients, it is more realistic to choose appropriate imaging methods to distinguish obstructive angina pectoris from CMVD. It can also reduce the economic burden on patients. With the continuous development of medical imaging, we must look for high-sensitivity detection measures for early detection and intervention to reduce cardiovascular events in diabetic patients.

REFERENCES

- Kibel A, Selthofer-Relatic K, Drenjancevic I, Bacun T, Bosnjak I, Kibel D, et al. Coronary microvascular dysfunction in diabetes mellitus. *J Int Med Res.* (2017) 45:1901–29. doi: 10.1177/0300060516675504
- An J, Nichols GA, Qian L, Munis MA, Harrison TN, Li Z, et al. Prevalence and incidence of microvascular and macrovascular complications over 15 years among patients with incident type 2 diabetes. *BMJ Open Diabetes Res Care.* (2021) 9:1–10. doi: 10.1136/bmjdr-2020-001847
- Kemp HG. Left ventricular function in patients with the anginal syndrome and normal coronary arteriograms. *Am J Cardiol.* (1973) 32:375–6. doi: 10.1016/S0002-9149(73)80150-X
- von Scholten BJ, Hasbak P, Christensen TE, Ghotbi AA, Kjaer A, Rossing P, et al. Cardiac 82Rb PET/CT for fast and non-invasive assessment of microvascular function and structure in asymptomatic patients with type 2 diabetes. *Diabetologia.* (2016) 59:371–8. doi: 10.1007/s00125-015-3799-x
- Naito R. Coronary artery disease in type 2 diabetes mellitus: recent treatment strategies and future perspectives. *World J Cardiol.* (2015) 7:119. doi: 10.4330/wjc.v7.i3.119
- Sorop O, van den Heuvel M, van Ditzhuijzen NS, de Beer VJ, Heinonen I, van Duin RWB, et al. Coronary microvascular dysfunction after long-term diabetes and hypercholesterolemia. *Am J Physiol Heart Circ Physiol.* (2016) 311:H1339–51. doi: 10.1152/ajpheart.00458.2015
- Haas AV, Rosner BA, Kwong RY, Rao AD, Garg R, Di Carli MF, et al. Sex differences in coronary microvascular function in individuals with type 2 diabetes. *Diabetes.* (2019) 68:631–6. doi: 10.2337/db18-0650
- Sattar A, Mondragon J, Clegg S, Sheldon M, Ahmed B. Prevalence and predictors of coronary microvascular dysfunction among patients with ischemia and non-obstructive CAD. *J Am Coll Cardiol.* (2016) 67:268. doi: 10.1016/S0735-1097(16)30269-8
- Sakuma H, Ishida M. Advances in myocardial perfusion MR imaging: physiological implications, the importance of quantitative analysis, and impact on patient care in coronary artery disease. *Magn Reson Med Sci.* (2021). doi: 10.2463/mrms.rev.2021-0033. [Epub ahead of print].
- Baumgart D, Haude M, Liu F, Ge J, Goerge G, Erbel R, et al. Current concepts of coronary flow reserve for clinical decision making during cardiac catheterization. *Interv Cardiol.* (1998) 136:136–49. doi: 10.1016/S0002-8703(98)70194-2
- Taqeti VR, Carli M. Coronary microvascular disease pathogenic mechanisms and therapeutic options. *J Am Coll Cardiol.* (2018) 72:2625–41. doi: 10.1016/j.jacc.2018.09.042
- Di Carli MF, Janisse J, Grunberger G, Ager J. Role of chronic hyperglycemia in the pathogenesis of coronary microvascular dysfunction in diabetes. *J Am Coll Cardiol.* (2003) 41:1387–93. doi: 10.1016/S0735-1097(03)00166-9
- Teclazich F. Microvascular Disease in Diabetes. Hoboken, NJ: Wiley-Blackwell (2020). 258 pp.
- Picchi A. Coronary microvascular dysfunction in diabetes mellitus: a review. *World J Cardiol.* (2010) 2:377. doi: 10.4330/wjc.v2.i11.377
- Luo E, Wang D, Yan G, Qiao Y, Tang C. The NF- κ B/miR-425-5p/MCT4 axis: a novel insight into diabetes-induced endothelial dysfunction. *Mol Cell Endocrinol.* (2019) 500:110641. doi: 10.1016/j.mce.2019.110641
- Shimokawa H, Suda A, Takahashi J, Berry C, Camici PG, Crea F, et al. Clinical characteristics and prognosis of patients with microvascular angina: an international and prospective cohort study by the coronary vasomotor disorders international study (COVADIS) group. *Eur Heart J.* (2021). doi: 10.1093/eurheartj/ehab282. [Epub ahead of print].
- Camici PG, Crea F. Coronary microvascular dysfunction. *N Engl J Med.* (2007) 356:830–40. doi: 10.1056/NEJMc070666
- Ong P, Camici PG, Beltrame JF, Crea F, Shimokawa H, Sechtem U, et al. International standardization of diagnostic criteria for microvascular angina. *Int J Cardiol.* (2017) 250:16–20. doi: 10.1016/j.ijcard.2017.08.068
- Camici PG, Olivetto I, Rimoldi OE. The coronary circulation and blood flow in left ventricular hypertrophy. *J Mol Cell Cardiol.* (2012) 52:857–64. doi: 10.1016/j.yjmcc.2011.08.028
- Radico F, Cicchitti V, Zimarino M, Caterina RD. Angina pectoris and myocardial ischemia in the absence of obstructive coronary artery disease: practical considerations for diagnostic tests. *Jacc Cardiovasc Interv.* (2014) 7:453–63. doi: 10.1016/j.jcin.2014.01.157
- Gutiérrez E. Microvascular function, diabetes and coronary risk - ScienceDirect. *Int J Cardiol.* (2020) 307:176–7. doi: 10.1016/j.ijcard.2020.02.038
- Sezer M, Kocaaga M, Aslanger E, Atici A, Demirkiran A, Bugra Z, et al. Bimodal pattern of coronary microvascular involvement in diabetes mellitus. *J Am Heart Assoc.* (2016) 5:e003995. doi: 10.1161/JAHA.116.003995
- Murthy VL, Naya M, Foster CR, Gaber M, Hainer J, Klein J, et al. Association between coronary vascular dysfunction and cardiac mortality in patients with and without diabetes mellitus. (2012) 126:1858–68. doi: 10.1161/CIRCULATIONAHA.112.120402
- Feher A, Sinusas AJ. Quantitative assessment of coronary microvascular function. *Circ Cardiovasc Imag.* (2017) 10:e006427. doi: 10.1161/CIRCIMAGING.117.006427
- Appleby MA, Michaels A, Chen M, Michael CG. Importance of the TIMI frame count: implications for future trials. *Curr Control Trials Cardiovasc Med.* (2000) 1:31–4. doi: 10.1186/CVM-1-1-031
- Kunadian V, Harrigan C, Zorkun C, Palmer AM, Ogando KJ, Biller LH, et al. Use of the TIMI frame count in the assessment of coronary artery blood flow and microvascular function over the past 15 years. *J Thromb Thrombol.* (2009) 27:316–28. doi: 10.1007/s11239-008-0220-3
- Ding S, Pu J, Qiao Z-q, Shan P, Song W, Du Y, et al. TIMI myocardial perfusion frame count: a new method to assess myocardial perfusion and its predictive value for short-term prognosis. *Catheterizat Cardiovasc Inte.* (2009) 75:722–32. doi: 10.1002/ccd.22298
- Ge H, Song D, An D, Zheng L, He B. Frame counting improves the assessment of post-reperfusion microvascular patency by TIMI myocardial perfusion grade: evidence from cardiac magnetic resonance imaging. *Int J Cardiol.* (2015) 203:360. doi: 10.1016/j.ijcard.2015.10.194

AUTHOR CONTRIBUTIONS

ZW and YQ conceived the topic and wrote the first draft. LL, GF, CS, and YC went through the manuscript and tables. All authors revised and approved of the final draft.

FUNDING

This work was supported as follows: Jiangsu Provincial Health Commission Project (M2020016); the Open Project Program of Guangxi Key Laboratory of Centre of Diabetic Systems Medicine (GKLCDSM-20210101-02); Zhenjiang social development (SH2018030).

29. Hesse B, Tãgil K, Cuocolo A, Anagnostopoulos C, Bardiés M, Bax J, et al. EANM/ESC procedural guidelines for myocardial perfusion imaging in nuclear cardiology. *Eur J Nucl Med Mol Imag.* (2005) 32:855. doi: 10.1007/s00259-005-1779-y
30. Stirrup JE, Underwood SR. PET should not replace routine SPECT MPS for the assessment of patients with known or suspected CAD. *J Nucl Cardiol.* (2017) 24:1960–4. doi: 10.1007/s12350-017-1023-8
31. Khoshakhlagh M, Islamian JP, Abedi SM, Mahmoudian B. Development of scintillators in nuclear medicine. *World J Nucl Med.* (2015) 14:156–9. doi: 10.4103/1450-1147.163241
32. Malhotra S, Doukky R. Dual isotope stress Tl-201 and rest Tc-99m CZT SPECT: are we truly leveraging CZT technology? *J Nucl Cardiol.* (2018) 26:1280–83. doi: 10.1007/s12350-018-1242-7
33. Duvall WL, Croft LB, Godiwala T, Ginsberg E, George T, Henzlova MJ, et al. Reduced isotope dose with rapid SPECT MPI imaging: initial experience with a CZT SPECT camera. *J Nucl Cardiol.* (2010) 17:1009–14. doi: 10.1007/s12350-010-9215-5
34. Nakazato R, Berman DS, Hayes SW, Fish M, Padgett R, Xu Y, et al. Myocardial perfusion imaging with a solid-state camera: simulation of a very low dose imaging protocol. *J Nucl Med.* (2013) 54:373–9. doi: 10.2967/jnumed.112.110601
35. Zavadvovsky KV, Mochula AV, Boshchenko AA, Vru Blevsky AV, Baev AE, Krylov AL, et al. Absolute myocardial blood flows derived by dynamic CZT scan vs invasive fractional flow reserve: correlation and accuracy. *J Nucl Cardiol.* (2021) 28:249–59. doi: 10.1007/s12350-019-01678-z
36. Acampa W, Zampella E, Assante R, Genova A, Simini GD, Mannarino T, et al. Quantification of myocardial perfusion reserve by CZT-SPECT: a head to head comparison with 82 rubidium PET imaging. *J Nucl Cardiol.* (2020). doi: 10.1007/s12350-020-02129-w. [Epub ahead of print].
37. Otaki Y, Manabe O, Miller R, Manrique A, Agostini D. Quantification of myocardial blood flow by CZT-SPECT with motion correction and comparison with 15O-water PET. *J Nucl Cardiol.* (2019). doi: 10.1007/s12350-019-01854-1. [Epub ahead of print].
38. Zampella E, Nappi C, Acampa W. Simultaneous dual isotope (201)Tl/(99m)Tc myocardial perfusion imaging using CZT cameras: clinical utility or technical challenge? *J Nucl Cardiol.* (2020) 27:748–50. doi: 10.1007/s12350-018-01522-w
39. Songy B, Guernou M, Lussato D, Queneau M, Bonardel G, Grellier JF, et al. Feasibility of simultaneous dual isotope acquisition for myocardial perfusion imaging with a cadmium zinc telluride camera. *J Nucl Cardiol.* (2020) 27:737–47. doi: 10.1007/s12350-018-1452-z
40. Taillefer R, Harel F. Radiopharmaceuticals for cardiac imaging: current status and future trends. *J Nucl Cardiol.* (2018) 25:1242–6. doi: 10.1007/s12350-018-1194-y
41. Debasis M, Mahmoud A, Rostyslav B, Chang H, Uttam S, Elias B, et al. Comparison of sparse domain approaches for 4D SPECT dynamic image reconstruction. *Med Phys.* (2018) 45:4493–509. doi: 10.1002/mp.13099
42. Arabi H, Akhavanallaf A, Sanaat A, Shiri I, Zaidi H. The promise of artificial intelligence and deep learning in PET and SPECT imaging. *Physica Medica.* (2021) 83:122–37. doi: 10.1016/j.ejmp.2021.03.008
43. Pelletier-Galarneau M, Martineau P, El Fakhri G. Quantification of PET myocardial blood flow. *Curr Cardiol Rep.* (2019) 21:11. doi: 10.1007/s11886-019-1096-x
44. Salata BM, Singh P. Role of cardiac PET in clinical practice. *Curr Treat Options Cardiovasc Med.* (2017) 19:93. doi: 10.1007/s11936-017-0591-x
45. Singh V, Carli M. SPECT versus PET myocardial perfusion imaging in patients with equivocal CT. *Curr Cardiol Rep.* (2020) 22:43. doi: 10.1007/s11886-020-01287-0
46. Bateman TM. Advantages and disadvantages of PET and SPECT in a busy clinical practice. *J Nucl Cardiol Offic Public Am Soc Nucl Cardiol.* (2012) 19(Suppl. 1):S3. doi: 10.1007/s12350-011-9490-9
47. Wanli G, Ping W, Yunliang L, Qiong W, Zhifang W, Huanzhen C, et al. Value of PET quantitative analysis of coronary physiology for the diagnosis and risk factors assessment of non-obstructive coronary microvascular disease. *Chin J Nucl Med Mol Imagin.* (2019) 39:478–83. doi: 10.3760/cma.j.issn.2095-2848.2019.08.007
48. Taqeti VR, Hachamovitch R, Murthy VL, Naya M, Foster CR, Hainer J, et al. Global coronary flow reserve is associated with adverse cardiovascular events independently of luminal angiographic severity and modifies the effect of early revascularization. *Circulation.* (2015) 131:19–27. doi: 10.1161/CIRCULATIONAHA.114.011939
49. Liga R, Neglia D. Emerging F-18-labelled PET myocardial perfusion tracers. *Curr Cardiol Rep.* (2020) 22:116. doi: 10.1007/s11886-020-01368-0
50. Davidson CQ, Phenix CP, Tai TC, Khaper N, Lees SJ. Searching for novel PET radiotracers: imaging. *Am J Nucl Med Mol Imag.* (2018) 8:200–27.
51. Werner RA, Chen X, Rowe SP, Lapa C, Javadi MS, Higuchi T. Moving into the next era of PET myocardial perfusion imaging: introduction of novel 18F-labeled tracers. *Int J Cardiovasc Imag.* (2018) 35:569–77. doi: 10.1007/s10554-018-1469-z
52. Li Y, Wei Z, Hua W, Gang L. Advanced tracers in PET imaging of cardiovascular disease. *Bio Res Int.* (2014) 2014:504532. doi: 10.1155/2014/504532
53. Yao Y, Li YM, He ZX, Civelek AC, Li XF. Likely common role of hypoxia in driving (18)F-FDG uptake in cancer, myocardial ischemia, inflammation and infection. *Can Biother Radiopharm.* (2021). doi: 10.1089/cbr.2020.4716. [Epub ahead of print].
54. Jain D, He ZX, Lele V. Cardiac hot spot imaging with (18)FDG. *Semin Nucl Med.* (2014) 44:375–85. doi: 10.1053/j.semnuclmed.2014.06.010
55. Bowei L, Yanfang W, Jie Y, Jingjing X, Dongyue S, Xue L, et al. Advancement of imaging technology for coronary microcirculation dysfunction assessment. *J Bio Eng.* (2020) 37:892–6. doi: 10.7507/1001-5515.202005003
56. Kawamura K, Kumata K, Takei M, Furutsuka K, Hashimoto H, Ito T, et al. Efficient radiosynthesis and non-clinical safety tests of the TSPO radioprobe [18F]FEDAC: prerequisites for clinical application. *Nucl Med Biol.* (2016) 43:445–53. doi: 10.1016/j.nucmedbio.2016.04.004
57. Luo R, Wang L, Ye F, Wang Y-R, Fang W, Zhang M-R, et al. [18F]FEDAC translocator protein positron emission tomography-computed tomography for early detection of mitochondrial dysfunction secondary to myocardial ischemia. *Ann Nucl Med.* (2021) 35:927–36. doi: 10.1007/s12149-021-01630-7
58. Qayyum AA, Kastrup J. Measuring myocardial perfusion: the role of PET, MRI and CT. *Clin Radiol.* (2015) 70:576–84. doi: 10.1016/j.crad.2014.12.017
59. Manabe O, Ran K, Katoh C, Magota K, Yoshinaga K. Validation of regional myocardial blood flow quantification using three-dimensional PET with rubidium-82: repeatability and comparison with two-dimensional PET data acquisition. *Nucl Med Commun.* (2020) 41:768–75. doi: 10.1097/MNM.0000000000001218
60. Xu J, Lo S, Juergens CP, Leung DY. Assessing coronary microvascular dysfunction in ischaemic heart disease: little things can make a big difference. *Heart Lung Circ.* (2019) 29:118–27. doi: 10.1016/j.hlc.2019.05.187
61. Kotecha T, Martinez-Naharro A, Boldrini M, Knight D, Hawkins P, Kalra S, et al. Automated pixel-wise quantitative myocardial perfusion mapping by CMR to detect obstructive coronary artery disease and coronary microvascular dysfunction. *JACC Cardiovasc Imag.* (2019) 12:1958–69. doi: 10.1016/j.jcmg.2018.12.022
62. Indorkar R, Kwong RY, Romano S, White BE, Farzaneh-Far A. Global coronary flow reserve measured during stress cardiac magnetic resonance imaging is an independent predictor of adverse cardiovascular events. *JACC Cardiovasc Imag.* (2019) 12(8 Pt 2):1686–95. doi: 10.1016/j.jcmg.2018.08.018
63. Zorach B, Shaw PW, Bourque J, Kuruvilla S, Balfour PC, Yang Y, et al. Quantitative cardiovascular magnetic resonance perfusion imaging identifies reduced flow reserve in microvascular coronary artery disease. *J Cardiovasc Mag Res.* (2018) 20:14. doi: 10.1186/s12968-018-0435-1
64. Levelt E, Piechnik SK, Liu A, Wijesurendra RS, Mahmood M, Ariga R, et al. Adenosine stress CMR T1-mapping detects early microvascular dysfunction in patients with type 2 diabetes mellitus without obstructive coronary artery disease. *J Cardiovasc Mag Res.* (2017) 19:81. doi: 10.1186/s12968-017-0397-8
65. Liu A, Wijesurendra RS, Liu JM, Greiser A, Jerosch-Herold M, Forfar JC, et al. RETRACTED: gadolinium-free cardiac MR stress T1-mapping to distinguish epicardial from microvascular coronary disease. *J Am Coll Cardiol.* (2018) 71:957–68. doi: 10.1016/j.jacc.2017.11.071
66. Chatzantonis G, Bietenbeck M, Florian A, Meier C, Yilmaz A. “Myocardial transit-time” (MyoTT): a novel and easy-to-perform CMR parameter to assess microvascular disease. *Clin Res Cardiol.* (2020) 109:488–97. doi: 10.1007/s00392-019-01530-x

67. Chatzantonis G, Bietenbeck M, Florian A, Meier C, Yilmaz A. Diagnostic value of the novel CMR parameter “myocardial transit-time” (MyoTT) for the assessment of microvascular changes in cardiac amyloidosis and hypertrophic cardiomyopathy. *Clin Res Cardiol.* (2021) 110:136–45. doi: 10.1007/s00392-020-01661-6
68. Zhou W, Chun J, Yin L, Leung ST, Ng MY. Long-term prognosis of patients with coronary microvascular disease using stress perfusion cardiac magnetic resonance. *JACC Cardiovasc Imag.* (2020) 14:602–11. doi: 10.1016/j.jcmg.2020.09.034
69. Verma A, Ha AC, Dennie C, Essebag V, Exner DV, Khan N, et al. Canadian heart rhythm society and Canadian association of radiologists consensus statement on magnetic resonance imaging with cardiac implantable electronic devices. *Can Assoc Radiol J.* (2014) 65:290–300. doi: 10.1016/j.carj.2014.08.001
70. Rahman H, Scannell CM, Demir OM, Ryan M, Chiribiri A. High-resolution cardiac magnetic resonance imaging techniques for the identification of coronary microvascular dysfunction. *JACC Cardiovasc Imag.* (2021) 14:978–86. doi: 10.1016/j.jcmg.2020.10.015
71. Kording F, Yamamura J, Lund G, U Eb Erle F, Jung C, Adam G, et al. Doppler ultrasound triggering for cardiovascular MRI at 3T in a healthy volunteer study. *Mag Res Med Sci.* (2017) 16:98–108. doi: 10.2463/mrms.mp.2015-0104
72. Xu L, Chen Y, Jin Q, Wu Y, Deng C, Zhong Y, et al. Biomimetic PLGA microbubbles coated with platelet membranes for early detection of myocardial ischaemia-reperfusion injury. *Mol Pharmacol.* (2021) 18:2974–85. doi: 10.1021/acs.molpharmaceut.1c00145
73. Thomas, James D. Myocardial contrast echocardiography perfusion imaging. *J Am Coll Cardiol.* (2013) 62:1362–4. doi: 10.1016/j.jacc.2013.05.053
74. Barletta G, Bene M. Myocardial perfusion echocardiography and coronary microvascular dysfunction. *World J Cardiol.* (2015) 7:861–74. doi: 10.4330/wjcv.v7.i12.861
75. Yang N, Su YF, Li WW, Wang SS, Zhao CQ, Wang BY, et al. Microcirculation function assessed by adenosine triphosphate stress myocardial contrast echocardiography and prognosis in patients with nonobstructive coronary artery disease. *Medicine.* (2019) 98:e15990. doi: 10.1097/MD.00000000000015990
76. Cortigiani L, Rigo F, Gherardi S, Sicari R, Galderisi M, Bovenzi F, et al. Additional prognostic value of coronary flow reserve in diabetic and nondiabetic patients with negative dipyridamole stress echocardiography by wall motion criteria. *J Am Coll Cardiol.* (2007) 50:1354–61. doi: 10.1016/j.jacc.2007.06.027
77. Moccetti M, Belcik T, Latifi Y, Xie A, Ozawa K, Brown E, et al. Flow augmentation in the myocardium by ultrasound cavitation of microbubbles: role of shear-mediated purinergic signaling. *J Am Soc Echocardiogr.* (2020) 33:1023–31. doi: 10.1016/j.echo.2020.03.016
78. Lei Z, Li SC, Min LJ, Lei MY, Ning Y, Qiao TX, et al. Assessment of the preventive effect against diabetic cardiomyopathy of FGF1-loaded nanoliposomes combined with microbubble cavitation by ultrasound. *Front Pharmacol.* (2020) 10:1535. doi: 10.3389/fphar.2019.01535
79. Ayub MT, Kalra D. Coronary microvascular dysfunction and the role of noninvasive cardiovascular imaging. *Diagnostics.* (2020) 10:679. doi: 10.3390/diagnostics10090679
80. Wong D, Ko BS, Cameron JD, Nerlekar N, Leung M, Malaipan Y, et al. Transluminal attenuation gradient in coronary computed tomography angiography is a novel noninvasive approach to the identification of functionally significant coronary artery stenosis: a comparison with fractional flow reserve. *J Am Coll Cardiol.* (2013) 61:1271–9. doi: 10.1016/j.jacc.2012.12.029
81. Takx R, Celeng C, Schoepf UJ. CT myocardial perfusion imaging: ready for prime time? *Eur Radiol.* (2018) 28:1253–6. doi: 10.1007/s00330-017-5057-8
82. Xu Y, Yu L, Shen C, Lu Z, Zhu X, Zhang J. Prevalence and disease features of myocardial ischemia with non-obstructive coronary arteries: insights from a dynamic CT myocardial perfusion imaging study. *Int J Cardiol.* (2021) 334:142–7. doi: 10.1016/j.ijcard.2021.04.055
83. Yu L, Tao X, Dai X, Liu T, Zhang JJKJoR. Dynamic CT myocardial perfusion imaging in patients without obstructive coronary artery disease: quantification of myocardial blood flow according to varied heart rate increments after stress. *Korean J Radiol.* (2021) 22:97. doi: 10.3348/kjr.2020.0249
84. Choi JH, Min JK, Labounty TM, Lin FY, Mendoza DD, Shin DH, et al. Intracoronary transluminal attenuation gradient in coronary CT angiography for determining coronary artery stenosis. *JACC: Cardiovasc Imag.* (2011) 4:1149–57. doi: 10.1016/j.jcmg.2011.09.006
85. Kojima T, Nagao M, Yabuuchi H, Yamasaki Y, Shirasaka T, Kawakubo M, et al. New transluminal attenuation gradient derived from dynamic coronary CT angiography: diagnostic ability of ischemia detected by ¹³N-ammonia PET. *Heart Vessels.* (2021) 36:433–41. doi: 10.1007/s00380-020-01712-y
86. Alam MS, Green R, Kemp RD, Beanlands RS, Chow B. Epicardial adipose tissue thickness as a predictor of impaired microvascular function in patients with non-obstructive coronary artery disease. *J Nucl Cardiol.* (2013) 20:804–12. doi: 10.1007/s12350-013-9739-6
87. Iwata K, Ogasawara K. Assessment of non-invasive diagnostic imaging modalities efficiency for detecting myocardial ischemia in patients suspected of having stable angina. *Preprint.* (2021). doi: 10.21203/rs.3.rs-495125/v1

Conflict of Interest: The authors declare that the research was conducted in the absence of any commercial or financial relationships that could be construed as a potential conflict of interest.

Publisher's Note: All claims expressed in this article are solely those of the authors and do not necessarily represent those of their affiliated organizations, or those of the publisher, the editors and the reviewers. Any product that may be evaluated in this article, or claim that may be made by its manufacturer, is not guaranteed or endorsed by the publisher.

Copyright © 2021 Qi, Li, Feng, Shao, Cai and Wang. This is an open-access article distributed under the terms of the Creative Commons Attribution License (CC BY). The use, distribution or reproduction in other forums is permitted, provided the original author(s) and the copyright owner(s) are credited and that the original publication in this journal is cited, in accordance with accepted academic practice. No use, distribution or reproduction is permitted which does not comply with these terms.



Sex Differences in the Non-infarct-Related Artery-Based Quantitative Flow Ratio in Patients With ST-Elevation Myocardial Infarction: A Retrospective Study

Hongli Hou^{1,2}, Qi Zhao³, Chao Qu⁴, Meng Sun⁵, Qi Liu¹, Xingtao Huang¹, Xuedong Wang¹, Ruoxi Zhang^{1*}, Lifeng Du⁶, Jingbo Hou^{1*} and Bo Yu¹

¹ Department of Cardiology, The 2nd Affiliated Hospital of Harbin Medical University, Harbin, China, ² Department of Cardiology, Chenjiaqiao Hospital of Chongqing Medical and Pharmaceutical College, Chongqing, China, ³ Department of Cardiology, The 1st Affiliated Hospital of Harbin Medical University, Harbin, China, ⁴ Department of Cardiology, Heilongjiang Provincial People's Hospital, Harbin, China, ⁵ The Key Laboratory of Myocardial Ischemia, Harbin Medical University, Ministry of Education, Harbin, China, ⁶ Department of Cardiology, Hegang People's Hospital, Hegang, China

OPEN ACCESS

Edited by:

Zhao Wang,
University of Electronic Science and
Technology of China, China

Reviewed by:

Krishnaraj Sinhji Rathod,
Queen Mary University of London,
United Kingdom
Taishi Yonetsu,
Tokyo Medical and Dental
University, Japan

*Correspondence:

Jingbo Hou
jingbohhou@163.com
Ruoxi Zhang
898717372@qq.com

Specialty section:

This article was submitted to
Cardiovascular Imaging,
a section of the journal
Frontiers in Cardiovascular Medicine

Received: 16 June 2021

Accepted: 31 August 2021

Published: 24 September 2021

Citation:

Hou H, Zhao Q, Qu C, Sun M, Liu Q,
Huang X, Wang X, Zhang R, Du L,
Hou J and Yu B (2021) Sex
Differences in the Non-infarct-Related
Artery-Based Quantitative Flow Ratio
in Patients With ST-Elevation
Myocardial Infarction: A Retrospective
Study.
Front. Cardiovasc. Med. 8:726307.
doi: 10.3389/fcvm.2021.726307

Introduction: It has been reported that sex has well-established relationships with the prevalence of coronary artery disease (CAD) and the major adverse cardiovascular events. Compared with men, the difference of coronary artery and myocardial characteristics in women has effects on anatomical and functional evaluations. Quantitative flow ratio (QFR) has been shown to be effective in assessing the hemodynamic relevance of lesions in stable coronary disease. However, its suitability in acute myocardial infarction patients is unknown. This study aimed to evaluate the sex differences in the non-infarct-related artery (NIRA)-based QFR in patients with ST-elevation myocardial infarction (STEMI).

Methods: In this study, 353 patients with STEMI who underwent angiographic cQFR assessment and interventional therapy were included. According to contrast-flow QFR (cQFR) standard operating procedures: reliable software was used to modeling the hyperemic flow velocity derived from coronary angiography in the absence of pharmacologically induced hyperemia. 353 patients were divided into two groups according to sex. A cQFR ≤ 0.80 was considered hemodynamically significant, whereas invasive coronary angiography (ICA) luminal stenosis $\geq 50\%$ was considered obstructive. Demographics, clinical data, NIRA-related anatomy, and functional cQFR values were recorded. Clinical outcomes included the NIRA reclassification rate between men and women, according to the ICA and cQFR assessments.

Results: Women were older and had a higher body mass index (BMI) than men. The levels of diastolic blood pressure, troponin I, peak creatine kinase-MB, low-density lipoprotein cholesterol, N terminal pro B-type natriuretic peptide, stent diameter, and current smoking rate were found to be significantly lower in the female group than in the male group. Women had a lower likelihood of a positive cQFR ≤ 0.80 for the same degree of stenosis and a lower rate of NIRA revascularization. Independent predictors of positive cQFR included male sex and diameter stenosis (DS) $> 70\%$.

Conclusions: cQFR values differ between the sexes, as women have a higher cQFR value for the same degree of stenosis. The findings suggest that QFR variations by sex require specific interpretation, as these differences may affect therapeutic decision-making and clinical outcomes.

Keywords: gender differences, non-infarct-related artery, ST-elevation myocardial infarction, quantitative flow ratio, revascularization

INTRODUCTION

Coronary artery disease (CAD) is the leading cause of death globally, with the majority of affected individuals dying of acute myocardial infarction (1). Evidence from pathologic studies suggest that there are significant differences in coronary obstructive lesions between man and women (2, 3). Women are diagnosed with CAD at a greater age compared to men. In addition, women diagnosed with CAD have specific clinical symptoms, lower cardiovascular risk assessment scores, and a lower incidence of obstructive coronary heart disease, however, they appear to have a worse prognosis. Studies have shown lower utilization of conventional non-invasive imaging in female patients with suspected diagnosis of CAD, which may be related to breast attenuation, the decrease of peak exercise ability, small body size, and lower incidence of obstructive CAD (4). Therefore, sex-specific strategies and interpretations are recommended in the guidelines (5).

More recent evidence suggests that patients with non-infarct-related artery disease (NIRA) may in fact have a worse prognosis, including a higher 30-day mortality, than patients without NIRA disease (6). In addition, there is a lack of consensus regarding the treatment approach (aggressive vs. conservative) that should be implemented in these patients with NIRA disease. For some special research projects, patients with ST-elevation myocardial infarction (STEMI) underwent complete revascularization show lower rates of major cardiovascular events than infarct-related artery (IRA)-only revascularization (7, 8).

In recent years, fractional flow reserve (FFR) testing has become an important step in flow reconstruction decisions in patients with CAD, with the aim of assessing the functional significance of epicardial coronary stenosis on angiography.

Studies have shown that the choice of an FFR-based revascularization strategy is superior to percutaneous coronary intervention (PCI) for infarct-related vessels alone, both in STEMI procedure or in a staged manner (9, 10). However, the cost of the pressure wire and limitations associated with the induction of hyperemia have limited the wide application of FFR. A novel practical tool which calculates FFR indirectly and guides revascularization decision-making without a pressure wire or hyperemic induction was established. Recent studies have shown that the contrast-flow quantitative flow ratio (cQFR) can accurately and reproducibly predict FFR values (11). Mechanically, the cQFR was calculated based on a contrast-flow hyperemic flow velocity model derived from coronary angiography without pharmacologically induced hyperemia. The accuracy of the cQFR in comparison with the conventional FFR

has already been reported (12), and the software for the cQFR measurement is now commercially available.

Therefore, study aimed to evaluate the sex differences in the NIRA-based cQFR in patients with STEMI. We hypothesized that sex differences in NIRA might be related to the difference in revascularization decision-making based on the quantitative flow ratio (QFR) in patients with STEMI.

MATERIALS AND METHODS

Ethics Statements

This study protocol conforms to the ethical guidelines of the 1975 Declaration of Helsinki, as reflected in a priori approval from the institution's human research committee. This study was also approved by the Research Ethics Committee of the 2nd Affiliated Hospital of Harbin Medical University, China. Informed consent was obtained from all patients.

Study Population

We identified 353 patients admitted for STEMI who underwent angiographic QFR assessment and interventional therapy at the 2nd Affiliated Hospital of Harbin Medical University between January 2018 and December 2019. The inclusion criteria were as follows: (1) patients presenting within 12 h of symptom onset, defined as typical chest pain lasting for >30 min; (2) ST-segment elevation ≥ 1 mm in two contiguous electrocardiographic leads or new onset of complete left bundle branch block; and (3) primary PCI including balloon angioplasty, thrombus aspiration, and/or stent implantation. The exclusion criterion included any chronic illness, such as cancer, liver cirrhosis, heart failure, or end-stage renal failure (13).

Coronary Angiography and Percutaneous Coronary Angiography

All primary PCIs were performed at our hospital [Department of Cardiology, The 2nd Affiliated Hospital of Harbin Medical University, a single tertiary interventional treatment center [>5,000 PCI cases per year]] by experienced interventional cardiologists, with experience with >1,000 PCI cases per year, who were not involved in the present study (13, 14). Baseline demographics and angiographic characteristics, as well as laboratory and physical examination data during hospitalization, were recorded by systematically reviewing the patients' files.

Primary PCI was usually performed using the percutaneous radial artery approach; the femoral approach was used when an intra-aortic balloon pump needed to be inserted. All patients' angiographic data from catheterization laboratory records were

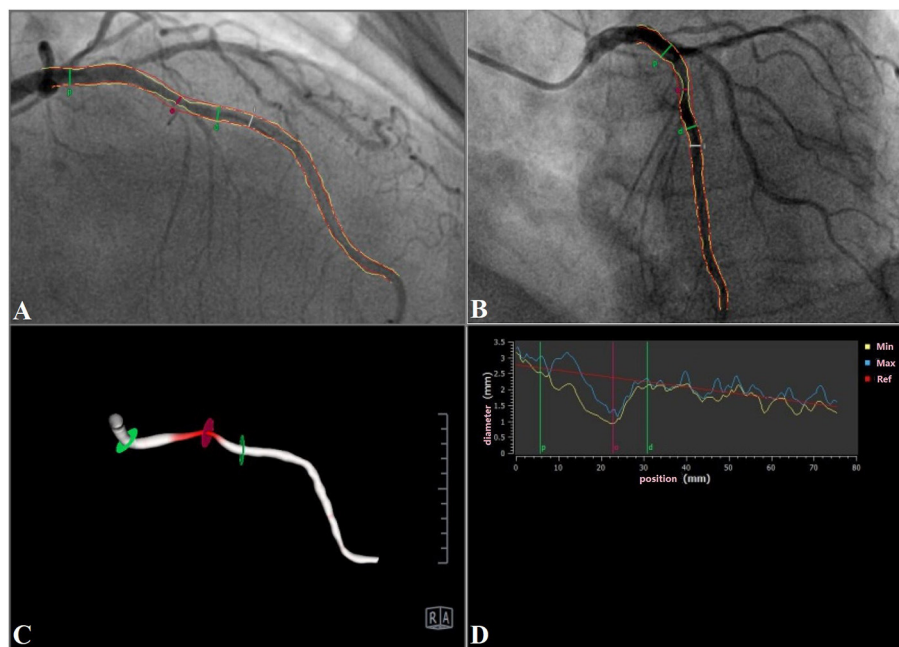


FIGURE 1 | A representative case of LAD (cQFR = 0.71). **(A,B)** Two-dimensional images; **(C)** three-dimensional reconstruction (right anterior oblique 50°, caudal 9°); **(D)** diameter diagram. LAD, left anterior descending artery; cQFR, contrast-flow quantitative flow ratio.

assessed using the conventional technique. The target artery was defined as clinically significant when vessel stenosis was $\geq 50\%$. Blood flow in the IRA that received only primary PCI was graded based on the thrombolysis in myocardial infarction (TIMI) grade. A chewable loading dose of 300 mg of aspirin and 600 mg of clopidogrel was administered before PCI. Success of the procedure was defined as $<20\%$ stenosis of the IRA with TIMI grade III flow after primary PCI. Post-operatively, all patients were transferred to our cardiac care unit and received standard treatment for STEMI, which consisted of 100 mg of aspirin, 20 mg of atorvastatin, and 75 mg of clopidogrel once a day (15).

Figures Computation of the Contrast-Flow Quantitative Flow Ratio

Three-dimensional quantitative coronary angiography (QCA) and QFR analyses were performed by an independent core laboratory with dedicated software (QAngio XA 3D prototype, Medis special by, Leiden, the Netherlands) (Figures 1A–D). Briefly, end-diastolic frames of two optimal angiography projections, which were separated with angles of at least 25° , were selected and used for three-dimensional model reconstruction. Fifteen frames/second acquisition in our software that performs QFR was require. The three-dimensional contour model of the segment of interest and its reference vessel were constructed in an automated manner, and manual correction of the contour was performed. After acquisition of the fixed QFR, estimated contrast coronary flow was calculated using the TIMI frame-count adjustment, which indicated the frames where contrast entered and exited the segmented part of the vessel (12). With

the application of the TIMI frame-count adjustment in the calculation method, the software automatically calculated the cQFR value. The cutoff value of the $cQFR \leq 0.80$ was used in the current study (16).

Blood Sampling

Venous blood was collected from all patients within 72 h of hospitalization. N terminal pro B-type natriuretic peptide (NT-proBNP), creatine kinase-MB (CK-MB), and troponin I levels were measured daily. Blood samples were collected on admission and at 24 and 48 h in every patient. Plasma NT-proBNP levels were measured using an Elecsys 2010 analyzer, a commercially available electrochemiluminescent sandwich immunoassay (Elecsys proBNP; Roche Diagnostics, Mannheim, Germany) (14). High-sensitivity-C-reactive protein levels were measured using a commercially available immunonephelometric kinetic assay (BN ProSpec; Siemens, Tarrytown, NY, USA). The 12-h fasting serum levels of triglycerides, total cholesterol, low-density lipoprotein cholesterol (LDL-C), and high-density lipoprotein cholesterol (HDL-C) were measured using standard methods (15). Other biochemical measurements were performed using the standard methods.

Definitions

Reperfusion time was defined as the symptom-to-balloon time, and the door-to-balloon time was defined as the time between hospitalization and balloon dilation (14). Diabetes mellitus was diagnosed when a patient was on insulin or oral hypoglycemic drugs or in patients not on insulin or oral hypoglycemic drugs but with a casual plasma glucose level >11.1 mmol/L, fasting plasma

glucose level >7 mmol/L, or glycated A1c hemoglobin level $>6.5\%$. Hypertension was diagnosed when the systolic arterial pressure was ≥ 140 mmHg and/or diastolic arterial pressure was ≥ 90 mmHg, and when the patient had been on antihypertensive drugs for a long time. Hyperlipidemia was defined as a fasting total serum cholesterol level >5.17 mmol/L, LDL-C level >3.15 mmol/L, or serum triglyceride level >1.70 mmol/L, or if the patient was on lipid-lowering agents owing to a medical history of hypercholesterolemia (15). Smoking was defined as current regular use of cigarettes or if the patient had quit smoking within the previous year. Cardiac function deterioration was defined as New York Heart Association (NYHA) functional class leveled up in follow-up compared to in hospital.

Statistical Analyses

Quantitative variables are expressed as the mean \pm standard deviation, and qualitative variables are expressed as the total number and percentage. The independent two-sample *t*-test was used to assess the differences between multiple sets of data. Categorical variables were compared using the chi-square or Fisher exact tests. Independent predictors of NIRA revascularization were identified using multivariate logistic regression analysis. Statistical significance was defined as a two-sided *p*-value <0.05 . All statistical analyses were performed using SPSS version 19.0 (IBM Corp., Armonk, NY, USA).

RESULTS

Basic Characteristics

In our single-center study, we initially screened 515 STEMI patients who underwent angiographic QFR assessment between January 2018 and December 2019. One hundred and sixty-two patients with angiography were excluded because of limited quality of the images or inappropriate angle of projections. A total of 353 patients (224 men and 129 women) were enrolled in the study. Patients were categorized into two groups according to different sex. The baseline demographic and angiographic characteristics of the two groups are presented in **Tables 1, 2**, respectively. Compared to men, women were older and had a higher body mass index (BMI). The levels of diastolic blood pressure, troponin I, peak CK-MB, LDL cholesterol, and NT-proBNP, stent diameter, and current smoking rate were found to be significantly lower in the female group than in the male group.

Characteristics of the Quantitative Flow Ratio

There was no significant statistical difference in each anatomical stenosis group (**Table 3**). Compared to men, women had a lower likelihood of a positive cQFR ≤ 0.80 , a higher cQFR value in similar range of diameter stenosis (DS) ($DS \leq 30\%$ and $DS > 70\%$), and a higher diameter stenosis while cQFR > 0.80 (**Figure 2**). Multivariate logistic regression analysis showed that male sex [odds ratio [OR] = 2.240, 95% confidence interval [CI]: 1.237–3.941, $P = 0.005$], and DS $> 70\%$ (OR = 9.407, 95% CI: 2.709–23.178, $P = 0.001$) were independently associated with positive cQFR (**Table 4**).

TABLE 1 | Patient demographics and clinical data.

	Male group (<i>n</i> = 224)	Female group (<i>n</i> = 129)	<i>P</i> -value
Age, years	64.69 \pm 5.67	68.28 \pm 8.38	<0.001
BMI, kg/m ²	26.02 \pm 4.32	27.17 \pm 2.93	0.003
Obesity, BMI ≥ 30 kg/m ²	38 (16.96)	22 (17.05)	1.000
Cardiovascular risk factors			
Hypertension	141 (62.95)	88 (68.22)	0.355
Diabetes mellitus	40 (17.86)	26 (20.16)	0.671
Hyperlipidaemia	134 (59.82)	90 (69.77)	0.069
Current smoking	108 (48.21)	11 (8.53)	<0.001
Previous MI	27 (12.05)	9 (6.98)	0.147
Previous PCI	43 (19.20)	15 (11.63)	0.074
Killip class on admission			
I	170 (75.89)	94 (72.86)	0.528
II	33 (14.73)	23 (17.83)	0.453
III	13 (5.81)	7 (5.43)	1.000
IV	8 (3.57)	5 (3.88)	1.000
SBP, mmHg	123.05 \pm 20.09	126.42 \pm 34.30	0.309
DBP, mmHg	77.73 \pm 12.30	73.33 \pm 14.63	0.003
Platelet counts, $\times 10^9$ /L	218.50 \pm 83.78	218.78 \pm 55.20	0.966
WBC, $\times 10^9$ /L	10.89 \pm 1.91	11.06 \pm 5.53	0.732
Hemoglobin, g/L	134.20 \pm 26.78	131.83 \pm 20.73	0.354
Creatinine, μ mol/L	85.44 \pm 11.72	87.02 \pm 27.37	0.533
Troponin I, μ g/L	15.74 \pm 3.50	14.14 \pm 3.53	<0.001
Peak CK-MB, μ g/L	35.29 \pm 16.22	27.47 \pm 11.15	<0.001
Total cholesterol, mol/L	4.50 \pm 0.79	4.67 \pm 1.43	0.240
LDL-cholesterol, mol/L	3.00 \pm 1.15	2.74 \pm 0.73	0.010
HDL-cholesterol, mol/L	1.18 \pm 0.39	1.30 \pm 0.47	0.008
Triglyceride, mol/L	2.24 \pm 1.22	2.09 \pm 0.84	0.173
hs-CRP	10.09 \pm 3.31	10.21 \pm 4.44	0.792
NT-proBNP, pg/mL	701.07 \pm 75.56	666.29 \pm 49.66	<0.001

Data are presented as *n* (%) or mean \pm SD. BMI, body mass index; MI, myocardial infarction; PCI, percutaneous coronary intervention; SBP, systolic blood pressure; DBP, diastolic blood pressure; WBC, white blood cell; CK-MB, creatine kinase-MB; HDL, high-density lipoprotein; hs-CRP, high-sensitivity C-reactive protein; LDL, low-density lipoprotein; NT-proBNP, N-terminal pro-brain natriuretic peptide.

One Year Follow-Up

One-year follow-up the cardiac function deterioration events was trendly, but not significantly, higher in male group compared to female group (81.0 vs. 93.2%, $P = 0.389$; **Figure 3**).

DISCUSSION

QCA plays an important role in evaluating the degree of coronary artery stenosis and guiding the operation of PCI (17). However, limitations of anatomy-based techniques have required for a novel physiological technology to assess the severity of coronary stenosis (18, 19). The deep understanding of the anatomy and physiology of coronary circulation is necessary for clinical doctors to assess the hemodynamic consequences of epicardial stenosis and discover the personal clinical treatment strategy (20).

TABLE 2 | Primary angiographic and interventional therapy characteristics.

	Male group (n = 224)	Female group (n = 129)	P-value
Reperfusion time, min	280.41 ± 116.17	287.32 ± 167.82	0.679
Door-to-balloon time, min	69.19 ± 14.79	67.81 ± 15.95	0.412
IRA, n (%)			
LAD	109 (48.66)	71 (55.04)	0.270
LCX	42 (18.75)	32 (24.81)	0.221
RCA	73 (32.59)	26 (20.16)	0.014
Stents per patient	0.97 ± 0.23	0.95 ± 0.29	0.355
Stent length, mm	23.75 ± 7.84	23.52 ± 7.78	0.793
Stent diameter, mm	2.72 ± 0.69	2.43 ± 0.69	<0.001
IABP, n (%)	18 (8.04)	6 (4.65)	0.276
Femoral approach, n (%)	22 (9.83)	14 (10.85)	0.855

Data are presented as n (%) or mean ± SD. IRA, infarct-related artery; LAD, left anterior descending coronary artery; LCX, left circumflex coronary artery; RCA, right coronary artery; IABP, intraaortic balloon pump.

TABLE 3 | Clinical characteristics on QCA and cQFR.

	Male group (n = 224)	Female group (n = 129)	P-value
Anatomical stenosis per patients			
DS <30%	8 (3.57)	2 (1.55)	0.337
DS 30–50%	146 (65.18)	95 (73.64)	0.122
DS >70%	70 (31.25)	32 (24.81)	0.224
Coronary vessel cQFR			
LAD	0.84 ± 0.05	0.86 ± 0.04	0.003
LCX	0.83 ± 0.05	0.85 ± 0.05	0.018
RCA	0.82 ± 0.05	0.85 ± 0.04	<0.001
Overall	0.83 ± 0.05	0.86 ± 0.04	<0.001
cQFR ≤ 0.8	82 (36.61)	22 (17.05)	<0.001
NIRA revascularization performed, n (%)	75 (33.48)	21 (16.30)	<0.001

Data are presented as n (%) or mean ± SD. QCA, quantitative coronary angiography; cQFR, contrast-flow quantitative flow ratio; NIRA, non-infarct-related artery; LAD, left anterior descending coronary artery; LCX, left circumflex coronary artery; RCA, right coronary artery; DS, diameter stenosis.

In fact, the adoption rates of invasive FFR-guided PCI remain low in real-world practice (21). In recent years, functional coronary imaging has been progressively applied, which is a new method based on mathematical assumptions of computational fluid dynamics models or coronary blood flow and thus assessing the degree of coronary artery stenosis (22). QFR is a three-dimensional QCA-based computation of FFR, moreover, previous studies have demonstrated excellent correlations and diagnostic agreements with FFR (23, 24). In addition, in some proof-of-concept studies, compared with FFR, QFR showed same excellent diagnostic ability whether in the acute physiological evaluation of non-culprit lesions in patients with STEMI or multivessel disease (25, 26).

Studies have shown that QFR showed good diagnostic agreement with FFR measured in the acute physiological

evaluation of non-culprit lesions in patients with ST-segment elevation myocardial infarction (STEMI) and multivessel disease (26). To the best of our knowledge, this is the first time to investigate sex differences in NIRA-based QFR among patients with STEMI. Our results demonstrated several important sex-related differences. Compared to men, women have an inherently higher QFR value, independent of anatomical stenosis, and are less likely to receive revascularization of the NIRA. In the FAME substudy, it was found that the FFR value in women was 0.75 ± 0.18 , whereas that in men was 0.71 ± 0.17 ($P = 0.001$). It is also reported that the proportion of functionally significant stenoses, defined as $FFR < 0.80$, was lower in women than in men (27). For the patient cohort in our study, one-third of the patients were women. Compared to men, women were older, characteristic with higher BMI, and less cardiovascular risk factors (smoking, hypertension, and hypercholesterolemia). The above situation led to women might present with a lower number of coronary segments containing calcified or mixed plaques than men. Previous studies have highlighted sex differences in coronary stenoses, coronary plaque burden, and plaque composition, which may impact functional stenosis evaluation (28). For example, women presented with a lower number of coronary segments containing calcified or mixed plaques than men (29). In some quantitative and qualitative plaque characteristics studies, the number of high-risk plaque characteristics increased with decrease in FFR, and vice versa. Physiological disease burden (FFR) and the number of high-risk plaque characteristics were closely related, and both components had significant association with the risk of clinical events (28, 29). Furthermore, microvascular dysfunction is the most recognized reason for the higher FFR value in women, which is assessed by the coronary flow reserve, and it was reported to be more frequent in women than in men (30, 31). Accordingly, the blunted hyperemic response is considered as the major reason for the higher FFR value in women (20). Besides, compared with man, the smaller heart and myocardial perfusion territories are also important factors that cannot be ignored (32), which result in a relatively lower myocardial mass to coronary volume in women and a higher FFR value compared to men.

As expected in instances of disease severity, our results demonstrate that the average of QFR significantly higher in women, but importantly, the proportion of QFR-positive stenoses was also lower in women than in men (17.05 vs. 36.61%, $P < 0.001$). These results are highly consistent with those of the invasive Fractional Flow Reserve vs. Angiography for Multivessel Evaluation substudy (27). This difference in the sex-specific QFR/FFR offers new insights that may help to determine the appropriate treatment for women with CAD on interventional therapy. Our results emphasize that a high QFR value in women predicts a reduced likelihood of revascularization. Thus, our study confirms our hypothesis that sex differences in NIRA might be related to the difference in revascularization decision-making based on the QFR in patients with STEMI. Furthermore, because of women have a higher intrinsic FFR value, special consideration is required during PCI procedure: the strategies for revascularization need to be considered from multiple perspectives rather than using dichotomous cutoffs

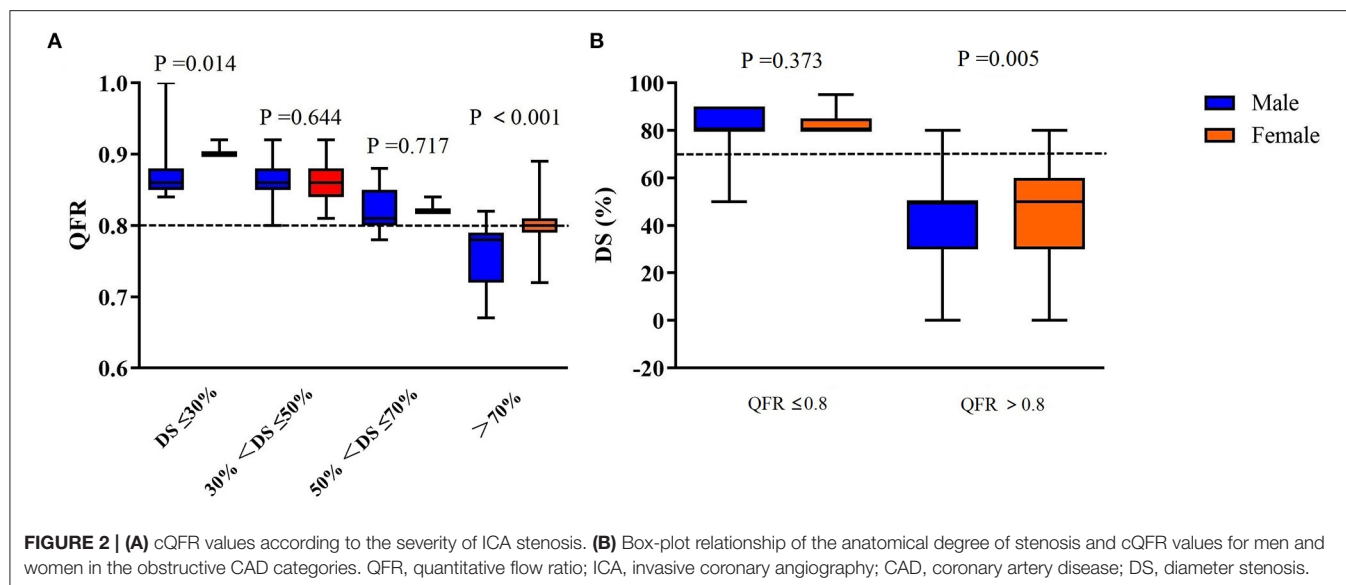


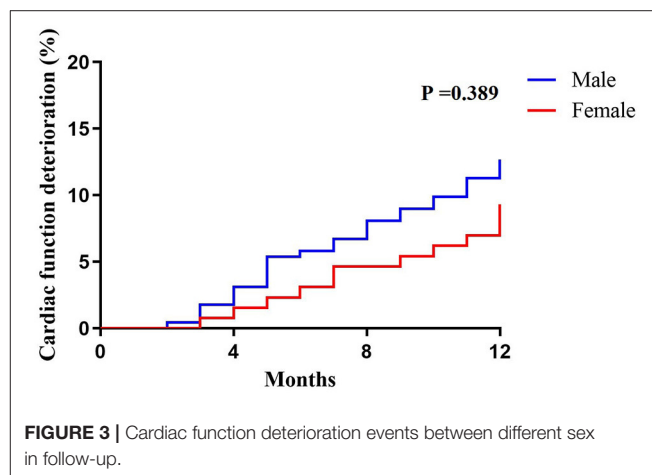
TABLE 4 | Univariate and multivariate regression analysis for predicting positive cQFR.

	Univariate		Multivariate	
	OR (95% CI)	P-value	OR (95% CI)	P-value
Male	2.809 (1.648–4.787)	<0.001	2.240 (1.273–3.941)	0.005
DS > 70%	9.694 (4.657–20.285)	<0.001	9.407 (2.709–23.178)	0.001
Previous MI	3.051 (1.515–6.142)	0.002		
Previous PCI	2.071 (1.160–3.700)	0.014		
Troponin I	1.088 (1.018–1.162)	0.012		
NT-proBNP	1.005 (1.001–1.008)	0.007		

OR, odds ratio; CI, confidence interval; MI, myocardial infarction; PCI, percutaneous coronary intervention; DS, diameter stenosis.

for invasive or non-invasive FFR (4). In our study, actual NIRA management for 90 days showed that women were more likely to receive medical treatment than men (83.70 vs. 66.52%, $P < 0.001$), and men were more likely to undergo NIRA revascularization than women (33.48 vs. 16.30%, $P < 0.001$). Therefore, the knowledge that women have a higher intrinsic physiological test value requiring special consideration, leading to suggestions that decisions of revascularization need to be nuanced and multifaceted rather than using dichotomous cutoffs for cQFR.

In previous studies, beyond sex and (as expected) % degree of stenosis, age, the presence of diabetes and vessel under study also showed a weak independent association with FFR data (33). In our study, female sex was significantly associated with positive cQFR after adjustment by DS (Table 4). In follow-up data, cardiac function deterioration rates were trendily, but not significantly, higher in male group compared to female group. There was also paradox that exists in female CAD, characterized by a lower prevalence of obstructive disease but higher prevalence of clinical presentation, ischemia, symptomatic



complaints, complications and mortality compared to men (34). However, this difference in sex did not translate into a difference in cardiac function in our study. This might be due to recent advances in revascularization techniques, stent technology and medical therapies and the relatively low-risk population of this study.

STUDY LIMITATIONS

The present study has some limitations. First, the number of patients was relatively small. There is a possibility of significant referral bias because of the retrospective and single-center design of the study. Second, we didn't measurement microvascular dysfunction, which leads to a lack of clarity understanding the differences in FFR values between men and women. Third, neither the physicians nor the patients were blinded to the QFR results and

whether revascularization was performed. Finally, there is relatively insufficient in data on long-term events and follow-up, and we plan to include this information in a future study.

CONCLUSIONS

There is significant different in QFR values between the male and female, as women have higher QFR values for the same degree of stenosis than men. Our findings suggest that QFR variations by sex needs more clinical and basic studies to explain the reasons, as these differences may affect clinical treatment strategy and long-term prognosis. However, the relative paucity of data supports the use of QFR at the NIRA in STEMI, and further investigation of the reliability of the non-culprit vessel QFR in this clinical setting is warranted.

DATA AVAILABILITY STATEMENT

The raw data supporting the conclusions of this article will be made available by the authors, without undue reservation.

ETHICS STATEMENT

The studies involving human participants were reviewed and approved by The Research Ethics Committee of the 2nd Affiliated Hospital of Harbin Medical University. The patients/participants

provided their written informed consent to participate in this study.

AUTHOR CONTRIBUTIONS

HH, RZ, JH, and BY were responsible for the conception and design of the study. HH, RZ, QZ, QL, XW, and XH contributed substantially to data acquisition. HH, QZ, CQ, QL, XW, LD, and XH contributed to data interpretation. MS was responsible for statistical analysis. HH and RZ drafted and revised the manuscript. All authors contributed to the article and approved the submitted version.

FUNDING

This study was supported by the National Natural Science Foundation of China (grant nos. 81900309 to QL; 81801803 to XH; 82000330 to XW; and 8197020581 to JH), China Postdoctoral Science Foundation (grant nos. 2019M661306 to QL and 2018M640310 to XH), and Heilongjiang Postdoctoral Science Foundation (grant no. LBH-Z19032 to XH).

SUPPLEMENTARY MATERIAL

The Supplementary Material for this article can be found online at: <https://www.frontiersin.org/articles/10.3389/fcvm.2021.726307/full#supplementary-material>

REFERENCES

- Goff Dc Jr, Lloyd-Jones DM, Bennett G, Coady S, D'Agostino RB, Gibbons R, et al. 2013 ACC/AHA guideline on the assessment of cardiovascular risk: a report of the American College of Cardiology/American Heart Association Task Force on Practice Guidelines. *Circulation*. (2014) 129 (25 Suppl. 2):S49–73. doi: 10.1161/01.cir.0000437741.48606.98
- Mautner SL, Lin F, Mautner GC, Roberts WC. Comparison in women versus men of composition of atherosclerotic plaques in native coronary arteries and in saphenous veins used as aortocoronary conduits. *J Am Coll Cardiol*. (1993) 21:1312–8. doi: 10.1016/0735-1097(93)90302-H
- Burke AP, Farb A, Malcom GT, Liang Y, Smialek J, Virmani R. Effect of risk factors on the mechanism of acute thrombosis and sudden coronary death in women. *Circulation*. (1998) 97:2110–6. doi: 10.1161/01.CIR.97.21.2110
- Fairbairn TA, Dobson R, Hurwitz-Koweek L, Matsuo H, Norgaard BL, Ronnow Sand NP, et al. Sex differences in coronary computed tomography angiography-derived fractional flow reserve: lessons from ADVANCE. *JACC Cardiovasc Imaging*. (2020) 13:2576–87. doi: 10.1016/j.jcmg.2020.07.008
- Mieres JH, Gulati M, Merz NB, Berman DS, Gerber TC, Hayes SN, et al. Role of noninvasive testing in the clinical evaluation of women with suspected ischemic heart disease: a consensus statement from the American Heart Association. *Circulation*. (2014) 130:350–79. doi: 10.1161/CIR.0000000000000061
- Park D-W, Clare RM, Schulte PJ, Pieper KS, Shaw LK, Califf RM, et al. Extent, location, and clinical significance of non-infarct-related coronary artery disease among patients with ST-elevation myocardial infarction. *JAMA*. (2014) 312:2019–27. doi: 10.1001/jama.2014.15095
- Wald DS, Morris JK, Wald NJ, Chase AJ, Edwards RJ, Hughes LO, et al. Randomized trial of preventive angioplasty in myocardial infarction. *N Engl J Med*. (2013) 369:1115–23. doi: 10.1056/NEJMoa1305520
- Gershlick AH, Khan JN, Kelly DJ, Greenwood JP, Sasikaran T, Curzen N, et al. Randomized trial of complete versus lesion-only revascularization in patients undergoing primary percutaneous coronary intervention for STEMI and multivessel disease: the CvLPRIT trial. *J Am Coll Cardiol*. (2015) 65:963–72. doi: 10.1016/j.jacc.2014.12.038
- Smits PC, Abdel-Wahab M, Neumann F-J, Boxma-de Klerk BM, Lunde K, Schotborgh CE, et al. Fractional flow reserve-guided multivessel angioplasty in myocardial infarction. *N Engl J Med*. (2017) 376:1234–44. doi: 10.1056/NEJMoa1701067
- Engström T, Kelbæk H, Helqvist S, Höfsten DE, Kløvgaard L, Holmvang L, et al. Complete revascularisation versus treatment of the culprit lesion only in patients with ST-segment elevation myocardial infarction and multivessel disease (DANAMI-3—PRIMULTI): an open-label, randomised controlled trial. *Lancet*. (2015) 386:665–71. doi: 10.1016/S0140-6736(15)60648-1
- Tu S, Barbato E, Kőszegi Z, Yang J, Sun J, Holm NR, et al. Fractional flow reserve calculation from 3-dimensional quantitative coronary angiography and TIMI frame count: a fast computer model to quantify the functional significance of moderately obstructed coronary arteries. *JACC Cardiovasc Interv*. (2014) 7:768–77. doi: 10.1016/j.jcin.2014.03.004
- Tu S, Westra J, Yang J, von Birgelen C, Ferrara A, Pellicano M, et al. Diagnostic accuracy of fast computational approaches to derive fractional flow reserve from diagnostic coronary angiography: the international multicenter FAVOR pilot study. *JACC Cardiovasc Interv*. (2016) 9:2024–35. doi: 10.1016/j.jcin.2016.07.013
- Jiang Z, Zhang R, Sun M, Liu Q, Wang S, Wang W, et al. Effect of clopidogrel vs ticagrelor on platelet aggregation and inflammation markers after percutaneous coronary intervention for ST-elevation myocardial infarction. *Can J Cardiol*. (2018) 34:1606–12. doi: 10.1016/j.cjca.2018.08.024
- Zhang R, Chen S, Zhao Q, Sun M, Yu B, Hou J. Fragmented QRS complex is a prognostic marker of microvascular reperfusion and changes in LV function occur in patients with ST elevation myocardial infarction who underwent primary percutaneous coronary intervention. *Exp Ther Med*. (2017) 13:2331–8. doi: 10.3892/etm.2017.4380

15. Zhao Q, Zhang R, Hou J, Yu B. Relationship between fragmented QRS and NT-proBNP in patients with ST elevation myocardial infarction who underwent primary percutaneous coronary intervention. *Acta Cardiol Sin.* (2018) 34:13–22. doi: 10.6515/ACS.201801_34(1).20170903A
16. Xu B, Tu S, Qiao S, Qu X, Chen Y, Yang J, et al. Diagnostic accuracy of angiography-based quantitative flow ratio measurements for online assessment of coronary stenosis. *J Am Coll Cardiol.* (2017) 70:3077–87. doi: 10.1016/j.jacc.2017.10.035
17. Collet C, Grundeken MJ, Asano T, Onuma Y, Wijns W, Serruys PW. State of the art: coronary angiography. *EuroIntervention.* (2017) 13:634–43. doi: 10.4244/EIJ-D-17-00465
18. White CW, Wright CB, Doty DB, Hiratzka LF, Eastham CL, Harrison DG, et al. Does visual interpretation of the coronary arteriogram predict the physiologic importance of a coronary stenosis? *N Engl J Med.* (1984) 310:819–24. doi: 10.1056/NEJM198403293101304
19. Lance Gould K, Johnson NP, Bateman TM, Beanlands RS, Bengel FM, Bober R, et al. Anatomic versus physiologic assessment of coronary artery disease. Role of coronary flow reserve, fractional flow reserve, and positron emission tomography imaging in revascularization decision-making. *J Am Coll Cardiol.* (2013) 62:1639–53. doi: 10.1016/j.jacc.2013.07.076
20. Crystal GJ, Klein LW. Fractional flow reserve: physiological basis, advantages and limitations, and potential gender differences. *Curr Cardiol Rev.* (2015) 11:209–19. doi: 10.2174/1573403X10666141020113318
21. Dehmer GJ, Weaver D, Roe MT, Milford-Beland S, Fitzgerald S, Hermann A, et al. A contemporary view of diagnostic cardiac catheterization and percutaneous coronary intervention in the United States: a report from the CathPCI Registry of the National Cardiovascular Data Registry, 2010 through June 2011. *J Am Coll Cardiol.* (2012) 60:2017–31. doi: 10.1016/j.jacc.2012.08.966
22. Hwang D, Choi KH, Lee JM, Mejía-Rentería H, Kim J, Park J, et al. Diagnostic agreement of quantitative flow ratio with fractional flow reserve and instantaneous wave-free ratio. *J Am Heart Assoc.* (2019) 8:e011605. doi: 10.1161/JAHA.118.011605
23. Collet C, Onuma Y, Sonck J, Asano T, Vandeloo B, Kornowski R, et al. Diagnostic performance of angiography-derived fractional flow reserve: a systematic review and Bayesian meta-analysis. *Eur Heart J.* (2018) 39:3314–21. doi: 10.1093/eurheartj/ehy445
24. Westra J, Andersen BK, Campo G, Matsuo H, Koltowski L, Eftekhari A, et al. diagnostic performance of in-procedure angiography-derived quantitative flow reserve compared to pressure-derived fractional flow reserve: the FAVOR II Europe-Japan study. *J Am Heart Assoc.* (2018) 7:e009603. doi: 10.1161/JAHA.118.009603
25. Sejr-Hansen M, Westra J, Thim T, Christiansen EH, Eftekhari A, Kristensen SD, et al. Quantitative flow ratio for immediate assessment of nonculprit lesions in patients with ST-segment elevation myocardial infarction—An iSTEMI substudy. *Catheter Cardiovasc Interv.* (2019) 94:686–92. doi: 10.1002/ccd.28208
26. Spitaleri G, Tebaldi M, Biscaglia S, Westra J, Brugaletta S, Erriquez A, et al. Quantitative flow ratio identifies nonculprit coronary lesions requiring revascularization in patients with ST-segment-elevation myocardial infarction and multivessel disease. *Circ Cardiovasc Interv.* (2018) 11:e006023. doi: 10.1161/CIRCINTERVENTIONS.117.006023
27. Kim H-S, Tonino PAL, De Bruyne B, Yong ASC, Tremmel JA, Pijls NHJ. The impact of sex differences on fractional flow reserve-guided percutaneous coronary intervention: a FAME (Fractional Flow Reserve Versus Angiography for Multivessel Evaluation) substudy. *JACC Cardiovasc Interv.* (2012) 5:1037–42. doi: 10.1016/j.jcin.2012.06.016
28. Lee JM, Choi KH, Koo BK, Park J, Kim J, Hwang D, et al. Prognostic implications of plaque characteristics and stenosis severity in patients with coronary artery disease. *J Am Coll Cardiol.* (2019) 73:2413–24. doi: 10.1016/j.jacc.2019.02.060
29. Douglas PS, Hoffmann U, Patel MR, Mark DB, Al-Khalidi HR, Cavanaugh B, et al. Outcomes of anatomical versus functional testing for coronary artery disease. *N Engl J Med.* (2015) 372:1291–300. doi: 10.1056/NEJMoa1415516
30. Noel Bairey Merz C, Shaw LJ, Reis SE, Bittner V, Kelsey SE, Olson M, et al. Insights from the NHLBI-sponsored women's ischemia syndrome evaluation (WISE) study: part II: gender differences in presentation, diagnosis, and outcome with regard to gender-based pathophysiology of atherosclerosis and macrovascular and microvascular coronary disease. *J Am Coll Cardiol.* (2006) 47(3 Suppl.):S21–9. doi: 10.1016/j.jacc.2004.12.084
31. Reis SE, Holubkov R, Conrad Smith AJ, Kelsey SE, Sharaf BL, Reichek N, et al. Coronary microvascular dysfunction is highly prevalent in women with chest pain in the absence of coronary artery disease: results from the NHLBI WISE study. *Am Heart J.* (2001) 141:735–41. doi: 10.1067/mhj.2001.114198
32. Lin FY, Devereux RB, Roman MJ, Meng J, Jow VM, Jacobs A, et al. Cardiac chamber volumes, function, and mass as determined by 64-multidetector row computed tomography: mean values among healthy adults free of hypertension and obesity. *JACC Cardiovasc Imaging.* (2008) 1:782–6. doi: 10.1016/j.jcmg.2008.04.015
33. Fineschi M, Guerrieri G, Orphal D, Palmerini E, Münzel T, Warnholtz A, et al. The impact of gender on fractional flow reserve measurements. *EuroIntervention.* (2013) 9:360–6. doi: 10.4244/EIJV9I3A58
34. Baumann S, Renker M, Schoepf UJ, De Cecco CN, Coenen A, De Geer J, et al. Gender differences in the diagnostic performance of machine learning coronary CT angiography-derived fractional flow reserve—results from the MACHINE registry. *Eur J Radiol.* (2019) 119:108657. doi: 10.1016/j.ejrad.2019.108657

Conflict of Interest: The authors declare that the research was conducted in the absence of any commercial or financial relationships that could be construed as a potential conflict of interest.

Publisher's Note: All claims expressed in this article are solely those of the authors and do not necessarily represent those of their affiliated organizations, or those of the publisher, the editors and the reviewers. Any product that may be evaluated in this article, or claim that may be made by its manufacturer, is not guaranteed or endorsed by the publisher.

Copyright © 2021 Hou, Zhao, Qu, Sun, Liu, Huang, Wang, Zhang, Du, Hou and Yu. This is an open-access article distributed under the terms of the Creative Commons Attribution License (CC BY). The use, distribution or reproduction in other forums is permitted, provided the original author(s) and the copyright owner(s) are credited and that the original publication in this journal is cited, in accordance with accepted academic practice. No use, distribution or reproduction is permitted which does not comply with these terms.



Relationship Between Immunoinflammation and Coronary Physiology Evaluated by Quantitative Flow Ratio in Patients With Coronary Artery Disease

Chengzhe Liu^{1,2,3,4†}, Zhiyao Yu^{1,2,3,4†}, Huaqiang Chen^{1,2,3,4†}, Jun Wang^{1,2,3,4}, Wei Liu^{1,2,3,4}, Liping Zhou^{1,2,3,4}, Yueyi Wang^{1,2,3,4}, Hu Chen^{1,2,3,4}, Huixin Zhou^{1,2,3,4}, Zhihao Liu^{1,2,3,4}, Jiapeng Han^{1,2,3,4}, Hong Jiang^{1,2,3,4*} and Lilei Yu^{1,2,3,4*}

OPEN ACCESS

Edited by:

Jinwei Tian,
The Second Affiliated Hospital of
Harbin Medical University, China

Reviewed by:

Song Ding,
Shanghai JiaoTong University, China
Régis Guieu,
Aix Marseille Université, France

*Correspondence:

Lilei Yu
lileiyu@whu.edu.cn;
whuyulilei@163.com
Hong Jiang
hong-jiang@whu.edu.cn

†These authors have contributed
equally to this work

Specialty section:

This article was submitted to
Cardiovascular Imaging,
a section of the journal
Frontiers in Cardiovascular Medicine

Received: 25 May 2021

Accepted: 06 September 2021

Published: 29 September 2021

Citation:

Liu C, Yu Z, Chen H, Wang J, Liu W,
Zhou L, Wang Y, Chen H, Zhou H,
Liu Z, Han J, Jiang H and Yu L (2021)
Relationship Between
Immunoinflammation and Coronary
Physiology Evaluated by Quantitative
Flow Ratio in Patients With Coronary
Artery Disease.
Front. Cardiovasc. Med. 8:714276.
doi: 10.3389/fcvm.2021.714276

¹ Department of Cardiology, Renmin Hospital of Wuhan University, Wuhan, China, ² Cardiac Autonomic Nervous System Research Center of Wuhan University, Wuhan, China, ³ Cardiovascular Research Institute, Wuhan University, Wuhan, China, ⁴ Hubei Key Laboratory of Cardiology, Wuhan, China

Background: The association between coronary physiology and immunoinflammation has not been investigated. We performed a retrospective study using quantitative flow ratio (QFR) to evaluate the interaction between immunoinflammatory biomarkers and coronary physiology.

Methods: A total of 172 patients with CAD who underwent coronary arteriography (CAG) and QFR were continuously enrolled from May 2020 to February 2021. As a quantitative indicator of coronary physiology, QFR can reflect the functional severity of coronary artery stenosis. The target vessel measured by QFR was defined as that with the most severe lesions. Significant coronary anatomical stenosis was defined as 70% stenosis in the target vessel.

Results: Compared with the QFR > 0.8 group, interleukin (IL)-6, IL-10, tumor necrosis factor (TNF)- α , and interferon (IFN)- γ were increased and CD3⁺ and CD4⁺ T lymphocyte counts were decreased in the QFR \leq 0.8 group. In addition, patients with DS \leq 70% had higher IL-6, IL-10, and TNF- α levels and decreased CD3⁺ and CD4⁺ T lymphocyte counts than those with DS > 70%. Logistic regression analysis indicated IL-6 to be an independent predictor of significant coronary functional and anatomic stenosis (odds ratio, 1.125; 95% CI, 1.059–1.196; $P < 0.001$). Receiver operating characteristic (ROC) analyses showed that IL-6 > 6.36 was predictive of QFR \leq 0.8 of the target vessel. The combination of IL-6, IL-10 and CD4 improved the value for predicting QFR \leq 0.8 of the target vessel (AUC, 0.737; 95% CI, 0.661–0.810).

Conclusion: Among immunoinflammatory biomarkers, IL-6 was independently associated with a higher risk of QFR \leq 0.8 of the target vessel. The combination of immunoinflammatory biomarkers was highly predictive of significant coronary functional and anatomic stenosis.

Keywords: quantitative flow ratio, coronary physiology, coronary artery disease, immuno, inflammation

INTRODUCTION

Coronary artery disease (CAD) remains the most common cause of death worldwide, with atherosclerosis being the most common manifestation (1). Atherosclerosis is considered a chronic inflammatory disease, and both the immune system and inflammatory cells play a major role in its pathogenesis (2). The immune system influences the state of inflammatory cells by transforming them into proinflammatory or anti-inflammatory functional units and guiding interaction between different immune and inflammatory cells (3). Different inflammatory cells enter into the vascular wall and interact with each other to cause release of proinflammatory factors, which is a key step in the initiation and progression of plaque (4). Furthermore, plaque stability correlates with inflammatory cell levels. Immune cell-filled plaques are less stable and more prone to rupture, inducing major cardiovascular adverse events (5). A high level of inflammatory cytokines in CAD is closely associated with poor prognosis (6).

In addition, myocardial ischemia caused by substantial coronary stenosis has a strong influence on prognosis (3, 4), and physiological ischemia is important than anatomical stenosis in guiding the treatment of patients. In general, if coronary artery stenosis does not cause ischemia, the incidence of adverse cardiovascular events is low, and the prognosis is good (7, 8). Both increased inflammatory activity and the presence of coronary ischemia have a strong impact on the progression and prognosis of CAD. We hypothesized that markers of systemic immune function and inflammation are related to parameters reflecting the severity of coronary functional and anatomic stenosis.

Invasive fractional flow reserve (FFR) is currently considered the gold standard for evaluating the ischemic potential of CAD (8). However, due to the additional pressure guidewire requirements, invasive nature of the operation, and side effects of adenosine, the use of FFR in daily clinical practice is limited (9). QFR is a non-invasive angiographically derived FFR measurement. Previous studies have shown good agreement between measured values of QFR and FFR (10, 11), and QFR has a clear cutoff value for the diagnosis of coronary functional stenosis and demonstrates excellent reproducibility (11, 12). It has also been shown that QFR has high predictive value for prognosis (13, 14). Nevertheless, there is no evidence to date of the effects of immunity and inflammation on coronary physiology as detected by QFR in patients with CAD. In the current study, we evaluated the relationship between markers based on immune function and inflammatory activity and functional coronary lesions using QFR.

METHODS

Study Population

This retrospective observational study included 172 consecutive patients with CAD who underwent coronary arteriography (CAG) and QFR from May 2020 to March 2021 at the Department of Cardiology of Renmin Hospital of Wuhan University. CAD was diagnosed according to previously

established guidelines (15). The main exclusion criteria were as follows: a diagnosis of ST-segment elevation myocardial infarction (STEMI), non-ST-segment elevation myocardial infarction (NSTEMI), coronary artery occlusion, or myocardial bridge; unqualified coronary angiographic images included ostial lesion, severe vessel tortuosity, diffuse long lesions, and poor coronary image quality; a lack of two images with a difference of more than 25 angles, overlap in the target lesion, excessive shortening or insufficient contrast agent filling, previous coronary artery bypass grafting (CABG); severe heart failure; cardiogenic shock; severe valvular disease; and previously known liver or kidney failure (estimated glomerular filtration rate <30 ml/min). In addition, patients with chronic inflammatory states, autoimmune disease, active infection, and malignancies were excluded. The flow chart for patient inclusion and exclusion is shown in **Figure 1A**. The study protocol was approved by the ethics committee of the Renmin Hospital of Wuhan University before patient enrollment.

Coronary Angiography

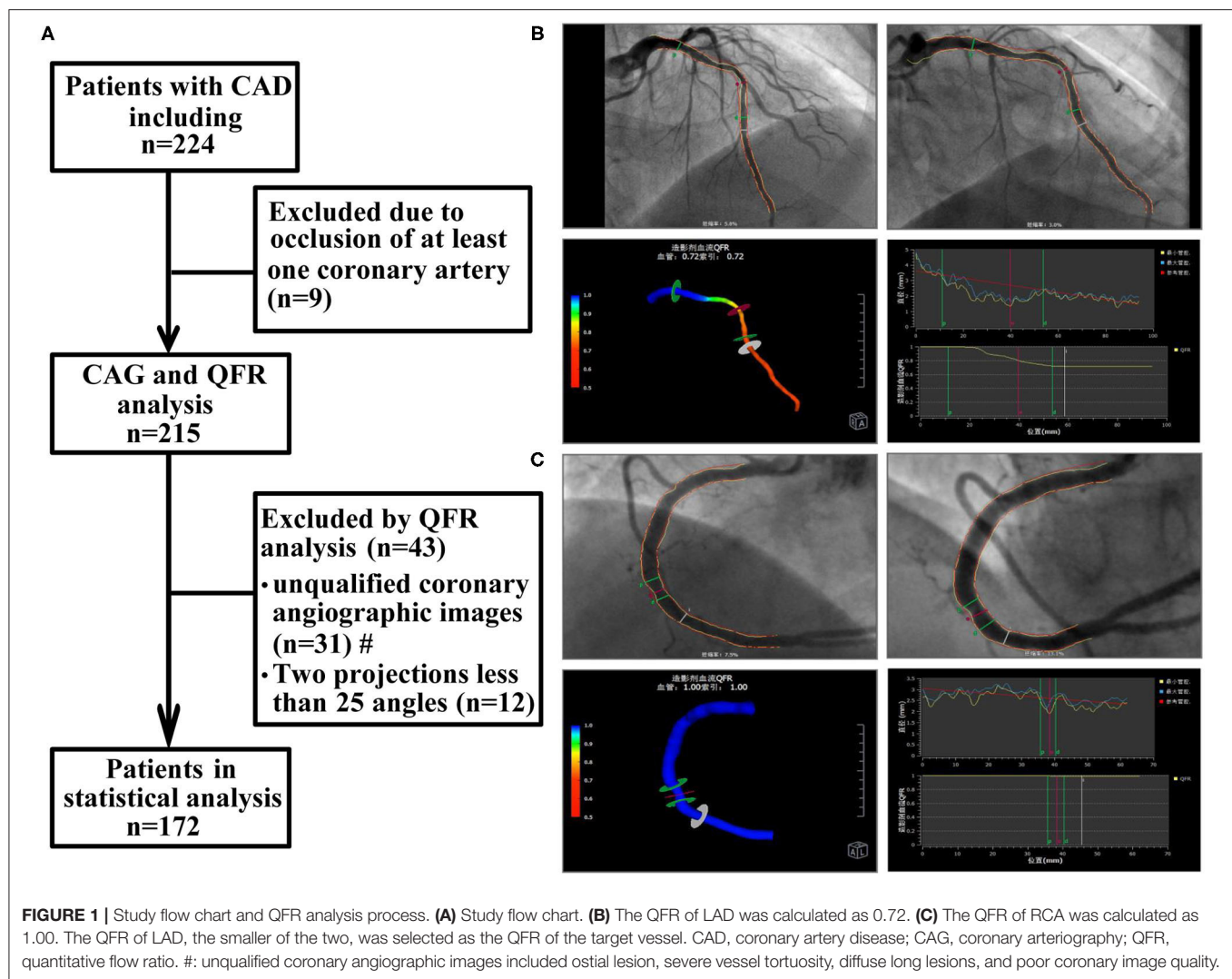
All patients underwent CAG in accordance with standard procedures. Two independent cardiologists with clinical experience assessed the degree of stenosis of each coronary lesion. Consensus with a third investigator was indicated if disagreement occurred. Significant coronary anatomical stenosis was defined as 70% stenosis of the target vessel (16). Target vessels were defined as those with the most severe lesions.

Computation of QFR

Offline QFR analysis was performed by a professional technician using the AngioPlus system (Pulse Medical Imaging Technology, Shanghai, China) following previously described procedures (10). Two angiographic images of the same coronary artery >25 degrees were selected for measurement. In the case of poor angiographic image quality, manual correction was performed according to standard operating procedures. Next, the contrast flow rate was obtained from coronary angiography images using the frame counting method, and then the contrast flow model was established for calculation. The QFR value obtained from the analysis was defined as the contrast-flow quantitative flow ratio (cQFR). Extensive studies have demonstrated that the cutoff value of QFR in coronary blood flow function is 0.8 (11, 17). For each patient, the coronary artery with the most clinically relevant or most severe stenosis was selected as the target vessel for subsequent analysis. The specific operation process is depicted in **Figures 1B,C**.

Blood Collection and Laboratory Tests

Venous blood samples were collected from all patients before they underwent CAG. All samples were sent immediately to the hospital laboratory for direct testing to prevent any potential storage effects. The samples of all participants were subjected to routine whole blood analysis, including analysis of liver and kidney function, lipids, C-reactive protein (CRP), and N-terminal pro-brain natriuretic peptide (NT-pro-BNP). Concentrations of inflammatory cytokines, including IL-2, IL-4, IL-6, IL-10, TNF- α , and IFN- γ , were determined by



flow cytometry (Becton Dickinson, FACSCalibur, USA) using a multiplex bead-based flow fluorescence immunoassay. Lymphocyte subsets were analyzed by flow cytometry (Becton Dickinson, FACSCanto II, USA). Additionally, multiple lymphocyte surface antigens were detected to distinguish different lymphocyte subsets ($CD3^+$, $CD4^+$, $CD8^+$, $CD19^+$, $CD16^+$ + 56^+); the number of cells in each subset was counted, and the value of $CD4^+/CD8^+$ was obtained. Levels of immunoglobulin (Ig)G, IgM, IgA, and complement C3 and C4 were measured by turbidimetric inhibition immunoassay using a specialized protein analysis system (IMMAGE 800 Automatic Special Protein Analyzer, Beckman, USA). A BN II protein meter (Siemens, Germany) was used to determine the concentration of IgE.

Statistical Analysis

Categorical variables are represented by frequencies and percentages (%), and the frequencies of each index were compared using the chi-square test. Continuous variables are

described in terms of the median and interquartile range (IQR) values. Unpaired *t*-tests and the Mann-Whitney test were used for comparisons, as appropriate. And correlation was determined by Pearson and Spearman rank analyses. Logistic regression analysis was also employed to evaluate independent predictors. Binary logistic regression analysis was used to obtain the prediction probability of single or multiple factors. ROC curve was drawn with the corresponding probability to analyze the prediction ability of each evaluation index. GraphPad Prism 7.0 software (GraphPad Software Inc.) and SPSS statistical software (version 26.0, IBM) were used for statistical analysis and chart drawing. *P* values < 0.05 were considered significant.

RESULTS

Baseline Characteristics

As presented in Table 1, the 172 patients included in the study were divided into two groups according to baseline

TABLE 1 | Baseline characteristics of QFR > 0.8 of the target vessel and QFR ≤ 0.8 of the target vessel.

Patients	All subjects (n = 172)	QFR > 0.8 (n = 106)	QFR ≤ 0.8 (n = 66)	P-value
Age, y	61.00 (53.00–68.00)	60.00 (52.00–68.00)	63.00 (55.00–69.00)	0.203
Male, %	114 (66.3)	62 (58.5)	52 (78.8)	0.006*
Current smoking, %	56 (32.6)	32 (30.2)	24 (36.4)	0.401
Family history of CAD, %	14 (8.1)	8 (7.5)	6 (9.1)	0.719
Diabetes mellitus, %	58 (33.7)	35 (33.0)	23 (34.8)	0.850
Hypertension, %	96 (55.8)	54 (50.9)	42 (63.6)	0.103
Hyperlipidemia, %	57 (33.1)	36 (34.0)	21 (31.8)	0.771
Previous MI, %	11 (6.4)	5 (4.7)	6 (9.1)	0.254
Previous PCI, %	61 (35.5)	27 (25.5)	34 (51.5)	0.001*
BMI, kg/m ²	24.49 (22.70–26.35)	24.77 (22.75–26.57)	24.22 (22.49–26.12)	0.314
CRP, mg/L	2.60 (0.5–5.00)	1.50 (0.5–5.00)	5.00 (0.5–5.00)	0.001*
NT pro-BNP, pg/mL	65.21 (34.85–135.20)	53.51 (31.77–103.70)	88.77 (47.72–334.50)	0.001*
Total cholesterol, mmol/L	3.90 (3.13–4.86)	3.95 (3.14–4.98)	3.79 (3.07–4.72)	0.294
Triglyceride, mmol/L	1.50 (1.01–2.14)	1.49 (0.96–2.17)	1.50 (1.09–2.11)	0.82
HDL-c, mmol/L	0.99 (0.89–1.22)	1.01 (0.90–1.23)	0.98 (0.87–1.13)	0.204
LDL-c, mmol/L	2.18 (1.59–3.13)	2.17 (1.66–3.20)	2.21 (1.54–2.91)	0.583
Location of lesions vessel				0.872
LAD	91 (52.9)	55 (51.9)	36 (54.5)	
LCX	32 (18.6)	21 (19.8)	11 (16.7)	
RCA	49 (28.5)	30 (28.3)	19 (28.8)	

Parameters were expressed as proportion and median IQR.

*A *p*-value <0.05 was considered a statistically significant difference between the two groups.

QFR, quantitative flow ratio; BMI, body mass index; CAD, coronary artery disease; CRP, C-reactive protein; NT pro-BNP, N-terminal pro-B-type natriuretic peptide; HDL-c, High density lipoprotein-cholesterol; LDL, low density lipoprotein-cholesterol; MI, myocardial infarction; PCI, percutaneous coronary intervention; CABG, coronary artery bypass grafting; LAD, left anterior descending branch; LCX, left circumferential branch; RCA, right coronary artery; IQR, interquartile range.

measurements: target vessel QFR > 0.8 (*n* = 66) and ≤ 0.8 (*n* = 106). Compared with the QFR > 0.8 of the target vessel group, the proportion of male patients in the QFR ≤ 0.8 of the target vessel group was higher (54.5 vs. 78.8%, *p* = 0.006); CRP and NT-pro BNP, markers of inflammatory response and cardiac impairment, were significantly increased (both *p* = 0.001). The proportion of patients with QFR ≤ 0.8 who had ever received percutaneous coronary intervention (PCI) was higher than that in patients with QFR > 0.8 (51.5 vs. 25.5%, *p* = 0.001). However, there was no correlation between other indicators and QFR of the target vessel (Table 1).

Comparison of Immunoinflammatory Biomarkers Between Patients With QFR > 0.8 of the Target Vessel and QFR ≤ 0.8 of the Target Vessel

The QFR ≤ 0.8 of the target vessel group showed statistically significant increases in levels of inflammatory factors, including IL-6 (*p* < 0.001), IL-10 (*p* = 0.011), TNF-α (*p* = 0.040), and IFN-γ (*p* = 0.018). However, CD3⁺ and CD4⁺ T lymphocytes were significantly reduced in patients with QFR ≤ 0.8 in the target vessel group (*p* = 0.015 and *p* = 0.011) (Figure 2). No other variables were significantly different (all *p* > 0.05).

Correlations Between QFR and Immunoinflammatory Biomarkers

IL-6 (*r* = −0.386, *p* < 0.001) and IL-10 (*r* = −0.169, *p* = 0.027) correlated negatively with QFR. In contrast, biomarkers of immune function correlated positively with QFR. Among these biomarkers, CD4⁺ T lymphocytes (*r* = 0.225, *p* = 0.003) had a higher correlation with QFR than CD3⁺ T lymphocytes (*r* = 0.215, *p* = 0.005) (Supplementary Figure 1).

Predictive Effects of Immunoinflammatory Biomarkers for QFR ≤ 0.8 of the Target Vessel

According to binary logistic regression analysis, IL-6, IL-10, and CD4⁺ T lymphocytes were predictors of QFR ≤ 0.8 of the target vessel. In addition, the significant predictive value of IL-6 was maintained after adjusting for traditional variables associated with coronary ischemia (Table 2). The CD3⁺ T lymphocyte count represents the number of all T cells, including CD4⁺ T lymphocytes and CD8⁺ T lymphocytes. As CD4⁺ T lymphocytes correlated more strongly with QFR than CD3⁺ T lymphocytes (Figure 3), we substituted CD4⁺ T lymphocytes for CD3⁺ T lymphocytes.

IL-6 had high predictive value for QFR ≤ 0.8 of the target vessel, with an area under the ROC curve of 0.709 (95% CI: 0.628–0.791). Moreover, the number of CD4⁺ T lymphocytes and

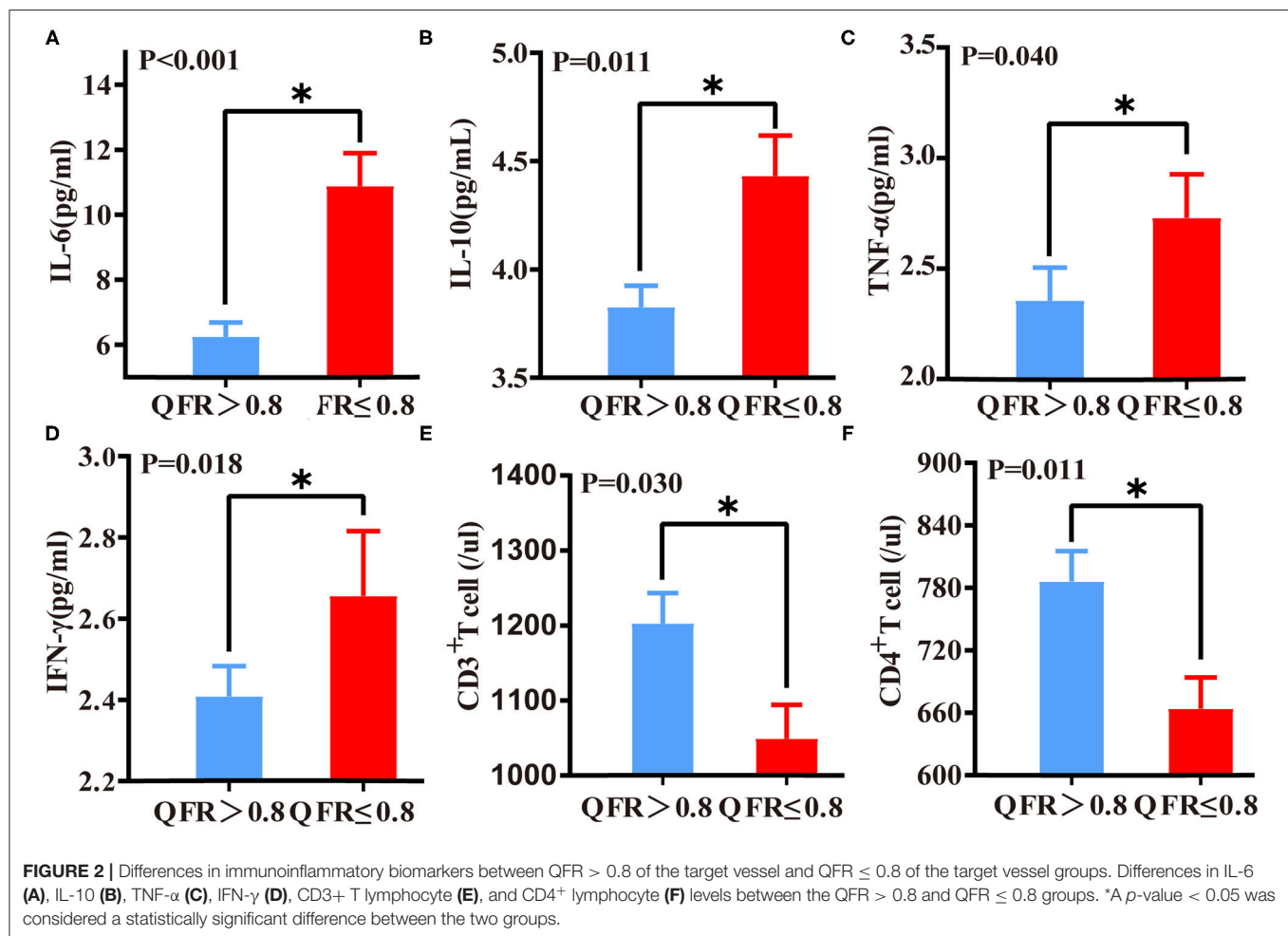


TABLE 2 | Logistic regression analyses of immunoinflammatory biomarker levels for QFR ≤ 0.8 of the target vessel.

Factor	Unadjusted		Model 1		Model 2		Model 3	
	Odds ratio (95%CI)	<i>p</i> -value	Odds ratio (95% CI)	<i>p</i> -value	Odds Ratio (95% CI)	<i>p</i> -value	Odds Ratio (95% CI)	<i>p</i> -value
IL-6	1.126 (1.062–1.194)	<0.001*	1.116 (1.055–1.182)	<0.001*	1.116 (1.052–1.183)	<0.001*	1.125 (1.059–1.196)	<0.001*
IL-10	1.429 (1.103–1.852)	0.007*	1.230 (0.929–1.630)	0.149	1.189 (0.890–1.588)	0.242	1.133 (0.838–1.531)	0.417
CD4	0.998 (0.997–0.999)	0.045*	0.998 (0.996–1.000)	0.016*	0.998 (0.997–1.000)	0.031*	0.999 (0.997–1.000)	0.110

Odds ratio shown were for immuno-inflammatory biomarker level as a continuous variable.

*A *p*-value < 0.05 was considered significant for statistical significance.

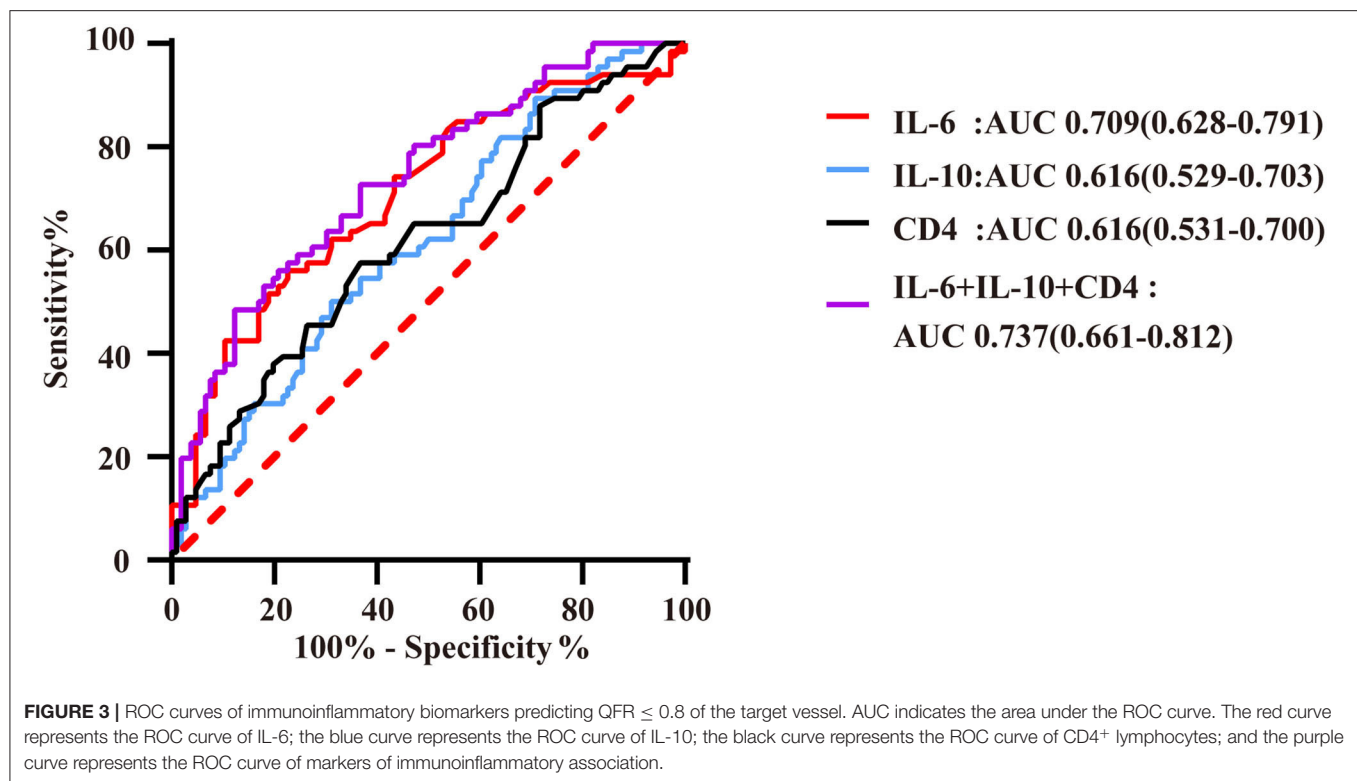
Unadjusted model performed univariate regression analysis on biomarkers. Model 1 put IL-6, IL-10, CD4 and together for multivariate regression analysis. Model 2 adjusted for NT pro-BNP and CRP. Model 3 adjusted for all factors in model 2 plus age, sex, BMI, hypertension, diabetes mellitus, smoking, and blood lipids.

IL-10 level had a certain predictive value for QFR, with AUCs of 0.616 (95% CI: 0.531–0.700) and 0.616 (95% CI: 0.529–0.703), respectively. In this study, the combination of these biomarkers resulted in a higher predictive value for QFR ≤ 0.8 of the target vessel, with an area under the ROC curve that increased to 0.737 (95% CI: 0.661–0.812) (Figure 4). The cutoff threshold of IL-6 to generate the maximum summation of sensitivity and specificity in discriminating QFR ≤ 0.8 of the target vessel was 6.36; the corresponding sensitivity and specificity were 56.1 and 77.4%, respectively. In addition, the cutoff value of the

combination of immunoinflammatory biomarkers (IL-6, IL-10 and CD4) was associated with 48.5% sensitivity and 88.7% specificity (Supplementary Table 1).

Association of Immunoinflammatory Biomarkers With Coronary Target Vessel Lesions

Based on the results of the corresponding CAG, the patients were grouped according to the 70% degree of coronary artery



diameter stenosis (DS) of the target vessel. The proportions of male patients and patients who underwent PCI, as well as CRP and BNP levels, were significantly higher among those with DS > 70% than those with DS \leq 70% ($p = 0.001$, $p < 0.001$, $p = 0.004$, $p = 0.008$, respectively). Compared with the DS \leq 70% of the target vessel group, the DS > 70% of the target vessel group had lower levels of total cholesterol ($p = 0.045$) and high-density lipoprotein (HDL) ($p = 0.034$). There was no significant difference between other indicators and DS of the target vessel (Supplementary Table 2).

Levels of IL-6 ($P < 0.001$), IL-10 ($p = 0.016$), and TNF- α ($P = 0.044$) in the DS > 70% target vessel group were much higher than those in the DS \leq 70% target vessel group. Conversely, levels of CD3⁺ T lymphocytes ($P = 0.012$) and CD4⁺ T lymphocytes ($P = 0.010$) in the DS > 70% of the target vessel group were significantly lower than those in the DS \leq 70% of the target vessel group (Figure 5).

Logistic regression analysis showed that IL-6, IL-10, and TNF- α levels and the CD4⁺ T lymphocyte count were able to predict DS > 70% of the target vessel. According to multivariate regression analysis, IL-6 was an independent predictor of DS > 70% of the target vessel (Supplementary Table 3). ROC curve analysis indicated that the combination of IL-6, IL-10, TNF- α , and CD4⁺ T lymphocyte biomarkers had a high predictive value for DS > 70% of the target vessel, with an AUC of 0.735 (95% CI, 0.661–0.810) (Figure 5). In addition, the cutoff value of IL-6 (5.62) was associated with 60.8% sensitivity and 72% specificity, with that of the combination of immunoinflammatory biomarkers

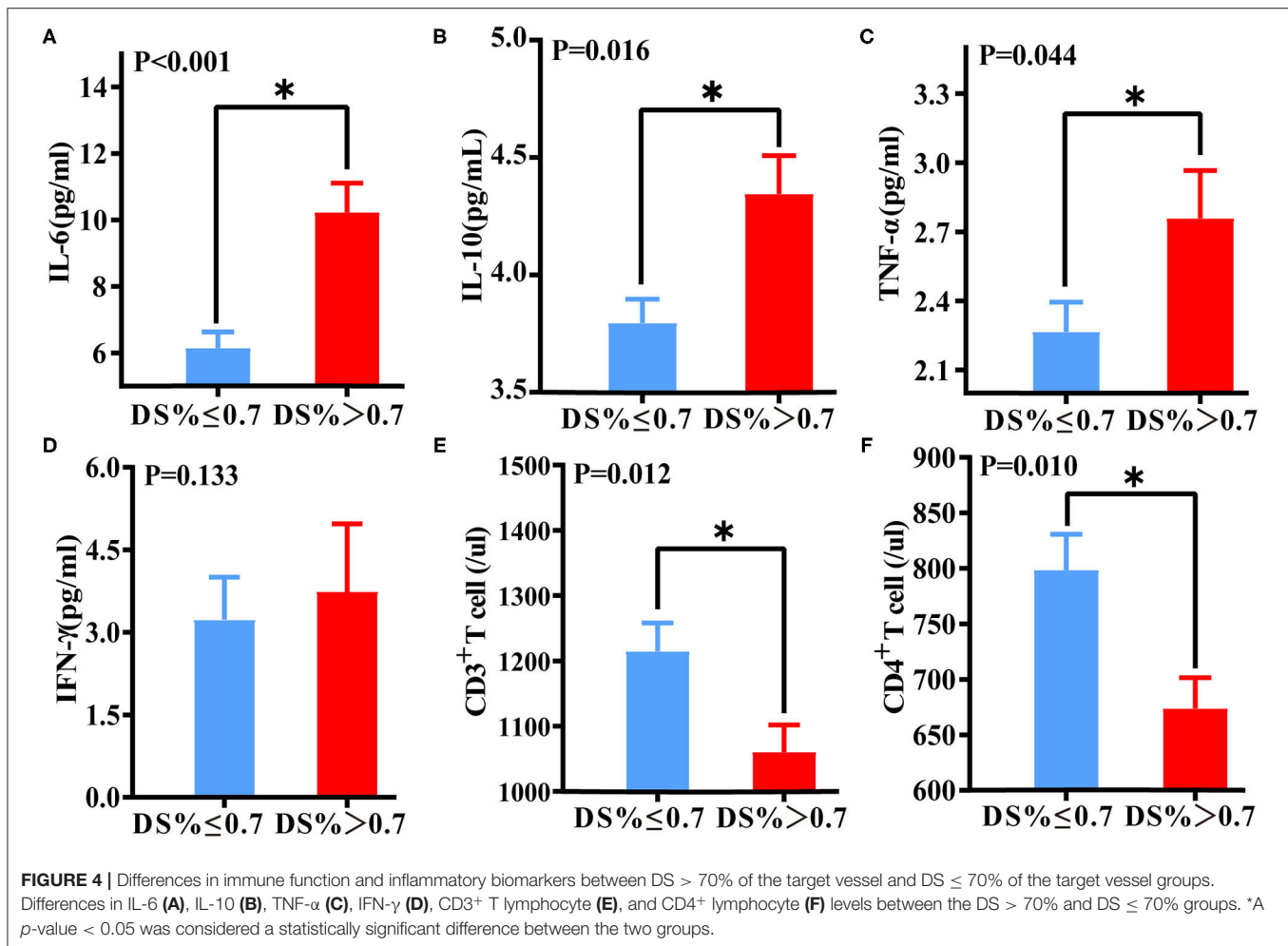
(0.403) related to 73.4% sensitivity and 62.4% specificity (Supplementary Table 4).

DISCUSSION

This study suggests that specific biomarkers of immune function and inflammatory factors, which are traditional biomarkers, are independent predictors of significant coronary anatomical and functional stenosis in patients with CAD. High levels of IL-6 and IL-10 and low CD4⁺ T lymphocyte counts were significantly associated with decreased coronary hemodynamics (QFR ≤ 0.8). Moreover, a combination of these biomarkers was superior to the individual markers in predicting functional coronary stenosis, with the largest area under the ROC curve (Figure 4). Furthermore, this study shows that these biomarkers have a certain predictive value for coronary artery anatomic stenosis.

Inflammation and Coronary Physiology

The relationship between inflammation and atherosclerosis is well-established, and various immune system cells and inflammatory factors are known to play a crucial role in the initiation and progression of CAD (1, 2). However, the link between inflammation and coronary physiology remains unclear. Our results are consistent with previous studies showing that inflammatory markers used for CAD focus on downstream inflammatory markers such as CRP (18). Upstream inflammatory markers, such as proinflammatory factors, have recently been suggested to control the inflammatory cascade, which may be more directly related to CAD (19). A large number of studies



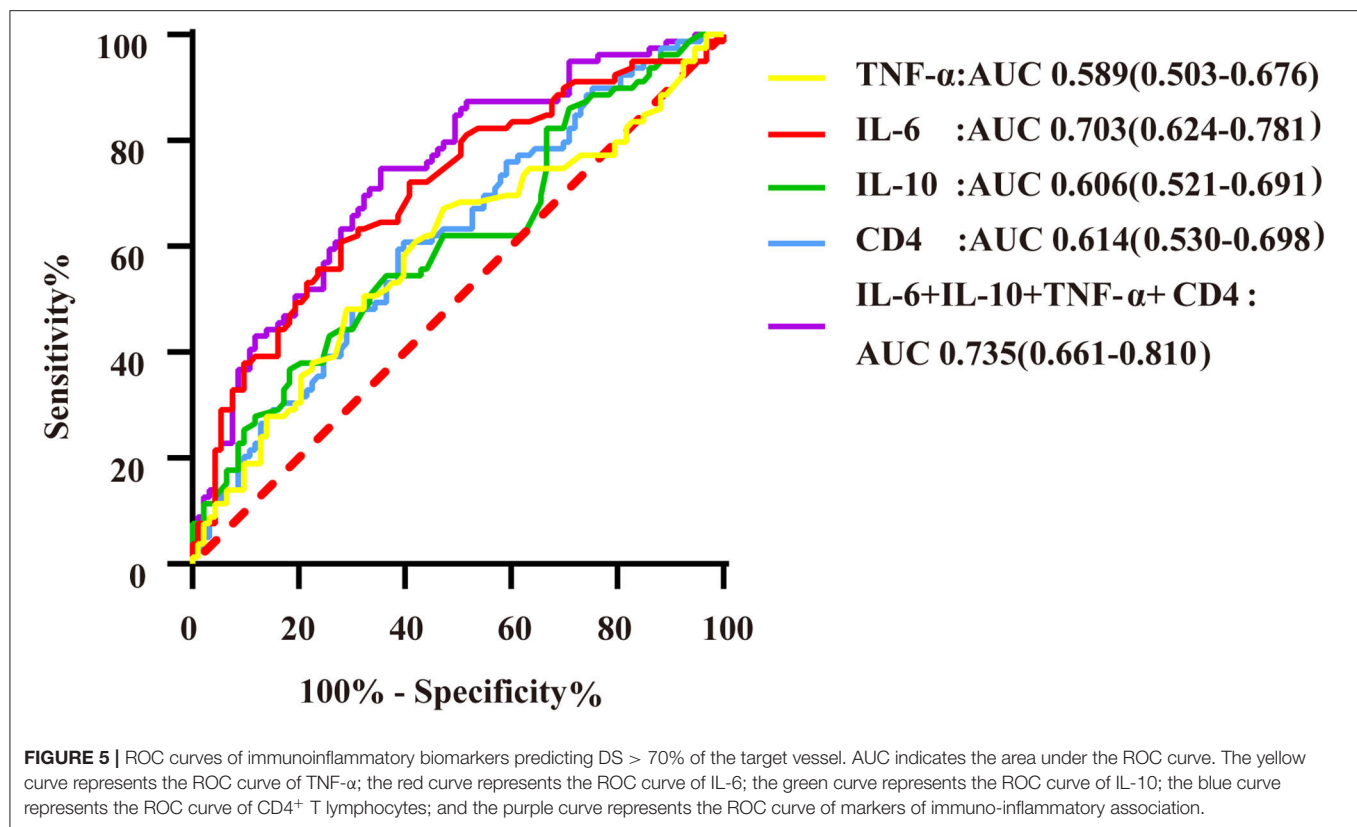
have shown that IL-6 plays a key role in the progression of coronary atherosclerosis (20, 21). IL-6 promotes the proliferation of neutrophils and monocytes as well as expression of adhesion molecules by vascular endothelial cells to enhance the local inflammatory response (22). In addition, IL-6 induces liver cells to synthesize fibrinogen and CRP (23). IL-6 correlated independently with functional and anatomic coronary stenosis in our study. Tocilizumab, an inhibitor of the IL-6 receptor, is being analyzed in clinical trials with respect to its therapeutic effect and mechanism in CAD (24, 25). Tocilizumab may affect the prognosis of CAD not only by inhibiting inflammation but also by directly regulating the severity of coronary physiology. The mechanism deserves further investigation.

Numerous studies have shown that IL-10 is a cytokine secreted mainly by monocyte macrophages and lymphocytes with inflammatory protective effects (26). Interestingly, our results revealed increased levels of IL-10 in a group of patients with more severe functional ($p = 0.011$) and anatomical ($p = 0.016$) coronary stenosis, and even elevated IL-10 levels were somewhat predictive of significant functional and anatomical coronary lesions. Similarly, some studies have reported a long-term increase in serum IL-10 levels in patients with unstable CAD

or myocardial infarction compared to levels in healthy subjects or those with stable CAD (27, 28), and IL-10 levels are higher in high-risk patients with atherosclerosis (29). We speculate that elevated IL-10 may be associated with inflammatory activation of local coronary vessels or the immune system. In addition, increased IL-10 levels can reduce the inflammatory response in coronary plaques, stabilize plaques and improve the prognosis of patients with CAD (30). In the CAPTURE trial, elevated serum IL-10 levels correlated with significant improvement in prognosis in those with acute coronary syndrome (ACS) (31).

Immunity and Coronary Physiology

A low lymphocyte count is a common manifestation of the inflammatory response, and both basic and clinical studies have suggested that a low lymphocyte count plays an important role in the progression of CAD (32, 33). The direct effectors that play a major role in inflammation are neutrophils and monocytes, whereas lymphocytes play a more extensive role in the regulation of an inflammatory response at various stages of atherosclerosis (34). Reduced lymphocyte counts are also associated with poor prognosis in patients with a variety of cardiovascular diseases, such as stable CAD (35) and ACS, including STEMI and NSTEMI



(36–38), and unstable angina pectoris (39). In this study, the numbers of CD3⁺ lymphocytes (indicating the total number of lymphocytes) and CD4⁺ lymphocytes (indicating the number of CD4⁺ T lymphocytes) were significantly reduced in patients with QFR ≤ 0.8 of the target vessel. At present, it is believed that the lymphocyte number may be reduced for the following reasons. On the one hand, lymphocyte apoptosis is increased in the inflammatory state. Under pathological conditions, inflammation indiscriminately damages lymphocytes, including Th1 cells (proinflammatory CD4⁺ lymphocytes) and Th2 cells (anti-inflammatory CD4⁺ lymphocytes). In the presence of uncleared phagocytic apoptotic cells, some heat shock proteins that interact with Toll-like receptors (TLRs) are released through cell lysis, thereby promoting secretion of proinflammatory factors by macrophages. There is a vicious cycle between the inflammatory cascade and immune cell apoptosis (40). On the other hand, patients with CAD are in a state of systemic stress response, during which the secretion of serum cortisol and catecholamine increases, which may directly lead to a decrease in lymphocyte count (41).

The Relationship Between Immunity, Inflammation and FFR

Previous studies on the link between inflammation and FFR have produced similar results. Versteeg et al. (42) demonstrated that TLRs, which play a key role in innate immunity, are significantly associated with stenosis of the tube diameter, the number of disaffected vessels, and FFR outcomes. In addition, Erdogan et al. (43) found that an increase in the number of

inflammatory cells and a decrease in the number of lymphocytes had a certain predictive power for FFR in patients with chronic coronary syndrome. In the present study, we demonstrated that immunoinflammatory biomarkers are closely related to coronary artery functional and anatomical stenosis. Therefore, our data confirm that immunoinflammatory biomarkers can serve as a therapeutic target in atherosclerosis (44, 45) and appear to be independent of and at least as powerful as traditional risk factors for myocardial infarction and atherosclerosis (46).

Limitations

This study has some limitations. First, this study involved a retrospective and observational design with a limited sample size. Second, follow-up data and endpoint event analysis were lacking. Third, other inflammatory markers, such as high-sensitivity CRP, were not included in the analysis because parameters with missing data were not included. Fourth, a gold standard control (FFR) was not included. Fifth, the QFR data were derived from the most severe stenosis observed in each of the main coronary vessels assessed. Thus, our study may not have fully taken the overall flow of the patient's coronary arteries into account, and further analysis should be performed in future well-designed clinical trials.

CONCLUSIONS

Inflammatory factors and immune function are associated with coronary artery anatomic stenosis and functional ischemia. IL-6 was found to be the most significant independent predictor

of functional coronary artery stenosis detected through QFR. Furthermore, the combination of IL-6, IL-10, and CD4⁺ T lymphocytes is a better predictor of functional coronary stenosis than any single biomarker. The combination of multiple indicators significantly increases the probability of identifying functional severe coronary artery disease, which is worthy of investigation in a broader and more specific state of heart disease.

DATA AVAILABILITY STATEMENT

The original contributions presented in the study are included in the article/**Supplementary Material**, further inquiries can be directed to the corresponding author/s.

ETHICS STATEMENT

Ethical review and approval was not required for this study with human participants, in accordance with the local legislation and institutional requirements.

AUTHOR CONTRIBUTIONS

LY and HJ: substantial contributions to conception and design, data acquisition, or data analysis, and interpretation.

REFERENCES

- Libby P, Ridker PM, Hansson GK. Progress and challenges in translating the biology of atherosclerosis. *Nature*. (2011) 473:317–25. doi: 10.1038/nature10146
- Hansson GK. Inflammation, atherosclerosis, and coronary artery disease. *New Eng J Med*. (2005) 352:1685–95. doi: 10.1056/NEJMra043430
- Legein B, Temmerman L, Biessen EA, Lutgens E. Inflammation and immune system interactions in atherosclerosis. *Cell Mol Life Sci*. (2013) 70:3847–69. doi: 10.1007/s00018-013-1289-1
- Chávez-Sánchez L, Espinosa-Luna JE, Chávez-Rueda K, Legorreta-Haquet MV, Montoya-Díaz E, Blanco-Favela F. Innate immune system cells in atherosclerosis. *Arch Med Res*. (2014) 45:1–14. doi: 10.1016/j.arcmed.2013.11.007
- Kobiyama K, Ley K. Atherosclerosis. *Circ Res*. (2018) 123:1118–20. doi: 10.1161/CIRCRESAHA.118.313816
- Libby P, Ridker PM, Hansson GK. Inflammation in atherosclerosis: from pathophysiology to practice. *J Am Coll Cardiol*. (2009) 54:2129–38. doi: 10.1016/j.jacc.2009.09.009
- Pijls NH, van Schaardenburgh P, Manoharan G, Boersma E, Bech JW, van't Veer M, et al. Percutaneous coronary intervention of functionally nonsignificant stenosis: 5-year follow-up of the DEFER Study. *J Am Coll Cardiol*. (2007) 49:2105–11. doi: 10.1016/j.jacc.2007.01.087
- Tonino PA, De Bruyne B, Pijls NH, Siebert U, Ikeno F, van't Veer M, et al. Fractional flow reserve versus angiography for guiding percutaneous coronary intervention. *N Eng J Med*. (2009) 360:213–24. doi: 10.1056/NEJMoa0807611
- De Maria GL, Garcia-Garcia HM, Scarsini R, Hideo-Kajita A, Gonzalo López N, Leone AM, et al. Novel indices of coronary physiology: do we need alternatives to fractional flow reserve? *Circ Cardiovasc Interv*. (2020) 13:e008487. doi: 10.1161/CIRCINTERVENTIONS.119.008487
- Tu S, Westra J, Yang J, von Birgelen C, Ferrara A, Pellicano M, et al. Diagnostic accuracy of fast computational approaches to derive fractional flow reserve from diagnostic coronary angiography: the international multicenter FAVOR pilot study. *JACC. Cardiovasc Int*. (2016) 9:2024–35. doi: 10.1016/j.jacc.2016.09.888
- Xu B, Tu S, Qiao S, Qu X, Chen Y, Yang J et al. Diagnostic accuracy of angiography-based quantitative flow ratio measurements for online assessment of coronary stenosis. *J Am Coll Cardiol*. (2017) 70:3077–87. doi: 10.1016/j.jacc.2017.10.035
- Chang Y, Chen L, Westra J, Sun Z, Guan C, Zhang Y, et al. Reproducibility of quantitative flow ratio: an inter-core laboratory variability study. *Cardiol J*. (2020) 27:230–7. doi: 10.5603/CJ.a2018.0105
- Biscaglia S, Tebaldi M, Brugaletta S, Cerrato E, Erriquez A, Passarini G, et al. Prognostic value of QFR measured immediately after successful stent implantation: the international multicenter prospective HAWKEYE study. *JACC. Cardiovasc Int*. (2019) 12:2079–88. doi: 10.1016/j.jcin.2019.06.003
- Kogame N, Ono M, Kawashima H, Tomaniak M, Hara H, Leipsic J, et al. The impact of coronary physiology on contemporary clinical decision making. *JACC Cardiovasc Interv*. (2020) 13:1617–38. doi: 10.1016/j.jcin.2020.04.040
- Mendis S, Thygesen K, Kuulasmaa K, Giampaoli S, Mähönen M, Ngu Blackett K, et al. World health organization definition of myocardial infarction: 2008–09 revision. *Int J Epidemiol*. (2011) 40:139–46. doi: 10.1093/ije/dyq165
- Neeland IJ, Patel RS, Eshtehardi P, Dhawan S, McDaniel MC, Rab ST, et al. Coronary angiographic scoring systems: an evaluation of their equivalence and validity. *Am Heart J*. (2012) 164:547–52.e1. doi: 10.1016/j.ahj.2012.07.007
- Song L, Tu S, Sun Z, Wang Y, Ding D, Guan C, et al. Quantitative flow ratio-guided strategy versus angiography-guided strategy for percutaneous coronary intervention: rationale and design of the FAVOR III China trial. *Am Heart J*. (2020) 223:72–80. doi: 10.1016/j.ahj.2020.02.015
- Kaptoge S I, Angelantonio E D, Lowe G. C-reactive protein concentration and risk of coronary heart disease, stroke, and mortality: an individual participant meta-analysis. *Lancet*. (2010) 375:132–40. doi: 10.1016/S0140-6736(09)61717-7
- Libby P. Inflammatory mechanisms: the molecular basis of inflammation and disease. *Nutr Rev*. (2007) 65:S140–S6. doi: 10.1301/nr.2007.dec.S140-S146
- Zegeye MM, Andersson JSO, Wennberg P, Repsilber D, Sirsjo A, Ljungberg LU. IL-6 as a mediator of the association between traditional risk factors and future myocardial infarction: a nested case-control study. *Arterioscler Thromb Vasc Biol*. (2021) 41:1570–9. doi: 10.1161/ATVBAHA.120.315793

CL, ZY, HuaC, JW, WL, ZL, YW, HuC, HZ, ZL, and JH: drafting the article or critically revising it for important intellectual content. CL, ZY, HuC, JW and WL: final approval of the version to be published and agreement to be accountable for all aspects of the work in ensuring that questions related to the accuracy or integrity of the work are appropriately investigated and resolved. All authors contributed to the article and approved the submitted version.

FUNDING

This work was supported by the National Key R&D Program of China [2017YFC1307802], and the National Natural Science Foundation of China [81970287, 81530011, 81770364, 81871486, and 82100530].

SUPPLEMENTARY MATERIAL

The Supplementary Material for this article can be found online at: <https://www.frontiersin.org/articles/10.3389/fcvm.2021.714276/full#supplementary-material>

21. Tyrrell DJ, Goldstein DR. Ageing and atherosclerosis: vascular intrinsic and extrinsic factors and potential role of IL-6. *Nature reviews. Cardiology*. (2021) 18:58–68. doi: 10.1038/s41569-020-0431-7
22. Villar-Fincheira P, Sanhueza-Olivares F, Norambuena-Soto I, Cancino-Arenas N, Hernandez-Vargas F, Troncoso R, et al. Role of interleukin-6 in vascular health and disease. *Front Mol Biosci*. (2021) 8:641734. doi: 10.3389/fmolb.2021.641734
23. Schmidt-Arras D, Rose-John S. IL-6 pathway in the liver: from physiopathology to therapy. *J Hepatol*. (2016) 64:1403–15. doi: 10.1016/j.jhep.2016.02.004
24. Kleveland O, Ueland T, Kunszt G, Bratlie M, Yndestad A, Broch K, et al. Interleukin-6 receptor inhibition with tocilizumab induces a selective and substantial increase in plasma IP-10 and MIP-1 β in non-ST-elevation myocardial infarction. *Int J Cardiol*. (2018) 271:1–7. doi: 10.1016/j.ijcard.2018.04.136
25. Giles JT, Sattar N, Gabriel S, Ridker PM, Gay S, Warne C, et al. Cardiovascular safety of tocilizumab versus etanercept in rheumatoid arthritis: a randomized controlled trial. *Arthr Rheumatol*. (2020) 72:31–40. doi: 10.1002/art.41095
26. Mallat Z, Besnard Z, Duriez M, Deleuze V, Emmanuel F, Bureau MF, et al. Protective role of interleukin-10 in atherosclerosis. *Circ Res*. (1999) 85:e17–24. doi: 10.1161/01.RES.85.8.e17
27. Lindmark E, Wallentin L, Siegbahn A. Blood cell activation, coagulation, and inflammation in men and women with coronary artery disease. *Thromb Res*. (2001) 103:249–59. doi: 10.1016/S0049-3848(01)00313-9
28. Cavusoglu E, Marmur JD, Hojjati MR, Chopra V, Butala M, Subnani R et al. Plasma interleukin-10 levels and adverse outcomes in acute coronary syndrome. *Am J Med*. (2011) 124:724–30. doi: 10.1016/j.amjmed.2011.02.040
29. Heiskanen M, Kähönen M, Hurme M, Lehtimäki T, Mononen N, Juonala M, et al. Polymorphism in the IL10 promoter region and early markers of atherosclerosis: the cardiovascular risk in young finns study. *Atherosclerosis*. (2010) 208:190–6. doi: 10.1016/j.atherosclerosis.2009.06.032
30. Tedgui A, Mallat Z. Cytokines in atherosclerosis: pathogenic and regulatory pathways. *Physiol Rev*. (2006) 86:515–81. doi: 10.1152/physrev.00024.2005
31. Heeschen C, Dimmeler S, Hamm CW, Fichtlscherer S, Boersma E, Simoons ML, et al. Serum level of the antiinflammatory cytokine interleukin-10 is an important prognostic determinant in patients with acute coronary syndromes. *Circulation*. (2003) 107:2109–14. doi: 10.1161/01.CIR.0000065232.57371.25
32. Haybar H, Pezeshki SMS, Saki N. Evaluation of complete blood count parameters in cardiovascular diseases: an early indicator of prognosis? *Exp Mol Pathol*. (2019) 110:104267. doi: 10.1016/j.yexmp.2019.104267
33. Verdoia M, Nardin M, Gioscia R, Negro F, Marcolongo M, Suryapranata H, et al. Higher neutrophil-to-lymphocyte ratio (NLR) increases the risk of suboptimal platelet inhibition and major cardiovascular ischemic events among ACS patients receiving dual antiplatelet therapy with ticagrelor. *Vascul Pharmacol*. (2020) 132:106765. doi: 10.1016/j.vph.2020.106765
34. Bodi V, Sanchis J, Nunez J, Mainar L, Minana G, Benet I, et al. Uncontrolled immune response in acute myocardial infarction: unraveling the thread. *Am Heart J*. (2008) 156:1065–73. doi: 10.1016/j.ahj.2008.07.008
35. Ommen SR, Gibbons RJ, Hodge DO, Thomson SP. Usefulness of the lymphocyte concentration as a prognostic marker in coronary artery disease. *Am J Cardiol*. (1997) 79:812–4. doi: 10.1016/S0002-9149(96)00878-8
36. Tamhane UU, Aneja S, Montgomery D, Rogers EK, Eagle KA, Gurm HS. Association between admission neutrophil to lymphocyte ratio and outcomes in patients with acute coronary syndrome. *Am J Cardiol*. (2008) 102:653–7. doi: 10.1016/j.amjcard.2008.05.006
37. Núñez J, Sastre C, D'Ascoli G, Ruiz V, Bonanad C, Miñana G, et al. Relation of low lymphocyte count to frailty and its usefulness as a prognostic biomarker in patients >65 years of age with acute coronary syndrome. *Am J Cardiol*. (2020) 125:1033–8. doi: 10.1016/j.amjcard.2020.01.006
38. Núñez J, Sanchis J, Bodí V, Núñez E, Heatta AM, Miñana G, et al. Therapeutic implications of low lymphocyte count in non-ST segment elevation acute coronary syndromes. *Eur J Int Med*. (2009) 20:768–74. doi: 10.1016/j.ejim.2009.09.006
39. Zouridakis EG, Garcia-Moll X, Kaski JC. Usefulness of the blood lymphocyte count in predicting recurrent instability and death in patients with unstable angina pectoris. *Am J Cardiol*. (2000) 86:449–51. doi: 10.1016/S0002-9149(00)00963-2
40. Gupta S, Agrawal A, Agrawal S, Su H, Gollapudi S. A paradox of immunodeficiency and inflammation in human aging: lessons learned from apoptosis. *Immun Ageing*. (2006) 3:5. doi: 10.1186/1742-4933-3-5
41. Thomson SP, McMahon LJ, Nugent CA. Endogenous cortisol: a regulator of the number of lymphocytes in peripheral blood. *Clin Immunol Immunopathol*. (1980) 17:506–14. doi: 10.1016/0090-1229(80)90146-4
42. Versteeg D, Hoefer IE, Schoneveld AH, de Kleijn DP, Busser E, Strijder C, et al. Monocyte toll-like receptor 2 and 4 responses and expression following percutaneous coronary intervention: association with lesion stenosis and fractional flow reserve. *Heart*. (2008) 94:770–6. doi: 10.1136/hrt.2007.117259
43. Erdogan M, Erdöl MA, Öztürk S, Durmaz T. Systemic immune-inflammation index is a novel marker to predict functionally significant coronary artery stenosis. *Bio Med*. (2020) 14:1553–61. doi: 10.2217/bmm-2020-0274
44. Yu L, Huang B, Po SS, Tan T, Wang M, Zhou L, et al. Low-level tragus stimulation for the treatment of ischemia and reperfusion injury in patients with ST-segment elevation myocardial infarction: a proof-of-concept study. *JACC Cardiovasc Int*. (2017) 10:1511–20. doi: 10.1016/j.jcin.2017.04.036
45. Goldfine AB, Shoelson SE. Therapeutic approaches targeting inflammation for diabetes and associated cardiovascular risk. *J Clin Invest*. (2017) 127:83–93. doi: 10.1172/JCI88884
46. Lorenzo C, Delgado P, Busse CE, Sanz-Bravo A, Martos-Folgado I, Bonzon-Kulichenko E, et al. ALDH4A1 is an atherosclerosis auto-antigen targeted by protective antibodies. *Nature*. (2021) 589:287–92. doi: 10.1038/s41586-020-2993-2

Conflict of Interest: The authors declare that the research was conducted in the absence of any commercial or financial relationships that could be construed as a potential conflict of interest.

Publisher's Note: All claims expressed in this article are solely those of the authors and do not necessarily represent those of their affiliated organizations, or those of the publisher, the editors and the reviewers. Any product that may be evaluated in this article, or claim that may be made by its manufacturer, is not guaranteed or endorsed by the publisher.

Copyright © 2021 Liu, Yu, Chen, Wang, Liu, Zhou, Wang, Chen, Zhou, Liu, Han, Jiang and Yu. This is an open-access article distributed under the terms of the Creative Commons Attribution License (CC BY). The use, distribution or reproduction in other forums is permitted, provided the original author(s) and the copyright owner(s) are credited and that the original publication in this journal is cited, in accordance with accepted academic practice. No use, distribution or reproduction is permitted which does not comply with these terms.



Advances in CT Techniques in Vascular Calcification

Lijie Zhang¹, Lihua Li², Guoquan Feng³, Tingpan Fan¹, Han Jiang¹ and Zhongqun Wang^{1*}

¹ Department of Cardiology, Affiliated Hospital of Jiangsu University, Zhenjiang, China, ² Department of Pathology, Affiliated Hospital of Jiangsu University, Zhenjiang, China, ³ Department of Radiology, Affiliated Hospital of Jiangsu University, Zhenjiang, China

Vascular calcification, a common pathological phenomenon in atherosclerosis, diabetes, hypertension, and other diseases, increases the incidence and mortality of cardiovascular diseases. Therefore, the prevention and detection of vascular calcification play an important role. At present, various techniques have been applied to the analysis of vascular calcification, but clinical examination mainly depends on non-invasive and invasive imaging methods to detect and quantify. Computed tomography (CT), as a commonly used clinical examination method, can analyze vascular calcification. In recent years, with the development of technology, in addition to traditional CT, some emerging types of CT, such as dual-energy CT and micro CT, have emerged for vascular imaging and providing anatomical information for calcification. This review focuses on the latest application of various CT techniques in vascular calcification.

Keywords: vascular calcification, calcification score, micro CT, dual energy CT, multi-slice spiral CT

OPEN ACCESS

Edited by:

Zhao Wang,
University of Electronic Science and
Technology of China, China

Reviewed by:

Atsushi Sakamoto,
CVPath Institute, United States
Yuanli Chen,
Hefei University of Technology, China
Meixiu Jiang,
Nanchang University, China

*Correspondence:

Zhongqun Wang
wangtsmc@126.com

Specialty section:

This article was submitted to
Cardiovascular Imaging,
a section of the journal
Frontiers in Cardiovascular Medicine

Received: 29 May 2021

Accepted: 30 August 2021

Published: 29 September 2021

Citation:

Zhang L, Li L, Feng G, Fan T, Jiang H
and Wang Z (2021) Advances in CT
Techniques in Vascular Calcification.
Front. Cardiovasc. Med. 8:716822.
doi: 10.3389/fcvm.2021.716822

INTRODUCTION

In hypertension, diabetes, atherosclerosis, and other diseases, vascular calcification, which severely affects human health, must not be ignored (1). Currently, there are many quantitative methods to calculate a vascular calcification level score. The most commonly used process is the Agatston (2), in which lesions with CT value ≥ 130 Hu and area ≥ 1 mm² (3) are defined as calcification. It is worth noting that the Agatston score is for the assessment of calcification in the coronary artery. As a clinically accessible imaging technique, CT is the most advanced non-invasive tool for detecting coronary calcification (4). CT can quickly and easily image and analyze the calcification. Bradley et al. (5) divided calcification into three characteristics: perimeter, length, and morphology, and the score accorded each feature. Multiple studies (6) have verified the accuracy and importance of calcification score derived by CT. In this review, recent development in various CT techniques in evaluating vascular calcification is stated. Moreover, we discuss the application and future development of CT in vascular calcification.

THE SIGNIFICANCE OF VASCULAR CALCIFICATION ASSESSED BY CT, ESPECIALLY IN THE CORONARY ARTERY

CT is a non-invasive imaging method for evaluating and analyzing vascular calcification. It is considered the gold standard for analyzing and quantifying vascular calcification (7, 8). Many studies have shown that the coronary calcium score is an essential and reliable predictor as levels of calcium increase with the morbidity and mortality of cardiovascular disease in patients (9–11). In a feasibility study, patients with a calcium score over 400 had a high risk of cardiovascular disease,

while those who scored 1 to 400 were at twice the risk of cardiovascular disease as those with a zero score (12). Rennenberg et al. analyzed the results of 30 different studies. They found a three to four times higher risk of incidence and mortality of cardiovascular disease in patients with vascular calcification (13).

Coronary calcium scoring is useful for a wide range of factors such as age and risk. It can assist risk stratification for clinical cardiovascular events (14, 15). Furthermore, the coronary artery calcium score (CACS) helps improve risk prediction in intermediate-risk groups when combined with other traditional clinical risk classification methods (16). This was confirmed by Tamar et al. (17). They found a greater redistribution of risk for middle-grade patients. This suggests that middle-risk patients may be more appropriate for coronary calcium scores. CACS was verified as optimizing the risk classification of cardiovascular events. It has significantly improved the accuracy of cardiovascular risk stratification. More importantly, CACS can help some patients at risk of cardiovascular disease be treated with statins at a secondary prevention level (18).

As a relatively inexpensive non-invasive imaging method (19), coronary computed tomography (CCTA) has become a vital examination method of patients with coronary disease in the clinical diagnosis and treatment plans due to its advantages of high spatial resolution, high sensitivity (95–99%), and high negative predictive value (97–99%) (20). The resolution of currently available CCTA is 0.5–1 mm, and CCTA is widely used to prevent and examine coronary heart disease (21). As a non-invasive examination method, compared with invasive coronary angiography, the visualization of blood vessels is the main advantage of CCTA (22). It provides information about coronary arteries' structure and information about the shape and composition of vascular plaques. Furthermore, the severity of coronary plaques estimated by imaging is consistent with intravascular ultrasound (IVUS) (23). However, it cannot detect minute elements such as macrophage accumulation and prominent plaque characteristics (24).

Using the traditional CT scanner, coronary artery calcium (CAC) is defined as (3) a lesion above the threshold of 130 sound field units with an area $\geq 1 \text{ mm}^2$. Studies have shown that (25) for lesions with calcification score ≥ 400 , the sensitivity and specificity of conventional CT in the diagnosis of coronary heart disease are lower than those of CCTA technology. Furthermore, as CCTA provides less information when the calcification score is high, severely calcified plaques cause beam hardening and blooming artifacts, resulting in inaccurate diagnoses of coronary artery stenosis (26). Skinner et al. (27) recommended invasive coronary angiography for patients with a CAC score >400 . It has been proved that (28) adding the transluminal attenuation gradient of a transverse optical lumen to CCTA can improve the diagnostic accuracy of CCTA. Experiments show that (29) a higher heart rate will affect the repeatability of CCTA plaque measurement. Higher heart rates will produce motion artifacts, leading to poor plaque image quality. Some strategies have been developed to improve CCTA diagnostic performance in calcified plaque recognition (30, 31). These methods include using image post-processing methods and iterative reconstruction (IR)

algorithms to suppress the influence of severe calcification on coronary artery lumen evaluation. Li et al. (32) found that the blooming removal algorithm significantly reduced blooming artifacts caused by calcified plaque, reduced the occurrence of false-positive coronary artery lesions, and improved CCTA diagnostic accuracy. It is worth noting that a study found that (33) the relationship between calcium volume and density and subsequent clinical diseases varies. Coronary artery calcification volume is positively correlated with both coronary heart disease and cardiovascular disease, while calcification density is inversely proportional to both. Several other studies have supported this view, concluding that stabilization has a greater density of calcification plaques than acute coronary heart disease (34–37). These results suggest that the density of calcification plaques may be protective and that high densities of calcification plaques are associated with stability. The mechanism by which this phenomenon occurs is currently unknown (38), and further investigation is needed.

CAC degree is closely associated with age, sex, and other factors, and the extent and prevalence of calcification increase with age (39). CCTA can detect CAC before patient symptoms appear, thus shortening hospital stay and saving costs (40). However, its main disadvantages are the need for iodized contrast media and radiation exposure, and consequently, there may be a potential risk of radiation-related malignant tumors (41).

WHAT ARE THE INADEQUACIES AND WEAK POINTS OF CALCIFICATION DETECTION BY EXISTING CT?

Depending on the vessel site involved, vascular calcification can be classified into medial and intimal calcification (42). As the spatial resolution of normal CT is not ideal, distinguishing between intimal and medial calcification is challenging. Normal CT does not detect microcalcification effectively (8). Additionally, with the widespread use of CT in vascular calcification imaging, radiation exposure is a significant concern. Consequently, reducing radiation exposure while maintaining image quality has become the focus of subsequent technical improvements (43). Currently, four techniques are used to optimize the radiation dose in multi-slice spiral CT (MSCT) arterial imaging: an ECG control tube technique, automatic exposure technique, tube voltage adjustment, and extensive pitch selection technique. It has also been proved that (44) 640-slice CT technology can reduce the radiation dose using wide-area detector technology. However, the expensive CT equipment and high detection cost also limit its wider use (45).

Imaging by CT, high-risk plaques include napkin ring signs, spot calcification, low attenuation plaques, and positive remodeling. The density of the napkin ring sign area is characterized by a high outer and low inner density (46), spot calcification of $<3 \text{ mm}$ (47), low attenuation feature patches $<150 \text{ HU}$ (48), and positive remodeling $\text{RI} > 1.1$ (47). If two of these are satisfied, it is defined as high-risk plaque (47). High-risk plaques are undesirable characteristics and can significantly increase the risk of cardiovascular disease.

Contrastingly, significant calcification can stabilize the plaque and rarely rupture, reflecting the disease stability (49).

CURRENT CLINICALLY AVAILABLE CT TECHNIQUES

MSCT

With the development of medical technology, MSCT has been constantly updated and improved, expanding from its previous 16-slice system to 128-, 256-, 320-, and 640-slice, or more (21). The development of multilayer spiral CT significantly reduces the patient's breath-holding time. At the same time, the improvement in temporal resolution reduces cardiac motion artifacts (50). After long-term clinical application, MSCT is a non-invasive, highly safe, operationally simple technique that can analyze coronary artery calcification and accurately assess the severity of coronary artery stenosis and plaque composition (21). This provides a variety of information for follow-up treatments.

With the gradual improvement in spatial resolution, MSCT allows the complete imaging analysis of minute calcification, and repeated examinations can be performed (21). MSCT is not only fast, simple, and non-invasive with high diagnostic accuracy but also uses many post-processing technologies (51), including volume rendering (VR), maximum intensity projection (MIP), multiplanar reconstruction (MPR), and curved planar reconstruction (CPR). However, these post-processing techniques also have their shortcomings. The role of each post-processing technique is different; for example, VR is beneficial to the observation of the overall arterial anatomy, while CPR is useful in plaque estimation (51). Many post-processing techniques are often used in combination to avoid misdiagnosis or no diagnosis at all.

Over the past decade, MSCT techniques can accurately detect and quantify the degree of arterial calcification. It has been used to monitor the progress of vascular calcification and evaluate and compare the effectiveness of various treatment regimens (45), including assessing the role of vitamin D in CAC (52). Medical staff can integrate CT into the decision-making process and improve work efficiency. Importantly, MSCT has been used to examine vascular calcification, distinguish between patients with different cardiovascular disease incidences and mortality risks,

and conduct timely clinical interventions to improve patient disease management and improve patient care.

The dual-source CT (DSCT) is a new technology developed based on 64-slice spiral CT. DSCT with two x-ray tubes and two detectors and the systems can work simultaneously (53). DSCT improves temporal resolution compared to single-source CT, which allows for imaging at higher heart rates. **Table 1** compares the main parameters of the first-, second-, and third-generation DSCT (54, 55). With the introduction of third-generation DSCT, its focus is smaller than that of previous generations. Even small anatomy can be displayed with a superior image quality, compared to the previous CT (56). Recently, it was found that the third-generation DSCT can be combined with tin filtering to reduce the radiation dose during calcification image acquisition (57, 58). In another study, Manta et al. (59) used the third-generation DSCT to image calcification in mice, and the scanning time was only 40 s. The total calcium content of detected calcified aortic plaques was as low as 0.71 $\mu\text{g Ca}^{2+}/\text{mg}$, proving the feasibility of imaging human-calcified plaques using the CT system. Moreover, the experimental results of Philip et al. showed that the radiation dose during CCTA, using third-generation DSCT, was reduced, and image quality was better than with the second-generation DSCT. They propose that the latest third-generation DSCT CCTA can be performed on patients with a radiation dose of <1 mSv (60).

Dual-Energy CT

Dual-energy CT (DECT), also called (61) spectral CT, can image the exact location using two different kVp so that two other datasets are obtained (62). Presently, DECT uses six methods and techniques (63), namely, dual-source DECT, single-source helical DECT, single-source twin-beam DECT, single-source sequential DECT, single-source rapid switching DECT, and dual-layer DECT. Dual-source DECT has a two-source CT system. Each X-ray tube produces a different X-ray energy spectrum. Single-source helical DECT is performed with two spiral scans under different kVp conditions, and single-source twin-beam DECT features the use of split-filter technology. Single-source sequential DECT data are obtained twice with two different kVp, single-source rapid switching DECT features an immediate change in the tube voltage between 80 and 140 kVp, and dual-layer DECT has a unique dual-layer energy-resolving detector (63).

TABLE 1 | Comparison of first-, second-, and third-generation dual-source CT.

Main parameter	First generation	Second generation	Third generation
Minimum frame rotation time (s)	0.33	0.28	0.25
Time resolution (ms)	83	75	66
Max scan speed (cm/s)	20.0	45.8	73.7
Maximum number of image layers (layer)	64	128	96
Optional kV value (KV)	80.100.120.140	70.80.100.120.140	70.80.100.120.140.150
Imaging vision (cm)	26	33	50
Ball tube max. power (kW)	2 × 80	2 × 100	2 × 120
Maximum collimation beam width (mm)	19.2	34.8	52.5

DECT features two different grades of images which can be obtained by one scan and can distinguish between the calcified and non-calcified plaque as well as show the stenosis degree of coronary artery lumen (64). Another advantage of DECT (65) is that it simplifies the workflow. Its data apply to all imaged patients; there is no need to select patients before scanning. DECT can remove artifacts and clearly show the components that produce artifacts such as coronary calcification and metals (66). DECT application technology (67) includes virtual monochromatic imaging (VMI) and virtual non-contrast (VNC) reconstruction. VMI is the synthetic image at a specific single energy level from two spectral x-ray projections, and VNC removes some imaging components (68). Using VMI to reduce the contrast agent dose is considered one of the most promising DECT applications (67). Additionally, VMI has the advantages of improving image contrast (69) and reducing artifacts (70), consequently improving the overall image quality and diagnostic performance. However, VMI has several limitations in reducing artifacts (71); the effect is best at high keV, but this also suppresses the iodine contrast. In addition, the removal of metal artifacts at high keV depends on the properties of the metal itself. VNC can be used to obtain the calcium score of coronary arteries (72). Compared with using calcium score acquisition alone, the radiation dose was reduced, but the displayed calcification was smaller than the actual calcification (73). Therefore, further research is still needed to determine the specific deviation of the VNC from reality (68). In a phantom study, researchers used a plaque similar to human vascular calcification and demonstrated strong agreement between the calcium integration calculated by DECT and the conventional mono-energy CT (74). It takes some time to use these techniques in fast-paced clinical work, which makes it challenging to get the maximum advantages of DECT (75).

DECT uses material decomposition to reduce the calcified components of plaque, thereby improving the visualization of the optical cavity (68). It also enhances plaque visualization to enable the accurate assessment of high-risk plaque features (76). DECT achieves a high-pitch spiral acquisition protocol of 3.0 and higher, shortens the scanning time, and thus reduces the effective radiation dose (77). DECT has a unique acquisition method called high-pitch spiral acquisition. It has a pair of dual-energy detectors. It only uses a quarter of the rotation time to obtain an image, thus providing a higher time resolution (78). According to a study (79), the imaging of ultrasmall superparamagnetic iron oxide by DECT may be helpful to visualize and quantify the accumulation of macrophages in plaque. It is expected that this technique will become a new technique in coronary plaque imaging. Ultrasmall superparamagnetic iron oxide is a negatively charged contrast agent that can stay in the circulatory system for a long time (80).

Logically, the total radiation dose of DECT is twice that of traditional scanning because it needs to obtain data at two different energy levels. However, DECT uses some methods to divide the total radiation dose into high- and low-energy components so that the total dose is no higher than in conventional scanning (81, 82). DECT can subtract calcified plaques from the images, which may improve the assessment

of the vascular system, especially with severely calcified plaques (71). Similarly, Domenic et al. (83) evaluated the DECT scanning calcium subtraction algorithm and its influence on the intracavity visualization of patients with severely calcified coronary arteries. They found that compared with the standard linear mixed non-subtraction image, the image with calcium subtraction provided better visibility of the coronary artery lumen and improved the reliability of diagnosis without affecting image quality and contrast noise. However, Michael et al. (84) found that DECT is not effective in evaluating the integrity of blood vessels and the plaque subtraction results are biased. Consequently, additional research is also needed to assess the role of this technique under specific clinical conditions.

In conclusion, further research is still needed in using DECT to identify coronary plaque and evaluate its diagnostic performance and potential clinical value.

CURRENT AVAILABLE NON-CLINICAL NEW CT TECHNIQUES

Micro-CT

Micro-CT has received wide attention as a newly developed imaging method for examining vascular calcification. Microcalcification in the fibrous cap destroys plaque stability by promoting rupture and is not easily detected by the two-dimensional histological method (85). A microcalcification size of only between 5 and 65 μm is sufficient to make the plaque unstable (86). However, ordinary CT cannot effectively detect microcalcification due to spatial resolution limitations. The spatial resolution of micro-CT can reach 1–10 μm (87), which can distinguish and quantify microscopic and macroscopic calcification. Moreover, micro-CT can detect microcalcifications in blood vessels which are normally difficult to find. In animal research, histological methods have been used for calcification analysis, but they have some shortcomings, such as the inability to check for complete vascular calcification. However, using micro-CT surmounts these limitations and calcification can be visualized and quantified three-dimensionally (88). Micro-CT can quantify calcification volume and calcification load, and there was no experimental deviation in the localization and distribution of calcification (88). Calcification load has a strong correlation with the calcification score. The volume represents the spatial size of the calcification plaque and the unit of calcification volume in mm^3 (89). Although micro-CT is reliable in detecting calcified plaque, it cannot effectively visualize the calcified internal structure, limiting the imaging of small structures such as calcified cell recesses and cell cracks (90). As previously stated, the disadvantages of micro-CT (91) include a long acquisition time, the need for deep anesthesia, poor soft tissue contrast, and high radiation dose, and the radiation doses can reach 760 mGy per scan. However, the CCTA radiation dose is usually around 100–450 mGy (92).

Non-destructive 3D micro-CT has been used in some studies on preclinical vascular calcification. Current CT 3D imaging technology can completely reconstruct calcified arteries

and provide accurate quantitative information. 3D micro-CT can detect arterial calcification with an intact vascular structure and accurately quantify calcification by the threshold method (93). 3D micro-CT can be combined with histology, immunohistochemistry, and proteomic methods and can be used as a supplementary means of histological examination. It provides a method of obtaining additional information about calcification volume and load from the same artery segment of the same animal (88). Moreover, the increasing practicality and technological development of the 3D Micro CT also provides a new opportunity to visualize and quantify intimal and medial calcification.

Carbon Nanotube–Based Micro-CT

Carbon nanotube-based (CNT) micro-CT can accurately generate microsecond transmission pulses and control transmission rays and provide higher temporal and spatial resolution. Compared with traditional micro-CT, the sharpness of the CNT calcification image with micro-CT in mouse models increased (94). This is a helpful tool for evaluating vascular calcification in living mice. However, only a few relevant studies have been conducted, and further research is needed to ensure clinical availability.

Combining Micro-CT With ^{18}F -NaF Micro-PET/CT

^{18}F -NaF micro-PET/CT can distinguish between macrocalcification and microcalcification (95). ^{18}F -NaF can bind to the calcified surface of small blood vessels (96). It is an essential method in measuring the calcified surface area and metabolic activity degree of calcified plaque according to the uptake of ^{18}F -NaF (97). This is an area where micro-CT does not perform well. Therefore, combining micro-CT with ^{18}F -NaF micro-PET/CT may become an excellent method to detect vascular calcification. However, its use may be inhibited by the expensive costs and the lack of standard analysis protocols in its clinical application (98).

Nano-CT

The spatial resolution of nano-CT can be as high as 400 nm, which exceeds micro-CT and can be imaged in the submicron range (90). With nano-CT imaging, the non-calcified groove of a single plaque cell can be detected, and its histopathological correlation corresponds to chondrocyte-like cells. Currently, the possibility of using nano-CT in the body is remote, as it requires inhibiting human physiological activity. Hence, the technology is likely to be used as an imaging method for *in vitro* analysis (90).

Synchrotron Radiation CT

The essence of a synchrotron is a circulating particle accelerator, and the X-rays generated by the synchrotron can be used to create 3D images with resolution up to 1 μm (99). Synchrotron radiation CT is an imaging technology belonging to phase-contrast computed tomography (PCCT), combining phase contrast with micron resolution, promoting superior spatial resolution. Differential phase-contrast imaging, a newly developed synchrotron imaging technology, allows the

evaluation of large structures and microscopic details of mouse atherosclerotic plaques and is a detailed three-dimensional morphological evaluation. The three-dimensional characteristics of imaging technology also allow detailed evaluation from different angles (100).

PCCT has high spatial resolution and soft-tissue contrast, which can accurately estimate the constituent and shape of plaque, and reliably classify it, and the results are consistent with histopathology (101). Some studies have shown that (102) phase-contrast CT can accurately identify lipid-rich, fibrous, or calcified plaques and has high diagnostic accuracy (sensitivity ≥ 0.95 ; specificity ≥ 0.94). Pfeiffer et al. (103) used phase-contrast CT to examine coronary arteries. The images showed densely calcified plaques and various narrow areas, which were difficult to identify with conventional CT examination (104). However, this technology has not been applied in humans, only *in vitro* or animal research (105).

Future micro-CT studies are needed if its use can be extended to clinical practice. Suppose micro-CT can suitably integrate three-dimensional data of vascular calcification with a manageable and analyzable platform. In that case, it can be more widely applied and is expected to become a conventional method for vascular calcification analysis in the future.

Ultra-High Resolution CT

The recently developed ultra-high resolution CT (106) allows images with a slice thickness of 0.25 mm, with a higher spatial resolution than traditional CT, and improves the diagnostic accuracy of CCTA in coronary heart disease and the evaluation of coronary stenosis. However, it has the disadvantage of increasing image noise, and the radiation dose is higher than in CT with the latest wide-coverage detector. A recent study shows that (107) material density imaging based on iodine and calcium improves the diagnostic ability of calcified coronary artery disease in patients with a high calcification score. In recent years, subtraction technology has been combined with CCTA. By removing the interference of artifacts caused by calcified plaque and metal stents, subtraction CCTA can improve the accuracy and efficiency of assessing the stenosis of diseased coronary artery segments (108). Recently, pieces of literature have reported that compared with traditional CCTA, subtraction CCTA can significantly improve the imaging quality of coronary artery calcification.

3D virtual intravascular endoscopy is a less invasive tool, which can be used to analyze the morphology of calcified coronary plaque and improve the assessment of coronary stenosis by CCTA (109).

CONCLUSION AND PROSPECT

With the development of science and society, imaging inspection equipment, such as CT technology, has been continuously developing since its advent. Different types of CT have their advantages and disadvantages in evaluating vascular calcification (Table 2). Vascular calcification is related to many diseases which seriously affect human health and life. Therefore, early detection and treatment of calcification are of great

TABLE 2 | Comparison of different CT technologies.

CT type	Advantages	Disadvantages	Macrocalcification	Microcalcification
Dual energy CT	Ability to eliminate artifacts Reduce radiation dose (limited) Improve image quality and contrast Less contrast dose Simplify the workflow	Assess poor vascular integrity Proof of VNC images in calcification less evidence of role	YES	NO
Multi-layer spiral CT	Some post-processing technologies Non-invasive; Simple; fast high diagnostic accuracy	Radiation exposure Increasing odds of associated cancer	YES	NO
Micro-CT	High spatial resolution Microcalcification can be detected	Long acquisition time Need deep anesthesia Poor contrast of the soft tissue High radiation dose Not in clinical	YES	YES

significance. KDIGO experts noted that any patient with vascular calcification that might affect treatment decisions might require an assessment of vascular calcification (45). Increasingly perfect CT examination makes the diagnostic information captured from images by doctors more accurate and convenient. Also, the evaluation technology of vascular calcification is gradually improving. In the future, it is hoped that CT technology will continue to develop and eventually combine high-definition and low radiation exposure. This will lead to a more extensive application and consequently bring new hope to more patients.

AUTHOR CONTRIBUTIONS

ZW and LZ conceived the topic and wrote the first draft. LL, GF, TF, and HJ went through the manuscript and tables. All authors contributed to the article and approved the submitted version.

FUNDING

This work was supported as follows the National Natural Science Foundation of China (82070455 and 81770450) the Projects from Social Development of Zhenjiang (SH2019087 and SH2018030).

REFERENCES

- Barrett H, O'Keeffe M, Kavanagh E, Walsh M, O'Connor EM. Is matrix gla protein associated with vascular calcification? A systematic review. *Nutrients*. (2018) 10:415. doi: 10.3390/nu10040415
- Ornellas NP, Joalbo A, Henry M. Coronary artery calcium score: current status. *Radiol Brasil*. (2017) 50:182–9. doi: 10.1590/0100-3984.2015.0235
- Agatston A, Janowitz W, Hildner FJ. Quantification of coronary artery calcium using ultrafast computed tomography. *J Am Coll Cardiol*. (1990) 15:827–32. doi: 10.1016/0735-1097(90)90282-T
- Becker CR, Knez A, Ohnesorge B, Schoepf UJ, Flohr T, Bruening R, et al. Visualization and quantification of coronary calcifications with electron beam and spiral computed tomography. *Eur Radiol*. (2000) 10:629–35. doi: 10.1007/s0033000050975
- Davis B, Marin D, Hurwitz LM, Ronald J, Ellis MJ, Ravindra KV, et al. Application of a novel CT-based iliac artery calcification scoring system for predicting renal transplant outcomes. *Ajr Am J Roentgenol*. (2016) 206:436. doi: 10.2214/AJR.15.14794
- Iluri K, Joshi PH, Henry TS, Blumenthal RS, Nasir K, Blaha MJ. Scoring of coronary artery calcium scans: history, assumptions, current limitations, and future directions. *Atherosclerosis*. (2015) 239:109–17. doi: 10.1016/j.atherosclerosis.2014.12.040
- Raggi P, O'Neill WC. Imaging for vascular calcification. *Semin Dial*. (2017) 30:347–52. doi: 10.1111/sdi.12596
- Smith ER, Hewitson TD, Holt SG. Diagnostic tests for vascular calcification. *Adv Chronic Kidney Dis*. (2019) 26:445–63. doi: 10.1053/j.ackd.2019.07.001
- Wilson PW, Kauppila LI, O'Donnell CJ, Kiel DP, Hannan M, Polak JM, et al. Abdominal aortic calcific deposits are an important predictor of vascular morbidity and mortality. *Circulation*. (2001) 103:1529–34. doi: 10.1161/01.CIR.103.11.1529
- Wayhs R, Zelinger A, Raggi P. High coronary artery calcium scores pose an extremely elevated risk for hard events. *J Am Coll Cardiol*. (2002) 39:225–30. doi: 10.1016/S0735-1097(01)01737-5
- Genders TS, Pugliese F, Mollet NR, Meijboom WB, Weustink AC, van Mieghem CA, et al. Incremental value of the CT coronary calcium score for the prediction of coronary artery disease. *Eur Radiol*. (2010) 20:2331–40. doi: 10.1007/s00330-010-1802-y
- Asafu Adjaye Frimpong G, Owusu IK, Anyitey-Kokor IC, Wiafe-Kwakye C, Aboagye E, Coleman NE, et al. Age-gender distribution of coronary artery calcium score in a black African population in Ghana. *Vasc Health Risk Manag*. (2018) 14:75–80. doi: 10.2147/VHRM.S160669
- Rennenberg RJ, Kessels AG, Schurgers LJ, van Engelshoven JM, de Leeuw PW, Kroon AA. Vascular calcifications as a marker of increased cardiovascular risk: a meta-analysis. *Vasc Health Risk Manag*. (2009) 5:185–97. doi: 10.2147/VHRM.S4822
- Mori H, Torii S, Kutyna M, Sakamoto A, Finn AV, Virmani R. Coronary artery calcification and its progression: what does it really mean? *JACC Cardiovasc Imag*. (2018) 11:127–42. doi: 10.1016/j.jcmg.2017.10.012
- Sarwar A, Shaw LJ, Shapiro MD, Blankstein R, Hoffmann U, Cury RC, et al. Diagnostic and prognostic value of absence of coronary artery calcification. *JACC Cardiovasc Imag*. (2009) 2:675–88. doi: 10.1016/j.jcmg.2008.12.031
- Rajiah P, Abbasa S. CT coronary imaging-a fast evolving world. *Qjm*. (2018) 111:595–604. doi: 10.1093/qjmed/hcx175
- Polonsky TS, McClelland RL, Jorgensen NW, Bild DE, Burke GL, Guerci AD, et al. Coronary artery calcium score and risk classification for coronary heart disease prediction. *JAMA*. (2010) 303:1610–6. doi: 10.1001/jama.2010.461
- Grundy SM, Stone NJ. 2018 American heart association/American college of cardiology/multisociety guideline on the management of blood cholesterol-secondary prevention. *JAMA Cardiol*. (2019) 4:589–91. doi: 10.1001/jamacardio.2019.0911

19. Han D, Ji HL, Hartaigh B, Min JK. Role of computed tomography screening for detection of coronary artery disease. *Clin Imag.* (2016) 40:307–10. doi: 10.1016/j.clinimag.2015.07.002
20. Dewey M. Coronary CT versus MR angiography: pro CT—the role of CT angiography. *Radiology.* (2011) 258:329–39. doi: 10.1148/radiol.10100161
21. Ngam PI, Ong CC, Chai P, Wong SS, Liang CR, Teo LLS. Computed tomography coronary angiography - past, present and future. *Singapore Med J.* (2020) 61:109–15. doi: 10.11622/smedj.2020028
22. Eckert J, Schmidt M, Magedanz A, Voigtlander T, Schmermund A. Coronary CT angiography in managing atherosclerosis. *Int J Mol Sci.* (2015) 16:3740–56. doi: 10.3390/ijms16023740
23. Lee SE, Villines TC, Chang HJ. Should CT replace IVUS for evaluation of CAD in large-scale clinical trials: effects of medical therapy on atherosclerotic plaque. *J Cardiovasc Comp Tomog.* (2019) 13:248–53. doi: 10.1016/j.jcct.2019.06.017
24. Rn A, Sm B, Jl C, Mjb D. How accurate is atherosclerosis imaging by coronary computed tomography angiography? *J Cardiovasc Comp Tomog.* (2019) 13:254–60. doi: 10.1016/j.jcct.2019.06.005
25. Amanuma M, Kondo T, Sano T, Sekine T, Takase S. Subtraction coronary computed tomography in patients with severe calcification. *Int J Cardiovasc Imag.* (2015) 31:1635–42. doi: 10.1007/s10554-015-0746-3
26. Park MJ, Jung JI, Choi YS, Ann SH, Youn HJ, Jeon GN, et al. Coronary CT angiography in patients with high calcium score: evaluation of plaque characteristics and diagnostic accuracy. *Int J Cardiovasc Imag.* (2011) 27(Suppl. 1):43–51. doi: 10.1007/s10554-011-9970-7
27. Skinner JS, Smeeth L, Kendall JM, Adams PC, Timmis A. NICE guidance. Chest pain of recent onset: assessment and diagnosis of recent onset chest pain or discomfort of suspected cardiac origin. *Heart.* (2010) 96:974–8. doi: 10.1136/hrt.2009.190066
28. Zheng M, Wei M, Wen D, Zhao H, Liu Y, Li J, et al. Translumenal attenuation gradient in coronary computed tomography angiography for determining stenosis severity of calcified coronary artery: a primary study with dual-source CT. *Eur Radiol.* (2015) 25:1219–28. doi: 10.1007/s00330-014-3519-9
29. Ping L, Lei X, Lin Y, Rui W, Jiang H, Sun Z, et al. Blooming artifact reduction in coronary artery calcification by a new de-blooming algorithm: initial study. *Sci Rep.* (2018) 8:6945. doi: 10.1038/s41598-018-25352-5
30. Osch JV, Mouden M, Dalen JV, Timmer JR, Reiffers S, Knollemas S, et al. Influence of iterative image reconstruction on CT-based calcium score measurements. *Int J Cardiovasc Imag.* (2014) 30:961–7. doi: 10.1007/s10554-014-0409-9
31. Sun Z, Ng C, Xu L, Fan Z, Lei J. Coronary CT angiography in heavily calcified coronary arteries: improvement of coronary lumen visualization and coronary stenosis assessment with image postprocessing methods. *Medicine.* (2015) 94:e2148. doi: 10.1097/MD.0000000000002148
32. Fuchs A, Kühl JT, Chen MY, Viladés Medel D, Alomar X, Shanbhag SM, et al. Subtraction CT angiography improves evaluation of significant coronary artery disease in patients with severe calcifications or stents—the C-Sub 320 multicenter trial. *Eur Radiol.* (2018) 28:4077–85. doi: 10.1007/s00330-018-5418-y
33. Criqui MH, Denenberg JO, Ix JH, M Cc Lelland RL, Wassel CL, Rifkin DE, et al. Calcium density of coronary artery plaque and risk of incident cardiovascular events. *JAMA.* (2015) 311:271–8. doi: 10.1001/jama.2013.282535
34. Schoenhagen P, Ziada KM, Kapadia SR, Crowe TD, Nissen SE, Tuzcu EM. Extent and direction of arterial remodeling in stable versus unstable coronary syndromes: an intravascular ultrasound study. *Circulation.* (2000) 101:598–603. doi: 10.1161/01.CIR.101.6.598
35. Shemesh J, Apter S, Itzhak Y, Motro M. Coronary calcification compared in patients with acute versus in those with chronic coronary events by using dual-sector spiral CT. *Radiology.* (2003) 226:483–8. doi: 10.1148/radiol.2262011903
36. Jinnouchi H, Sato Y, Sakamoto A, Cornelissen A, Mori M, Kawakami R, et al. Calcium deposition within coronary atherosclerotic lesion: implications for plaque stability. *Atherosclerosis.* (2020) 306:85–95. doi: 10.1016/j.atherosclerosis.2020.05.017
37. Nakahara T, Dweck MR, Narula N, Pisapia D, Narula J, Strauss HW. Coronary artery calcification: from mechanism to molecular imaging. *JACC Cardiovasc Imag.* (2017) 10:582–93. doi: 10.1016/j.jcmg.2017.03.005
38. Bailey G, Meadows J, Morrison AR. Imaging atherosclerotic plaque calcification: translating biology. *Curr Atheroscler Rep.* (2016) 18:51. doi: 10.1007/s11883-016-0601-6
39. McClelland RL. Distribution of coronary artery calcium by race, gender, and age: results from the multi-ethnic study of atherosclerosis (MESA). *Circulation.* (2006) 113:30–7. doi: 10.1161/CIRCULATIONAHA.105.580696
40. Waltz J, Kocher M, Kahn J, Dirr MK, Burt JR. The future of concurrent automated coronary artery calcium scoring on screening low-dose computed tomography. *Cureus.* (2020) 12:e8574. doi: 10.7759/cureus.8574
41. Harden SP, Bull RK, Bury RW, Castellano EA, Clayton B, Hamilton MC, et al. The safe practice of CT coronary angiography in adult patients in UK imaging departments. *Clin Radiol.* (2016) 71:722–8. doi: 10.1016/j.crad.2016.04.008
42. Lee SJ, Lee IK, Jeon JH. Vascular calcification-new insights into its mechanism. *Int J Mol Sci.* (2020) 21:2685. doi: 10.3390/ijms21082685
43. Runge VM, Marquez H, Andreisek G, Valavanis A, Alkadhi H. Recent technological advances in computed tomography and the clinical impact therein. *Invest Radiol.* (2015) 50:119–27. doi: 10.1097/RLI.0000000000000125
44. Shamsul S, Sabarudin A, Hamid HA, Bakar NA, Karim M. Evaluation of radiation dose from coronary CT angiography (CCTA) examination associated with prospective ECG-triggering technique in multidetector 640-slice scanner. *J Phys Confer Series.* (2020) 1505:012073. doi: 10.1088/1742-6596/1505/1/012073
45. Karohl C, D'Marco Gascón L, Raggi P. Noninvasive imaging for assessment of calcification in chronic kidney disease. *Nat Rev Nephrol.* (2011) 7:567–77. doi: 10.1038/nrneph.2011.110
46. Maurovich-Horvat P, Schlett CL, Alkadhi H, Nakano M, Otsuka F, Stolzmann P, et al. The napkin-ring sign indicates advanced atherosclerotic lesions in coronary CT angiography. *JACC Cardiovasc Imag.* (2012) 5:1243–52. doi: 10.1016/j.jcmg.2012.03.019
47. Senoner T, Plank F, Beyer C, Langer C, Birkel K, Steinkohl F, et al. Gender differences in the atherosclerosis profile by coronary CTA in coronary artery calcium score zero patients. *J Clin Med.* (2021) 10:1220. doi: 10.3390/jcm10061220
48. Leber AW, Knez A, Becker A, Becker C, von Ziegler F, Nikolaou K, et al. Accuracy of multidetector spiral computed tomography in identifying and differentiating the composition of coronary atherosclerotic plaques: a comparative study with intracoronary ultrasound. *J Am Coll Cardiol.* (2004) 43:1241–7. doi: 10.1016/j.jacc.2003.10.059
49. Nicoll R, Henein MY. Arterial calcification: friend or foe? *Int J Cardiol.* (2013) 167:322–7. doi: 10.1016/j.ijcard.2012.06.110
50. Toia P, La Grutta L, Sollami G, Clemente A, Gagliardo C, Galia M, et al. Technical development in cardiac CT: current standards and future improvements—a narrative review. *Cardiovasc Diagn Ther.* (2020) 10:2018–35. doi: 10.21037/cdt-20-527
51. Cellina M, Gibelli D, Martinenghi C, Oliva G, Floridi C. CT angiography of lower extremities from anatomy to traumatic and nontraumatic lesions: a pictorial review. *Emerg Radiol.* (2020) 27:441–50. doi: 10.1007/s10140-020-01770-9
52. Raggi P, Chertow GM, Torres PU, Csiky B, Naso A, Nossuli K, et al. The ADVANCE study: a randomized study to evaluate the effects of cinacalcet plus low-dose vitamin D on vascular calcification in patients on hemodialysis. *Nephrol Dial Transplant.* (2011) 26:1327–39. doi: 10.1093/ndt/gfq725
53. Schmidt B, Flohr T. Principles and applications of dual source CT. *Physica Medica.* (2020) 79:36–46. doi: 10.1016/j.ejmp.2020.10.014
54. Gottumukkala RV, Kalra MK, Tabari A, Otrakji A, Gee MS. Advanced CT techniques for decreasing radiation dose, reducing sedation requirements, and optimizing image quality in children. *Radiographics.* (2019) 39:709–26. doi: 10.1148/rg.2019180082
55. Lee HA, Lee YH, Yoon KH, Bang DH, Park DE. Comparison of virtual unenhanced images derived from dual-energy CT with true unenhanced images in evaluation of gallstone disease. *AJR Am J Roentgenol.* (2016) 206:74–80. doi: 10.2214/AJR.15.14570

56. Meyer M, Haubenreisser H, Raupach R, Schmidt B, Lietzmann F, Leidecker C, et al. Initial results of a new generation dual source CT system using only an in-plane comb filter for ultra-high resolution temporal bone imaging. *Eur Radiol.* (2015) 25:178–85. doi: 10.1007/s00330-014-3406-4
57. Tesche C, De Cecco CN, Vliegthart R, Albrecht MH, Varga-Szemes A, Duguay TM, et al. Accuracy and radiation dose reduction using low-voltage computed tomography coronary artery calcium scoring with tin filtration. *Am J Cardiol.* (2017) 119:675–80. doi: 10.1016/j.amjcard.2016.10.051
58. Tesche C, De Cecco CN, Schoepf UJ, Duguay TM, Albrecht MH, De Santis D, et al. CT coronary calcium scoring with tin filtration using iterative beam-hardening calcium correction reconstruction - ScienceDirect. *Euro J Radiol.* (2017) 91:29–34. doi: 10.1016/j.ejrad.2017.03.011
59. Manta C, Meyer M, Géraud C, Roscher M, Goerdts S, Schoenberg SO, et al. Detection of calcified aortic plaques in an apolipoprotein e animal model using a human computed tomography system for ultra-high-resolution imaging: a feasibility study. *J Thorac Imag.* (2019) 34:41–7. doi: 10.1097/RJT.0000000000000375
60. Linsen P, Coenen A, Lubbers MM, Dijkshoorn M, Nieman K. Computed tomography angiography with a 192-slice dual-source computed tomography system: improvements in image quality and radiation dose. *J Clin Imag Sci.* (2016) 6:44. doi: 10.4103/2156-7514.192840
61. Rajiah P, Parakh A, Kay F, Baruah D, Shuai L. Update on multienergy CT: physics, principles, and applications. *Radiographics.* (2020) 40:200038. doi: 10.1148/rq.2020200038
62. Karçaaltincaba M, Aktaş A. Dual-energy CT revisited with multidetector CT: review of principles and clinical applications. *Diag Int Radiol.* (2011) 17:181–94. doi: 10.4261/1305-3825.DIR.3860-10.0
63. Siegel MJ, Kaza RK, Bolus DN, Boll DT, Berland LL. White paper of the society of computed body tomography and magnetic resonance on dual-energy CT, part 1: technology and terminology. *J Comp Assis Tomogr.* (2016) 40:841. doi: 10.1097/RCT.0000000000000531
64. Goo HW, Goo JM. Dual-energy CT: new horizon in medical imaging. *Korean J Radiol.* (2017) 18:555–69. doi: 10.3348/kjr.2017.18.4.555
65. Rassouli N, Etesami M, Dhanantwari A, Rajiah P. Detector-based spectral CT with a novel dual-layer technology: principles and applications. *Insights Into Imag.* (2017) 8:589–98. doi: 10.1007/s13244-017-0571-4
66. Machida H, Tanaka I, Fukui R, Shen Y, Ishikawa T, Tate E, et al. Dual-energy spectral CT: various clinical vascular applications. *Radiographics.* (2016) 36:1215–32. doi: 10.1148/rq.2016150185
67. Albrecht MH, De C, Joseph SU, Adam S, Marwen E, Domenico DS, et al. Dual-energy CT of the heart current and future status. *Eur J Radiol.* (2018) 105:110–8. doi: 10.1016/j.ejrad.2018.05.028
68. Kay FU. Dual-energy CT and coronary imaging. *Cardiovasc Diagn Ther.* (2020) 10:1090–107. doi: 10.21037/cdt.2020.04.04
69. Grant KL, Flohr TG, Krauss B, Sedlmair M, Thomas C, Schmidt B. Assessment of an advanced image-based technique to calculate virtual monoenergetic computed tomographic images from a dual-energy examination to improve contrast-to-noise ratio in examinations using iodinated contrast media. *Inv Radiol.* (2014) 49:586–92. doi: 10.1097/RLI.0000000000000060
70. So A, Jiang H, Narayanan S, Thibault JB, Imai Y, Dutta S, et al. Dual-energy CT and its potential use for quantitative myocardial CT perfusion. *J Cardiovasc Comp Tomogr.* (2012) 6:308–17. doi: 10.1016/j.jcct.2012.07.002
71. Wortman JR, Sodickson AD. Pearls, pitfalls, and problems in dual-energy computed tomography imaging of the body. *Radiol Clin North Am.* (2018) 56:625–40. doi: 10.1016/j.rcl.2018.03.007
72. Schwarz F, Nance JW, Ruzsics B, Bastarrika G, Sterzik A, Schoepf UJ. Quantification of coronary artery calcium on the basis of dual-energy coronary CT angiography. *Radiology.* (2012) 264:700–7. doi: 10.1148/radiol.12112455
73. Chae EJ, Song JW, Seo JB, Krauss B, Jang YM, Song KS. Clinical utility of dual-energy CT in the evaluation of solitary pulmonary nodules: initial experience. *Radiology.* (2008) 249:671–81. doi: 10.1148/radiol.24.92071956
74. Kumar V, Min JK, He X, Raman SV. Computation of calcium score with dual-energy computed tomography: a phantom study. *J Comput Assist Tomogr.* (2017) 41:156–8. doi: 10.1097/RCT.0000000000000480
75. Sodickson AD. Editor Driving CT developments the last mile: case examples of successful and somewhat less successful translations into clinical practice. *SPIE Med Imag.* (2017) 10:132. doi: 10.1117/12.2260235
76. Danad I, B ÓH, Min JK. Dual-energy computed tomography for detection of coronary artery disease. *Expert Rev Cardiovasc Ther.* (2015) 13:1345–56. doi: 10.1586/14779072.2015.1102055
77. Achenbach S, Goroll T, Seltmann M, Pflederer T, Anders K, Ropers D, et al. Detection of coronary artery stenoses by low-dose, prospectively ECG-triggered, high-pitch spiral coronary CT angiography. *JACC Cardiovasc Imag.* (2011) 4:328–37. doi: 10.1016/j.jcmg.2011.01.012
78. Danad I, Fayad ZA, Willemink MJ, Min JK. New applications of cardiac computed tomography: dual-energy, spectral, and molecular CT imaging. *JACC Cardiovasc Imag.* (2015) 8:710–23. doi: 10.1016/j.jcmg.2015.03.005
79. Hideyuki S, Shinichiro F, Yosuke K, Hiroyuki D. Feasibility of macrophage plaque imaging using novel ultrasmall superparamagnetic iron oxide in dual energy CT. *Eur J Radiol Open.* (2018) 5:87–91. doi: 10.1016/j.ejro.2018.05.003
80. Nitta N, Tsuchiya K, Sonoda A, Ota S, Ushio N, Takahashi M, et al. Negatively charged superparamagnetic iron oxide nanoparticles: a new blood-pooling magnetic resonance contrast agent. *Japan J Radiol.* (2012) 30:832–9. doi: 10.1007/s11604-012-0133-0
81. Wortman JR, Shyu JY, Dileo J, Uyeda JW, Sodickson AD. Dual-energy CT for routine imaging of the abdomen and pelvis: radiation dose and image quality. *Emerg Radiol.* (2019) 27:45–50. doi: 10.1007/s10140-019-01733-9
82. Duan X, Ananthakrishnan L, Guild JB, Xi Y, Rajiah P. Radiation doses and image quality of abdominal CT scans at different patient sizes using spectral detector CT scanner: a phantom and clinical study. *Abdom Radiol.* (2020) 45:3361–368. doi: 10.1007/s00261-019-02247-1
83. Santis D, Domenico, Nam K, Schoepf, Joseph U, Grant, et al. Heavily calcified coronary arteries advanced calcium subtraction improves luminal visualization and diagnostic confidence in dual-energy coronary computed tomography angiography. *Invest Radiol.* (2018) 53:103–9. doi: 10.1097/RLI.0000000000000416
84. Lell MM, Kramer M, Klotz E, Villablanca P, Ruehm SG. Carotid computed tomography angiography with automated bone suppression: a comparative study between dual energy and bone subtraction techniques. *Inv Radiol.* (2009) 44:322. doi: 10.1097/RLI.0b013e31819e8ad9
85. Maldonado N, Kellyarnold A, Vengrenyuk Y, Laudier D, Fallon JT, Virmani R, et al. A mechanistic analysis of the role of microcalcifications in atherosclerotic plaque stability: potential implications for plaque rupture. *Am J Physiol Heart Circ Physiol.* (2012) 303:619–28. doi: 10.1152/ajpheart.00036.2012
86. Danial JSH, Murad F, Saez AG, Moawad MR, Urrico GS, Vancheri F, et al. Computed histological quantification of atherosclerotic plaque microcalcifications. *Angiology.* (2020) 71:916–9. doi: 10.1177/0003319720939466
87. Badea CT, Drangova M, Holdsworth DW, Johnson GA. In vivo small-animal imaging using micro-CT and digital subtraction angiography. *Phys Med Biol.* (2008) 53:R319–50. doi: 10.1088/0031-9155/53/19/R01
88. Borland SJ, Behnson J, Ashton N, Francis SE, Canfield AE. X-ray micro-computed tomography: an emerging technology to analyze vascular calcification in animal models. *Int J Mol Sci.* (2020) 21:4538. doi: 10.3390/ijms21124538
89. Bos D, Ikram MA, Elias-Smale SE, Krestin GP, Hofman A, Witteman JC, et al. Calcification in major vessel beds relates to vascular brain disease. *Arterioscl Thromb Vasc Biol.* (2011) 31:2331–7. doi: 10.1161/ATVBAHA.111.232728
90. Kampschulte M, Langheinrich AC, Sender J, Litzlbauer HD, Krombach GA. Nano-computed tomography: technique and applications. *RöFo Fortschritte Gebiet.* (2016) 188:146–54. doi: 10.1055/s-0041-106541
91. Vrigneaud JM, Courteau A, Ranouil J, Morgand L, Raguin O, Walker P, et al. Application of the optically stimulated luminescence (OSL) technique for mouse dosimetry in micro-CT imaging. *Med Phys.* (2013) 40:122102. doi: 10.1118/1.4829499
92. Tamaoki H, Yoshimachi F, Sakurai T, Shin T, Ikari Y. Simultaneous computed tomographic angiography of the coronary and radial arteries. *Cardiovasc Int Ther.* (2020) 35:185–93. doi: 10.1007/s12928-019-00598-6

93. Maldonado N, Kelly-Arnold A, Laudier D, Weinbaum S, Cardoso L. Imaging and analysis of microcalcifications and lipid/necrotic core calcification in fibrous cap atheroma. *Int J Cardiovasc Imag.* (2015) 31:1079–87. doi: 10.1007/s10554-015-0650-x
94. Wait J, Tomita H, Burk LM, Lu J, Zhou OZ, Maeda N, et al. Detection of aortic arch calcification in apolipoprotein E-null mice using carbon nanotube-based micro-CT system. *J Am Heart Assoc Cardiovasc Cerebrovasc Dis.* (2013) 2:e003358. doi: 10.1161/JAHA.112.003358
95. Vgberg W, Persson J, Szekely L, Hertz HM. Cellular-resolution 3D virtual histology of human coronary arteries using x-ray phase tomography. *Sci Rep.* (2018) 8:11014. doi: 10.1038/s41598-018-29344-3
96. Hsu JJ, Fong F, Patel R, Qiao R, Lo K, Soundia A, et al. Changes in microarchitecture of atherosclerotic calcification assessed by (18)F-NaF PET and CT after a progressive exercise regimen in hyperlipidemic mice. *J Nucl Cardiol.* (2020). doi: 10.1007/s12350-019-02004-3. [Epub ahead of print].
97. Demer LL, Yin T. Interactive and multifactorial mechanisms of calcific vascular and valvular disease. *Trends Endocrinol Metab.* (2019) 30:646–57. doi: 10.1016/j.tem.2019.06.001
98. Andrews J, Psaltis PJ, Bartolo BAD, Nicholls SJ, Puri R. Coronary arterial calcification: a review of mechanisms, promoters and imaging. *Trends Cardiovasc Med.* (2018) 28:491–501. doi: 10.1016/j.tcm.2018.04.007
99. Heinzer S, Krucker T, Stampanoni M, Abela R, Meyer EP, Schuler A, et al. Hierarchical microimaging for multiscale analysis of large vascular networks. *Neuroimage.* (2006) 32:626–36. doi: 10.1016/j.neuroimage.2006.03.043
100. Bonanno G, Coppo S, Modregger P, Pellegrin M, Stuber A, Stampanoni M, et al. Ultra-high-resolution 3D imaging of atherosclerosis in mice with synchrotron differential phase contrast: a proof of concept study. *Sci Rep.* (2015) 5:11980. doi: 10.1038/srep11980
101. Hetterich H, Webber N, Willner M, Herzen J, Birnbacher L, Hipp A, et al. AHA classification of coronary and carotid atherosclerotic plaques by grating-based phase-contrast computed tomography. *Eur Radiol.* (2016) 26:3223–33. doi: 10.1007/s00330-015-4143-z
102. Habbel C, Hetterich H, Willner M, Herzen J, Steigerwald K, Auweter S, et al. Ex Vivo assessment of coronary atherosclerotic plaque by grating-based phase-contrast computed tomography: correlation with optical coherence tomography. *Invest Radiol.* (2017) 52:223–31. doi: 10.1097/RLI.0000000000000346
103. Pfeiffer F, Reiser M, Rummeny E. [X-ray Phase Contrast: Principles, potential and advances in clinical translation]. *Der Radiol.* (2018) 58:218–25. doi: 10.1007/s00117-018-0357-9
104. Hetterich H, Willner M, Habbel C, Herzen J, Hoffmann VS, Fill S, et al. X-ray phase-contrast computed tomography of human coronary arteries. *Invest Radiol.* (2015) 50:686–94. doi: 10.1097/RLI.0000000000000169
105. Kwan AC, Pourmorteza A, Dan S, Bluemke DA, Lima J. Next-generation hardware advances in CT: cardiac applications. *Radiology.* (2020) 298:192791. doi: 10.1148/radiol.2020192791
106. Takagi H, Tanaka R, Nagata K, Ninomiya R, Arakita K, Schuijff JD, et al. Diagnostic performance of coronary CT angiography with ultra-high-resolution CT: comparison with invasive coronary angiography. *Eur J Radiol.* (2018) 101:30. doi: 10.1016/j.ejrad.2018.01.030
107. Andreini D, Pontone G, Mushtaq S, Bertella E, Conte E, Segurini C, et al. Diagnostic accuracy of rapid kilovolt peak-switching dual-energy CT coronary angiography in patients with a high calcium score. *JACC Cardiovasc Imag.* (2015) 8:746–8. doi: 10.1016/j.jcmg.2014.10.013
108. Masafumi K, Daisuke U, Yoshinori F, Daisuke S, Seitaro O, Takeshi N, et al. The effect of heart rate on coronary plaque measurements in 320-row coronary CT angiography. *Int J Cardiovasc Imag.* (2018) 34:1977–985. doi: 10.1007/s10554-018-1415-0
109. Xu L, Sun Z. Virtual intravascular endoscopy visualization of calcified coronary plaques: a novel approach of identifying plaque features for more accurate assessment of coronary lumen stenosis. *Medicine.* (2015) 94:e805. doi: 10.1097/MD.00000000000000805

Conflict of Interest: The authors declare that the research was conducted in the absence of any commercial or financial relationships that could be construed as a potential conflict of interest.

Publisher's Note: All claims expressed in this article are solely those of the authors and do not necessarily represent those of their affiliated organizations, or those of the publisher, the editors and the reviewers. Any product that may be evaluated in this article, or claim that may be made by its manufacturer, is not guaranteed or endorsed by the publisher.

Copyright © 2021 Zhang, Li, Feng, Fan, Jiang and Wang. This is an open-access article distributed under the terms of the Creative Commons Attribution License (CC BY). The use, distribution or reproduction in other forums is permitted, provided the original author(s) and the copyright owner(s) are credited and that the original publication in this journal is cited, in accordance with accepted academic practice. No use, distribution or reproduction is permitted which does not comply with these terms.



Coronary Computed Tomography Angiography Assessment of High-Risk Plaques in Predicting Acute Coronary Syndrome

Guanyu Lu^{1,2}, Weitao Ye¹, Jiehao Ou¹, Xinyun Li¹, Zekun Tan¹, Tingyu Li¹ and Hui Liu^{1,2*}

¹ Department of Radiology, Guangdong Provincial People's Hospital, Guangdong Academy of Medical Sciences, Guangzhou, China, ² College of Medicine, Shantou University, Shantou, China

OPEN ACCESS

Edited by:

Zhao Wang,
University of Electronic Science and
Technology of China, China

Reviewed by:

Kenichiro Otsuka,
Massachusetts General Hospital,
United States
Shady Abohashem,
Massachusetts General Hospital and
Harvard Medical School,
United States

*Correspondence:

Hui Liu
liuhuijiu@gmail.com

Specialty section:

This article was submitted to
Cardiovascular Imaging,
a section of the journal
Frontiers in Cardiovascular Medicine

Received: 18 July 2021

Accepted: 07 September 2021

Published: 01 October 2021

Citation:

Lu G, Ye W, Ou J, Li X, Tan Z, Li T and
Liu H (2021) Coronary Computed
Tomography Angiography
Assessment of High-Risk Plaques in
Predicting Acute Coronary Syndrome.
Front. Cardiovasc. Med. 8:743538.
doi: 10.3389/fcvm.2021.743538

Coronary computed tomography angiography (CCTA) is a comprehensive, non-invasive and cost-effective imaging assessment approach, which can provide the ability to identify the characteristics and morphology of high-risk atherosclerotic plaques associated with acute coronary syndrome (ACS). The development of CCTA and latest advances in emerging technologies, such as computational fluid dynamics (CFD), have made it possible not only to identify the morphological characteristics of high-risk plaques non-invasively, but also to assess the hemodynamic parameters, the environment surrounding coronaries and so on, which may help to predict the risk of ACS. In this review, we present how CCTA was used to characterize the composition and morphology of high-risk plaques prone to ACS and the current role of CCTA, including emerging CCTA technologies, advanced analysis, and characterization techniques in prognosticating the occurrence of ACS.

Keywords: coronary computed tomography angiography (CCTA), high-risk plaque, acute coronary syndrome (ACS), computational fluid dynamics–CFD, pericoronary adipose tissue attenuation, coronary artery

INTRODUCTION

Acute coronary syndrome (ACS) may be the first manifestation of coronary artery disease (CAD), mainly caused by the rupture or erosion of unstable plaques (1–4), which is the leading cause of death for most of the world's population. Therefore, it has been a driving force to identify these high-risk plaques prone to rupture which may lead to ACS. Substantial study efforts have confirmed that virtual histology intravascular ultrasound (IVUS) or optical coherence tomography (OCT) can be valuable (5).

However, these invasive diagnostic approaches with low positive predictive value and unclear cost-effectiveness have not been widely used in clinical practice (6). Coronary computed tomography angiography (CCTA), as a comprehensive non-invasive imaging assessment approach, which allows for the quantification and characterization of coronary atherosclerosis, can effectively evaluate the condition of all coronary arteries and the branches in the whole-heart, and has great clinical application value in identifying adverse plaque characteristics (7, 8). The high accuracy and high efficiency of CCTA are well-confirmed in previous studies, as well as its higher diagnostic performance compared with invasive reference standards (7, 9, 10). CCTA has been used to identify the characteristics and morphology of high-risk atherosclerotic plaques associated with ACS in previous studies, including positive remodeling, low attenuation, spotty calcification, and

the napkin-ring sign (8, 10, 11). The development of CCTA and latest advances in emerging technologies, such as computational fluid dynamics (CFD), have made it possible to simultaneously perform the comprehensive evaluation of anatomical severity degree, lesion geometry, plaque characteristics, quantification of hemodynamic parameters and detection of vascular inflammation, which may help to identify the high-risk plaques and predict the risk of ACS (12).

In this review, we delineate the current understanding of the pathology of the atherosclerotic plaques associated with ACS and corresponding manifestations on CCTA in clinical practice. The application of CCTA in characterizing the composition and morphology of high-risk plaques prone to ACS and prognosticating the occurrence of ACS are further described. Finally, the progress in emerging CCTA technologies, advanced analysis and characterization techniques are also reviewed. The new techniques can provide the comprehensive assessment of high-risk plaques and surrounding environment, and may provide personalized risk assessment of future ACS events and further guide clinical decision-making.

FROM HIGH-RISK PLAQUE HISTOPATHOLOGY TO CCTA

The detection and characterization of plaque by CCTA is based on histopathology, therefore, and therefore it is vital to grasp the histopathological characteristics and evolution process of high-risk atherosclerotic plaque.

Atherosclerosis, most often observed at the branch points and low shear stress areas of blood vessels, is a multifactorial systemic disease and has a chronic and progressive process (13). About two-thirds of ACS results from the rupture of atherosclerotic plaque (14, 15). The early manifestations of atherosclerosis are non-atherosclerotic intimal lesions, which include intimal thickening and xanthoma. Subsequently, starting from pathological intimal thickening, they further develop into increasingly vulnerable and rupture-prone lesions, and progress into fibroatheroma or even thin cap fibroatheroma, which is considered to be the precursor of plaque rupture (16). Moreover, the development of lesions before rupture can be explained by the histopathological nature of unstable lesions, including intraplaque hemorrhage, neo-vascularization, plaque healing, and recurrent rupture (17, 18). Compared with plaque erosion and stable CAD, intraplaque hemorrhage is the most common finding in plaque rupture, which includes numerous foam cells (lipid-laden macrophage), cholesterol clefts, and an expanding necrotic core, contributing to the vulnerability of plaque (19).

The characteristics of high-risk plaques are related to the vulnerability of plaques (18). Based on the histopathologic composition of vulnerable plaques, including thin cap fibroatheroma, macrophage infiltration, and necrotic core (20, 21), the corresponding typical manifestations of high-risk plaques in CCTA are listed as follows: positive remodeling, low attenuation, spotty calcification, and napkin-ring sign (22–24) (Figure 1).

FROM HIGH-RISK PLAQUE CCTA FEATURES TO ACUTE CORONARY SYNDROME

CCTA Assessment of High-Risk Plaque Features

The percentage of stenosis is important information on CCTA. When coronary heart disease cannot be ruled out clinically, the percentage of stenosis on CCTA can help to rule out patients in stable condition and with low possibility of coronary heart disease (25–27). However, the main cause of ACS is plaque rupture and erosion rather than fixed stenosis. Given that plaque instability and plaque progression are important factors leading to subsequent acute coronary events, identifying high-risk plaque characteristics is necessary (17, 25, 28–31). As a comprehensive non-invasive imaging assessment approach, CCTA has been used to identify the morphological characteristics of high-risk plaques prone to rupture that may lead to ACS (32–35).

Positive Remodeling

Clinically, coronary artery remodeling refers to be the compensatory changes of cross-sectional area and structure of coronary artery in the progression of coronary atherosclerosis. In pathological findings, the lumen of some coronary arteries was found to be increased during atherogenesis in autopsy (36). For *in vivo* detection of coronary artery, IVUS examination confirmed that the cross-sectional area of the vessel at the atherosclerotic site was significantly larger than that at the proximal reference segment, then the concept of positive remodeling was proposed which refers to the compensatory increase of vessel wall when atherosclerotic plaque volume increases continuously, thus maintaining the effective area in the lumen (37). While on CT, the outer vessel wall dimension could be measured. The remodeling index (RI) is calculated by dividing the vessel cross-sectional area/diameter of the largest stenosis (or maximum vessel area/diameter) by the average cross-sectional area/diameter of the proximal and distal reference segments (7, 38, 39) (Figure 2Aa). At present, positive remodeling is generally defined as $RI \geq 1.1$ in CCTA (8, 40, 41), while some researchers prefer other cut-off point (42, 43). In addition, automatic software makes it easier to quantify the RI (44).

Low Attenuation

The composition of plaques can be reflected by CT attenuation value, with the highest CT attenuation value for calcification, followed by fibrous tissue, and the lowest CT value for lipid. Low-attenuation plaques refer to those with the lowest CT attenuation value and the most easily ruptured lipid composition (a lipid-rich necrotic core), which is defined as mean attenuation <30 Hounsfield units (HU) of at least three regions of interest (ROIs) in general (39, 45) (Figure 2Bb). However, the CT attenuation value of lipid plaques overlaps with that of fibrous plaques, so it is difficult to distinguish the plaques only by CT attenuation value alone. In addition, the CT value of plaques is affected by many factors, such as contrast agent, plaque volume, slice

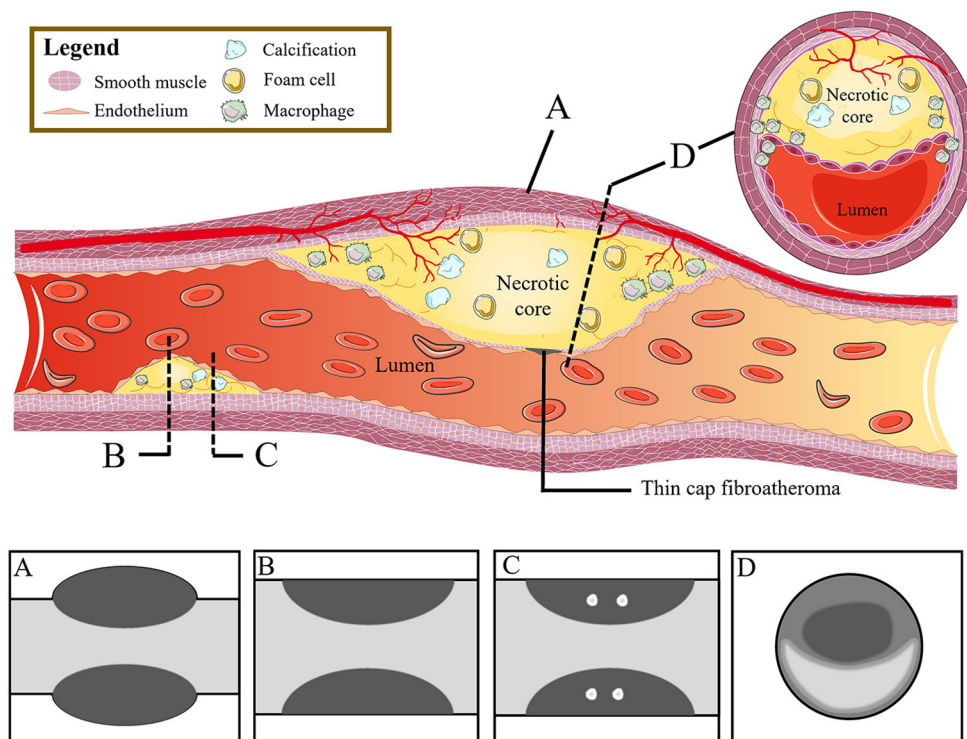


FIGURE 1 | From high-risk plaque histopathology to CCTA. The figure shows the histopathologic components of vulnerable plaques (colored illustrations) and the corresponding typical CT features of high-risk plaques: **(A)** positive remodeling, **(B)** low attenuation, **(C)** spotty calcification, and **(D)** napkin-ring sign. CCTA, coronary computed tomography angiography.

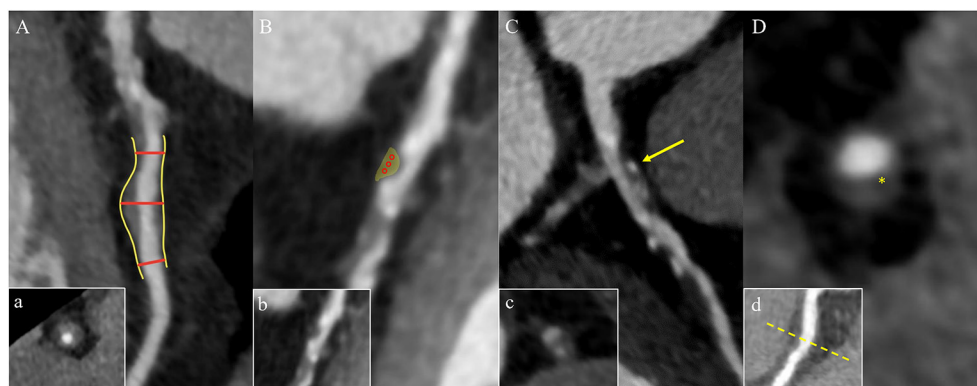


FIGURE 2 | High-risk plaque characteristics on CCTA. **(A)** Positive remodeling of a non-calcified plaque in the proximal left anterior descending coronary artery. The two short red lines indicate the vessel diameters of the proximal and distal of the plaque (both 1.0 mm), and the long red line indicates the maximum vessel diameter in the middle of the plaque (1.6 mm). The remodeling index is 1.6. Picture a is the cross section of picture **(A)**. **(B)** A low-attenuation plaque (yellow area) in the mid segment of the left anterior descending coronary artery with a mean CT attenuation value of 21 HU in the three regions of interest (red circles). Picture b is the original picture **(B)**. **(C)** Spotty calcification of a partially calcified plaque surrounded by non-calcified components in the proximal left anterior descending coronary artery with a diameter <3 mm in all directions (yellow arrow). Picture c is the cross section of picture **(C)**. **(D)** A napkin-ring sign plaque in the proximal right coronary artery. The yellow star shows the central area of the plaque with a low HU close to the lumen, which is surrounded by the peripheral edge of higher CT attenuation. Picture d is the multiplanar reconstructed image of picture **(D)**. CCTA, coronary computed tomography angiography; HU, Hounsfield units.

thickness, tube voltage, and so on. Therefore, the current research mainly relies on special procedures to identify which plaque is low-attenuation (7, 45).

Spotty Calcification

Spotty calcification is the initial state of calcification. Since calcification is one of the consequences of local inflammation,

spotty calcification may indicate active local inflammation. Mechanical stimulation on fibrous cap caused by spotty calcification and local inflammation may lead to the plaque with spotty calcification easy to rupture, thereby accelerating disease progression (46–48). Therefore, spotty calcification is considered to be one of the characteristics of high-risk plaques. In CCTA, spotty calcification is generally manifested as calcification in plaques with a density of more than 130 HU and a diameter of <3 mm surrounded by non-calcified components (42, 49, 50) (**Figure 2Cc**). However, only calcification more than 0.5 mm in diameter is visible on CT, so nearly two-thirds of the calcifications cannot be recognized on CT (51, 52).

Napkin-Ring Sign

The napkin ring sign is a qualitative plaque feature that can be defined by the presence of two features on the cross section of non-calcified plaques: the low-attenuation central area obviously contacting with the coronary artery lumen and the annular high attenuation plaque tissue surrounding the central area (7, 34) (**Figure 2Dd**). Histologically, the low-density area corresponds to the large necrotic nucleus, while the “annular” outer area is associated with fibrous tissue. The necrotic core area in plaque with the napkin-ring sign may be more than twice that without napkin ring sign (1.10 vs. 0.46 mm²) (53) corresponding to some studies’ indications that a necrotic core area >1 mm² when plaque is prone to rupture (14). The density of the ring is greater than that of the inner core but <130 HU in CT scans. Currently, the napkin-ring sign is considered to be a special CT feature of plaque with a large necrotic core, and it is a reliable marker of plaque instability (7, 14).

High-Risk Plaque Features on CCTA in Prediction of Acute Coronary Syndrome

Although the risk of plaque instability increases with the degree of coronary stenosis, most of the culprit lesions found in ACS are considered non-obstructive before rupture. Previous studies indicated that the characteristics of high-risk plaques identified by CCTA have a prognostic value independent of stenosis and atherosclerotic burden (41) (see **Table 1**).

In 2007, Motoyama et al. found that compared with SA lesions, the frequency of positive remodeling, non-calcified plaques or low-attenuation plaques (<30 HU) and spotty calcification on CCTA was higher in ACS culprit lesions, and these three characteristics could independently predict the occurrence of ACS. Moreover, among the three plaque features, positive remodeling has the highest accuracy in ACS prediction (22). In addition, an increase in the RI of culprit lesions in ACS patients compared with stable plaques in ACS and stable angina (SA) patients was also observed in other cross-sectional studies (11, 43, 54, 55).

In a subsequent study, Ozaki et al. compared the characteristics of lesions with intact fibrous caps and ruptured fibrous cap in ACS patients. The results revealed 88% of ruptured plaques had low-attenuation characteristics ($P = 0.01$) (56). These results were consistent with previous studies (43, 54, 55). Recently, a post-mortem multiple comparison analysis based on the SCOT-HEART study which included 1,769 patients with

median follow up of 4.7 years identified the predictive effect of low-attenuation plaques on future cardiovascular events. They found that 4% was the cut-off value of low-attenuation plaque load as well as the strongest predictor of myocardial infarction. The predictive effect was independent of cardiovascular risk factors, calcification score and percentage of stenosis (45).

In a number of cross-sectional studies, investigators found that spotty calcification was associated with culprit lesions in ACS (49–52, 55). Compared with ACS, large calcification (≥ 3 mm) was more common in SA (22, 43). However, the predictive value of spotty calcification for plaque rupture is still controversial due to the huge heterogeneity in results (57). In addition, the definition and pathophysiological role of spotty calcification were questioned in studies using other imaging technologies such as OCT (58).

On CCTA, another manifestation of high-risk plaques is napkin ring sign. In a prospective study, Otsuka et al. recruited 895 patients and found that the hazard ratio (HR) of ACS in patients with the napkin ring sign was 5.55 [95% confidence interval (CI), 2.0–14.70; $P < 0.001$], which indicated napkin ring sign was an independent predictor of ACS (34). In a long-term follow-up study using ACS as one of the primary points, a strong prognostic implication of napkin-ring sign was also demonstrated by Feuchtnner et al. (59).

Combining the characteristics of high-risk plaques could better predict the risk of ACS in the future (10, 42). The result of another study, which included 1,059 patients with follow-up for 27 ± 10 months also showed that PR or low-attenuation plaques, especially in combination, was independent predictors of future ACS events (49). Subsequently, this result was confirmed in a follow-up study (8). Furthermore, in the *post-hoc* analysis of the SCOT-HEART study, the adverse plaque was defined as a plaque with one or more of the features above observed. The results revealed that patients with adverse plaques had three times higher risk of myocardial infarction than patients without adverse plaques, and the prediction effect was stronger when combined with the presence of stenosis (23).

Although there remain some controversies regarding the definition of high-risk plaques on CCTA and the predictive efficacy of different high-risk plaque characteristics in future ACS events to date (5, 8, 25, 41, 60–63), the correlation between the existence of high-risk plaques and the occurrence of future ACS events is generally obtained.

EMERGING CCTA TECHNOLOGIES AND ACUTE CORONARY SYNDROME

The emerging technologies have promoted the clinical application of CCTA. Right now, CCTA can not only identify the morphological characteristics of high-risk plaques non-invasively, but also enable the intracoronary and extracoronary imaging, so as to realize the comprehensive assessment of high-risk plaques and surrounding environment, which may provide personalized risk assessment of future ACS events and further guide clinical decision-making (12).

TABLE 1 | Prediction of acute coronary syndrome by high-risk plaque CCTA features.

Study author	Study method	Number of included patients	Type of CT equipment	Analyzed high-risk plaque features
Hoffmann et al. (11)	ACS vs. SA	14/9	16-slice	Positive remodeling
Motoyama et al. (22)	ACS vs. SA	38/33	16-slice	Positive remodeling, low-attenuation NCP (<30 HU), and spotty calcification
Motoyama et al. (49)	ACS vs. non-ACS	15/1,044	16/64-slice	Positive remodeling and low attenuation
Kitagawa et al. (54)	ACS vs. non-ACS	21/80	64-slice	NCPs (<40 HU), positive remodeling and spotty calcification
Pflederer et al. (55)	ACS vs. SA	55/55	DSCT	Positive remodeling, lower attenuation and spotty calcification
Kim et al. (43)	ACS vs. SA	35/36	64-slice	Spotty calcification, low attenuation (≤ 60 HU) and positive remodeling ($RI \geq 1.05$)
Ferencik et al. (42)	ACS vs. non-ACS	21/13	64-slice	Positive remodeling ($RI > 1.05$), low attenuation (< 90/30HU) and spotty calcification
Otsuka et al. (34)	ACS vs. non-ACS	24/871	64-slice	Positive remodeling ($RI > 1.1$), low attenuation (<30 HU), and napkin-ring sign
Puchner et al. (10)	ACS vs. non-ACS	37/435	64/128/256-slice/DSCT	Positive remodeling, low attenuation (<30 HU), napkin-ring sign and spotty calcification
Motoyama et al. (8)	ACS vs. non-ACS	88/3,070	16/64/320-slice	Positive remodeling ($RI \geq 1.1$), low attenuation (≤ 30 HU) and plaque progression
Chang et al. (41)	ACS vs. non-ACS	234/234	64-slice/DSCT/Other	Positive remodeling ($RI \geq 1.1$), low attenuation (<30 HU) and spotty calcification
Williams et al. (45)	MI vs. non-MI	41/1,728	64/320-slice	low attenuation (<30 HU)

ACS, acute coronary syndrome; CCTA, coronary computed tomography angiography; SA, stable angina; NCP, non-calcified plaque; HU, Hounsfield units; DSCT, dual-source computed tomography; RI, remodeling index; MI, myocardial infarction.

Computational Fluid Dynamics and Acute Coronary Syndrome

Plaque rupture happens when the stress inside the plaque exceeds its strength (64), while rupture of plaques is a complex biomechanical process, which is affected by the plaque structure and composition, external forces, and hemodynamic factors. Even if the plaque manifests the same vulnerable characteristics, the risk of rupture is different due to the heterogeneity of hemodynamic press exerting on the plaque (13, 65). Therefore, in addition to the assessment of plaque characteristics, accurate evaluation of plaque hemodynamic parameters is also vital for the identification of high-risk plaques and the prediction of ACS risk.

Fractional flow reserve (FFR) is the ratio of the pressure at the distal end of the stenosis to the pressure at the proximal end of the normal vessel in a state of maximum hyperemic condition. In recent years, FFR derived from CCTA (FFR_{CT}) has used advanced fluid dynamics analysis method which combines the advantages of CCTA and traditional FFR (Figure 3). It is an image post-processing technology that applies hemodynamics to CCTA examination, which uses conventional standardized CCTA image data to evaluate the hemodynamic differences of coronary artery stenosis (66). Assuming that blood is an incompressible Newtonian fluid with constant density and viscosity, the flow and pressure in the coronary model volume can be calculated by the Navier-Stokes equations (12, 58). Three prospective clinical trials (67–69) all have verified that FFR_{CT} can evaluate coronary artery stenosis from both anatomy and function. In addition, it has avoided the invasive operations of traditional FFR and the complications such as coronary artery tearing, bleeding, arrhythmia, myocardial infarction, and

so on (70). This “one-stop” technology can fundamentally avoid unnecessary coronary angiography and revascularization. Moreover, it can provide more information for clinical practice and has the potential to replace other traditional methods recommended in clinical guidelines. As a long-term gatekeeper to guide revascularization, FFR_{CT} is a new hot spot in clinical research (69, 71, 72).

FFR_{CT}, change in FFR_{CT} across the lesion (ΔFFR_{CT}), wall shear stress (WSS) and axial plaque stress are important hemodynamic parameters, which has been reported to be associated with the occurrence of adverse clinical events (13, 65, 66, 73–75). Lee et al. had demonstrated the role of these non-invasive hemodynamic parameters in identifying high-risk plaques leading to ACS by comparing adverse plaque characteristics and non-invasive hemodynamics parameters between culprit and non-culprit lesions (76). The adverse hemodynamics were defined as $FFR_{CT} \leq 0.80$, $\Delta FFR_{CT} \geq 0.06$, $WSS \geq 154.7$ dyn/cm² or axial play stress ≥ 1606.6 dyn/cm². The results showed that the FFR_{CT} of culprit lesions was lower compared with non-culprit lesions, which was consistent with the findings of Ferencik et al. (77). While ΔFFR_{CT} , WSS, and axial plaque stress are higher in culprit lesions, and ΔFFR_{CT} has the highest incremental value. Moreover, Park et al. proved that ΔFFR_{CT} has a powerful value in ACS risk prediction (78), indicating that lesion-specific hemodynamic parameters have greater influence on the occurrence of plaque rupture and ACS than that in vascular level. The value of WSS in identifying high-risk plaques has also been confirmed (79–81).

Compared with plaques with high-risk anatomical characteristics or high-risk hemodynamic characteristics,

plaques with both characteristics have a significantly higher risk of progressing to ACS (HR: 3.22; 95%CI: 1.86 to 5.55; $P < 0.001$; and HR: 11.75; 95%CI: 2.85–48.51; $P = 0.001$, respectively) (76). These studies are very valuable because they identified adverse hemodynamic characteristics before the onset of ACS. On the basis of anatomic severity and adverse plaque characteristics, the non-invasive evaluation of hemodynamic parameters was added, which improved the C-index and reclassification ability in identifying the high-risk plaques that led to ACS. In the future, the evaluation of non-invasive hemodynamic parameters may improve the identification of plaques prone to rupture as well as the prediction efficiency of high-risk plaques for ACS, and help to make the risk stratification. Further studies need to explore and determine the optimal hemodynamic parameters or combination of different patients and lesion subgroups.

Pericoronary Fat and Acute Coronary Syndrome

Vascular inflammation can promote the progression of coronary atherosclerosis and vulnerable plaque rupture, leading to the occurrence of ACS (64). Epicardial pericoronary adipose tissue (PCAT) is a special type of adipose tissue. It interacts with the adjacent vascular wall, regulates the cardiovascular biological function in a paracrine manner, and changes its phenotype in response to signals from vascular walls (82–86). Antonopoulos et al. (84) studied the gene expression, histology and CT imaging of adipose tissue samples collected during cardiac surgery, and considered that the CT density of adipose tissue (usually defined as -190 to -30 HU) reflects the balance of lipid and water phase, which is a marker of adipocyte size and lipid content. Inflammatory signals released by inflamed blood vessels are directly spread to PCAT, which can induce local lipolysis and inhibit fat formation, and also increase microvascular permeability, thus promoting perivascular edema. With the decrease of lipid content and morphology in adipocytes of PCAT, the lipid phase in adipose tissue decreases and the water phase increases, resulting in different gradients of adipocytes around the coronary artery. A further study confirmed that PCAT CT attenuation measured by CCTA can detect vascular inflammation confirmed by biopsy, and the fat attenuation index (FAI) was proposed (84). Pericoronary FAI was used to track and quantify the composition changes of PCAT by evaluating the spatial changes of peripheral fat attenuation by CCTA, which was the average density of adipose tissue in the target area (84) (Figure 4), reflecting inflammatory burden of target coronary segment (A higher pericoronary FAI was associated with a higher inflammatory burden).

Inflammation of adipose tissue around the plaque will directly affect the formation and stability of coronary plaque. Therefore, PCAT attenuation measured by CCTA is a promising indicator for identifying high-risk plaques. In patients with ACS, cases of PCAT stranding have been reported around culprit lesions (87). Goeller et al. retrospectively recruited 19 patients with ACS and 16 patients with stable CAD (88). They found that culprit lesions were associated with increased FAI around the lesions. The frequency of pericoronary FAI ≥ -68.2 HU of culprit lesions

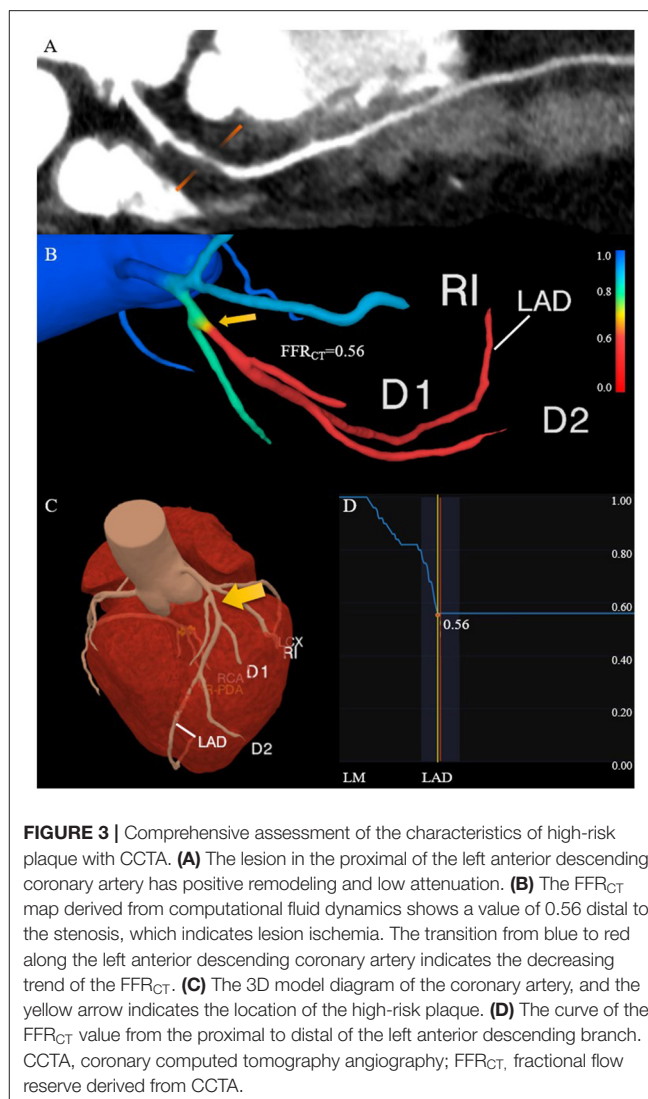


FIGURE 3 | Comprehensive assessment of the characteristics of high-risk plaque with CCTA. **(A)** The lesion in the proximal of the left anterior descending coronary artery has positive remodeling and low attenuation. **(B)** The FFR_{CT} map derived from computational fluid dynamics shows a value of 0.56 distal to the stenosis, which indicates lesion ischemia. The transition from blue to red along the left anterior descending coronary artery indicates the decreasing trend of the FFR_{CT} . **(C)** The 3D model diagram of the coronary artery, and the yellow arrow indicates the location of the high-risk plaque. **(D)** The curve of the FFR_{CT} value from the proximal to distal of the left anterior descending branch. CCTA, coronary computed tomography angiography; FFR_{CT} , fractional flow reserve derived from CCTA.

in ACS is higher, which can be used as a potential cut-off value to distinguish culprit lesions and non-culprit lesions. Therefore, combining the characteristics of high-risk plaques with the FAI around the plaques can be more reliable in identifying the high-risk plaques leading to ACS. Goeller et al. further studied the correlation between pericoronary FAI and coronary plaque progression (89). They found that the increased non-calcified plaque burden was related to the increased FAI, on the contrary, the decreased non-calcified plaque burden was related to the decreased FAI, and FAI ≥ -75 HU around the proximal end of right coronary artery (RCA) was an independent predictor of increased load of non-calcified plaques and total plaques. Therefore, PCAT is helpful to identify patients with high risk of plaque progression.

Although FAI can detect the changes of PCAT composition caused by coronary artery inflammation, it can only measure the average density of the ROI and cannot fully reflect the fine structural characteristics of the ROI. Inflammation, fibrosis, and

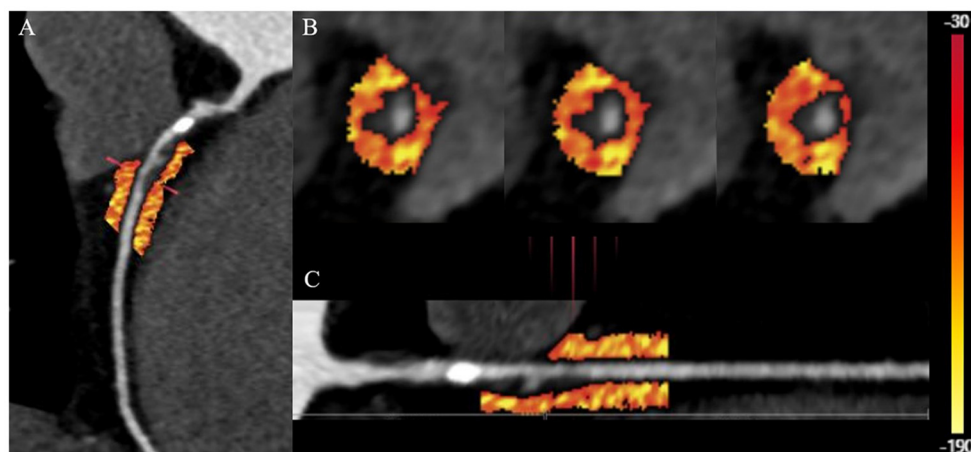


FIGURE 4 | Quantification of PCAT CT attenuation of low-attenuation plaques in the proximal-mid right coronary artery. **(A)** The multiplanar reconstructed image of PCAT measured with the range from -190 to -30 HU. **(B)** Cross-section images of PCAT measure. **(C)** Straightened image of PCAT measure. PCAT, pericoronary adipose tissue; HU, Hounsfield units.

angiogenesis are three main causes of adipose tissue dysfunction (90). Advanced imaging omics analysis can supplement the deficiency of FAI, revealing the structural changes of PCAT that cannot be recognized by the naked eye, so as to carry out more personalized assessment, and finally provide new biological insights into the pathogenesis of the disease. Recently, some researchers have verified the feasibility of PCAT image transcriptomics (91). They collected adipose tissue biopsies from 167 patients undergoing CCTA and cardiac surgery. In addition, they used image transcriptomics to correlate the gene expression of inflammation, fibrosis, and microvascular remodeling with the image omics features extracted from CT images. They proposed a new machine learning derived biomarker-fat radiomic profile (FRP), which was trained and validated to discover the PCAT imaging features related to inflammation, fibrosis, and microvascular remodeling associated with an increased cardiovascular risk. The FRP turned out to be affected by a series of factors such as scanning conditions, and the analysis was time-consuming (91). At present, a new application is being developed to automatically detect the coronary artery and pericardium, and may realize pericoronary space segmentation and feature extraction, so as to calculate FRP and FAI, and simultaneously correct the technical and anatomical information. The calculation time can be reduced to 5 min. In conclusion, PCAT imaging analysis is a new field, and its application in assessing the risk of ACS needs to be explored.

LIMITATIONS AND FUTURE DIRECTIONS OF CCTA IN ACUTE CORONARY SYNDROME

Modern CCTA assessment provides a series of advantages by combining the coronary anatomy, plaque morphology, atherosclerotic plaque load and coronary blood flow, which

allows for the evaluation of morphological and functional characteristics of high-risk plaques, and the individual risk of ACS.

In addition to CCTA, positron emission tomography (PET), magnetic resonance coronary angiography (MRCA), IVUS, OCT, and other imaging modalities are also effective methods to assess coronary atherosclerotic plaques (92–98). Notably, CCTA has irreplaceable advantages over other examinations. Firstly, CCTA can quickly provide powerful diagnostic information. Secondly, compared to coronary angiography, IVUS, and OCT, CCTA is a relatively non-invasive method with low requirements for practitioners and high universality of clinical application. In addition, CCTA has a higher spatial resolution in identifying high-risk plaque characteristics and more stable image quality than MRCA and PET. With the development of advanced hardware technology, such as photon count detectors and novel contrast agents, potential applications of multi-parameter techniques may make the plaque characterization more precise. Moreover, in previous studies, CCTA has been confirmed as a cost-effective imaging strategy (99–103).

However, there still remain certain drawbacks in CCTA. Compared with IVUS and OCT (92–98), CCTA has relatively lower spatial resolution, which hindered the detection of microscopic structure in histology (9, 104), such as the fibrous cap thickness or plaque rupture. Further CCTA studies are needed to investigate pathophysiology of rapid progression of high-risk coronary plaques leading to ACS, which will offer clinical utility on the management of patients with CAD. Recent development of intravascular imaging enables to evaluate biomechanical plaque rupture stress *in vivo*, offering prognostic implication of patients at higher risk of ACS (105, 106). The combination of intravascular imaging and CCTA may help development a novel methodology for plaque assessment of the probability of coronary plaque rupture. In addition, the beam hardening and related halo caused by the high attenuation

structure may affect the image quality (107–109), causing reduced accuracy when identifying heavily calcified lesions. Moreover, the temporal resolution of CCTA can be affected by heart cycle as well as respiration, and it is not uncommon to find the motion artifacts in images of CCTA. Another limitation is the potential increased radiation exposure (110). While recent development of CCTA enables to reduce radiation doses by increasing the use of low-end potential scans, high-pitch scan protocols, and iterative image reconstruction. The true cardiac-capable photon-count detector will be likely available soon (111–113). The emergence of wide-detector technology, dual source X-ray and high-pitch acquisition platforms has made it possible for end-diastolic and end-systolic acquisition in a single heartbeat and with sub-millisievert dose (114–116).

Although the presence of high-risk plaque features has been widely recognized in the prediction of clinical ACS, its positive predictive value for ACS is still limited (60). In previous studies, there was a relatively long-time span between CCTA and ACS events, so the changes in drug treatment during this period have considerable heterogeneity. In addition, the clinical significance of these findings may be uncertain in the case of patients having received the effective medication. Therefore, these high-risk plaque characteristics should be further investigated in cohort studies and prospective ACS prevention trials. In addition, multicenter randomized controlled trials are needed to determine whether drug treatment and/or intervention based on high-risk plaque CCTA characteristics can improve the clinical outcomes of patients.

Recently, some technological innovations in image acquisition, post-processing and other imaging biomarkers have become more and more important, which may affect the implementation, interpretation and clinical application of CCTA. To achieve high image quality should continue to be emphasized in the future, so as to accurately apply new methods such as functional assessment and plaque quantification to CCTA imaging (117). Moreover, artificial intelligence and machine learning methods may get more attention (118–120). Currently, emerging technologies such as CCTA-based identification of high-risk plaque features and FAI have not been verified in randomized controlled trials. Therefore, in the future, further studies are needed to prove the clinical benefits of CCTA application. Furthermore, with the development of hardware and advanced analysis tools, and true clinical and cost-effectiveness data, it will continue to popularize in clinical practice (121).

REFERENCES

- Virmani R, Kolodgie FD, Burke AP, Finn AV, Gold HK, Tufenkji TN, et al. Atherosclerotic plaque progression and vulnerability to rupture: angiogenesis as a source of intraplaque hemorrhage. *Arterioscler Thromb Vasc Biol.* (2005) 25:2054–61. doi: 10.1161/01.ATV.0000178991.71605.18
- Virmani R, Kolodgie FD, Burke AP, Farb A, Schwartz SM. Lessons from sudden coronary death: a comprehensive morphological classification

CONCLUSION

Current findings support more attention and careful management of patients with high-risk atherosclerotic lesions, and monitoring plaque progression for individualized treatment. CCTA has an important significance in research and daily clinical practice, which allows for not only predicting the occurrence of ACS by analyzing the characteristics of high-risk plaques but also improving the predictive value in future ACS through emerging technologies such as computational fluid dynamics and evaluation of pericoronary radiation group characteristics (such as pericoronary FAI). Furthermore, combining multi-dimensional methods can comprehensively evaluate the anatomy and biology of the coronary artery, and further integrate CCTA into clinical practice. However, the identification of high-risk plaque characteristics based on CCTA and emerging technologies such as FAI have not been verified in randomized controlled trials with definite results, which requires verification of the clinical benefits of CCTA applications in the future.

AUTHOR CONTRIBUTIONS

GL substantially planned, wrote, and revised the manuscript and made illustrates and the table. WY polished and revised the manuscript. JO and XL contributed to the collection of CT images. ZT and TL contributed to linguistic revision of the manuscript. HL substantially contributed to instruction of the writing and revision of the manuscript. All authors read and approved the final manuscript.

FUNDING

The work was supported by the Key R&D Program of Guangdong Province of China (No. 2018B030339001 to HL), the National Natural Science Foundation of China (No. 81974262 to HL), Guangdong Basic and Applied Basic Research Foundation (No. 2020A1515010650 to HL), and Guangdong Nurses Association Research Foundation (No. gdshsxh2021b077 to XL).

ACKNOWLEDGMENTS

We thank Fei Peng from Beijing Tiantan Hospital, Yuelong Yang, Xiaoyu Wei, Xiaobing Zhou from Guangdong Provincial People's Hospital for giving instructions and sharing experience to the manuscript. We thank all participants who were recruited in this work.

scheme for atherosclerotic lesions. *Arterioscler Thromb Vasc Biol.* (2000) 20:1262–75. doi: 10.1161/01.atv.20.5.1262

- Virani SS, Alonso A, Aparicio HJ, Benjamin EJ, Bittencourt MS, Callaway CW, et al. Heart disease and stroke statistics-2021 update: a report from the American Heart Association. *Circulation.* (2021) 143:e254–743. doi: 10.1161/CIR.0000000000000950
- Fishbein MC, Siegel RJ. How big are coronary atherosclerotic plaques that rupture? *Circulation.* (1996) 94:2662–6. doi: 10.1161/01.cir.94.10.2662

5. Stone GW, Maehara A, Lansky AJ, De Bruyne B, Cristea E, Mintz GS, et al. PROSPECT Investigators. A prospective natural-history study of coronary atherosclerosis. *N Engl J Med.* (2011) 364:226–35. doi: 10.1056/NEJMoa1002358
6. Koskinas KC, Ughi GJ, Windecker S, Tearney GJ, Raber L. Intracoronary imaging of coronary atherosclerosis: validation for diagnosis, prognosis and treatment. *Eur Heart J.* (2016) 37:524–35a–c. doi: 10.1093/eurheartj/ehv642
7. Maurovich-Horvat P, Ferencik M, Voros S, Merkely B, Hoffmann U. Comprehensive plaque assessment by coronary CT angiography. *Nat Rev Cardiol.* (2014) 11:390–402. doi: 10.1038/nrcardio.2014.60
8. Motoyama S, Ito H, Sarai M, Kondo T, Kawai H, Nagahara Y, et al. Plaque characterization by coronary computed tomography angiography and the likelihood of acute coronary events in mid-term follow-up. *J Am Coll Cardiol.* (2015) 66:337–46. doi: 10.1016/j.jacc.2015.05.069
9. Budoff MJ, Dowe D, Jollis JG, Gitter M, Sutherland J, Halamert E, et al. Diagnostic performance of 64-multidetector row coronary computed tomographic angiography for evaluation of coronary artery stenosis in individuals without known coronary artery disease: results from the prospective multicenter ACCURACY (Assessment by Coronary Computed Tomographic Angiography of Individuals Undergoing Invasive Coronary Angiography) trial. *J Am Coll Cardiol.* (2008) 52:1724–32. doi: 10.1016/j.jacc.2008.07.031
10. Puchner SB, Liu T, Mayrhofer T, Truong QA, Lee H, Fleg JL, et al. High-risk plaque detected on coronary CT angiography predicts acute coronary syndromes independent of significant stenosis in acute chest pain: results from the ROMICAT-II trial. *J Am Coll Cardiol.* (2014) 64:684–92. doi: 10.1016/j.jacc.2014.05.039
11. Hoffmann U, Moselewski F, Nieman K, Jang IK, Ferencik M, Rahman AM, et al. Noninvasive assessment of plaque morphology and composition in culprit and stable lesions in acute coronary syndrome and stable lesions in stable angina by multidetector computed tomography. *J Am Coll Cardiol.* (2006) 47:1655–62. doi: 10.1016/j.jacc.2006.01.041
12. Taylor CA, Fonte TA, Min JK. Computational fluid dynamics applied to cardiac computed tomography for noninvasive quantification of fractional flow reserve: scientific basis. *J Am Coll Cardiol.* (2013) 61:2233–41. doi: 10.1016/j.jacc.2012.11.083
13. Kwak BR, Back M, Bochaton-Piallat ML, Caligiuri G, Daemen MJ, Davies PF, et al. Biomechanical factors in atherosclerosis: mechanisms and clinical implications. *Eur Heart J.* (2014) 35:3013–20, 3020a–d. doi: 10.1093/eurheartj/ehu353
14. Virmani R, Burke AP, Farb A, Kolodgie FD. Pathology of the vulnerable plaque. *J Am Coll Cardiol.* (2006) 47:C13–8. doi: 10.1016/j.jacc.2005.10.065
15. Otsuka F, Yasuda S, Noguchi T, Ishibashi-Ueda H. Pathology of coronary atherosclerosis and thrombosis. *Cardiovasc Diagn Ther.* (2016) 6:396–408. doi: 10.21037/cdt.2016.06.01
16. Yahagi K, Kolodgie FD, Otsuka F, Finn AV, Davis HR, Joner M, et al. Pathophysiology of native coronary, vein graft, and in-stent atherosclerosis. *Nat Rev Cardiol.* (2016) 13:79–98. doi: 10.1038/nrcardio.2015.164
17. Ahmadi A, Leipsic J, Blankstein R, Taylor C, Hecht H, Stone GW, et al. Do plaques rapidly progress prior to myocardial infarction? The interplay between plaque vulnerability and progression. *Circ Res.* (2015) 117:99–104. doi: 10.1161/CIRCRESAHA.117.305637
18. Ahmadi A, Argulian E, Leipsic J, Newby DE, Narula J. From subclinical atherosclerosis to plaque progression and acute coronary events: jacc state-of-the-art review. *J Am Coll Cardiol.* (2019) 74:1608–17. doi: 10.1016/j.jacc.2019.08.012
19. Kolodgie FD, Gold HK, Burke AP, Fowler DR, Kruth HS, Weber DK, et al. Intraplaque hemorrhage and progression of coronary atheroma. *N Engl J Med.* (2003) 349:2316–25. doi: 10.1056/NEJMoa035655
20. Kolodgie FD, Burke AP, Farb A, Gold HK, Yuan J, Narula J, et al. The thin-cap fibroatheroma: a type of vulnerable plaque: the major precursor lesion to acute coronary syndromes. *Curr Opin Cardiol.* (2001) 16:285–92. doi: 10.1097/00001573-200109000-00006
21. Narula J, Finn AV, Demaria AN. Picking plaques that pop. *J Am Coll Cardiol.* (2005) 45:1970–3. doi: 10.1016/j.jacc.2005.03.034
22. Motoyama S, Kondo T, Sarai M, Sugiura A, Harigaya H, Sato T, et al. Multislice computed tomographic characteristics of coronary lesions in acute coronary syndromes. *J Am Coll Cardiol.* (2007) 50:319–26. doi: 10.1016/j.jacc.2007.03.044
23. Williams MC, Moss AJ, Dweck M, Adamson PD, Alam S, Hunter A, et al. Coronary artery plaque characteristics associated with adverse outcomes in the SCOT-HEART study. *J Am Coll Cardiol.* (2019) 73:291–301. doi: 10.1016/j.jacc.2018.10.066
24. Joshi NV, Vesey AT, Williams MC, Shah AS, Calvert PA, Craighead FH, et al. 18F-fluoride positron emission tomography for identification of ruptured and high-risk coronary atherosclerotic plaques: a prospective clinical trial. *Lancet.* (2014) 383:705–13. doi: 10.1016/S0140-6736(13)61754-7
25. Arbab-Zadeh A, Fuster V. From detecting the vulnerable plaque to managing the vulnerable patient: JACC state-of-the-art review. *J Am Coll Cardiol.* (2019) 74:1582–93. doi: 10.1016/j.jacc.2019.07.062
26. Hulten E, Pickett C, Bittencourt MS, Villines TC, Petrillo S, Di Carli MF, et al. Outcomes after coronary computed tomography angiography in the emergency department: a systematic review and meta-analysis of randomized, controlled trials. *J Am Coll Cardiol.* (2013) 61:880–92. doi: 10.1016/j.jacc.2012.11.061
27. Goldstein JA, Chinnaiyan KM, Abidov A, Achenbach S, Berman DS, Hayes SW, et al. The CT-STAT (Coronary Computed Tomographic Angiography for Systematic Triage of Acute Chest Pain Patients to Treatment) trial. *J Am Coll Cardiol.* (2011) 58:1414–22. doi: 10.1016/j.jacc.2011.03.068
28. Zaman T, Agarwal S, Anabtawi AG, Patel NS, Ellis SG, Tuzcu EM, et al. Angiographic lesion severity and subsequent myocardial infarction. *Am J Cardiol.* (2012) 110:167–72. doi: 10.1016/j.amjcard.2012.03.008
29. Ojio S, Takatsu H, Tanaka T, Ueno K, Yokoya K, Matsubara T, et al. Considerable time from the onset of plaque rupture and/or thrombi until the onset of acute myocardial infarction in humans: coronary angiographic findings within 1 week before the onset of infarction. *Circulation.* (2000) 102:2063–9. doi: 10.1161/01.cir.102.17.2063
30. Yokoya K, Takatsu H, Suzuki T, Hosokawa H, Ojio S, Matsubara T, et al. Process of progression of coronary artery lesions from mild or moderate stenosis to moderate or severe stenosis: a study based on four serial coronary arteriograms per year. *Circulation.* (1999) 100:903–9. doi: 10.1161/01.cir.100.9.903
31. Fracassi F, Crea F, Sugiyama T, Yamamoto E, Uemura S, Vergallo R, et al. Healed culprit plaques in patients with acute coronary syndromes. *J Am Coll Cardiol.* (2019) 73:2253–63. doi: 10.1016/j.jacc.2018.10.093
32. Kolossvary M, Szilveszter B, Merkely B, Maurovich-Horvat P. Plaque imaging with CT—a comprehensive review on coronary CT angiography based risk assessment. *Cardiovasc Diagn Ther.* (2017) 7:489–506. doi: 10.21037/cdt.2016.11.06
33. Conte E, Annoni A, Pontone G, Mushtaq S, Guglielmo M, Baggiano A, et al. Evaluation of coronary plaque characteristics with coronary computed tomography angiography in patients with non-obstructive coronary artery disease: a long-term follow-up study. *Eur Heart J Cardiovasc Imaging.* (2017) 18:1170–8. doi: 10.1093/ehjci/jew200
34. Otsuka K, Fukuda S, Tanaka A, Nakanishi K, Taguchi H, Yoshikawa J, et al. Napkin-ring sign on coronary CT angiography for the prediction of acute coronary syndrome. *JACC Cardiovasc Imaging.* (2013) 6:448–57. doi: 10.1016/j.jcmg.2012.09.016
35. Kroner ES, van Velzen JE, Boogers MJ, Siebelink HM, Schalij MJ, Kroft LJ, et al. Positive remodeling on coronary computed tomography as a marker for plaque vulnerability on virtual histology intravascular ultrasound. *Am J Cardiol.* (2011) 107:1725–9. doi: 10.1016/j.amjcard.2011.02.337
36. Glagov S, Weisenberg E, Zarins CK, Stankunavicius R, Koletts GJ. Compensatory enlargement of human atherosclerotic coronary arteries. *N Engl J Med.* (1987) 316:1371–5. doi: 10.1056/NEJM198705283162204
37. Nakamura M, Nishikawa H, Mukai S, Setsuda M, Nakajima K, Tamada H, et al. Impact of coronary artery remodeling on clinical presentation of coronary artery disease: an intravascular ultrasound study. *J Am Coll Cardiol.* (2001) 37:63–9. doi: 10.1016/s0735-1097(00)01097-4
38. Varnava AM, Mills PG, Davies MJ. Relationship between coronary artery remodeling and plaque vulnerability. *Circulation.* (2002) 105:939–43. doi: 10.1161/hc0802.104327
39. Oikonomou EK, West HW, Antoniades C. Cardiac computed tomography: assessment of coronary inflammation and other plaque features. *Arterioscler Thromb Vasc Biol.* (2019) 39:2207–19. doi: 10.1161/ATVBAHA.119.312899

40. Achenbach S, Ropers D, Hoffmann U, MacNeill B, Baum U, Pohle K, et al. Assessment of coronary remodeling in stenotic and nonstenotic coronary atherosclerotic lesions by multidetector spiral computed tomography. *J Am Coll Cardiol.* (2004) 43:842–7. doi: 10.1016/j.jacc.2003.09.053
41. Chang HJ, Lin FY, Lee SE, Andreini D, Bax J, Cademartiri F, et al. Coronary atherosclerotic precursors of acute coronary syndromes. *J Am Coll Cardiol.* (2018) 71:2511–22. doi: 10.1016/j.jacc.2018.02.079
42. Ferencik M, Schlett CL, Ghoshhajra BB, Kriegel MF, Joshi SB, Maurovich-Horvat P, et al. A computed tomography-based coronary lesion score to predict acute coronary syndrome among patients with acute chest pain and significant coronary stenosis on coronary computed tomographic angiogram. *Am J Cardiol.* (2012) 110:183–9. doi: 10.1016/j.amjcard.2012.02.066
43. Kim SY, Kim KS, Seung MJ, Chung JW, Kim JH, Mun SH, et al. The culprit lesion score on multi-detector computed tomography can detect vulnerable coronary artery plaque. *Int J Cardiovasc Imaging.* (2010) 26:245–52. doi: 10.1007/s10554-010-9712-2
44. Boogers MJ, Broersen A, van Velzen JE, de Graaf FR, El-Naggar HM, Kitslaar PH, et al. Automated quantification of coronary plaque with computed tomography: comparison with intravascular ultrasound using a dedicated registration algorithm for fusion-based quantification. *Eur Heart J.* (2012) 33:1007–16. doi: 10.1093/eurheartj/ehr465
45. Williams MC, Kwiecinski J, Doris M, McElhinney P, D'Souza MS, Cadet S, et al. Low-attenuation noncalcified plaque on coronary computed tomography angiography predicts myocardial infarction: results from the multicenter SCOT-HEART trial (Scottish Computed Tomography of the HEART). *Circulation.* (2020) 141:1452–62. doi: 10.1161/CIRCULATIONAHA.119.044720
46. Mori H, Torii S, Kutyna M, Sakamoto A, Finn AV, Virmani R. Coronary artery calcification and its progression: what does it really mean? *JACC Cardiovasc Imaging.* (2018) 11:127–42. doi: 10.1016/j.jcmg.2017.10.012
47. van Velzen JE, de Graaf FR, de Graaf MA, Schuijf JD, Kroft LJ, de Roos A, et al. Comprehensive assessment of spotty calcifications on computed tomography angiography: comparison to plaque characteristics on intravascular ultrasound with radiofrequency backscatter analysis. *J Nucl Cardiol.* (2011) 18:893–903. doi: 10.1007/s12350-011-9428-2
48. Vancheri F, Longo G, Vancheri S, Danial JSH, Henein MY. Coronary artery microcalcification: imaging and clinical implications. *Diagnostics.* (2019) 9:125. doi: 10.3390/diagnostics9040125
49. Motoyama S, Sarai M, Harigaya H, Anno H, Inoue K, Hara T, et al. Computed tomographic angiography characteristics of atherosclerotic plaques subsequently resulting in acute coronary syndrome. *J Am Coll Cardiol.* (2009) 54:49–57. doi: 10.1016/j.jacc.2009.02.068
50. Benedek T, Gyongyosi M, Benedek I. Multislice computed tomographic coronary angiography for quantitative assessment of culprit lesions in acute coronary syndromes. *Can J Cardiol.* (2013) 29:364–71. doi: 10.1016/j.cjca.2012.11.004
51. Saremi F, Achenbach S. Coronary plaque characterization using CT. *Am J Roentgenol.* (2015) 204:W249–60. doi: 10.2214/AJR.14.13760
52. Burke AP, Weber DK, Kolodgie FD, Farb A, Taylor AJ, Virmani R. Pathophysiology of calcium deposition in coronary arteries. *Herz.* (2001) 26:239–44. doi: 10.1007/pl00002026
53. Seifarth H, Schlett CL, Nakano M, Otsuka F, Karolyi M, Liew G, et al. Histopathological correlates of the napkin-ring sign plaque in coronary CT angiography. *Atherosclerosis.* (2012) 224:90–6. doi: 10.1016/j.atherosclerosis.2012.06.021
54. Kitagawa T, Yamamoto H, Horiguchi J, Ohhashi N, Tadehara F, Shokawa T, et al. Characterization of noncalcified coronary plaques and identification of culprit lesions in patients with acute coronary syndrome by 64-slice computed tomography. *JACC Cardiovasc Imaging.* (2009) 2:153–60. doi: 10.1016/j.jcmg.2008.09.015
55. Pfleiderer T, Marwan M, Schepis T, Ropers D, Selmann M, Muschiol G, et al. Characterization of culprit lesions in acute coronary syndromes using coronary dual-source CT angiography. *Atherosclerosis.* (2010) 211:437–44. doi: 10.1016/j.atherosclerosis.2010.02.001
56. Ozaki Y, Okumura M, Ismail TF, Motoyama S, Naruse H, Hattori K, et al. Coronary CT angiographic characteristics of culprit lesions in acute coronary syndromes not related to plaque rupture as defined by optical coherence tomography and angiography. *Eur Heart J.* (2011) 32:2814–23. doi: 10.1093/eurheartj/ehr189
57. Otsuka F, Finn AV, Virmani R. Do vulnerable and ruptured plaques hide in heavily calcified arteries? *Atherosclerosis.* (2013) 229:34–7. doi: 10.1016/j.atherosclerosis.2012.12.032
58. Ong DS, Lee JS, Soeda T, Higuma T, Minami Y, Wang Z, et al. Coronary calcification and plaque vulnerability: an optical coherence tomographic study. *Circ Cardiovasc Imaging.* (2016) 9:e003929. doi: 10.1161/CIRCIMAGING.115.003929
59. Feuchtnner G, Kerber J, Burghard P, Dichtl W, Friedrich G, Bonaros N, et al. The high-risk criteria low-attenuation plaque <60 HU and the napkin-ring sign are the most powerful predictors of MACE: a long-term follow-up study. *Eur Heart J Cardiovasc Imaging.* (2017) 18:772–779. doi: 10.1093/ehjci/jew167
60. Achenbach S. Imaging the vulnerable plaque on coronary CTA. *JACC Cardiovasc Imaging.* (2020) 13:1418–21. doi: 10.1016/j.jcmg.2019.11.006
61. Arbab-Zadeh A, Fuster V. The myth of the “vulnerable plaque”: transitioning from a focus on individual lesions to atherosclerotic disease burden for coronary artery disease risk assessment. *J Am Coll Cardiol.* (2015) 65:846–55. doi: 10.1016/j.jacc.2014.11.041
62. Schuurman AS, Vroegindewey MM, Kardys I, Oemrawsingh RM, Garcia-Garcia HM, van Geuns RJ, et al. Prognostic value of intravascular ultrasound in patients with coronary artery disease. *J Am Coll Cardiol.* (2018) 72:2003–11. doi: 10.1016/j.jacc.2018.08.2140
63. Lee SE, Sung JM, Rizvi A, Lin FY, Kumar A, Hadamitzky M, et al. Quantification of coronary atherosclerosis in the assessment of coronary artery disease. *Circ Cardiovasc Imaging.* (2018) 11:e007562. doi: 10.1161/CIRCIMAGING.117.007562
64. Weissberg PL, Bennett MR. Atherosclerosis—an inflammatory disease. *N Engl J Med.* (1999) 340:1928–9. doi: 10.1056/nejm199906173402418
65. Choi G, Lee JM, Kim HJ, Park JB, Sankaran S, Otake H, et al. Coronary artery axial plaque stress and its relationship with lesion geometry: application of computational fluid dynamics to coronary CT angiography. *JACC Cardiovasc Imaging.* (2015) 8:1156–66. doi: 10.1016/j.jcmg.2015.04.024
66. De Bruyne B, Fearon WF, Pijls NH, Barbato E, Tonino P, Piroth Z, et al. Fractional flow reserve-guided PCI for stable coronary artery disease. *N Engl J Med.* (2014) 371:1208–17. doi: 10.1056/NEJMoa1408758
67. Fairbairn TA, Nieman K, Akasaka T, Norgaard BL, Berman DS, Raff G, et al. Real-world clinical utility and impact on clinical decision-making of coronary computed tomography angiography-derived fractional flow reserve: lessons from the ADVANCE Registry. *Eur Heart J.* (2018) 39:3701–11. doi: 10.1093/eurheartj/ehy530
68. Leipsic J, Yang TH, Thompson A, Koo BK, Mancini GB, Taylor C, et al. CT angiography (CTA) and diagnostic performance of noninvasive fractional flow reserve: results from the Determination of Fractional Flow Reserve by Anatomic CTA (DeFACTO) study. *AJR Am J Roentgenol.* (2014) 202:989–94. doi: 10.2214/AJR.13.11441
69. Norgaard BL, Leipsic J, Gaur S, Seneviratne S, Ko BS, Ito H, et al. Diagnostic performance of noninvasive fractional flow reserve derived from coronary computed tomography angiography in suspected coronary artery disease: the NXT trial (Analysis of Coronary Blood Flow Using CT Angiography: Next Steps). *J Am Coll Cardiol.* (2014) 63:1145–55. doi: 10.1016/j.jacc.2013.11.043
70. Fearon WF, Bornschein B, Tonino PA, Gothe RM, Bruyne BD, Pijls NH, et al. Economic evaluation of fractional flow reserve-guided percutaneous coronary intervention in patients with multivessel disease. *Circulation.* (2010) 122:2545–50. doi: 10.1161/CIRCULATIONAHA.109.925396
71. Koo BK, Erglis A, Doh JH, Daniels DV, Jegere S, Kim HS, et al. Diagnosis of ischemia-causing coronary stenoses by noninvasive fractional flow reserve computed from coronary computed tomographic angiograms. Results from the prospective multicenter DISCOVER-FLOW (Diagnosis of Ischemia-Causing Stenoses Obtained Via Noninvasive Fractional Flow Reserve) study. *J Am Coll Cardiol.* (2011) 58:1989–97. doi: 10.1016/j.jacc.2011.06.066
72. Min JK, Leipsic J, Pencina MJ, Berman DS, Koo BK, van Mieghem C, et al. Diagnostic accuracy of fractional flow reserve from anatomic CT angiography. *JAMA.* (2012) 308:1237–45. doi: 10.1001/2012.jama.11274
73. Lee JM, Choi G, Hwang D, Park J, Kim HJ, Doh JH, et al. Impact of Longitudinal Lesion Geometry on Location of Plaque Rupture

- and Clinical Presentations. *JACC Cardiovasc Imaging*. (2017) 10:677–88. doi: 10.1016/j.jcmg.2016.04.012
74. Samady H, Eshetehardi P, McDaniel MC, Suo J, Dhawan SS, Maynard C, et al. Coronary artery wall shear stress is associated with progression and transformation of atherosclerotic plaque and arterial remodeling in patients with coronary artery disease. *Circulation*. (2011) 124:779–88. doi: 10.1161/CIRCULATIONAHA.111.021824
 75. Fukumoto Y, Hiro T, Fujii T, Hashimoto G, Fujimura T, Yamada J, et al. Localized elevation of shear stress is related to coronary plaque rupture: a 3-dimensional intravascular ultrasound study with *in-vivo* color mapping of shear stress distribution. *J Am Coll Cardiol*. (2008) 51:645–50. doi: 10.1016/j.jacc.2007.10.030
 76. Lee JM, Choi G, Koo BK, Hwang D, Park J, Zhang J, et al. Identification of high-risk plaques destined to cause acute coronary syndrome using coronary computed tomographic angiography and computational fluid dynamics. *JACC Cardiovasc Imaging*. (2019) 12:1032–43. doi: 10.1016/j.jcmg.2018.01.023
 77. Ferencik M, Lu MT, Mayrhofer T, Puchner SB, Liu T, Maurovich-Horvat P, et al. Non-invasive fractional flow reserve derived from coronary computed tomography angiography in patients with acute chest pain: subgroup analysis of the ROMICAT II trial. *J Cardiovasc Comput Tomogr*. (2019) 13:196–202. doi: 10.1016/j.jcct.2019.05.009
 78. Park J, Lee JM, Koo BK, Choi G, Hwang D, Rhee TM, et al. Relevance of anatomical, plaque, and hemodynamic characteristics of non-obstructive coronary lesions in the prediction of risk for acute coronary syndrome. *Eur Radiol*. (2019) 29:6119–28. doi: 10.1007/s00330-019-06221-9
 79. Park JB, Choi G, Chun EJ, Kim HJ, Park J, Jung JH, et al. Computational fluid dynamic measures of wall shear stress are related to coronary lesion characteristics. *Heart*. (2016) 102:1655–61. doi: 10.1136/heartjnl-2016-309299
 80. Han D, Starikov A, O'Hartagh B, Gransar H, Kolli KK, Lee JH, et al. Relationship between endothelial wall shear stress and high-risk atherosclerotic plaque characteristics for identification of coronary lesions that cause ischemia: a direct comparison with fractional flow. *Reserve J Am Heart Assoc*. (2016) 5:e004186. doi: 10.1161/JAHA.116.004186
 81. Bourantas CV, Papadopolou SL, Serruys PW, Sakellarios A, Kitslaar PH, Bizopoulos P, et al. Noninvasive prediction of atherosclerotic progression: the PROSPECT-MSCT study. *JACC Cardiovasc Imaging*. (2016) 9:1009–11. doi: 10.1016/j.jcmg.2015.07.005
 82. Verhagen SN, Visseren FL. Perivascular adipose tissue as a cause of atherosclerosis. *Atherosclerosis*. (2011) 214:3–10. doi: 10.1016/j.atherosclerosis.2010.05.034
 83. Tanaka K, Sata M. Roles of perivascular adipose tissue in the pathogenesis of atherosclerosis. *Front Physiol*. (2018) 9:3. doi: 10.3389/fphys.2018.00003
 84. Antonopoulos AS, Sanna F, Sabharwal N, Thomas S, Oikonomou EK, Herdman L, et al. Detecting human coronary inflammation by imaging perivascular fat. *Sci Transl Med*. (2017) 9:eal2658. doi: 10.1126/scitranslmed.aal2658
 85. Margaritis M, Antonopoulos AS, Digby J, Lee R, Reilly S, Coutinho P, et al. Interactions between vascular wall and perivascular adipose tissue reveal novel roles for adiponectin in the regulation of endothelial nitric oxide synthase function in human vessels. *Circulation*. (2013) 127:2209–21. doi: 10.1161/CIRCULATIONAHA.112.001133
 86. Akoumianakis I, Antoniadou C. The interplay between adipose tissue and the cardiovascular system: is fat always bad? *Cardiovasc Res*. (2017) 113:999–1008. doi: 10.1093/cvr/cvx111
 87. Hedgire Sa, Baliyan V, Zucker EJ, Bittner DO, Staziaki PV, Takx RAP, et al. Perivascular epicardial fat stranding at coronary CT angiography: a marker of acute plaque rupture and spontaneous coronary artery dissection. *radiology*. (2018) 287:808–15. doi: 10.1148/radiol.2017171568
 88. Goeller M, Achenbach S, Cadet S, Kwan AC, Commandeur F, Slomka PJ, et al. Pericoronary adipose tissue computed tomography attenuation and high-risk plaque characteristics in acute coronary syndrome compared with stable coronary artery disease. *JAMA Cardiol*. (2018) 3:858–63. doi: 10.1001/jamacardio.2018.1997
 89. Goeller M, Tamarappoo BK, Kwan AC, Cadet S, Commandeur F, Razipour A, et al. Relationship between changes in pericoronary adipose tissue attenuation and coronary plaque burden quantified from coronary computed tomography angiography. *Eur Heart J Cardiovasc Imaging*. (2019) 20:636–43. doi: 10.1093/ehjci/jez013
 90. Crewe C, An YA, Scherer PE. The ominous triad of adipose tissue dysfunction: inflammation, fibrosis, and impaired angiogenesis. *J Clin Invest*. (2017) 127:74–82. doi: 10.1172/JCI88883
 91. Oikonomou EK, Williams MC, Kotanidis CP, Desai MY, Marwan M, Antonopoulos AS, et al. A novel machine learning-derived radiotranscriptomic signature of perivascular fat improves cardiac risk prediction using coronary CT angiography. *Eur Heart J*. (2019) 40:3529–43. doi: 10.1093/eurheartj/ehz592
 92. Lin FY, Villines TC, Narula J, Shaw LJ. What is the clinical role of non-invasive atherosclerosis imaging? *J Cardiovasc Comput Tomogr*. (2019) 13:261–6. doi: 10.1016/j.jcct.2019.05.010
 93. Adamson PD, Newby DE. Non-invasive imaging of the coronary arteries. *Eur Heart J*. (2019) 40:2444–54. doi: 10.1093/eurheartj/ehy670
 94. Erlinge D, Maehara A, Ben-Yehuda O, Botker HE, Maeng M, Kjoller-Hansen L, et al. Identification of vulnerable plaques and patients by intracoronary near-infrared spectroscopy and ultrasound (PROSPECT II): a prospective natural history study. *Lancet*. (2021) 397:985–95. doi: 10.1016/S0140-6736(21)00249-X
 95. Daghem M, Bing R, Fayad ZA, Dweck MR. Noninvasive imaging to assess atherosclerotic plaque composition and disease activity: coronary and carotid applications. *JACC Cardiovasc Imaging*. (2020) 13:1055–68. doi: 10.1016/j.jcmg.2019.03.033
 96. Li J, Montarello NJ, Hoogendoorn A, Verjans JW, Bursill CA, Peter K, et al. Multimodality intravascular imaging of high-risk coronary plaque. *JACC Cardiovasc Imaging*. (2021) 12:28. doi: 10.1016/j.jcmg.2021.03.028
 97. Otsuka K, Villiger M, Karanasos A, van Zandvoort LJC, Doradla P, Ren J, et al. Intravascular polarimetry in patients with coronary artery disease. *JACC Cardiovasc Imaging*. (2020) 13:790–801. doi: 10.1016/j.jcmg.2019.06.015
 98. Otsuka K, Villiger M, Nadkarni SK, Bouma BE. Intravascular polarimetry: clinical translation and future applications of catheter-based polarization sensitive optical frequency domain imaging. *Front Cardiovasc Med*. (2020) 7:146. doi: 10.3389/fcvm.2020.00146
 99. Mark DB, Federspiel JJ, Cowper PA, Anstrom KJ, Hoffmann U, Patel MR, et al. Economic outcomes with anatomical versus functional diagnostic testing for coronary artery disease. *Ann Intern Med*. (2016) 165:94–102. doi: 10.7326/M15-2639
 100. Levin DC, Parker L, Halpern EJ, Rao VM. Coronary CT angiography: reversal of earlier utilization trends. *J Am Coll Radiol*. (2019) 16:147–55. doi: 10.1016/j.jacr.2018.07.022
 101. Chang HJ, Lin FY, Gebow D, An HY, Andreini D, Bathina R, et al. Selective referral using CCTA versus direct referral for individuals referred to invasive coronary angiography for suspected CAD: a randomized, controlled, open-label trial. *JACC Cardiovasc Imaging*. (2019) 12:1303–12. doi: 10.1016/j.jcmg.2018.09.018
 102. Tarkin JM, Dweck MR, Evans NR, Takx RA, Brown AJ, Tawakol A, et al. Imaging atherosclerosis. *Circ Res*. (2016) 118:750–69. doi: 10.1161/CIRCRESAHA.115.306247
 103. Goehler A, Mayrhofer T, Pursnani A, Ferencik M, Lumish HS, Barth C, et al. Long-term health outcomes and cost-effectiveness of coronary CT angiography in patients with suspicion for acute coronary syndrome. *J Cardiovasc Comput Tomogr*. (2020) 14:44–54. doi: 10.1016/j.jcct.2019.06.008
 104. Cury RC, Abbara S, Achenbach S, Agatston A, Berman DS, Budoff MJ, et al. Coronary Artery Disease - Reporting and Data System (CAD-RADS): an expert consensus document of SCCT, ACR and NASCI: endorsed by the ACC. *JACC Cardiovasc Imaging*. (2016) 9:1099–113. doi: 10.1016/j.jcmg.2016.05.005
 105. Costopoulos C, Maehara A, Huang Y, Brown AJ, Gillard JH, Teng Z, et al. Heterogeneity of plaque structural stress is increased in plaques leading to MACE: insights from the PROSPECT study. *JACC Cardiovasc Imaging*. (2020) 13:1206–18. doi: 10.1016/j.jcmg.2019.05.024
 106. Doradla P, Otsuka K, Nadkarni A, Villiger M, Karanasos A, Zandvoort LJC, et al. Biomechanical stress profiling of coronary atherosclerosis: identifying a multifactorial metric to evaluate plaque rupture risk. *JACC Cardiovasc Imaging*. (2020) 13:804–16. doi: 10.1016/j.jcmg.2019.01.033

107. Lee SE, Chang HJ, Sung JM, Park HB, Heo R, Rizvi A, et al. Effects of statins on coronary atherosclerotic plaques: the PARADIGM study. *JACC Cardiovasc Imaging*. (2018) 11:1475–84. doi: 10.1016/j.jcmg.2018.04.015
108. Ghekiere O, Salgado R, Buls N, Leiner T, Mancini I, Vanhoenacker P, et al. Image quality in coronary CT angiography: challenges and technical solutions. *Br J Radiol*. (2017) 90:20160567. doi: 10.1259/bjr.20160567
109. Cury RC, Abbara S, Achenbach S, Agatston A, Berman DS, Budoff MJ, et al. CAD-RADS(TM) coronary artery disease - reporting and data system. An expert consensus document of the Society of Cardiovascular Computed Tomography (SCCT), the American College of Radiology (ACR) and the North American Society for Cardiovascular Imaging (NASCI) endorsed by the American College of Cardiology. *J Cardiovasc Comput Tomogr*. (2016) 10:269–81. doi: 10.1016/j.jcct.2016.04.005
110. Smulders MW, Kietselaer BLJH, Wildberger JE, Dagnelie PC, Brunner-La Rocca HP, Mingels AMA, et al. Initial imaging-guided strategy versus routine care in patients with non-ST-segment elevation myocardial infarction. *J Am Coll Cardiol*. (2019) 74:2466–77. doi: 10.1016/j.jacc.2019.09.027
111. Stocker TJ, Deseive S, Leipsic J, Hadamitzky M, Chen MY, Rubinshtein R, et al. Reduction in radiation exposure in cardiovascular computed tomography imaging: results from the PROspective multicenter registry on radiation dose Estimates of cardiac CT angiography in daily practice in 2017 (PROTECTION VI). *Eur Heart J*. (2018) 39:3715–23. doi: 10.1093/eurheartj/ehy546
112. Pessis E, Campagna R, Sverzut JM, Bach F, Rodallec M, Guerini H, et al. Virtual monochromatic spectral imaging with fast kilovoltage switching: reduction of metal artifacts at CT. *Radiographics*. (2013) 33:573–83. doi: 10.1148/rg.332125124
113. Kalisz K, Halliburton S, Abbara S, Leipsic JA, Albrecht MH, Schoepf UJ, et al. Update on cardiovascular applications of multienergy CT. *Radiographics*. (2017) 37:1955–74. doi: 10.1148/rg.2017170100
114. Hill KD, Frush DP, Han BK, Abbott BG, Armstrong AK, DeKemp RA, et al. Radiation safety in children with congenital and acquired heart disease: a scientific position statement on multimodality dose optimization from the image gently alliance. *JACC Cardiovasc Imaging*. (2017) 10:797–818. doi: 10.1016/j.jcmg.2017.04.003
115. Cauldwell C. Anesthesia risks associated with pediatric imaging. *Pediatr Radiol*. (2011) 41:949–50. doi: 10.1007/s00247-011-2160-x
116. Greenberg SB. Rebalancing the risks of computed tomography and magnetic resonance imaging. *Pediatr Radiol*. (2011) 41:951–2. doi: 10.1007/s00247-011-2159-3
117. Choi AD, Thomas DM, Lee J, Abbara S, Cury RC, Leipsic JA, et al. 2020 SCCT guideline for training cardiology and radiology trainees as independent practitioners (level II) and advanced practitioners (Level III) in cardiovascular computed tomography: a statement from the Society of Cardiovascular Computed Tomography. *JACC Cardiovasc Imaging*. (2021) 14:272–87. doi: 10.1016/j.jcmg.2020.09.004
118. Weir-McCall JR, Branch K, Ferencik M, Blankstein R, Choi AD, Ghoshhajra BB, et al. Highlights of the 15th annual scientific meeting of the Society of Cardiovascular Computed Tomography. *J Cardiovasc Comput Tomogr*. (2020) 14:466–70. doi: 10.1016/j.jcct.2020.09.008
119. Abdelrahman KM, Chen MY, Dey AK, Virmani R, Finn AV, Khamis RY, et al. Coronary computed tomography angiography from clinical uses to emerging technologies: JACC state-of-the-art review. *J Am Coll Cardiol*. (2020) 76:1226–43. doi: 10.1016/j.jacc.2020.06.076
120. Kumar V, Weerakoon S, Dey AK, Earls JP, Katz RJ, Reiner JS, et al. The evolving role of coronary CT angiography in Acute Coronary Syndromes. *J Cardiovasc Comput Tomogr*. (2021) 15:384–93. doi: 10.1016/j.jcct.2021.02.002
121. Nicol ED, Norgaard BL, Blanke P, Ahmadi A, Weir-McCall J, Horvat PM, et al. The future of cardiovascular computed tomography: advanced analytics and clinical insights. *JACC Cardiovasc Imaging*. (2019) 12:1058–72. doi: 10.1016/j.jcmg.2018.11.037

Conflict of Interest: The authors declare that the research was conducted in the absence of any commercial or financial relationships that could be construed as a potential conflict of interest.

Publisher's Note: All claims expressed in this article are solely those of the authors and do not necessarily represent those of their affiliated organizations, or those of the publisher, the editors and the reviewers. Any product that may be evaluated in this article, or claim that may be made by its manufacturer, is not guaranteed or endorsed by the publisher.

Copyright © 2021 Lu, Ye, Ou, Li, Tan, Li and Liu. This is an open-access article distributed under the terms of the Creative Commons Attribution License (CC BY). The use, distribution or reproduction in other forums is permitted, provided the original author(s) and the copyright owner(s) are credited and that the original publication in this journal is cited, in accordance with accepted academic practice. No use, distribution or reproduction is permitted which does not comply with these terms.



Combined Use of Multiple Intravascular Imaging Techniques in Acute Coronary Syndrome

Takashi Kubo^{1,2*}, Kosei Terada¹, Yasushi Ino^{1,3}, Yasutsugu Shiono¹, Shengxian Tu⁴, Tien-Ping Tsao⁵, Yundai Chen⁶ and Duk-Woo Park⁷

¹ Department of Cardiovascular Medicine, Wakayama Medical University, Wakayama, Japan, ² Department of Cardiovascular Medicine, Naga Municipal Hospital, Kinokawa, Japan, ³ Department of Cardiovascular Medicine, Shingu Municipal Hospital, Shingu, Japan, ⁴ School of Biomedical Engineering, Biomedical Instrument Institute, Shanghai Jiao Tong University, Shanghai, China, ⁵ Division of Cardiology, Heart Center, Cheng Hsin General Hospital, Taipei, Taiwan, ⁶ Department of Cardiology, Chinese PLA General Hospital, Beijing, China, ⁷ Division of Cardiology, Asan Medical Center, University of Ulsan College of Medicine, Seoul, South Korea

OPEN ACCESS

Edited by:

Jinwei Tian,
The Second Affiliated Hospital of
Harbin Medical University, China

Reviewed by:

Kensuke Nishimiya,
Tohoku University, Japan
Suma Victor,
Madras Medical Mission, India

*Correspondence:

Takashi Kubo
kubo.takashi@yahoo.com

Specialty section:

This article was submitted to
Cardiovascular Imaging,
a section of the journal
Frontiers in Cardiovascular Medicine

Received: 29 November 2021

Accepted: 20 December 2021

Published: 17 January 2022

Citation:

Kubo T, Terada K, Ino Y, Shiono Y,
Tu S, Tsao T-P, Chen Y and Park D-W
(2022) Combined Use of Multiple
Intravascular Imaging Techniques in
Acute Coronary Syndrome.
Front. Cardiovasc. Med. 8:824128.
doi: 10.3389/fcvm.2021.824128

Recent advances in intravascular imaging techniques have made it possible to assess the culprit lesions of acute coronary syndrome (ACS) in the clinical setting. Intravascular ultrasound (IVUS) is the most commonly used intravascular imaging technique that provides cross-sectional images of coronary arteries. IVUS can assess plaque burden and vessel remodeling. Optical coherence tomography (OCT) is a high-resolution (10 μm) intravascular imaging technique that uses near-infrared light. OCT can identify key features of atheroma, such as lipid core and thin fibrous cap. Near-infrared spectroscopy (NIRS) can detect lipid composition by analyzing the near-infrared absorption properties of coronary plaques. NIRS provides a chemogram of the coronary artery wall, which allows for specific quantification of lipid accumulation. These intravascular imaging techniques can depict histological features of plaque rupture, plaque erosion, and calcified nodule in ACS culprit lesions. However, no single imaging technique is perfect and each has its respective strengths and limitations. In this review, we summarize the implications of combined use of multiple intravascular imaging techniques to assess the pathology of ACS and guide lesion-specific treatment.

Keywords: acute coronary syndrome, plaque rupture, plaque erosion, calcified nodule, intravascular ultrasound, optical coherence tomography, near-infrared spectroscopy

INTRODUCTION

Several autopsy studies have revealed the pathology of culprit lesions of acute coronary syndrome (ACS). ACS is caused by three main mechanisms: plaque rupture, plaque erosion, and calcified nodule. Plaque rupture is the most common (55–60%) mechanism for ACS (1). Plaque rupture usually has an extensive lipid core containing large numbers of cholesterol crystals and a thin fibrous cap (<65 μm) infiltrated by foamy macrophages. Plaque erosion is found in 30–35% of ACS (1). Most of plaque erosion occurs over areas of intimal thickening, with minimal or no evidence of a lipid. Calcified nodule is identified in 2–7% of ACS (1). Calcified nodule is a plaque with luminal thrombi showing calcific nodules protruding into the lumen through a disrupted thin fibrous cap.

Recent advances in intravascular imaging techniques have made it possible to assess the culprit lesions of ACS in the clinical setting. In the early 1990s, intravascular ultrasound (IVUS) became

clinically available, enabling morphological evaluation of coronary artery walls. In the mid-2000s, optical coherence tomography (OCT) was developed and its high resolution allows for more precise observations of coronary atherosclerosis. In the late 2000s, near-infrared spectroscopy (NIRS) was clinically applied, which permits to diagnose plaque composition. These intravascular imaging techniques can depict histological features of plaque rupture, plaque erosion, and calcified nodule in ACS culprit lesions (2).

IVUS

IVUS is the most commonly used intravascular imaging technique in the world. IVUS provides cross-sectional images of coronary arteries. IVUS can identify plaque rupture and calcified nodule, but not plaque erosion. Plaque rupture is identified as ulceration with a recess in the plaque beginning at the luminal-intimal border (3, 4). The lesions with plaque rupture usually have a large plaque burden with positive vascular remodeling and exhibit a hypoechoic plaque with acoustic shadow derived from the lipid core (so-called attenuated plaque) (5). The coarse-resolution (100–200 μm) of IVUS cannot determine the presence or absence of small rupture, therefore this technique cannot diagnose plaque erosion. Calcified nodule is identified by a convex shape of the luminal surface with a bright echo, bulgy shape, irregular surface, and acoustic shadowing (6). The lesions with calcified nodule often have an extensive calcium sheet.

OCT

OCT is a high-resolution (10 μm) intravascular imaging technique that uses near-infrared light. OCT is the most reliable technique for evaluating the complex morphology of ACS culprit lesions, although this technique requires some complicated procedures such as intracoronary contrast injection to remove red blood cells for image acquisition. OCT can identify lipid core (characterized by signal-poor regions with diffuse borders), thin fibrous cap (characterized by homogeneous, signal-rich regions), and calcification (characterized by well-delineated, signal-poor regions with sharp borders) in atherosclerotic plaques (7). Plaque rupture is defined as a disruption of thin fibrous cap with a clear cavity formed inside the plaque (8). The lesions with plaque rupture often have macrophages (defined by signal-rich, distinct or confluent punctuate regions with shadowing), vasa vasorum (defined by signal-poor, well-delineated voids within plaque), cholesterol crystals (defined as thin, linear regions of high signal intensity within the lipid plaque), and healed plaques (defined as plaques with 1 or more layers with different optical density) (9, 10). Plaque erosion is identified by the presence of attached thrombus overlying an intact (i.e. absence of fibrous cap disruption) plaque without superficial lipid or calcification (11). The absence of endothelial cells is a key pathological criterion for erosion, however the resolution of current OCT cannot detect individual endothelial cells. Since the OCT metrics of plaque erosion are different from the pathological definition, the term “OCT-derived erosion” is used instead of erosion.

TABLE 1 | Diagnostic criteria for plaque rupture, erosion, and calcified nodules.

	IVUS	OCT	NIRS
Plaque rupture	Fibrous cap disruption Intra-plaque cavity Attenuated plaque	Fibrous cap disruption Intra-plaque cavity Large lipid plaque Macrophages Vasa vasorum Cholesterol crystals Healed plaque	High maxLCBI 4mm (>400)
Plaque erosion		Intact fibrous cap Fibrotic plaque	Low maxLCBI 4mm (<400)
Calcified nodule	Convex calcium Large calcium sheet	Convex calcium Large calcium sheet	Moderate maxLCBI 4mm

IVUS, intravascular ultrasound; LCBI, lipid core burden index; NIRS, near-infrared spectroscopy; OCT, optical coherence tomography.

Calcified nodule is defined by fibrous cap disruption detected over a calcified plaque characterized by protruding calcification (11). Most of calcified nodule have superficially located large calcification. In ACS culprit lesions, a large amount of thrombus may cause a strong attenuation of the near-infrared light and interfere with accurate OCT assessment of plaque morphology.

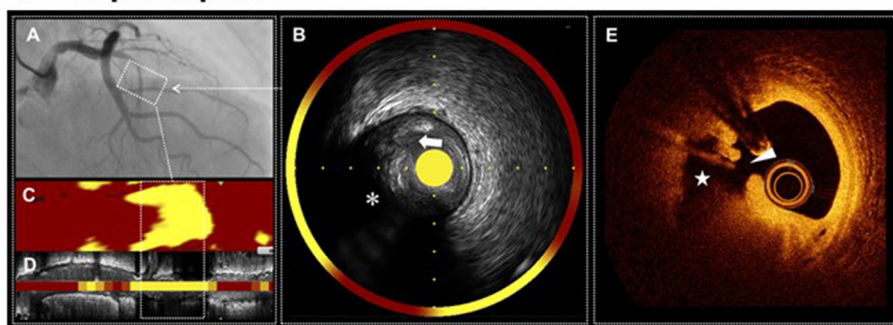
NIRS

NIRS can identify lipid composition by analyzing the near-infrared absorption properties of coronary plaques. NIRS provides a chemogram of the coronary artery wall, which enables the detection of lipid core and specific quantification of lipid accumulation measured as the lipid core burden index (LCBI) and maximal LCBI over any 4 mm segment (maxLCBI4mm). Unlike IVUS and OCT, NIRS can accurately measure lipid component even in the presence of thrombi. NIRS is currently available as a combination catheter with IVUS. NIRS can compensate for the lack of IVUS ability to detect plaque erosion. Plaque erosion has a significantly lower maxLCBI4mm than plaque rupture and calcified nodule (12, 13). The optimal cutoff value for maxLCBI4mm to differentiate between plaque erosion and other plaque types is ~ 400 (12). By assessing plaque cavity, convex calcium, and maxLCBI4mm, NIRS-IVUS can accurately identify plaque rupture (sensitivity = 97% and specificity = 96%), plaque erosion (sensitivity = 93% and specificity = 99%), and calcified nodule (sensitivity = 100% and specificity = 99%) (13).

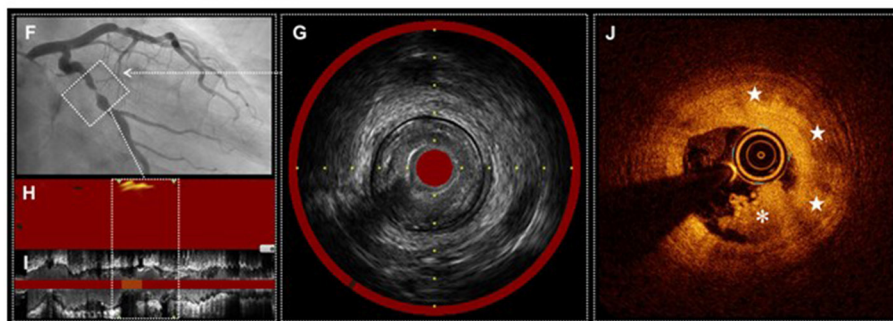
MULTIMODALITY IMAGING

Information obtained from multiple imaging techniques can complement each other. In fact, in addition to morphological evaluation, plaque tissue characterization is useful for differentiating plaque rupture, plaque erosion, and calcified

I. Plaque rupture



II. Plaque erosion



III. Calcified nodule

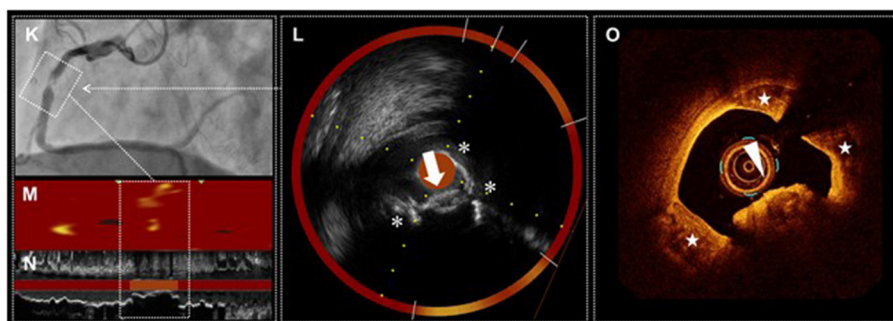


FIGURE 1 | Multimodality imaging of plaque rupture, plaque erosion, and calcified nodule. Plaque rupture (I) Angiogram shows occlusion of proximal LAD, the culprit lesion of STEMI (A). IVUS demonstrates ulceration (arrow) with a recess on the surface of attenuated plaque (asterisk) (B,D). NIRS identifies a large lipid content (maxLCBI4mm = 920) (B–D). OCT reveals plaque rupture characterized by a fibrous cap disruption (arrowhead) and a cavity (star) formation inside the plaque (E). Plaque erosion (II) Angiogram shows severe stenosis in mid LCX, the culprit lesion of STEMI (F). IVUS demonstrates the absence of plaque ulceration (G,I). NIRS identifies a small lipid content (maxLCBI4mm = 129) (G–I). OCT reveals plaque erosion characterized by the presence of attached thrombus (asterisk) overlying an intact fibrotic plaque (stars) (J). Calcified nodule (III) Angiogram shows severe stenosis and intraluminal filling defect in mid RCA, the culprit lesion of non-STEMI (K). IVUS demonstrates a convex calcium with irregular surface (arrow) and large superficial calcium (asterisks) (L,N). NIRS identifies a moderate lipid content (maxLCBI4mm = 208) (L–N). OCT reveals calcified nodule characterized by a protruding calcium with thrombi (arrowhead) and large superficial calcium (stars) (O). IVUS, intravascular ultrasound; LAD, left anterior descending artery; LCBI, lipid core burden index; LCX, left circumflex artery; NIRS, near-infrared spectroscopy; OCT, optical coherence tomography; RCA, right coronary artery; STEMI, ST-segment elevation myocardial infarction.

nodule (Table 1). Plaque rupture is identified by fibrous cap disruption and intra-plaque cavity in IVUS/OCT, attenuated plaque in IVUS, large lipid plaque in OCT, and high maxLCBI4mm (>400) in NIRS (Figure 1-I). Plaque erosion is identified by intact fibrous cap and fibrotic plaque in OCT, and low maxLCBI4mm (<400) in NIRS (Figure 1-II). Calcified nodule is identified by convex calcium and large

calcium sheet in IVUS/OCT, and intermediate maxLCBI4mm in NIRS (Figure 1-III).

IMPACT ON TREATMENT STRATEGY

Information from multiple imaging techniques influence percutaneous coronary intervention (PCI) strategies and risk

stratification in ACS. Plaque rupture is at high risk of slow flow or no-reflow, distal embolization, and microvascular obstruction associated with PCI (14–16). This is because the lesions with plaque rupture are rich in thrombi and lipid cores that can be embolic sources. A prospective randomized controlled trial using IVUS showed that the use of distal protection device was effective in preventing slow flow during PCI for attenuated plaques (17). Plaque erosion has a better prognosis after PCI compared with plaque rupture (18, 19). Non-stent strategy may be an option for plaque erosion if sufficient lumen is obtained by thrombus aspiration alone. A prospective observational OCT study demonstrated that a majority (92.5%) of patients with ACS caused by plaque erosion managed with dual antiplatelet therapy without stenting remained free of major adverse cardiovascular event during 1-year follow-up period (20). Calcified nodule is associated with stent underexpansion that is a well-known predictor of poor clinical outcome. An OCT-guided PCI registry disclosed that the minimum stent area at post-PCI was significantly smaller in calcified nodule than in plaque rupture and plaque erosion, with half of calcified nodule having a stent expansion index (calculated by minimum stent area / reference lumen area \times 100) of $<80\%$ (21). Further research is needed to evaluate the effectiveness of more aggressive procedures such as rotational atherectomy, excimer laser coronary angioplasty, and shockwave intravascular lithotripsy for calcified nodules.

LIMITATIONS

Each intravascular imaging technique has its inherent limitations. IVUS has a coarse-resolution that is insufficient to detect ruptured thin fibrous caps and small ulcers on plaque surface. OCT has a small field of view and shallow imaging depth that often preclude assessment of the plaque burden and remodeling pattern. NIRS is unable to identify fibrous caps, in addition to its lack of morphological evaluation ability.

REFERENCES

1. Virmani R, Burke AP, Farb A, Kolodgie FD. Pathology of the vulnerable plaque. *J Am Coll Cardiol.* (2006) 47:C13–8. doi: 10.1016/j.jacc.2005.10.065
2. Johnson TW, Räber L, di Mario C, Bourantas C, Jia H, Mattesini A, et al. Clinical use of intracoronary imaging. Part 2: acute coronary syndromes, ambiguous coronary angiography findings, and guiding interventional decision-making: an expert consensus document of the European Association of Percutaneous Cardiovascular Interventions. *Eur Heart J.* (2019) 40:2566–84. doi: 10.1093/eurheartj/ehz332
3. Mintz GS, Nissen SE, Anderson WD, Bailey SR, Erbel R, Fitzgerald PJ, et al. American college of cardiology clinical expert consensus document on standards for acquisition, measurement and reporting of Intravascular Ultrasound Studies (IVUS). A report of the American College of Cardiology Task Force on Clinical Expert Consensus Documents. *J Am Coll Cardiol.* (2001) 37:1478–92. doi: 10.1016/s0735-1097(01)01175-5
4. Saito Y, Kobayashi Y, Fujii K, Sonoda S, Tsujita K, Hibi K, et al. Clinical expert consensus document on standards for measurements and assessment of intravascular ultrasound from the Japanese Association of Cardiovascular Intervention and Therapeutics. *Cardiovasc Interv Ther.* (2020) 35:1–12. doi: 10.1007/s12928-019-00625-6

FUTURE PERSPECTIVES

To overcome the limitations of each imaging technique, new efforts have been developed for data fusion methodologies and designs for hybrid dual-probe catheters. Combined IVUS-OCT imaging provides a fusional image of OCT with a high resolution for the plaque surface and IVUS with a large imaging depth (22). Combined IVUS-OCT imaging enables a comprehensive depiction of coronary atherosclerotic plaque. Combined NIRS-OCT imaging allows the detection of lipid core by spectroscopy and structural features, including cap thickness, by OCT (23). Combined NIRS-OCT imaging will facilitate the identification of thin-capped fibroatheroma, which is recognized as a precursor to plaque rupture.

CONCLUSION

At this time, there is no single imaging technique that is perfect for evaluating atherosclerosis. The combination of multiple imaging techniques provides a lot of information about the morphology and composition of atherosclerosis. Detailed coronary evaluation with multiple imaging techniques allows a better understanding of the pathology of ACS and guides lesion-specific treatment.

AUTHOR CONTRIBUTIONS

TK wrote the manuscript. KT, YI, and YS collected images of IVUS, OCT, and NIRS. ST, T-PT, YC, and D-WP reviewed and revised the manuscript. All authors approved the final manuscript.

FUNDING

This work was partially supported by JSPS KAKENHI Grant Number JP19K12846.

5. Wu X, Mintz GS, Xu K, Lansky AJ, Witzensbichler B, Guagliumi G, et al. The relationship between attenuated plaque identified by intravascular ultrasound and no-reflow after stenting in acute myocardial infarction: the HORIZONS-AMI (Harmonizing Outcomes With Revascularization and Stents in Acute Myocardial Infarction) trial. *JACC Cardiovasc Interv.* (2011) 4:495–502. doi: 10.1016/j.jcin.2010.12.012
6. Lee JB, Mintz GS, Lissauskas JB, Biro SG, Pu J, Sum ST, et al. Histopathologic validation of the intravascular ultrasound diagnosis of calcified coronary artery nodules. *Am J Cardiol.* (2011) 108:1547–51. doi: 10.1016/j.amjcard.2011.07.014
7. Fujii K, Kubo T, Otake H, Nakazawa G, Sonoda S, Hibi K, et al. Expert consensus statement for quantitative measurement and morphological assessment of optical coherence tomography. *Cardiovasc Interv Ther.* (2020) 35:13–8. doi: 10.1007/s12928-019-00626-5
8. Kubo T, Imanishi T, Takarada S, Kuroi A, Ueno S, Yamano T, et al. Assessment of culprit lesion morphology in acute myocardial infarction: ability of optical coherence tomography compared with intravascular ultrasound and coronary angiography. *J Am Coll Cardiol.* (2007) 50:933–9. doi: 10.1016/j.jacc.2007.04.082
9. Tearney GJ, Regar E, Akasaka T, Adriaenssens T, Barlis P, Bezerra HG, et al. Consensus standards for acquisition, measurement, and reporting

- of intravascular optical coherence tomography studies: a report from the international working group for intravascular optical coherence tomography standardization and validation. *J Am Coll Cardiol.* (2012) 59:1058–72. doi: 10.1016/j.jacc.2011.09.079
10. Kubo T, Tanaka A, Ino Y, Kitabata H, Shiono Y, Akasaka T. Assessment of coronary atherosclerosis using optical coherence tomography. *J Atheroscler Thromb.* (2014) 21:895–903. doi: 10.5551/jat.25452
 11. Jia H, Abtahian F, Aguirre AD, Lee S, Chia S, Lowe H, et al. *In vivo* diagnosis of plaque erosion and calcified nodule in patients with acute coronary syndrome by intravascular optical coherence tomography. *J Am Coll Cardiol.* (2013) 62:1748–58. doi: 10.1016/j.jacc.2013.05.071
 12. Madder RD, Goldstein JA, Madden SP, Puri R, Wolski K, Hendricks M, et al. Detection by near-infrared spectroscopy of large lipid core plaques at culprit sites in patients with acute ST-segment elevation myocardial infarction. *JACC Cardiovasc Interv.* (2013) 6:838–46. doi: 10.1016/j.jcin.2013.04.012
 13. Terada K, Kubo T, Kameyama T, Matsuo Y, Ino Y, Emori H, et al. NIRS-IVUS for differentiating coronary plaque rupture, erosion, and calcified nodule in acute myocardial infarction. *JACC Cardiovasc Imaging.* (2021) 14:1440–50. doi: 10.1016/j.jcmg.2020.08.030
 14. Shiono Y, Kubo T, Tanaka A, Tanimoto T, Ota S, Ino Y, et al. Impact of attenuated plaque as detected by intravascular ultrasound on the occurrence of microvascular obstruction after percutaneous coronary intervention in patients with ST-segment elevation myocardial infarction. *JACC Cardiovasc Interv.* (2013) 6:847–53. doi: 10.1016/j.jcin.2013.01.142
 15. Tanaka A, Imanishi T, Kitabata H, Kubo T, Takarada S, Tanimoto T, et al. Lipid-rich plaque and myocardial perfusion after successful stenting in patients with non-ST-segment elevation acute coronary syndrome: an optical coherence tomography study. *Eur Heart J.* (2009) 30:1348–55. doi: 10.1093/eurheartj/ehp122
 16. Terada K, Kubo T, Madder RD, Ino Y, Takahata M, Shimamura K, et al. Near-infrared spectroscopy to predict microvascular obstruction after primary percutaneous coronary intervention. *EuroIntervention.* (2021) 17:e999–e1006. doi: 10.4244/EIJ-D-20-01421
 17. Hibi K, Kozuma K, Sonoda S, Endo T, Tanaka H, Kyono H, et al. A Randomized study of distal filter protection versus conventional treatment during percutaneous coronary intervention in patients with attenuated plaque identified by intravascular ultrasound. *JACC Cardiovasc Interv.* (2018) 11:1545–55. doi: 10.1016/j.jcin.2018.03.021
 18. Niccoli G, Montone RA, Di Vito L, Gramegna M, Refaat H, Scalone G, et al. Plaque rupture and intact fibrous cap assessed by optical coherence tomography portend different outcomes in patients with acute coronary syndrome. *Eur Heart J.* (2015) 36:1377–84. doi: 10.1093/eurheartj/ehv029
 19. Yonetsu T, Lee T, Murai T, Suzuki M, Matsumura A, Hashimoto Y, et al. Plaque morphologies and the clinical prognosis of acute coronary syndrome caused by lesions with intact fibrous cap diagnosed by optical coherence tomography. *Int J Cardiol.* (2016) 203:766–74. doi: 10.1016/j.ijcard.2015.11.030
 20. Xing L, Yamamoto E, Sugiyama T, Jia H, Ma L, Hu S, et al. EROSION Study (effective anti-thrombotic therapy without stenting: intravascular optical coherence tomography-based management in plaque erosion): a 1-year follow-up report. *Circ Cardiovasc Interv.* (2017) 10:e005860. doi: 10.1161/CIRCINTERVENTIONS.117.005860
 21. Khalifa AKM, Kubo T, Ino Y, Terada K, Emori H, Higashioka D, et al. Optical coherence tomography comparison of percutaneous coronary intervention among plaque rupture, erosion, and calcified nodule in acute myocardial infarction. *Circ J.* (2020) 84:911–6. doi: 10.1253/circj.CJ-20-0014
 22. Ono M, Kawashima H, Hara H, Gao C, Wang R, Kogame N, et al. Advances in IVUS/OCT and future clinical perspective of novel hybrid catheter system in coronary imaging. *Front Cardiovasc Med.* (2020) 7:119. doi: 10.3389/fcvm.2020.00119
 23. Bourantas CV, Jaffer FA, Gijzen FJ, van Soest G, Madden SP, Courtney BK, et al. Hybrid intravascular imaging: recent advances, technical considerations, and current applications in the study of plaque pathophysiology. *Eur Heart J.* (2017) 38:400–12. doi: 10.1093/eurheartj/ehw097

Conflict of Interest: The authors declare that the research was conducted in the absence of any commercial or financial relationships that could be construed as a potential conflict of interest.

Publisher's Note: All claims expressed in this article are solely those of the authors and do not necessarily represent those of their affiliated organizations, or those of the publisher, the editors and the reviewers. Any product that may be evaluated in this article, or claim that may be made by its manufacturer, is not guaranteed or endorsed by the publisher.

Copyright © 2022 Kubo, Terada, Ino, Shiono, Tu, Tsao, Chen and Park. This is an open-access article distributed under the terms of the Creative Commons Attribution License (CC BY). The use, distribution or reproduction in other forums is permitted, provided the original author(s) and the copyright owner(s) are credited and that the original publication in this journal is cited, in accordance with accepted academic practice. No use, distribution or reproduction is permitted which does not comply with these terms.



Comparison of Myocardial Layer-Specific Strain and Global Myocardial Work Efficiency During Treadmill Exercise Stress in Detecting Significant Coronary Artery Disease

Jingru Lin¹, Lijian Gao², Jia He³, Mengyi Liu¹, Yuqi Cai¹, Lili Niu¹, Ying Zhao¹, Xiaoni Li¹, Jiangtao Wang⁴, Weichun Wu^{1,5*}, Zhenhui Zhu^{1*} and Hao Wang^{1*}

OPEN ACCESS

Edited by:

Minjie Lu,
Chinese Academy of Medical
Sciences and Peking Union Medical
College, China

Reviewed by:

Stefano Coiro,
Hospital of Santa Maria della
Misericordia in Perugia, Italy
Katarzyna Mizia-Stec,
Medical University of Silesia, Poland

*Correspondence:

Weichun Wu
achunductor@163.com
Zhenhui Zhu
dr.zhu@139.com
Hao Wang
hal6112@163.com

Specialty section:

This article was submitted to
Cardiovascular Imaging,
a section of the journal
Frontiers in Cardiovascular Medicine

Received: 30 September 2021

Accepted: 13 December 2021

Published: 17 January 2022

Citation:

Lin J, Gao L, He J, Liu M, Cai Y, Niu L,
Zhao Y, Li X, Wang J, Wu W, Zhu Z
and Wang H (2022) Comparison of
Myocardial Layer-Specific Strain and
Global Myocardial Work Efficiency
During Treadmill Exercise Stress in
Detecting Significant Coronary Artery
Disease.
Front. Cardiovasc. Med. 8:786943.
doi: 10.3389/fcvm.2021.786943

¹ Department of Echocardiography, National Center for Cardiovascular Diseases, Fuwai Hospital, Chinese Academy of Medical Sciences and Peking Union Medical College, Beijing, China, ² Department of Cardiology, National Center for Cardiovascular Diseases, Fuwai Hospital, Chinese Academy of Medical Sciences and Peking Union Medical College, Beijing, China, ³ Cardiac Arrhythmia Center, National Center for Cardiovascular Diseases, Fuwai Hospital, Chinese Academy of Medical Sciences and Peking Union Medical College, Beijing, China, ⁴ General Electric Healthcare, Beijing, China, ⁵ Key Laboratory of Cardiovascular Imaging (Cultivation), Chinese Academy of Medical Sciences, Beijing, China

Background: Myocardial layer-specific strain can identify myocardial ischemia. Global myocardial work efficiency (GWE) based on non-invasive left ventricular (LV) pressure-strain loops is a novel parameter to determine LV function considering afterload. The study aimed to compare the diagnostic value of GWE and myocardial layer-specific strain during treadmill exercise stress testing to detect significant coronary artery disease (CAD) with normal baseline wall motion.

Methods: Eighty-nine patients who referred for coronary angiography due to suspected of CAD were included. Forty patients with severe coronary artery stenosis were diagnosed with significant CAD, and 49 were defined as non-significant CAD. Stress echocardiography was performed 24 h before angiography. Layer-specific longitudinal strains were assessed from the endocardium, mid-myocardium, and epicardium by 2D speckle-tracking echocardiography. Binary logistic regression analyses were performed to evaluate the association between significant CAD and echocardiographic parameters. A receiver operating characteristic curve was used to assess the capability of layer-specific strain and GWE to diagnose significant CAD.

Results: Patients with significant CAD had the worse function in all three myocardial layers at peak exercise compared with those with non-significant CAD when assessed with global longitudinal strain (GLS). At the peak exercise and recovery periods, GWE was lower in patients with significant CAD than in patients with non-significant CAD. In multivariable binary logistic regression analysis, peak endocardial GLS (OR: 1.35, $p = 0.006$) and peak GWE (OR: 0.76, $p = 0.001$) were associated with significant CAD. Receiver operating characteristic curves showed peak GWE to be superior to mid-myocardial, epicardial, and endocardial GLS in identifying significant CAD. Further,

adding peak GWE to endocardial GLS could improve diagnostic capabilities.

Conclusions: Both GWE and endocardial GLS contribute to improving the diagnostic performance of exercise stress echocardiography. Furthermore, adding peak GWE to peak endocardial GLS provides incremental diagnostic value during a non-invasive screening of significant CAD before radioactive or invasive examinations.

Keywords: myocardial work efficiency, layer-specific strain, speckle-tracking echocardiography, treadmill exercise stress, coronary artery disease

INTRODUCTION

Coronary artery disease (CAD) is one of the leading global causes of mortality and morbidity. Concerning the diagnostics of CAD, coronary angiography (CAG), which despite being considered the gold standard, only confirmed significant CAD in 38% of suspected patients (1). Stress echocardiography, which is recommended as a first-line diagnostic test in patients with suspected of CAD, showed a limited specificity and sensitivity due to lacking quantitative and objective methods (2). Non-invasive, quantitative, and objective imaging techniques are necessary for an optimal decision on diagnosis and therapy in patients suspected of CAD without known heart disease to improve clinical outcomes and enhance the diagnostic yield of cardiac catheterization.

The newly developed and explored (3–5) quantitatively objective method of layer-specific strain evaluation could increase the diagnostic accuracy for CAD (5) by evaluating the endocardial myocardium's longitudinal function, which was more susceptible to ischemic injury.

However, as strain is load-dependent, increasing the afterload may underestimate the left ventricular (LV) function; therefore, myocardial work (MW), which combines strain and non-invasive LV pressure, could overcome the limitation. Global myocardial work efficiency (GWE) is one of the major MW parameters and is derived from the percentage ratio of constructive work to the sum of constructive work and wasted work. Recently, significantly lower GWE values were reported in patients with CAD, heart failure, hypertension with left ventricle hypertrophy, and COVID-19 (6–10), and the prognostic value of GWE was found to predict the long-term outcomes of patients after ST-segment elevation myocardial infarction (11) or patients after cardiac resynchronization therapy (12).

Due to the limited data available, this study aims to compare the diagnostic value of GWE with myocardial layer-specific global longitudinal strain during exercise stress to detect significant CAD with normal baseline wall motion.

Abbreviations: CAD, coronary artery disease; 2D, two-dimensional; MW, myocardial work; LV, left ventricular; GWE, global myocardial work efficiency; GLS, global longitudinal strain; CAG, coronary angiography; ECG, electrocardiography; WMSI, wall motion score index; AFI, automated function imaging; AUC, area under the curve.

MATERIALS AND METHODS

Study Population

The study was conducted in a single tertiary coronary care center with 89 patients without known ischemic heart disease who were referred with angina pectoris and had plans to undergo treadmill exercise stress testing and CAG. Patients with the following criteria were excluded: age < 18 years; baseline LV ejection fraction <50%; abnormal baseline wall motion; previous myocardial infarction; prior coronary artery bypass grafting or coronary interventional therapy; left bundle branch block; atrial fibrillation; sustained severe arrhythmia; severe valvular dysfunction; inability to undergo exercise testing; absence of any of apical four-chamber, three-chamber, and two-chamber views; and inadequate image quality. All patients underwent two-dimensional (2D) echocardiography (speckle-tracking echocardiography and MW analysis), and a treadmill exercise stress test followed by CAG.

Written informed consent was given by all study participants or their legal representatives. The study complied with the Declaration of Helsinki and was approved by the Ethics Committees of Fuwai Hospital (no. 2018-1121).

Conventional Echocardiography

Comprehensive conventional echocardiography was performed (13) using a commercially available ultrasound system (Vivid E9 or Vivid E95, GE Healthcare, Horton, Norway) with a 3.5-MHz transducer. Images were analyzed offline using dedicated software (EchoPAC 203, GE Healthcare, Horton, Norway). LV dimensions, LV septal thickness, and LV posterior wall thickness were measured from the parasternal long-axis view. LV mass was calculated as $\{0.8 \times 1.04 \times [(LV \text{ end-diastolic diameter} + LV \text{ end-diastolic posterior wall thickness} + \text{end-diastolic septal wall thickness})^3 - (LV \text{ end-diastolic diameter})^3] + 0.6\}$. LV mass was then indexed for body surface area to generate the LV mass index. LV ejection fraction was measured using Simpson's biplane method from apical four- and two-chamber views. Early trans-mitral velocity (E wave) and late trans-mitral velocity (A wave) were measured by pulsed-wave Doppler from the apical four-chamber view with the sample volume positioned at the tip of the mitral leaflets. Mitral inflow E/A ratio was calculated as E wave divided by A wave.

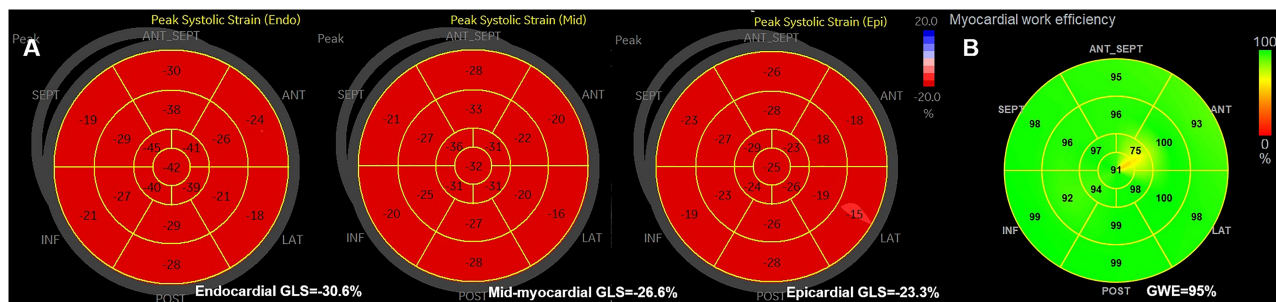


FIGURE 1 | (A) The example of bull's eyes of the global myocardial longitudinal layer-specific strain. **(B)** The example of global myocardial work efficiency. GLS, global longitudinal strain; GWE, global myocardial work efficiency.

Treadmill Exercise Stress Echocardiography

The treadmill exercise stress test was conducted utilizing the standard Bruce protocol (14) whereby the patient's heart rate, blood pressure, and 12-lead electrocardiography (ECG) were recorded. Cine loops (2D) from the four-, two-, and three-chamber apical views were taken during the rest (before exercise), peak exercise (<1 min after exercise), and recovery (3 min after exercise) periods. Criteria for terminating the test were achieving a target heart rate of 85% of the age-predicted maximum, development of wall motion abnormality, development of intolerant symptoms, severe ischemic electrocardiographic changes, severe hypertension (systolic blood pressure >220 mmHg or diastolic blood pressure >120 mmHg), symptomatic hypotension, or significant arrhythmia (14). The ECGs were categorized as either normal or abnormal by two blinded investigators. A positive exercise ECG was defined as ST-segment horizontal or down-sloping depression ≥ 1 mm with duration >2 min or ST-segment elevation ≥ 1 mm with duration >1 min in the leads dominated by R waves. The regional myocardial functional abnormality was assessed based on the observed wall thickening and endocardial motion of the myocardial segment in exercise stress echocardiography (15). A 17-segment model was used to assess wall motion from the apical four-, two-, and three-chamber views during the rest, peak exertion, and recovery periods, and a semiquantitative scoring system was used to analyze each segment (1 = normal wall motion, 2 = hypokinesia, 3 = akinesia, and 4 = dyskinesia) (15, 16). The wall motion score index (WMSI) was calculated for each patient as the average of the analyzed segmental values, and patients with wall motion abnormality (WMSI > 1) during exercise were considered as positive stress echocardiogram.

Speckle-Tracking Echocardiography and Myocardial Layer-Specific Strain

From each of the three apical views at rest and during exercise, the cardiac loop with the best representation of the LV wall was identified and analyzed in the commercially available

software (EchoPAC version 203, GE Healthcare); initially with automated function imaging (AFI) and subsequently with the 2D strain software. AFI identified and tracked the endocardium automatically to generate the LV global longitudinal strain (GLS), and the regional speckle area of interest was adjusted manually where the tracking was poor. For 2D strain analysis, the endocardial borders were manually delineated by the operator and then traced by the software in the end-systolic frame for the analyses of longitudinal endocardial, mid-myocardial, and epicardial strains (Figure 1). Images with low tracking quality in more than two segments in a single view were excluded from further analysis. The Δ -value of the LV myocardial layer-specific measurements was calculated as the difference between the values at peak exercise stress and at rest.

Global LV Myocardial Work Efficiency Analysis

Global myocardial work efficiency was calculated from a combination of the 2D LV GLS (based on AFI) and a non-invasively estimated LV pressure, using the commercially obtained software (EchoPAC version 203, GE Healthcare) (17). Brachial blood pressure was measured immediately after the echocardiography test, as a surrogate of non-invasive peak LV pressure. A non-invasive pressure-strain loop was constructed from the software adjusted to the timing of valvular events, mitral valve closure, aortic valve opening, aortic valve closure, and mitral valve opening (18). Myocardial work index corresponds to the area of the pressure-strain loop during the cardiac cycle. Myocardial constructive work was defined as work performed by the myocardium during segmental shortening in systole or during lengthening in isovolumic relaxation. Myocardial wasted work was defined as work performed by the myocardium during segmental lengthening in systole or during segmental shortening against a closed aortic valve in isovolumic relaxation. GWE was calculated as the sum of constructive work in all LV segments, divided by the sum of constructive and wasted work in all LV segments, expressed as a percentage (Figure 1).

TABLE 1 | Clinical characteristics and conventional echocardiographic variables of patients.

Variable	Non-Significant CAD (n = 49)	Significant CAD (n = 40)	p-value
Age, years	56 ± 8	58 ± 8	0.202
Male, n (%)	30 (61)	31 (78)	0.100
Body surface area, m ²	1.79 ± 0.17	1.87 ± 0.18	0.033
Body mass index, kg/m ²	25.3 ± 3.1	27.4 ± 3.1	0.002
Medical history, n (%)			
Hypertension	23 (47)	27 (68)	0.052
Diabetes mellitus	14 (29)	14 (35)	0.516
Dyslipidemia	40 (82)	39 (98)	0.043
Medication, n (%)			
Platelet inhibitors	34 (69)	37 (93)	0.007
Beta-Blockers	25 (51)	33 (83)	0.002
Calcium channel blockers	22 (45)	15 (38)	0.481
ACE inhibitors or ARBs	11 (22)	20 (50)	0.007
Statins	42 (86)	38 (95)	0.275
Coronary angiography, n (%)			
One-Vessel disease	–	27 (68)	–
Two-Vessel disease	–	9 (23)	–
Three-Vessel disease	–	4 (10)	–
Left main coronary artery	–	2 (5)	–
Left anterior descending artery	–	29 (73)	–
Left circumflex artery	–	10 (25)	–
Right coronary artery	–	16 (40)	–
Coronary dominance, n (%)			
Right coronary dominance	45 (92)	36 (90)	>0.999
Left coronary dominance	3 (6)	3 (8)	>0.999
Codominance	1 (2)	1 (3)	>0.999
ECG positive, n (%)	15 (31)	7 (18)	0.154
Echocardiographic parameters			
LVDd, mm	47 ± 3	48 ± 5	0.239
LVDs, mm	32 ± 3	31 ± 3	0.325
IVSd, mm	9 ± 1	9 ± 1	0.338
LVPWd, mm	8 ± 1	9 ± 1	0.016
LV mass index, g/m ²	78 ± 16	82 ± 15	0.173
Mitral E, m/s	0.8 ± 0.2	0.8 ± 0.2	0.509
Mitral A, m/s	0.8 ± 0.2	0.8 ± 0.1	0.531
Mitral E/A	1.0 ± 0.3	1.0 ± 0.3	0.683

ACE, angiotensin-converting enzyme; ARB, angiotensin II receptor blocker; CAD, coronary artery disease; ECG, electrocardiography; LV, left ventricular; LVDd, LV end-diastolic diameter; LVDs, LV end-systolic diameter; LVPWd, LV posterior wall thickness in end-diastole; Mitral E, mitral early-diastole velocity; Mitral A, mitral late-diastole velocity; IVSd, interventricular septum thickness in end-diastole.

Data are expressed as mean ± SD or as number (percentage).

Coronary Angiography

The images from CAG were interpreted visually by an experienced cardiologist blinded to patients' echocardiographic data. Significant CAD was defined as ≥70% luminal diameter narrowing in one or more major epicardial vessels or ≥50% in the left main coronary (19).

TABLE 2 | Hemodynamic and echocardiographic parameters at rest and during treadmill exercise stress.

Variable	Non-Significant CAD (n = 49)	Significant CAD (n = 40)	P-Value
Rest			
Heart rate, beats/min	77 ± 15	75 ± 13	0.523
SBP, mm Hg	132 ± 20	131 ± 18	0.914
DBP, mm Hg	78 ± 12	79 ± 12	0.581
LVEF, %	64 ± 5	62 ± 4	0.203
Rest GLS(AFI), %	−19.6 ± 2.3	−19.2 ± 1.8	0.323
Rest endocardial GLS, %	−24.0 ± 3.0	−23.9 ± 2.6	0.867
Rest mid-myocardial GLS, %	−21.0 ± 2.9	−20.9 ± 2.3	0.853
Rest epicardial GLS, %	−18.5 ± 2.8	−18.4 ± 2.1	0.825
Rest GWE, %	95 (93, 96)	94 (92, 96)	0.060
Peak exercise			
Heart rate, beats/min	140 ± 8	138 ± 7	0.161
SBP, mmHg	176 ± 20	171 ± 22	0.268
DBP, mmHg	77 ± 14	77 ± 15	0.966
LVEF, %	67 ± 3	66 ± 4	0.180
Peak WMSI	1.00 (1.00, 1.00)	1.00 (1.00, 1.06)	0.079
Peak GLS(AFI), %	−21.5 ± 2.3	−20.0 ± 1.9	0.001
Peak endocardial GLS, %	−28.8 ± 2.7	−26.0 ± 3.0	<0.001
Peak mid-myocardial GLS, %	−25.0 ± 2.4	−22.8 ± 2.7	<0.001
Peak epicardial GLS, %	−21.8 ± 2.3	−19.9 ± 2.4	<0.001
ΔEndocardial GLS, %	−4.86 ± 3.00	−2.17 ± 3.49	<0.001
ΔMid-myocardial GLS, %	−4.02 ± 2.72	−1.90 ± 3.12	0.001
ΔEpicardial GLS, %	−3.30 ± 2.67	−1.57 ± 2.84	0.004
Peak GWE, %	94 (93, 95)	90 (87, 93)	<0.001
Recovery			
Heart rate, beats/min	84 ± 12	83 ± 10	0.564
SBP, mmHg	155 ± 22	159 ± 26	0.409
DBP, mmHg	69 ± 11	72 ± 16	0.377
LVEF, %	67 ± 5	66 ± 6	0.354
Recovery WMSI	1.00 (1.00, 1.03)	1.00 (1.00, 1.06)	0.702
Recovery GLS(AFI), %	−21.4 ± 2.7	−20.7 ± 2.0	0.195
Recovery endocardial GLS, %	−27.0 ± 3.5	−26.9 ± 2.8	0.855
Recovery mid-myocardial GLS, %	−23.4 ± 3.0	−23.6 ± 2.6	0.841
Recovery epicardial GLS, %	−20.4 ± 2.5	−20.8 ± 2.4	0.562
Recovery GWE, %	95 (94, 96)	93 (91, 95)	0.001

AFI, Automated function imaging; CAD, coronary artery disease; DBP, diastolic blood pressure; EF, ejection fraction; GLS, global longitudinal strain; GWE, global myocardial work efficiency; LV, left ventricular; SBP, systolic blood pressure; WMSI, wall motion score index.

Δ-value, stress value—rest value. Data are expressed as mean ± SD or as median (interquartile range).

Intra- and Interobserver Variability for Myocardial Layer-Specific Strain and GWE

Intra- and interobserver variabilities were determined with 15 randomly selected patients, where the analysis was repeated by the same investigator 2 weeks later and by a second investigator blinded to the initial results of the first investigator, respectively.

Statistical Analysis

Normally distributed continuous variables are presented as mean values \pm standard deviation or as the median value (interquartile range) when not normally distributed. Categorical variables are presented as absolute numbers and percentages. Normal distribution was verified by the Shapiro–Wilk test. Continuous variables were compared using Student's *t*-test or Mann–Whitney *U*-test, as appropriate, whereas categorical variables were compared with the chi-squared test or Fisher's exact test. Correlation between continuous variables was performed using Pearson's or Spearman's correlation coefficient. Univariate binary logistic regression analyses were performed to evaluate the association between the presence of significant CAD and the echocardiographic variables. After excluding variables that showed collinearity (Pearson's or Spearman's correlation coefficient ≥ 0.60 or variance inflation factor > 10), all variables that found to be significant on univariate binary logistic regression were considered for multiple binary regression analysis using the forward selection method. Receiver operating characteristic curve analysis and Youden's index were used to assess the optimal cutoff points for layer-specific strain and GWE in predicting significant CAD. The comparisons of AUCs were performed using the method described by DeLong et al. (20). Intraclass correlation coefficients and coefficients of variation were calculated during the inter- and intraobserver variability tests to evaluate the reproducibility.

Analyses were performed using SPSS, version 25.0 (IBM Corp., Armonk, NJ, USA), MedCalc, version 18.2.1 (MedCalc Software, Ltd., Ostend, Belgium), and GraphPad Prism 8 (GraphPad Software, San Diego, CA, USA). All statistical tests were two-sided, and a $p < 0.05$ was considered statistically significant.

RESULTS

Clinical Characteristics

Of the 89 patients, 40 and 49 patients were diagnosed with significant and non-significant CAD by CAG. The demographic information, angiographic results, and exercise ECG results of both groups are presented in **Table 1**, and hemodynamic data during treadmill exercise testing are shown in **Table 2**. No statistically significant differences were observed (all $p > 0.05$) between the two groups regarding age, gender, heart rate, blood pressure, coronary dominance, and exercise ECG results. Patients with significant CAD showed a larger body surface area and body mass index (both $p < 0.05$) and a higher incidence of dyslipidemia ($p < 0.05$) compared with those in the non-significant CAD group (**Table 1**).

Conventional Echocardiography

No significant differences were observed (all $p > 0.05$) between the two groups for the conventional echocardiographic parameters of LV end-diastolic or end-systolic dimensions, LV septal thickness in end-diastole, LV mass index, mitral early-diastole velocity, mitral late-diastole velocity, and the ratio of mitral early-diastole velocity to late-diastole velocity. LV

posterior wall thickness in end-diastole was significantly larger in the significant CAD group than that of the non-significant CAD group ($p < 0.05$; **Table 1**).

GLS and Myocardial Layer-Specific Strain Analysis

The LV GLS (AFI) had significantly lower absolute values during peak exercise in the significant CAD group ($p = 0.001$) compared with those in the non-significant group, although there were no significant differences observed during the rest or recovery periods (all $p > 0.05$; **Table 2**).

Patients with significant CAD had a significantly worse function than those with non-significant CAD at peak exercise in all three myocardial layers when assessed with GLS (all $p < 0.001$), although the differences between the two groups were not significant at rest or during recovery ($p > 0.05$; **Figure 2**, **Table 2**). The difference (Δ -value) in endocardial, mid-myocardial, and epicardial GLS from rest to peak exercise were, respectively significantly smaller in the significant CAD group than that of patients with non-significant CAD (all $p < 0.01$; **Table 2**).

Global LV Myocardial Work Efficiency Analysis

The GWE value was minimal during peak exercise and increased in the recovery period (**Figure 2**) in both groups. At peak exercise and recovery period, the values of GWE in patients with significant CAD were significantly lower than those of the non-significant CAD group (all $p < 0.01$), although at rest, the values of the two groups had no significant differences ($p > 0.05$; **Table 2**).

Correlation Between GWE and Myocardial Strain at Peak Exercise

Peak GWE showed modest negative correlations with peak endocardial, mid-myocardial, and epicardial GLS ($r = -0.44$, -0.43 , and -0.43 , respectively; all $p < 0.001$) and a good negative correlation with peak GLS using AFI ($r = -0.63$, $p < 0.001$; **Supplementary Figure 1**). Peak endocardial, mid-myocardial, and epicardial GLS ($r = 0.46$, 0.47 , and 0.45 , respectively, all $p < 0.001$) all presented modest positive correlations with peak GLS using AFI (**Supplementary Figure 2**). Peak endocardial GLS showed great correlations with both peak mid-myocardial GLS and peak epicardial GLS ($r = 0.98$, and 0.93 , respectively, both $p < 0.001$).

Binary Logistic Regression Analyses for the Detection of Significant CAD

In univariable binary logistic regression analysis, body surface area, body mass index, dyslipidemia, LV posterior wall thickness in end-diastole, peak endocardial, mid-myocardial, epicardial GLS, peak GLS (AFI), peak GWE, and recovery GWE were significantly associated with significant CAD (**Table 3**).

In multivariable binary logistic regression analysis, peak endocardial GLS (odds ratio: 1.35, $p = 0.006$) and peak GWE (odds ratio: 0.76, $p < 0.001$) were significantly associated with significant CAD (**Table 3**).

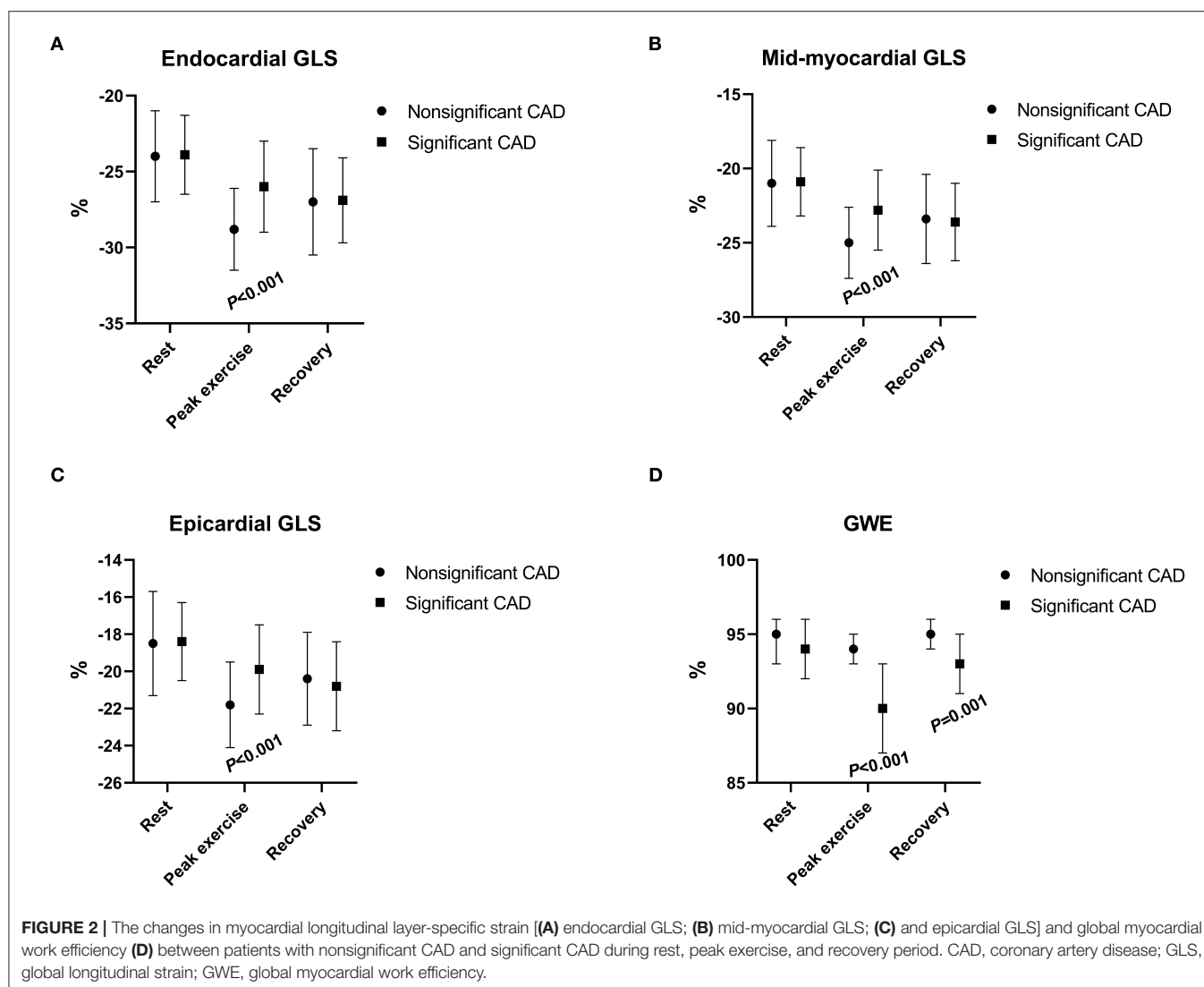


TABLE 3 | Univariate and multivariate binary logistic regression analyses for detection of significant CAD.

Parameters	Univariate binary logistic regression		Multivariate binary logistic regression	
	OR [95% CI]	p-value	OR [95% CI]	p-value
Body surface area, m ²	14.97 [1.19–189.02]	0.036		
Body mass index, kg/m ²	1.24 [1.07–1.44]	0.004		
Dyslipidemia	8.78 [1.06–72.56]	0.044		
LVPWd, mm	1.57 [1.07–2.30]	0.021		
Peak endocardial GLS, %	1.44 [1.19–1.75]	<0.001	1.35 [1.09–1.67]	0.006
Peak mid-myocardial GLS, %	1.44 [1.18–1.78]	0.001		
Peak epicardial GLS, %	1.43 [1.15–1.77]	0.001		
Peak GLS(AFI), %	1.39 [1.13–1.72]	0.002		
Peak GWE, %	0.71 [0.60–0.84]	<0.001	0.76 [0.64–0.90]	0.001
Recovery GWE, %	0.81 [0.68–0.96]	0.013		

CI, confidence interval; OR, odds ratio; for other abbreviations see **Tables 1, 2**.

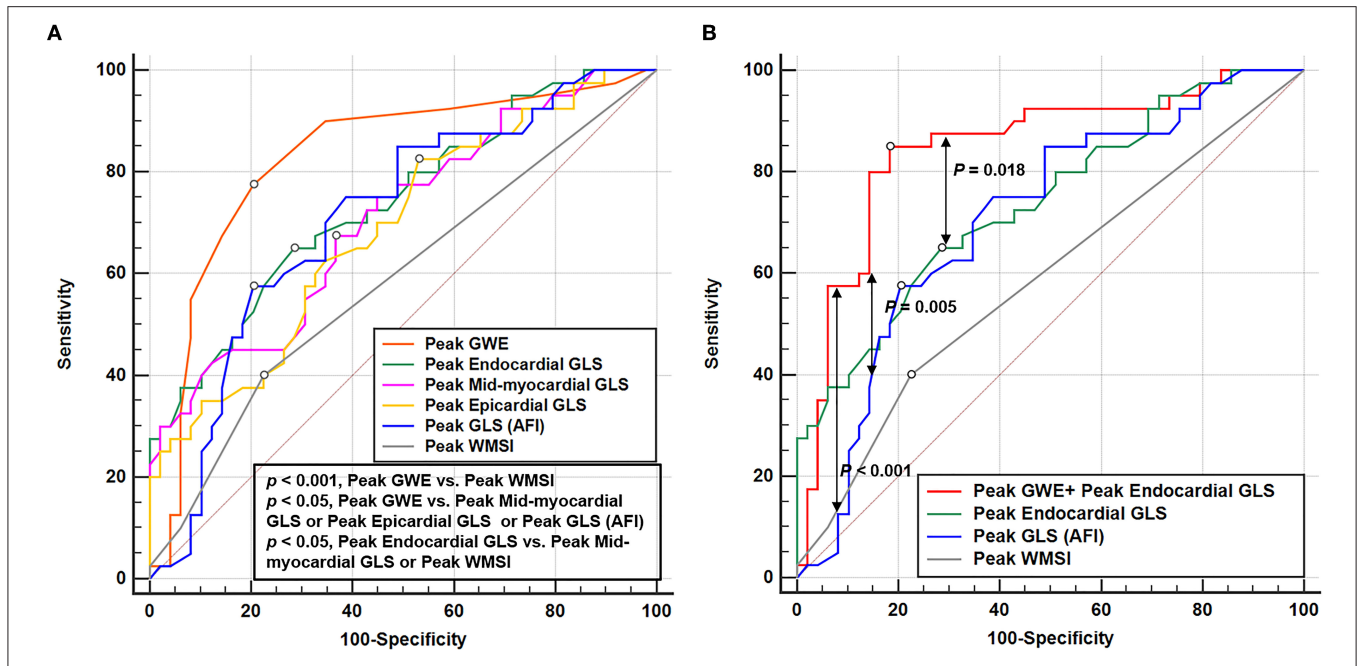


FIGURE 3 | Receiver operating characteristic curves of echocardiographic parameters at peak exercise to detect the significant CAD. **(A)** Receiver operating characteristic curves of GWE, layer-specific strain, GLS (AFI), and WMSI at peak exercise in identifying significant CAD. **(B)** Receiver operating characteristic curve of the parameter combined peak GWE and peak endocardial GLS, peak endocardial GLS, peak GLS (AFI), and peak WMSI in detecting significant CAD. CAD, coronary artery disease; GLS, global longitudinal strain; GWE, global myocardial work efficiency; AFI, automated function imaging; WMSI, wall motion score index.

TABLE 4 | Receiver operating characteristic curve analysis for the detection of significant CAD.

Parameters	AUC	95%CI	p-value	Cutoff value	Sensitivity (%)	Specificity (%)	Youden's index
Peak GWE + Peak endocardial GLS	0.848	0.756–0.915	<0.001	>0.406	85.0	81.6	0.666
Peak GWE, %	0.827	0.733–0.899	<0.001	≤92	77.5	79.6	0.571
Peak endocardial GLS, %	0.739	0.635–0.827	<0.001	>-27.0	65.0	71.4	0.364
Peak mid-myocardial GLS, %	0.708	0.602–0.800	<0.001	>-24.0	67.5	63.3	0.308
Peak epicardial GLS, %	0.688	0.581–0.782	0.001	>-21.8	82.5	46.9	0.294
Peak GLS (AFI), %	0.708	0.603–0.800	<0.001	>-20.0	57.5	79.6	0.371
Peak WMSI	0.587	0.478–0.691	0.080	>1.00	40.0	77.6	0.176
ΔEndocardial GLS, %	0.721	0.616–0.811	<0.001	>-3.6	67.5	71.4	0.389
ΔMid-myocardial GLS, %	0.702	0.596–0.795	<0.001	>-1.5	50.0	85.7	0.357
ΔEpicardial GLS, %	0.684	0.577–0.778	0.001	>-4.4	85.0	49.0	0.340

AUC, area under the curve; CI, confidence interval; Δ-value, stress value—rest value; for other abbreviations see as **Tables 1, 2**.

Receiver Operating Characteristic Curve Analysis for the Detection of Significant CAD

According to receiver operating characteristic curve analysis, the cutoff value for the best possible detection of peak GWE in the significant CAD group was 92%. Peak GWE had the highest area under the curve (AUC) for the detection of significant CAD (AUC, 0.827; $p < 0.001$) that was superior to peak mid-myocardial and epicardial GLS (AUC, 0.708, and 0.688, respectively, both $p < 0.05$; **Figure 3A**, **Table 4**), although it was not statistically better than endocardial GLS (AUC: 0.739, $p > 0.05$). However, the addition of peak GWE to peak

endocardial GLS significantly increased the AUC over that of peak endocardial GLS (AUC: 0.848 vs. 0.739, $p = 0.018$; **Figure 3B**, **Table 4**). The AUCs of the combination of peak GWE and peak endocardial GLS or peak GWE alone were significantly higher than that of peak GLS using AFI (**Figures 3A,B**, **Table 4**). The AUC of peak GLS (AFI) was similar to those of peak myocardial layer-specific GLS (0.708 vs. endocardial, 0.739; mid-myocardial, 0.708, and epicardial, 0.688; all $p > 0.05$; **Figure 3A**, **Table 4**). The AUCs of peak myocardial layer-specific GLS and peak GWE were better than peak WMSI, which represented the conventional exercise stress echocardiography (**Figure 3A**, **Table 4**). The Δ-value of myocardial layer-specific GLS also had

high AUCs to identify significant CAD (endocardial, 0.721; mid-myocardial, 0.702; and epicardial, 0.684; **Table 4**).

Intra- and Interobserver Variabilities for Layer-Specific Strain Parameters and GWE

The intra- and interobserver variabilities for peak myocardial layer-specific GLS and peak GWE, which showed good repeatability and reproducibility, are summarized in **Supplementary Table 1**.

DISCUSSION

This is the first study to compare the ability of myocardial layer-specific strain and GWE in identifying significant CAD in patients with angina pectoris without a known history of CAD. The primary findings were that both myocardial layer-specific GLS and GWE at peak exercise can discriminate significant CAD. At peak exercise, GWE was superior to myocardial layer-specific GLS as a non-invasive measure for the detection of significant CAD. Furthermore, the combination of peak GWE and peak endocardial GLS had incremental diagnostic value for the detection of significant CAD when compared to that of myocardial layer-specific GLS at peak exercise alone.

Myocardial Layer-Specific Strain for the Detection of Significant CAD Compared With GLS Based on AFI or WMSI During Exercise Stress

Previous studies have reported excellent intra- and interobserver reproducibilities of layer-specific strain (21, 22). In addition, studies have also investigated the diagnostic value of layer-specific strain on stress echocardiography in patients suspected of CAD (23–26). Nishi et al. suggested that layer-specific GLS at the early recovery phase after cycle ergometer exercise stress was significantly more impaired in the ischemic territories than in non-ischemic territories (26). However, in our research, the differences in layer-specific strain during the rest or recovery periods between significant and non-significant CAD groups were less pronounced. Only layer-specific strain at peak exercise after treadmill exercise stress testing provided a high value for the non-invasive identification of significant CAD. Despite the statement of the stress period is different, the definition of the early recovery period in the study of Nishi et al. was similar to the definition of peak exercise in our research (from immediate cessation to <3 min after exercise vs. <1 min after treadmill exercise), and the definition of the recovery period in our research was >3 min after treadmill exercise. Therefore, the results are consistent.

The LV heart wall comprises three layers: the oblique endocardial, the circular mid-myocardial, and the oblique epicardial layer. Since the endocardial layer of the myocardium is more susceptible to ischemia than the epicardial layer, and the endocardial-layer fibers are mainly oriented in the longitudinal direction (27, 28), it is likely to expect in patients with CAD that ischemia extends from endocardium to epicardium and endocardial GLS deteriorates before epicardial GLS abnormalities become apparent (29). However, the previous

studies did not demonstrate clear superiority for endocardial-layer strain over other layers on stress echocardiography for the detection of significant CAD (23, 26). Nishi et al. found that the diagnostic ability of the endocardial, mid-myocardial, and epicardial GLS at the early recovery phase on cycle ergometer exercise stress echocardiography (AUC; 0.621, 0.619, and 0.616, respectively), are comparable (26), which was also found by Ejlersen et al. (23). Similarly, in this study, the myocardial layer-specific GLS analysis revealed that all myocardial layers were affected in patients with significant CAD at peak exercise. However, the AUCs for the detection of significant CAD were not statistically different among the three layers at peak exercise although the AUC of endocardial GLS was the highest among all three layers.

In line with previous research (23, 26, 30), myocardial layer-specific GLS was better than the semiquantitative method of WMSI in stress echocardiography to identify significant CAD. Besides, with previous studies demonstrated that GLS added value to exercise stress testing to diagnose various cardiac diseases, including myocardial ischemia (30, 31). We also compared the diagnostic value of layer-specific GLS and GLS (AFI) during exercise stress to identify significant CAD and found that myocardial layer-specific GLS was relative to GLS (AFI). However, no statistical differences were observed in the diagnostic value of the three layer-specific GLS and GLS (AFI) when applied to treadmill exercise stress echocardiography, although the AUC of endocardial GLS was better than that of GLS (AFI), which were consistent with previous studies (23, 25). Therefore, it was confirmed that endocardial GLS at peak exercise was superior to the conventional stress echocardiography and has no significant superiority over GLS (AFI) or other layer-specific strain in identifying myocardial ischemia.

In addition, we also explored the difference in endocardial, mid-myocardial, and epicardial GLS from rest to peak exercise and found that significant CAD can be effectively identified. The diagnostic value of the differences in endocardial, mid-myocardial, and epicardial GLS from rest to peak exercise was comparable to endocardial, mid-myocardial, and epicardial GLS at peak exercise.

Incremental Diagnostic Value of GWE

The myocardial layer-specific GLS had a high diagnostic value for significant CAD, but these parameters were still limited by load dependency. An increase in afterload would lead to a reduction in strain, which may underestimate the true myocardial contractility, especially in the context of stress echocardiography (32). MW can overcome this limitation and reflect the true contractility of the myocardium by establishing the GWE, which combines the global constructive and wasted work of the myocardium, which can better reflect the myocardial changes affected by ischemia.

Recently, various studies have proved the diagnostic and prognostic values of GWE (6–12). However, the comparison of the diagnostic capability of GWE and myocardial layer-specific GLS during peak exercise in identifying significant CAD in patients without a history of CAD has not been explored prior to our study. We observed that the GWE was moderately correlated with the myocardial layer-specific GLS at peak exercise but

stronger with the GLS obtained by AFI, because MW derived from GLS (based on AFI) and brachial artery blood pressure. The peak GWE was superior in the detection of significant CAD when compared to that of the WMSI, GLS (AFI), mid-myocardial, and epicardial GLS at peak. However, the diagnostic capability of peak GWE did not show statistically significant superiority over peak endocardial GLS, although the AUC of peak GWE was higher than that of peak endocardial GLS. The combination of peak GWE and peak endocardial GLS could significantly improve the discrimination ability for significant CAD when compared to endocardial GLS alone. The present research extends the usefulness of peak GWE to patients with CAD with normal LV ejection fraction and baseline wall motion and suggests an incremental diagnostic value of peak GWE over the myocardial layer-specific GLS in patients whose rest echocardiography does not suggest CAD. The MW can only indicate overall-layer myocardial function but could not reflect each layer's MW at present, which can be explored in future studies.

Clinical Implications

In patients with angina pectoris and no history of CAD, conventional echocardiography during exercise stress was not accurate enough to detect significant CAD. The use of GWE or myocardial layer-specific GLS at peak exercise, especially the combination of peak GWE and peak endocardial GLS, provided a better non-invasive screening method to identify significant CAD before radioactive or invasive exams. Peak GWE is particularly important in measurements performed during exercise stress testing, or in patients with inadequate blood pressure control. However, the practical applicability of these new parameters to assist the decision-making process for significant CAD needs to be verified in further studies.

LIMITATIONS

This was a retrospective, single-center study, and prospective validation is needed. Selection bias inherent in any study comparing stress echocardiography with invasive angiography may have occurred in our research since only patients with chest pain who underwent invasive angiography were included. The circumferential and radial strains were not investigated in this study, since the myocardial fibers most vulnerable to ischemia are the longitudinally orientated fibers that are located subendocardial, and longitudinal strain is thought to be the most sensitive parameter to detect CAD (33). Since LV GWE is predicated on the measurement of GLS, it is not a vendor-independent measure and is still influenced by the image quality. Fractional flow reserve measurements were not taken in this study, and therefore, the true hemodynamic relevance of the stenoses is not known. Despite this limitation, the fraction of patients with non-flow limiting stenosis may have been reduced since a high cutoff for significant CAD was used.

CONCLUSION

In patients with angina pectoris and normal baseline wall motion, both peak GWE and peak endocardial GLS are independent predictors of significant CAD that can significantly improve the diagnostic performance of exercise stress echocardiography. Furthermore, adding peak GWE to peak endocardial GLS provides incremental diagnostic value in non-invasive screening for significant CAD before radioactive or invasive examinations.

DATA AVAILABILITY STATEMENT

The raw data supporting the conclusions of this article will be made available by the authors, without undue reservation.

ETHICS STATEMENT

The studies involving human participants were reviewed and approved by Ethics Committees of Fuwai Hospital (No. 2018-1121). The participants or their legal representatives provided their written informed consent to participate in this study.

AUTHOR CONTRIBUTIONS

WW, ZZ, and HW contributed to the conception, design, supervision of the study, and revised the manuscript critically for intellectual content. JL drafted the manuscript. LG, JH, LN, YZ, XL, and JW contributed to the collection and interpretation of data. JL, ML, and YC contributed to statistical analysis. All authors contributed to the article and approved the submitted version.

FUNDING

This study was supported by the Beijing Municipal Science and Technology Commission (Grant No. Z171100001017213) and Construction Research Project of Key Laboratory (Cultivation) of Chinese Academy of Medical Sciences (Grant No. 2019PT310025).

ACKNOWLEDGMENTS

We sincerely thank the colleagues of the Department of Echocardiography, Cardiology, and the Functional Testing Center of Fuwai Hospital for their effort and assistance. We would like to thank Editage (www.editage.cn) for English language editing.

SUPPLEMENTARY MATERIAL

The Supplementary Material for this article can be found online at: <https://www.frontiersin.org/articles/10.3389/fcvm.2021.786943/full#supplementary-material>

Supplementary Figure 1 | Correlation between GWE and layer-specific strain, GLS (AFI) at peak exercise. **(A)** Correlation between peak GWE and peak endocardial GLS. **(B)** Correlation between peak GWE and peak mid-myocardial

GLS. **(C)** Correlation between peak GWE and peak epicardial GLS. **(D)** Correlation between peak GWE and peak GLS (AFI). GLS, global longitudinal strain; GWE, global myocardial work efficiency; AFI, automated function imaging.

Supplementary Figure 2 | Correlation between layer-specific strain and GLS (AFI) at peak exercise. **(A)** Correlation between peak endocardial GLS and peak GLS (AFI). **(B)** Correlation between peak mid-myocardial GLS and peak GLS (AFI).

(C) Correlation between peak epicardial GLS and peak GLS (AFI). GLS, global longitudinal strain; AFI, automated function imaging.

Supplementary Table 1 | Intra- and inter-observer variabilities for peak layer-specific strain parameters and peak GWE. ICC, Intraclass correlation coefficient; CI, confidence interval; CV, coefficient of variation; GLS, global longitudinal strain; GWE, global myocardial work efficiency.

REFERENCES

- Patel MR, Peterson ED, Dai D, Brennan JM, Redberg RF, Anderson HV, et al. Low diagnostic yield of elective coronary angiography. *N Engl J Med*. (2010) 362:886–95. doi: 10.1056/NEJMoa0907272
- Task Force M, Montalescot G, Sechtem U, Achenbach S, Andreotti F, Arden C, et al. 2013 ESC guidelines on the management of stable coronary artery disease: the task force on the management of stable coronary artery disease of the European society of cardiology. *Eur Heart J*. (2013) 34:2949–3003. doi: 10.1093/eurheartj/ehz296
- Illardi F, Marchetta S, Martinez C, Sprynger M, Ancion A, Manganaro R, et al. Impact of aortic stenosis on layer-specific longitudinal strain: relationship with symptoms and outcome. *Eur Heart J Cardiovasc Imaging*. (2020) 21:408–16. doi: 10.1093/ehjci/jez215
- Huttin O, Girerd N, Coiro S, Bozec E, Selton-Suty C, Lamiral Z, et al. Association between layer-specific longitudinal strain and risk factors of heart failure and dyspnea: a population-based study. *J Am Soc Echocardiogr*. (2019) 32:854–65.e8. doi: 10.1016/j.echo.2019.03.011
- Sarvari SI, Haugaa KH, Zahid W, Bendz B, Aakhus S, Aaberge L, et al. Layer-specific quantification of myocardial deformation by strain echocardiography may reveal significant CAD in patients with non-ST-segment elevation acute coronary syndrome. *JACC Cardiovasc Imaging*. (2013) 6:535–44. doi: 10.1016/j.jcmg.2013.01.009
- Minhas AS, Gilotra NA, Goerlich E, Metkus T, Garibaldi BT, Sharma G, et al. Myocardial work efficiency, a novel measure of myocardial dysfunction, is reduced in COVID-19 patients and associated with in-hospital mortality. *Front Cardiovasc Med*. (2021) 8:667721. doi: 10.3389/fcvm.2021.667721
- Lin J, Wu W, Gao L, He J, Zhu Z, Pang K, et al. Global myocardial work combined with treadmill exercise stress to detect significant coronary artery disease. *J Am Soc Echocardiogr*. (2021). doi: 10.1016/j.echo.2021.10.009. [Epub ahead of print].
- Huang J, Yang C, Yan ZN, Fan L, Ni CF. Global myocardial work: a new way to detect subclinical myocardial dysfunction with normal left ventricle ejection fraction in essential hypertension patients: compared with myocardial layer-specific strain analysis. *Echocardiography*. (2021) 38:850–60. doi: 10.1111/echo.15063
- D'Andrea A, Illardi F, D'Ascenzi F, Bandera F, Benfari G, Esposito R, et al. Impaired myocardial work efficiency in heart failure with preserved ejection fraction. *Eur Heart J Cardiovasc Imaging*. (2021) 22:1312–20. doi: 10.1093/ehjci/jeab153
- El Mahdoui M, van der Bijl P, Abou R, Ajmone Marsan N, Delgado V, Bax JJ. Global left ventricular myocardial work efficiency in healthy individuals and patients with cardiovascular disease. *J Am Soc Echocardiogr*. (2019) 32:1120–7. doi: 10.1016/j.echo.2019.05.002
- Lustosa RP, Butcher SC, van der Bijl P, El Mahdoui M, Montero-Cabezas JM, Kostyukevich MV, et al. Global left ventricular myocardial work efficiency and long-term prognosis in patients after ST-segment-elevation myocardial infarction. *Circ Cardiovasc Imaging*. (2021) 14:e012072. doi: 10.1161/CIRCIMAGING.120.012072
- van der Bijl P, Vo NM, Kostyukevich MV, Mertens B, Ajmone Marsan N, Delgado V, et al. Prognostic implications of global, left ventricular myocardial work efficiency before cardiac resynchronization therapy. *Eur Heart J Cardiovasc Imaging*. (2019) 20:1388–1394. doi: 10.1093/ehjci/jez095
- Mitchell C, Rahko PS, Blauwet LA, Canaday B, Finstuen JA, Foster MC, et al. Guidelines for performing a comprehensive transthoracic echocardiographic examination in adults: recommendations from the American society of echocardiography. *J Am Soc Echocardiogr*. (2019) 32:1–64. doi: 10.1016/j.echo.2018.06.004
- Pellikka PA, Arruda-Olson A, Chaudhry FA, Chen MH, Marshall JE, Porter TR, et al. Guidelines for performance, interpretation, and application of stress echocardiography in ischemic heart disease: from the American society of echocardiography. *J Am Soc Echocardiogr*. (2020) 33:1–41.e8. doi: 10.1016/j.echo.2019.07.001
- Lang RM, Badano LP, Mor-Avi V, Afkalo J, Armstrong A, Ernande L, et al. Recommendations for cardiac chamber quantification by echocardiography in adults: an update from the American society of echocardiography and the European association of cardiovascular imaging. *J Am Soc Echocardiogr*. (2015) 28:1–39.e14. doi: 10.1016/j.echo.2014.10.003
- Eek C, Grenne B, Brunvand H, Aakhus S, Endresen K, Hol PK, et al. Strain echocardiography and wall motion score index predicts final infarct size in patients with non-ST-segment-elevation myocardial infarction. *Circ Cardiovasc Imaging*. (2010) 3:187–94. doi: 10.1161/CIRCIMAGING.109.910521
- Smiseth OA, Donal E, Penicka M, Sletten OJ. How to measure left ventricular myocardial work by pressure-strain loops. *Eur Heart J Cardiovasc Imaging*. (2021) 22:259–61. doi: 10.1093/ehjci/jeaa301
- Russell K, Eriksen M, Aaberge L, Wilhelmsen N, Skulstad H, Remme EW, et al. A novel clinical method for quantification of regional left ventricular pressure-strain loop area: a non-invasive index of myocardial work. *Eur Heart J*. (2012) 33:724–33. doi: 10.1093/eurheartj/ehs016
- Patel MR, Dehmer GJ, Hirshfeld JW, Smith PK, Spertus JA. ACCF/SCAI/STS/AATS/AHA/ASNC/HFSA/SCCT 2012 appropriate use criteria for coronary revascularization focused update: a report of the American college of cardiology foundation appropriate use criteria task force, society for cardiovascular angiography and interventions, society of thoracic surgeons, American association for thoracic surgery, American heart association, American society of nuclear cardiology, and the society of cardiovascular computed tomography. *J Am Coll Cardiol*. (2012) 59:857–81. doi: 10.1016/j.jtcvs.2012.01.061
- DeLong ER, DeLong DM, Clarke-Pearson DL. Comparing the areas under two or more correlated receiver operating characteristic curves: a nonparametric approach. *Biometrics*. (1988) 44:837–45. doi: 10.2307/2531595
- Ramlogan S, Aly D, France R, Schmidt S, Hinzman J, Sherman A, et al. Reproducibility and intervendor agreement of left ventricular global systolic strain in children using a layer-specific analysis. *J Am Soc Echocardiogr*. (2020) 33:110–9. doi: 10.1016/j.echo.2019.08.004
- Coiro S, Huttin O, Bozec E, Selton-Suty C, Lamiral Z, Carluccio E, et al. Reproducibility of echocardiographic assessment of 2D-derived longitudinal strain parameters in a population-based study (the STANISLAS Cohort study). *Int J Cardiovasc Imaging*. (2017) 33:1361–9. doi: 10.1007/s10554-017-1117-z
- Ejlertsen JA, Poulsen SH, Mortensen J, May O. Diagnostic value of layer-specific global longitudinal strain during adenosine stress in patients suspected of coronary artery disease. *Int J Cardiovasc Imaging*. (2017) 33:473–80. doi: 10.1007/s10554-016-1022-x
- Mandoli GE, Cameli M, Minardi S, Crudele F, Lunghetti S, Mondillo S. Layer-specific strain in dipyridamole stress echo: a new tool for the diagnosis of microvascular angina. *Echocardiography*. (2018) 35:2005–13. doi: 10.1111/echo.14180
- Cadeddu Dessalvi C, Deidda M, Farci S, Longu G, Mercurio G. Early ischemia identification employing 2D speckle tracking selective layers analysis during dobutamine stress echocardiography. *Echocardiography*. (2019) 36:2202–8. doi: 10.1111/echo.14535

26. Nishi T, Funabashi N, Ozawa K, Nishi T, Kamata T, Fujimoto Y, et al. Regional layer-specific longitudinal peak systolic strain using exercise stress two-dimensional speckle-tracking echocardiography for the detection of functionally significant coronary artery disease. *Heart Vessels*. (2019) 34:1394–403. doi: 10.1007/s00380-019-01361-w
27. Oh BH, Volpini M, Kambayashi M, Murata K, Rockman HA, Kassab GS, et al. Myocardial function and transmural blood flow during coronary venous retroperfusion in pigs. *Circulation*. (1992) 86:1265–79. doi: 10.1161/01.CIR.86.4.1265
28. Reimer KA, Lowe JE, Rasmussen MM, Jennings RB. The wavefront phenomenon of ischemic cell death. 1. Myocardial infarct size vs duration of coronary occlusion in dogs. *Circulation*. (1977) 56:786–94. doi: 10.1161/01.CIR.56.5.786
29. Nishi T, Funabashi N, Ozawa K, Takahara M, Fujimoto Y, Kamata T, et al. Resting multilayer 2D speckle-tracking transthoracic echocardiography for the detection of clinically stable myocardial ischemic segments confirmed by invasive fractional flow reserve. Part 1: Vessel-by-vessel analysis. *Int J Cardiol*. (2016) 218:324–32. doi: 10.1016/j.ijcard.2016.05.016
30. Biering-Sorensen T, Hoffmann S, Mogelvang R, Zeeberg Iversen A, Galatius S, Fritz-Hansen T, et al. Myocardial strain analysis by 2-dimensional speckle tracking echocardiography improves diagnostics of coronary artery stenosis in stable angina pectoris. *Circ Cardiovasc Imaging*. (2014) 7:58–65. doi: 10.1161/CIRCIMAGING.113.000989
31. Simonovic D, Coiro S, Deljanin-Ilic M, Kobayashi M, Carluccio E, Girerd N, et al. Exercise-induced B-lines in heart failure with preserved ejection fraction occur along with diastolic function worsening. *ESC Heart Fail*. (2021) 8:5068–80. doi: 10.1002/ehf2.13575
32. Boe E, Russell K, Eek C, Eriksen M, Remme EW, Smiseth OA, et al. Non-invasive myocardial work index identifies acute coronary occlusion in patients with non-ST-segment elevation-acute coronary syndrome. *Eur Heart J Cardiovasc Imaging*. (2015) 16:1247–55. doi: 10.1093/ehjci/jev078
33. Geyer H, Caracciolo G, Abe H, Wilansky S, Carerj S, Gentile F, et al. Assessment of myocardial mechanics using speckle tracking echocardiography: fundamentals and clinical applications. *J Am Soc Echocardiogr*. (2010) 23:351–69; quiz 453–5. doi: 10.1016/j.echo.2010.02.015

Conflict of Interest: The authors declare that the research was conducted in the absence of any commercial or financial relationships that could be construed as a potential conflict of interest.

Publisher's Note: All claims expressed in this article are solely those of the authors and do not necessarily represent those of their affiliated organizations, or those of the publisher, the editors and the reviewers. Any product that may be evaluated in this article, or claim that may be made by its manufacturer, is not guaranteed or endorsed by the publisher.

Copyright © 2022 Lin, Gao, He, Liu, Cai, Niu, Zhao, Li, Wang, Wu, Zhu and Wang. This is an open-access article distributed under the terms of the Creative Commons Attribution License (CC BY). The use, distribution or reproduction in other forums is permitted, provided the original author(s) and the copyright owner(s) are credited and that the original publication in this journal is cited, in accordance with accepted academic practice. No use, distribution or reproduction is permitted which does not comply with these terms.



Coronary Computed Tomography Angiographic Predictors of Non-culprit Territory Unrecognized Myocardial Infarction Assessed by Cardiac Magnetic Resonance in Non-ST-elevation Acute Coronary Syndrome

OPEN ACCESS

Edited by:

Jinwei Tian,
The Second Affiliated Hospital of
Harbin Medical University, China

Reviewed by:

Qi Zhao,
Capital Medical University, China
Gaetano Antonio Lanza,
Agostino Gemelli University Polyclinic
(IRCCS), Italy

*Correspondence:

Tsunekazu Kakuta
kaz@joy.email.ne.jp

[†]These authors have contributed
equally to this work

Specialty section:

This article was submitted to
Cardiovascular Imaging,
a section of the journal
Frontiers in Cardiovascular Medicine

Received: 30 November 2021

Accepted: 24 December 2021

Published: 31 January 2022

Citation:

Matsuda K, Hoshino M, Kanaji Y,
Sugiyama T, Misawa T, Hada M,
Nagamine T, Nogami K, Sayama K,
Teng Y, Ueno H, Yonetsu T, Sasano T
and Kakuta T (2022) Coronary
Computed Tomography Angiographic
Predictors of Non-culprit Territory
Unrecognized Myocardial Infarction
Assessed by Cardiac Magnetic
Resonance in Non-ST-elevation Acute
Coronary Syndrome.
Front. Cardiovasc. Med. 8:825523.
doi: 10.3389/fcvm.2021.825523

Kazuki Matsuda^{1†}, Masahiro Hoshino^{1†}, Yoshihisa Kanaji¹, Tomoyo Sugiyama¹,
Toru Misawa¹, Masahiro Hada¹, Tatsuhiko Nagamine¹, Kai Nogami¹, Kodai Sayama¹,
Yun Teng¹, Hiroki Ueno¹, Taishi Yonetsu², Tetsuo Sasano² and Tsunekazu Kakuta^{1*}

¹ Division of Cardiovascular Medicine, Tsuchiura Kyodo General Hospital, Ibaraki, Japan, ² Department of Cardiovascular
Medicine, Tokyo Medical and Dental University, Tokyo, Japan

Objectives: This study sought to assess the predictors of coronary computed tomography angiographic findings for non-infarct-related (non-IR) territory unrecognized myocardial infarction (UMI) in patients with a first episode of non-ST-elevation acute coronary syndrome (NSTEMI-ACS).

Background: UMI detected by cardiac magnetic resonance imaging (CMR) is associated with adverse outcomes in patients with both acute coronary syndrome and chronic coronary syndrome. However, the association between the presence of UMI and coronary computed tomography angiographic (CCTA) findings remains unknown.

Methods: We investigated 158 patients with a first clinical episode of NSTEMI-ACS, who underwent pre-PCI 320-slice CCTA and uncomplicated urgent percutaneous coronary intervention (PCI) within 48 h of admission. In these patients, post-PCI CMR was performed within 30 days from urgent PCI and before non-IR lesion staged PCI. UMI was assessed using late gadolinium enhancement (LGE)-CMR by identifying regions of hyperenhancement with an ischemic distribution pattern in non-IR territories (non-IR UMI). CCTA analysis included qualitative and quantitative assessments of the culprit segment, Agatston score, mean peri-coronary fat attenuation index (FAI), epicardial fat volume (EFV) and epicardial fat attenuation (EFA).

Results: Non-IR UMI was detected in 30 vessel territories (9.7%, 30/308 vessels) of 28 patients (17.7%, 28/158 patients). The presence of low-attenuation plaque, spotty calcification, napkin ring sign, and positive remodeling was not significantly different between vessels with and without subtended non-IR UMI. Agatston score >30.0 (OR: 8.39, 95% confidence interval (CI): 2.17 to 32.45, $p = 0.002$), mean FAI >-64.3 (OR: 3.23, 95% CI: 1.34 to 7.81, $p = 0.009$), and stenosis severity (OR: 1.04, 95% CI: 1.02 to 1.06, $p < 0.001$) were

independently associated with non-IR UMI. Neither EFV ($p = 0.340$) nor EFA ($p = 0.700$) was associated with non-IR UMI.

Conclusion: The prevalence of non-IR UMI was 17.7 % in patients with first NSTEMI-ACS presentation. Agatston score, mean FAI, and coronary stenosis severity were independent CCTA predictors of the presence of non-IR UMI. The integrated CCTA assessment may help identify the presence of non-IR UMI before urgent PCI.

Keywords: acute coronary syndrome, percutaneous coronary intervention, unrecognized myocardial infarction, cardiac magnetic resonance imaging, coronary computed tomography angiography

INTRODUCTION

A large proportion of acute myocardial infarction (MI) is asymptomatic or atypically presented without clinical recognition (1–3). Unrecognized myocardial infarction (UMI) has been reported to constitute up to more than 50% of all MI in the general population and in the cohort older than 60 years or in patients with chronic coronary syndrome, depending on the cardiovascular risk and modalities to detect UMI (4, 5). Recently, the presence of unrecognized myocardial scar detected by late gadolinium enhancement (LGE) in patients presenting with the first acute AMI has been reported to be associated with worse outcomes (6, 7). The prevalence of UMI in these studies were 8.2–13%, and the majority of the patients in these studies exhibited ST-elevation myocardial infarction (STEMI) treated with primary percutaneous coronary intervention (PCI). In contrast, there are limited data available regarding the prevalence of UMI in patients with non-ST-elevation acute coronary syndrome (NSTEMI-ACS). Currently, although coronary computed tomography angiography (CCTA) has not been recommended as a risk-stratifying tool of ACS, recent reports supported the clinical potentials and implications of CCTA in the ACS setting (8, 9). Therefore, in this study, we sought to assess the prevalence of non-infarct-related territory UMI (non-IR UMI) in patients presenting with a first episode of NSTEMI-ACS without a history of MI, PCI, or coronary artery bypass graft (CABG). We further evaluated the association between the presence of non-IR UMI and CCTA findings including qualitative and quantitative assessments including the stenosis severity, Agatston score, peri-coronary fat attenuation index (FAI), epicardial fat volume (EFV) and epicardial fat attenuation (EFA) to assess if CCTA findings including peri-coronary adipose tissue and pericardial fat assessments could predict the presence of non-IR UMI before invasive coronary angiography.

MATERIALS AND METHODS

Study Design and Patient Population

This study was a retrospective analysis of prospectively, but non-consecutively enrolled patients in the institutional NSTEMI-ACS CCTA research registry at Tsuchiura Kyodo General Hospital, which tested the hypothesis that CCTA before invasive coronary angiography may provide the diagnostic and therapeutic information of atherosclerotic burden, lesion location and procedural planning of revascularization in patients

with suspected NSTEMI-ACS. From this registry data, 169 patients with the first episode of NSTEMI-ACS who underwent subsequent coronary angiography with *ad-hoc* uncomplicated PCI and cardiac magnetic resonance imaging (CMR) within 30 days after the index PCI and before non-IR significant lesion staged PCI were enrolled in the present study. Uncomplicated PCI was defined as post-PCI Thrombolysis in Myocardial Infarction flow grade ≥ 3 , residual angiographic diameter stenosis less than 20%, no side branch occlusion with a diameter more than 1.5 mm or visible distal embolization, and no PCI-related myocardial infarction according to current guidelines (10). Diagnosis of NSTEMI-ACS was made by symptoms, biomarker elevation, and ECG changes. Patients with NSTEMI-ACS were enrolled according to the ESC guidelines for the management of acute coronary syndromes in patients presenting without persistent ST-segment elevation (11). We included patients aged at least 20 years who were admitted to the intensive care unit with a diagnosis of NSTEMI-ACS within 48 h of the last appearance of symptoms suggestive of myocardial ischemia and/or ST-T segment change in at least 2 leads. All patients subsequently underwent uncomplicated PCI with an early invasive strategy less than 48 h after admission (12). We included patients with unstable angina pectoris (UAP) and non-ST-elevation myocardial infarction (NSTEMI) when the single culprit lesion was identifiable and considered suitable for PCI. We excluded patients with significant left main coronary artery disease (CAD), chronic total occlusion, unidentifiable culprit lesions, significant valvular disease, previous CABG, previous MI, significant arrhythmia, renal insufficiency with a baseline serum creatinine level >1.5 mg/dL, and contraindication to CMR (eg, pacemaker, internal defibrillator, or other incompatible intracorporeal foreign bodies, pregnancy, and claustrophobia). In the case of multivessel disease, delayed enhancement (DE)-CMR imaging was performed before staged non-IR lesion revascularization. Patients treated with multivessel PCI for not only culprit but non-culprit territory lesions at the index urgent PCI were excluded from the final analysis. A representative case undergoing urgent PCI with preprocedural CCTA and postprocedural CMR is shown (Figure 1). The study protocol agreed with the Declaration of Helsinki and was approved by the institutional ethics committee (TKGH-IRB 2021FY85). All patients provided written informed consent for future enrollment in the institutional clinical studies. Prompt optimal medical therapy was initiated in all patients before urgent PCI and guideline-directed medical therapy was continued thereafter.

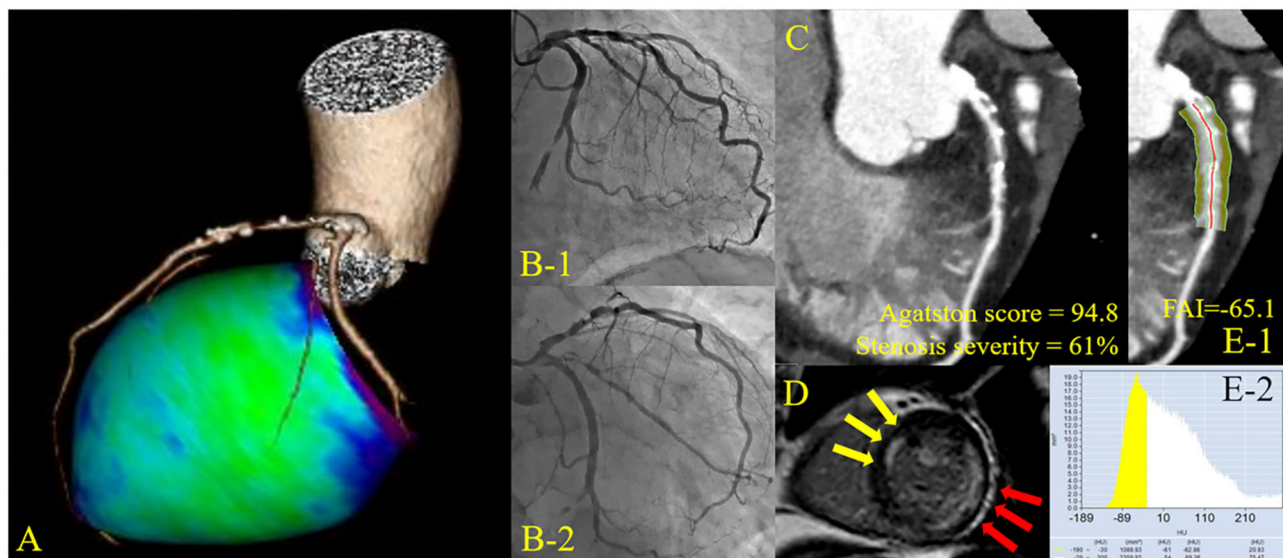


FIGURE 1 | Representative cardiac images of a patient with non-infarct-related unrecognized myocardial infarction. A 72-year-old man with a history of diabetes mellitus. **(A)** Three-dimensional reconstruction of the coronary artery. **(B)** Pre-percutaneous coronary intervention (PCI) angiogram reveals 99% stenosis in the left circumflex artery #13 (culprit lesion) and 75% stenosis in the left anterior descending artery #6 (non-culprit lesion). **(C)** Curved planar reconstruction view with Agatston score and computed tomography-derived stenosis severity. **(D)** Delayed enhancement cardiac magnetic resonance imaging shows infarct-related late gadolinium enhancement (LGE) in the lateral territory and non-infarct-related LGE in the anterior territory. **(E)** Peri-coronary fat attenuation index (FAI) at the proximal 40 mm segment of non-infarct-related vessel (left anterior descending artery) was traced.

Urgent Coronary Angiography and PCI

Invasive coronary angiography (CAG) and revascularization of the IR lesion were performed by *ad-hoc* PCI via the routine use of drug-eluting stents with a 6-French system. Before the PCI procedure, all patients received a loading dose of 200 mg aspirin and 300 mg clopidogrel or 20 mg prasugrel. Coronary angiograms were analyzed quantitatively using QAngio XA system (Medis Medical Imaging Systems, The Netherlands). The IR lesion was identified by the combination of electrocardiography (ECG), echocardiography, and coronary angiographic findings by two expert interventionalists. The stent type and procedure strategy selected were at the operator's discretion.

CCTA Acquisition

CCTA imaging was performed before PCI, indicating that the median value of the interval between CCTA and PCI was 4.3 (2.1–7.2) h. Computed tomography (CT) imaging was performed using a 320-slice CT scanner (Aquilion ONE; Canon Medical Systems Corporation, Japan) in accordance with the Society of Cardiovascular Computed Tomography guidelines (13) in all patients. All CCTA examinations were performed using a single CT system during the present study period. When needed, oral and/or intravenous beta-blockers were administered to achieve a target heart rate ≤ 65 bpm. A non-contrast enhanced CT-scan for the assessment of coronary artery calcification, prospectively triggered at 75% of the RR-interval with 3 mm slice thickness, was followed by CCTA. Immediately before CCTA scanning, 0.3 or 0.6 mg of sublingual nitroglycerine was administered. The

scan was triggered using an automatic bolus-tracking technique with a region of interest placed in the ascending aorta. Images were acquired after a bolus injection of 40 to 60 mL contrast (iopamidol, Bayer Yakuhin, Ltd., Japan) at a rate of 3–6 mL/s, using prospective ECG-triggering or retrospective ECG gating with tube current modulation. Acquisition and reconstruction parameters for the patients were 120 kVp, tube current of 50 to 750 mA, gantry rotation speed of 350 ms per rotation, helical pitch of 8 to 18, field matrix of 512×512 , and scan thickness of 0.5 mm. All scans were performed during a single breath-hold. Images were reconstructed at a window centered at 75% of the R-R interval to coincide with left ventricular diastasis.

Analyses of FAI, Epicardial Fat, CCTA Plaque, and Agatston Score

In the present study, the crude analysis of FAI of all three main coronary vessels was performed. The mean FAI of three main coronary vessels or the vessel specific FAI value was used for the analysis. FAI analysis was performed in the proximal 40 mm segments of left anterior descending coronary artery and left circumflex coronary artery and the proximal 10 to 50 mm segment of the right coronary artery using a dedicated workstation Aquarius iNtuition Edition version 4.4.13; TeraRecon Inc., USA), as previously described (14, 15). Within the pre-identified segment of interest, the lumen as well as the inner and outer vessel wall border were tracked in an automated manner with additional manual optimization. Adipose tissue was defined as all voxels with attenuation between -190 HU and -30 HU. The FAI value was defined as the average CT attenuation in

HU of the adipose tissue located within a radial distance from the outer vessel wall equal to the diameter of the coronary vessel (Figure 1).

EFV and EFA was quantified offline on non-contrast CT images in all patients, using a semiautomatic software equipped in the dedicated workstation (AZE Virtual Place, Canon Medical Systems Corporation, Japan). Region of interest (ROI) were drawn by manual tracing of the pericardium in axial planes from the take-off of right pulmonary artery to apex of the heart. Then, EFV and EFA were automatically calculated as the sum of all pixels within a window of -190 and -30 HU in the ROI. FAI and epicardial fat analysis were separately performed as a *post-hoc* analysis blinded to CMR results at the institutional imaging and physiology laboratory by the expert investigators for FAI analysis (KM and M. Hoshino). Plaque assessment on CCTA was independently performed by two experienced readers (M. Hada and TM) using the reconstructed CCTA images transferred to an offline workstation (Ziostation2, Ziosoft Inc., Japan).

Coronary artery calcium (CAC) quantification was performed on non-contrast CT images by Agatston method using the software facilitating semi-automatic assessment (Ziostation2, Ziosoft Inc., Japan). This software can allow the user to relate calcification to the specific coronary arteries by locating area with attenuation ≥ 130 HU.

CMR Examination

CMR Acquisition and Assessment of IR (ACS Culprit) Scar and Non-IR UMI

Images were acquired on a 1.5-T scanner (Philips Achieva, Philips Medical Systems, The Netherlands) with 32-channel cardiac coils within 30 (8–32) days after the IR lesion PCI and before the staged PCI of non-IR significant lesions. Cardiac gating and heart rate recording were achieved using the vector-cardiogram device. Blood pressure and heart rate were monitored throughout the protocol. Cine-CMR was performed using a retrospectively gated steady-state free precession sequence. Twelve short-axis slices of the left ventricle (LV) were acquired from the apex to the base. The cine-CMR parameters were as follows: repetition time/echo time, 4.1 ms/1.4 ms; slice thickness, 6 mm; flip angle, 55° ; field of view, 350×350 mm²; matrix size, 128×128 ; and number of phases per cardiac cycle, 20. LV mass and volumes were calculated according to the Simpson's rule using CMR data (16). Gadolinium contrast was infused intravenously at a total dose of 0.10 mmol/kg. Fifteen min after this injection, LGE images were acquired in the same planes as cine images and imaging parameters were as follows: repetition time/echo time, 3.8 ms/1.28 ms; flip angle, 15° ; field of view, 350×350 mm²; acquisition matrix, 200×175 ; number of phases per cardiac cycle, and slice thickness, 8 mm. The infarcted myocardium was quantified on the LGE images as myocardium with a signal intensity exceeding the mean signal intensity of the remote myocardium by >5 standard deviation (SD) and using a semi-automatic algorithm. Non-IR UMI was defined as absence of MI/PCI/CABG history on medical records, but the presence of LGE on the non-IR territories by a consensus of two experienced cardiologists (KS and YK) and controlled by an expert reader (TK) masked to the patient data. High signal intensity lesion

located in subendocardial territories with a ischemic distribution consistent of specific epicardial coronary arteries on LGE images were considered to represent non-IR UMI or IR scar. Infarct size of both ACS (IR) and UMI (non-IR) was measured using the full width at one-half maximum method. Microvascular obstruction (MVO) was defined as the hypo-enhanced region within and included in the infarcted myocardium. LV mass was normalized to body surface area as LV mass index (LVMI). All CMR images were analyzed using dedicated off-line software (AZE Virtual Place, Canon Medical Systems Corporation, Japan).

Statistical Analysis

Statistical analyses were performed using SPSS version 25.0 (IBM Corporation, USA) and R version 4.0.3 (The R Foundation for Statistical Computing, Austria) software. Both patient-based and vessel-based analyses were tried to identify the predictors of non-IR UMI. Categorical data were expressed as numbers and percentages and compared by the chi-square or Fisher's exact tests. Continuous data were expressed as median (interquartile range [IQR]) and analyzed using Mann–Whitney U test. Receiver operating curves were analyzed to assess the best cut-off values of significant predictors for the presence of non-IR UMI using CCTA variables. The optimal cut-off value was calculated using the Youden index.

Univariable and multivariable linear regression analyses were performed to determine predictive factors of non-IR UMI size. Univariable and multivariable logistic regression analyses were performed to predict the presence of non-IR UMI using CCTA variables. The covariates with $p < 0.10$ in the univariable analysis were included in the multivariable analysis. A collinearity index was used for checking linear combinations among covariates, and Akaike information criterion for avoiding overfitting. The Generalized estimating equations approach was used to take into account the within-subject correlation due to multiple vessels analyzed within a single patient.

The prediction model for non-IR UMI was constructed to determine the incremental discriminatory and reclassification performance of FAI, by using relative integrated discrimination improvement (IDI) and category-free net reclassification index (NRI) when FAI was added to the clinical risk model including GRACE score, ejection fraction (EF), Agatston score, and CCTA-derived stenosis severity. A two-sided $p < 0.05$ was considered statistically significant.

RESULTS

Baseline Patient Characteristics, CCTA and CMR Findings

Of 169 initially enrolled patients, 5 and 6 patients were excluded from the final analysis because of unsatisfactory CCTA and DE-CMR data acquisition, respectively. Thus, the final analysis was performed on 158 patients with complete pre-PCI CCTA and post-PCI DE-CMR data. Of 158 patients for the final analysis, 8 non-IR lesions were treated at the index urgent PCI of NSTEMI-ACS. These vessels were excluded from the vessel-based UMI assessment because PCI-related myocardial injury could not be differentiated from that by UMI-related scar. Therefore, the

TABLE 1 | Baseline characteristics.

	Total	Patients with non-IR UMI	Patients without non-IR UMI	P value
	(n = 158)	(n = 28)	(n = 130)	
Age (years)	66 (58 to 72)	65 (59 to 72)	66 (58 to 72)	0.819
Male, n (%)	121 (76.6%)	28 (80.0%)	97 (75.2%)	0.658
Hypertension, n (%)	110 (69.6%)	20 (66.7%)	90 (70.3%)	0.667
Diabetes mellitus, n (%)	50 (31.7%)	11 (36.7%)	39 (30.5%)	0.519
Hyperlipidemia, n (%)	96 (60.8%)	14 (46.7%)	82 (64.1%)	0.097
Smoker, n (%)	70 (44.3%)	16 (53.3%)	54 (41.1%)	0.310
LDL cholesterol (mg/dl)	120 (104 to 151)	112 (95 to 140)	122 (105 to 152)	0.673
eGFR (ml/min/1.73m ²)	75.1 (62.2 to 84.8)	66.6 (55.5 to 79.6)	75.3 (64.1 to 85.4)	0.117
EF (%)	62.0 (55 to 66)	55 (51 to 60)	63 (58 to 66)	<0.001
Peak Troponin (ng/l)	3,269 (730 to 14869)	6,269 (2162 to 22204)	2,565 (674 to 12362)	0.172
Peak CK (U/l)	250 (129 to 655)	345 (174 to 983)	247 (120 to 608)	0.339
Peak CK-MB (U/l)	24 (12 to 56)	38 (18 to 58)	22 (12 to 55)	0.043
CRP (mg/dl)	0.14 (0.06 to 0.60)	0.25 (0.11 to 0.95)	0.13 (0.05 to 0.54)	0.191
GRACE score	115 (95 to 146)	124 (104 to 149)	113 (93 to 144)	0.078
SYNTAX score	12 (8 to 20)	16 (11 to 23)	11 (8 to 19)	0.054
Lesion location				
RCA culprit, n (%)	42 (26.6%)	4 (14.3%)	38 (29.2%)	0.156
LAD culprit, n (%)	79 (50.0%)	16 (57.1%)	63 (48.5%)	0.533
LCX culprit, n (%)	37 (23.4%)	8 (28.6%)	29 (22.3%)	0.469
Multivessel disease, n (%)	49 (31.0%)	11 (39.3%)	38 (29.2%)	0.368
Clinical status				0.029
NSTEMI, n (%)	129 (81.6%)	27 (20.9%)	102 (78.5%)	
UAP, n (%)	29 (18.4%)	1 (3.4%)	28 (96.6%)	

Values are n (%) or median (interquartile range). Non-IR UMI, non-infarct-related unrecognized myocardial infarction; LDL, low density lipoprotein; eGFR, estimated glomerular filtration rate; EF, ejection fraction; CK, creatine kinase; CK-MB, creatine kinase-MB; CRP, C-reactive protein; RCA, right coronary artery; LAD, left anterior descending coronary artery; LCX, left circumflex coronary artery; NSTEMI, non-ST-elevation myocardial infarction; UAP, unstable angina pectoris.

vessel-based analysis was performed in 308 vessels and territories on CCTA after excluding 8 territories from the vessel-based non-IR UMI analysis. The patients' clinical characteristics, CCTA and CMR findings according to the presence or absence of non-IR UMI are presented in **Tables 1, 2**. In 158 patients, median age was 66 (58–72) years, and 76.6 % were men. Non-IR UMI was detected in 30 territories of 28 (17.7%) patients, two of which had multiple non-IR-UMI on two different territories. The patients with non-IR UMI, when compared with those without non-IR UMI, showed significantly lower EF. The prevalence of non-IR UMI was significantly higher in patients with NSTEMI in comparison with those with UAP [27/129 (20.9%) vs. 1/29 (3.4%), $P = 0.029$]. On the vessel-based analysis of CCTA, non-IR UMI was significantly associated stenosis severity represented by CCTA-derived area stenosis and quantitative coronary angiography (QCA)-derived diameter stenosis. Vessels with non-IR UMI showed significantly higher total Agatston scores and the vessel-specific Agatston score. Of note, the vessel-specific FAI values of vessels with non-IR UMI tended to be higher than those without. On a patient-based analysis, the mean FAI values were significantly elevated in patients with non-IR UMI (**Table 2**). EFV and EFA showed no significant association with the presence of non-IR UMI, for both patient-based and

vessel-based analyses. The degree of IR myocardial injury post PCI evaluated by creatine kinase (CK)-MB was significantly higher in patients with non-IR UMI than in those without unrecognized non-IR UMI ($p = 0.043$). Furthermore, the degree of IR-LGE was weakly albeit significantly correlated with the degree of non-IR LGE ($r = 0.204$, $p = 0.010$).

Determinant of the Presence of Non-IR UMI on CCTA

The results of univariable and multivariable logistic regression analyses to determine the predictors of the presence of non-IR UMI are presented in **Table 3**. When using CCTA variables, stenosis severity, Agatston score, and mean FAI were independently predictive of the presence of non-IR UMI. The best cut-off values of the FAI and Agatston score to predict the presence of non-IR UMI were -64.3 and 30.0 , respectively. Multivariable linear regression analysis revealed that FAI and CT-derived stenosis were independent predictors of non-IR LGE volume (**Table 4**). For the prediction of non-IR UMI volume, **Figure 2** shows the non-IR UMI volume stratified by the best cut-off values of FAI (-64.3) and CT-derived stenosis severity (55.2%). For the presence or absence of non-IR UMI, the prevalence stratified by the numbers of significant CCTA

TABLE 2 | QCA, CCTA, and CMR findings.

	Total	Vessels with non-IR UMI	Vessels without non-IR UMI	P value
	(n = 308)	(n = 30)	(n = 278)	
QCA				
Diameter stenosis (%)	27.3 (14.7 to 46.6)	51.3 (27.1 to 73.1)	26.5 (14.6 to 41.9)	<0.001
MLD (mm)	2.16 (1.47 to 2.78)	1.85 (0.96 to 2.79)	2.18 (1.51 to 2.78)	0.185
CCTA				
Plaque features				
Low attenuation plaque, n (%)	40 (13.0%)	4 (13.3%)	36 (12.9%)	>0.999
Napkin ring sign, n (%)	5 (1.6%)	1 (3.3%)	4 (1.4%)	0.424
Spotty calcification, n (%)	118 (38.3%)	11 (36.7%)	107 (38.5%)	0.704
Positive remodeling ≥ 1.10 , n (%)	62 (20.1%)	6 (20.0%)	56 (20.1%)	>0.999
Remodeling index	0.94 (0.83 to 1.06)	0.98 (0.82 to 1.05)	0.94 (0.83 to 1.06)	0.446
Agatston score				
Agatston score total	217 (61 to 714)	356 (180 to 1047)	202 (56 to 659)	0.015
Agatston score in each vessel	135 (34 to 135)	57 (32 to 171)	30 (0 to 134)	0.034
Agatston score of non-IR vessels average	49 (14 to 212)	91 (42 to 309)	43 (6 to 157)	0.043
Epicardial fat				
Epicardial fat attenuation (HU)	-77.3 (-80.6 to -73.5)	-75.6 (-79.2 to -73.9)	-77.7 (-80.7 to -73.5)	0.340
Epicardial fat volume (cm ³)	126 (96 to 167)	118 (95 to 161)	125 (96 to 167)	0.700
FAI				
FAI average (HU)	-69.5 (-74.0 to -64.5)	-64.9 (-71.5 to -60.3)	-69.7 (-74.4 to -64.7)	0.005
FAI in each vessel (HU)	-69.4 (-75.0 to -63.1)	-68.2 (-72.8 to -59.8)	-69.6 (-75.3 to -63.5)	0.078
CT-derived stenosis				
CT-derived stenosis severity (%)	35.9 (28.0 to 45.0)	43.6 (32.7 to 100.0)	35.0 (28.5 to 44.0)	<0.001
MLA (mm ²)	4.2 (2.9 to 6.4)	2.9 (0.0 to 4.9)	4.3 (2.9 to 6.6)	0.001
CMR				
Total LGE volume (ml)	2.7 (0.0 to 7.3)	7.8 (2.9 to 14.1)	2.4 (0.0 to 6.2)	<0.001
IR LGE volume (ml)	1.9 (0.0 to 5.6)	2.7 (0.7 to 5.2)	1.9 (0.0 to 5.6)	0.694
Non-IR LGE volume (ml)	0.0 (0.0 to 0.0)	3.2 (1.4 to 5.0)		
Non-IR RCA LGE volume (ml)	0.0 (0.0 to 0.0)	2.8 (0.9 to 4.6)		
Non-IR LAD LGE volume (ml)	0.0 (0.0 to 0.0)	2.3 (0.7 to 3.6)		
Non-IR LCX LGE volume (ml)	0.0 (0.0 to 0.0)	5.1 (4.4 to 8.4)		

Values are n (%) or median (interquartile range). QCA, quantitative coronary angiography; CCTA, coronary computed tomography angiographic; CMR, cardiac magnetic resonance; UMI, unrecognized myocardial infarction; MLD, minimal lumen diameter; non-IR, non-infarct-related; FAI, peri-coronary fat attenuation index; CT, computed tomography; MLA, minimum lumen area; LGE, late gadolinium enhancement; IR, infarct-related; RCA, right coronary artery; LAD, left anterior descending coronary artery; LCX, left circumflex coronary artery.

predictors ([1] FAI >-64.3 , [2] Agatston score >30.0 , and [3] CT-derived stenosis $>55.2\%$) was presented in **Figure 3**. The discriminant efficacy (IDI and NRI) of predicting non-IR UMI was significantly improved when FAI was added to the clinical risk model (**Table 5**).

DISCUSSION

This study investigated the prevalence of non-IR UMI and its CCTA-derived predictors in patients with a first clinical episode of NSTEMI-ACS. The main findings of this study are summarized as follows: (1) the prevalence of non-IR UMI was 17.7 %; (2) on CCTA performed before urgent PCI, non-IR UMI was significantly associated with EF on the patient-based analysis; (3) the median volume of non-IR UMI was

3.2 (1.4–5.0) ml; (4) on the vessel-based analysis, non-IR UMI was significantly associated with CT-derived stenosis severity, Agatston score, and FAI; (5) peak cardiac marker elevation (CK-MB) post PCI was significantly higher in patients with non-IR UMI compared with those without non-IR UMI; (6) on multivariable linear regression model, vessel-based FAI and CT-derived stenosis were significant predictors of non-IR UMI volume; (7) FAI significantly improved NRI and IDI over the reference prediction model including GRACE score, EF, CCTA-derived stenosis severity, and Agatston score.

Previous studies reporting the prevalence of CMR-derived non-IR UMI in patients with ACS are scarce and this is the first study to investigate CCTA-derived predictors of non-IR UMI by DE-CMR and its prevalence in patients with a first clinical episode of NSTEMI-ACS. The presence of unrecognized myocardial scar detected by LGE in patients presenting with first acute AMI

TABLE 3 | Univariable and multivariable logistic analysis of predicting non-IR UMI.

	Univariable analysis			Multivariable analysis		
	OR	95% CI	P value	OR	95% CI	P value
Age	1.00	0.97 to 1.04	0.963			
Male	1.12	0.43 to 2.90	0.812			
EF	0.94	0.92 to 0.97	<0.001			not selected
Agatston score of non-IR vessels average	1.00	1.00 to 1.00	0.018			
Agatston score of non-IR vessels average >30.0	12.06	2.86 to 50.84	0.001	8.39	2.17 to 32.45	0.002
FAI average	1.09	1.02 to 1.17	0.012			
FAI average >-64.3	3.32	1.55 to 7.12	0.002	3.23	1.34 to 7.81	0.009
MLA	0.76	0.60 to 0.96	0.021			
CT-derived stenosis	1.05	1.03 to 1.07	<0.001	1.04	1.02 to 1.06	<0.001
QCA-derived diameter stenosis	1.04	1.03 to 1.06	<0.001			not selected
SYNTAX score	1.04	1.01 to 1.07	0.011			
GRACE score	1.01	1.00 to 1.03	0.043			not selected
NSTEMI	7.32	0.99 to 53.98	0.051			

Non-IR, non-infarct-related; UMI, unrecognized myocardial infarction; OR, odds ratio; CI, confidence interval; EF, ejection fraction; FAI, peri-coronary fat attenuation index; MLA, minimum lumen area; CT, computed tomography; QCA, quantitative coronary angiography; NSTEMI, non-ST-elevation myocardial infarction.

TABLE 4 | Univariable and multivariable linear regression analysis of predicting non-IR LGE volume.

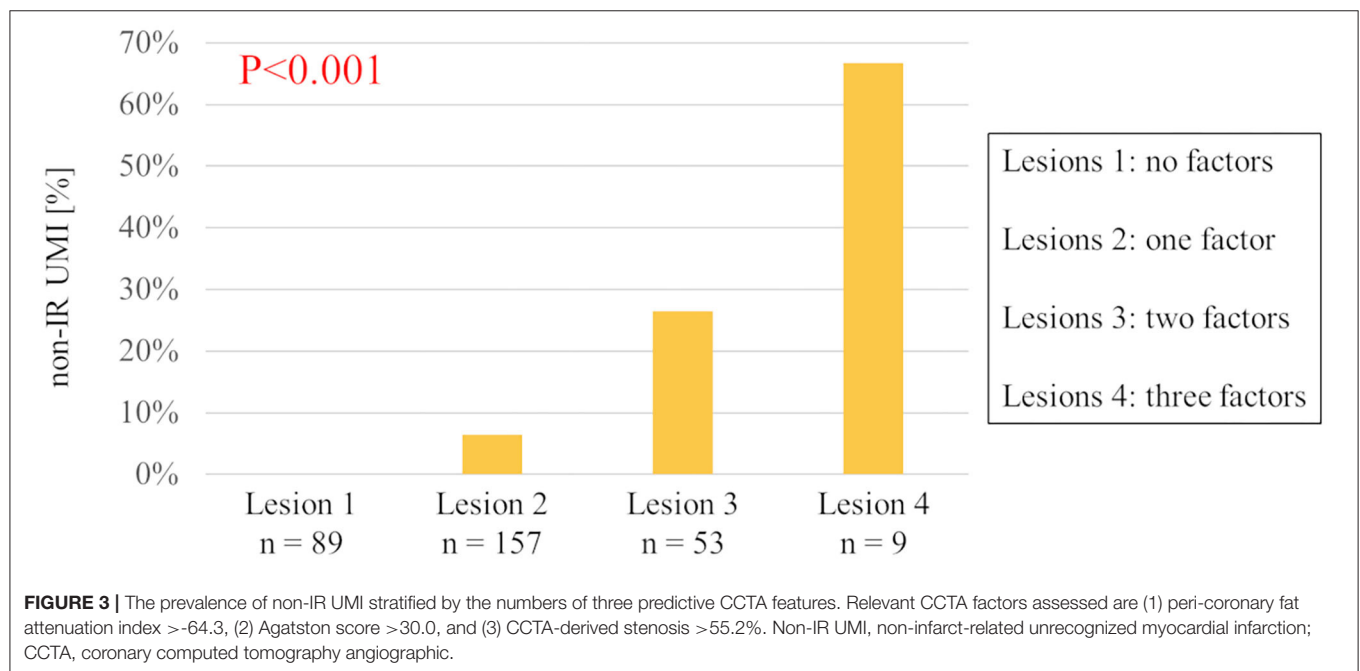
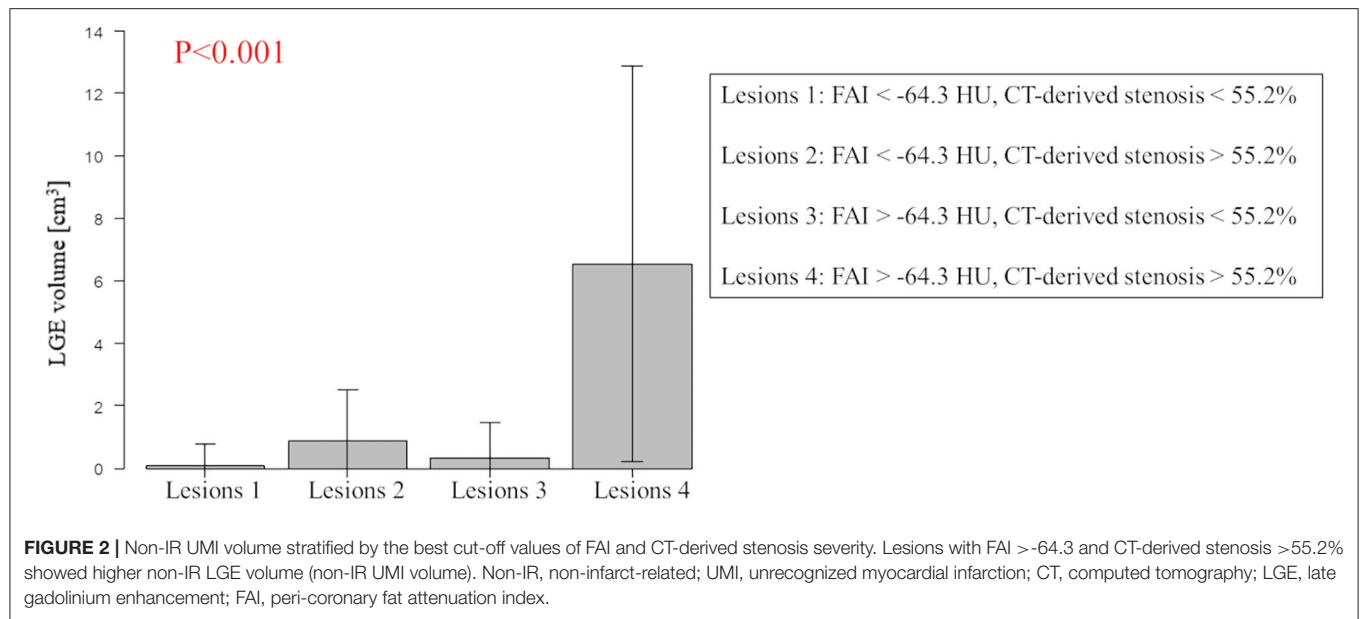
	Univariable analysis			Multivariable analysis		
	β	95% CI	P value	β	95% CI	P value
Age	-0.010	-0.028 to 0.009	0.326			
Male	0.014	-0.491 to 0.462	0.952			
EF	-0.043	-0.064 to -0.022	<0.001	-0.011	-0.032 to 0.011	0.341
Agatston score of non-IR vessels average	0.001	0.000 to 0.002	0.015			
Agatston score of non-IR vessels average >30.0	0.443	0.033 to 0.852	0.034	-0.057	-0.459 to 0.345	0.779
FAI average	0.046	0.015 to 0.077	0.003			
FAI average >-64.3	1.007	0.544 to 1.469	<0.001	0.666	0.209 to 1.124	0.004
MLA	-0.137	-0.204 to -0.069	<0.001			
CT-derived stenosis	0.042	0.032 to 0.052	<0.001	0.037	0.026 to 0.049	<0.001
QCA-derived diameter stenosis	0.031	0.022 to 0.040	<0.001			
SYNTAX score	0.019	-0.003 to 0.041	0.087			
GRACE score	0.011	0.005 to 0.016	<0.001	0.004	-0.002 to 0.009	0.124
NSTEMI	0.458	-0.062 to -0.977	0.084			

Non-IR, non-infarct-related; LGE, late gadolinium enhancement; CI, confidence interval; EF, ejection fraction; FAI, peri-coronary fat attenuation index; MLA, minimum lumen area; CT, computed tomography; QCA, quantitative coronary angiography; NSTEMI, non-ST-elevation myocardial infarction.

has been reported to be 8.2–13.0% (6, 7). The majority of the patients in these studies exhibited STEMI treated with primary PCI. In contrast, our results indicated that the prevalence of UMI in NSTE-ACS was higher than these previous reports.

Currently, CCTA is a class I (level of evidence A) recommendation as an alternative to coronary angiography for exclusion of ACS in patients at low-to-intermediate risk of CAD with suspected acute coronary syndrome to confirm the diagnosis and evaluate the risk of future events (11). Although CAC quantification on non-contrast CT is widely acknowledged as an important decision tool for identifying

stable patients with coronary atherosclerosis who would benefit from preventive treatments, it is not used as a gatekeeper in patients with chest pain in the emergency department. Our results suggested that Agatston score-defined CAC on CCTA in the setting of NSTE-ACS may help risk stratify high-risk patients with non-IR UMI in combination of FAI assessment independent of stenosis assessment and high-risk plaque features. Further studies are needed to test if the prediction of non-IR UMI could be associated with worse prognosis after PCI in patients with a first clinical episode of NSTE-ACS.



Association of Agatston Score, Stenosis Severity, and FAI With Non-IR UMI

Agatston score-defined CAC quantification has emerged as one of the most reliable ways to estimate cardiovascular risk (17). Although the exact pathophysiological mechanisms causing UMI remain to be determined, our results agreed with the previous studies which demonstrated a significant association of angiographic stenosis severity and Agatston score with the presence of UMI (18, 19) in patients with stable CAD. Agatston score and stenosis severity could be the signature of the advanced

atherosclerotic burden, and the presence of UMI might represent the inter-relationship of the high-risk patient characteristics. The progression of atherosclerosis including plaque healing after asymptomatic rupture or erosion may lead to distal thrombosis and an increase in plaque burden and stenosis progression, resulting in the potential occurrence of UMI in the subtended territory (20–22).

It has been recently reported that the mean peri-coronary adipose tissue attenuation value expressed by FAI on CCTA is associated with cardiac mortality (14). FAI, a marker of

TABLE 5 | Prediction models for the presence of non-IR UMI.

Prediction model	C-statistics	P value	IDI	P value	NRI	P value
Clinical model 1	0.783	–	Reference	–	Reference	–
Clinical model 2	0.846	0.008	0.062	0.015	0.583	0.002

Clinical model 1 (EF + GRACE score + Agatston score + CT-derived stenosis). Clinical model 2 (EF + GRACE score + Agatston score + CT-derived stenosis + FAI). Non-IR UMI, non-infarct-related unrecognized myocardial infarction; IDI, integrated discrimination improvement; NRI, net reclassification index; EF, ejection fraction; CT, computed tomography; FAI, peri-coronary fat attenuation index.

perivascular inflammation, was significantly associated with the presence of non-IR UMI in this study. This finding may suggest that local inflammation caused by plaque instability could link with the occurrence of non-IR UMI. Recent studies reported the relationship between FAI and CCTA-derived unstable plaque features (23, 24). These vulnerable plaques with high inflammation may occasionally cause rupture or erosion, leading to debris liberation, distal embolization of the myocardium, and the occurrence of UMI. Recent studies have focused on the detection of vascular inflammation by using non-invasive imaging modalities such as positron emission tomography imaging (25, 26). A recent study reported that FAI was associated with 18F-fluorodeoxyglucose uptake (27), indicating the feasibility of CT attenuation of peri-coronary adipose tissue for detecting peri-coronary inflammation. Our study supports this notion and extends that vascular inflammation could be linked with non-IR UMI in patients with a first clinical episode of NSTEMI-ACS. Given the well-accepted association between atherosclerosis and inflammation, and the recently reported CANTOS study (28) and COLCOT trial (29) showing the link with anti-inflammatory therapy and the reduction of recurrent cardiovascular events, further studies are needed to test our hypothesis generating results and if anti-inflammatory intervention could reduce the FAI values and the occurrence of UMI.

Clinical Implications

Recent reports supported the clinical potentials and implications of CCTA in the ACS setting (8, 9). Previous investigations have suggested that the presence of UMI confers an increased risk of adverse events (2, 3, 7). Recently, the presence of unrecognized myocardial scar detected by LGE in patients presenting with first acute AMI has been reported to be associated with worse outcomes (6, 7). Although the current study lacks prognostic information, our findings suggest that CCTA in the setting of NSTEMI-ACS could provide the information of the previous occurrence of non-IR UMI and the status of vascular inflammation, potentially resulting in the risk stratification in these patients showing a wide heterogeneity in its symptoms and prognosis reported in patients with NSTEMI-ACS (30, 31). A recent study by Antiochos et al. reported, in a multicenter cohort study of patients with suspected coronary artery disease, that presence of UMI or clinically recognized MI portended an equally significant risk for death and MI, independently of the presence of ischemia (2). Further studies are required to test the clinical significance of CCTA in the setting of NSTEMI-ACS,

particularly with respect to the inflammatory status by FAI and the predictability of non-IR UMI and its prognostication.

Limitations

This study was a single center analysis of prospectively enrolled from the registry data and pertains an observational nature, and its inherent limitation exists. Rigorous exclusion criteria and the CMR protocol limited the number of study patients and may have resulted in a certain level of selection bias. Patients were screened after knowing the contraindications to CMR and the importance of ECG gating, leading to further selection bias, because we had no patients with metallic device implants, bronchospasm, claustrophobia, or atrioventricular block. Because patients are more likely to present with multivessel coronary artery disease in NSTEMI-ACS, compared with those with STEMI, determining the IR vessel in patients with NSTEMI-ACS can be challenging. The final call was discretion of the operator and consensus reading of two expert interventionalists, which was an important limitation of the present study. Although this study included a relatively large number of patients with pre-PCI CCTA and post-PCI CMR data, the present sample size still limited the confidence of the overall statistical analyses, as well as extensive subgroup analyses. The assessment of involved myocardial segments by a coronary stenosis was determined by the coronary anatomy, and no objective method was applied, although there are no universally accepted criteria for this purpose. Finally, this study lacks prognostic information and further large sample studies are needed to test the results obtained from the present study.

CONCLUSION

In patients with a first clinical episode of NSTEMI-ACS who underwent urgent PCI, the prevalence of non-IR UMI was 17.7 %. The comprehensive CCTA assessment including FAI, Agatston score, and stenosis severity could identify patients with non-IR UMI before invasive CAG. Our findings warrant further investigation to test if comprehensive CCTA assessment for the presence of non-IR UMI may provide prognostic information or guide intensive therapeutic strategy.

DATA AVAILABILITY STATEMENT

The raw data supporting the conclusions of this article will be made available by the authors, without undue reservation.

ETHICS STATEMENT

The studies involving human participants were reviewed and approved by Tsuchiura Kyodo General Hospital Ethics Committee. The patients/participants provided their written informed consent to participate in this study.

REFERENCES

- Boland LL, Folsom AR, Sorlie PD, Taylor HA, Rosamond WD, Chambless LE, et al. Occurrence of unrecognized myocardial infarction in subjects aged 45 to 65 years (the ARIC study). *Am J Cardiol.* (2002) 90:927–31. doi: 10.1016/S0002-9149(02)02655-3
- Antiochos P, Ge Y, Steel K, Bingham S, Abdullah S, Mikolich JR, et al. Imaging of clinically unrecognized myocardial fibrosis in patients with suspected coronary artery disease. *J Am Coll Cardiol.* (2020) 76:945–57. doi: 10.1016/j.jacc.2020.06.063
- Acharya T, Aspelund T, Jonasson TF, Schelbert EB, Cao JJ, Sathya B, et al. Association of unrecognized myocardial infarction with long-term outcomes in community-dwelling older adults: the ICELAND MI study. *JAMA Cardiol.* (2018) 3:1101–6. doi: 10.1001/jamacardio.2018.3285
- Schelbert EB, Cao JJ, Sigurdsson S, Aspelund T, Kellman P, Aletras AH, et al. Prevalence and prognosis of unrecognized myocardial infarction determined by cardiac magnetic resonance in older adults. *Jama.* (2012) 308:890–6. doi: 10.1001/2012.jama.11089
- Pride YB, Piccirillo BJ, Gibson CM. Prevalence, consequences, and implications for clinical trials of unrecognized myocardial infarction. *Am J Cardiol.* (2013) 111:914–8. doi: 10.1016/j.amjcard.2012.11.042
- Omori T, Kurita T, Dohi K, Takasaki A, Nakata T, Nakamori S, et al. Prognostic impact of unrecognized myocardial scar in the non-culprit territories by cardiac magnetic resonance imaging in patients with acute myocardial infarction. *Eur Heart J Cardiovasc Imaging.* (2018) 19:108–16. doi: 10.1093/ehjci/jex194
- Amier RP, Smulders MW, van der Flier WM, Bekkers S, Zweerink A, Allaart CP, et al. Long-term prognostic implications of previous silent myocardial infarction in patients presenting with acute myocardial infarction. *JACC Cardiovasc Imaging.* (2018) 11:1773–81. doi: 10.1016/j.jcmg.2018.02.009
- Kofoed KE, Kelbæk H, Hansen PR, Torp-Pedersen C, Høfsten D, Kløvgaard L, et al. Early versus standard care invasive examination and treatment of patients with non-ST-segment elevation acute coronary syndrome. *Circulation.* (2018) 138:2741–50. doi: 10.1161/CIRCULATIONAHA.118.037152
- Linde JJ, Kelbæk H, Hansen TF, Sigvardsen PE, Torp-Pedersen C, Bech J, et al. Coronary CT angiography in patients with non-ST-segment elevation acute coronary syndrome. *J Am Coll Cardiol.* (2020) 75:453–63. doi: 10.1016/j.jacc.2019.12.012
- Thygesen K, Alpert JS, Jaffe AS, Chaitman BR, Bax JJ, Morrow DA, et al. Fourth universal definition of myocardial infarction (2018). *Circulation.* (2018) 138:e618–e51. doi: 10.1161/CIR.0000000000000617
- Collet JP, Thiele H, Barbato E, Barthélémy O, Bauersachs J, Bhatt DL, et al. 2020 ESC Guidelines for the management of acute coronary syndromes in patients presenting without persistent ST-segment elevation. *Eur Heart J.* (2021) 42:1289–367. doi: 10.1093/eurheartj/ehab088
- Puymirat E, Taldir G, Aissaoui N, Lemesle G, Lorgis L, Cuisset T, et al. Use of invasive strategy in non-ST-segment elevation myocardial infarction is a major determinant of improved long-term survival: FAST-MI (French Registry of Acute Coronary Syndrome). *JACC Cardiovasc Interv.* (2012) 5:893–902. doi: 10.1016/j.jcin.2012.05.008
- Abbara S, Blanke P, Maroules CD, Cheezum M, Choi AD, Han BK, et al. SCCT guidelines for the performance and acquisition of coronary computed tomographic angiography: a report of the society of Cardiovascular Computed Tomography Guidelines Committee: Endorsed by the North American Society for Cardiovascular Imaging (NASCI). *J Cardiovasc Comput Tomogr.* (2016) 10:435–49. doi: 10.1016/j.jcct.2016.10.002
- Oikonomou EK, Marwan M, Desai MY, Mancio J, Alashi A, Hutt Centeno E, et al. Non-invasive detection of coronary inflammation using computed tomography and prediction of residual cardiovascular risk (the CRISP CT study): a post-hoc analysis of prospective outcome data. *Lancet.* (2018) 392:929–39. doi: 10.1016/S0140-6736(18)31114-0
- Sugiyama T, Kanaji Y, Hoshino M, Yamaguchi M, Hada M, Ohya H, et al. Determinants of pericoronary adipose tissue attenuation on computed tomography angiography in coronary artery disease. *J Am Heart Assoc.* (2020) 9:e016202. doi: 10.1161/JAHA.120.016202
- Schwitzer J, DeMarco T, Kneifel S, von Schulthess GK, Jörg MC, Arheden H, et al. Magnetic resonance-based assessment of global coronary flow and flow reserve and its relation to left ventricular functional parameters: a comparison with positron emission tomography. *Circulation.* (2000) 101:2696–702. doi: 10.1161/01.CIR.101.23.2696
- Budoff MJ, Shaw LJ, Liu ST, Weinstein SR, Mosler TP, Tseng PH, et al. Long-term prognosis associated with coronary calcification: observations from a registry of 25,253 patients. *J Am Coll Cardiol.* (2007) 49:1860–70. doi: 10.1016/j.jacc.2006.10.079
- Nordenskjöld AM, Hammar P, Ahlström H, Bjerner T, Duvernoy O, Eggers KM, et al. Unrecognized myocardial infarction assessed by cardiac magnetic resonance imaging—prognostic implications. *PLoS ONE.* (2016) 11:e0148803. doi: 10.1371/journal.pone.0148803
- Cha MJ, Kim SM, Kim Y, Kim HS, Cho SJ, Sung J, et al. Unrecognized myocardial infarction detected on cardiac magnetic resonance imaging: Association with coronary artery calcium score and cardiovascular risk prediction scores in asymptomatic Asian cohort. *PLoS ONE.* (2018) 13:e0204040. doi: 10.1371/journal.pone.0204040
- Burke AP, Kolodgie FD, Farb A, Weber DK, Malcom GT, Smialek J, et al. Healed plaque ruptures and sudden coronary death: evidence that subclinical rupture has a role in plaque progression. *Circulation.* (2001) 103:934–40. doi: 10.1161/01.CIR.103.7.934
- Mann J, Davies MJ. Mechanisms of progression in native coronary artery disease: role of healed plaque disruption. *Heart.* (1999) 82:265–8. doi: 10.1136/hrt.82.3.265
- Usui E, Yonetsu T, Kanaji Y, Hoshino M, Yamaguchi M, Hada M, et al. Optical coherence tomography-defined plaque vulnerability in relation to functional stenosis severity and microvascular dysfunction. *JACC Cardiovasc Interv.* (2018) 11:2058–68. doi: 10.1016/j.jcin.2018.07.012
- Goeller M, Tamarappoo BK, Kwan AC, Cadet S, Commandeur F, Razipour A, et al. Relationship between changes in pericoronary adipose tissue attenuation and coronary plaque burden quantified from coronary computed tomography angiography. *Eur Heart J Cardiovasc Imaging.* (2019) 20:636–43. doi: 10.1093/ehjci/jez013
- Goeller M, Achenbach S, Cadet S, Kwan AC, Commandeur F, Slomka PJ, et al. Pericoronary adipose tissue computed tomography attenuation and high-risk plaque characteristics in acute coronary syndrome compared with stable coronary artery disease. *JAMA Cardiol.* (2018) 3:858–63. doi: 10.1001/jamacardio.2018.1997
- Rudd JH, Warburton EA, Fryer TD, Jones HA, Clark JC, Antoun N, et al. Imaging atherosclerotic plaque inflammation with [18F]-fluorodeoxyglucose positron emission tomography. *Circulation.* (2002) 105:2708–11. doi: 10.1161/01.CIR.0000020548.60110.76
- Tawakol A, Migrino RQ, Bashian GG, Bedri S, Vermeylen D, Cury RC, et al. In vivo 18F-fluorodeoxyglucose positron emission tomography imaging provides a noninvasive measure of carotid plaque inflammation in patients. *J Am Coll Cardiol.* (2006) 48:1818–24. doi: 10.1016/j.jacc.2006.05.076

AUTHOR CONTRIBUTIONS

KM, MHo, and TK contributed to conception and design of the study. KM and MHo organized the database, performed the statistical analysis, and wrote the first draft of the manuscript. All authors contributed to manuscript revision, read, and approved the submitted version.

27. Antonopoulos AS, Sanna F, Sabharwal N, Thomas S, Oikonomou EK, Herdman L, et al. Detecting human coronary inflammation by imaging perivascular fat. *Sci Transl Med.* (2017) 9. doi: 10.1126/scitranslmed.aal2658
28. Ridker PM, Everett BM, Thuren T, MacFadyen JG, Chang WH, Ballantyne C, et al. CANTOS Trial Group: Anti-inflammatory Therapy with Canakinumab for Atherosclerotic Disease. *N Engl J Med.* (2017) 377:1119–31. doi: 10.1056/NEJMoa1707914
29. Tardif JC, Kouz S, Waters DD, Bertrand OF, Diaz R, Maggioni AP, et al. Efficacy and safety of low-dose colchicine after myocardial infarction. *N Engl J Med.* (2019) 381:2497–505. doi: 10.1056/NEJMoa1912388
30. McManus DD, Gore J, Yarzebski J, Spencer F, Lessard D, Goldberg RJ. Recent trends in the incidence, treatment, and outcomes of patients with STEMI and NSTEMI. *Am J Med.* (2011) 124:40–7. doi: 10.1016/j.amjmed.2010.07.023
31. Chan MY, Sun JL, Newby LK, Shaw LK, Lin M, Peterson ED, et al. Long-term mortality of patients undergoing cardiac catheterization for ST-elevation and non-ST-elevation myocardial infarction. *Circulation.* (2009) 119:3110–7. doi: 10.1161/CIRCULATIONAHA.108.799981

Conflict of Interest: The authors declare that the research was conducted in the absence of any commercial or financial relationships that could be construed as a potential conflict of interest.

Publisher's Note: All claims expressed in this article are solely those of the authors and do not necessarily represent those of their affiliated organizations, or those of the publisher, the editors and the reviewers. Any product that may be evaluated in this article, or claim that may be made by its manufacturer, is not guaranteed or endorsed by the publisher.

Copyright © 2022 Matsuda, Hoshino, Kanaji, Sugiyama, Misawa, Hada, Nagamine, Nogami, Sayama, Teng, Ueno, Yonetsu, Sasano and Kakuta. This is an open-access article distributed under the terms of the Creative Commons Attribution License (CC BY). The use, distribution or reproduction in other forums is permitted, provided the original author(s) and the copyright owner(s) are credited and that the original publication in this journal is cited, in accordance with accepted academic practice. No use, distribution or reproduction is permitted which does not comply with these terms.



Knowledge of Hyperemic Myocardial Blood Flow in Healthy Subjects Helps Identify Myocardial Ischemia in Patients With Coronary Artery Disease

OPEN ACCESS

Edited by:

Jinwei Tian,
The Second Affiliated Hospital of
Harbin Medical University, China

Reviewed by:

Francesca Pugliese,
Queen Mary University of London,
United Kingdom
Koen Nieman,
Stanford University, United States
Filippo Cademartiri,
Guglielmo Monasterio Tuscany
Foundation (CNR), Italy

*Correspondence:

Mei Zhang
daixh@vip.sina.com
Pengfei Zhang
pengf-zhang@163.com

[†]These authors have contributed
equally to this work and share senior
authorship

Specialty section:

This article was submitted to
Cardiovascular Imaging,
a section of the journal
Frontiers in Cardiovascular Medicine

Received: 18 November 2021

Accepted: 14 January 2022

Published: 03 February 2022

Citation:

Lyu L, Pan J, Li D, Li X, Yang W,
Dong M, Guo C, Lin P, Han Y, Liang Y,
Sun J, Yu D, Zhang P and Zhang M
(2022) Knowledge of Hyperemic
Myocardial Blood Flow in Healthy
Subjects Helps Identify Myocardial
Ischemia in Patients With Coronary
Artery Disease.
Front. Cardiovasc. Med. 9:817911.
doi: 10.3389/fcvm.2022.817911

Lijuan Lyu¹, Jichen Pan¹, Dumin Li², Xinhao Li¹, Wei Yang¹, Mei Dong¹, Chenghu Guo¹,
Peixin Lin¹, Yeming Han², Yongfeng Liang², Junyan Sun², Dexin Yu², Pengfei Zhang^{1*†}
and Mei Zhang^{1*†}

¹ The Key Laboratory of Cardiovascular Remodeling and Function Research, The State and Shandong Province Joint Key
Laboratory of Translational Cardiovascular Medicine, Department of Cardiology, Chinese Ministry of Education, Chinese
National Health Commission and Chinese Academy of Medical Sciences, Qilu Hospital, Cheeloo College of Medicine,
Shandong University, Jinan, China, ² Department of Radiology, Qilu Hospital, Cheeloo College of Medicine, Shandong
University, Jinan, China

Backgrounds: Dynamic CT myocardial perfusion imaging (CT-MPI) allows absolute quantification of myocardial blood flow (MBF). Although appealing, CT-MPI has not yet been widely applied in clinical practice, partly due to our relatively limited knowledge of CT-MPI. Knowledge of distribution and variability of MBF in healthy subjects helps in recognition of physiological and pathological states of coronary artery disease (CAD).

Objectives: To describe the distribution and normal range of hyperemic MBF in healthy subjects obtained by dynamic CT-MPI and validate whether it can accurately identify functional myocardial ischemia when the cut-off value of hyperemia MBF is set to the lower limit of the normal range.

Materials and Methods: Fifty-one healthy volunteers (age, 38 ± 12 years; 15 men) were prospectively recruited. Eighty patients (age, 58 ± 10 years; 55 men) with suspected or known CAD who underwent interventional coronary angiography (ICA) examinations were retrospectively recruited. Comprehensive CCTA + dynamic CT-MPI protocol was performed by the third – generation dual-source CT scanner. Invasive fractional flow reserve (FFR) measurements were performed in vessels with 30–90% diameter reduction. ICA/FFR was used as the reference standard for diagnosing functional ischemia. The normal range for the hyperemic MBF were defined as the mean ± 1.96 SD. The cut-off value of hyperemic MBF was set to the lower limit of the normal range.

Results: The global hyperemic MBF were 164 ± 24 ml/100 ml/min and 123 ± 26 ml/100 ml/min for healthy participants and patients. The normal range of the hyperemic MBF was 116–211 ml/100 ml/min. Of vessels with an ICA/FFR result ($n = 198$), 67 (34%) were functionally significant. In the per-vessel analysis, an MBF cutoff value of <116 ml/100 ml/min can identify myocardial ischemia with a diagnostic accuracy, sensitivity,

specificity, positive predictive value, and negative predictive value of 85.9% (170/198), 91.0% (61/67), 83.2% (109/131), 73.5% (61/83), and 94.8% (109/115). CT-MPI showed good consistency with ICA/FFR in diagnosing functional ischemia, with a Cohen's kappa statistic of 0.7016 (95%CI, 0.6009 – 0.8023).

Conclusion: Recognizing hyperemic MBF in healthy subjects helps better understand myocardial ischemia in CAD patients.

Keywords: computed tomography myocardial perfusion imaging, myocardial blood flow, fractional flow reserve, myocardial ischemia, coronary artery disease

INTRODUCTION

Coronary computed tomography angiography (CCTA) has become a reliable diagnostic technique to evaluate coronary artery disease (CAD) with high sensitivity and a negative predictive value (1–3). However, CCTA provides only anatomic information and tends to overestimate stenosis severity (2–4) and is limited in its ability to diagnose myocardial ischemia. Thus, CT myocardial perfusion imaging (CT-MPI) has been developed for myocardial blood flow (MBF) evaluation (5, 6). Combination of CCTA with CT-MPI can merge anatomical and physiological information, and provide a comprehensive interpretation of CAD.

Although appealing, CT-MPI has not yet been widely applied in clinical practice, partly due to our relatively limited knowledge of CT-MPI. In contrast to static perfusion imaging protocol, dynamic CT-MPI allows quantitative assessment of MBF. Beyond the assessment of the physiologic importance of a known epicardial stenosis, absolute MBF quantification offers potential advantages in identifying balanced ischemia and detection of microvascular disease. However, it is difficult to definitively classify quantitative MBF as normal or abnormal based on available knowledge. Understanding the normal blood flow distribution of the myocardial may have a role in the further delineation of these disease state. Previous publications with positron emission computed tomography (PET) (7, 8)

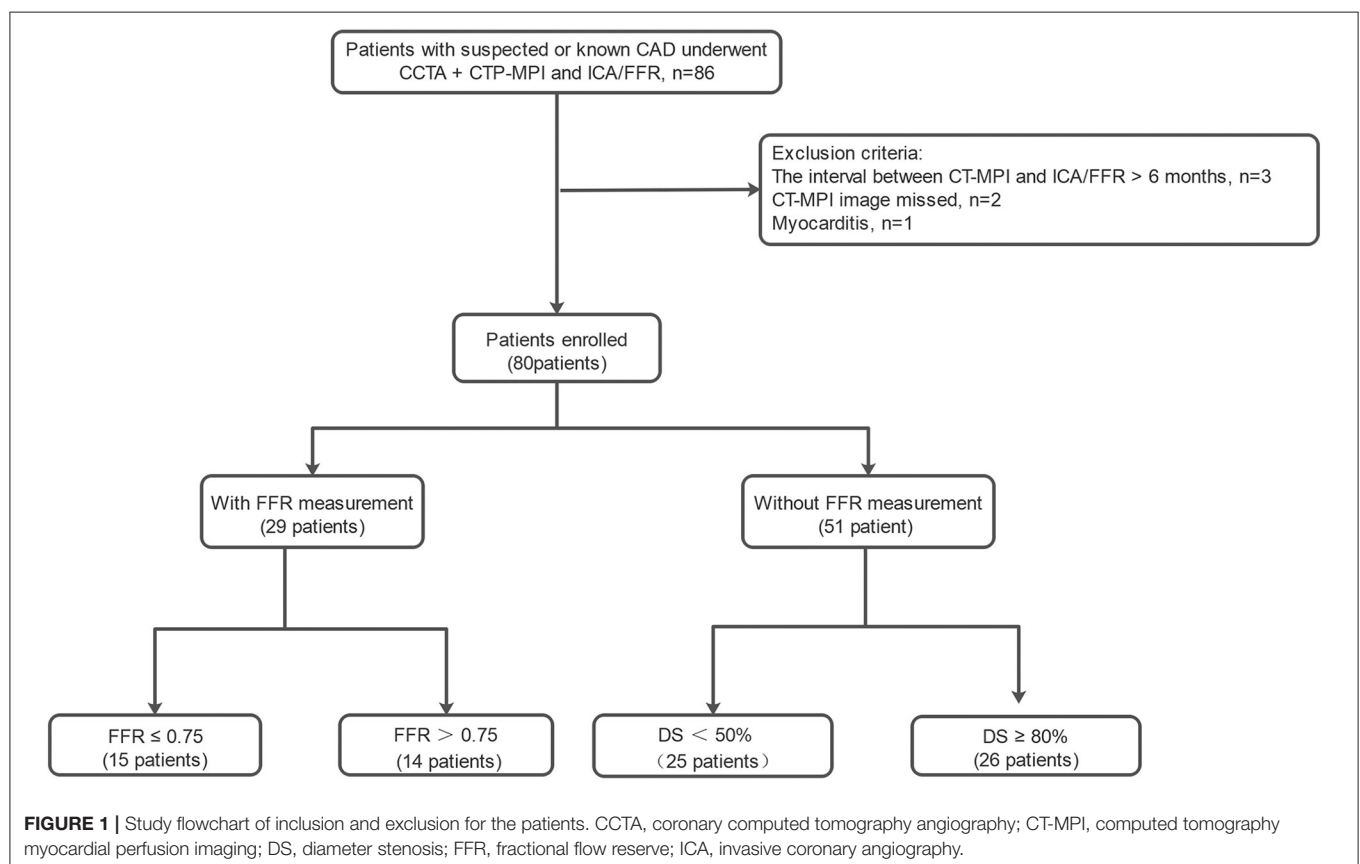


TABLE 1 | The demographic, clinical and imaging characteristics of healthy participants and patients.

Characteristics	Healthy participants (n = 51)	Patients (n = 80)	P-value
Age, years	38 ± 11.5	58 ± 10.1	<0.001*
Male gender (%)	16/51 (31)	55/80 (69)	<0.001*
Body mass index (kg/m ²)	22.7 ± 2.6	25.9 ± 3.0	<0.001*
Coronary risk factors			
Hypertension (%)	-	55/80 (69)	
Dyslipidemia (%)	-	73/80 (91)	
Diabetes (%)	-	19/80 (24)	
Smoking (%)	-	42/80 (53)	
Family history of CAD (%)	4/51 (8)	16/80 (20)	0.059
Symptoms			
Typical angina (%)	-	38/80 (48)	
Atypical angina (%)	-	35/80 (44)	
Non-cardiac chest pain (%)	-	7/80 (9)	
Distribution of coronary artery			
Right dominance (%)	49/51 (96)	77/80 (96)	
Left dominance (%)	1/51 (2)	2/80 (3)	
Balanced (%)	1/51 (2)	1/80 (1)	
Stenosis extent (diameter stenosis, %)			
<50 (%)	-	121/198 (61)	
50–90 (%)	-	36/198 (18)	
≥90 (%)	-	41/198 (21)	
Vessels with ischemic lesion	-	67/198 (34)	
Left anterior descending artery (%)	-	33/198 (17)	
Left circumflex coronary artery (%)	-	15/198 (8)	
Right coronary artery (%)	-	19/198 (10)	
Serum markers			
Cholesterol (mmol/L)	4.14 (3.45–4.86)	3.39 (2.99–4.25)	0.006*
HDL-C (mmol/L)	1.44 ± 0.30	1.11 ± 0.25	<0.001*
LDL-C (mmol/L)	2.24 (1.80–2.99)	1.86 (1.53–2.61)	0.119
Triglyceride (mmol/L)	0.86 (0.59–1.24)	1.31 (0.90–1.78)	<0.001*
Fasting plasma glucose (mmol/L)	4.83 (4.58–5.06)	5.13 (4.61–5.58)	0.034*
Creatinine (μmol/L)	63 (55–77)	68 (57–77)	0.254
Hemodynamic changes in CT-MPI scan protocol			
Rest heart rate (beats/min)	77 ± 12	72 ± 12	0.234
Stress heart rate (beats/min)	100 (89–109)	91 (78–103)	0.007*
Δ Heart rate (beats/min)	29 (20–32)	23 (17–29)	0.003*
Rest SBP (mmHg)	120 ± 13	136 ± 14	<0.001*
Rest DBP (mmHg)	73 ± 8	81 ± 10	<0.001*
Hyperemic MBF (ml/100 ml/min)	164 ± 24	123 ± 26	<0.001*

Measurement data are means ± standard deviations, or medians, with interquartile ranges in parentheses. Categorical data are numbers of patients or vessels, with percentages in parentheses. CAD, coronary artery disease; HDL-C, high density lipoprotein cholesterol; LDL-C, low density lipoprotein cholesterol; Δ Heart rate, Stress heart rate -Rest heart rate; CCTA, coronary computed tomography angiography; CT-MPI, computed tomography myocardial perfusion imaging; SBP, systolic pressure; DBP, diastolic pressure; MBF, myocardial blood flow.

*P-values < 0.05 refers to results of Student's t-tests for normal distribution data, Mann-Whitney U-tests for non-normal distribution data, and Chi-square test for Categorical data.

and magnetic resonance imaging (MRI) (9) have suggested absolute MBF values for normal participants and thresholds for discriminating ischemic myocardial disease. However, previous studies have shown that MBF values vary with different imaging modalities, and that CT underestimates the stress MBF of normal myocardia compared with PET (5, 7, 8, 10–13). Therefore, it is necessary to establish the normal range of MBF through

dynamic CT-MPI. To the best of our knowledge, only a few small-sample studies have reported the value ranges of MBF in normal subjects based on CT-MPI (11, 13). However, the results were inconsistent. The studies mentioned above were both performed on previous generation CT scanners but were conducted using different stressor. Apart from true variability, variability in MBF measurements can be affected by many

TABLE 2 | Regional distribution of hyperemic MBF.

	Hyperemic MBF (ml/100 ml/min)	P-value
Vessel territories		0.399
LAD	167 ± 24 (116–233)	
RCA	164 ± 24 (108–225)	
LCX	160 ± 25 (113–226)	
Regions		0.606
Anterior	165 ± 24 (117–218)	
Septum	165 ± 22 (115–243)	
Inferior	167 ± 28 (107–225)	
Lateral	160 ± 25 (108–225)	
Axial level		0.478
Basal	161 ± 23 (113–227)	
Middle	167 ± 25 (112–238)	
Apical	164 ± 25 (119–223)	

Data are means ± standard deviations; numbers in parentheses are ranges. The AHA 17 segments model of left ventricular were assigned to 3 major coronary arteries territories: LAD (segments 1, 2, 7, 8, 13, 14, and 17), RCA (segments 3, 4, 9, 10, and 15), LCX (segments 5, 6, 11, 12, and 16); four myocardial regions: anterior (Segments 1, 7, 13, 17), septum (Segments 2, 3, 8, 9, and 14), inferior (segments 4, 10, and 15), and lateral (segments 5, 6, 11, 12, and 16); and basal (segment 1–6), middle (segment 7–12), and apical (segment 13–16) for the analysis. MBF, myocardial blood flow; LAD, left anterior descending coronary artery; LCX, left circumflex coronary artery; RCA, right coronary artery.

P-values were derived from one-way ANOVA.

TABLE 3 | Hyperemic MBF of 17 segments.

Segments	Hyperemic MBF (ml/100 ml/min)
Basal anterior ^a	169 ± 27 (117–234)
Basal anteroseptal ^a	164 ± 25 (114–243)
Basal inferoseptal ^b	145 ± 20 (108–207)
Basal inferior ^a	169 ± 27 (108–221)
Basal inferolateral ^{ab}	158 ± 26 (94–237)
Basal anterolateral ^a	164 ± 27 (106–231)
Mid anterior ^a	169 ± 28 (104–229)
Mid anteroseptal ^a	177 ± 27 (114–272)
Mid inferoseptal ^a	171 ± 26 (121–250)
Mid inferior ^a	167 ± 29 (100–228)
Mid inferolateral ^{ab}	161 ± 27 (107–208)
Mid anterolateral ^{ab}	159 ± 25 (108–222)
Apical anterior ^{ab}	163 ± 24 (120–223)
Apical septal ^a	169 ± 26 (113–243)
Apical inferior ^a	165 ± 31 (105–233)
Apical lateral ^{ab}	160 ± 26 (112–209)
Apex ^{ab}	158 ± 26 (108–205)

Data are means ± standard deviations, numbers in parentheses are ranges. P-values were calculated with a one-way ANOVA and post-hoc Bonferroni to assess significance. MBF, myocardial blood flow; Min, minimum value; Max, maximum value.

Letter a and b indicate significant difference between segmental MBF values ($p < 0.05$), and letter ab represents the value has no significant difference with a and b ($p > 0.05$).

factors, such as heterogeneity of included patients, scanner, image acquisition and reconstruction, postprocessing software, and calculation algorithms. Nonetheless, as revealed by previous studies, scanner- and software-specific normal values of MBF is still of clinical importance to guide image interpretation of dynamic CT-MPI (14). To date, there is no report on the normal range of the hyperemic MBF in healthy subjects using a third – generation dual-source CT (DSCT) scanner.

In this study, we aimed to explore the normal range of the hyperemic MBF from dynamic CT-MPI in healthy individuals using the third – generation DSCT scanner. Based on the determined range of the hyperemic MBF, we also aimed to validate the diagnostic value of the lower limit of normal range of MBF for diagnosing myocardial ischemia defined by invasive coronary angiography (ICA)/fractional flow reserve (FFR).

MATERIALS AND METHODS

Study Population

Fifty-one healthy volunteers [age, 38 ± 12 years (22 – 59 years); 15 men] that completed adenosine-stressed dynamic CT-MPI between August 2019 and January 2021 were prospectively recruited by public advertising or from hospital staff. The inclusion criteria required that all volunteers be aged between 18 and 60 years, with normal blood pressure, normal blood lipid level, normal blood sugar level, normal effort tolerance, normal results upon physical examination and normal electrocardiogram, and transthoracic echocardiogram examination. The exclusion criteria were as follows: (a) any

medical history of heart disease; (b) risk factors for coronary artery disease; (c) angina pectoris or equivalent symptoms; (d) contraindications to adenosine or iodine contrast media; (e) any history of endocrine diseases, respiratory diseases, connective tissue disease, and anemia and severe abnormal liver function; (f) history of alcoholism; (g) pregnancy; (h) coronary with any stenosis by CCTA.

A total of 80 consecutive symptomatic patients [age, 58 ± 10 years (37–82 years); 55 men] who completed CT-MPI and invasive coronary angiography (ICA)/fractional flow reserve (FFR) examinations between August 2016 and January 2021 were retrospectively recruited and constituted the validation data set (**Figure 1**). The median interval between CT-MPI and ICA/FFR examinations was 9 (4–26) days. The inclusion criteria were suspected or known CAD with stable angina or angina-equivalent symptoms and being aged 18 years or older. The exclusion criteria were as follows: (a) acute coronary syndrome or clinical instability, (b) non-ischemic cardiomyopathy, (c) contraindications to adenosine or iodine contrast media, (d) pregnancy, (e) missed image, (f) the interval between CT-MPI and ICA/FFR more than 6 months.

The study was approved by the local institutional ethical committee. All enrolled participants gave written informed consent.

Sample Size Calculation

According to the diagnostic performance of dynamic CT MPI on the third – generation DSCT scanner reported by Li et al. (12) the vessel-based sensitivity and specificity of hyperemic myocardial

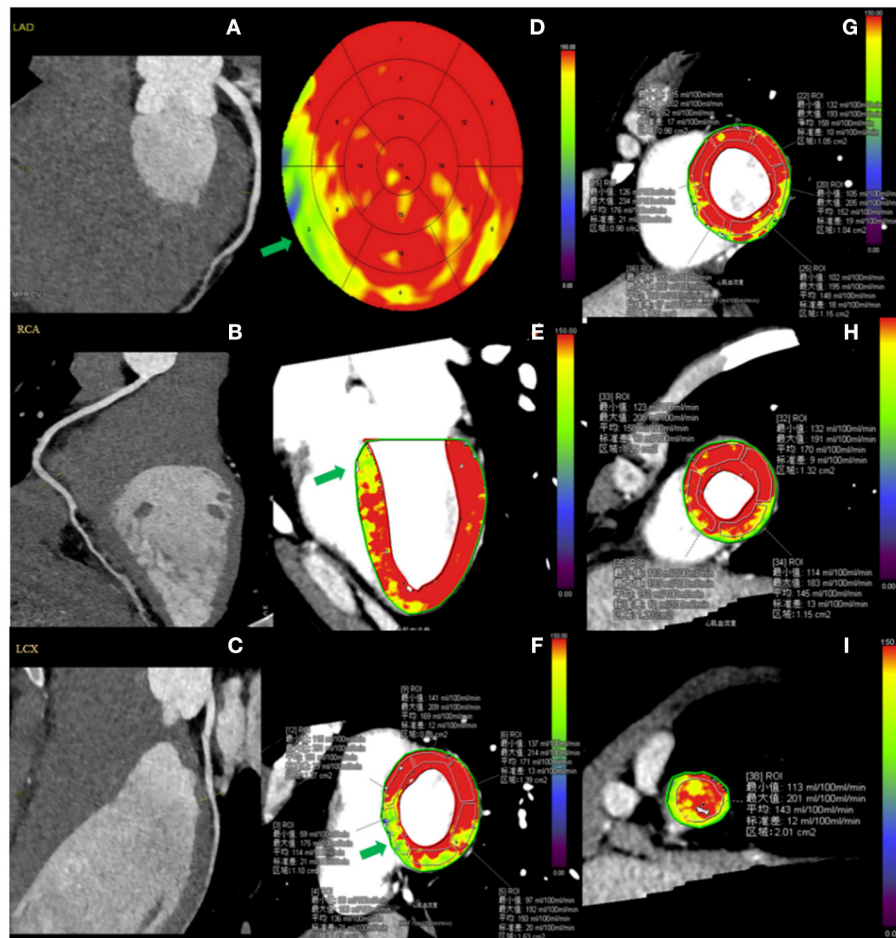


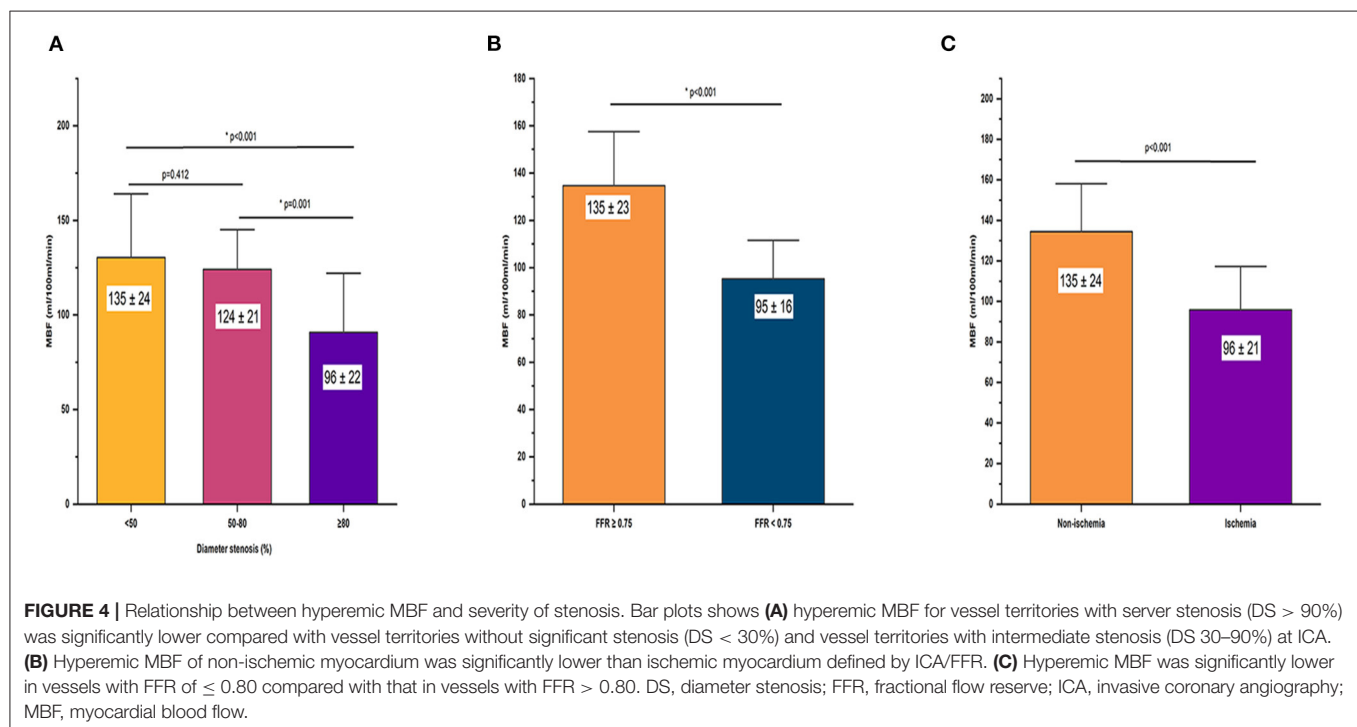
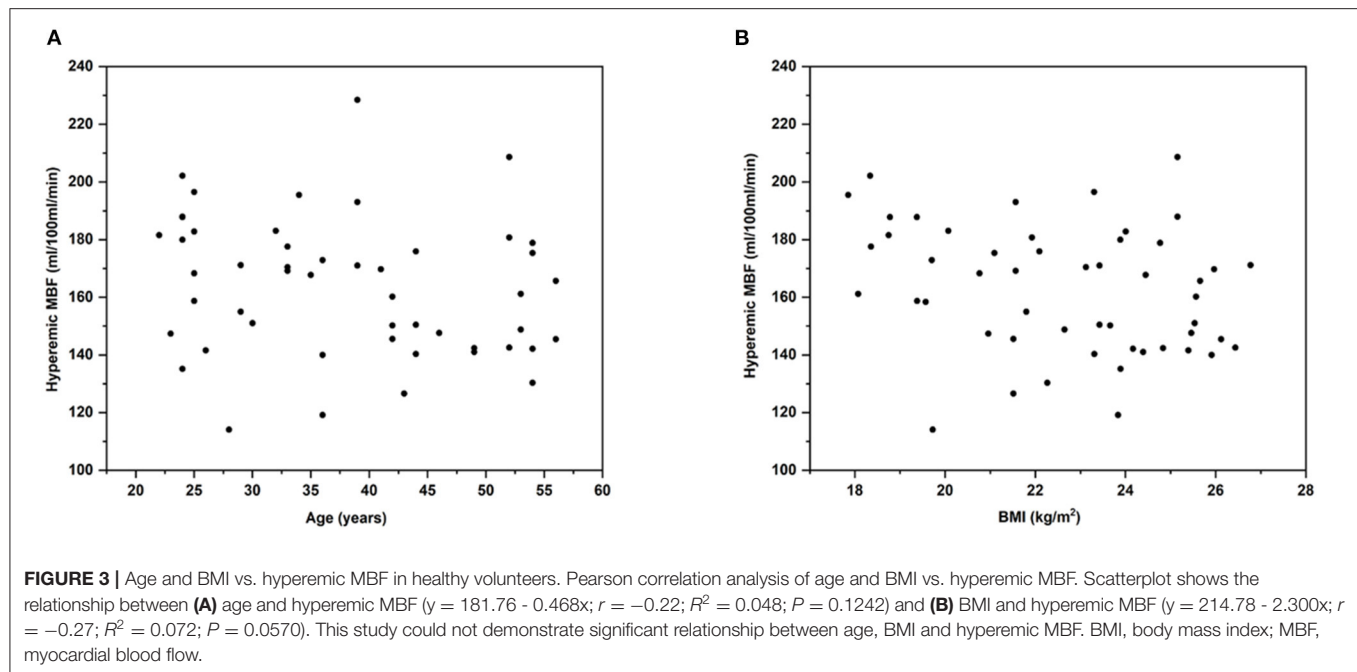
FIGURE 2 | Case example of CCTA and hyperemic MBF distribution in a healthy participant. A 29-year-old male healthy volunteer. (A–C) Resting CCTA shows no calcified plaque or stenosis in the coronary arteries. (D–I) Stress CT-MPI during adenosine infusion showed normal myocardial perfusion, as shown by relatively homogeneous color-coded images in the bull's eye diagram (D) and left ventricular long-axis view (E) and short-axis views (F–I). (D–F) The green arrow shows that the hyperemic MBF of basal-septum was lower than that of other segments. (F–G) ROI was manually placed in each myocardial segment as large as possible, excluding a 1 mm endocardial and epicardial borders to avoid image artifacts. CCTA, coronary computed tomography angiography; CT-MPI, computed tomography myocardial perfusion imaging; MBF, myocardial blood flow; ROI, Region of interest.

blood flow (MBF) for detecting hemodynamically significant stenosis are 96 and 93%, respectively. We assumed the sensitivity and specificity for hyperemic MBF to be equal to 95 and 90%. Based on these assumptions, using a two-sided binomial test, a total of 160 vessel participants were required to achieve 80% efficacy for rejecting the null hypothesis. The target significance level is 0.05. A total of 198 vessels were included, which provided >90% power. The sample size was estimated using Power Analysis and Sample Size software (version 15.0.5; PASS).

Dynamic CT-MPI and CCTA Protocol

All participants were scanned with a third – generation DSCT scanner (SOMATOM Force; Siemens Healthineers, Germany). A “one-stop” CT-MPI + CCTA protocol integrating calcium score, dynamic CT-MPI, and CCTA was employed. Initially,

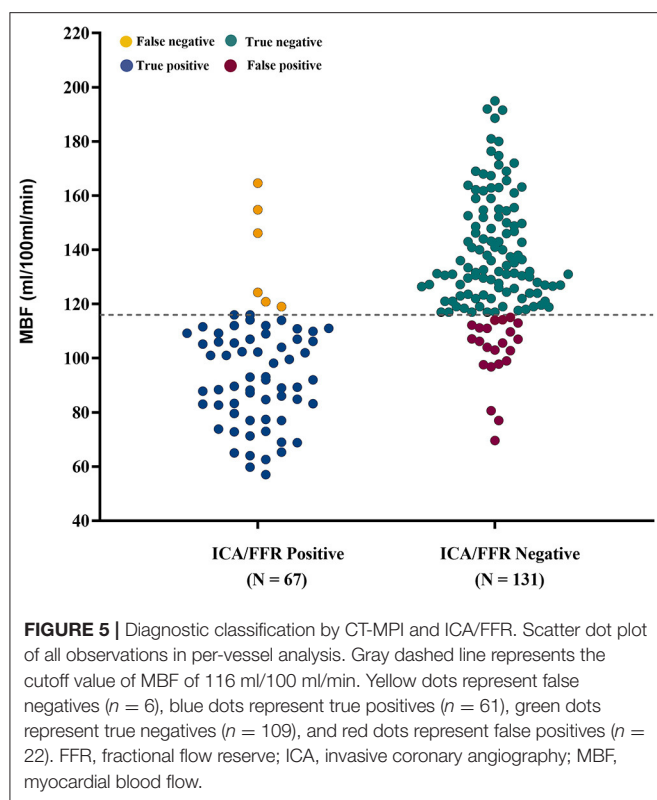
calcium score scan was performed. Then, dynamic CT-MPI was performed after 3 min of continuous adenosine administration at an infusion rate of 160 $\mu\text{g/kg/min}$. Iodinated contrast agent (100 mL; Ultravist, 370 mg iodine/mL, Bayer, Germany) was given in a bolus injection at a flow rate of 5.2 mL/s, followed by a 40 mL saline flush. Dynamic CT-MPI image acquisitions were started 4 s after contrast injection was started. The shuttle-mode acquisition technique is used to image the complete left ventricle. By moving the table back and forth after each acquisition, two series of images were collected, which together covered the entire myocardium. Dynamic image acquisition was performed in systole, 250 ms after the R - wave. Depending on heart rate, scans were launched every second or third heart cycle, resulting in a series of 10–15 data samples acquired over a period of ~32 s. The following scan parameters were used: collimation = 192×0.6 mm, gantry rotation time = 250 ms, temporal resolution =



66 ms, shuttle-mode z-axis coverage of 105 mm, tube voltage = 70 kV, and automated tube current scaling. CARE kV and CARE dose 4D was used to reduce radiation dose.

Nitroglycerin was given sublingually to all participants 5 min after CT-MPI. Subsequently, a bolus of contrast media was injected into the antecubital vein at a rate of 4–5 ml/s, followed by a 40 mL saline flush using a dual-barrel

power injector. Retrospective electrocardiography—triggered sequential acquisition was carried out in all patients undergoing CCTA, with the center of the triggering window set at diastole or systole, depending on the heart rate. With application of automated tube voltage and current modulation, the reference tube current was set as 320 mAs, and the reference tube voltage was set as 100 kV.



CCTA and CT-MPI Image Processing

The CT-MPI images were reconstructed with CT-MPI software package (VPCT body, Siemens Healthineers) using a dedicated kernel to reduce iodine beam-hardening artifacts (b23f, Qr36). All reconstructed images were transferred to a workstation (Syngo.Via VB10B; Siemens Healthineers) for analysis. Motion correction was performed for all images. Quantification of MBF was performed using a hybrid deconvolution model, as previously reported by Coenen et al. (15). To sample the MBF, the region of interest (ROI) was manually placed on short-axis view on a segment basis according to the American Heart Association (AHA) 17-segment model (16). The ROI was drawn to cover the whole segment without perfusion defect or cover the whole area of suspected perfusion defects within the segment. According to AHA recommendation, individual myocardial segments were assigned to the three major coronary arteries territories and was adjusted for differences in dominance (16). The global MBF was the mean MBF value of all 17 myocardial segments, and regional MBF was calculated as the average MBF value of the myocardial segments it included. Two experienced cardiovascular radiologists who were blinded to the participants' clinical history independently analyzed the CCTA and CT-MPI data. Image quality for each segment was assessed with a 4-point scale as previously described (17).

ICA and Invasive FFR

All patients underwent ICA with standard methods. All coronary arteries and main branches were evaluated by two

interventional cardiologists. During steady-state hyperemia, FFR was measured using a 0.014-inch pressure guidewire (Prime Wire Prestige PLUS, Volcano Corporation). Hyperemia was induced by intravenous infusion of adenosine at 140 mg/kg/min. FFR measurements were performed in intermediate stenosis (defined as a diameter reduction between 30 and 90% on visual assessment). Ischemic lesions were defined as lesions with more than 90% stenosis or intermediate lesions with $\text{FFR} \leq 0.80$. Non-ischemic lesions were defined as lesions with $<30\%$ stenosis or intermediate lesions with $\text{FFR} > 0.80$. Vessels causing ischemia were defined as arteries with one or more ischemic lesions. The most severe stenosis was considered for analysis in the same perfusion territory.

Statistical Analysis

The Shapiro–Wilk test was used to determine if the data had a normal distribution. Continuous variables were presented as the mean \pm standard deviation (SD) or as the median and quartile. ANOVA or Student's t -test was used for normally distributed data, and the Mann–Whitney U -test was used for non-normally distributed data. Bonferroni correction was applied for multiple comparisons. Categorical variables were presented as the number and proportion. The coefficient of variation (CV, %) of hyperemic MBF in both the volunteer group and patient group were calculated as $(\text{SD}/\text{mean}) \times 100\%$. Bivariate Pearson correlation analyses were performed between the age and hyperemic MBF and between BMI and hyperemic MBF. The normal range for hyperemic MBF was defined as that which would include 95% of the population. On the basis of the normality of data distribution, the normal range was calculated as the mean \pm SD \times 1.96. Cut-off value was defined as the lower limit of the normal range. Cohen's Kappa statistic was used to compare the MBF derived from CT-MPI with the ICA/FFR in diagnosing myocardial ischemia. Intra-observer and inter-observer agreements of MBF measurements were manually tested for intraclass correlation coefficients and by using Bland–Altman plots. Effective radiation dose was calculated by multiplying the dose-length product by a constant conversion factor ($k = 0.026 \text{ mSv/mGy/cm}$) (18). A 2-sided $p < 0.05$ was considered statistically significant. All statistical analyses were performed using an SPSS software package (SPSS 26.0; IBM) and a MedCalc software package (MedCalc 15.2.0).

RESULTS

Baseline Characteristics of Healthy Participants and Patients

Details of excluded patients are presented in **Figure 1**. Forty-two vessels from 80 enrolled patients with 30–90% luminal stenosis but without FFR were excluded from the analysis. A total of 198 vessels from 80 enrolled patients were ultimately included for the analysis. As shown in **Table 1**, the enrolled patients were mainly male and were significantly older and more overweight than the volunteers.

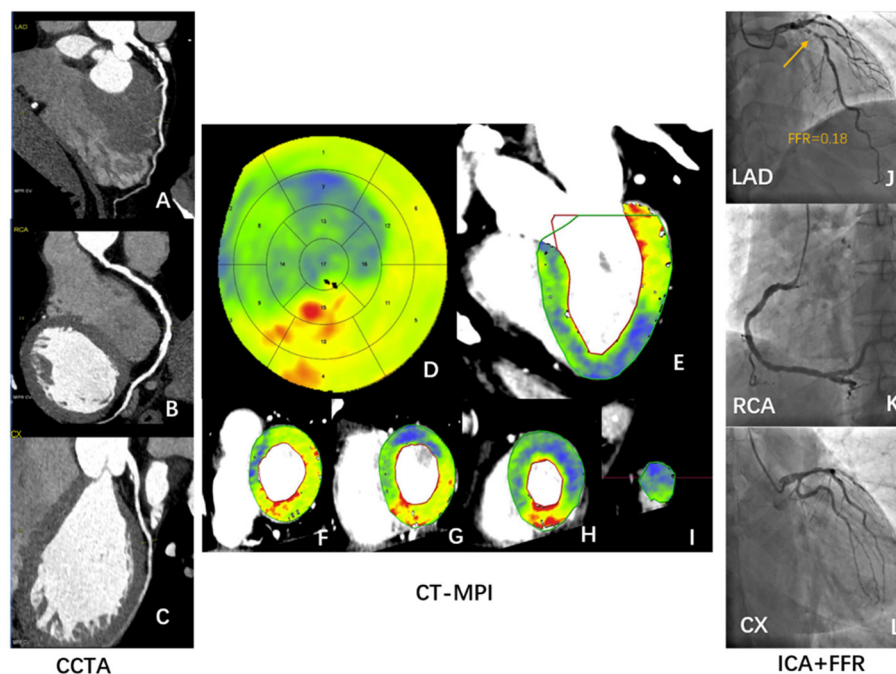


FIGURE 6 | Case illustrating hyperemic MBF can identify ischemic stenosis confirmed by ICA/FFR. A 56-year-old man who presented with a history of hypertension, current smoking, symptomatic for suspected angina, and a recent inconclusive 24 h' DCG. (A–C) Rest CCTA shows severe stenosis of distal LAD (A) and multiple mild stenosis of RCA (B). (D–I) Dynamic stress CT-MPI bull's eye diagram (D), long axis view (E), and short axis view (F–I) all show severe induced perfusion defects in the anterior wall, septum, and apical wall of left ventricle. The regional hyperemic MBF of LAD, RCA, LCX are 77 ml/100 ml/min, 126 ml/100 ml/min, and 107 ml/100 ml/min, respectively. (J–L) ICA shows severe proximal LAD stenosis (J) with positive invasive FFR (J). ICA shows multiple mild stenosis in RCA (K) and no stenosis of LCX (L). CCTA, coronary computed tomography angiography; CT-MPI, computed tomography myocardial perfusion imaging; DCG, dynamic cardiogram; FFR, fractional flow reserve; ICA, invasive coronary angiography; LAD, left anterior descending coronary artery; LCX, left circumflex coronary artery; MBF, myocardial blood flow; RCA, right coronary artery.

Image Quality and Radiation Dose of CCTA and CT-MPI

All participants tolerated the procedures well. **Supplementary Table E1** shows the image quality of CT-MPI. The proportion of non-diagnostic segments with poor image quality for the volunteer group and the patient group was 0.1 and 0.3%, respectively. The radiation doses of CCTA in healthy participants and patients were 11.1 (8.8 – 13.9) mSv and 13.6 (11.2 – 16.1) mSv, respectively. The radiation doses of dynamic stress CT-MPI in healthy participants and patients were 5.9 (4.6 – 9.0) mSv and 7.1 (5.6 – 9.0) mSv, respectively.

Hyperemic MBF of Healthy Participants

In healthy participants, the global hyperemic MBF was 164 ± 24 ml/100 ml/min (range 114–228 ml/100 ml/min; CV, 14.6%). Hyperemic MBF values were homogeneously distributed among myocardial regions (all $P > 0.05$, **Table 2**), but not among 17 myocardial segments ($P = 0.006$; **Table 3**). The hyperemic MBF of the basal inferoseptal (segment 3) was significantly lower than that of the other segments. Representative case examples are illustrated in **Figure 2**. There was no significant difference in the MBF between other myocardial segments.

Effect of Age, Gender, and BMI on Hyperemic MBF of Healthy Subjects

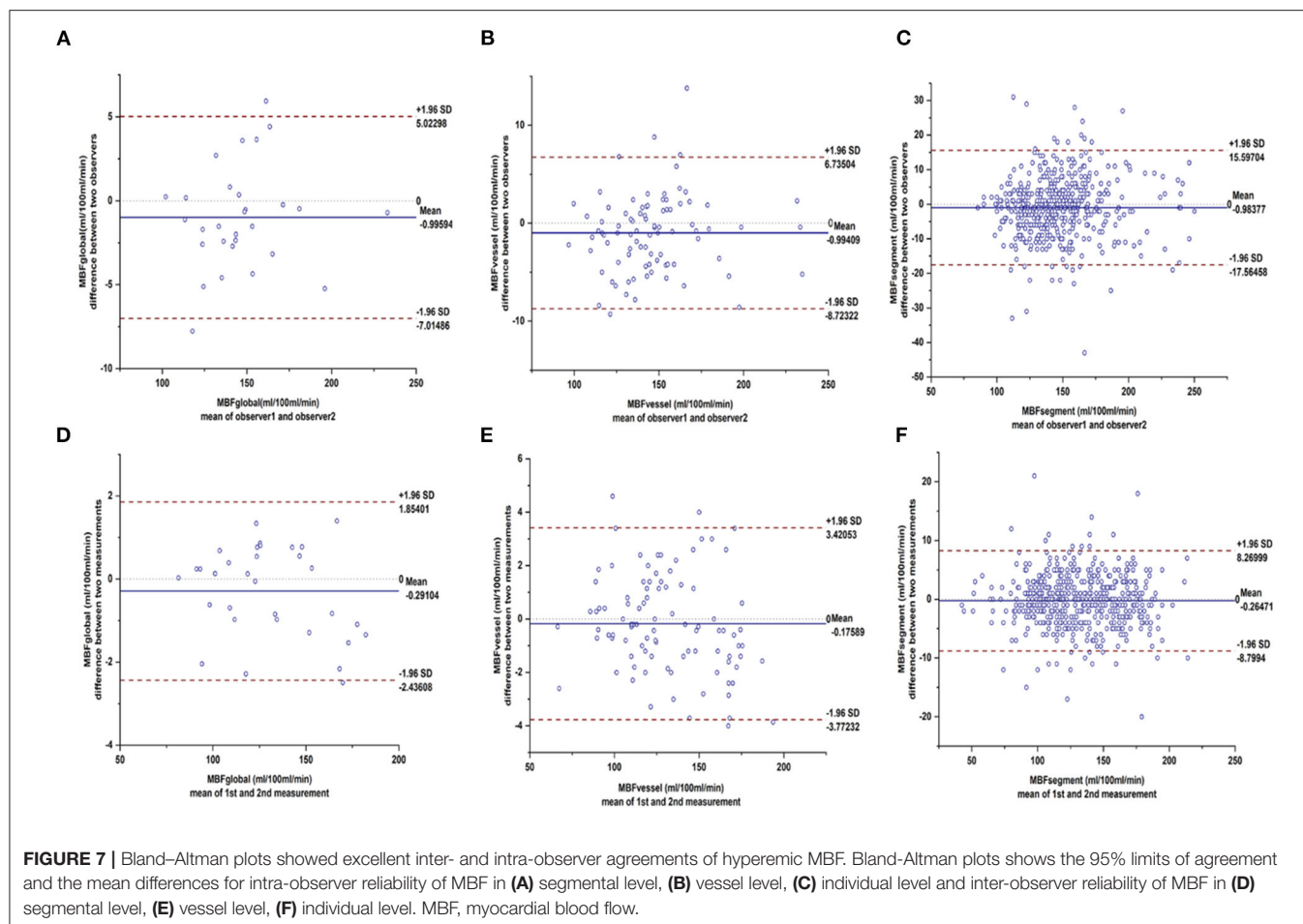
The hyperemic MBF in females appeared to be higher than that of males (168 ± 24 ml/100 ml/min vs. 155 ± 20 ml/100 ml/min, $P = 0.082$), but the difference was not statistically significant. No significant correlation between hyperemia MBF and age (**Figure 3A**) was observed. Similarly, no significant correlation between hyperemia MBF and body mass index (BMI) was observed normal volunteers (**Figure 3B**).

Normal Reference Range of Hyperemic MBF

According to the Shapiro-Wilk test, at the per-patient, per-vessel and per-segment levels, MBF were all normally distributed. In the per-vessel analysis, the regional MBF was 164 ± 24 ml/100 ml/min (range 108–233 ml/100 ml/min). The reference range of the regional MBF was 116–211 ml/100 ml/min.

Hyperemic MBF of Patients

Patients had lower global hyperemic MBF values (123 ± 26 ml/100 ml/min) and greater heterogeneity (CV, 21%) than healthy volunteers. In per-vessel analysis, the regional MBF of non-ischemic vessels was significantly lower than that of healthy



people (135 ± 24 ml/100 ml/min vs. 164 ± 24 ml/100 ml/min, $p < 0.001$) and higher than that of ischemic vessels (96 ± 201 ml/100 ml/min vs. 135 ± 24 ml/100 ml/min, $p < 0.001$). Details of the relationship between the MBF and stenosis severity were shown in Figure 4.

Diagnostic Performance of the Calculated Normal MBF Range for Predicting Ischemic Stenosis

Of the 198 vessels, 67 vessels were diagnosed as ischemic lesions by ICA/FFR. MBF with a cutoff value of <116 ml/100 ml/min showed good diagnostic performance in diagnosing ischemic lesions. The diagnostic accuracy, sensitivity, specificity, PPV, NPV and area under the curve (AUC) were 85.9% (170/198), 91.0% (61/67), 83.2% (109/131), 73.5% (61/83), 94.8% (109/115), and 0.871 [CI, 0.817 – 0.926], $p < 0.001$, respectively (Figure 5). With a cutoff value of 116 ml/100 ml/min, CT-MPI showed good consistency with ICA/FFR, with a Cohen's kappa statistic of 0.7016 (95% CI, 0.6009 – 0.8023). A representative case is illustrated in Figure 6.

Reproducibility of MBF Measurements

As shown in Figure 7, there was excellent intra- and inter-observer reproducibility of manual MBF measurements. The

intraclass correlation coefficients for the global MBF, regional MBF, and segmental MBF were 0.996, 0.991, and 0.990, respectively (all $p < 0.001$). The interclass correlation coefficients for the global MBF, regional MBF, and segmental MBF were 0.993, 0.989, and 0.955, respectively (all $p < 0.001$).

DISCUSSION

The main findings of the present study can be summarized as follows: (a) the hyperemic MBF was heterogeneous in both healthy individuals and patients; (b) patients had lower hyperemic MBF and greater heterogeneity than healthy subjects; and (c) the normal range hyperemic MBF with third-generation DSCT was 116–211 ml/100 ml/min. The normal range of hyperemic MBF defined in healthy subjects can help in the diagnosis of myocardial ischemia defined by ICA/FFR.

Cut-Off Values of Hyperemic MBF Assessed by CT

The lower limit of the normal range of MBF derived from healthy volunteers can help identify ischemia, and the diagnostic efficacy is comparable to that of previous studies (Table 4). Both the optimal cutoff of MBF and the MBF of the remote myocardium reported by Bamberg et al. (5), Greif et al. (19), and Rossi

TABLE 4 | Quantitative myocardial blood flow and ischemic cut-off values of stress MBF assessed by CT-MPI.

References	Equipment	Normal MBF (ml/100 ml/min)	Ischemic MBF (ml/100 ml/min)	Cutoff value (ml/100 ml/min)	Reference standard	Diagnostic accuracy	Sen	Spe	PPV	NPV	Objects (MI, revascularization)
Bamberg et al. (5)	2nd DSCT	104.8 ± 34.0	73.2 ± 26.0	75	FFR ≤ 0.75 + ICA ≥ 85% DS	N/A	N/A	N/A	N/A	N/A	Yes, yes
Greif et al. (19)	2nd DSCT	122.7 ± 34.0	78.7 ± 26.1	75	FFR ≤ 0.80 + ICA ≥ 90% DS	78.2	95.1	74.0	49.3	98.3	Yes, yes
Rossi et al. (20)	2nd DSCT	109	62	78	FFR ≤ 0.75 + ICA ≥ 90% DS	90	88	90	77	95	No, yes
Kono et al. (21)	2nd DSCT	116.3 ± 27	25.6 ± 22.5	103.1	FFR ≤ 0.80	68.1	88.9	47.8	62.5	81.5	No, no
Wichmann et al. (25)	2nd DSCT	140 ± 38.4	80.7 ± 33.7	103	CCTA ≥ 50% DS	62.9	82.4	80.5	60.1	92.8	No, no
Li et al. (12)	3st DSCT	169 ± 34	75 ± 20	99	FFR ≤ 0.80 + ICA ≥ 90% DS	94	96	93	92	96	No, no
Li et al. (22)	3st DSCT	133	78	89.5	FFR ≤ 0.80	90.5	84.3	97.7	97.7	84.3	No, no
Coenen et al. (15)	3st DSCT	108	79	91	MRI	68	75	61	63	73	No, no
Rossi et al. (24)	2nd DSCT	161	92 (74–109)	106	FFR ≤ 0.80 + ICA ≥ 80% DS	N/A	75	88.3	68.3	91.3	No, no
Pontone et al. (23)	Revolution CT	130 ± 46	96 ± 32	101	FFR ≤ 0.80 + ICA ≥ 80% DS	78	86	75	60	93	No, no
Yi et al. (10)	3st DSCT	147.5 ± 25.6	91.5 ± 29.9	N/A	FFR ≤ 0.80 + ICA ≥ 80% DS	92	83	99	98	90	No, no
Current study	3st DSCT	164 ± 24	96 ± 21	116	FFR ≤ 0.75 + ICA ≥ 80% DS	85.9	91.0	83.2	94.8	73.5	No, no

CCTA, Coronary computed tomography angiography; CT-MPI, computed tomography myocardial perfusion imaging; DS, diameter stenosis; DSCT, dual-source CT scanner; FFR, fractional flow reserve; ICA, interventional coronary angiography; MBF, myocardial blood flow; MI, myocardial infarction; NPV, negative predictive value; N/A, not reported; PPV, positive predictive value; Sen, sensitivity; Spe, specificity.

et al. (20) was significantly lower, which may be due to the fact that these studies included patients with MI and a history of revascularization. Studies excluding patients with a history of MI and a history of revascularization reported a cutoff value of MBF ranging from 89.5 to 106 ml/100 ml/min, and the MBF of the remote myocardium ranged between 116 ml/100 ml/min and 169 ml/100 ml/min (10, 12, 15, 21–25), which are consistent with the present study. Obviously, the severity of myocardial ischemia in patients affects the optimal cutoff value of MBF. In addition, coronary microvascular dysfunction (CMVD) may be another main pathophysiological factor leading to decreased MBF.

Aging, Sex, Body Mass Index, and Hyperemic Myocardial Blood Flow

The present study showed the hyperemic MBF was not significantly different between males and females, and similar findings were reported in previous studies using either adenosine or dipyridamole infusion in normal subjects (7, 26). In normal volunteers aged 22–59 years, this study did not find that hyperemic MBF declines with increasing age. According to Chareonthaitawee et al. (7) and Uren et al. (26), there was a significant decrease in the hyperemic MBF among healthy subjects aged over 65 or 70 years. These changes are likely to result from various factors associated with aging including endothelial dysfunction. Whether MBF reduction in the elderly is a pathological change due to possible CMVD is worth considering. Studies have shown that the increase in BMI is accompanied by endothelial dysfunction (27). Obesity is one of the risk factors for atherosclerosis (28). To define the range of true normal human myocardial perfusion as physiological guides in clinical studies or management, we selected young volunteers who were <60 years old and were not obese.

Spatial Heterogeneity of Myocardial Blood Flow

Describing the distribution of MBF in normal humans may assist us in better recognizing and understanding ischemia. The present study showed that the hyperemic MBF of the basal septum was lower than that of other segments, while the hyperemic MBF of the middle septum was higher than that of other segments. A similar phenomenon in adenosine-stress dynamic CT-MPI has previously been reported (6, 29). This spatial heterogeneity may have occurred due to the following reasons: (a) At the interventricular junction area, the membranous part of the septum is mainly formed by fibrous tissue, and the middle and apical part of the septum are mainly composed of muscular tissues. The difference in tissue composition and capillary distribution may be the basis of the spatial heterogeneity of the MBF in the septum. (b) Beam-hardening and motion artifacts may have substantial impact on image interpretation. Clinicians should be fully aware of the spatial heterogeneity of the MBF distribution as described above, to avoid unnecessary economic burden and psychological pressure on patients due to incorrect interpretation of the results of myocardial perfusion.

Limitations

Our study has several limitations. Firstly, this study was a small, single-center study and all images were obtained by third-generation DSCT scanner. The MBF value might vary from a different CT scanner, different MBF calculation methods, different pharmacological stressors and different ethnicities. The normal reference value range of MBF reported by our study may only be applicable to the scenario with similar examination and postprocess protocols, and MBF calculation methods. Secondly, all participants were Chinese, our findings not be extrapolated to other ethnicities or populations. Therefore, further studies are needed to establish a normal-value database for MBF and the present study contributes to that effort. Thirdly, the MBF derived from CT-MPI does not represent the true blood flow of the myocardium. Specifically, in CT imaging iodinated contrast agents have an extraction fraction in the range of 10–40% depending on the actual flow. This is a major confounder of MBF quantification as compared to other more realistic methods and leads to a systematic underestimation of MBF in CTP imaging. In addition, the limited temporal sampling rate of the shuttle mode and the hybrid deconvolution also contribute to the underestimation of MBF (30–33). Finally, we verified the diagnostic value of the MBF optimal cutoff value in patients with non-CAD and with severe ischemia, which might result in an overestimation of its diagnostic performance.

CONCLUSION

This study provides the normal range of hyperemic MBF in healthy subjects using a third-generation DSCT scanner. Recognizing hyperemic MBF in healthy subjects helps better understand myocardial ischemia in CAD patients. Developing a dataset for CT-MPI in a large-sample, multi-center, multi-ethnic, multi-vendor sources study in the future is challenging but promising.

DATA AVAILABILITY STATEMENT

The original contributions presented in the study are included in the article/**Supplementary Material**, further inquiries can be directed to the corresponding authors.

ETHICS STATEMENT

The studies involving human participants were reviewed and approved by Ethics Committee on Scientific Research of Shandong University Qilu Hospital [KYL-2016-336]. The patients/participants provided their written informed consent to participate in this study. Written informed consent was obtained from the individual(s) for the publication of any potentially identifiable images or data included in this article.

AUTHOR CONTRIBUTIONS

MZ and PZ: conceived and designed study and performed critical revision of the manuscript. LL: conceived and designed study,

analyzed data, prepared first draft, and revised subsequent drafts. JP, XL, WY, CG, PL, and MD: assisted in acquisition of CT imaging and contributed to analysis of data. XL, WY, and MD: assisted in acquisition of ICA/FFR data and contributed to analysis of data. DL, YL, and DY: designed and implemented CCTA + CT-MPI protocols, assisted in acquisition of imaging, and analysis of data. YH and JS: contribution to analysis of CCTA and CT-MPI data. All authors contributed to the article and approved the submitted version.

FUNDING

This work was supported by the National Key Research and Development Program of China [2016YFC1300302]

REFERENCES

- Budoff MJ, Dowe D, Jollis JG, Gitter M, Sutherland J, Halamert E, et al. Diagnostic performance of 64-multidetector row coronary computed tomographic angiography for evaluation of coronary artery stenosis in individuals without known coronary artery disease: results from the prospective multicenter ACCURACY (Assessment by Coronary Computed Tomographic Angiography of Individuals Undergoing Invasive Coronary Angiography) trial. *J Am Coll Cardiol.* (2008) 52:1724–32. doi: 10.1016/j.jacc.2008.07.031
- Meijboom WB, Meijis MF, Schuijff JD, Cramer MJ, Mollet NR, van Mieghem CA, et al. Diagnostic accuracy of 64-slice computed tomography coronary angiography: a prospective, multicenter, multivendor study. *J Am Coll Cardiol.* (2008) 52:2135–44. doi: 10.1016/j.jacc.2008.08.058
- Miller JM, Rochitte CE, Dewey M, Arbab-Zadeh A, Niinuma H, Gottlieb I, et al. Diagnostic performance of coronary angiography by 64-row CT. *N Engl J Med.* (2008) 359:2324–36. doi: 10.1056/NEJMoa0806576
- Nissen L, Winther S, Westra J, Ejlersen JA, Isaksen C, Rossi A, et al. Diagnosing coronary artery disease after a positive coronary computed tomography angiography: the Dan-NICAD open label, parallel, head to head, randomized controlled diagnostic accuracy trial of cardiovascular magnetic resonance and myocardial perfusion scintigraphy. *Eur Heart J Cardiovasc Imaging.* (2018) 19:369–77. doi: 10.1093/ehjci/jex342
- Bamberg F, Becker A, Schwarz F, Marcus RP, Greif M, von Ziegler F, et al. Detection of hemodynamically significant coronary artery stenosis: incremental diagnostic value of dynamic CT-based myocardial perfusion imaging. *Radiology.* (2011) 260:689–98. doi: 10.1148/radiol.11110638
- Wang Y, Qin L, Shi X, Zeng Y, Jing H, Schoepf UJ, et al. Adenosine-stress dynamic myocardial perfusion imaging with second-generation dual-source CT: comparison with conventional catheter coronary angiography and SPECT nuclear myocardial perfusion imaging. *Am J Roentgenol.* (2012) 198:521–9. doi: 10.2214/AJR.11.7830
- Chareonthaitawee P, Kaufmann PA, Rimoldi O, Camici PG. Heterogeneity of resting and hyperemic myocardial blood flow in healthy humans. *Cardiovasc Res.* (2001) 50:151–61. doi: 10.1016/S0008-6363(01)00202-4
- Murthy VL, Bateman TM, Beanlands RS, Berman DS, Borges-Neto S, Chareonthaitawee P, et al. Clinical quantification of myocardial blood flow using PET: joint position paper of the SNMMI cardiovascular council and the ASNC. *J Nucl Cardiol.* (2018) 25:269–97. doi: 10.1007/s12350-017-1110-x
- Muehling OM, Jerosch-Herold M, Panse P, Zenovich A, Wilson BV, Wilson RF, et al. Regional heterogeneity of myocardial perfusion in healthy human myocardium: assessment with magnetic resonance perfusion imaging. *J Cardiovasc Magn Reson.* (2004) 6:499–507. doi: 10.1081/JCMR-120030570
- Yi Y, Xu C, Wu W, Shen ZJ, Lee W, Yun CH, et al. Low-dose CT perfusion with combined use of CTP and CTP-derived coronary CT angiography at 70 kVp: validation with invasive fractional flow reserve. *Eur Radiol.* (2020) 31:1119–29. doi: 10.1007/s00330-020-07096-x
- Kim EY, Chung WJ, Sung YM, Byun SS, Park JH, Kim JH, et al. Normal range and regional heterogeneity of myocardial perfusion in healthy human myocardium: assessment on dynamic perfusion CT using 128-slice dual-source CT. *Int J Cardiovasc Imaging.* (2014) 30 Suppl 1:33–40. doi: 10.1007/s10554-014-0432-x
- Li Y, Yu M, Dai X, Lu Z, Shen C, Wang Y, et al. Detection of hemodynamically significant coronary stenosis: CT myocardial perfusion versus machine learning CT fractional flow reserve. *Radiology.* (2019) 293:305–14. doi: 10.1148/radiol.2019190098
- Ho KT, Ong HY, Tan G, Yong QW. Dynamic CT myocardial perfusion measurements of resting and hyperaemic blood flow in low-risk subjects with 128-slice dual-source CT. *Eur Heart J Cardiovasc Imaging.* (2015) 16:300–6. doi: 10.1093/ehjci/jeu200
- Sunderland JJ, Pan X-B, Declercq J, Menda Y. Dependency of cardiac rubidium-82 imaging quantitative measures on age, gender, vascular territory, and software in a cardiovascular normal population. *J Nucl Cardiol.* (2015) 22:72–84. doi: 10.1007/s12350-014-9920-6
- Coenen A, Rossi A, Lubbers MM, Kurata A, Kono AK, Chelu RG, et al. Integrating CT myocardial perfusion and CT-FFR in the work-up of coronary artery disease. *JACC Cardiovasc Imaging.* (2017) 10:760–70. doi: 10.1016/j.jcmg.2016.09.028
- Cerqueira MD, Weissman NJ, Dilsizian V, Jacobs AK, Kaul S, Laskey WK, et al. Standardized myocardial segmentation and nomenclature for tomographic imaging of the heart. A statement for healthcare professionals from the Cardiac Imaging Committee of the Council on Clinical Cardiology of the American Heart Association. *Circulation.* (2002) 105:539–42. doi: 10.1161/hc0402.102975
- Feuchtnr G, Goetti R, Plass A, Wieser M, Scheffel H, Wyss C, et al. Adenosine stress high-pitch 128-slice dual-source myocardial computed tomography perfusion for imaging of reversible myocardial ischemia: comparison with magnetic resonance imaging. *Circ Cardiovasc Imaging.* (2011) 4:540–9. doi: 10.1161/CIRCIMAGING.110.961250
- Trattner S, Halliburton S, Thompson CM, Xu Y, Chelliah A, Jambawalikar SR, et al. Cardiac-specific conversion factors to estimate radiation effective dose from dose-length product in computed tomography. *J Am Coll Cardiol Img.* (2018) 11:64–74. doi: 10.1016/j.jcmg.2017.06.006
- Greif M, von Ziegler F, Bamberg F, Tittus J, Schwarz F, D'Anastasi M, et al. CT stress perfusion imaging for detection of haemodynamically relevant coronary stenosis as defined by FFR. *Heart.* (2013) 99:1004–11. doi: 10.1136/heartjnl-2013-303794
- Rossi A, Dharampala A, Wragg A, Davies LC, van Geuns RJ, Anagnostopoulos C, et al. Diagnostic performance of hyperaemic myocardial blood flow index obtained by dynamic computed tomography: does it predict functionally significant coronary lesions? *Eur Heart J Cardiovasc Imaging.* (2014) 15:85–94. doi: 10.1093/ehjci/jet133
- Kono AK, Coenen A, Lubbers M, Kurata A, Rossi A, Dharampala A, et al. Relative myocardial blood flow by dynamic computed

and the Fundamental Research Funds of Shandong University [2018JC009].

ACKNOWLEDGMENTS

The authors thank Dr. Jihan Huang from Shanghai University of Traditional Chinese Medicine for providing us with statistical analysis consultation. We are grateful to American Journal Experts for professional English language editing support.

SUPPLEMENTARY MATERIAL

The Supplementary Material for this article can be found online at: <https://www.frontiersin.org/articles/10.3389/fcvm.2022.817911/full#supplementary-material>

- tomographic perfusion imaging predicts hemodynamic significance of coronary stenosis better than absolute blood flow. *Invest Radiol.* (2014) 49:801–7. doi: 10.1097/RLI.0000000000000087
22. Li Y, Dai X, Lu Z, Shen C, Zhang J. Diagnostic performance of quantitative, semi-quantitative, and visual analysis of dynamic CT myocardial perfusion imaging: a validation study with invasive fractional flow reserve. *Eur Radiol.* (2020) 31:525–34. doi: 10.1007/s00330-020-07145-5
 23. Pontone G, Baggiano A, Andreini D, Guaricci AI, Guglielmo M, Muscogiuri G, et al. Dynamic stress computed tomography perfusion with a whole-heart coverage scanner in addition to coronary computed tomography angiography and fractional flow reserve computed tomography derived. *JACC Cardiovasc Imaging.* (2019) 12:2460–71. doi: 10.1016/j.jcmg.2019.02.015
 24. Rossi A, Wragg A, Klotz E, Pirro F, Moon JC, Nieman K, Pugliese F. Dynamic computed tomography myocardial perfusion imaging: comparison of clinical analysis methods for the detection of vessel-specific ischemia. *Circ Cardiovasc Imaging.* (2017) 10:5505. doi: 10.1161/CIRCIMAGING.116.005505
 25. Wichmann JL, Meinel FG, Schoepf UJ, Lo GG, Choe YH, Wang Y, et al. Absolute versus relative myocardial blood flow by dynamic CT myocardial perfusion imaging in patients with anatomic coronary artery disease. *Am J Roentgenol.* (2015) 205:W67–72. doi: 10.2214/AJR.14.14087
 26. Uren NG, Camici PG, Melin JA, Bol A, de Bruyne B, Radvan J, et al. Effect of aging on myocardial perfusion reserve. *J Nucl Med.* (1995) 36:2032–6.
 27. Patel AR, Hui H, Kuvin JT, Pandian NG, Karas RH. Modestly overweight women have vascular endothelial dysfunction. *Clin Cardiol.* (2009) 32:269–73. doi: 10.1002/clc.20451
 28. Eckel RH, Krauss RM. American Heart Association call to action: obesity as a major risk factor for coronary heart disease. AHA Nutrition Committee. *Circulation.* (1998) 97:2099–100. doi: 10.1161/01.CIR.97.21.2099
 29. Yu L, Tao X, Dai X, Liu T, Zhang J. Dynamic CT myocardial perfusion imaging in patients without obstructive coronary artery disease: quantification of myocardial blood flow according to varied heart rate increments after stress. *Kor J Radiol.* (2021) 22:249. doi: 10.3348/kjr.2020.0249
 30. Bindschadler M, Modgil D, Branch KR, La Riviere PJ, Alessio AM. Comparison of blood flow models and acquisitions for quantitative myocardial perfusion estimation from dynamic CT. *Phys Med Biol.* (2014) 59:1533–56. doi: 10.1088/0031-9155/59/7/1533
 31. Ishida M, Kitagawa K, Ichihara T, Natsume T, Nakayama R, Nagasawa N, et al. Underestimation of myocardial blood flow by dynamic perfusion CT: explanations by two-compartment model analysis and limited temporal sampling of dynamic CT. *J Cardiovasc Comput Tomogr.* (2016) 10:207–14. doi: 10.1016/j.jcct.2016.01.008
 32. van Assen M, Pelgrim GJ, De Cecco CN, Stijnen JMA, Zaki BM, Oudkerk M, et al. Intermodel disagreement of myocardial blood flow estimation from dynamic CT perfusion imaging. *Eur J Radiol.* (2019) 110:175–80. doi: 10.1016/j.ejrad.2018.11.029
 33. van Assen M, Pelgrim GJ, Slager E, van Tuijl S, Schoepf UJ, Vliegenthart R, et al. Low CT temporal sampling rates result in a substantial underestimation of myocardial blood flow measurements. *Int J Cardiovasc Imaging.* (2019) 35:539–47. doi: 10.1007/s10554-018-1451-9

Conflict of Interest: The authors declare that the research was conducted in the absence of any commercial or financial relationships that could be construed as a potential conflict of interest.

Publisher's Note: All claims expressed in this article are solely those of the authors and do not necessarily represent those of their affiliated organizations, or those of the publisher, the editors and the reviewers. Any product that may be evaluated in this article, or claim that may be made by its manufacturer, is not guaranteed or endorsed by the publisher.

Copyright © 2022 Lyu, Pan, Li, Li, Yang, Dong, Guo, Lin, Han, Liang, Sun, Yu, Zhang and Zhang. This is an open-access article distributed under the terms of the Creative Commons Attribution License (CC BY). The use, distribution or reproduction in other forums is permitted, provided the original author(s) and the copyright owner(s) are credited and that the original publication in this journal is cited, in accordance with accepted academic practice. No use, distribution or reproduction is permitted which does not comply with these terms.



Artificial Intelligence—A Good Assistant to Multi-Modality Imaging in Managing Acute Coronary Syndrome

Ming-hao Liu^{1,2}, Chen Zhao^{1,2}, Shengfang Wang^{1,2}, Haibo Jia^{1,2*} and Bo Yu^{1,2*}

¹ Department of Cardiology, The 2nd Affiliated Hospital of Harbin Medical University, Harbin, China, ² The Key Laboratory of Myocardial Ischemia, Chinese Ministry of Education, Harbin, China

OPEN ACCESS

Edited by:

Zhao Wang,
University of Electronic Science and
Technology of China, China

Reviewed by:

Yasutomi Higashikuni,
University of Tokyo, Japan
Natalia Maroz-Vadlazzhskaya,
Minsk, Belarus

*Correspondence:

Haibo Jia
jh101180@163.com
Bo Yu
yubodr@163.com

Specialty section:

This article was submitted to
Cardiovascular Imaging,
a section of the journal
Frontiers in Cardiovascular Medicine

Received: 25 September 2021

Accepted: 29 December 2021

Published: 16 February 2022

Citation:

Liu M-h, Zhao C, Wang S, Jia H and
Yu B (2022) Artificial Intelligence—A
Good Assistant to Multi-Modality
Imaging in Managing Acute Coronary
Syndrome.
Front. Cardiovasc. Med. 8:782971.
doi: 10.3389/fcvm.2021.782971

Acute coronary syndrome is the leading cause of cardiac death and has a significant impact on patient prognosis. Early identification and proper management are key to ensuring better outcomes and have improved significantly with the development of various cardiovascular imaging modalities. Recently, the use of artificial intelligence as a method of enhancing the capability of cardiovascular imaging has grown. AI can inform the decision-making process, as it enables existing modalities to perform more efficiently and make more accurate diagnoses. This review demonstrates recent applications of AI in cardiovascular imaging to facilitate better patient care.

Keywords: acute coronary syndrome, artificial intelligence, machine learning, computed tomography, magnetic resonance, coronary angiography, intravascular ultrasound, optical coherence tomography

INTRODUCTION

Acute coronary syndrome (ACS) is a common type of coronary artery disease, which often leads to devastating consequences (1–3). Therefore, researchers and clinical practitioners have devoted countless efforts to the prevention, diagnosis, treatment, and rehabilitation of it. Various imaging modalities have emerged in this context, including non-invasive methods such as coronary computed tomographic angiography (CCTA), cardiac magnetic resonance (CMR), single-photon emission computed tomography (SPECT) myocardial perfusion imaging, and invasive approaches such as coronary angiography (CAG), intravascular ultrasound (IVUS), optical coherence tomography (OCT), fractional flow reserve (FFR), and near-infrared spectroscopy (NIRS), etc. Even though patients with ACS benefit comprehensively from the application of the above-mentioned imaging modalities, there are still gaps in understanding.

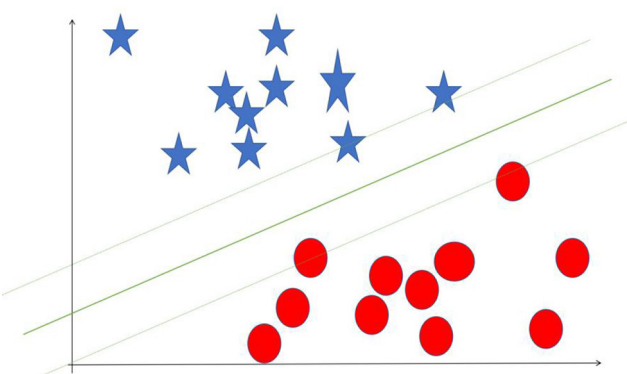
Artificial intelligence (AI) is a computerized program that resembles the human brain by collecting and processing data (4). With proper training, a variety of tasks that used to be undertaken by people can now be finished by AI. An overview of commonly used machine learning algorithms is shown in **Table 1**. Everyday life has already been extensively “infiltrated” by AI. A tremendous amount of work has already been put into cardiovascular imaging that combines AI, hoping to help clinicians achieve better healthcare for patients with ACS in particular. To date, scientific researchers have successfully developed AI to process imaging data, support diagnosis, interpret an image, provide treatment advice, recognize patterns of disease, and so on (**Figure 1**). Applications of AI in non-invasive modalities are summarized in **Table 2**, while applications in invasive ones are in **Table 3**. This review discusses recent applications of AI in cardiovascular imaging modalities related to ACS.

TABLE 1 | Overview of common AI algorithms.

Algorithm	Description	Illustration
Convolutional neural network (CNN)	A typical CNN consists of convolutional layer, max pooling layer and fully connected layer. Convolutional layer extracts features in the image, max pooling layer downsamples the features. Usually the former two layers repeat many times. Fully connected layer classifies the features from the former 2 layers	
eXtreme Gradient Boosting (XGBoost)	Based on gradient boosting decision tree, highly effective and flexible. It is a sparsity aware algorithm and a weighted quantile sketch for approximate learning	<div><div><p>Predict Disease</p><p>Tree 1</p><p>Chest pain</p><p>yes → cTnI ↑ → yes → AMI (+2) / no → Angina (+0.1)</p><p>no → Arrhythmia Heart Failure (-1)</p></div><div><p>Tree 2</p><p>ECG change</p><p>yes → ACS Arrhythmia (+0.9) / no → Cardiomyopathy (-0.9)</p></div></div> <p>$f(\text{AMI})=2.9$ $f(\text{dilated cardiomyopathy})=-1.9$</p>
Random forest (RF)	A supervised machine learning classifier. Consisted of many decision trees, it induces random feature selection during the training process. It output a single result after combining multiple decision trees	

(Continued)

TABLE 1 | Continued

Algorithm	Description	Illustration
Support vector machine (SVM)	A supervised machine learning method designed to solve two-group classification problem. It aims to find a hyperplane to mostly separate data of two groups	

APPLICATIONS OF AI IN NON-INVASIVE IMAGING MODALITIES

CT

CT-Derived FFR

CCTA has long been found to be a reliable method to give ACS an all-around evaluation. Cardiologists have used it to gain information, for example, relating to stenosis, calcification, plaque, lipid, and stent (40, 41). In recent years, a novel tool called computed tomography angiography-based fractional flow reserve (FFRCT) has emerged as a non-invasive alternative to traditional FFR obtained by pressure wire based on invasive CAG. Given that FFRCT involves a large amount of data collection and processing, artificial intelligence appears to have great potential for accomplishing such tasks.

Liu et al. acquired FFRCT in 243 symptomatic coronary artery disease (CAD) patients with deep learning (DL). In patients who had revascularization, major adverse cardiovascular event (MACE) rates in those with a DL-FFRCT value ≤ 0.8 (2.9%) were similar to those who had CAG-guided interventions (3.3%). If a DL-FFRCT value > 0.8 was interpreted as positive, calling for intervention as high as 72% of CAG should not be done (5).

According to recent studies (6, 7), CT-FFR could not only assist in deciding the intervention but also predict prognosis, as a non-invasive alternative to traditional FFR. Driessen et al. found the Pearson's and Spearman's correlation coefficients between CT-FFR and wire-based FFR were 0.80 and 0.67, respectively (42) although the automatic method was different in various studies.

Qiao et al. designed a "Functional SYNTAX score" (FSSCTA) to forecast prognosis in patients with three-vessel CAD. FSSCTA is a combination of anatomical characteristics and functional characteristics produced by machine learning (ML)-based CT-FFR evaluation. The MACE predicting ability of FSSCTA was compared with that of SSCTA and SSICA (based on CAG). The predictive accuracy of FSSCTA for MACE proved to be better. Revascularization strategies guided by traditional SS and FSSCTA were also compared. With FSSCTA, 52 (22.9%) patients

initially indicated for CABG guided by SSCTA would have been recommended to PCI (9).

With its non-invasive nature, CT-FFR significantly reduces costs by avoiding unnecessary CAG, as well as unnecessary anxiety and fear. Risk stratification tools should also consider updates by integrating with CT-FFR due to its easy accessibility and predictive power.

Markers Based on CT

Coronary artery calcium (CAC) has been shown to be powerful in predicting the extent and severity of CAD in symptomatic patients (43–45). Syntax score is used by interventionists and surgeons to assist in determining treating strategy as well as predicting outcome in patients who have had 3-vessel or left main CAD (46, 47). Studies have developed markers like CAC and Syntax score to assist in decision-making, prognosis predicting, and risk stratification, taking advantage of advances in artificial intelligence that have grown in recent decades.

A deep Convolutional Neural Network (CNN) is a powerful algorithm in image featuring. Zeleznik et al. confirmed that calcium on CCTA can be quantified automatically, moreover, the calcium score based on CNN can predict the outcome. CT readers localize the heart in cardiac CT, then segment the heart and the segment containing calcium, followed by the deep learning system automatically identifying and quantifying calcium. The AUC of the automatic method and manual approach was not different (8).

XGBoost is commonly applied in building predictive models, with the advantage of making weak classifiers into one single strong classifier. Featuring CT-based plaque qualitatively and quantitatively, Al' Aref et al. identified precursors of culprit lesion (CL) in ACS patients who had CAG. XGBoost algorithm was used to build a model predicting CLs. The predictive model performed well in discriminating CL precursors. The model also showed a specificity of up to 89.3% when tested in the non-ACS cohort (10). It may provide new insights into the target of secondary prevention of ACS.

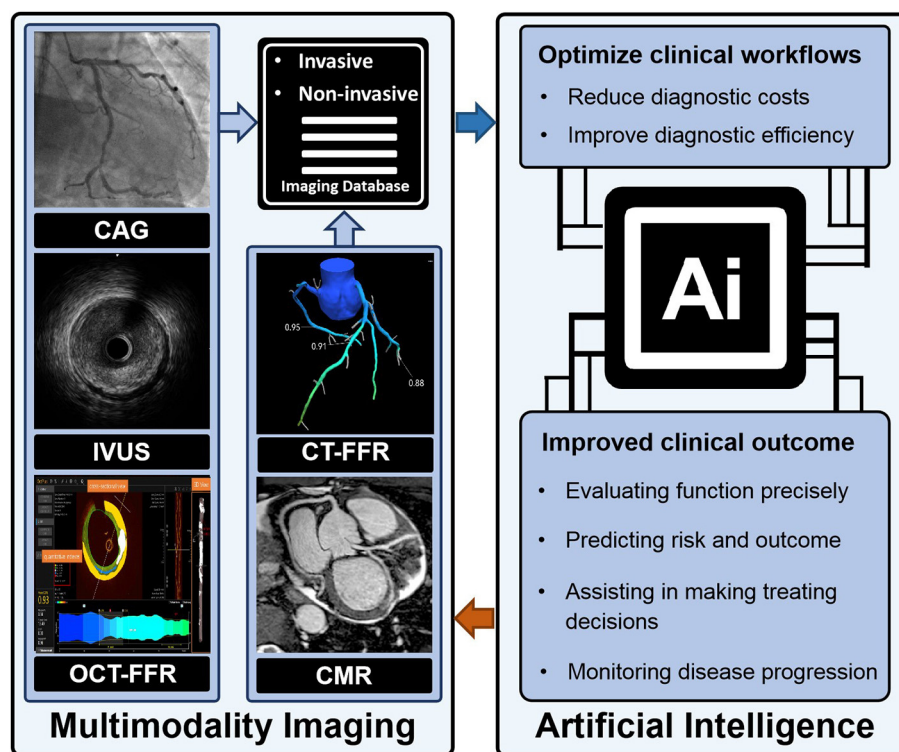


FIGURE 1 | AI and imaging.

Since XGBoost can identify culprit lesions, it can predict certain diseases theoretically, given the right data. CT radiomics have drawn attention from researchers who have then built models. Lin et al. successfully identified acute myocardial infarction (AMI) by building a machine learning model that combined a series of clinical factors and pericoronary adipose tissue attenuation with CT radiomic to identify AMI patients, achieving an AUC of 0.87 (11). With the help of powerful tools like XGBoost, radiomics can be of enormous use on multiple levels. We can expect that image biomarkers derived from CT radiomics will contribute to more precise diagnoses, risk stratification (29), and even clinical recommendations in the future.

Serum biomarkers also possess predicting capability, just like imaging biomarkers. XGboost was again proven to be capable of predicting cardiac events based on serum biomarkers integrating other data (12). We look forward to seeing what radiomics combining serum biomarkers can achieve.

Outcome Prediction

Atherosclerotic plaque features and stenosis can be evaluated qualitatively and quantitatively, providing comprehensive information to clinical practitioners, further enabling the prognostic prediction of ACS events (48–50).

A functional assessment like FFR and adverse cardiac events can both be predicted by CCTA features. Deciding on these features in a traditional way involves enormous statistical analysis. However, ML algorithms can finish the job, not only

saving time and costs but also providing important information on potential intervening targets.

Yang et al. used Boruta and hierarchical clustering to identify the relevant features correlated with low FFR. They then assessed the ability to predict vessel-level adverse incidents in 5 years. In total, six features were identified as associated with low FFR. With the 6 relevant features increasing, the risk of vessel level adverse incidents in 5 years increased. Additionally, it is a better prognostic predictor than percent diameter stenosis and FFR (13). Additionally, random forest (RF) can also pick up features out of 1,000 radiomics which can strengthen the power of predicting MACE (14).

Applications of AI in MR

Cardiac magnetic resonance (CMR) plays a pivotal part in comprehensively evaluating myocardial infarction (51). Cine and late gadolinium enhancement (LGE) sequences are most frequently referred to in this context. Functional evaluation is mainly performed by cine sequences because the movement can be captured by them (52). Detection of myocardial injury makes LGE sequence critical in diagnosing myocardial infarction (53).

Differentiating Diagnosis

In patients in whom AMI is complicated by chronic myocardial infarction (CMI) it is crucial to distinguish AMI and CMI for the sake of treatment and follow-up. However, ECG and coronary angiography provide limited information to pinpoint acute injury.

TABLE 2 | Applications of AI in non-invasive modalities.

References	Modality	Purpose	Samples	Algorithm	Results
Liu et al. (5)	CT	Investigate CT-FFR as an alternative in deciding on intervention	243 patients	Tree-structured RNN	MACE rate with a CT-FFR value ≤ 0.8 (2.9%) similar to that of CAG-guided interventions (3.3%) ($p = 0.838$)
Duguay et al. (6)	CT	Investigate the prognostic value of CT-FFR	48 patients	Deep neural network	CT-FFR ≤ 0.80 has a HR of 1.56 [1.01–2.83], ($p = 0.048$) to predict MACE
Eberhard et al. (7)	CT	Evaluate feasibility and clinical role of CT-FFR	56 patients	Deep neural network	Agreement of 81% in CT-FFR and clinical diagnosis of ACS
Zeleznik et al. (8)	CT	Validate an automatic method of quantifying coronary calcium	20,084 patients	Deep CNN (fully) of U-net architecture	Spearman's correlation of 0.92 ($P < 0.0001$) to manual measurement. Strong predictor of cardiovascular events (multivariable-adjusted HR up to 4.3)
Qiao et al. (9)	CT	Investigate if FSS _{CTA} can predict outcome in three vessel CAD patients	227 patients	Deep neural network	FSS _{CTA} (OR = 1.21, $P = 0.001$). Predictive accuracy for MACE of FSS _{CTA} AUC: 0.81, $P = 0.01$
Al'Aref et al. (10)	CT	Identify culprit lesion precursors among ACS patients based on CT-based plaque characteristics	468 patients	XGBoost	ML model's AUC of identifying culprit lesion precursors of 0.774 (CI: 0.758–0.790)
Lin et al. (11)	CT	Determine whether CT-based PCAT can distinguish patients with AMI with those with stable angina or no CAD	180 patients	XGBoost	AUC 0.87 in discriminating AMI
Tamarappoo et al. (12)	CT	Assess an ML risk score to predict long-term hard cardiac events	1,069 patients	XGBoost	The ML risk score AUC 0.81
Yang et al. (13)	CT	Lumen narrowing and plaque characteristics to predict ischaemia and outcome	1,013 vessels	Boruta and hierarchical clustering	Six features predicting low FFR AUC 0.797 ($P < 0.001$). AUC of them predicting vessel-oriented composite outcome 0.706 ($p = 0.031$)
Oikonomou et al. (14)	CT	Find FRP that can predict MACE	1,777 patients	RF	The coronary FRP signature can predict MACE (C-statistic 0.77 [95% CI: 0.62–0.93])
Larroza et al. (15)	CMR	Texture features to differentiate AMI	44 patients	RF SVM	Polynomial SVM AUC of 0.86 ± 0.06 on LGE MRI, AUC of 0.82 ± 0.06 on cine MRI
Schuster et al. (16)	CMR	Investigate feasibility and prognostic implications of AI-based software analysis	1,017 patients	suiteHEART, v4.0.6; Neosoft	Manual and automated volumetric assessments' impact on outcome (manual: HR, 0.93; automated: HR, 0.94)
Ma et al. (17)	CMR	Feature study on CMR to diagnose myocardial injury in AMI	68 patients	ML	Radiomics and T1 values AUC of 0.88 (training set) and 0.86 (test set) in diagnosing MVO
Knott et al. (18)	CMR	Explore the prognostic significance of MBF and MPR	1,049 patients	CNN	MBF: adjusted HR for death and MACE 1.93 and 2.14 MPR: adjusted HR for death and MACE 2.45 and 1.74
Groepenhoff et al. (19)	CCTA CMR integrated	Calculate the incidence of macrovascular and microvascular disease in women and men, develop a decision-support tool	400 patients expected	ML	Actively recruiting participants
Dekker et al. (20)	LDACCT during MPI	Investigate the association of automated CAC scores and MACE	747 patients	CNN	High CAC scores has HR of 2.19 in predicting MACE

CT, computed tomography; FFR, fractional flow reserve; RNN, recurrent neural network; RF, random forest; MACE, major adverse cardiovascular event; CAG, coronary angiography; HR, hazard ratio; ACS, acute coronary syndrome; CNN, convolutional neural network; FSS, functional syntax score; OR, odds ratio; AUC, area under curve; CI, confidence interval; PCAT, pericoronary adipose tissue; CAD, coronary artery disease; ML, FRP, fat radiomic profile; CMR, cardiac magnetic resonance; SVM, support vector machine; LGE, late gadolinium enhancement; MVO, microvascular obstruction; MBF, myocardial blood flow; MPR, myocardial perfusion reserve; LDACCT, low dose attenuation computed tomography; MPI, myocardial perfusion imaging; CAC, coronary artery calcium.

Larroza et al. used machine learning and extracted texture features in CMR images from 22 AMI patients and 22 CMI patients. They analyzed cine and LGE MRI separately to classify AMI and CMI. By evaluating the classification performance of three predictive models based on ML extracting texture features, the best performance was yielded by the polynomial SVM. It was demonstrated that feature analysis can be applied in differentiating AMI from CMI on both cine and LGE CMR (15).

The imaging features that can separate the two groups were carefully selected by SVM classifier.

Predicting Prognosis

CMR is regarded to be a gold-standard non-invasive modality for assessing cardiac function quantitatively and characterizing myocardium after MI (54, 55).

TABLE 3 | Applications of AI in invasive modalities.

References	Modality	Purpose	Samples	Algorithm	Results
Howard et al. (21)	CAG	Identify damping in arterial pressure waveform	5,709 beats	CNN	Sensitivity 100%, specificity 99.8%, positive predictive value 98.1%, negative predictive value 99.5%
Moon et al. (22)	CAG	Recognize and localize stenosis	452 movie clips	CNN	Frame-wise AUC 0.971, frame-wise accuracy 0.934, clip-wise accuracy 0.965
Roguin et al. (23)	CAG	Estimate FFR	31 patients	ANN	Sensitivity 88%, specificity 93%, positive predictive value 94%, negative predictive value 87%
Yabushita et al. (24)	CAG	Detect stenosis	199 patients, 1,838 videos	CNN	Predictive accuracy: AUC 0.61
Zhao et al. (25)	CAG	Calculate FFR	137,126 images	CNN	Correlation between CFR _{auto} and CFR _{manual} : $r = 0.51$
Du et al. (26)	CAG	Comprehensive analysis	20,612 angiograms	GAN CNN	F1-scores: stenosis, 0.829; total occlusion, 0.810; calcification, 0.802; thrombosis, 0.823; dissection, 0.854.
Lee et al. (27)	OCT	Developed an automated atherosclerotic plaque characterization method	6,556 images	CNN RF	Sensitivities/specificities: fibrolipidic plaques 84.8/97.8% fibrocalcific plaques 91.4/95.7%
Chu et al. (28)	OCT	Automatically characterize OCT plaques	509 pullbacks	CNN	Diagnostic accuracy: fibrous plaque 97.6%, lipid 90.5%, calcium 88.5%
Xu et al. (29)	OCT	Identify fibroatheroma with deep features	360 images	AlexNet, VGG-16, VGG-19, and GoogLeNet; SVM	Classification accuracy: Alexnet 0.7333, VGG-16 0.7611, VGG-19 0.7639, GoogLeNet 0.7333
Prabhu et al. (30)	OCT	Identify fibrolipidic and fibrocalcific A-lines in OCT images	6,556 images	SVM	Overall accuracy 81.58% sensitivity/specificity: other (81.43/89.59), fibrolipidic (94.48/87.32), fibrocalcific (74.82/95.28)
Shi et al. (31)	OCT	Boost the performance of recognizing vulnerable plaques	2,300 images	Fully CNN Deep CNN	Final score: 0.8767
Liu et al. (32)	OCT	Improve the detection quality of vulnerable plaque	2,300 images	Deep CNN	Precision rate 88.84%, recall rate 95.02%, overlap rate 85.09%; detection quality score 88.46%
Lee et al. (33)	OCT	Characterize coronary calcified plaque in OCT images	8,231 images	CNN	Sensitivity 97.7%, specificity 87.7%, F1 score 0.922
Cha et al. (34)	OCT	Compare OCT-FFR with wire-based FFR	125 patients	RF	Sensitivity 100%, specificity 92.9%, positive predictive value 87.5%, negative predictive value 100%, and accuracy 95.2%
Johnson et al. (35)	OCT	Use transcriptomic data to predict FCT change	69 patients	Elastic net K top scoring pair	Classification AUC = 0.969 and 0.972
Bae et al. (36)	IVUS	Develop ML models for predicting OCT-TCFA	517 patients	ANN SVM naïve Bayes	ANN: $81 \pm 5\%$ (AUC = 0.80 ± 0.08) SVM: $77 \pm 4\%$ (AUC = 0.74 ± 0.05) naïve Bayes: $78 \pm 2\%$ (AUC = 0.77 ± 0.04)
Jun et al. (37)	IVUS	Find the most accurate classifier to classify TCFA	12,325 images	FNN KNN RF CNN	AUC of: FNN: 0.859, KNN: 0.848, RF: 0.844, CNN: 0.911
Cho et al. (38)	IVUS	Develop IVUS-based algorithms for classifying attenuation and calcified plaques	113,746 frames	EfficientNet	Angle level dice similarity coefficients: calcification 0.79, attenuation 0.74 Frame level accuracy: attenuation 93%, calcification 96% Vessel level correlation with human measurement: attenuation $r = 0.89$, calcification $r = 0.95$
Wang et al. (39)	IVUS	1. Identify the most powerful predictor(s) for plaque vulnerability change 2. Test whether machine learning approaches could improve prediction accuracy	9 patients	SVM RF	Prediction accuracy: RF 91.47% SVM 90.78% MPVI the best single risk factor

CAG, coronary angiography; ANN, artificial neural network; GAN, generative adversarial network; CFR, coronary flow reserve; OCT, optical coherence tomography; FCT, fibrous cap thickness; IVUS, intravascular ultrasound; TCFA, thin cap fibroatheroma; FNN, feed-forward neural network; KNN, K-nearest neighbor; MPVI, morphological plaque vulnerability index.

One of the reasons artificial intelligence was developed is that it can replace human resources to some extent, on the premise that it can finish a human's job just as well, if not better. The CMR parameters of both ventricles can be analyzed both manually and computationally. Schuster et al. proved that automatic ventricle evaluation can predict MACE as well as manual evaluation. Volume parameters like left ventricular mass left and right ventricular ejection fraction and so on were automatically and manually analyzed. Parameters then entered regression models to predict MACE (16).

In a study conducted by Ma et al., 68 patients had CMR after PCI for AMI. The evaluation of the myocardial damage and prediction of left ventricular (LV) systolic contractility recovery were evaluated with radiomics signatures extracted by open-source software combining selected strongest features. Better diagnostic performance for microvascular obstruction (MVO) than T1 values alone was achieved by incorporating radiomics and T1 values. A greater predicting power for LV contractility recovery was also yielded by radiomics signature adding to T1 values compared to T1 values alone (17).

Derived from CMR perfusion images, myocardial stress-related metrics are used to predict MACE. During the process of deriving stress metrics, CNN was used to segment the contour of the ventricle and myocardium (18). Another example of artificial intelligence participating in predicting prognosis was exhibited.

Application of AI in Other Non-invasive Modalities

Various modalities other than those above-mentioned examples have been used to prevent, diagnose, and treat ACS. Additionally, some methods integrate the above-mentioned modalities serving the same purpose as the tools of machine learning.

Integration of CCTA, stress CMR perfusion imaging, and electronic medical record data is proposed for building decision-making assisting systems (19). Machine learning is destined to play a role in these systems, although it is uncertain which algorithm will be used.

Dekker et al. used deep learning on low-dose attenuation correction CT (LDAC) images from 747 patients with chest pain gathered during 82 Rubidium PET/CT in one single assessment, to get CAC scores. High CAC scores (>400) showed the higher predictive value of events. Both high CAC scores and ischemia were found to be independent predictors of MACE (20). This demonstrates that deep learning methods can also be applied to imaging systems derived from PET/CT.

APPLICATION OF AI IN INVASIVE MODALITIES

CAG

Arterial Waveform Analysis

Howard et al. implemented a 1-dimensional convolutional neural network to automatically analyze arterial pressure waveforms. With the algorithm, real-time identification of damping can be realized to guarantee the safety of intervention for ACS patients. The classification network achieved excellent accuracy,

specificity, sensitivity, positive, and negative predicting values (21). This indicates that, given the right circumstances, artificial intelligence can serve us in many ways.

Stenosis Recognizing

If we analyze CAG images with neural networks like ANN or CNN, in theory, stenosis or thrombus or calcification will be identified given sufficient labeling. Stenosis, as the most significant information extracted by interventionists, has naturally become the primary subject.

Moon et al. designed a three-step algorithm to recognize stenosis in coronary angiography automatically. The model was trained with 452 series of right coronary angiography. In internal and external validation sets, both frame-wise and series-wise satisfactory accuracy were achieved (22).

Yabushita et al. attempted to detect clinically significant stenosis in coronary angiography movies with a model. One hundred and ninety-nine patients with 1,838 movies were enrolled to produce the multi-layer 3D CNN model. A c-statistic value of 0.61 was achieved in the test set as well as the validation cohort in the training set (24).

CAG-FFR

ANN classifies lesions, as stated above. What surprised us is that software based on ANN can furthermore compute FFR instantaneously without any additional movement, while the respective vessel is being viewed (23). CNN was applied for the same purpose and achieved acceptable correlation (25).

Comprehensive Analysis

Since deep neural network (DNN) is widely used in CAG image processing, is it applicable for finishing comprehensive analysis, from segmentation to stenosis measurement, from calcification to dissection. Du et al. implemented two different DNNs to accomplish such tasks, which only took seconds. The labeling of coronary artery segments and lesion types is a key factor in training the network (26). We can expect to have a full analysis of CAG almost instantaneously for interventionists to make decisions in the near future.

OCT

Plaque Analysis

Owing to high spatial resolution (15 μm), OCT has an inherent advantage in morphological analysis of plaques (56, 57). Studies focusing on plaque characteristics or classification have grown in recent years. Accurately and efficiently identifying atherosclerotic plaques, in particular, vulnerable plaques which are often an alarming sign of successive cardiac events, which are of great significance in managing ACS (58). Additionally, with AI's prosperity, OCT combining AI are the proposed solutions to a series of clinical challenges.

CNN has repeatedly demonstrated its classifying ability in other imaging modalities and has also been proven in OCT. Furthermore, RF was combined with CNN, also serving as a classifier. For starters, RF is particularly efficient in a large data set. Secondly, RF has a relatively low risk of overfitting. Thirdly, RF is good at deciding the significance of features that

matter in classification. Lastly, RF is robust in noisy data and OCT data is “noisy.” As a result, Lee et al. mixed DL and manual lumen morphological characteristics to automatically feature atherosclerotic plaques. High sensitivities and specificities for fibrolipidic and fibrocalcific plaques were achieved after sequential pre-processing, training, testing, and post-processing. The hybrid approach performed better than the previous automatic or manual method alone. The training also depends on accurate labeling (27).

CNN was then widely tested in OCT modality to classify different plaques (28, 59), including vulnerable plaques (31, 32). SVM was also tested in the OCT modality to classify fibrolipidic and fibrocalcific plaques (30). If calcified plaque is the focus of classification, CNN could also accomplish the task, furthermore, to pursue excellence, other DL techniques can be integrated (33).

OCT-Based FFR

FFR is considered a highly specific tool for diagnosing myocardial ischemia in borderline angiographic stenosis (60, 61). However, it provides no information on the morphology of lesion characteristics like OCT. Researchers have sought to combine FFR with OCT via the application of artificial intelligence to acquire both functional and morphological information at the same time. Cha et al. obtained OCT data from 125 patients with typical angina and left anterior descending artery lesions of borderline stenosis (luminal diameter <70%), as well as their FFR data. Random forest extracted the six most important features to predict FFR. The OCT-based ML-FFR correlated well with the wire-based FFR (34). As introduced in the previous sections discussing CT-FFR, most FFR calculations are merely based on images but prediction models integrating both imaging and clinical data broaden our vision.

Predicting FCT Change

Fibrous cap thickness (FCT) precisely measured by OCT (56) is of utmost the importance in plaque rupture (62, 63). Statin is believed to make FCT grow so that acute coronary events are less likely to occur (64, 65). Nevertheless, statin is not effective in everyone by showing increased FCT (66). Hence a tool to predict FCT change in patients taking statin will undoubtedly optimize medical therapy in CAD patients to reduce incidents of ACS. ML models predict FCT changes measured by OCT via analyzing gene expression data (35). Once models like this are integrated, precision medicine can potentially be practiced.

IVUS

Plaque Analysis

According to previous studies, large lipid core and thin fibrous cap can independently predict cardiac events including ACS (58). Intravascular ultrasound (IVUS) is widely used in evaluating lesions and plaque. However, conventional frame-by-frame analysis is not efficient. Various artificially intelligent algorithms have been sought to assist in analyzing plaques.

High risk plaques are undoubtedly the first-choice target for classifying models in IVUS modality. A computational method called EfficientNet was introduced to identify “attenuated plaque, calcified plaque, and plaque without attenuation or calcification”

(38). This novel approach has potential and may be of assistance in “high risk” plaque recognition.

Thin-cap fibroatheroma (TCFA) is defined as “a lipid-rich plaque underlying a thin-fibrous cap whose thickness is <65 μm ” (67). The existence of TCFA independently predicts adverse cardiac events, especially ACS, as concluded by a few studies looking into the progress of non-culprit lesions. However, the relatively poor resolution of IVUS makes it impossible to identify TCFA. ML have appeared in predicting and classifying TCFA for its capability in finding patterns in a huge dataset and precise prediction with processed data.

Bae et al. collected IVUS and OCT images in patients with stable and unstable angina, respectively. They then separated them into the training and testing samples. Each of the IVUS-OCT co-registered frames was labeled as with TCFA and without TCFA. ANN, SVM, and naïve Bayes were used to predict OCT-derived TCFA, all of which showed accuracies of around 80% (36). Other forms of neural networks were also proven to possess similar capability (37).

Plaque Vulnerability Prediction

A genuine clinical challenge arises in predicting upcoming plaque rupture and related critical events like myocardial infarction. To solve this, some effort has been made to take advantage of artificial intelligence for its strength in image feature extraction, a huge quantity of data processing, complex pattern finding, and biomechanics for its advantage in studying the fluid environment in which vulnerable plaques reside in the perspective of fluid mechanics.

A “morphological plaque vulnerability index (MPVI)” has been proposed to evaluate plaque vulnerability using morphological features was obtained from *in vivo* IVUS images. Wang et al. acquired IVUS data from nine patients to reconstruct “fluid-structure interaction (FSI)” models in which hydrodynamic metrics were obtained. In total, 10 baseline risk factors were used by three models to forecast “MPVI change ($\Delta\text{MPVI} = \text{MPVI}_{\text{follow-up}} - \text{MPVI}_{\text{baseline}}$).” Model of RF performed best and MPVI was weighed most in the predictors (39).

PITFALLS AND LIMITATIONS

All kinds of novel methods/algorithms/models appear to be promising but there is still much work to be done before they can be translated for clinical use. No matter how well the newly developed models perform, strict external validation with cohorts from different centers other than the centers where that model was built is mandatory. Before proving satisfactory generalizability, clinical deployment is, at present, out of the question.

Overfitting is a common trap in a complex algorithm, although various techniques can be applied to avoid it. A model with good performance may yield misleading results when applying new data, leading to serious sequelae because of overfitting. Therefore, techniques like K-fold cross validation should be considered to reduce errors in prediction or pattern finding.

One of the major limitations of building an ML model is the quality of data. The incorrect selection of data and inaccurate measurements may produce flawed results that could be misleading. The same problem also applies to data that have too much noise.

Involving big data processing and a huge amount of calculations, conducting AI research undoubtedly involves demands both in terms of software and hardware. Further advances in AI study are anticipated but require a lot of investment.

To date, no guidelines or expert consensus has been issued. Standardization of AI research is urgently required to guarantee the quality of AI research.

CHALLENGES AND DIRECTIONS

Essentially AI is a science based on data. Generally speaking, more data means better AI research products. Although AI researches are prospering, the scarcity of data remains a challenge. One important reason for this is that clinical data often are stored in different systems. For example, images are in Picture Archiving and Communication Systems (PACS), electronic health records are stored in Hospital Information Systems (HIS), and electrocardiograms (ECG) are in paper format. Collecting integrated clinical data is therefore time consuming and demanding of human resources. A revolutionary data storing system is required in order to tackle this obstacle.

Legislation focusing on clinical AI products is still in development in most countries. Due to the complexity of AI in terms of legal and ethical issues, the process of legislation is expected to be long-term and difficult, given that there is no precedent in human history. There will likely be polarizing debates about whether the developer, the user, or the AI itself are accountable when the AI model produces negative results in the real world.

There have already been products integrating the collection of health-related information, such as smart wearable devices and hand-held diagnostic tools. Mobile devices possess an inherent advantage for obtaining clinical data. In the future, it is likely to be a popular direction with the potential to develop more accurate disease phenotyping and more personalized therapies.

It is noteworthy that ACS often requires timely management and AI products involving treatment schedules should take processing time into account. Similar to the example algorithms mentioned above, it is best to be able to display results simultaneously or within seconds along with the CAG or PCI.

Attempts have been made to integrate different imaging modalities to evaluate ACS comprehensively with efficiency in terms of time and cost, such as IVUS and OCT in fusion. Although large clinical trials are lacking, they may also be a prospective direction.

CONCLUSION

Many gaps are to be bridged in cardiovascular disease, ACS in particular, from the mechanism of disease to precise diagnosis and personalized optimal therapeutic strategy. AI has shown its potential in making accurate diagnoses, evaluating functions precisely, predicting risk and outcome, assisting in making treatment decisions, and monitoring disease progression, etc. based on its inherent advantages compared to human power. However, AI also has limitations to be addressed before being widely deployed clinically. Strenuous effort should be made to tackle overfitting, lack of generalizability, limited interpretability, robustness, and so on. Meanwhile, standardization of conducting AI research is an urgent matter. The application of AI to cardiovascular medicine in the future will provide supplemental options for clinicians and benefits to patients.

AUTHOR CONTRIBUTIONS

M-hL constructed the writing of the article. CZ made major revision on the structure and mostly made the Central figure. SW made major revision on the writing. All work were under HJ and BY's guidance. All authors contributed to the article and approved the submitted version.

FUNDING

This work was supported by the National Key R&D Program of China (grant No. 2016YFC1301104 to BY) and the National Natural Science Foundation of China (grants: 81722025, 82061130223, and 81827806).

REFERENCES

1. Steg PG, Goldberg RJ, Gore JM, Fox KA, Eagle KA, Flather MD, et al. Baseline characteristics, management practices, and in-hospital outcomes of patients hospitalized with acute coronary syndromes in the Global Registry of Acute Coronary Events (GRACE). *Am J Cardiol.* (2002) 90:358–63. doi: 10.1016/S0002-9149(02)02489-X
2. O'Gara PT, Kushner FG, Ascheim DD, Casey DE Jr, Chung MK, de Lemos JA, et al. 2013 ACCF/AHA guideline for the management of ST-elevation myocardial infarction: a report of the American College of Cardiology Foundation/American Heart Association Task Force on Practice Guidelines. *Circulation.* (2013) 127:e362–425. doi: 10.1161/CIR.0b013e3182742cf6
3. Amsterdam EA, Wenger NK, Brindis RG, Casey DE Jr, Ganiats TG, Holmes DR Jr, et al. 2014 AHA/ACC guideline for the management of patients with non-ST-elevation acute coronary syndromes: a report of the American College of Cardiology/American Heart Association Task Force on Practice Guidelines. *J Am Coll Cardiol.* (2014) 64:e139–228. doi: 10.1016/j.jacc.2014.09.017
4. Hamet P, Tremblay J. Artificial intelligence in medicine. *Metabolism.* (2017) 69S:S36–40. doi: 10.1016/j.metabol.2017.01.011
5. Liu X, Mo X, Zhang H, Yang G, Shi C, Hau WK. A 2-year investigation of the impact of the computed tomography-derived fractional flow reserve calculated using a deep learning algorithm on routine decision-making for coronary artery disease. *Eur Radiol.* (2021) 31:7039–46. doi: 10.1007/s00330-021-07771-7
6. Duguay TM, Tesche C, Vliegenthart R, De Cecco CN, Lin H, Albrecht MH, et al. Coronary computed tomographic angiography-derived fractional flow reserve based on machine learning for risk stratification of non-culprit

- coronary narrowings in patients with acute coronary syndrome. *Am J Cardiol.* (2017) 120:1260–6. doi: 10.1016/j.amjcard.2017.07.008
7. Eberhard M, Nadarevic T, Cousin A, von Spiczak J, Hinzpeter R, Euler A, et al. Machine learning-based CT fractional flow reserve assessment in acute chest pain: first experience. *Cardiovasc Diagn Ther.* (2020) 10:820–30. doi: 10.21037/cdt-20-381
 8. Zeleznik R, Foldyna B, Eslami P, Weiss J, Alexander I, Taron J, et al. Deep convolutional neural networks to predict cardiovascular risk from computed tomography. *Nat Commun.* (2021) 12:715. doi: 10.1038/s41467-021-20966-2
 9. Qiao HY, Li JH, Schoepf UJ, Bayer RR, Tinnfeld FC, Di Jiang M, et al. Prognostic implication of CT-FFR based functional SYNTAX score in patients with *de novo* three-vessel disease. *Eur Heart J Cardiovasc Imaging.* (2020) 2020:jeaa256. doi: 10.1093/ehjci/jeaa256
 10. Al'Aref SJ, Singh G, Choi JW, Xu Z, Maliakal G, van Rosendael AR, et al. A boosted ensemble algorithm for determination of plaque stability in high-risk patients on coronary CTA. *JACC Cardiovasc Imaging.* (2020) 13:2162–73. doi: 10.1016/j.jcmg.2020.03.025
 11. Lin A, Kolossváry M, Yuvaraj J, Cadet S, McElhinney PA, Jiang C, et al. Myocardial infarction associates with a distinct pericoronary adipose tissue radiomic phenotype: a prospective case-control study. *JACC Cardiovasc Imaging.* (2020) 13:2371–83. doi: 10.1016/j.jcmg.2020.06.033
 12. Tamarappoo BK, Lin A, Commandeur F, McElhinney PA, Cadet S, Goeller M, et al. Machine learning integration of circulating and imaging biomarkers for explainable patient-specific prediction of cardiac events: a prospective study. *Atherosclerosis.* (2021) 318:76–82. doi: 10.1016/j.atherosclerosis.2020.11.008
 13. Yang S, Koo BK, Hoshino M, Lee JM, Murai T, Park J, et al. CT angiographic and plaque predictors of functionally significant coronary disease and outcome using machine learning. *JACC Cardiovasc Imaging.* (2021) 14:629–41. doi: 10.1016/j.jcmg.2020.08.025
 14. Oikonomou EK, Williams MC, Kotanidis CP, Desai MY, Marwan M, Antonopoulos AS, et al. A novel machine learning-derived radiotranscriptomic signature of perivascular fat improves cardiac risk prediction using coronary CT angiography. *Eur Heart J.* (2019) 40:3529–43. doi: 10.1093/eurheartj/ehz592
 15. Larroza A, Materka A, López-Lereu MP, Monmeneu JV, Bodí V, Moratal D. Differentiation between acute and chronic myocardial infarction by means of texture analysis of late gadolinium enhancement and cine cardiac magnetic resonance imaging. *Eur J Radiol.* (2017) 92:78–83. doi: 10.1016/j.ejrad.2017.04.024
 16. Schuster A, Lange T, Backhaus SJ, Strohmeier C, Boom PC, Matz J, et al. Fully automated cardiac assessment for diagnostic and prognostic stratification following myocardial infarction. *J Am Heart Assoc.* (2020) 9:e016612. doi: 10.1161/JAHA.120.016612
 17. Ma Q, Ma Y, Yu T, Sun Z, Hou Y. Radiomics of non-contrast-enhanced T1 mapping: diagnostic and predictive performance for myocardial injury in acute ST-segment-elevation myocardial infarction. *Korean J Radiol.* (2021) 22:535–46. doi: 10.3348/kjr.2019.0969
 18. Knott KD, Seraphim A, Augusto JB, Xue H, Chacko L, Aung N, et al. The prognostic significance of quantitative myocardial perfusion: an artificial intelligence-based approach using perfusion mapping. *Circulation.* (2020) 141:1282–91. doi: 10.1161/CIRCULATIONAHA.119.044666
 19. Groepenhoff F, Eikendal ALM, Bots SH, van Ommen AM, Overmars LM, Kapteijn D, et al. Cardiovascular imaging of women and men visiting the outpatient clinic with chest pain or discomfort: design and rationale of the ARGUS Study. *BMJ Open.* (2020) 10:e040712. doi: 10.1136/bmjopen-2020-040712
 20. Dekker M, Waissi F, Bank IEM, Isgum I, Scholtens AM, Velthuis BK, et al. The prognostic value of automated coronary calcium derived by a deep learning approach on non-ECG gated CT images from 82Rb-PET/CT myocardial perfusion imaging. *Int J Cardiol.* (2021) 329:9–15. doi: 10.1016/j.ijcard.2020.12.079
 21. Howard JP, Cook CM, van de Hoef TP, Meuwissen M, de Waard GA, van Lavieren MA, et al. Artificial intelligence for aortic pressure waveform analysis during coronary angiography: machine learning for patient safety. *JACC Cardiovasc Interv.* (2019) 12:2093–101. doi: 10.1016/j.jcin.2019.06.036
 22. Moon JH, Lee DY, Cha WC, Chung MJ, Lee KS, Cho BH, et al. Automatic stenosis recognition from coronary angiography using convolutional neural networks. *Comput Methods Programs Biomed.* (2021) 198:105819. doi: 10.1016/j.cmpb.2020.105819
 23. Roguin A, Abu Dogosh A, Feld Y, Konigstein M, Lerman A, Koifman E. Early feasibility of automated artificial intelligence angiography based fractional flow reserve estimation. *Am J Cardiol.* (2021) 139:8–14. doi: 10.1016/j.amjcard.2020.10.022
 24. Yabushita H, Goto S, Nakamura S, Oka H, Nakayama M, Goto S. Development of novel artificial intelligence to detect the presence of clinically meaningful coronary atherosclerotic stenosis in major branch from coronary angiography video. *J Atheroscler Thromb.* (2021) 28:835–43. doi: 10.5551/jat.59675
 25. Zhao Q, Li C, Chu M, Gutiérrez-Chico JL, Tu S. Angiography-based coronary flow reserve: the feasibility of automatic computation by artificial intelligence. *Cardiol J.* (2021) doi: 10.5603/CJ.a2021.0087
 26. Du T, Xie L, Zhang H, Liu X, Wang X, Chen D, et al. Training and validation of a deep learning architecture for the automatic analysis of coronary angiography. *EuroIntervention.* (2021) 17:32–40. doi: 10.4244/EIJ-D-20-00570
 27. Lee J, Prabhu D, Kolluru C, Gharaibeh Y, Zimin VN, Dallen LAP, et al. Fully automated plaque characterization in intravascular OCT images using hybrid convolutional and lumen morphology features. *Sci Rep.* (2020) 10:2596. doi: 10.1038/s41598-020-59315-6
 28. Chu M, Jia H, Gutiérrez-Chico JL, Maehara A, Ali ZA, Zeng X, et al. Artificial intelligence and optical coherence tomography for the automatic characterisation of human atherosclerotic plaques. *EuroIntervention.* (2021) 17:41–50. doi: 10.4244/EIJ-D-20-01355
 29. Xu P, Xue Y, Schoepf UJ, Varga-Szemes A, Griffith J, Yacoub B, et al. Radiomics: the next frontier of cardiac computed tomography. *Circ Cardiovasc Imaging.* (2021) 14:e011747. doi: 10.1161/CIRCIMAGING.120.011747
 30. Prabhu D, Bezerra H, Kolluru C, Gharaibeh Y, Mehanna E, Wu H, et al. Automated A-line coronary plaque classification of intravascular optical coherence tomography images using handcrafted features and large datasets. *J Biomed Opt.* (2019) 24:1–15. doi: 10.1117/1.JBO.24.10.106002
 31. Shi P, Xin J, Liu S, Deng Y, Zheng N. Vulnerable plaque recognition based on attention model with deep convolutional neural network. *Annu Int Conf IEEE Eng Med Biol Soc.* (2018) 2018:834–7. doi: 10.1109/EMBC.2018.8512279
 32. Liu R, Zhang Y, Zheng Y, Liu Y, Zhao Y, Yi L. Automated detection of vulnerable plaque for intravascular optical coherence tomography images. *Cardiovasc Eng Technol.* (2019) 10:590–603. doi: 10.1007/s13239-019-00425-2
 33. Lee J, Gharaibeh Y, Kolluru C, Zimin VN, Dallen LAP, Kim JN, et al. Segmentation of coronary calcified plaque in intravascular OCT images using a two-step deep learning approach. *IEEE Access.* (2020) 8:225581–93. doi: 10.1109/ACCESS.2020.3045285
 34. Cha JJ, Son TD, Ha J, Kim JS, Hong SJ, Ahn CM, et al. Optical coherence tomography-based machine learning for predicting fractional flow reserve in intermediate coronary stenosis: a feasibility study. *Sci Rep.* (2020) 10:20421. doi: 10.1038/s41598-020-77507-y
 35. Johnson KW, Glicksberg BS, Shameer K, Vengrenyuk Y, Krittanawong C, Russak AJ, et al. A transcriptomic model to predict increase in fibrous cap thickness in response to high-dose statin treatment: Validation by serial intracoronary OCT imaging. *EBioMedicine.* (2019) 44:41–9. doi: 10.1016/j.ebiom.2019.05.007
 36. Bae Y, Kang SJ, Kim G, Lee JG, Min HS, Cho H, et al. Prediction of coronary thin-cap fibroatheroma by intravascular ultrasound-based machine learning. *Atherosclerosis.* (2019) 288:168–74. doi: 10.1016/j.atherosclerosis.2019.04.228
 37. Jun TJ, Kang SJ, Lee JG, Kweon J, Na W, Kang D, et al. Automated detection of vulnerable plaque in intravascular ultrasound images. *Med Biol Eng Comput.* (2019) 57:863–76. doi: 10.1007/s11517-018-1925-x
 38. Cho H, Kang SJ, Min HS, Lee JG, Kim WJ, Kang SH, et al. Intravascular ultrasound-based deep learning for plaque characterization in coronary artery disease. *Atherosclerosis.* (2021) 324:69–75. doi: 10.1016/j.atherosclerosis.2021.03.037
 39. Wang L, Tang D, Maehara A, Wu Z, Yang C, Muccigrosso D, et al. Using intravascular ultrasound image-based fluid-structure interaction models and machine learning methods to predict human coronary plaque vulnerability change. *Comput Methods Biomech Biomed Eng.* (2020) 23:1267–76. doi: 10.1080/10255842.2020.1795838

40. Moss AJ, Williams MC, Newby DE, Nicol ED. The updated NICE guidelines: cardiac CT as the first-line test for coronary artery disease. *Curr Cardiovasc Imaging Rep.* (2017) 10:15. doi: 10.1007/s12410-017-9412-6
41. Knuuti J, Wijns W, Saraste A, Capodanno D, Barbato E, Funck-Brentano C, et al. 2019 ESC Guidelines for the diagnosis and management of chronic coronary syndromes. *Eur Heart J.* (2020) 41:407–77. doi: 10.1093/eurheartj/ehz425
42. Driessen RS, Danad I, Stuijzand WJ, Raijmakers PG, Schumacher SP, van Diemen PA, et al. Comparison of coronary computed tomography angiography, fractional flow reserve, and perfusion imaging for ischemia diagnosis. *J Am Coll Cardiol.* (2019) 73:161–73. doi: 10.1016/j.jacc.2018.10.056
43. Detrano R, Guerci AD, Carr JJ, Bild DE, Burke G, Folsom AR, et al. Coronary calcium as a predictor of coronary events in four racial or ethnic groups. *N Engl J Med.* (2008) 358:1336–45. doi: 10.1056/NEJMoa072100
44. Pursnani A, Massaro JM, D'Agostino RB Sr, O'Donnell CJ, Hoffmann U. Guideline-based statin eligibility, coronary artery calcification, and cardiovascular events. *JAMA.* (2015) 314:134–41. doi: 10.1001/jama.2015.7515
45. Goff DC Jr, Lloyd-Jones DM, Bennett G, Coady S, D'Agostino RB, Gibbons R, et al. 2013 ACC/AHA guideline on the assessment of cardiovascular risk: a report of the American College of Cardiology/American Heart Association Task Force on Practice Guidelines. *Circulation.* (2014) 129(25 Suppl. 2):S49–73. doi: 10.1161/01.cir.0000437741.48606.98
46. Sianos G, Morel MA, Kappetein AP, Morice MC, Colombo A, Dawkins K, et al. The SYNTAX Score: an angiographic tool grading the complexity of coronary artery disease. *EuroIntervention.* (2005) 1:219–27.
47. Franzone A, Taniwaki M, Rigamonti F, Heg D, Piccolo R, Roffi M, et al. Angiographic complexity of coronary artery disease according to SYNTAX score and clinical outcomes after revascularisation with newer-generation drug-eluting stents: a substudy of the BIOSCIENCE trial. *EuroIntervention.* (2016) 12:e595–604. doi: 10.4244/EIJV12I5A99
48. Lee JM, Choi KH, Koo BK, Park J, Kim J, Hwang D, et al. Prognostic implications of plaque characteristics and stenosis severity in patients with coronary artery disease. *J Am Coll Cardiol.* (2019) 73:2413–24. doi: 10.1016/j.jacc.2019.02.060
49. Finck T, Stojanovic A, Will A, Hendrich E, Martinoff S, Hausleiter J, et al. Long-term prognostic value of morphological plaque features on coronary computed tomography angiography. *Eur Heart J Cardiovasc Imaging.* (2020) 21:237–48. doi: 10.1093/ehjci/jez238
50. Ateş AH, Yorgun H, Canpolat U, Kaya EB, Sahiner L, Hazirolan T, et al. Long-term prognostic value of coronary atherosclerotic plaque characteristics assessed by computerized tomographic angiography. *Angiology.* (2021) 72:252–9. doi: 10.1177/0003319720963677
51. Kim RJ, Wu E, Rafael A, Chen EL, Parker MA, Simonetti O, et al. The use of contrast-enhanced magnetic resonance imaging to identify reversible myocardial dysfunction. *N Engl J Med.* (2000) 343:1445–53. doi: 10.1056/NEJM200011163432003
52. Mojibian H, Pouraliakbar H. Chapter 8: Cardiac magnetic resonance imaging. In: Maleki M, Alizadehasl A, Haghighi M, editors. *Practical Cardiology.* Elsevier (2018) p. 159–66. doi: 10.1016/B978-0-323-51149-0.00008-0
53. Lintings PE, Nivet H, Clément-Guinaudeau S, Camaioni C, Sridi S, Corneloup O, et al. High-resolution late gadolinium enhancement magnetic resonance for the diagnosis of myocardial infarction with nonobstructed coronary arteries. *JACC Cardiovasc Imaging.* (2020) 13:1135–48. doi: 10.1016/j.jcmg.2019.11.020
54. Suzuki J, Caputo GR, Masui T, Chang JM, O'Sullivan M, Higgins CB. Assessment of right ventricular diastolic and systolic function in patients with dilated cardiomyopathy using cine magnetic resonance imaging. *Am Heart J.* (1991) 122(4 Pt 1):1035–40. doi: 10.1016/0002-8703(91)90469-X
55. Bottini PB, Carr AA, Prisant LM, Flickinger FW, Allison JD, Gottdiener JS. Magnetic resonance imaging compared to echocardiography to assess left ventricular mass in the hypertensive patient. *Am J Hypertens.* (1995) 8:221–8. doi: 10.1016/0895-7061(94)00178-E
56. Huang D, Swanson EA, Lin CP, Schuman JS, Stinson WG, Chang W, et al. Optical coherence tomography. *Science.* (1991) 254:1178–81. doi: 10.1126/science.1957169
57. Tearney GJ, Regar E, Akasaka T, Adriaenssens T, Barlis P, Bezerra HG, et al. Consensus standards for acquisition, measurement, and reporting of intravascular optical coherence tomography studies: a report from the International Working Group for intravascular optical coherence tomography standardization and validation. *J Am Coll Cardiol.* (2012) 59:1058–72. doi: 10.1016/j.jacc.2011.09.079
58. Virmani R, Burke AP, Farb A, Kolodgie FD. Pathology of the vulnerable plaque. *J Am Coll Cardiol.* (2006) 47(8 Suppl.):C13–8. doi: 10.1016/j.jacc.2005.10.065
59. Mengdi Xu, Jun Cheng, Annan Li, Lee JA, Wong DWK, Taruya A, et al. Fibroatheroma identification in Intravascular Optical Coherence Tomography images using deep features. *Annu Int Conf IEEE Eng Med Biol Soc.* (2017) 2017:1501–4. doi: 10.1109/EMBC.2017.8037120
60. Pijls NH, De Bruyne B, Peels K, Van Der Voort PH, Bonnier HJ, Bartunek J, et al. Measurement of fractional flow reserve to assess the functional severity of coronary-artery stenoses. *N Engl J Med.* (1996) 334:1703–8. doi: 10.1056/NEJM199606273342604
61. Pijls NH, Van Gelder B, Van der Voort P, Van Der Voort PH, Bonnier HJ, Bartunek J, et al. Fractional flow reserve. A useful index to evaluate the influence of an epicardial coronary stenosis on myocardial blood flow. *Circulation.* (1995) 92:3183–93. doi: 10.1161/01.CIR.92.11.3183
62. Burke AP, Farb A, Malcom GT, Liang YH, Smialek J, Virmani R. Coronary risk factors and plaque morphology in men with coronary disease who died suddenly. *N Engl J Med.* (1997) 336:1276–82. doi: 10.1056/NEJM199705013361802
63. Tian J, Ren X, Vergallo R, Xing L, Yu H, Jia H, et al. Distinct morphological features of ruptured culprit plaque for acute coronary events compared to those with silent rupture and thin-cap fibroatheroma: a combined optical coherence tomography and intravascular ultrasound study. *J Am Coll Cardiol.* (2014) 63:2209–16. doi: 10.1016/j.jacc.2014.01.061
64. Takarada S, Imanishi T, Kubo T, Tanimoto T, Kitabata H, Nakamura N, et al. Effect of statin therapy on coronary fibrous-cap thickness in patients with acute coronary syndrome: assessment by optical coherence tomography study. *Atherosclerosis.* (2009) 202:491–7. doi: 10.1016/j.atherosclerosis.2008.05.014
65. Takarada S, Imanishi T, Ishibashi K, Tanimoto T, Komukai K, Ino Y, et al. The effect of lipid and inflammatory profiles on the morphological changes of lipid-rich plaques in patients with non-ST-segment elevated acute coronary syndrome: follow-up study by optical coherence tomography and intravascular ultrasound. *JACC Cardiovasc Interv.* (2010) 3:766–72. doi: 10.1016/j.jcin.2010.05.001
66. Kataoka Y, St John J, Wolski K, Uno K, Puri R, Tuzcu EM, et al. Atheroma progression in hyporesponders to statin therapy. *Arterioscler Thromb Vasc Biol.* (2015) 35:990–5. doi: 10.1161/ATVBAHA.114.304477
67. Fujii K, Hao H, Shibuya M, Imanaka T, Fukunaga M, Miki K, et al. Accuracy of OCT, grayscale IVUS, and their combination for the diagnosis of coronary TCFA: an ex vivo validation study. *JACC Cardiovasc Imaging.* (2015) 8:451–60. doi: 10.1016/j.jcmg.2014.10.015

Conflict of Interest: The authors declare that the research was conducted in the absence of any commercial or financial relationships that could be construed as a potential conflict of interest.

Publisher's Note: All claims expressed in this article are solely those of the authors and do not necessarily represent those of their affiliated organizations, or those of the publisher, the editors and the reviewers. Any product that may be evaluated in this article, or claim that may be made by its manufacturer, is not guaranteed or endorsed by the publisher.

Copyright © 2022 Liu, Zhao, Wang, Jia and Yu. This is an open-access article distributed under the terms of the Creative Commons Attribution License (CC BY). The use, distribution or reproduction in other forums is permitted, provided the original author(s) and the copyright owner(s) are credited and that the original publication in this journal is cited, in accordance with accepted academic practice. No use, distribution or reproduction is permitted which does not comply with these terms.



Predictors of Near-Infrared Spectroscopy-Detected Lipid-Rich Plaques by Optical Coherence Tomography-Defined Morphological Features in Patients With Acute Coronary Syndrome

OPEN ACCESS

Edited by:

Zhao Wang,
University of Electronic Science and
Technology of China, China

Reviewed by:

Seung-Yul Lee,
Wonkwang University, South Korea
Wojciech Warha,
Medical University of Silesia, Poland

*Correspondence:

Taishi Yonetsu
yonetsu@gmail.com

Specialty section:

This article was submitted to
Cardiovascular Imaging,
a section of the journal
Frontiers in Cardiovascular Medicine

Received: 24 December 2021

Accepted: 18 January 2022

Published: 21 February 2022

Citation:

Usui E, Yonetsu T, Ohmori M,
Kanno Y, Nakao M, Niida T,
Matsuda Y, Matsuda J, Umemoto T,
Misawa T, Hada M, Hoshino M,
Kanaji Y, Sugiyama T, Kakuta T and
Sasano T (2022) Predictors of
Near-Infrared Spectroscopy-Detected
Lipid-Rich Plaques by Optical
Coherence Tomography-Defined
Morphological Features in Patients
With Acute Coronary Syndrome.
Front. Cardiovasc. Med. 9:842914.
doi: 10.3389/fcvm.2022.842914

Eisuke Usui¹, Taishi Yonetsu^{1*}, Mari Ohmori¹, Yoshinori Kanno¹, Masahiko Nakao²,
Takayuki Niida¹, Yuji Matsuda¹, Junji Matsuda¹, Tomoyuki Umemoto¹, Toru Misawa²,
Masahiro Hada², Masahiro Hoshino², Yoshihisa Kanaji², Tomoyo Sugiyama²,
Tsuneakazu Kakuta² and Tetsuo Sasano¹

¹ Cardiovascular Medicine, Tokyo Medical and Dental University, Tokyo, Japan, ² Cardiovascular Medicine, Tsuchiura Kyodo General Hospital, Ibaraki, Japan

Background: Near-infrared spectroscopy (NIRS) provides the localization of lipid-rich components in coronary plaques. However, morphological features in NIRS-detected lipid-rich plaques (LRP) are unclear.

Methods: A total of 140 *de novo* culprit lesions in 140 patients with the acute coronary syndrome (ACS) who underwent NIRS and optical coherence tomography (OCT) examinations for the culprit lesions at the time of percutaneous coronary interventions were investigated. We defined a NIRS-LRP as a lesion with a maximum lipid core burden index of 4 mm [LCBI_{4mm}] > 500 in the culprit plaque. Clinical demographics, angiographic, and OCT findings were compared between the patients with NIRS-LRP (*n* = 54) vs. those without NIRS-LRP (*n* = 86). Uni- and multivariable logistic regression analyses were performed to examine the independent OCT morphological predictors for NIRS-LRP.

Results: Clinical demographics showed no significant differences between the two groups. The angiographic minimum lumen diameter was smaller in the NIRS-LRP group than in the non- NIRS-LRP group. In OCT analysis, the minimum flow area was smaller; lipid angle, lipid length, the prevalence of thin-cap fibroatheroma, and cholesterol crystals were greater in the NIRS-LRP group than in the non-NIRS-LRP group. Plaque rupture and thrombi were more frequent in the NIRS-LRP group, albeit not significant. In a multivariable logistic regression analysis, presence of thin-cap fibroatheroma [odds ratio (OR): 2.56; 95% CI: 1.12 to 5.84; *p* = 0.03] and cholesterol crystals (OR: 2.90; 95% CI: 1.20 to 6.99; *p* = 0.02) were independently predictive of NIRS-LRP.

Conclusions: In ACS culprit lesions, OCT-detected thin-cap fibroatheroma and cholesterol crystals rather than plaque rupture and thrombi were closely associated with a great lipid-core burden.

Keywords: acute coronary syndrome (ACS), cholesterol crystal, lipid-rich plaque, near-infrared spectroscopy (NIRS), optical coherence tomography, thin-cap fibroatheroma (TCFA)

INTRODUCTION

Near-infrared spectroscopy (NIRS) is a novel modality useful to identify lipid-rich plaques prone to progress (1, 2). NIRS system is combined in conventional intravascular ultrasound (IVUS) imaging catheters and could be used in daily catheterization procedures. Optical coherence tomography is an imaging modality that enables us to identify coronary plaque features with high-resolution imaging quality (3, 4). Several previous studies compared NIRS-IVUS and optical coherence tomography (OCT) findings and showed associations between NIRS-detected great lipid core burden index (LCBI) and OCT-detected plaque vulnerability in stable patients (5) and non-infarct-related arteries (6). Recently, a NIRS-IVUS and OCT study (7) has proposed NIRS-IVUS-derived criteria to predict the OCT-derived plaque morphologies of the culprit lesions of acute myocardial infarction. Nevertheless, OCT-derived predictive variables of NIRS-detected great LCBI are still unknown in culprit lesions of the acute coronary syndrome (ACS) despite great LCBI in ACS culprit lesions has been known to be predictive of periprocedural myocardial injury after stenting (8–12). Thus, this study aimed to examine (i) the relation between OCT-derived plaque morphologies and great LCBI and (ii) the OCT-derived lipid-related predictors of great LCBI in culprit lesions in patients with ACS.

METHODS

Study Population

This was a multicenter, retrospective, observational study from two hospitals in Japan. In the institutional database of Tokyo Medical and Dental University and Tsuchiura Kyodo General Hospital between July 2015 and October 2021, a total of 506 culprit lesions in 506 patients who underwent both OCT and NIRS examinations before revascularization were investigated. Exclusion criteria were patients with stable coronary artery disease ($n = 301$), in-stent restenosis ($n = 25$), lesions with pre-imaging ballooning or atherectomy ($n = 32$), and poor imaging quality ($n = 8$). In the present study, myocardial infarction was defined as type I or II myocardial infarction in the fourth universal definition (13). In brief, it was defined when there is clinical evidence of acute myocardial ischemia (symptoms of myocardial ischemia; new ischemic electrocardiographic changes; development of pathological Q waves; imaging evidence of new loss of viable myocardium or new regional wall motion abnormality in a pattern consistent with an ischemic etiology; identification of a coronary thrombus by angiography or autopsy) and with

detection of a rise and/or fall of cardiac troponin values with at least one value above the 99th percentile URL. ST-segment elevation myocardial infarction was defined as myocardial infarction with ST-segment elevation >0.1 mV in > 2 contiguous leads or a new left bundle-branch block on the electrocardiogram. Non-ST-segment elevation myocardial infarction was defined as myocardial infarction in the absence of ST-segment elevation on the electrocardiogram. Unstable angina was defined as having newly developed/accelerating chest symptoms on exertion or rest angina within 2 weeks without elevated cardiac biomarkers. The culprit lesion was determined by the operator's discretions, employing angiography, electrocardiographic changes, or left ventricular wall motion abnormalities. In patients with multiple stenoses, the culprit lesion was determined as the lesion with the tightest stenosis. Finally, 140 ACS culprit lesions in 140 patients comprised the final dataset. The study complied with the Declaration of Helsinki and was approved by the institutional review boards of Tokyo Medical and Dental University and Tsuchiura Kyodo General Hospital. All the patients provided written informed consent before imaging and subsequent intervention for possible data use in future studies.

Cardiac Catheterization

Each patient initially underwent standard selective coronary angiography for the assessment of coronary anatomy *via* radial or femoral artery using a 6- or 7-Fr system. Coronary angiograms were analyzed quantitatively using a CMS-MEDIS quantitative coronary angiography (QCA) system (Medis Medical Imaging Systems, Leiden, The Netherlands) to measure the minimum lumen diameter and reference the lumen diameter, percent diameter stenosis, and lesion length at the culprit lesion. All the patients had received a bolus injection of heparin (5,000 IU) before the procedure, and an additional bolus injection of 2,000 IU was administered every hour as needed to maintain an activated clotting time > 250 s. QCA measurements were performed in diastolic frames from orthogonal projections. Post-PCI coronary flow was assessed according to the Thrombolysis in Myocardial Infarction (TIMI) flow grade (14). OCT and NIRS-IVUS imaging were performed before PCI for the culprit lesion.

OCT Imaging Acquisition and Analysis

OCT was performed after intracoronary nitroglycerin (100–200 μ g). Frequency-domain OCT (ILUMIEN OPTIS, Abbott Vascular, Santa Clara, California in 137 patients or Optical Frequency Domain Imaging System, Terumo Corporation, Tokyo, Japan, in three patients) was used. The technique for OCT imaging has been described previously (3, 4). In brief, for frequency-domain OCT systems, a 2.7-Fr (Dragonfly OPTIS or Dragonfly OpStar Abbott Vascular) or a 2.6-Fr (Fastview,

Terumo Corporation) catheter was advanced over a guidewire, followed by an automated pullback with a speed of 18–36 mm/s and 180 frames/s (Dragonfly OPTIS and Dragonfly OpStar) or 20–40 mm/s and 160 frames/s (Fastview) with continuous contrast injection (4 ml/s, 14–18 ml total).

Optical coherence tomography images were analyzed using proprietary software (Abbott or Terumo) by two experienced investigators (EU and TY). A 30-mm segment of the culprit lesion (15-mm proximal and 15-mm distal to the most stenotic lesion site) was examined in all the culprit vessels. Proximal and distal references were defined as the cross-sections with the largest lumen area before major side branches within the examined segment. The reference lumen area was defined as an average of the largest lumen area proximal and distal to the stenosis. The flow area was calculated in each frame as the lumen area minus the thrombus area (15). Percent area stenosis was calculated according to the following formula: [(mean reference lumen area minus minimal lumen area)/mean reference lumen area]. The plaque was categorized as lipidic, fibrous, or calcified. The lipidic plaque had a region with strong signal attenuation and a diffuse border, and a plaque was considered lipid rich if the lipidic angle was $> 90^\circ$. Plaque rupture was defined as a disrupted fibrous cap with intraplaque cavity formation (**Figure 1A**). Thin-cap fibroatheroma (TCFA) had a fibrous cap thickness $< 65 \mu\text{m}$ with a lipid-rich plaque (**Figure 1B**) (4). The fibrous plaque had a homogeneous signal-rich region. The calcified plaque was defined as a signal-poor or heterogeneous region with sharply delineated borders. Thrombus was defined as an irregular mass (diameter $> 250 \mu\text{m}$) either attached to the luminal surface or floating within the lumen (**Figure 1C**) (4). We defined a low-intensity area (LIA) as a homogeneous signal-poor region without attenuation that was $\geq 0.5 \text{ mm}$ in length (**Figure 1D**) (3, 16, 17). Cholesterol crystal (CC) was defined as a thin linear region of high intensity, having a clear border with adjacent tissue, not present within or at the border of the calcified plaque (**Figure 1D**) (18). The layered plaque was defined as a layer of tissue located close to the luminal surface with clear demarcation from the underlying plaque (**Figure 1E**) (19). Macrophages were defined as signal-rich, distinct, or confluent punctate regions accompanied by heterogenic signal shadows. Microvessels were non-signal tubuloluminal structures in a plaque without a connection to the lumen (20).

NIRS-IVUS Imaging Acquisition

Following the OCT imaging, NIRS-IVUS imaging was performed by using the TVC Imaging System (InfraReDx, Burlington, Massachusetts), including MC8 on a 40-MHz TVC Insight catheter ($n = 31$) or MC10 on a 50-MHz Dualpro catheter ($n = 109$). The NIRS-IVUS catheter was advanced distally to the culprit lesion over a workhorse guidewire, followed by an automated pullback with a speed of 0.5 mm/s for the TVC Insight catheter or 2 mm/s for the Dualpro catheter. The TVC Imaging System provided concurrent color-coded data of a near-infrared spectrum co-registered with IVUS grayscale images. NIRS-IVUS images were stored digitally and analyzed with offline software (echoPlaque 4, INDEC Medical Systems, Inc., Mountain View,

California) by an investigator who was blinded to the OCT findings (M.Hada.).

Near-infrared spectroscopy (NIRS) data were denoted on a chemogram, demonstrating the color-coded distribution of lipid in the vessel combined with IVUS images. The chemogram indicated the probability of lipid every 1 pixel (0.1 mm in a longitudinal image and 1° in a circumferential image) by using red (low probability of lipid) and yellow (high probability of lipid). The lipid core burden index (LCBI) was defined as the fraction of pixels, indicating lipid at the probability > 0.6 within the region of interest, multiplied by 1,000. The maximum LCBI in 4 mm ($\text{maxLCBI}_{4\text{mm}}$) was defined as the maximum value of the LCBI for any 4-mm region in the culprit lesion. We defined NIRS-LRP as a lesion having $\text{max LCBI}_{4\text{mm}}$ of > 500 (8, 10, 11).

Statistical Analysis

Categorical variables were presented as frequency and were compared with χ^2 statistics or the Fisher exact test. Continuous variables were presented as median and interquartile range and were compared with the Mann–Whitney U test. Prevalence of OCT-derived plaque morphologies in relation to $\text{max LCBI}_{4\text{mm}}$ on tertiles was compared using Cochran–Armitage trend test with $p < 0.05$ as significant. Multivariable logistic regression analyses were performed to identify the independent predictors of NIRS-LRP. We used a generalized estimating equation approach to compensate for clustering effects of multiple lesions in the same patient. A multivariable model comprised age, gender, and associated variables in the univariate analyses ($p < 0.10$) in clinical demographics and OCT characteristics. Although a presence of calcification was positively associated with NIRS-LRP in the univariable analysis, we did not include calcification in the multivariable analysis for the purpose of building a prediction model, which is composed of lipid-related OCT findings. Inter- and intra-observer variability of diagnosis of TCFA and CC was tested by two independent observers and repeated by one observer 4 weeks apart in 50 randomly selected cases using Kappa statistics. A 2-sided $p < 0.05$ was considered statistically significant. Statistical analysis was performed with R statistics version 3.5.3 (R Foundation for Statistical Computing, Vienna, Austria).

RESULTS

Baseline Clinical Demographics

Patient age was median 66 (interquartile range; 56.8–73.) years, and 82.9% (116/140) were men. More than half (56.4%) of the patients presented with non-ST-segment elevation myocardial elevation (43 ST-segment elevation MI, 79 non-ST-segment elevation MI, and 18 unstable angina). The prevalence of diabetes mellitus and pre-PCI statin treatment was 30 and 29.3%, respectively. Baseline clinical demographics showed no significant differences between patients with NIRS-LRP and those without NIRS-LRP in culprit lesions (**Table 1**).

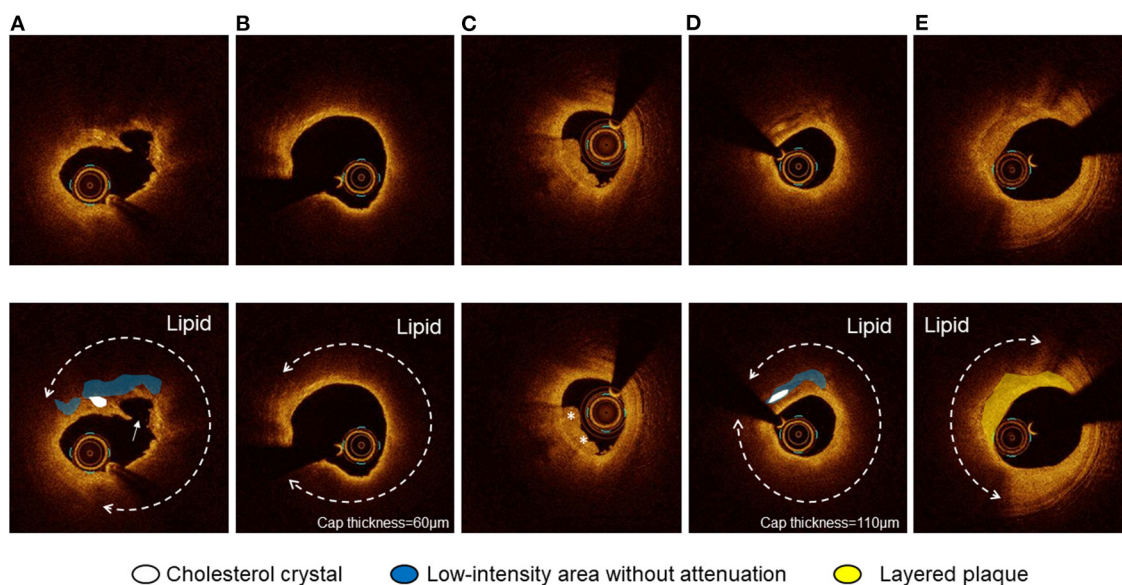


FIGURE 1 | Optical coherence tomography (OCT) images of plaque rupture, thin-cap fibroatheroma (TCFA), thrombus, cholesterol crystal (CC), and layered plaque. **(A)** Plaque rupture with a lipidic plaque and cholesterol crystal accompanying a homogeneous low-intensity area without attenuation. CC was defined as a thin linear region of high intensity, having a clear border with adjacent tissue, not present within or at the border of a calcified plaque. **(B)** TCFA was defined as a lipidic plaque with a lipid angle of $> 90^\circ$ with a fibrous cap thickness $< 65 \mu\text{m}$. **(C)** Thrombus was defined as an irregular mass (diameter $> 250 \mu\text{m}$) either attached to the luminal surface or floating within the lumen. **(D)** CC accompanying a homogeneous low-intensity area without attenuation. The thinnest fibrous cap thickness was $110 \mu\text{m}$. **(E)** The layered plaque was defined as a layer of tissue located close to the luminal surface with clear demarcation from the underlying plaque.

Angiographic and OCT Findings According to Max LCBI_{4mm}

Overall, the mean and median values of max LCBI_{4mm} were 438 ± 266 and 443 [223–631], respectively. There was good concordance of inter- and intra-observer agreement for the identification of TCFA ($\kappa = 0.77, 0.91$) and CC ($\kappa = 0.88, 0.92$). All 95 culprit lesions with OCT-detected CCs also had LIAs in the culprit plaque (**Supplementary Figure 1**). **Table 1** shows the angiographic and OCT findings according to the presence or absence of NIRS-LRP in culprit lesions. The angiographic minimum lumen diameter was smaller in patients with NIRS-LRP than in patients without NIRS-LRP. By OCT, the minimum flow area was smaller; lipidic plaque, TCFA, CC, and calcification were more frequent; maximum lipid angle and lipid length were longer in patients with NIRS-LRP than in patients without NIRS-LRP. The final angiogram showed deteriorated post-PCI TIMI flow grade (Grade 2 or worse) in 3.7% (2/54) of the patients with NIRS-LRP and in 1.2% (1/86) of those without NIRS-LRP ($p = 0.68$). All the other patients showed normal flow grades (Grade 3). The prevalence of thrombus, plaque rupture, low-intensity area without attenuation, layered plaque, macrophage accumulation, and microvessels showed no significant differences between the two groups. The prevalence of OCT-detected TCFA and cholesterol crystals increased according to the increase of max LCBI_{4mm}, whereas those of plaque rupture, thrombus, macrophage, layered plaque, microvessel, and calcification

were statistically similar irrespective of max LCBI_{4mm} (**Figure 2**).

Supplementary Figure 2A shows the max LCBI_{4mm} according to the presence or absence of TCFA and cholesterol crystals. Median max LCBI_{4mm} was 608 [428–738], 494 [247–655], 419 [284, 644], and 267 [31–478] in culprit lesions with TCFA and CC, lesions with TCFA without CC, lesions with CC without TCFA, and lesions without TCFA and CC. The absence of both TCFA and CCs showed smaller max LCBI_{4mm} compared with patients having at least 1 characteristic. The presence of CCs was not associated with the prevalence of NIRS-LRP in patients having TCFA, whereas NIRS-LRP was more frequent in patients with CCs under the absence of TCFA (**Supplementary Figure 2B**). A representative case with NIRS-LRP with a thick fibrous cap is shown in **Supplementary Figure 3**.

Predictors of NIRS-LRP

Table 2 shows uni- and multivariable logistic regression analyses to predict the presence of NIRS-LRP in the culprit lesions. TCFA and CC were independently predictive of the presence of NIRS-LRP after adjusting for confounding factors.

DISCUSSION

The major findings of this study are as follows: In the multimodality assessment of the culprit lesions of ACS, (i) prevalence of TCFA and CC increased as max LCBI_{4mm}

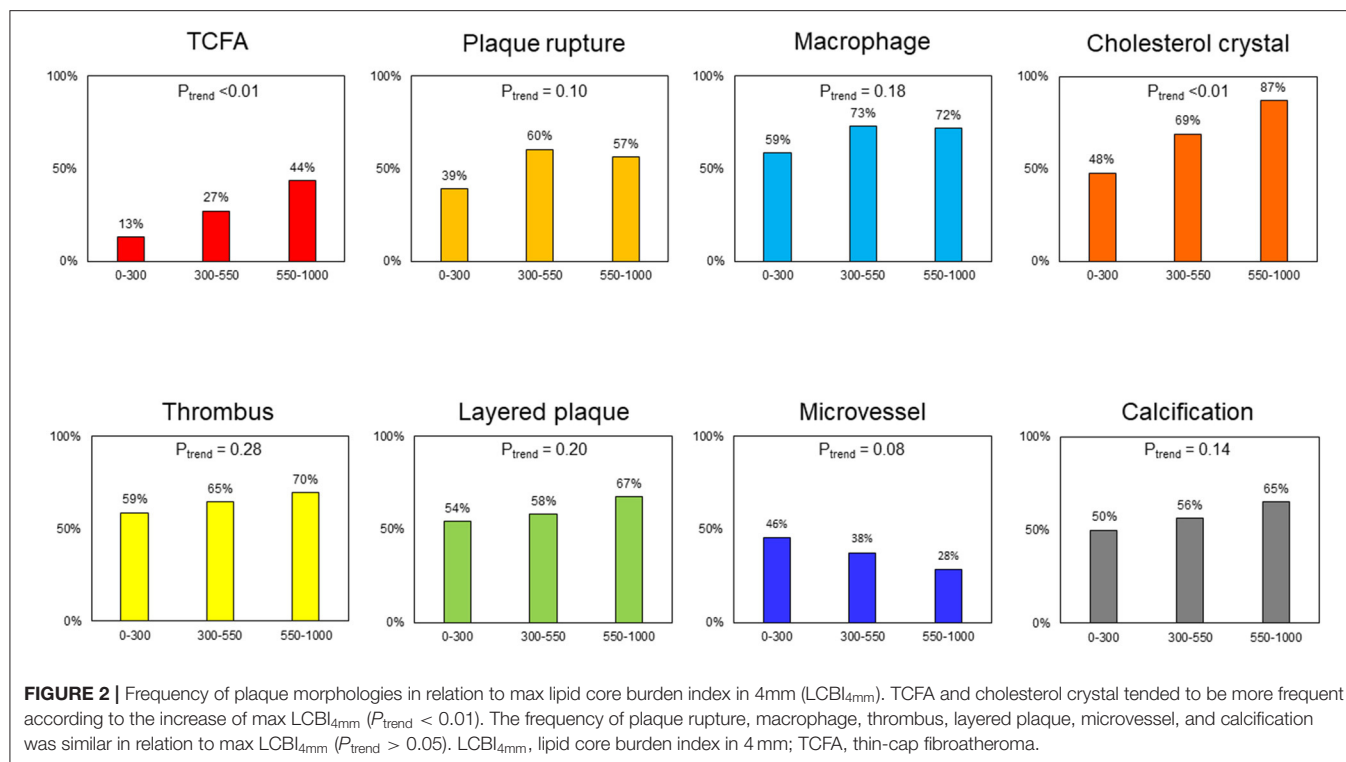
TABLE 1 | Clinical demographics, angiographic, and optical coherence tomography findings.

	Patients with NIRS-LRP (n = 54)	Patients without NIRS-LRP (n = 86)	p value
Clinical demographics			
Age, years	67.0 [58.3, 75.0]	65.5 [55.3, 72.0]	0.30
Male	43 (79.6)	73 (84.9)	0.57
Diabetes mellitus	17 (31.5)	25 (29.1)	0.91
Hypertension	36 (66.7)	57 (66.3)	1.00
Dyslipidemia	27 (50.0)	42 (48.8)	1.00
Current smoking	19 (35.2)	37 (43.0)	0.46
Renal insufficiency*	19 (35.2)	27 (31.4)	0.78
Prior myocardial infarction	2 (3.7)	6 (7.0)	0.66
Prior percutaneous coronary intervention	0 (0.0)	8 (9.3)	0.053
Clinical presentation			0.11
STEMI	22 (40.7)	21 (24.4)	
Non-STEMI	27 (50.0)	52 (60.5)	
Unstable angina	5 (9.3)	13 (15.1)	
Total cholesterol, mg/dL	195.5 [168.3, 221.8]	192.0 [163.3, 211.8]	0.55
LDL cholesterol, mg/dL	123.0 [103.3, 144.5]	111.0 [90.0, 134.0]	0.053
HDL cholesterol, mg/dL	44.0 [36.0, 54.8]	46.0 [41.0, 55.0]	0.20
Triglycerides, mg/dL	112.0 [69.8, 176.5]	109.0 [81.0, 183.0]	0.34
C-reactive protein, mg/dL	0.14 [0.07, 0.39]	0.16 [0.05, 0.38]	0.99
Pre-admission statin treatment	11 (20.4)	30 (34.9)	0.10
Statin on discharge	52 (96.3)	86 (100.0)	0.29
Angiographic findings			
Target vessel			0.25
Left anterior descending artery	37 (68.5)	47 (54.7)	
Left circumflex artery	7 (13.0)	10 (11.6)	
Right coronary artery	10 (18.5)	28 (32.6)	
Left main	0 (0.0)	1 (0.1)	
Minimum lumen diameter, mm	0.66 [0.47, 0.85]	0.80 [0.57, 1.00]	0.02
Reference diameter, mm	2.71 [2.32, 3.21]	2.92 [2.40, 3.36]	0.11
Diameter stenosis, %	74.7 [68.9, 83.0]	74.3 [63.3, 78.9]	0.15
Lesion length, mm	12.8 [10.4, 17.1]	12.3 [9.3, 16.1]	0.30
Optical coherence tomographic findings			
Minimum flow area, mm ²	1.02 [0.82, 1.15]	1.09 [1.00, 1.42]	<0.01
Area stenosis, %	82.8 [78.9, 87.4]	82.4 [75.1, 87.6]	0.44
Lipidic plaque	53 (98.1)	71 (82.6)	0.01
TCFA	23 (42.6)	16 (18.6)	<0.01
Maximum lipid angle, °	287.6 [222.5, 360.0]	199.0 [122.9, 296.8]	<0.01
Thinnest fibrous cap, mm	0.07 [0.06, 0.10]	0.07 [0.06, 0.14]	0.54
Lipid length, mm	12.55 [8.40, 17.30]	8.55 [4.62, 12.38]	<0.01
Thrombus	37 (68.5)	53 (61.6)	0.52
Plaque rupture	31 (57.4)	42 (48.8)	0.42
Low-intensity area without attenuation	49 (90.7)	69 (80.2)	0.15
Cholesterol crystal	44 (81.5)	51 (59.3)	0.01
Layered plaque	37 (68.5)	47 (54.7)	0.15
Macrophage accumulation	38 (70.4)	57 (66.3)	0.75
Microvessels	17 (31.5)	35 (40.7)	0.36
Calcification	37 (68.5)	43 (50.0)	0.048
Maximum calcification angle, °	97.5 [78.0, 130.3]	88.3 [57.0, 136.9]	0.35
Maximum calcification thickness, mm	0.75 [0.53, 1.08]	0.79 [0.59, 1.06]	0.98
Calcified nodule	0 (0)	2 (2)	0.69

Values are n (%) or median [interquartile range].

*Estimated glomerular filtration rate <60 mL/min/1.73 m² using the Modification of Diet in Renal Disease study equation.

HDL, high-density lipoprotein; LDL, low-density lipoprotein; LRP, lipid-rich plaque; NIRS, near-infrared spectroscopy; STEMI, ST-segment elevation myocardial infarction; TCFA, thin-cap fibroatheroma.

**TABLE 2 |** Predictors of NIRS-LRP.

	OR	95% CI	p value	OR	95% CI	p value
Age, per 10 years	1.22	0.90–1.63	0.32	1.31	0.93–1.84	0.13
Male	0.70	0.29–1.69	0.42	0.64	0.23–1.84	0.41
STEMI	2.13	1.02–4.43	0.04	1.90	0.83–4.32	0.13
LDL cholesterol, per 10 mg/dL	1.07	0.99–1.17	0.10	–	–	–
Pre-admission statin treatment	0.48	0.22–1.06	0.07	0.47	0.20–1.14	0.09
Thin-cap fibroatheroma	3.25	1.51–6.98	< 0.01	2.56	1.12–5.84	0.03
Thrombus	1.36	0.66–2.79	0.41	–	–	–
Plaque rupture	1.41	0.71–2.80	0.32	–	–	–
Low-intensity area without attenuation	2.41	0.84–6.99	0.10	–	–	–
Cholesterol crystal	3.02	1.34–6.79	< 0.01	2.90	1.20–6.99	0.02
Layered plaque	1.81	0.88–3.69	0.11	–	–	–
Calcification	2.18	1.07–4.44	0.03	–	–	–

CI, confidence interval; LDL, low-density lipoprotein; LRP, lipid-rich plaque; NIRS, near-infrared spectroscopy; OR, odds ratio; STEMI, ST-segment-elevation myocardial infarction.

increased; (ii) prevalence of plaque rupture, thrombus, macrophage, and a layered plaque was similar in any tertiles of max LCBI_{4mm}; (iii) TCFA and CC were independently predictive of the presence of NIRS-LRP after a multivariable adjustment.

In the pathological process of coronary atherosclerotic lesion progression, focal macrophage infiltration into an intimal lipid pool triggers loss of matrix and extensive cellular debris with an overlying fibrous cap, leading to the necrotic core formation in the plaque. Intraplaque hemorrhage originated from leaky neoangiogenesis and/or plaque fissure promotes the necrotic core expansion coupled with cholesterol crystallization, followed by fibrous cap thinning and rupture (21, 22). Although OCT

provides a high-resolution image and enables us to observe intraplaque structures, the penetration depth is limited and leads to misinterpretation of lipid extent. Thus, we performed a multimodality study to examine OCT-detected plaque features, representing a large amount of lipid using NIRS-detected LCBI as a gold standard.

Jinnouchi et al. reported in an *ex vivo* study (18) that OCT-detected cholesterol crystals were associated with histological stacked cholesterol clefts with high positive and negative predictive values (100 and 84%, respectively) and the presence of intraplaque hemorrhage and late necrotic core, suggesting an ability of OCT-detected cholesterol crystal to identify advanced

plaques. Our results that cholesterol crystal was independently associated with large lipid are supported by these pathological data and may help physicians to detect unstable plaques by OCT. Although we tried to detect intraplaque hemorrhage as OCT-detected LIAs (3, 16, 17), this morphology alone did not significantly relate to NIRS-LRP, and 81% (95/118) of them had concomitant CCs. Furthermore, all CCs were concomitant with LIAs (**Supplementary Figure 1**). LIAs may not always represent intraplaque hemorrhage, and the differential diagnosis can be calcifications and lipid pools in pathological intimal thickening (3). Given that erythrocyte membranes are a principal localized source of free cholesterol in plaques (22, 23), our results suggest that CCs are helpful to identify true intraplaque hemorrhage in OCT-detected LIAs. This explains why we used CCs, not LIA, as one of the vulnerable morphologies in this study.

On the other hand, the prevalence of plaque rupture, thrombus, macrophage, and layered plaque had no significant trend with increasing max LCBI_{4mm}. Although plaque rupture should occur based on TCFA with a large amount of lipid, the plaque components could flow out through the rupture, and OCT-detected plaque rupture may sometimes represent a cavity after an old rupture with a small residual lipid. Indeed, 16% (12/73) of OCT-detected plaque ruptures had max LCBI_{4mm} of < 200 in this population. This may be the reason why plaque rupture was not associated with NIRS-LRP. Thrombus can be presented not only by plaque rupture due to a large amount of lipid but also by plaque erosion and a calcified nodule (21, 22). Similarly, layered plaques are formed by the healing process after ruptured or erosive thrombotic events (21, 22, 24), which is plausible to be irrelevant with max LCBI_{4mm}. In other words, thrombotic events can occur in the absence of a large amount of lipids. Macrophages infiltrate into the lipid pool in pathological intimal thickening and can be observed both in early- and late-stage plaques.

Since TCFA is known to be one of the vulnerable plaque features prone to rupture (21, 22), several studies have tested the effects of intensive medical treatments on fibrous cap thickness (25–27). However, as shown in **Supplementary Figure 3**, our results suggested that a CC could be a marker of unstable lipid-rich plaques even in the absence of a thin fibrous cap and may help predict distal embolization during PCI procedures (8–12).

Study Limitations

First, a selection bias cannot be avoided because this was a retrospective observational study at two centers, having a relatively small sample size. Second, the study comprised patients who had undergone both NIRS and OCT examinations before PCI. Thus, we excluded the patients with severe conditions

making it hard to undergo these imaging examinations, such as chronic kidney disease, cardiogenic shock, or heavily calcified or tortuous lesions, which may also lead to selection bias. Third, we may not identify intraplaque structures, particularly in the case of lipidic plaques due to the signal attenuation and/or limited penetration depth of OCT. Fourth, OCT findings may not always represent the mechanism of the event because a ruptured plaque may not contain a large amount of lipids after the lipid discharge. Fourth Fifth, the findings can be applied only in culprit lesions in patients with ACS. Fifth Sixth, we need further analyses with clinical outcome data to investigate the prognostic impact of PCI for lesions with NIRS-LRP.

CONCLUSION

In ACS culprit lesions, OCT-detected TCFA and CCs rather than plaque rupture and thrombi were closely associated with a great lipid-core burden.

DATA AVAILABILITY STATEMENT

The original contributions presented in the study are included in the article/**Supplementary Material**, further inquiries can be directed to the corresponding author.

ETHICS STATEMENT

The studies involving human participants were reviewed and approved by Tsuchiura Kyodo General Hospital, Tokyo Medical and Dental University. The patients/participants provided their written informed consent to participate in this study.

AUTHOR CONTRIBUTIONS

EU contributed to resources, data curation, investigation, statistical analysis, and writing. TY contributed to resources, investigation, review, and editing. MHa contributed to resources and investigation. MO, YKann, MN, TN, YM, JM, TU, TM, MHo, TSu, and YKana contributed to resources. TK contributed to resources, review, and editing. TSa contributed to review and editing and supervision. All authors contributed to the article and approved the submitted version.

SUPPLEMENTARY MATERIAL

The Supplementary Material for this article can be found online at: <https://www.frontiersin.org/articles/10.3389/fcvm.2022.842914/full#supplementary-material>

REFERENCES

1. Waksman R, Di Mario C, Torguson R, Ali ZA, Singh V, Skinner WH, et al. Identification of patients and plaques vulnerable to future coronary events with near-infrared spectroscopy intravascular ultrasound imaging: a prospective, cohort study. *Lancet*. (2019) 394:1629–37. doi: 10.1016/S0140-6736(19)31794-5
2. Erlinge D, Maehara A, Ben-Yehuda O, Botker HE, Maeng M, Kjoller-Hansen L, et al. Identification of vulnerable plaques and patients by intracoronary near-infrared spectroscopy and ultrasound (PROSPECT II): a prospective natural history study. *Lancet*. (2021) 397:985–95. doi: 10.1016/S0140-6736(21)00249-X
3. Prati F, Regar E, Mintz GS, Arbustini E, Di Mario C, Jang IK, et al. Expert review document on methodology, terminology, and clinical applications of

- optical coherence tomography: Physical principles, methodology of image acquisition, and clinical application for assessment of coronary arteries and atherosclerosis. *Eur Heart J*. (2010) 31:401–15. doi: 10.1093/eurheartj/ehp433
4. Tearney GJ, Regar E, Akasaka T, Adriaenssens T, Barlis P, Bezerra HG, et al. Consensus standards for acquisition, measurement, and reporting of intravascular optical coherence tomography studies: A report from the International Working Group for Intravascular Optical Coherence Tomography Standardization and Validation. *J Am Coll Cardiol*. (2012) 59:1058–72. doi: 10.1016/j.jacc.2011.09.079
 5. Roleder T, Kovacic JC, Ali Z, Sharma R, Cristea E, Moreno P, et al. Combined NIRS and IVUS imaging detects vulnerable plaque using a single catheter system: A head-to-head comparison with OCT. *EuroIntervention*. (2014) 10:303–11. doi: 10.4244/EIJV10I3A53
 6. Zanchin C, Ueki Y, Losdat S, Fahrni G, Daemen J, Ondracek AS, et al. In vivo relationship between near-infrared spectroscopy-detected lipid-rich plaques and morphological plaque characteristics by optical coherence tomography and intravascular ultrasound: A multimodality intravascular imaging study. *Eur Heart J Cardiovasc Imaging*. (2021) 22:824–34. doi: 10.1093/ehjci/jez318
 7. Terada K, Kubo T, Kameyama T, Matsuo Y, Ino Y, Emori H, et al. NIRS-IVUS for differentiating coronary plaque rupture, erosion, and calcified nodule in acute myocardial infarction. *J Am Coll Cardiol Img*. (2021) 14:1440–50. doi: 10.1016/j.jcmg.2020.08.030
 8. Goldstein JA, Maini B, Dixon SR, Brilakis ES, Grines CL, Rizik DG, et al. Detection of lipid-core plaques by intracoronary near-infrared spectroscopy identifies high risk of periprocedural myocardial infarction. *Circ Cardiovasc Interv*. (2011) 4:429–37. doi: 10.1161/CIRCINTERVENTIONS.111.963264
 9. Stone GW, Maehara A, Muller JE, Rizik DG, Shunk KA, Ben-Yehuda O, et al. Plaque characterization to inform the prediction and prevention of periprocedural myocardial infarction during percutaneous coronary intervention: The CANARY trial (Coronary Assessment by Near-infrared of Atherosclerotic Rupture-prone Yellow). *J Am Coll Cardiol Interv*. (2015) 8:927–36. doi: 10.1016/j.jcin.2015.01.032
 10. Kini AS, Motoyama S, Vengrenyuk Y, Feig JE, Pena J, Baber U, et al. Multimodality intravascular imaging to predict periprocedural myocardial infarction during percutaneous coronary intervention. *J Am Coll Cardiol Interv*. (2015) 8:937–45. doi: 10.1016/j.jcin.2015.03.016
 11. Yang HM, Yoon MH, Lim HS, Seo KW, Choi BJ, Choi SY, et al. Lipid-core plaque assessed by near-infrared spectroscopy and procedure related microvascular injury. *Korean Circ J*. (2019) 49:1010–8. doi: 10.4070/kcj.2019.0072
 12. Matsuoka T, Kitahara H, Saito K, Mori N, Tateishi K, Fujimoto Y, et al. Utility of near-infrared spectroscopy to detect the extent of lipid core plaque leading to periprocedural myocardial infarction. *Catheter Cardiovasc Interv*. (2021) 1–10. doi: 10.1002/ccd.29927
 13. Thygesen K, Alpert JS, Jaffe AS, Chaitman BR, Bax JJ, Morrow DA, et al. Fourth universal definition of myocardial infarction (2018). *J Am Coll Cardiol*. (2018) 72:2231–64. doi: 10.1016/j.jacc.2018.08.1038
 14. TIMI Study Group. The Thrombolysis in myocardial infarction (TIMI) trial. Phase I findings. *N Engl J Med*. (1985) 312:932–6. doi: 10.1056/NEJM198504043121437
 15. Xing L, Yamamoto E, Sugiyama T, Jia H, Ma L, Hu S, et al. EROSION study (Effective Anti-thrombotic therapy without stenting: intravascular optical coherence tomography-based management in plaque erosion): A 1-year follow-up report. *Circ Cardiovasc Interv*. (2017) 10:1–8. doi: 10.1161/CIRCINTERVENTIONS.117.005860
 16. Usui E, Matsumura M, Mintz GS, Zhou Z, Hada M, Yamaguchi M, et al. Clinical outcomes of low-intensity area without attenuation and cholesterol crystals in non-culprit lesions assessed by optical coherence tomography. *Atherosclerosis*. (2021) 332:41–7. doi: 10.1016/j.atherosclerosis.2021.08.003
 17. Hoshino M, Yonetsu T, Yuki Y, Inoue K, Kanaji Y, Usui E, et al. Optical coherence tomographic features of unstable coronary lesions corresponding to histopathological intraplate hemorrhage evaluated by directional coronary atherectomy specimens. *J Am Coll Cardiol Interv*. (2018) 11:1414–5. doi: 10.1016/j.jcin.2018.04.013
 18. Jinnouchi H, Sato Y, Torii S, Sakamoto A, Cornelissen A, Bhoite RR, et al. Detection of cholesterol crystals by optical coherence tomography. *EuroIntervention*. (2020) 16:395–403. doi: 10.4244/EIJ-D-20-00202
 19. Shimokado A, Matsuo Y, Kubo T, Nishiguchi T, Taruya A, Teraguchi I, et al. In vivo optical coherence tomography imaging and histopathology of healed coronary plaques. *Atherosclerosis*. (2018) 275:35–42. doi: 10.1016/j.atherosclerosis.2018.05.025
 20. Uemura S, Ishigami KI, Soeda T, Okayama S, Sung JH, Nakagawa H, et al. Thin-cap fibroatheroma and microchannel findings in optical coherence tomography correlate with subsequent progression of coronary atherosclerotic plaques. *Eur Heart J*. (2012) 33:78–85. doi: 10.1093/eurheartj/ehr284
 21. Virmani R, Kolodgie FD, Burke AP, Farb A, Schwartz SM. Lessons from sudden coronary death. *Arterioscler Thromb Vasc Biol*. (2000) 20:1262–75. doi: 10.1161/01.atv.20.5.1262
 22. Yahagi K, Kolodgie FD, Otsuka F, Finn A V, Davis HR, Joner M, et al. Pathophysiology of native coronary, vein graft, and in-stent atherosclerosis. *Nat Rev Cardiol*. (2016) 13:79–98. doi: 10.1038/nrcardio.2015.164
 23. Kolodgie FD, Gold HK, Burke AP, Fowler DR, Kruth HS, Weber DK, et al. Intraplate hemorrhage and progression of coronary atheroma. *N Engl J Med*. (2003) 349:2316–25. doi: 10.1056/nejmoa035655
 24. Burke AP, Kolodgie FD, Farb A, Weber DK, Malcom GT, Smialek J, et al. Healed plaque ruptures and sudden coronary death: Evidence that subclinical rupture has a role in plaque progression. *Circulation*. (2001) 103:934–40. doi: 10.1161/01.CIR.103.7.934
 25. Hattori K, Ozaki Y, Ismail TF, Okumura M, Naruse H, Kan S, et al. Impact of statin therapy on plaque characteristics as assessed by serial OCT, grayscale and integrated backscatter-IVUS. *J Am Coll Cardiol Img*. (2012) 5:169–77. doi: 10.1016/j.jcmg.2011.11.012
 26. Komukai K, Kubo T, Kitabata H, Matsuo Y, Ozaki Y, Takarada S, et al. Effect of atorvastatin therapy on fibrous cap thickness in coronary atherosclerotic plaque as assessed by optical coherence tomography: The EASY-FIT study. *J Am Coll Cardiol*. (2014) 64:2207–17. doi: 10.1016/j.jacc.2014.08.045
 27. Yano H, Horinaka S, Ishimitsu T. Effect of evolocumab therapy on coronary fibrous cap thickness assessed by optical coherence tomography in patients with acute coronary syndrome. *J Cardiol*. (2020) 75:289–95. doi: 10.1016/j.jcc.2019.08.002

Conflict of Interest: The authors declare that the research was conducted in the absence of any commercial or financial relationships that could be construed as a potential conflict of interest.

Publisher's Note: All claims expressed in this article are solely those of the authors and do not necessarily represent those of their affiliated organizations, or those of the publisher, the editors and the reviewers. Any product that may be evaluated in this article, or claim that may be made by its manufacturer, is not guaranteed or endorsed by the publisher.

Copyright © 2022 Usui, Yonetsu, Ohmori, Kanno, Nakao, Niida, Matsuda, Matsuda, Umemoto, Misawa, Hada, Hoshino, Kanaji, Sugiyama, Kakuta and Sasano. This is an open-access article distributed under the terms of the Creative Commons Attribution License (CC BY). The use, distribution or reproduction in other forums is permitted, provided the original author(s) and the copyright owner(s) are credited and that the original publication in this journal is cited, in accordance with accepted academic practice. No use, distribution or reproduction is permitted which does not comply with these terms.



Protective Value of Aspirin Loading Dose on Left Ventricular Remodeling After ST-Elevation Myocardial Infarction

Camilla Calvieri^{1†}, Nicola Galea^{2,3*†}, Francesco Cilia³, Giacomo Pambianchi³, Giuseppe Mancuso³, Domenico Filomena¹, Sara Cimino¹, Iacopo Carbone³, Marco Francone^{4,5}, Luciano Agati¹ and Carlo Catalano³

¹ Department of Clinical, Internal, Anesthesiological and Cardiovascular Sciences, "Policlinico Umberto I" Hospital, Sapienza University of Rome, Rome, Italy, ² Department of Experimental Medicine, Sapienza University of Rome, Rome, Italy, ³ Department of Radiological, Oncological and Pathological Sciences, Sapienza University of Rome, Rome, Italy, ⁴ Department of Biomedical Sciences, Humanitas University, Milan, Italy, ⁵ Humanitas Research Hospital, Istituti di Ricovero e Cura a Carattere Scientifico (IRCCS), Milan, Italy

OPEN ACCESS

Edited by:

Jinwei Tian,

The Second Affiliated Hospital of Harbin Medical University, China

Reviewed by:

Emanuele Monda,

University of Campania Luigi

Vanvitelli, Italy

Carmen Chan,

Queen Mary Hospital, Hong Kong SAR, China

Ali Hosseinsabet,

Tehran University of Medical Sciences, Iran

*Correspondence:

Nicola Galea

nicola.galea@uniroma1.it

[†]These authors have contributed equally to this work and share first authorship

Specialty section:

This article was submitted to Cardiovascular Imaging, a section of the journal *Frontiers in Cardiovascular Medicine*

Received: 30 September 2021

Accepted: 07 February 2022

Published: 16 March 2022

Citation:

Calvieri C, Galea N, Cilia F, Pambianchi G, Mancuso G, Filomena D, Cimino S, Carbone I, Francone M, Agati L and Catalano C (2022) Protective Value of Aspirin Loading Dose on Left Ventricular Remodeling After ST-Elevation Myocardial Infarction. *Front. Cardiovasc. Med.* 9:786509. doi: 10.3389/fcvm.2022.786509

Aims: Left ventricular (LV) remodeling after ST-elevation myocardial infarction (STEMI) is a complex process, defined as changes of LV volumes over time. CMR feature tracking analysis (CMR-FT) offers an accurate quantitative assessment of LV wall deformation and myocardial contractile function. This study aimed to evaluate the role of myocardial strain parameters in predicting LV remodeling and to investigate the effect of Aspirin (ASA) dose before primary coronary angioplasty (pPCI) on myocardial injury and early LV remodeling.

Methods and Results: Seventy-eight patients undergoing CMR, within 9 days from symptom onset and after 6 months, were enrolled in this cohort retrospective study. We divided the study population into three groups based on a revised Bullock's classification and we evaluated the role of baseline CMR features in predicting early LV remodeling. Regarding CMR strain analysis, worse global circumferential and longitudinal strain (GCS and GLS) values were associated with adverse LV remodeling. Patients were also divided based on pre-pPCI ASA dosage. Significant differences were detected in patients receiving ASA 500 mg dose before pPCI, which showed lower infarct size extent and better strain values compared to those treated with ASA 250 mg. The stepwise multivariate logistic regression analysis, adjusted for covariates, indicated that a 500 mg ASA dose remained an inverse independent predictor of early adverse LV remodeling.

Conclusion: GCS and GLS have high specificity to detect early LV adverse remodeling. We first reported a protective effect of ASA loading dose of 500 mg before pPCI on LV myocardial damage and in reducing early LV adverse remodeling.

Keywords: myocardial infarction, feature tracking, cardiac magnetic resonance, myocardial strain, aspirin, ventricular remodeling

INTRODUCTION

Left ventricular (LV) remodeling after ST-elevation myocardial infarction (STEMI) is a complex and multifactorial process, beginning within the first week and lasting almost until 1 year (1). Despite improvements in dual antiplatelet therapy and the reperfusion strategies of STEMI patients, adverse LV remodeling remains an open issue predisposing patients to poor cardiovascular

outcomes (2, 3). “Early” LV adverse remodeling, an LV ventricular maladaptive process occurring until 6 months after myocardial infarction, has been widely described (4, 5), whereas few studies have also described reverse remodeling in those patients (6). The latter is a favorable LV remodeling process, which has been correlated with good clinical outcomes (2, 6). Cardiac magnetic resonance (CMR) is widely considered the gold-standard imaging modality to assess LV volumes and LV ejection fraction (LVEF), to quantify myocardial infarct size (IS), and to predict improvement in regional and global contractile function (2, 4). Different thresholds have been proposed to classify LV remodeling by using CMR (3, 7). Recently, Bulluck et al. have proved that a cut off of 12% of volume increase in left ventricular end-diastolic volume (LVEDV) and/or left ventricular end-systolic volume (LVESV) is more accurate to detect early LV remodeling, compared to other cut-offs (7). This criterion has been proved to identify a high-risk group of STEMI patients for the composite end point of all-cause mortality and heart failure (HF) at a median follow-up of 5.8 years (8). Moreover, different factors assessed by CMR within the first week of an acute STEMI, such as LVEF, IS, and microvascular obstruction (MVO), have been reported to be independent strong predictors of LV adverse remodeling and clinical outcomes after STEMI (9, 10). The quantitative assessment of myocardial contractile deformation enabled by CMR feature tracking analysis (CMR-FT) offers deeper information on regional and global LV function other than LVEF, helping to predict LV remodeling (11, 12). Furthermore, CMR-FT has been increasingly used in STEMI patients to assess the efficacy of cardioprotective therapies in preventing post-infarction LV remodeling (12–14), such as to evaluate the effect of intravenous administration of metoprolol on long term prognostic effect in the randomized METOCARD-CNIC trial (13).

Among cardioprotective drugs, antiplatelet agents play a pivotal role in improving myocardial reperfusion after STEMI (15). To date, a wide dose range of aspirin (ASA) is recommended by current guidelines before primary percutaneous coronary intervention (pPCI) in STEMI patients (16). However, it has been poorly investigated whether the pre-pPCI ASA dose may have an impact on LV remodeling.

The present study aimed to confirm the predictive role of myocardial strain parameters by CMR-FT in detecting LV adverse remodeling and assess the effect of ASA dose before pPCI on IS extent, LV global contractility, and adverse LV remodeling in a population of reperfused STEMI.

METHODS

Study Design

This is a retrospective single-center observational study. All STEMI patients included in this study were treated by pPCI within 12 h after symptoms onset and had undergone CMR in the early post-infarction phase (within 9 days from hospital admission) and after 6 months (FU). We retrospectively selected participants from our Institution’s STEMI CMR registry of 177 patients, 78 patients, admitted to our Coronary Care Unit

between January 2010 and February 2019, who met the inclusion criteria (10).

Demographic, clinical, and pharmacological data were registered in the emergency room before any drug administration and before pPCI reperfusion. STEMI was defined as previously reported (16). Body mass index (BMI) was measured in each patient and we defined obesity as BMI > 25 kg/m². Cardiac troponin I levels were measured within 12 h of admission with acute myocardial infarction defined according to ESC guidelines (16). The normal range for troponin I was between 0 and 0.04 ng/mL. Among angiographic parameters: culprit lesion infarct related artery, TIMI flow before and after PCI, time to reperfusion, pre- and post-pPCI systolic blood pressure (SBP), and diastolic blood pressure (DBP) were collected. Post-pPCI SBP, DBP, and HR values were measured within 2 h post-PCI. The above parameters were not evaluated at the CMR time (neither in the first exam nor at follow-up). Exclusion criteria were previously reported (10).

For LV early remodeling categories, we divided the population into three groups, based on a revised Bullock’s classification scheme for LV remodeling (7) by comparing baseline and 6-month follow-up CMR (FU-CMR) exams: “*adverse remodeling*” defined as an increase of LVEDV and/or LVESV > 12%, “*reverse remodeling*” as a decrease of 12% of LVESV, and “*null remodeling*” as other volume percentage increase or decrease < 12%.

To evaluate the effect of ASA loading dose on IS and LV remodeling, we analyzed a subgroup of 45 STEMI patients, according to oral ASA dose at hospital admission before PCI (we included only patients who received a traceable ASA dose). We divided the population into two groups, one receiving 250 mg and the other treated with a loading dose of 500 mg. ASA dosage was decided according to the preference of the emergency department physicians who treated the patients.

This study complied with the Declaration of Helsinki. All participants gave written informed consent to the protocol and the study was approved by the local ethical committee.

Patients or the public were not involved in the design, conduct, reporting, or dissemination plans of our research.

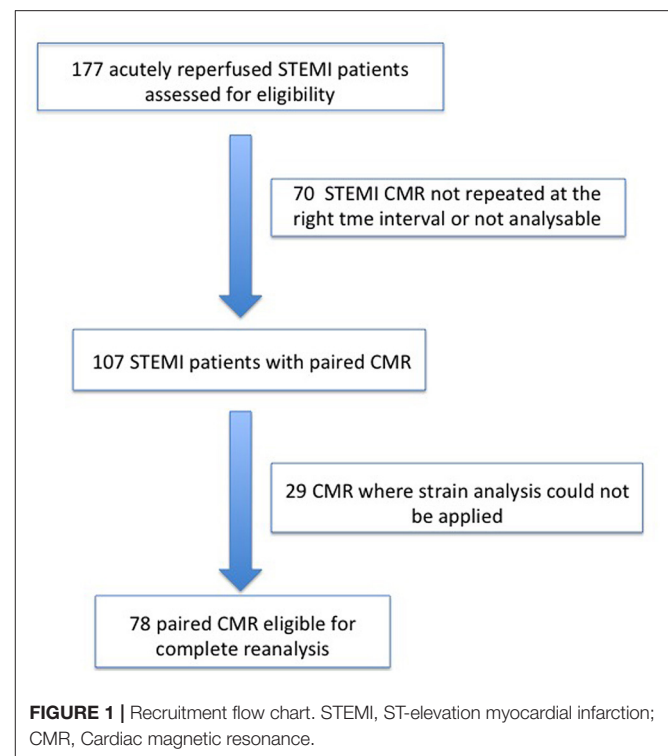
CMR Imaging Protocol and Analysis

CMR exams were performed by using a 1.5-T scanner (Magnetom Avanto, Siemens Healthcare) equipped with a multichannel phase-array cardiac coil. A standardized CMR protocol, including the ECG-gated cine steady-state free precession (cine-MR), T2-weighted short tau inversion recovery (T2w-STIR) for the evaluation of area-at-risk (AAR), and late gadolinium enhancement sequences (LGE) for infarct size (IS), was performed in all patients. Technical parameters and image analysis details have been previously described (10, 17). Image analysis was performed using dedicated commercial software (cvi42 v. 5.3, Circle Cardiovascular Imaging, Calgary, AB, Canada). LV remodeling index (LV-RI) was obtained by dividing LV mass for LVEDV at baseline and FU-CMR exam. Myocardial salvage was quantified by the difference between AAR and IS (18, 19). Feature tracking (CMR-FT) analysis was performed offline using dedicated commercial software (cvi42 v. 5.3, Circle Cardiovascular Imaging, Calgary, AB, Canada) as

detailed elsewhere (11). CMR-FT analysis was applied using basal, mid, and apical ventricular short-axis, vertical-, and horizontal long-axis views in cine-SSFP images. LV endocardial and epicardial contours were traced in a semiautomatic way on short- and long-axis cine-SSFP images in all the phases of the cardiac cycle. LV myocardial tracking was then visually reviewed and the contouring errors were corrected and the analysis repeated. We measured global radial (GRS), circumferential (GCS), and longitudinal (GLS) components of the different LV strain parameters to detect any alteration in myocardial fibers deformability during the cardiac cycle. Furthermore, all measurements of CMR parameters (left and right ventricular volumes, AAR, IS, MVO, GRS, GCS, and GLS) were performed in consensus between two observers with 15 (N.G.) and 6 years (F.C.) of experience in CMR. Intra-observer and inter-observer variability for measurements of GRS, GCS, and GLS were assessed in a sample of 10 patients; two investigators measured blinded the same exam, and one investigator repeated the analysis 1 week later, blinded to the previous measurements. To assess the inter- and intra-observer variability Wilcoxon signed rank test and the intraclass correlation coefficients (ICC) were determined for each parameter (GCS, GLS, GRS).

Statistical Analysis

All continuous variables were assessed for normality with the Shapiro-Wilk test and by examination of their histogram. Data are presented as frequencies and percentages, mean \pm standard deviation (SD) or median and interquartile ranges (IQRs), as appropriate. Comparison of continuous variables was performed using the one-way ANOVA test with the *post-hoc* Bonferroni test or Kruskal-Wallis test, when appropriate. Unadjusted differences between two continuous variables were compared using the Wilcoxon Sum Rank Test or *t*-test di Student, as appropriate. Comparison of normally distributed data between baseline and FU-CMR was performed using paired *t*-test. Correlation between parameters was assessed using either Pearson's correlation coefficient (r) or Spearman's rank coefficient (ρ), where appropriate. Differences in categorical variables were compared using the Chi Square test or Fisher exact test, as appropriate. Comparisons of the CMR-derived parameters (deformation parameters, ventricular volumes, and LVEF) between different groups were evaluated by analysis of covariance (ANCOVA) with Bonferroni-adjusted *post-hoc* tests, after adjusting for age, sex, body mass index (BMI). Interclass correlation coefficients were calculated to assess inter-observer and intra-observer agreement of LV volumes and strain measurements. The primary end-point was defined as LV adverse remodeling. Receiver operating characteristic (ROC) analysis was performed to compare AAR, MVO, LGE, and myocardial strain values in detecting LV adverse remodeling and assess their predictive power. Continuous variables were dichotomized based on Youden's J statistic to allow for comparison of the odds ratios (ORs) in the univariate and multivariate models. In order to identify predictors of LV adverse remodeling, univariate and multivariate logistic regression models were used. Variables with a $p < 0.10$ at univariate logistic analysis were subsequently introduced into the multivariate logistic regression model. To



select the best fit, the stepwise logistic regression method was applied. Associations between the investigated variables and the likelihood of LV adverse remodeling were estimated using hazard ratios (OR) and their 95% confidence intervals (95% CI). The Hosmer-Lemeshow test was performed to show the good calibration of the logistic regression model. Only $p < 0.05$ were considered statistically significant. All tests were 2-tailed and analyses were performed using computer software packages (SPSS-24.0, IBM, NY, USA).

RESULTS

From 2010 to 2019, a total of 1,285 STEMI patients underwent pPCI in Policlinico Umberto I Hospital, of which $\sim 15\%$ had CMR performed and 78 were recruited as reported in the flow chart (Figure 1). According to our internal procedures, when allowed by the clinical condition of the patient, the availability of the scanner/staff, and in the absence of contraindications, CMR was performed in reperfused STEMI patients for the assessment of post-infarction myocardial injury during the acute phase and to detect complications at short and long term follow up. Among the study population of enrolled STEMI patients, 38 (49%) showed adverse, 22 (28%) reverse, and 18 (23%) null LV remodeling, assessed by paired CMR exams (baseline and FU-CMR). Demographic, clinical, angiographic, and pharmacological characteristics of the STEMI population according to the three groups are illustrated in Table 1. No differences in demographic data, cardiovascular risk factors, angiographic presentation, or laboratory findings were found.

TABLE 1 | Demographic, clinical, pharmacological, and angiographic characteristics according to LV remodeling groups.

	Adverse remodeling (n = 38)	Reverse remodeling (n = 22)	Null remodeling (n = 18)	p-value
Demographic data and CAD comorbidities				
Male sex n, %	36 (95)	21 (95)	16 (89)	0.646
Age yrs	59 ± 13	54 ± 10	58 ± 12	0.289
BSA m ²	1.88 ± 0.2	1.97 ± 0.2	1.95 ± 0.1	0.215
BMI kg/m ²	25.6 ± 3.7	27.9 ± 4.5	26.05 ± 3	0.089
Hypertension n, %	15 (40)	12 (55)	11 (61)	0.304
Obesity n, %	24 (63.2)	15 (68.2)	12 (66.7)	0.917
Dislipidemia n, %	20 (54)	7 (32)	11 (61)	0.133
CAD familiarity n, %	23 (62)	14 (64)	13 (72)	0.755
Diabetes n, %	5 (13)	2 (9)	2 (11)	0.874
Smoking habitus n, %	21 (58)	14 (64)	10 (56)	0.881
pPCI characteristics				
LAD IRA n, %	23 (60)	11 (50)	13 (72)	0.568
LCX IRA n, %	7 (18)	5 (23)	1 (6)	
RCA IRA n, %	8 (21)	6 (27)	4 (22)	
Thromboaspiration n, %	20 (71)	8 (53)	6 (46)	0.241
Time to reperfusion min	95 (55–165)	120 (90–256)	120 (95–266)	0.197
TIMI flow pre-pPCI 0 n, %	21 (72)	15 (88)	9 (64)	0.259
TIMI flow pre-pPCI 1 n, %	8 (28)	2 (12)	4 (29)	
TIMI flow post-pPCI 2 n, %	1 (3)	0 (0)	0 (0)	0.583
TIMI flow post-pPCI 3 n, %	31 (97)	18 (100)	16 (100)	
SBP pre-pPCI mmHg	125 ± 24	132 ± 21	141 ± 24	0.071
DBP pre-pPCI mmHg	77 ± 13	80 ± 12	85 ± 11	0.183
HR pre-pPCI bpm	70 (62–80)	60 (65–77)	78 (65–90)	0.517
SBP post-pPCI mmHg	130 ± 15	126 ± 18	131 ± 16	0.674
DBP post-pPCI mmHg	79 ± 9	78 ± 12	76 ± 13	0.856
HR post-pPCI bpm	75 (65–85)	72 (70–80)	75 (59–80)	0.600
Pharmacological therapy before and after pPCI				
ASA 250 mg n, %	15 (71.4)	5 (45.5)	3 (23.1)	0.021
ASA 500 mg n, %	6 (28.6)	6 (54.5)	10 (77)	
Clopidogrel n, %	25 (66)	16 (73)	14 (78)	0.632
GbIIb-IIIa inhibitors n, %	15 (54)	10 (63)	7 (54)	0.833
ACE-inhibitors n, %	31 (86)	21 (96)	17 (94)	0.406
Spironolactone n, %	19 (53)	11 (50)	9 (50)	0.971
β-blockers n, %	32 (91)	20 (91)	18 (100)	0.428
Statins n, %	33 (92)	22 (100)	18 (100)	0.176
Antidiabetics n, %	3 (7.9)	1 (4.5)	1 (5.6)	0.989
Laboratory parameters				
Hb g/dl	13.7 ± 1.8	14.2 ± 1.3	14 ± 1.8	0.635
CK MB peak ng/mL	163.2 ± 127	150.4 ± 141	192.2 ± 228	0.707
Tnl peak ng/ml	30.3 ± 44	9.3 ± 17	37.5 ± 80	0.165
Creatinine mg/dL	0.88 ± 0.2	0.92 ± 0.2	0.89 ± 0.2	0.784

CAD, coronary artery disease; BSA, body mass index; pPCI, primary percutaneous coronary intervention; LAD, left anterior descending artery; IRA, infarct related artery; LCX, left circumflex artery; RCA, right coronary artery; TIMI, Thrombolysis in Myocardial Infarction; SBP, systolic blood pressure; DBP, diastolic blood pressure; HR, heart rate; bpm, beat per minute; ASA, Aspirin; ACE, angiotensin converting enzyme; Hb, hemoglobin; CK MB, creatine kinase isoenzymes MB; Tnl, troponin I. Bold values are those statistically significant, as well as those with a p value < 0.05.

Agreement in strain measurements was excellent with ICC between 0.922 and 0.943 ($p < 0.001$, **Supplementary Material**) and $p > 0.43$ (range 0.43–0.85) at Wilcoxon's test. Regarding pharmacological therapy, no differences were noted about beta-blocker, antidiabetics, statins, ACE-inhibitors, spironolactone, GbIIb-IIIa inhibitors, and clopidogrel use among the three LV remodeling categories, except for the pre-pPCI ASA administration. At the first CMR exam, patients with LV adverse remodeling showed higher AAR, IS, and MVO, if compared to the other two groups (**Table 2**). Meanwhile, at FU-CMR, the adverse remodeling group had lower LVEF, greater IS extent, and lower LV-RI. At CMR strain analysis, significantly worse GCS and GLS values at baseline and FU-CMRs in the adverse LV remodeling group, compared to the sum of the other two groups, were found (**Figure 2**, **Table 2**). After adjusting for age, sex, BMI by ANCOVA analysis, the only CMR derived parameters that reported a different statistical significance if compared with ANOVA analysis, according to the three remodeling groups, were baseline AAR, baseline MVO, FU IS, baseline GRS, and baseline GLS.

At ROC curve analysis (**Figure 3**), AAR, IS, MVO, GLS, and GCS values, measured at baseline CMR, showed significant sensitivity (Se) and specificity (Sp) to detect adverse remodeling at FU-CMR (AAR AUC 0.684, 95% CI 0.563–0.789, $p = 0.0040$ Youden index J 0.3476 with Se: 51% and Sp: 83%; LGE AUC 0.747, 95% CI 0.635–0.859, $p < 0.001$ Youden index J for LGE > 9.7% with Se: 93% and Sp: 40%; MVO AUC 0.637, 95% CI 0.514–0.747, $p = 0.0405$ Youden index J for MVO 0.39 gr with a Se: 42% and Sp: 97%; GLS AUC 0.639, 95% CI 0.521–0.745, $p = 0.0306$ Youden index J > −10.21 % with Se: 35% and Sp: 90%; GCS AUC 0.660 95% CI 0.543–0.764, $p = 0.0138$ Youden index J > −11.09 % with Se: 43% and Sp: 92%). In pairwise comparisons, there were no significant differences between the AUC of ROC curves of the measured CMR parameters by DeLong et al. (20) method ($p > 0.05$ for all). About infarct related artery, significantly worse GCS and GLS were observed in those having, as the culprit lesion, the left anterior descending artery (LAD) compared to circumflex (LCX) and right coronary arteries (RCA) (GCS values in LAD -13.0 ± 4 vs. $-16.0 \pm 3\%$ in LCX vs. $-15.1 \pm 3\%$ in RCA, $p = 0.014$; GLS values $-12 \pm 4\%$ in LAD vs. $-16.1 \pm 3\%$ in LCX vs. $-15.4 \pm 2\%$ in RCA, $p < 0.001$).

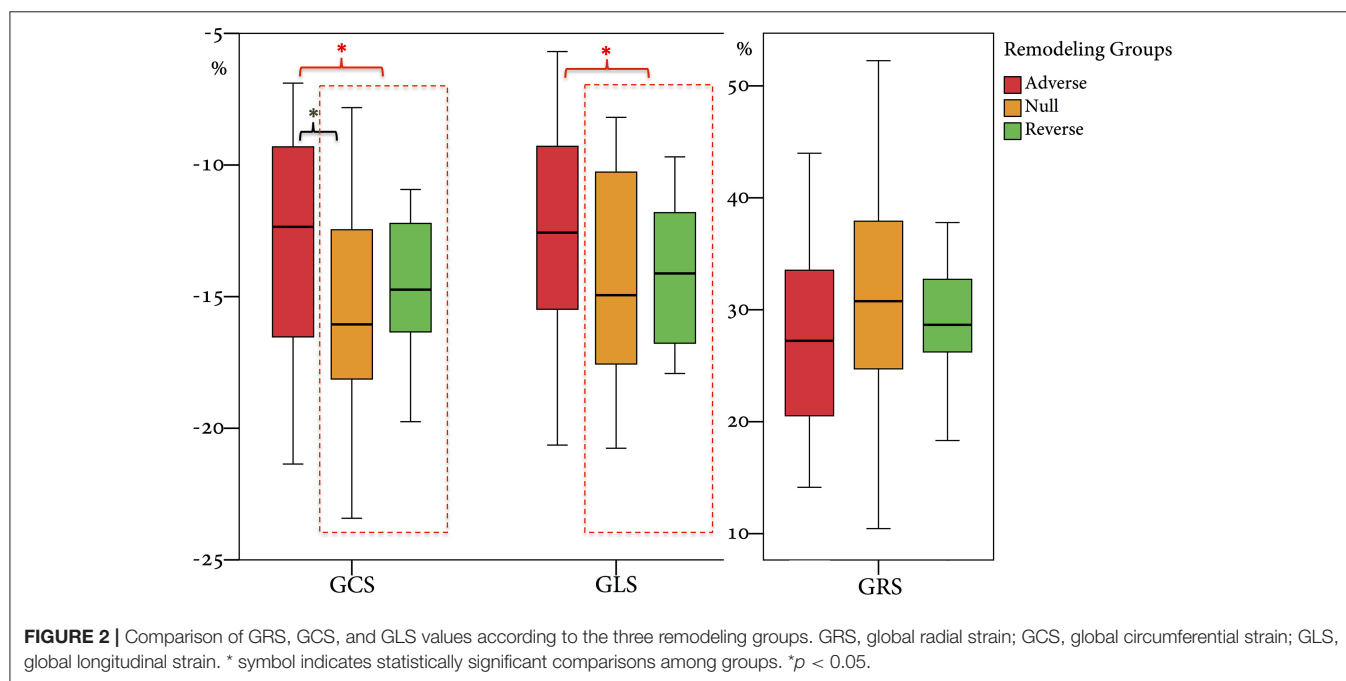
ASA Loading Dose Effects

Among cardiovascular drugs administered before PCI, patients with LV adverse remodeling were less frequently treated with ASA loading dose (500 mg), compared to those with reverse or null remodeling (**Table 1**). Thus, we decided to assess the ASA loading dose effect according to LV remodeling groups. Among the 45 STEMI patients who received a traceable dose of ASA before PCI, 22 STEMI underwent to ASA loading dose, and 23 patients to ASA 250 mg. No differences according to demographic and clinical variables between the two groups were found (**Table 3**). Patients receiving ASA loading dose before PCI had lower MVO and lower IS extent at baseline and FU-CMR and better strain values (GRS and GCS) compared to those treated with ASA 250 mg (**Table 4**). Moreover, in the ASA loading group a significant improvement of GCS and GLS, but not GRS values,

TABLE 2 | CMR parameters at baseline and 6-month follow-up, according to LV remodeling categories.

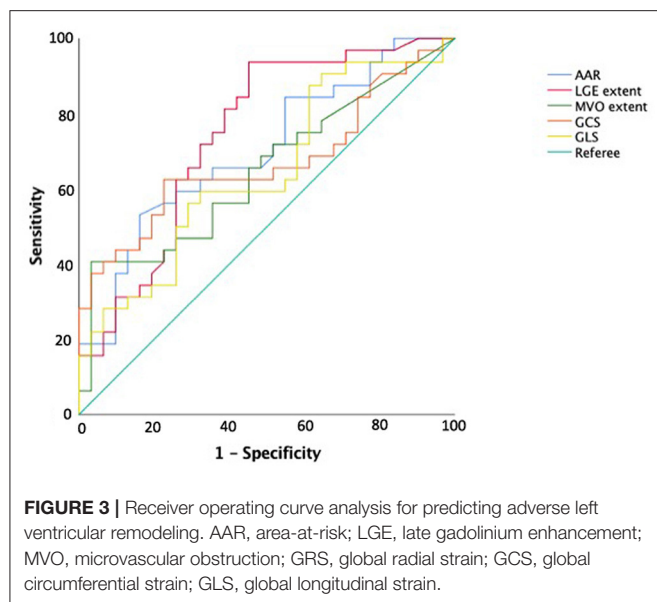
	Adverse remodeling (n = 38)	Reverse remodeling (n = 22)	Null remodeling (n = 18)	p^A vs. R	p^R vs. N	p^A vs. N	p^A vs. (R + N)	p^{overall}
LVEDVi at baseline, ml/m ²	69.3 (55–76)	66.8 (55–82)	72.3 (61–79)	0.939	0.765	0.563	0.749	0.866
LVESVi at baseline, ml/m ²	34 (26–50)	33 (28–42)	36 (29–39)	0.902	0.935	0.687	0.757	0.940
LVMi at baseline, gr/m ²	60.7 (54–73)	61.5 (54–71)	58.8 (44–71)	0.899	0.414	0.207	0.415	0.470
LVEF at baseline, %	46 ± 12	48 ± 9	51 ± 7	1.000	0.863	0.191	0.126	0.177
LV-RI at baseline	0.96 ± 0.2	0.93 ± 0.2	0.86 ± 0.2	1.000	0.907	0.242	0.156	0.215
AAR at baseline, %	30.6 ± 19	19.3 ± 14	18.4 ± 13	0.052	1.000	0.065	0.004	0.017
IS at baseline, %	18.5 (12.5–29.6)	10.8 (4.2–19.7)	9.9 (6.2–21.9)	0.004	0.663	0.027	0.002	0.007
Myocardial salvage, %	9.3 ± 18	7.6 ± 10	6.02 ± 9	0.700	0.627	0.512	0.497	0.755
MVO at baseline, %	0.78 (0.08–3.31)	0.83 (0.075–1.44)	0.24 (0.0–0.79)	0.410	0.207	0.017	0.046	0.058
LVEDVi at FU, ml/m ²	87.7 (75–105)	54.9 (48–69)	72.5(61–78)	<0.001	0.011	0.005	<0.001	<0.001
LVESVi at FU, ml/m ²	42.4 (33–65)	24.3 (20–31)	34.9(30–41)	<0.001	0.002	0.028	<0.001	<0.001
LVMi at FU, gr/m ²	59.4 (51–73)	55.6 (47–62)	56.1 (49–64)	0.221	0.688	0.262	0.149	0.347
LVEF at FU, %	46 ± 12	56 ± 8	50 ± 8	0.005	0.288	0.821	0.007	0.006
LV-RI at FU	0.69 ± 0.2	1.01 ± 0.2	0.82 ± 0.2	<0.001	0.018	0.084	<0.001	<0.001
IS at FU, gr	12.8 (8.5–24.4)	7.2 (3.5–15.4)	10 (5.8–19.5)	0.007	0.413	0.090	0.006	0.016
GRS at baseline, %	26.9 ± 8.2	29.4 ± 5	30.9 ± 9	0.699	0.475	0.198	0.068	0.154
GRS at FU, %	28.8 ± 9	31.4 ± 7	33.4 ± 8	0.762	0.418	0.184	0.074	0.153
GCS at baseline, %	−12.9 ± 4	−14.7 ± 2	−15.5 ± 4	0.225	0.426	0.048	0.012	0.034
GCS at FU, %	−14.2 ± 4	−16.4 ± 3	−16.8 ± 3	0.130	0.668	0.074	0.010	0.036
GLS at baseline, %	−12.4 ± 4	−14.0 ± 3	−14.8 ± 4	0.338	0.483	0.087	0.023	0.063
GLS at FU, %	−13.9 ± 4	−16.0 ± 3	−15.3 ± 4	0.141	0.494	0.676	0.049	0.122

A, adverse remodeling; R, reverse remodeling; N, null remodeling; B, baseline; FU, follow-up; LVEDVi, left ventricular end-diastolic volume index; LVESVi, left ventricular end-systolic volume index; LVMi, Left ventricular mass index; LVEF, left ventricular ejection fraction; LV-RI, left ventricular remodeling index; AAR, area at risk; IS, infarct size; FU, follow-up; MVO, microvascular obstruction; LGE, late gadolinium enhancement; GRS, global radial strain; GCS, global circumferential strain; GLS, global longitudinal strain. Bold values are those statistically significant, as well as those with a p value < 0.05.



between baseline and FU-CMR exams (GCS -15.09 ± 3.8 to $-16.7 \pm 3.2\%$, $p = 0.010$, GLS -14.1 ± 3.9 to $-15.7 \pm 3.2\%$, p

$= 0.011$, GRS 31.0 ± 7.8 to $32.9 \pm 7\%$, $p = 0.104$) was noted. Meanwhile, no significant differences of GCS and GLS values



between two paired CMR exams within the group treated with lower ASA doses (GCS -13.8 ± 3.5 to $-14.1 \pm 3.9\%$, $p = 0.612$, GLS -12.9 ± 3.3 to $-13.8 \pm 3.7\%$, $p = 0.232$, GRS 28.2 ± 6.6 to $27.4 \pm 7.9\%$, $p = 0.594$) were observed (**Figure 4**).

The stepwise multivariate logistic regression analysis was adjusted for IS, GCS, and GLS cut-offs and related to adverse remodeling. An ASA loading dose of 500 mg remained an inverse independent predictor of early adverse LV remodeling (**Table 5**). The Hosmer-Lemeshow test demonstrated good calibration of the logistic regression model ($\chi^2 = 1.095$, $p = 0.955$).

DISCUSSION

Our study confirmed the value of the strain analysis provided by CMR-FT in assessing the risk of LV early adverse remodeling, according to Bulluck's definition (7). In particular, we demonstrated that cut-offs of -11.09% for GCS and -10.21 for GLS, measured at baseline CMR, are highly specific in predicting LV adverse remodeling whereas those parameters do not differ between patients with null and reverse remodeling. Although both strain CMR parameters have been used previously to predict adverse LV remodeling (11, 12, 21), they have never been applied to these new categories (7). Furthermore, we retrospectively evaluated the effect of ASA dose before pPCI in STEMI patients for the first time, and described a positive effect of a loading dose of 500 mg on early LV remodeling.

CMR Parameters in Predicting LV Remodeling

In this study, we categorized the population using the three LV remodeling patterns based on Bulluck's definition (7), observing a similar percentage distribution (adverse remodeling 49 vs. 45%, reverse remodeling 28 vs. 29%, and null remodeling 19 vs. 23%). For CMR parameters, the adverse remodeling group showed

TABLE 3 | Demographic, clinical, pharmacological, and angiographic characteristics according to the ASA group.

	ASA 250 mg (n = 23)	ASA 500 mg (n = 22)	p-value
Male sex n, %	22 (95.7)	20 (90.9)	0.524
Age yrs	59 (51–65)	54 (46–68)	0.658
BSA m ²	1.96 (1.79–2.01)	1.94 (1.82–2.07)	0.708
BMI kg/m ²	25.9 \pm 3.2	26.6 \pm 3.8	0.561
Hypertension n, %	13 (56.5)	11 (52.4)	0.783
Obesity n, %	17 (73.9)	13 (59.1)	0.292
Dislipidemia n, %	14 (60.9)	10 (47.6)	0.378
CAD familiarity n, %	17 (73.9)	11 (52.4)	0.138
Diabetes n, %	4 (17.4)	2 (10.0)	0.669
Smoking habitus n, %	17 (77.3)	14 (66.7)	0.438
LAD n, %	16 (69.5)	15 (68.2)	0.862
LCX n, %	4 (17.4)	3 (13.6)	
RCA n, %	3 (13)	4 (18.2)	
Thromboaspiration n, %	15 (65.2)	8 (36.4)	0.047
Time to reperfusion min	120 (90–210)	120 (80–163)	0.445
TIMI flow pre PCI 0 n, %	17 (73.9)	11 (50)	0.098
TIMI flow pre PCI 1 n, %	6 (26.1)	11 (50)	
TIMI flow post PCI 2 n, %	5 (21.7)	3 (13.6)	0.477
TIMI flow post PCI 3 n, %	18 (78.3)	19 (86.4)	
SBP pre PCI mmHg	130 (112–150)	135 (124–151)	0.510
DBP pre PCI mmHg	80 (70–89)	80 (77–96)	0.412
HR pre PCI bpm	74 (65–81)	67 (61–77)	0.153
SBP post PCI mmHg	130 (120–135)	132 (111–147)	0.522
DBP post PCI mmHg	75 (70–80)	75 (70–88)	0.800
HR post PCI bpm	75 (65–82)	73 (63–80)	0.463
Hb g/dl	13.7 (12.5–15)	13.9 (12.7–15.5)	0.426
CK MB peak ng/mL	123.6 (67–213)	107.3 (26–333)	0.876
TnI peak ng/ml	3.8 (1.9–27.2)	4.4 (0.7–10.7)	0.669

CAD, coronary artery disease; BSA, body mass index; pPCI, primary percutaneous coronary intervention; LAD, left anterior descending artery; IRA, infarct related artery; LCX, left circumflex artery; RCA, right coronary artery; TIMI, Thrombolysis in Myocardial Infarction; SBP, systolic blood pressure; DBP, diastolic blood pressure; HR, heart rate; bpm, beat per minute; ASA, Aspirin; ACE, angiotensin converting enzyme; Hb, hemoglobin; CK MB, creatine kinase isoenzymes MB; TnI, troponin I. Bold values are those statistically significant, as well as those with a p value < 0.05.

greater AAR, IS, and MVO at baseline CMR and greater IS at FU-CMR, as already reported (7). Otherwise, no differences in IS and MVO between reverse and null remodeling groups were found in our study. Notably, there were no differences in salvage myocardium extent among the three groups. Although IS and MVO are known predictors of adverse remodeling (7), the relationship between them and myocardial recovery is still an open issue (6, 7). Moreover, at FU-CMR, the adverse remodeling group showed lower LVEF, LV-RI, and greater IS, as compared to the other two groups. Regarding FT-CMR strain analysis, the adverse remodeling group showed worse GCS and GLS values at baseline and FU-CMR (**Figure 5**), if compared to reverse and null remodeling categories as one. Various studies investigated the value of FT-CMR features in predicting adverse remodeling (11, 12, 22), using different cut-off values and follow-up periods. For the definition of adverse LV remodeling, we considered LVEDV

TABLE 4 | CMR parameters at baseline and 6-month follow-up, according to ASA groups.

	ASA 250 mg (n = 23)	ASA 500 mg (n = 22)	p-value
LVEDV _B ml/m ²	69.2 (54–80)	73.0 (60–82)	0.892
LVESV _B ml/m ²	36.4 (25–49)	35.8 (27–42)	0.716
LVM _B gr/m ²	54.7 (49–65)	59.5 (48–75)	0.716
LVEF _B %	46 ± 10	50 ± 9	0.284
LV-Rl _B	0.9 ± 0.2	0.9 ± 0.2	0.502
LVEF _{FU} %	47.5 ± 10	52.6 ± 10	0.100
LVM _{FU} gr/m ²	54.9 (46–69)	57.5 (48–64)	0.880
LV-Rl _{FU}	0.76 ± 0.2	0.82 ± 0.2	0.342
Adverse remodeling n, %	15 (65)	6 (27)	0.011
AAR _B %	28.4 ± 12	29.4 ± 12	0.888
MVO _B %	0.7 (0.09–2.26)	0.59 (0.00–1.57)	0.555
IS _B %	19.0 (12–29)	12.0 (6–19.7)	0.031
Myocardial salvage %	7.2 (1.9–13.4)	10.4 (2.8–17.4)	0.375
IS _{FU} %	12.6 (9–28)	7.3 (4–17)	0.009
GRS _B %	28.1 ± 6	31.1 ± 8	0.157
GRS _{FU} %	27.4 ± 8	32.9 ± 7	0.022
GCS _B %	−13.9 ± 3	−15.2 ± 4	0.240
GCS _{FU} %	−14.1 ± 4	−16.7 ± 3	0.028
GLS _B %	−12.8 ± 3	−14.2 ± 4	0.204
GLS _{FU} %	−13.8 ± 4	−15.7 ± 3	0.094

ASA, Aspirin; A, adverse remodeling; R, reverse remodeling; N, null remodeling; B, baseline; FU, follow-up; LVEDV_B, left ventricular end-diastolic volume index; LVESV_B, left ventricular end-systolic volume index; LVM_B, Left ventricular mass index; LVEF, left ventricular ejection fraction; LV-Rl, left ventricular remodeling index; AAR, area at risk; IS, infarct size; FU, follow-up; MVO, microvascular obstruction; LGE, late gadolinium enhancement; GRS, global radial strain; GCS, global circumferential strain; GLS, global longitudinal strain. Bold values are those statistically significant, as well as those with a p value < 0.05.

and/or an LVESV delta change of 12%, which is lower than most reports, and 6 months for follow-up, longer if compared to other studies, mostly around 3/4 months. Thus, this issue may have induced a larger rate of adverse remodeling in our population (49%), as compared to other cohorts (17–24.4%) (11, 12, 22, 23). In the majority of studies, baseline GLS was the best predictor of adverse remodeling among all strain values (11, 22–24). In particular, Reindl et al. (22) reported significant differences in baseline strain values and infarct size/MVO percentage between no remodeling and remodeling groups, as observed in our cohort. Moreover, they showed that a GLS-value > −14% was the best independent predictor of 4 months LV adverse remodeling (LVEDV delta change of 10%) with an AUC of 0.610, which do not differ substantially from our GLS AUC value of 0.639 using LVEDV/LVESV delta change of 12%. In the retrospective study of Cha et al. (11), at ROC curve analysis (AUC: 0.756, 95% CI = 0.636–0.887, *p* < 0.001), the GLS cut-off of −12.84% resulted in high sensitivity (Se: 85%) and low specificity (Sp: 61%) in predicting adverse remodeling at 6 months (LVEDV delta change of 20%), whereas in our study the optimal cut-off was lower (GLS > −10.21%), with lower sensitivity (Se: 35%) and higher specificity (Sp: 90%), likely reflecting the different criteria

in classifying the remodeling groups. Interestingly, in our study GCS was the strongest predictor of adverse remodeling among the baseline strain values, as already reported by other authors (12, 25, 26). Holmes et al. (12) found that GCS was a superior predictor of LV adverse remodeling at 3 months follow-up than MVO, GLS, and GRS, although they considered a cohort of both STEMI and non-STEMI patients (12), differently from our population of STEMI only. Similarly, Buss et al. demonstrated that GCS is useful in predicting preserved LV function at 6 months follow-up but they did not evaluate LV remodeling groups (25).

For the other CMR factors, we compared strain parameters and IS in predicting adverse remodeling, demonstrating high sensitivity for IS cut-off of 9.7% (Se: 93%), whereas the GCS and GLS may offer high specificity at the optimal cut-off values (Sp: 92 and 90%, respectively). These results support the evidence that both GCS and GLS values are both useful in the prognostic stratification of STEMI patients and should be interpreted in combination with other CMR parameters, to improve risk profiling and tailoring of therapies.

Lastly, we observed worse GCS and GLS values in patients with LAD culprit artery, compared to LCX and RCA, even if no difference of infarct related artery distribution according to LV remodeling groups was noted. These findings confirmed that the anterior location of myocardial infarction may be responsible for a greater myocardial injury and function impairment, as reported by Masci et al. (27).

Protective Effect of 500 mg Aspirin Administration Prior to PCI

Regarding clinical and procedural characteristics, among the LV remodeling groups, a strong difference in pre-pPCI ASA loading dose was found, suggesting its potentially protective role in preventing early adverse remodeling. Besides, a lower IS extent in patients who received a 500 mg dose of ASA at baseline and FU-CMR was found. These findings are in agreement with those reported in elective procedures, where an ASA reload of 325 mg before PCI improved reperfusion indices, reduced myocardial “no reflow” and periprocedural myocardial injury, by blunting post-PCI increase of thromboxane B₂ production (28). Moreover, a higher ASA dose before revascularization was also associated with an improvement of LVEF (28). A possible explanation could be due to the effect of high ASA doses in inhibiting post-ischemic LV remodeling process (29), by suppression of proinflammatory cytokines, reduction of collagen deposition, and left ventricular hypertrophy as demonstrated in animal models (30). Indeed, Muller et al. (31) observed a reduction of collagen production and LV hypertrophy in a model of angiotensin II induced organ damage in rats pretreated with 600 mg of aspirin, reporting that high ASA doses decreased mortality, cardiac hypertrophy, fibrosis, and albuminuria independently of blood pressure, by inhibition of IKK/NF-κB pathway. Meanwhile, Adamek et al. (29) demonstrated that high ASA doses, after left coronary artery ligation, suppressed inflammatory response in animal experiments, by inhibiting proinflammatory cytokines such IL-1β and TNF, even though not affecting LV remodeling.

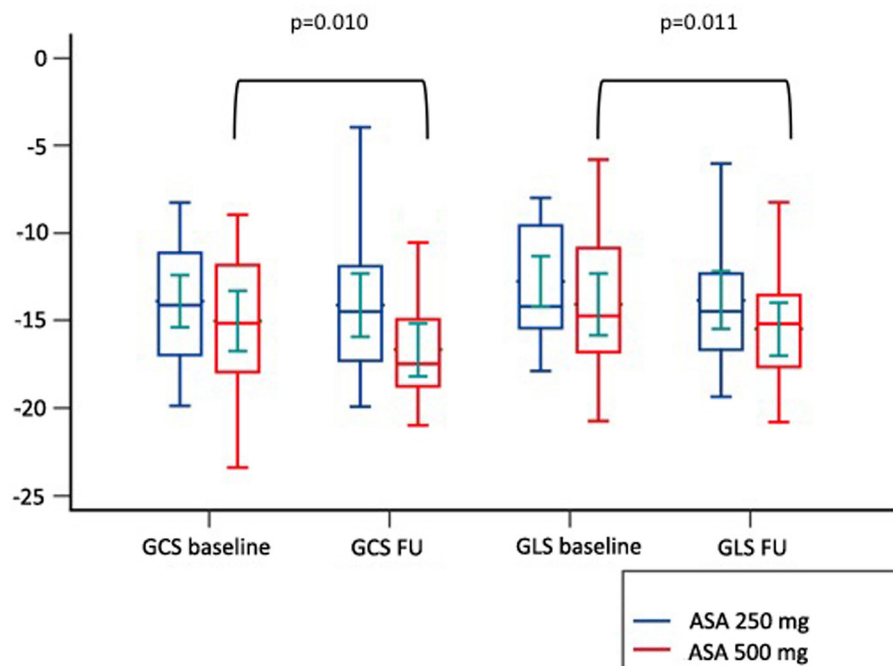


FIGURE 4 | Comparison of paired GLS and GCS values between CMR at baseline and at follow up according to pre-pPCI ASA loading dose. GCS, global circumferential strain; GLS, global longitudinal strain; ASA, aspirin.

TABLE 5 | Stepwise multivariate logistic regression analysis of predictors of LV adverse remodeling.

	Univariate analysis				Multivariate analysis			
	O.R.	Lower	upper	p-value	O.R.	Lower	upper	p-value
ASA 500 mg	0.243	0.073	0.811	0.021	0.243	0.073	0.811	0.021
IS	10.254	2.702	38.912	0.001				
GCS	6.857	2.023	23.243	0.002				
GLS	3.069	1.022	9.216	0.046				
Thromboasp	2.500	0.828	7.548	0.104				
Time to reperfusion	0.998	0.995	1.001	0.207				

ASA, aspirin; IS, infarct size; GCS, global circumferential strain at baseline CMR; GLS, global longitudinal strain at baseline CMR; Thromboasp, thromboaspiration.

As previously reported, a longer time to reperfusion as well as poor reperfusion indices can determine myocardial injury and LV adverse remodeling (19). In our study, although the greater percentage of thrombo-aspiration might explain the higher rate of adverse remodeling in the lower ASA dose group, an ASA loading dose of 500 mg remained, at multivariate analysis, a significant protective factor independently from IS.

Furthermore, for the first time, ASA's role in improving myocardial contractility at FU-CMR has been examined. As FT-CMR has been demonstrated to be a valid and accurate tool to assess short and long term efficacy of cardioprotective drugs such as metoprolol (13, 32), no data about the effect of ASA on early LV remodeling and myocardial strain have been reported previously. Indeed, few clinical studies investigated the optimal ASA dose before pPCI in STEMI patients (16), which remains to

be defined. In a retrospective study by Berger et al., the higher ASA dose in STEMI patients was associated with a greater risk of moderate-to-severe bleeding than lower doses, but there was no difference in 30 day mortality or ischemic related outcomes (33). The CURRENT-OASIS 7 trial compared open-label high-dose (300–325 mg daily) to low-dose (75–100 mg) aspirin in patients with acute coronary syndromes undergoing planned PCI (34). In a recent retrospective study by Rossi et al. (35), a high intravenous ASA dose in STEMI patients increased in-hospital mortality if compared to patients treated with intravenous low doses or oral doses, but it did not influence cardiovascular events after 1-year follow up. Recently, a clinical randomized trial demonstrated that an intravenous ASA dose of 250–500 mg compared to 300 mg orally can lead to complete inhibition of thromboxane generation and platelet aggregation, indicating the efficacy of higher doses

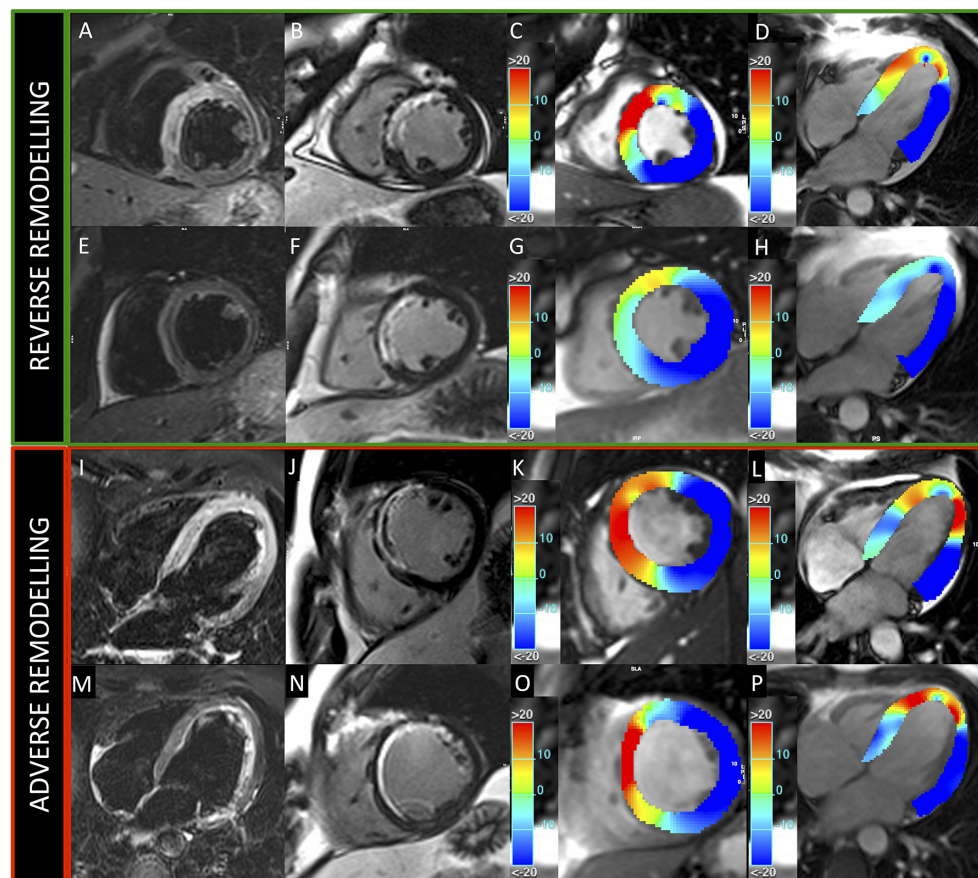


FIGURE 5 | Patients presenting reverse and adverse remodeling at baseline and follow-up CMRs. Images acquired in two patients with reverse (upper green panel) and adverse (lower red panel) remodeling, treated, respectively, with 500 and 250 mg ASA dose. Upper and lower rows represent exams acquired at baseline and 6-month follow-up, respectively. T2-weighted (**A,E,I,M**) and LGE (**B,F,J,N**) images show anterior myocardial infarction in both cases. GCS (**C,G,K,O**) and GLS (**D,H,L,P**) colored maps demonstrate better baseline values and higher recovery of myocardial contractility at follow-up in the patient with reverse remodeling.

in ameliorating myocardial reperfusion (36). The effect of higher ASA doses in ameliorating IS and contractility and in preventing LV adverse remodeling in our study may be interpreted by a complete inhibition of platelet cyclooxygenase 1 activity (COX1) (28). Indeed, as demonstrated in the REMODELING prospective cohort trial in STEMI patients treated with antiplatelet agents, increased levels of platelet activation and inflammation may be responsible for post-STEMI LV adverse remodeling processes (37). High platelet reactivity is frequent after STEMI and is associated with major adverse cardiovascular and cerebral events, especially if associated with P2Y12 inhibitors platelet activity (38). Moreover, plasma thromboxane B₂ has been reported to have a role in modulating myocardial reperfusion and has been hypothesized to have a vasoconstriction effect, modulated by COX-1 (39).

In our study, the protective effect of ASA high loading doses in preventing adverse LV remodeling was independent of IS and myocardial strain values at multivariate analysis. Nonetheless, if confirmed, these data could have a relevant clinical impact, with potential implications on the clinical course and prognosis of a large number of STEMI patients. Therefore, further pharmacological interventional clinical trials that are

adequately powered and possibly multicenter in approach, with a larger population and longer follow-up, are required.

LIMITATIONS

This study has several limitations. First, it is a retrospective and not an interventional-randomized study about ASA dose before pPCI. ASA dose before pPCI has been arbitrarily decided by the emergency room physician or cardiologist on call, introducing a selection bias. Second, considering the nature of the study, no preliminary statistical power analysis was performed and in particular, the statistical significance of the prognostic value of ASA loading dose at multivariate analysis should be interpreted with caution. Third, due to the vast heterogeneity of the study population, we cannot exclude the interference of the effect of other pre-existing drug treatments (in particular chronic administration of ASA). Third, no laboratory assessment of platelet aggregation was performed because it was not foreseen in our routine clinical practices; therefore, it could be only hypothesized that the positive effects of ASA loading dose are mediated by the complete inhibition of Cox1. Fourth, in our study, we considered only global strain values, which represent

validated and reproducible indices of the whole LV contractile function. Regional strain analysis was not included in the analysis, therefore it was not possible to assess whether the positive effect of ASA is exerted directly on the infarcted tissue, in the peri-infarct region, or the remote tissue.

CONCLUSION

Our findings reported that CMR strain parameters (GCS and GLS) have high specificity to detect early adverse remodeling, compared to other CMR imaging indices (IS, AAR, and MVO). The present study described a protective effect of 500 mg ASA loading dose before pPCI in improving LV contractility, myocardial damage, and in reducing early LV adverse remodeling for the first time. Further randomized multicentric studies using CMR analysis are needed to clarify this issue.

DATA AVAILABILITY STATEMENT

The raw data supporting the conclusions of this article will be made available by the authors, without undue reservation.

ETHICS STATEMENT

The studies involving human participants were reviewed and approved by Policlinico Umberto I Hospital - Rome. The

patients/participants provided their written informed consent to participate in this study.

AUTHOR CONTRIBUTIONS

CCal, NG, MF, and LA conceived and designed the study. CCal, FC, DF, and SC collected the clinical, laboratory, and CMR data. NG, GP, GM, FC, and IC performed and independently analyzed CMR exams. NG, FC, and MF interpreted CMR results. CCal performed statistical analyses. CCal, NG, MF, LA, and CCat interpreted the results. CCal, NG, and FC co-wrote the manuscript and prepared the figures. IC, MF, LA, and CCat contributed to the revision of the manuscript. All authors have read and approved the final manuscript.

FUNDING

Publication fee was funded by Sapienza University of Rome – Progetti di Ricerca Prot. RM11916B88D7811D.

SUPPLEMENTARY MATERIAL

The Supplementary Material for this article can be found online at: <https://www.frontiersin.org/articles/10.3389/fcvm.2022.786509/full#supplementary-material>

REFERENCES

- Cohn JN, Ferrari R, Sharpe N. Cardiac remodeling—concepts and clinical implications: a consensus paper from an international forum on cardiac remodeling. Behalf of an International Forum on cardiac remodeling. *J Am Coll Cardiol.* (2000) 35:569–82. doi: 10.1016/S0735-1097(99)00630-0
- Funaro S, La Torre G, Madonna M, Galiuto L, Scara A, Labbadia A, et al. Incidence, determinants, and prognostic value of reverse left ventricular remodelling after primary percutaneous coronary intervention: results of the Acute Myocardial Infarction Contrast Imaging (AMICI) multicenter study. *Eur Heart J.* (2009) 30:566–75. doi: 10.1093/eurheartj/ehn529
- Rodriguez-Palomares JF, Gavara J, Ferreira-Gonzalez I, Valente F, Rios C, Rodriguez-Garcia J, et al. Prognostic value of initial left ventricular remodeling in patients with reperfused STEMI. *JACC Cardiovasc Imaging.* (2019) 12:2445–56. doi: 10.1016/j.jcmg.2019.02.025
- Masci PG, Pavon AG, Pontone G, Symons R, Lorenzoni V, Francone M, et al. Early or deferred cardiovascular magnetic resonance after ST-segment-elevation myocardial infarction for effective risk stratification. *Eur Heart J Cardiovasc Imaging.* (2020) 21:632–9. doi: 10.1093/ehjci/jez179
- Canali E, Masci P, Bogaert J, Bucciarelli Ducci C, Francone M, McAlindon E, et al. Impact of gender differences on myocardial salvage and post-ischaemic left ventricular remodelling after primary coronary angioplasty: new insights from cardiovascular magnetic resonance. *Eur Heart J Cardiovasc Imaging.* (2012) 13:948–53. doi: 10.1093/ehjci/jes087
- Bodi V, Monmeneu JV, Ortiz-Perez JT, Lopez-Lereu MP, Bonanad C, Huser O, et al. Prediction of reverse remodeling at cardiac MR imaging soon after first st-segment-elevation myocardial infarction: results of a large prospective registry. *Radiology.* (2016) 278:54–63. doi: 10.1148/radiol.2015142674
- Bulluck H, Go YY, Crimi G, Ludman AJ, Rosmini S, Abdel-Gadir A, et al. Defining left ventricular remodeling following acute ST-segment elevation myocardial infarction using cardiovascular magnetic resonance. *J Cardiovasc Magn Reson.* (2017) 19:26. doi: 10.1186/s12968-017-0343-9
- Bulluck H, Carberry J, Carrick D, McEntegart M, Petrie MC, Eteiba H, et al. Redefining adverse and reverse left ventricular remodeling by cardiovascular magnetic resonance following st-segment-elevation myocardial infarction and their implications on long-term prognosis. *Circ Cardiovasc Imaging.* (2020) 13:e009937. doi: 10.1161/CIRCIMAGING.119.009937
- Carrick D, Haig C, Rauhalampi S, Ahmed N, Mordi I, McEntegart M, et al. Prognostic significance of infarct core pathology revealed by quantitative non-contrast in comparison with contrast cardiac magnetic resonance imaging in reperfused ST-elevation myocardial infarction survivors. *Eur Heart J.* (2016) 37:1044–59. doi: 10.1093/eurheartj/ehv372
- Galea N, Dacquino GM, Ammendola RM, Coco S, Agati L, De Luca L, et al. Microvascular obstruction extent predicts major adverse cardiovascular events in patients with acute myocardial infarction and preserved ejection fraction. *Eur Radiol.* (2019) 29:2369–77. doi: 10.1007/s00330-018-5895-z
- Cha MJ, Lee JH, Jung HN, Kim Y, Choe YH, Kim SM. Cardiac magnetic resonance-tissue tracking for the early prediction of adverse left ventricular remodeling after ST-segment elevation myocardial infarction. *Int J Cardiovasc Imaging.* (2019) 35:2095–102. doi: 10.1007/s10554-019-01659-w
- Holmes AA, Romero J, Levsky JM, Haramati LB, Phuong N, Rezai-Gharai L, et al. Circumferential strain acquired by CMR early after acute myocardial infarction adds incremental predictive value to late gadolinium enhancement imaging to predict late myocardial remodeling and subsequent risk of sudden cardiac death. *J Interv Card Electrophysiol.* (2017) 50:211–8. doi: 10.1007/s10840-017-0296-9
- Podlesnikar T, Pizarro G, Fernandez-Jimenez R, Montero-Cabezas JM, Sanchez-Gonzalez J, Bucciarelli-Ducci C, et al. Effect of early metoprolol during ST-segment elevation myocardial infarction on left ventricular strain: feature-tracking cardiovascular magnetic resonance substudy from the METOCARD-CNIC trial. *JACC Cardiovasc Imaging.* (2019) 12:1188–98. doi: 10.1016/j.jcmg.2018.07.019
- Bulluck H, Hammond-Haley M, Weinmann S, Martinez-Macias R, Hausenloy DJ. Myocardial infarct size by CMR in clinical cardioprotection studies:

- insights from randomized controlled trials. *JACC Cardiovasc Imaging*. (2017) 10:230–40. doi: 10.1016/j.jcmg.2017.01.008
15. Sardella G, Sangiorgi GM, Mancone M, Colantonio R, Donahue M, Politi L, et al. A multicenter randomized study to evaluate intracoronary abiximab with the ClearWay catheter to improve outcomes with Lysis (IC ClearLy): trial study design and rationale. *J Cardiovasc Med*. (2010) 11:529–35. doi: 10.2459/JCM.0b013e3283341c1c
 16. Ibanez B, James S, Agewall S, Antunes MJ, Bucciarelli-Ducci C, Bueno H, et al. 2017 ESC Guidelines for the management of acute myocardial infarction in patients presenting with ST-segment elevation: the Task Force for the management of acute myocardial infarction in patients presenting with ST-segment elevation of the European Society of Cardiology (ESC). *Eur Heart J*. (2018) 39:119–77. doi: 10.1093/eurheartj/ehx393
 17. Symons R, Masci PG, Francone M, Claus P, Barison A, Carbone I, et al. Impact of active smoking on myocardial infarction severity in reperfused ST-segment elevation myocardial infarction patients: the smoker's paradox revisited. *Eur Heart J*. (2016) 37:2756–64. doi: 10.1093/eurheartj/ehv738
 18. Francone M, Carbone I, Agati L, Bucciarelli Ducci C, Mangia M, Iacucci I, et al. Utility of T2-weighted short-tau inversion recovery (STIR) sequences in cardiac MRI: an overview of clinical applications in ischaemic and non-ischaemic heart disease. *Radiol Med*. (2011) 116:32–46. doi: 10.1007/s11547-010-0594-0
 19. Francone M, Bucciarelli-Ducci C, Carbone I, Canali E, Scardala R, Calabrese FA, et al. Impact of primary coronary angioplasty delay on myocardial salvage, infarct size, and microvascular damage in patients with ST-segment elevation myocardial infarction: insight from cardiovascular magnetic resonance. *J Am Coll Cardiol*. (2009) 54:2145–53. doi: 10.1016/j.jacc.2009.08.024
 20. DeLong ER, DeLong DM, Clarke-Pearson DL. Comparing the areas under two or more correlated receiver operating characteristic curves: a nonparametric approach. *Biometrics*. (1988) 44:837–45.
 21. Khan JN, Singh A, Nazir SA, Kanagala P, Gershlick AH, McCann GP. Comparison of cardiovascular magnetic resonance feature tracking and tagging for the assessment of left ventricular systolic strain in acute myocardial infarction. *Eur J Radiol*. (2015) 84:840–8. doi: 10.1016/j.ejrad.2015.02.002
 22. Reindl M, Tiller C, Holzknacht M, Lechner I, Eisner D, Riepl L, et al. Global longitudinal strain by feature tracking for optimized prediction of adverse remodeling after ST-elevation myocardial infarction. *Clin Res Cardiol*. (2021) 110:61–71. doi: 10.1007/s00392-020-01649-2
 23. Shetye AM, Nazir SA, Razvi NA, Price N, Khan JN, Lai FY, et al. Comparison of global myocardial strain assessed by cardiovascular magnetic resonance tagging and feature tracking to infarct size at predicting remodelling following STEMI. *BMC Cardiovasc Disord*. (2017) 17:7. doi: 10.1186/s12872-016-0461-6
 24. Garg P, Kidambi A, Swoboda PP, Foley JR, Musa TA, Ripley DP, et al. The role of left ventricular deformation in the assessment of microvascular obstruction and intramyocardial haemorrhage. *Int J Cardiovasc Imaging*. (2017) 33:361–70. doi: 10.1007/s10554-016-1006-x
 25. Buss SJ, Krautz B, Hofmann N, Sander Y, Rust L, Giusca S, et al. Prediction of functional recovery by cardiac magnetic resonance feature tracking imaging in first time ST-elevation myocardial infarction. Comparison to infarct size and transmural by late gadolinium enhancement. *Int J Cardiol*. (2015) 183:162–70. doi: 10.1016/j.ijcard.2015.01.022
 26. Mordi I, Bezerra H, Carrick D, Tzemos N. The combined incremental prognostic value of LVEF, late gadolinium enhancement, and global circumferential strain assessed by CMR. *JACC Cardiovasc Imaging*. (2015) 8:540–9. doi: 10.1016/j.jcmg.2015.02.005
 27. Masci PG, Ganame J, Francone M, Desmet W, Lorenzoni V, Iacucci I, et al. Relationship between location and size of myocardial infarction and their reciprocal influences on post-infarction left ventricular remodelling. *Eur Heart J*. (2011) 32:1640–8. doi: 10.1093/eurheartj/ehr064
 28. Basili S, Tanzilli G, Raparelli V, Calvieri C, Pignatelli P, Carnevale R, et al. Aspirin reload before elective percutaneous coronary intervention: impact on serum thromboxane b2 and myocardial reperfusion indexes. *Circ Cardiovasc Interv*. (2014) 7:577–84. doi: 10.1161/CIRCINTERVENTIONS.113.001197
 29. Adamek A, Hu K, Bayer B, Wagner H, Ertl G, Bauersachs J, et al. High dose aspirin and left ventricular remodeling after myocardial infarction: aspirin and myocardial infarction. *Basic Res Cardiol*. (2007) 102:334–40. doi: 10.1007/s00395-007-0647-2
 30. Saito T, Rodger IW, Hu F, Robinson R, Huynh T, Giaid A. Inhibition of COX pathway in experimental myocardial infarction. *J Mol Cell Cardiol*. (2004) 37:71–7. doi: 10.1016/j.yjmcc.2004.04.002
 31. Muller DN, Heissmeyer V, Dechend R, Hampich F, Park JK, Fiebeler A, et al. Aspirin inhibits NF-kappaB and protects from angiotensin II-induced organ damage. *FASEB J*. (2001) 15:1822–4. doi: 10.1096/fj.00-0843fje
 32. Podlesnikar T, Pizarro G, Fernandez-Jimenez R, Montero-Cabezas JM, Sanchez-Gonzalez J, Bucciarelli-Ducci C, et al. Five-year outcomes and prognostic value of feature-tracking cardiovascular magnetic resonance in patients receiving early prereperfusion metoprolol in acute myocardial infarction. *Am J Cardiol*. (2020) 133:39–47. doi: 10.1016/j.amjcard.2020.07.037
 33. Berger JS, Stebbins A, Granger CB, Ohman EM, Armstrong PW, Van de Werf F, et al. Initial aspirin dose and outcome among ST-elevation myocardial infarction patients treated with fibrinolytic therapy. *Circulation*. (2008) 117:192–9. doi: 10.1161/CIRCULATIONAHA.107.729558
 34. Mehta SR, Tanguay JF, Eikelboom JW, Jolly SS, Joyner CD, Granger CB, et al. Double-dose versus standard-dose clopidogrel and high-dose versus low-dose aspirin in individuals undergoing percutaneous coronary intervention for acute coronary syndromes (CURRENT-OASIS 7): a randomised factorial trial. *Lancet*. (2010) 376:1233–43. doi: 10.1016/S0140-6736(10)61088-4
 35. Rossi R, Bagnacani A, Sgura F, Enrique Monopoli D, Coppi F, Talarico M, et al. Effect on mortality of different routes of administration and loading dose of aspirin in patients with ST-segment elevation acute myocardial infarction treated with primary angioplasty. *Coron Artery Dis*. (2020) 31:348–53. doi: 10.1097/MCA.0000000000000840
 36. Zeymer U, Hohlfeld T, Vom Dahl J, Erbel R, Munzel T, Zahn R, et al. Prospective, randomised trial of the time dependent antiplatelet effects of 500 mg and 250 mg acetylsalicylic acid i.v and 300 mg p.o in ACS (ACUTE). *Thromb Haemost*. (2017) 117:625–35. doi: 10.1160/TH16-08-0650
 37. Park Y, Tantry US, Koh JS, Ahn JH, Kang MG, Kim KH, et al. Novel role of platelet reactivity in adverse left ventricular remodelling after ST-segment elevation myocardial infarction: the REMODELING Trial. *Thromb Haemost*. (2017) 117:911–22. doi: 10.1160/TH16-10-0744
 38. Dillinger JG, Saeed A, Spagnoli V, Sollier CB, Sideris G, Silberman SM, et al. High platelet reactivity on aspirin in patients with acute ST elevation myocardial infarction. *Thromb Res*. (2016) 144:56–61. doi: 10.1016/j.thromres.2016.05.002
 39. Niccoli G, Giubilato S, Russo E, Spaziani C, Leo A, Porto I, et al. Plasma levels of thromboxane A2 on admission are associated with no-reflow after primary percutaneous coronary intervention. *Eur Heart J*. (2008) 29:1843–50. doi: 10.1093/eurheartj/ehn325

Conflict of Interest: The authors declare that the research was conducted in the absence of any commercial or financial relationships that could be construed as a potential conflict of interest.

Publisher's Note: All claims expressed in this article are solely those of the authors and do not necessarily represent those of their affiliated organizations, or those of the publisher, the editors and the reviewers. Any product that may be evaluated in this article, or claim that may be made by its manufacturer, is not guaranteed or endorsed by the publisher.

Copyright © 2022 Calvieri, Galea, Cilia, Pambianchi, Mancuso, Filomena, Cimino, Carbone, Francone, Agati and Catalano. This is an open-access article distributed under the terms of the Creative Commons Attribution License (CC BY). The use, distribution or reproduction in other forums is permitted, provided the original author(s) and the copyright owner(s) are credited and that the original publication in this journal is cited, in accordance with accepted academic practice. No use, distribution or reproduction is permitted which does not comply with these terms.



Deceleration Capacity Improves Prognostic Accuracy of Relative Increase and Final Coronary Physiology in Patients With Non-ST-Elevation Acute Coronary Syndrome

OPEN ACCESS

Edited by:

Jinwei Tian,
The Second Affiliated Hospital of
Harbin Medical University, China

Reviewed by:

Xiaoxiang Yan,
Shanghai Jiao Tong University, China
Tong Liu,
Tianjin Medical University, China

*Correspondence:

Hong Jiang
hong-jiang@whu.edu.cn
Lilei Yu
lileiyu@whu.edu.cn

†These authors have contributed
equally to this work

Specialty section:

This article was submitted to
Cardiovascular Imaging,
a section of the journal
Frontiers in Cardiovascular Medicine

Received: 04 January 2022

Accepted: 04 February 2022

Published: 22 March 2022

Citation:

Wang J, Liu C, Guo F, Zhou Z, Zhou L,
Wang Y, Chen H, Zhou H, Liu Z,
Duan S, Sun J, Deng Q, Xu S, Jiang H
and Yu L (2022) Deceleration Capacity
Improves Prognostic Accuracy of
Relative Increase and Final Coronary
Physiology in Patients With
Non-ST-Elevation Acute Coronary
Syndrome.
Front. Cardiovasc. Med. 9:848499.
doi: 10.3389/fcvm.2022.848499

Jun Wang^{1,2,3,4†}, Chengzhe Liu^{1,2,3,4†}, Fuding Guo^{1,2,3,4†}, Zhen Zhou^{1,2,3,4}, Liping Zhou^{1,2,3,4},
Yueyi Wang^{1,2,3,4}, Huaqiang Chen^{1,2,3,4}, Huixin Zhou^{1,2,3,4}, Zhihao Liu^{1,2,3,4},
Shoupeng Duan^{1,2,3,4}, Ji Sun^{1,2,3,4}, Qiang Deng^{1,2,3,4}, Saiting Xu^{1,2,3,4}, Hong Jiang^{1,2,3,4*} and
Lilei Yu^{1,2,3,4*}

¹ Department of Cardiology, Renmin Hospital of Wuhan University, Wuhan, China, ² Cardiac Autonomic Nervous System
Research Centre of Wuhan University, Wuhan, China, ³ Cardiovascular Research Institute, Wuhan University, Wuhan, China,
⁴ Hubei Key Laboratory of Cardiology, Wuhan, China

Background: Both coronary physiology and deceleration capacity (DC) showed prognostic efficacy for patients with acute coronary syndrome (ACS). This retrospective cohort study was performed to evaluate the prognostic implication of DC combined with the relative increase and final coronary physiology as detected by quantitative flow ratio (QFR) for patients with non-ST-elevation ACS (NSTEMI-ACS) who underwent complete and successful percutaneous coronary intervention (PCI).

Methods: Patients with NSTEMI-ACS who underwent PCI with pre- and post-procedural QFR in our department between January 2018 and November 2019 were included. The 24-hour deceleration capacity (DC 24h) was obtained via Holter monitoring. The incidence of major adverse cardiac and cerebrovascular events (MACCEs) during follow up was defined as the primary outcome. The optimal cutoffs of the relative increase, final QFR, and DC 24h for prediction of MACCEs were determined via receiver operating characteristic (ROC) analysis and the predictive efficacies were evaluated with multivariate Cox regression analysis.

Results: Overall, 240 patients were included. During a mean follow up of 21.3 months, 31 patients had MACCEs. Results of multivariate Cox regression analyses showed that a higher post-PCI QFR [adjusted hazard ratio (HR): 0.318; 95% confidence interval (CI): 0.129–0.780], a higher relative QFR increase (HR: 0.161; 95% CI: 0.066–0.391), and a higher DC (HR: 0.306; 95% CI: 0.134–0.701) were all independent predictors of lower risk of MACCEs. Subsequently, incorporating low DC (≤ 2.42) into the risk predicting model with clinical variables, the predictive efficacies of low relative QFR increase ($\leq 23\%$) and low post-PCI QFR (≤ 0.88) for MACCEs were both significantly improved.

Conclusions: The DC combined with relative increase and final coronary physiology may improve the predictive efficacy of existing models based on clinical variables for MACCEs in NSTEMI-ACS patients who underwent complete and successful PCI.

Keywords: deceleration capacity, non-ST-elevation acute coronary syndrome (NSTEMI-ACS), coronary physiology, major adverse cardiac and cerebrovascular events (MACCEs), quantitative flow ratio (QFR)

INTRODUCTION

Currently, physiological assessment of coronary artery stenosis has become an important standard for decision making in percutaneous coronary intervention (PCI) (1–3). Indeed, it has been shown that up to 20% of patients with successful revascularization as evidenced by angiographic findings still suffer from subsequent adverse coronary events (4–6). Recently studies showed that these patients were likely to have residual or diffuse disease and/or stented segment, due to condition of anatomical revascularization, but not functional revascularization (4–6). Previous studies have shown that the relative increase and final fractional flow reserve (FFR) were reliable parameters for evaluating coronary functional revascularization and may confer prognostic efficacy for patients after PCI (4). Furthermore, recent studies suggest that quantitative flow ratio (QFR), a highly consistent parameter, with FFR indicating functional stenosis of coronary arteries, may also be a validated prognostic index after PCI (5–7). However, the current understanding of coronary artery disease (CAD) indicates that the progression of disease is not only determined by the anatomy or physiology of the coronary lesion alone but is also influenced by systemic factors, such as inflammation and autonomic dysfunction (8–10). In this regard, an integrated approach incorporating parameters of functional revascularization, such as QFR, may confer better prognostic implications in patients with non-ST-elevation acute coronary syndrome (NSTEMI-ACS) after PCI.

Our previous study revealed a significant association between parameters of heart rate variability (HRV), inflammation, and coronary artery physiology based on QFR (11). Specifically, the 24-hour deceleration capacity (DC 24h), a Holter-derived indicator of parasympathetic activity, has also been suggested as a strong predictor of mortality for patients with myocardial infarction (12). Physiologically, autonomic nervous system (ANS) carries the essential function in the formation of the heart and critical regulator of vascular development during

cardiovascular development (13). Moreover, pathologically, autonomic function, particularly the activity of the vagus nerve, has been correlated with systemic inflammation (13, 14) and vascular tension (15). Therefore, we hypothesized that an integrated approach incorporating the relative increase and final coronary physiology with DC 24h may improve the prognostic efficacy of current models based on clinical variables in NSTEMI-ACS patients who underwent complete and successful PCI.

METHODS

Patient Population

Patients with NSTEMI-ACS who underwent complete and successful PCI with adequate information of pre- and post-PCI QFR computation in the Department of Cardiology of Renmin Hospital of Wuhan University between January 2018 and November 2019 were retrospectively included. The diagnosis of NSTEMI-ACS was in accordance with the criteria of current guidelines (16), which include unstable angina pectoris (UA) and non-ST segment elevation myocardial infarction (NSTEMI). Complete and successful PCI was defined as the achievement of residual stenosis <20% and final thrombolysis in myocardial infarction (TIMI) flow grade 3. Patients with the following clinical conditions were excluded from the study: atrioventricular block, bundle branch blocks, pacemaker implantation, atrial fibrillation, atrial flutter, chronic coronary syndrome, acute ST-segment elevation myocardial infarction, hyperthyroidism, excessive alcohol intake, any malignancies, any systemic acute or chronic inflammation, use of any medications affecting autonomic function, scarcity of 24h Holter monitoring data, and nonstandard dual-antiplatelet therapy. Patients with the following coronary lesion characteristics which prevented QRS analysis were also excluded: prolonged occluded lesion, coronary bypass graft, left main coronary artery disease, coronary slow flow, unqualified coronary angiographic images including ostial lesion, myocardial bridge, severe vessel overlap or tortuosity at the stenotic segments, and poor coronary image quality where measurement of QFR was not applicable. The study was approved by the Ethics Committee of Renmin Hospital of Wuhan University (No. WDRY2021-K078) before the performance. The flowchart of patient enrollment is shown in Figure 1.

Holter Monitoring

Before the PCI procedure, all patients received Holter monitor examination for HRV analysis and derivation of DC 24h. Holter monitor data was analyzed as previously described (12, 17–20) to obtain the standard time-domain and frequency-domain parameters. Briefly, R peak detection was used to identify

Abbreviations: DC, deceleration capacity; DC 24h, 24-hour deceleration capacity; QFR, quantitative flow ratio; ACS, acute coronary syndrome; CAD, coronary artery disease; NSTEMI-ACS, non-ST-elevation ACS; NSTEMI, acute non-ST-segment elevation myocardial infarction; LAD, left anterior descending artery; LCX, left circumflex artery; RCA, right coronary artery; PCI, percutaneous coronary intervention; MACCEs, major adverse cardiac and cerebrovascular events; ROC, receiver operating characteristic; HR, hazard ratio; CI, confidence interval; ANS, autonomic nervous system; SDNN, standard deviation of all normal sinus RR intervals; RMSSD, root mean square successive difference; SDANN, standard deviation average of NN intervals; PNN50, percentage of the number of times that the difference between adjacent normal RR intervals >50 ms over the total number of NN intervals; HF, high-frequency power; LF, low-frequency power.

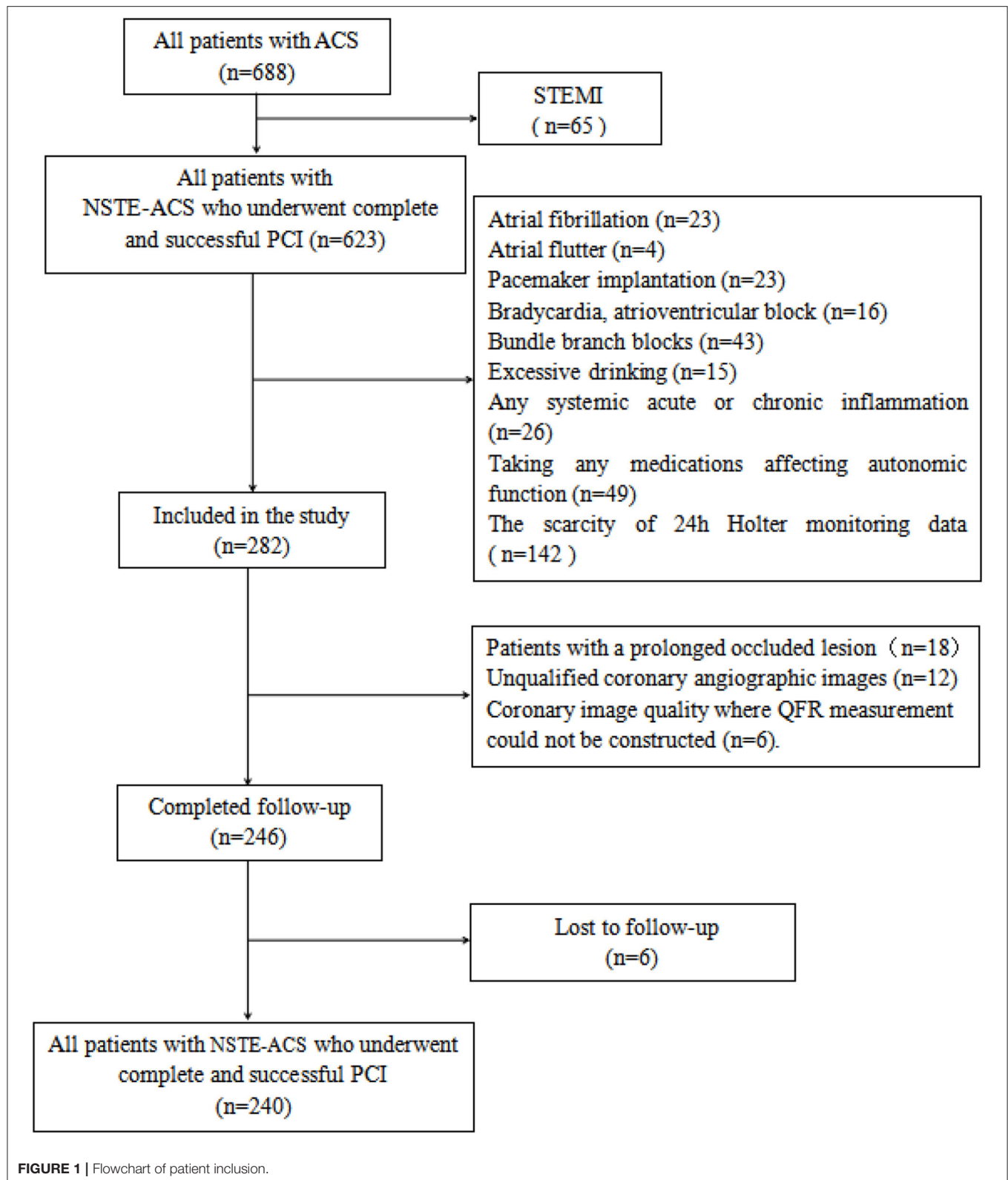


FIGURE 1 | Flowchart of patient inclusion.

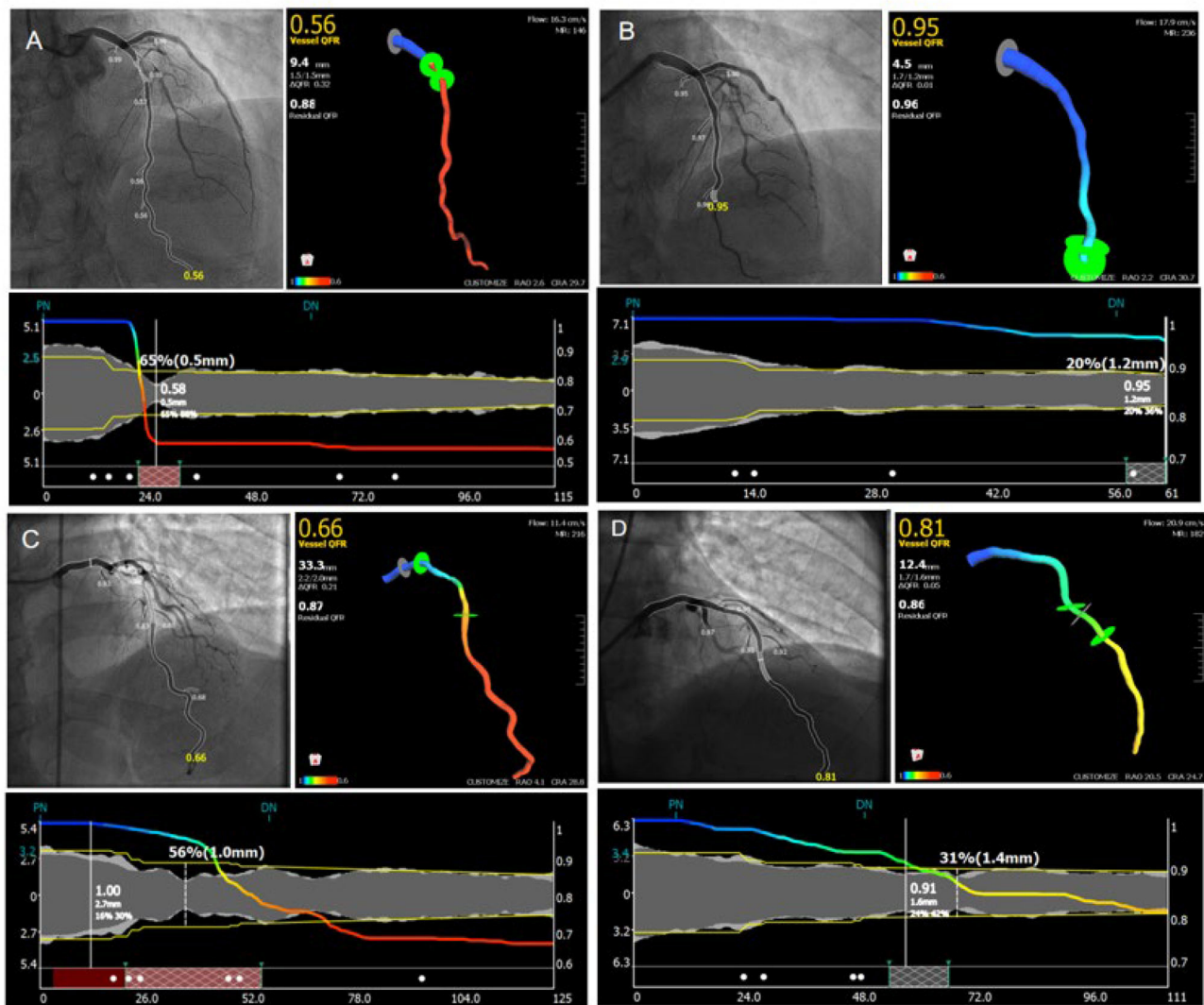


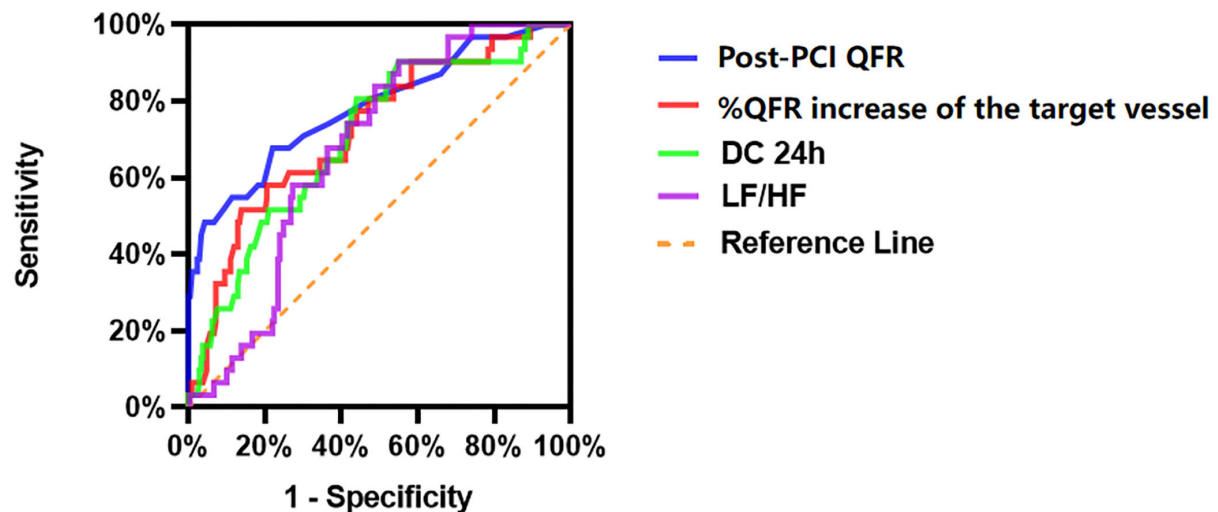
FIGURE 2 | Representative images for cQFR analysis. (A,C) Representative images for the measuring of pre-percutaneous coronary intervention quantitative flow ratio. (B,D) Representative images for the measuring of post-percutaneous coronary intervention quantitative flow ratio.

normal sinus RR intervals and then the standard deviation of all normal sinus RR intervals (SDNN), root mean square successive difference (RMSSD), and standard deviation average of NN intervals (SDANN) were calculated. PNN50 represents the percentage of the number of times that the difference between adjacent normal RR intervals is >50 ms over the total number of NN intervals. The high-frequency power (HF) was defined as high frequency spectra 0.15–0.4 Hz; low-frequency power (LF) as frequency spectra 0.04–0.15 Hz; and very low-frequency (VLF) as frequency spectra 0.003–0.04 Hz. Low-frequency/high-frequency (LF/HF) denotes the ratio of the parameters. Normalized LF and HF powers were calculated with the following equations: $LF_n = 100 \times LF / (\text{total power} - VLF)$ and $HF_n = 100 \times HF / (\text{total power} - VLF)$. DC 24h was calculated, following transformation of the RR intervals using phase-rectified signal averaging, by introducing anchor points (RR0) into the tachygram and generating a plot

of all RR intervals recorded. Four-beat segments were defined as two beats prior to and two beats after the anchor points. The preceding RR-intervals, defined as RR-1 and RR-2, and the RR-interval following RR0 (RR + 1) were used in the analysis. The mean values of RR-2, RR-1, RR0 and RR + 1 were used in the equation $DC\ 24h = [X(0) + X(1) - X(-1) - X(-2)] / 4$ to calculate DC 24h (12, 19, 20).

QFR Computation

For pre-PCI QFR and post-PCI QFR, analysis of all participants was performed offline and analyzed with the AngioPlus system (Pulse Medical Imaging Technology, Shanghai, China). Two selected views of the same coronary artery greater than 25° were transferred to the QFR system and the QFR was calculated by establishing the contrast flow model. Using a modified TIMI frame count method, the contrast flow rate was estimated



Variables	AUC	SE	P	95%CI	Cut-off	Sensitivity	Specificity	Youden index	C-index
Post-PCI the target vessel	0.784	0.049	< 0.001	0.687-0.881	0.88	67.7	78.0	0.457	0.792
%QFR increase of the target vessel	0.724	0.049	< 0.001	0.628-0.820	0.23	58.1	79.4	0.375	0.729
DC 24h	0.703	0.049	< 0.001	0.607-0.799	2.42	74.2	58.4	0.326	0.715
LF/HF	0.676	0.040	0.002	0.597-0.755	1.08	74.2	57.4	0.316	0.691

FIGURE 3 | ROC analysis comparing the predictive efficacies of related variables for the incidence of MACCEs during follow up.

from coronary angiography images and the contrast flow model was calculated.

In our study, the contrast-flow quantitative flow ratio (cQFR) was derived from routine coronary angiography of the target vessel that was most clinically relevant or with the most severe stenosis. The relative increase of QFR was calculated by %QFR increase with PCI [(post-PCI QFR-pre-PCI QFR) / pre-PCI QFR* 100]. Representative examples are shown in **Figure 2**.

Follow Up

Outcome data were obtained either by phone or by clinical visit after discharge. The incidence of major adverse cardiac and cerebrovascular events (MACCEs) during follow up was selected as the primary outcome, which was defined as a composite of cardiac mortality, stroke, revascularization and re-admission for UA. Cardiac mortality was defined as overall mortality from cardiac causes. Stroke was defined as fatal or non-fatal ischemic stroke. Revascularization was defined as revascularization on target or non-target vessels. Re-admission for UA was defined as a new admission for UA following discharge from the index hospitalization for successful PCI.

PCI was performed by an experienced senior interventional cardiologist according to standard procedures with a second-generation drug eluting stent (21). Each patient received a loading dose of either aspirin and clopidogrel prior to PCI. All patients were instructed to take aspirin indefinitely plus a P2Y12 inhibitor for at least 1 year after PCI in conformity with current guidelines with respect to recommended duration of drug therapy (21). After PCI, patients continued with optimized medical treatments and were followed up at clinics regularly after discharge.

Statistical Analysis

Continuous variables were presented as “mean \pm SD” for normal distribution, and medians and interquartile ranges (IQRs) for skewed distribution. A chi-square (χ^2) test was used to analyze the differences among categorical variables, and comparisons of means among multiple groups were performed with ANOVA. A Mann-Whitney U test or Kruskal-Wallis variance analysis was used for analyzing non-normal distribution. The Kaplan-Meier survival curve was used to analyze the potential associations between DC 24h, post-PCI QFR, and % QFR increase at baseline with the incidence of MACCEs in NSTEMI-ACS patients with stent placement. Univariate analysis was carried out first, followed by multivariate Cox regression analysis incorporating variables with significant findings in univariate analysis. The predictability of MACCEs using DC 24h, post PCI QFR, % QFR increase and LF/HF by ROC curve analysis. Moreover, comparisons were also performed to evaluate whether adding DC 24h, post PCI QFR and % QFR increase to the classic risk factors for cardiovascular disease could improve the predictive ability of the models. SPSS 23 was applied for the statistical analysis, with $p < 0.05$ indicating statistical significance.

RESULTS

Patient Characteristics

A total of 240 patients with NSTEMI-ACS who underwent PCI were retrospectively included. The mean age of the patients was 62.8 years and 75.4% of them were male. Most (88.3%) of the patients had UA. During a mean follow-up of 21.3 months, 31 patients had MACCEs.

TABLE 1 | Comparison of patient information and target vessel characteristics according to 24-hour deceleration capacity.

	DC 24h ≤ 2.42 (n = 110)	DC 24h > 2.42 (n = 130)	$t/Z/\chi^2$	p
Male (%)	86 (78.2)	95 (73.1)	0.838	0.360
Age (years)	64.32 \pm 10.76	61.58 \pm 9.20	2.127	0.034
Hypertension (%)	37 (33.6)	54 (41.5)	1.581	0.209
Duration of Hypertension (years)	11.00 (5.50, 16.50)	10.50 (3.00, 18.00)	0.635	0.525
Diabetes mellitus (%)	33 (30.0)	32 (24.6)	0.875	0.350
Duration of diabetes mellitus (years)	5.00 (3.00, 9.00)	5.00 (2.00, 9.75)	0.751	0.453
Current smoking (%)	55 (50.0)	52 (40.0)	2.412	0.120
Current smoking cigarettes per day	12.50 (6.25, 20.00)	20.00 (10.00, 20.00)	0.408	0.683
Duration of smoking (years)	18.00 (10.00, 23.75)	19.00 (12.25, 26.75)	1.009	0.313
Current drinking (%)	30 (27.3)	26 (20.0)	1.762	0.184
Family history of CAD (%)	11 (10.0)	18 (13.8)	0.830	0.362
History of myocardial infarction	8 (7.3)	11 (8.5)	0.116	0.734
Previous PCI (%)	32 (29.1)	35 (26.9)	0.139	0.709
Clinical presentation			0.113	0.737
Unstable angina pectoris	98 (89.1)	114 (87.7)		
NSTEMI	12 (10.9)	16 (12.3)		
Vessel characteristics				
Number of diseased vessels	2.13 \pm 0.86	2.15 \pm 0.82	0.245	0.807
Number of implanted stents	1.75 \pm 1.02	1.86 \pm 1.04	0.800	0.425
Target vascular location			2.054	0.358
LAD	55 (50.0)	59 (45.4)		
LCX	18 (16.4)	31 (23.8)		
RCA	37 (33.6)	40 (30.8)		
Minimal lumen diameter	0.86 \pm 0.40	0.84 \pm 0.37	0.421	0.674
Maximum area stenosis	83.94 \pm 9.86	84.38 \pm 9.70	0.346	0.730
Lesion length of target vessels	17.00 (11.45, 27.70)	15.90 (9.50, 22.70)	1.417	0.156
pre-PCI QFR	0.66 \pm 0.09	0.68 \pm 0.09	1.742	0.083
% QFR increase	0.33 (0.22, 0.50)	0.33 (0.23, 0.46)	0.244	0.808
Post-PCI QFR	0.92 (0.85, 0.96)	0.94 (0.90, 0.97)	1.934	0.053

CAD, coronary artery disease; NSTEMI: acute non-ST-segment elevation myocardial infarction; LAD, left anterior descending artery; LCX, left circumflex artery; RCA, right coronary artery; SDNN, standard deviation of all normal sinus RR intervals; RMSSD, root mean square successive difference; SDANN, standard deviation average of NN intervals; PNN50, percentage of the number of times that the difference between adjacent normal RR intervals > 50 ms over the total number of NN intervals; HF, high-frequency power; LF, low-frequency power; DC 24h, twenty-four-hour deceleration capacity; PCI, percutaneous coronary intervention; QFR, quantitative flow ratio.

TABLE 2 | Incidence of adverse outcomes according to 24-hour deceleration capacity.

	DC 24h ≤ 2.42 (n = 110)	DC 24h > 2.42 (n = 130)	χ^2	P
MACCEs, n (%)	23 (20.9)	8 (6.2)	11.533	0.001
Cardiac death, n (%)	2 (1.8)	1 (0.8)	0.021	0.884
Revascularization, n (%)	9 (8.2)	1 (0.8)	6.448	0.011
Stroke, n (%)	3 (2.7)	1 (0.8)	0.455	0.500
Re-admission for unstable angina, n (%)	10 (9.1)	4 (3.1)	3.923	0.048

ROC Analyses for MACCEs

As shown in **Figure 3**, ROC analyses showed that post-PCI QFR, percent QFR increase, DC 24h and LF/HF were all potential predictors for MACCEs, with the optimized cutoff values of 0.88, 23%, 2.42, and 1.08 and the area under the ROC (AUC) of 0.784, 0.724, 0.703, and 0.676, respectively.

Patient and Target Vessel Characteristics According to DC 24h

As shown in **Table 1**, patients with lower DC 24h were more likely to be older ($p < 0.05$). Moreover, patients with low DC 24h had higher incidence of MACCEs, revascularization, and re-admission for UA

TABLE 3 | Comparison of patient information and characteristics of target vessels in patients with NSTEMI-ACS according to post-PCI QFR of the target vessel.

	Low post-PCI ≤ 0.88 (<i>n</i> = 66)	High post-PCI > 0.88 (<i>n</i> = 174)	t/Z/ χ^2	<i>P</i>
Male (%)	46 (69.7)	135 (77.6)	1.606	0.205
Age (years)	62.41 \pm 10.44	62.99 \pm 9.88	0.403	0.687
Hypertension (%)	19 (28.8)	72 (41.4)	3.223	0.073
Duration of hypertension (years)	10.00 (5.00, 18.00)	11.00 (3.25, 16.00)	0.166	0.868
Diabetes mellitus (%)	18 (27.3)	47 (27.0)	0.002	0.968
Duration of diabetes mellitus (years)	5.00 (2.00, 8.00)	5.50 (3.00, 10.00)	1.391	0.164
Current smoking (%)	28 (42.4)	79 (45.4)	0.172	0.679
Current smoking cigarettes per day	10.00 (3.00, 20.00)	20.00 (10.00, 20.00)	0.880	0.379
Duration of smoking (years)	13.50 (9.25, 24.75)	19.00 (14.25, 25.00)	0.979	0.328
Current drinking (%)	12 (18.2)	44 (25.3)	1.350	0.245
Family history of CAD (%)	9 (13.6)	20 (11.5)	0.207	0.649
History of myocardial infarction	4 (6.1)	15 (8.6)	0.430	0.512
Previous PCI (%)	16 (24.2)	51 (29.3)	0.611	0.435
Clinical presentation			1.073	0.300
Unstable angina pectoris	56 (84.8)	156 (89.7)		
NSTEMI	10 (15.2)	18 (10.3)		
Average heart rate (beats/min)	71.47 \pm 7.12	69.91 \pm 6.71	1.577	0.116
SDNN	111.00 (80.00, 127.50)	112.00 (91.00, 135.25)	1.187	0.235
SDANN	95.00 (73.25, 113.50)	91.00 (73.00, 110.00)	1.181	0.238
rMSSD	38.00 (25.00, 67.75)	42.00 (28.75, 63.25)	0.570	0.569
Pnn50	6.00 (2.00, 15.25)	7.50 (3.00, 15.00)	0.711	0.477
Total power (ms ²)	1,976.45 (1,327.88, 2,842.18)	2,039.40 (1,361.50, 3,278.55)	0.574	0.566
LF (ms ²)	117.30 (66.38, 196.56)	151.21 (90.13, 265.64)	2.929	0.003
HF (ms ²)	116.90 (56.28, 248.03)	130.65 (68.38, 244.63)	0.799	0.425
LF/HF	0.92 (0.70, 1.45)	1.32 (0.76, 1.85)	3.015	0.003
DC 24h ms	2.43 \pm 1.10	2.95 \pm 1.46	2.959	0.004
Target vessel characteristics				
Number of diseased vessels	2.21 \pm 0.90	2.11 \pm 0.81	0.765	0.446
Number of implanted stents	1.88 \pm 1.00	1.79 \pm 1.05	0.612	0.541
Target vascular location			24.740	< 0.001
LAD	48 (72.7)	66 (37.9)		
LCX	10 (15.2)	39 (22.4)		
RCA	8 (12.1)	69 (39.7)		
Minimal lumen diameter	0.79 \pm 0.36	0.87 \pm 0.39	1.571	0.118
Maximum area stenosis	84.90 \pm 8.76	83.91 \pm 10.10	0.694	0.488
Lesion length (mm)	18.60 (11.20, 29.40)	15.95 (10.13, 23.53)	1.394	0.163
Pre-PCI QFR	0.64 \pm 0.10	0.68 \pm 0.08	3.077	0.002
% QFR increase	0.19 (0.13, 0.36)	0.37 (0.26, 0.52)	6.212	< 0.001
Post-PCI QFR	0.82 (0.75, 0.86)	0.95 (0.92, 0.97)	11.880	< 0.001

compared to patients with high DC 24h (all $p < 0.05$; Table 2).

Patient and Target Vessel Characteristics According to Post-PCI QFR

As shown in Table 3, patients with a post-PCI QFR ≤ 0.88 were more likely to have target lesions of the left anterior descending coronary artery, lower LFn, LF/HF, DC 24h, and pre-PCI QFR, and a smaller relative QFR increase compared to patients with post-PCI QFR > 0.88 of the target vessels (all $p < 0.05$). Besides,

patients with post-PCI QFR ≤ 0.88 had higher incidence of MACCEs, revascularization and re-admission for UA compared to those with post-PCI QFR > 0.88 of the target vessels (all $p < 0.05$; Table 4).

Patient and Target Vessel Characteristics According to Relative QFR Increase

As shown in Table 5, patients with smaller %QFR increase were more likely to have lower LFn, LF/HF, maximum area stenosis of the target vessel, post-PCI QFR and higher pre-PCI QFR (all

TABLE 4 | Incidence of adverse outcomes according to post-PCI QFR of the target vessel.

	Low post-PCI ≤ 0.88 (<i>n</i> = 66)	High post-PCI > 0.88 (<i>n</i> = 174)	χ^2	<i>P</i>
MACCEs, <i>n</i> (%)	21 (31.8)	10 (5.7)	28.914	< 0.001
Cardiac death, <i>n</i> (%)	1 (1.5)	2 (1.1)	0.000	1.000
Revascularization, <i>n</i> (%)	6 (9.1)	4 (2.3)	3.958	0.047
Stroke, <i>n</i> (%)	1 (1.5)	3 (1.7)	0.000	1.000
Re-admission for unstable angina, <i>n</i> (%)	11 (16.7)	3 (1.7)	16.825	< 0.001

$p < 0.05$). Moreover, those with smaller %QFR increase had a higher incidence of MACCEs and re-admission for UA compared to patients with larger %QFR increase (all $p < 0.05$; **Table 6**).

Association Between Relative Increase and Final QFR, and DC for MACCEs

The Kaplan-Meier analyses showed that the incidence of MACCEs was significantly different between patients with lower and higher of DC 24h (cutoff: 2.42, $\chi^2 = 11.531$, $p = 0.001$, **Figure 4**), post-PCI QFR (cutoff: 0.88, $\chi^2 = 31.159$, $p < 0.001$, **Figure 5**), and %QFR increase of the target vessel (cutoff: 23%, $\chi^2 = 20.420$, $p < 0.001$, **Figure 6**). Results of multivariate Cox regression analyses suggested that hypertension (HR: 6.816; 95% CI: 2.986–15.559), LF/HF > 1.08 (HR: 0.335; 95% CI: 0.144–0.779), DC 24h > 2.42 ms (HR: 0.306; 95% CI: 0.134–0.701), pre-PCI QFR (HR: 0.527; 95% CI: 0.346–0.802), post-PCI QFR > 0.88 (HR: 0.318; 95% CI: 0.129–0.780) and relative increase percentage of QFR $> 23\%$ (HR: 0.161; 95% CI: 0.066–0.391) were all independent predictors of MACCEs (**Table 7**, all $p < 0.05$).

Prognostic Implication of Relative Increase and Final QFR Combined With DC

As shown in **Figure 7**, incorporating post-PCI QFR (Model 2) significantly enhanced the ability to predict accurately the MACCEs compared with Model 1 which included traditional cardiovascular risk factors only (AUC: 0.858 versus 0.685). The predictive ability further increased in Model 3, which incorporated % QFR increase (AUC: 0.867; C-index: 0.881; Youden index: 0.665; sensitivity: 87.1%; specificity: 79.4%; $p < 0.001$). Moreover, Adding DC 24h ≤ 2.42 into Model 4 further improved the predictive efficacy of the model for MACCEs (AUC: 0.888; C-index: 0.903; Youden index: 0.684; sensitivity: 87.1%; specificity: 81.3%; CI: 0.829–0.947; $p < 0.001$, **Figure 8**).

As shown in **Supplementary Figure 1**, the C-index was 0.875 (95% CI: 0.799–0.916, $p < 0.001$) for prognostic model 5, containing model 1 plus post-PCI QFR of the target vessel ≤ 0.88 , and 0.802 (95% CI: 0.695–0.877, $p < 0.001$) for model 6, containing model 1 plus %QFR increase of the target vessel $\leq 23\%$. For model 7, containing model 1 plus DC 24h ≤ 2.42 ms, the C-index was 0.793 (95% CI: 0.689–0.865, $p < 0.001$). These results suggest that model 5 is a more powerful predictor of MACCEs than %QFR increase of the target vessel $\leq 23\%$ or DC 24h ≤ 2.42 ms.

DISCUSSION

In this retrospective cohort study, we included patients with NSTEMI who underwent complete revascularization with PCI and who had adequate information on pre- and post-procedural QFR and Holter-derived HRV data. We found that lower post-PCI QFR (≤ 0.88), smaller % QFR increase ($\leq 23\%$), and lower DC 24h (≤ 2.42) at baseline were all independent predictors for the risk of MACCEs during follow up. Moreover, incorporation of relative increase and final QFR combined with DC may improve the predictive efficacy of existing models based on clinical variables for MACCEs in patients with NSTEMI-ACS.

Risk stratification remains challenging in patients with NSTEMI-ACS, particularly for those after PCI (22, 23). Although multiple large observational studies have suggested a potential role of post-PCI FFR as a predictor for adverse events in the future, the optimal cutoff remains unknown and may be variable according to the different patient populations included (24–26). More importantly, FFR can only be obtained *via* invasive procedures with the assistance of an additional pressure guidewire and the use of adenosine, which significantly limits its use in clinical practice (27). In comparison, QFR, as a noninvasive angiographically-derived FFR measurement is more applicable in clinical settings. Previous studies have confirmed that QFR is highly consistent with FFR and could be used as a validated indicator of functional coronary stenosis (28, 29). A previous study that included 602 patients who underwent complete and successful revascularization with a mean follow-up of 629 days showed that lower values of QFR might be a risk factor for the increased incidence of vessel-oriented adverse events (5). Alternatively, a retrospective study that included 771 vessels with post-PCI QFR suggested a predictive efficacy and independent correlation between post-PCI QFR and long-term vessel-related clinical outcomes in state of the PCI practice (6). Our results, which showed a possible prognostic role of post-PCI QFR for MACCEs in NSTEMI-ACS patients after PCI, is consistent with the findings of these studies. Nevertheless, neither pre-PCI FFR nor post-PCI QFR alone could fully discriminate the degree of relative contribution of stented and non-stented segment disease burden. Therefore, in order to discriminate the relative contribution of each component of coronary artery lesions, previous studies showed that the percentage of increase of the FFR value before and after PCI has also been independently and significantly

TABLE 5 | Comparison of patient information and target vessel characteristics according to percent QFR increase of the target vessel.

	Low %QFR increase $\leq 23\%$ (<i>n</i> = 62)	High %QFR increase $> 23\%$ (<i>n</i> = 178)	t/Z/ χ^2	<i>P</i>
Male (%)	47 (75.8)	134 (75.3)	0.007	0.934
Age (years)	61.53 \pm 10.54	63.29 \pm 9.83	1.188	0.236
Hypertension (%)	20 (32.3)	71 (39.9)	1.137	0.286
Duration of hypertension (years)	12.00 (7.00, 15.75)	10.00 (3.00, 18.00)	0.062	0.950
Diabetes mellitus (%)	19 (30.6)	46 (25.8)	0.537	0.464
Duration of diabetes mellitus (years)	5.00 (2.00, 8.00)	5.00 (3.00, 9.00)	0.737	0.461
Current smoking (%)	30 (48.4)	77 (43.3)	0.490	0.484
Current smoking cigarettes per day	20.00 (10.00, 20.00)	15.00 (5.00, 20.00)	1.124	0.261
Duration of smoking (years)	15.00 (8.75, 23.50)	19.00 (13.75, 25.50)	1.788	0.074
Current drinking (%)	17 (27.4)	39 (21.9)	0.780	0.377
Family history of CAD (%)	8 (12.9)	21 (11.8)	0.053	0.818
History of myocardial infarction	6 (9.7)	13 (7.3)	0.356	0.551
Previous PCI (%)	16 (25.8)	51 (28.7)	0.185	0.667
Clinical presentation			2.994	0.084
Unstable angina pectoris	51 (82.3)	161 (90.4)		
NSTEMI	11 (17.7)	17 (9.6)		
Average heart rate (beats/min)	71.29 \pm 7.29	70.01 \pm 6.68	1.268	0.206
SDNN	113.50 (81.50, 136.00)	110.00 (90.75, 134.25)	0.120	0.904
SDANN	99.50 (73.25, 120.50)	90.50 (73.00, 109.25)	1.667	0.096
rMSSD	41.00 (25.75, 61.50)	41.50 (28.75, 66.00)	0.681	0.496
Pnn50	7.00 (2.75, 18.25)	7.00 (3.00, 15.00)	0.332	0.740
Total power (ms ²)	1,933.05 (1,290.48, 2,820.45)	2,039.40 (1,361.50, 3,251.30)	0.801	0.423
LF (ms ²)	119.65 (53.06, 212.74)	144.25 (93.51, 246.23)	2.658	0.008
HF (ms ²)	109.60 (60.85, 227.50)	131.20 (67.78, 252.13)	0.943	0.346
LF/HF	0.92 (0.62, 1.50)	1.28 (0.76, 1.82)	2.618	0.009
DC 24h ms	2.84 \pm 1.50	2.79 \pm 1.35	0.214	0.830
Target vessel characteristics				
Number of diseased vessels	2.15 \pm 0.88	2.14 \pm 0.82	0.038	0.970
Number of implanted stents	1.77 \pm 0.95	1.83 \pm 1.06	0.339	0.735
Target vascular location			3.776	0.151
LAD	35 (56.5)	79 (44.4)		
LCX	13 (21.0)	36 (20.2)		
RCA	14 (22.6)	63 (35.4)		
Minimal lumen diameter	0.87 \pm 0.38	0.84 \pm 0.38	0.549	0.583
Maximum area stenosis	81.43 \pm 9.07	85.11 \pm 9.83	2.552	0.011
Lesion length of target vessels	16.30 (11.30, 25.93)	16.40 (10.20, 25.90)	0.625	0.532
Pre-PCI QFR	0.72 \pm 0.08	0.65 \pm 0.08	5.989	<0.001
% QFR increase	0.16 (0.12, 0.20)	0.40 (0.31, 0.55)	11.473	<0.001
Post-PCI QFR	0.86 (0.80, 0.91)	0.94 (0.91, 0.97)	7.146	<0.001

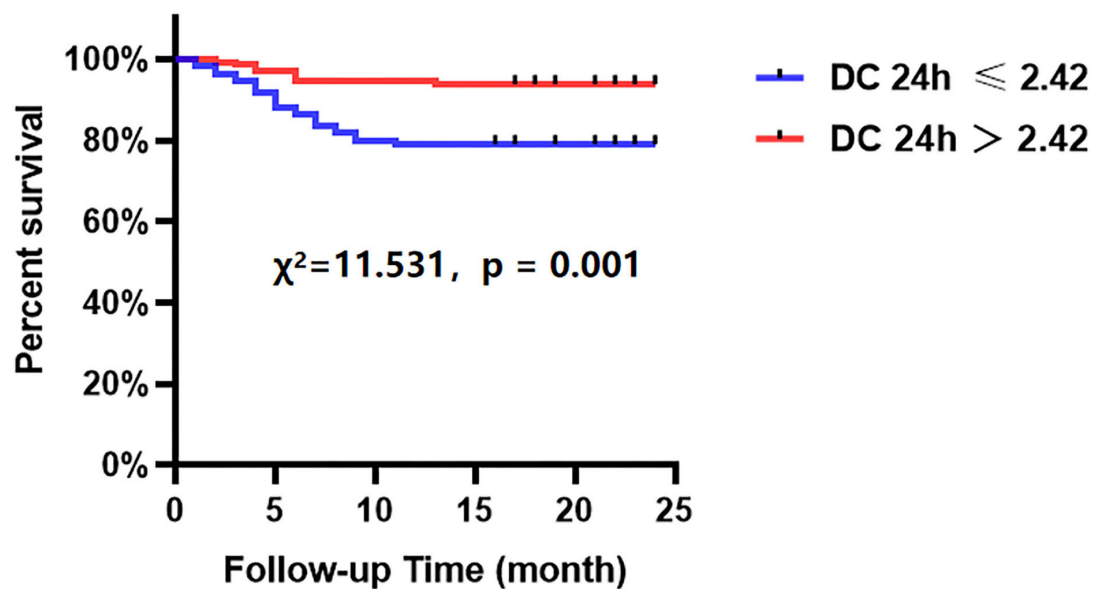
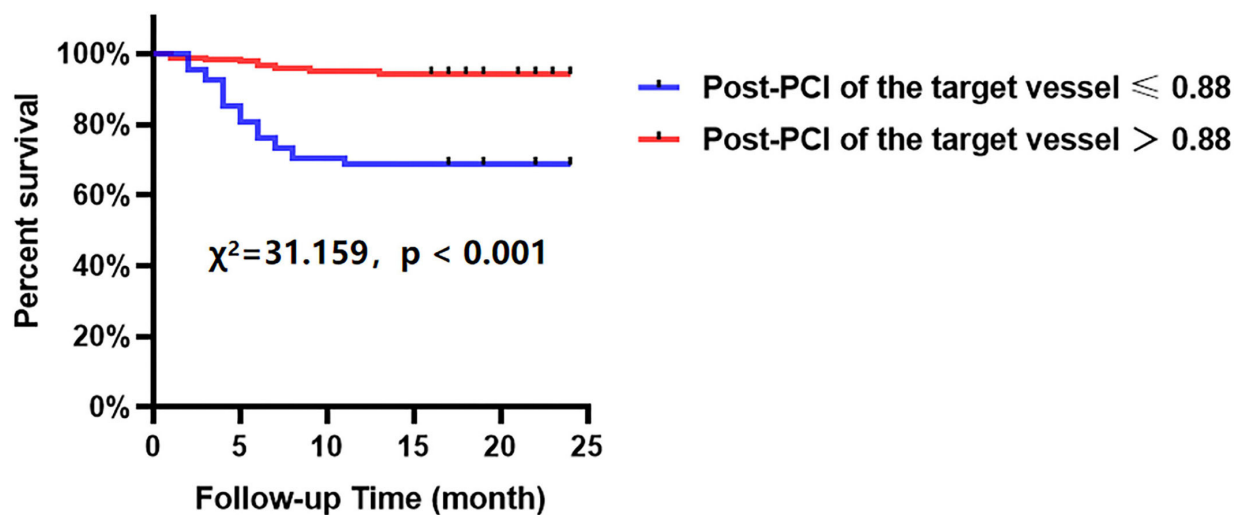
correlated with poor long-term prognosis (4), and integration of the concept of percent FFR increase and post-PCI FFR value allowed a better discrimination of high-risk patients after complete and successful PCI (4). In our study, significant associations were observed between percent QFR increase and post-PCI QFR with MACCEs after PCI. However, all these findings are focused on the local interaction between stents and targeted lesions. It could be hypothesized that incorporating parameters that indicated the systematic burden of CAD, such as systematic inflammation and autonomic dysregulation, may

further improve the prognostic efficacy of models based on current clinical variables.

Previous studies showed that the ANS is directly involved in cardiovascular development (30–32). Previous ex vivo studies showed that the imbalance of ANS may be an early marker of acute cardiovascular disease events (33–36). In addition, ANS is shown to have key effects on vasoconstriction and vasodilation, which influence vessel physiology (13, 37). Alternatively, the mechanism underlying persistently lowered shear stress appears to be the formation of vulnerable plaque (38). However, there

TABLE 6 | Incidence of adverse outcomes according to percent QFR increase of the target vessel.

	Low %QFR increase $\leq 23\%$ (<i>n</i> = 62)	High %QFR increase $> 23\%$ (<i>n</i> = 178)	χ^2	<i>P</i>
MACCEs, <i>n</i> (%)	18 (29.0)	13 (7.3)	19.301	<0.001
Cardiac death, <i>n</i> (%)	1 (1.6)	2 (1.1)	0.000	1.000
Revascularization, <i>n</i> (%)	5 (8.1)	5 (2.8)	2.001	0.157
Stroke, <i>n</i> (%)	2 (3.2)	2 (1.1)	0.289	0.591
Re-admission for unstable angina, <i>n</i> (%)	10 (16.1)	4 (2.2)	13.704	<0.001

**FIGURE 4 |** Cumulative event-free survival probability of MACCEs in patients with NSTEMI-ACS who underwent PCI according to the DC 24 h.**FIGURE 5 |** Cumulative event-free survival probability of MACCEs in patients with NSTEMI-ACS who underwent PCI according to post-PCI of the target vessel.

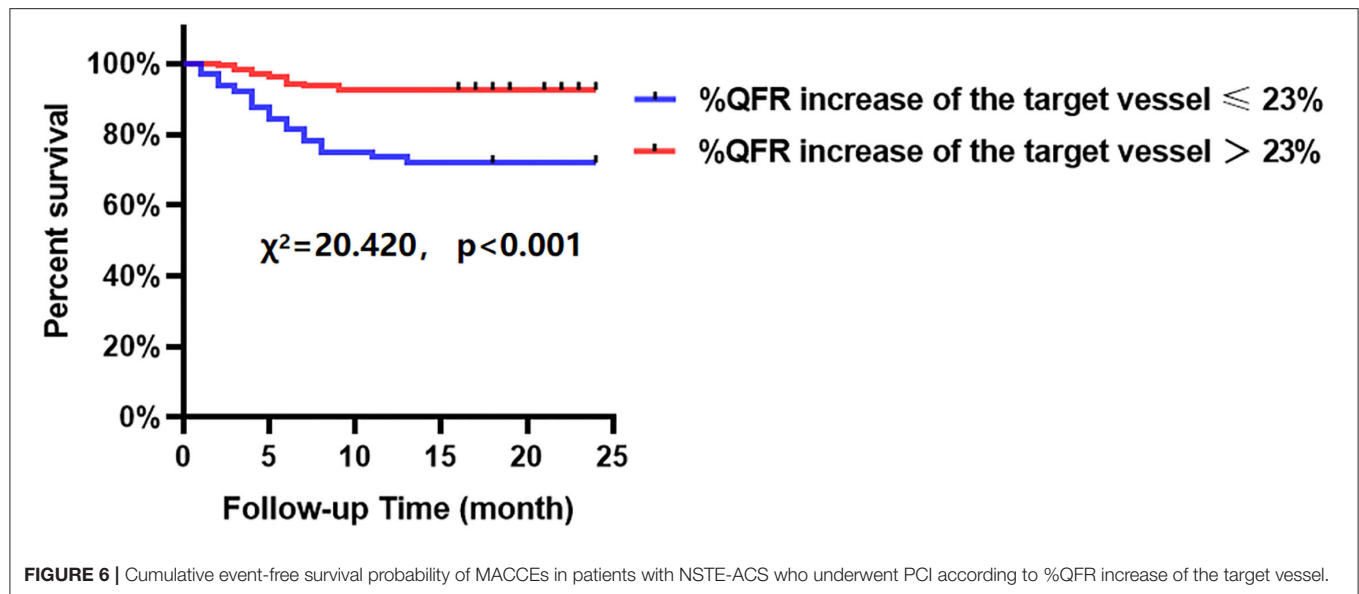
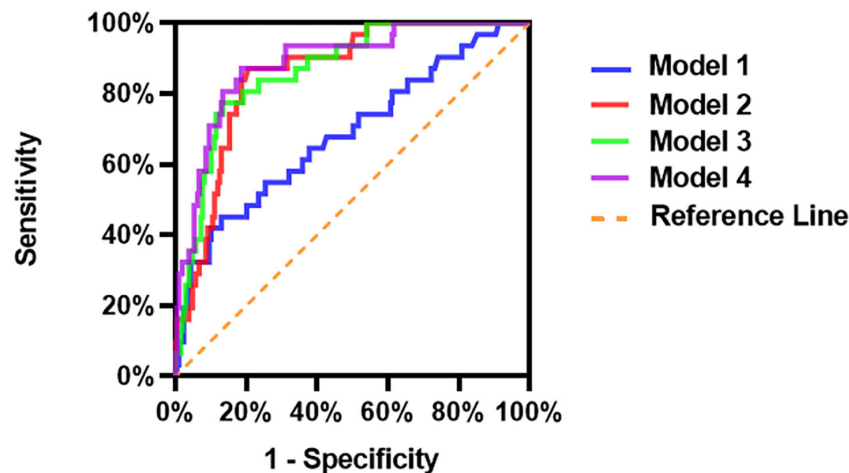


TABLE 7 | Potential predictors for the incidence of MACCEs in patients with NSTEMI-ACS who underwent PCI.

Variables	Univariate			Multivariate		
	HR	95% CI	P	HR	95% CI	P
Female	1.305	0.601–2.834	0.501			
Age (years)	0.976	0.943–1.010	0.163			
Hypertension (%)	2.425	1.188–4.950	0.015	6.816	2.986–15.559	<0.001
Diabetes mellitus (%)	1.804	0.876–3.717	0.110			
Current smoking (%)	1.022	0.504–2.073	0.952			
Current drinking (%)	0.972	0.419–2.257	0.948			
Family history of CAD (%)	0.783	0.238–2.576	0.688			
History of myocardial infarction	1.678	0.587–4.797	0.334			
Previous PCI (%)	1.427	0.684–2.979	0.343			
Average heart rate (beats/min)	1.035	0.988–1.085	0.147			
SDNN	1.003	0.996–1.011	0.412			
SDANN	1.006	0.995–1.018	0.276			
rMSSD	0.996	0.987–1.005	0.399			
Pnn50	1.012	0.991–1.034	0.246			
Total power (ms ²)	0.997	0.975–1.019	0.795			
LF (ms ²)	1.048	0.895–1.226	0.562			
HF (ms ²)	1.088	0.978–1.210	0.122			
High LF/HF (>1.08)	0.277	0.124–0.620	0.002	0.335	0.144–0.779	0.011
High DC 24h (>2.42 ms)	0.274	0.123–0.613	0.002	0.306	0.134–0.701	0.005
Number of diseased vessels	1.077	0.701–1.653	0.736			
Number of implanted stents	0.989	0.701–1.395	0.949			
Pre-PCI QFR	0.660	0.443–0.984	0.041	0.527	0.346–0.802	0.003
High post-PCI of the target vessel (>0.88)	0.156	0.073–0.331	< 0.001	0.318	0.129–0.780	0.012
High %QFR increase of the target vessel (>23%)	0.224	0.110–0.458	< 0.001	0.161	0.066–0.391	<0.001
Target vascular location	0.748	0.488–1.145	0.181			
Minimal lumen diameter of target vessel	1.869	0.751–4.647	0.179			
Maximum area stenosis of target vessel	0.982	0.950–1.016	0.295			
Lesion length of target vessels	1.002	0.968–1.036	0.924			



Model	AUC	SE	P	95%CI	Sensitivity	Specificity	Youden index	C-index
Model 1	0.685	0.055	0.001	0.578-0.793	45.2	87.1	0.323	0.702
Model 2	0.858	0.030	< 0.001	0.799-0.916	77.4	86.6	0.640	0.875
Model 3	0.867	0.031	< 0.001	0.807-0.928	87.1	79.4	0.665	0.881
Model 4	0.888	0.030	< 0.001	0.829-0.947	87.1	81.3	0.684	0.903

Model	B	SE	Wals	P	HR	95% CI
Model 1	0.061	0.015	17.400	<0.001	1.063	1.033-1.093
Model 2	0.046	0.007	42.055	<0.001	1.048	1.033-1.062
Model 3	0.045	0.006	50.917	<0.001	1.046	1.033-1.059
Model 4	0.049	0.006	65.642	<0.001	1.050	1.038-1.063

FIGURE 7 | Comparison of the predictive capacity and accuracy of predictive models for MACCEs. Model 1: Age + Sex + Hypertension + Diabetes mellitus + Current smoking + Family history of CAD + History of myocardial infarction. Model 2: Model 1 + Post-PCI QFR of the target vessel ≤ 0.88 . Model 3: Model 2 + %QFR increase of the target vessel $\leq 23\%$. Model 4: Model 3 + DC 24 h ≤ 2.42 ms.

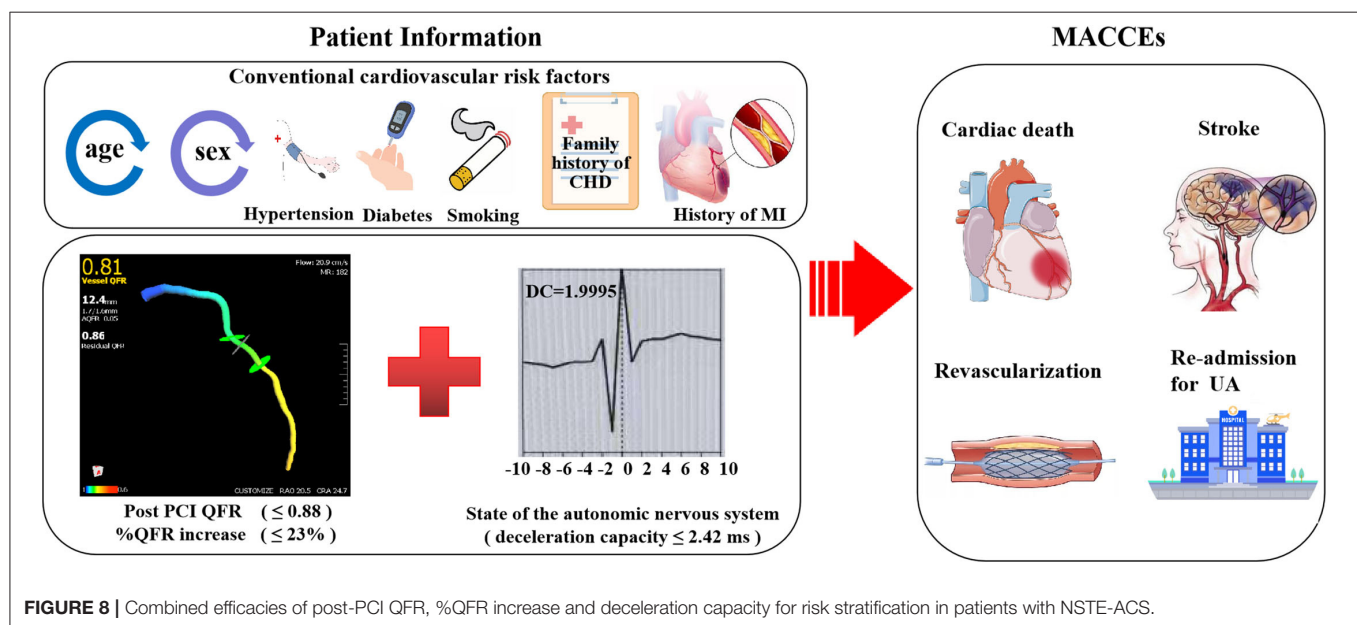


FIGURE 8 | Combined efficacies of post-PCI QFR, %QFR increase and deceleration capacity for risk stratification in patients with NSTEMI-ACS.

remains scant evidence from literature to indicate the potential association between ANS, hydrodynamic shear forces and the vulnerability of coronary plaque. Our results therefore support

the hypothesis that imbalance in cardiac ANS may affect local hydrodynamic shear forces and lead to vulnerability of coronary lesions, and may therefore play a key role in the pathogenesis

of acute coronary events. Interestingly, our previous studies showed a significant interaction between ANS and immune inflammation on coronary physiology evaluated by QFR (11, 39). These findings support the incorporation of ANS imbalance for risk stratification of patients with CAD. Notably, measurement of DC is refractory to external factors and premature beat, which could therefore objectively reflect the modulation of heart rate by the ANS and quantitatively analyze vagal nerve activity compared with HRV (12, 19, 20).

Our overall findings are in line with a previous prospective study including 2,111 patients with acute myocardial infarction, which demonstrated that impaired DC was a strong predictor of mortality after myocardial infarction, and the predictive efficacy of DC was even stronger than the conventional measures of HRV (12). In this study, we found that incorporation of relative increase and final QFR combined with DC is associated with stronger predictive efficacy of existing models based on clinical variables for MACCEs in patients with NSTEMI-ACS. Briefly, acute myocardial ischemia might impair cardiac vagal nerve and induce the production of inflammatory cytokines (14), and subsequently lead to endothelial dysfunction, lipid dysregulation, vascular smooth muscle cell activation, macrophage infiltration, thus accelerating coronary artery plaque rupture of residual lesions and effects on the burden of coronary heart disease (40, 41). Although the exact molecular pathways remain to be determined, the results of our study support the incorporation of relative increase and final QFR combined with DC to improve the predictive efficacy of existing models based on clinical variables for MACCEs in patients with NSTEMI-ACS.

STUDY LIMITATIONS

Due to the retrospective nature of the study, possible selection bias may overestimate the predictive value of DC 24h, post-PCI QFR or %QFR increase for MACCEs, particularly with the small sample size. In order to validate the predictive value of these parameters, prospective cohort studies with larger samples sizes will be required. Also, we evaluated the DC only once, on patient admission. It is unclear whether DC monitored for multiple times would be more valid as a predictor of MACCEs. In addition, it should be mentioned that the post-PCI QFR or %QFR increase has not yet been validated against post-PCI FFR or %FFR increase. Studies are warranted for further confirmation and optimization of the software and protocols for QFR measurement. Moreover, our findings might not be generalizable to other institutions due to the differences between offline and online analyses. Nevertheless, the concept regarding that “higher is better” for DC 24hr, post-PCI QFR or %QFR increase when undergoing complete revascularization with PCI is beyond doubt. In addition, intravascular ultrasound or optical coherence tomography may be considered to provide detailed assessment of culprit lesions and non-culprit lesions of the patients, and it might also improve the prognostic efficacy if parameters related to these examinations are incorporated. Due to methodological reasons, DC could not be applied to ACS patients with atrial fibrillation or other non-sinus rhythms.

Finally, no inflammatory markers were analyzed because we did not measure these markers in the included patients.

CONCLUSIONS

In conclusion, the results of our study showed that the relative increase and final coronary physiology combined with DC may improve the predictive efficacy of existing models based on clinical variables for MACCEs in NSTEMI-ACS patients who underwent complete and successful PCI. These results support the incorporation of relative increase and final coronary physiology combined with DC for risk stratification in NSTEMI-ACS patients, although validation will require larger prospective studies.

DATA AVAILABILITY STATEMENT

The datasets used and/or analyzed during this study are available from the corresponding author on reasonable request. Requests to access these datasets should be directed to LY, lileiyu@whu.edu.cn or HJ, hong-jiang@whu.edu.cn.

ETHICS STATEMENT

The studies involving human participants were reviewed and approved by the Ethics Committee of Renmin Hospital of Wuhan University (No. WDRY2021-K078). The Ethics Committee waived the requirement of written informed consent for participation.

AUTHOR CONTRIBUTIONS

LY and HJ: substantial contributions to conception and design, data acquisition, and data analysis and interpretation. JW, CL, FG, ZZ, HC, LZ, YW, HZ, ZL, SD, JS, QD, and SX: drafting the article or critically revising it for important intellectual content. JW, CL, and FG: final approval of the version to be published and agreement to be accountable for all aspects of the work in ensuring that questions related to the accuracy or integrity of the work are appropriately investigated and resolved. All authors contributed to the article and approved the submitted version.

FUNDING

This work was supported by the National Natural Science Foundation of China (81871486, 81970287, and 82100530).

SUPPLEMENTARY MATERIAL

The Supplementary Material for this article can be found online at: <https://www.frontiersin.org/articles/10.3389/fcvm.2022.848499/full#supplementary-material>

Supplementary Figure 1 | Comparison of the predictive capacity and accuracy of relative increase and final QFR and DC for MACCEs. Model 5: Model 1 + Post-PCI QFR of the target vessel ≤ 0.88 . Model 6: Model 1 + %QFR increase of the target vessel $\leq 23\%$. Model 7: Model 1 + DC 24h ≤ 2.42 ms.

REFERENCES

1. Tonino PA, De Bruyne B, Pijls NH, Siebert U, Ikeno F, van't Veer M, et al. Fractional flow reserve versus angiography for guiding percutaneous coronary intervention. *N Engl J Med*. (2009) 360:213–24. doi: 10.1056/NEJMoa0807611
2. De Bruyne B, Fearon WF, Pijls NH, Barbato E, Tonino P, Piroth Z, et al. Fractional flow reserve-guided PCI for stable coronary artery disease. *N Engl J Med*. (2014) 371:1208–17. doi: 10.1056/NEJMoa1408758
3. Xaplanteris P, Fournier S, Pijls NHJ, Fearon WF, Barbato E, Tonino PAL, et al. Five-year outcomes with PCI guided by fractional flow reserve. *N Engl J Med*. (2018) 379:250–9. doi: 10.1056/NEJMoa1803538
4. Lee JM, Hwang D, Choi KH, Rhee TM, Park J, Kim HY, et al. Prognostic implications of relative increase and final fractional flow reserve in patients with stent implantation. *JACC Cardiovasc Interv*. (2018) 11:2099–109. doi: 10.1016/j.jcin.2018.07.031
5. Biscaglia S, Tebaldi M, Brugaletta S, Cerrato E, Erriquez A, Passarini G, et al. Prognostic value of QFR measured immediately after successful stent implantation: the international multicenter prospective HAWKEYE study. *JACC Cardiovasc Interv*. (2019) 12:2079–88. doi: 10.1016/j.jcin.2019.06.003
6. Kogame N, Takahashi K, Tomaniak M, Chichareon P, Modolo R, Chang CC, et al. Clinical implication of quantitative flow ratio after percutaneous coronary intervention for 3-vessel disease. *JACC Cardiovasc Interv*. (2019) 12:2064–75. doi: 10.1016/j.jcin.2019.08.009
7. Kogame N, Ono M, Kawashima H, Tomaniak M, Hara H, Leipsic J, et al. The impact of coronary physiology on contemporary clinical decision making. *JACC Cardiovasc Interv*. (2020) 13:1617–38. doi: 10.1016/j.jcin.2020.04.040
8. Ridker PM, Everett BM, Thuren T, MacFadyen JG, Chang WH, Ballantyne C, et al. Antiinflammatory therapy with canakinumab for atherosclerotic disease. *N Engl J Med*. (2017) 377:1119–31. doi: 10.1056/NEJMoa1707914
9. Goldfine AB, Shoelson SE. Therapeutic approaches targeting inflammation for diabetes and associated cardiovascular risk. *J Clin Invest*. (2017) 127:83–93. doi: 10.1172/JCI88884
10. Hinterdobler J, Schott S, Jin H, Meesmann A, Steinsiek AL, Zimmermann AS, et al. Acute mental stress drives vascular inflammation and promotes plaque destabilization in mouse atherosclerosis. *Eur Heart J*. (2021) 19:ehab371. doi: 10.1093/eurheartj/ehab371
11. Wang J, Liu W, Chen H, Liu C, Wang M, Chen H, et al. Novel insights into the interaction between the autonomic nervous system and inflammation on coronary physiology: a quantitative flow ratio study. *Front Cardiovasc Med*. (2021) 8:700943. doi: 10.3389/fcvm.2021.700943
12. Bauer A, Kantelhardt JW, Barthel P, Schneider R, Mäkilä J, Ulm K, et al. Deceleration capacity of heart rate as a predictor of mortality after myocardial infarction: cohort study. *Lancet*. (2006) 367:1674–81. doi: 10.1016/S0140-6736(06)68735-7
13. Raab S, Plate KH. Different networks, common growth factors: shared growth factors and receptors of the vascular and the nervous system. *Acta Neuropathol*. (2007) 113:607–26. doi: 10.1007/s00401-007-0228-3
14. Borovikova LV, Ivanova S, Zhang M, Yang H, Botchkina GI, Watkins LR, et al. Vagus nerve stimulation attenuates the systemic inflammatory response to endotoxin. *Nature*. (2000) 405:458–62. doi: 10.1038/35013070
15. James JM, Mukoyama YS. Neuronal action on the developing blood vessel pattern. *Semin Cell Dev Biol*. (2011) 9:1019–27. doi: 10.1016/j.semdb.2011.09.010
16. Mendis S, Thygesen K, Kuulasmaa K, Giampaoli S, Mähönen M, Ngu Blackett K, et al. World Health Organization definition of myocardial infarction: 2008-09 revision. *Int J Epidemiol*. (2011) 40:139–46. doi: 10.1093/ije/dyq165
17. El Aarbaoui T, Méline J, Brondeel R, Chaix B. Short-term association between personal exposure to noise and heart rate variability: the RECORD MultiSensor Study. *Environ Pollut*. (2017) 231:703–11. doi: 10.1016/j.envpol.2017.08.031
18. Xhyheri B, Manfrini O, Mazzolini M, Pizzi C, Bugiardini R. Heart rate variability today. *Prog Cardiovasc Dis*. (2012) 55:321–31. doi: 10.1016/j.pcad.2012.09.001
19. Kantelhardt JW, Bauer A, Schumann AY, Barthel P, Schneider R, Malik M, et al. Phase-rectified signal averaging for the detection of quasi-periodicities and the prediction of cardiovascular risk. *Chaos*. (2007) 17:015112. doi: 10.1063/1.2430636
20. Liu Q, Chen YF, Fan SZ, Abbod MF, Shieh JS. Quasi-periodicities detection using phase-rectified signal averaging in EEG signals as a depth of anesthesia monitor. *IEEE Trans Neural Syst Rehabil Eng*. (2017) 25:1773–84. doi: 10.1109/TNSRE.2017.2690449
21. Authors/Task Force members., Windecker S, Kolh P, Alfonso F, Collet JP, Cremer J, et al. 2014 ESC/EACTS Guidelines on myocardial revascularization: the Task Force on Myocardial Revascularization of the European Society of Cardiology (ESC) and the European Association for Cardio-Thoracic Surgery (EACTS) developed with the special contribution of the European Association of Percutaneous Cardiovascular Interventions (EAPCI). *Eur Heart J*. (2014) 35:2541–619. doi: 10.1093/eurheartj/ehu278
22. Amsterdam EA, Wenger NK, Brindis RG, Casey DE Jr, Ganiats TG, Holmes DR Jr, et al. 2014 AHA/ACC guideline for the management of patients with non-ST-elevation acute coronary syndromes: a report of the American College of Cardiology/American Heart Association Task Force on Practice Guidelines. *J Am Coll Cardiol*. (2014) 64:e139–228. doi: 10.1016/j.jacc.2014.09.016
23. Tziakas D, Chalikias G, Al-Lamee R, Kaski JC. Total coronary occlusion in non ST elevation myocardial infarction: Time to change our practice? *Int J Cardiol*. (2021) 329:1–8. doi: 10.1016/j.ijcard.2020.12.082
24. Johnson NP, Tóth GG, Lai D, Zhu H, Açar G, Agostoni P, et al. Prognostic value of fractional flow reserve: linking physiologic severity to clinical outcomes. *J Am Coll Cardiol*. (2014) 64:1641–54. doi: 10.1016/j.jacc.2014.07.973
25. Li SJ, Ge Z, Kan J, Zhang JJ, Ye F, Kwan TW, et al. Cutoff value and longterm prediction of clinical events by FFR measured immediately after implantation of a drug-eluting stent in patients with coronary artery disease: 1-to 3-year results from the DKCRUSH VII registry study. *J Am Coll Cardiol Interv*. (2017) 10:986–95. doi: 10.1016/j.jacc.2017.09.197
26. Piroth Z, Toth GG, Tonino PAL, Barbato E, Aghlmandi S, Curzen N, et al. Prognostic value of fractional flow reserve measured immediately after drug-eluting stent implantation. *Circ Cardiovasc Interv*. (2017) 10:e005233. doi: 10.1161/CIRCINTERVENTIONS.116.005233
27. De Maria GL, Garcia-Garcia HM, Scarsini R, Hideo-Kajita A, Gonzalo López N, Leone AM, et al. Novel Indices of Coronary Physiology: Do We Need Alternatives to Fractional Flow Reserve? *Circ Cardiovasc Interv*. (2020) 13:e008487. doi: 10.1161/circinterventions.119.008487
28. Xu B, Tu S, Song L, Jin Z, Yu B, Fu G, et al. Angiographic quantitative flow ratio-guided coronary intervention (FAVOR III China): a multicentre, randomised, sham-controlled trial. *Lancet*. (2021) 3:50140-6736(21)02248-0. doi: 10.1016/S0140-6736(21)02248-0
29. Xu B, Tu S, Qiao S, Qu X, Chen Y, Yang J, et al. Diagnostic accuracy of angiography-based quantitative flow ratio measurements for online assessment of coronary stenosis. *J Am Coll Cardiol*. (2017) 70:3077–87. doi: 10.1016/j.jacc.2017.10.035
30. Honma Y, Araki T, Gianino S, Bruce A, Heuckeroth R, Johnson E, et al. Artemin is a vascular-derived neurotrophic factor for developing sympathetic neurons. *Neuron*. (2002) 35:267–82. doi: 10.1016/S0896-6273(02)00774-2
31. Zukowska Z, Grant DS, Lee EW. Neuropeptide Y: a novel mechanism for ischemic angiogenesis. *Trends Cardiovasc Med*. (2003) 13:86–92. doi: 10.1016/S1050-1738(02)00232-3
32. Pan L, Tang J, Liu H, Cheng B. Sympathetic nerves: how do they affect angiogenesis, particularly during wound healing of soft tissues? *Clin Hemorheol Microcirc*. (2016) 2:181–91. doi: 10.3233/CH-152019
33. Meng G, Zhou X, Wang M, Zhou L, Wang Z, Wang M, et al. Gut microbe-derived metabolite trimethylamine N-oxide activates the cardiac autonomic nervous system and facilitates ischemia-induced ventricular arrhythmia via two different pathways. *EBioMedicine*. (2019) 44:656–64. doi: 10.1016/j.ebiom.2019.03.066
34. Yu L, Wang Y, Zhou X, Huang B, Wang M, Li X, et al. Leptin injection into the left stellate ganglion augments ischemia-related ventricular arrhythmias via sympathetic nerve activation. *Heart Rhythm*. (2018) 15:597–606. doi: 10.1016/j.hrthm.2017.12.003
35. Yu L, Huang B, Zhou X, Wang S, Wang Z, Wang M, et al. Renal sympathetic stimulation and ablation affect ventricular arrhythmia by modulating autonomic activity in a cesium-induced long QT canine model. *Heart Rhythm*. (2017) 14:912–9. doi: 10.1016/j.hrthm.2017.02.010
36. Yu L, Huang B, Po SS, Tan T, Wang M, Zhou L, et al. Low-level tragus stimulation for the treatment of ischemia and reperfusion injury in patients

- with ST-segment elevation myocardial infarction: a proof-of-concept study. *JACC Cardiovasc Interv.* (2017) 10:1511–20. doi: 10.1016/j.jcin.2017.04.036
37. Florea VG, Cohn JN. The autonomic nervous system and heart failure. *Circ Res.* (2014) 114:1815–26. doi: 10.1161/CIRCRESAHA.114.302589
 38. Pedrigi RM, Poulsen CB, Mehta VV, Ramsing Holm N, Pareek N, Post AL, et al. Inducing persistent flow disturbances accelerates atherogenesis and promotes thin cap fibroatheroma development in D374Y-PCSK9 hypercholesterolemic minipigs. *Circulation.* (2015) 132:1003–12. doi: 10.1161/CIRCULATIONAHA.115.016270
 39. Liu C, Yu Z, Chen H, Wang J, Liu W, Zhou L, et al. Relationship between immunoinflammation and coronary physiology evaluated by quantitative flow ratio in patients with coronary artery disease. *Front Cardiovasc Med.* (2021) 2021:1223. doi: 10.3389/fcvm.2021.714276
 40. Tracey KJ. The inflammatory reflex. *Nature.* (2002) 420:853–9. doi: 10.1038/nature01321
 41. Dutta P, Courties G, Wei Y, Leuschner F, Gorbato R, Robbins CS, et al. Myocardial infarction accelerates atherosclerosis. *Nature.* (2012) 487:325–9. doi: 10.1038/nature11260

Conflict of Interest: The authors declare that the research was conducted in the absence of any commercial or financial relationships that could be construed as a potential conflict of interest.

Publisher's Note: All claims expressed in this article are solely those of the authors and do not necessarily represent those of their affiliated organizations, or those of the publisher, the editors and the reviewers. Any product that may be evaluated in this article, or claim that may be made by its manufacturer, is not guaranteed or endorsed by the publisher.

Copyright © 2022 Wang, Liu, Guo, Zhou, Zhou, Wang, Chen, Zhou, Liu, Duan, Sun, Deng, Xu, Jiang and Yu. This is an open-access article distributed under the terms of the Creative Commons Attribution License (CC BY). The use, distribution or reproduction in other forums is permitted, provided the original author(s) and the copyright owner(s) are credited and that the original publication in this journal is cited, in accordance with accepted academic practice. No use, distribution or reproduction is permitted which does not comply with these terms.

Advantages of publishing in Frontiers



OPEN ACCESS

Articles are free to read
for greatest visibility
and readership



FAST PUBLICATION

Around 90 days
from submission
to decision



HIGH QUALITY PEER-REVIEW

Rigorous, collaborative,
and constructive
peer-review



TRANSPARENT PEER-REVIEW

Editors and reviewers
acknowledged by name
on published articles

Frontiers

Avenue du Tribunal-Fédéral 34
1005 Lausanne | Switzerland

Visit us: www.frontiersin.org

Contact us: frontiersin.org/about/contact



REPRODUCIBILITY OF RESEARCH

Support open data
and methods to enhance
research reproducibility



DIGITAL PUBLISHING

Articles designed
for optimal readership
across devices



FOLLOW US

@frontiersin



IMPACT METRICS

Advanced article metrics
track visibility across
digital media



EXTENSIVE PROMOTION

Marketing
and promotion
of impactful research



LOOP RESEARCH NETWORK

Our network
increases your
article's readership